Sensible heat flux for estimating evaporation

by

MICHAEL J. SAVAGE

Submitted in fulfilment of the academic requirements of the degree of

Doctor of Science in Agriculture

in Agrometeorology

Soil-Plant-Atmosphere-Continuum Research Unit
School of Environmental Sciences
Faculty of Science and Agriculture
University of KwaZulu-Natal
Pietermaritzburg
South Africa

March, 2010

PREFACE

The research contained in this thesis was completed without supervision and carried out by the candidate while based in the Soil-Plant-Atmosphere Continuum Research Unit, Discipline of Agrometeorology, School of Environmental Sciences, Faculty of Science and Agriculture, University of KwaZulu-Natal, Pietermaritzburg, South Africa. The research was financially supported by the Water Research Commission, University of KwaZulu-Natal, the National Research Foundation, Texas A&M University and the United States Council for the International Exchange of Scholars (via a Senior Fulbright Scholarship) and in one part the research was contracted by the Council for Scientific and Industrial Research.

The contents of this work have not been submitted in any form to another university and, except where the work of others is acknowledged in the text, the results reported are due to investigations by the candidate.

As the candidate's administrative supervisor, I approve of this thesis.

Signed: ……

Date: 30 March 2010

DECLARATION 1: Plagiarism

I, Michael John Savage, declare that:

(i) the research reported in this thesis, except where otherwise indicated or acknowledged, is my original work;

(ii) this thesis has not been submitted in full or in part for any degree or examination to any other university;

(iii) this thesis does not contain other persons' data, pictures, graphs or other information, unless specifically acknowledged as being sourced from other persons;

(iv) this thesis does not contain other persons' writing, unless specifically acknowledged as being sourced from other researchers. Where other written sources have been quoted, then:

a) their words have been re-written but the general information attributed to them has been referenced

b) where their exact words have been used, their writing has been placed inside quotation marks, and referenced;

(v) where I have used material for which publications followed and of which I am an author or co-author, I have indicated in detail which part of the material was actually written by myself alone and have fully referenced such publications;

(vi) this thesis is primarily a collection of material, prepared by myself, published in various journals. In some cases, additional material has been included and in two cases, the contents of two journal submissions have been combined into a chapter. The reference style of the journal, for each chapter, has been retained and for convenience of the reader the references have been placed at the end of each chapter;

(vii) this thesis does not contain text, graphics or tables copied and pasted from the Internet, unless specifically acknowledged, and the source being detailed in the thesis and in the References sections.

Signed:  ……

Date: 30 March 2010

DECLARATION 2: Publications

1. Savage, M.J., K.J. McInnes and J.L. Heilman, 1995. Placement height of eddy correlation sensors above a short grassland surface. Agricultural and Forest Meteorology 74, 195–204.

This paper is an analysis of data I collected from a grassland site at Texas A & M University. I designed the experiment and collected and analysed the eddy covariance data, wrote the paper and was the corresponding author.
[Chapter 9]

2. Savage, M.J., K.J. McInnes and J.L. Heilman, 1996. The "footprints" of eddy correlation sensible heat flux density, and other micrometeorological measurements. South African Journal of Science 92, 137–142.

This paper is an analysis of data I collected from a grassland site at Texas A & M University. I wrote the paper and was the corresponding author.
[Chapter 9]

3. Savage, M.J., C.S. Everson and B.R. Metelerkamp, 1997. Evaporation measurement above vegetated surfaces using micrometeorological techniques. Water Research Commission Report No. 349/1/97, Pretoria, South Africa, p248, ISBN 1–86845–363–4.

I was project leader of this project, funded by the Water Research Commission (WRC), and instrumental in proposing the study, analysed the data and wrote the report. The second author, at the time based near the Catchment VI Cathedral Peak research site, played a major role in the data collection and site visits. The third author collected some of the data and did some of the Bowen ratio calculations under my supervision.
[Chapters 3, 8 and 9]

4. Savage, M.J., C.S. Everson, G.O. Odhiambo, M.G. Mengistu and C. Jarmain, 2004. Theory and practice of evaporation measurement, with special focus on surface layer scintillometry as an operational tool for the estimation of spatially averaged evaporation. Water Research Commission Report No. 1335/1/04, Pretoria, South Africa, p204, ISBN 1–77005–247–X.

I was project leader of this WRC-funded research, responsible for the site visitations, data collection and data analysis. I wrote the report.
[Chapters 4, 5, 6 and 7]

5. Odhiambo, G.O. and M.J. Savage, 2009. Surface layer scintillometer and eddy covariance sensible heat flux comparisons for a mixed grassland community as affected by Bowen ratio and MOST formulations. Journal of Hydrometeorology 10, 479–492.

I obtained the funding for this WRC-funded research, conducted and supervised the site visitations, undertook the data analysis, rewrote the first version submitted after the student indicated that he could not make the changes requested by the reviewers. For the rewriting, I recalculated the data and developed the theory presented in the second and final version of the paper and was the corresponding author.

[Chapter 5]

6. Odhiambo, G.O. and M.J. Savage, 2009. Surface layer scintillometry for estimating the sensible heat flux component of the surface energy balance. South African Journal of Science 105, 208–216.

This is a review of a topic that I pursued as part of a WRC project that I was responsible for. I initiated and finalised Table 2.1 which was used in the first version of the paper, rewrote the second and third versions of the paper, was corresponding author and undertook all changes requested by the journal.
[Chapter 2]

7. Savage, M.J., 2009. Estimation of evaporation using a dual-beam surface layer scintillometer and component energy balance measurements. Agricultural and Forest Meteorology 149, 501–517.

I was responsible for the WRC project on which this work was based. This entailed undertaking site visitations, data collection, data analysis, writing and submission of the work to the journal.
[Chapter 4]

8. Savage, M.J. and J.L. Heilman, 2009. Infrared calibration of net radiometers and infra red thermometers. Agricultural and Forest Meteorology 149, 1279–1293.
This work was started at Texas A & M University. I undertook all measurements. My co-author was shown early versions of the paper and was involved after the paper was returned by the journal for modification. I was the corresponding author.
[Chapter 3]

9. Mengistu, M.G. and M.J. Savage, 2010. Open water evaporation for a small shallow dam in winter using surface renewal and eddy covariance methods. Journal of Hydrology 380, 27–35.

This work was part of a larger WRC project awarded to the Council for Scientific and Industrial Research (CSIR). I was a member of the project team but also contracted by the CSIR for this research. We (the authors) depended heavily on support from staff of the CSIR during the field programme. I was instrumental in proposing this study, made the necessary fine-wire and water temperature sensors, was actively involved during the experimental setup, did all of the datalogger programming, error-checked the data, performed the eddy covariance and stored heat flux calculations and was the corresponding author responsible for the changes requested by the journal in consultation with the second author. I performed a complete reanalysis of the data following the first submission of the paper.
[Chapter 10]

10. Savage, M.J., C.S. Everson and B.R. Metelerkamp, 2009. Bowen ratio evaporation measurement in a remote montane grassland: Data integrity and fluxes. Journal of Hydrology 376, 249–260.

I was project leader of this research, funded by the WRC. I was instrumental in proposing the study, analysed the data, wrote the paper and was the corresponding author. The second author played a major role in the data collection and site visits. The third author collected some of the data and did some of the Bowen ratio calculations under my supervision.
[Chapter 8]

11. Savage, M.J., G.O. Odhiambo, M.G. Mengistu, C.S. Everson and C. Jarmain, 2010. Measurement of grassland evaporation using a surface-layer scintillometer. Water SA 36, 1–8.

I was project leader of this WRC-funded research. I was responsible for the site visitations, data collection, data analysis, writing and submission of the work to the journal. I was the corresponding author. I wrote the paper.
[Chapter 6]

12. Mengistu, M.G. and M.J. Savage, 2010. Surface renewal method for estimating sensible heat flux. Water SA 36, 9–17.

The surface renewal method was first used by me as part of the WRC surface-layer scintillometer project that I led. I was instrumental in proposing this review and was the corresponding author responsible for a substantial rewrite of the paper.
[Chapter 2a]

13. Savage, M.J., 2010. Flux estimation using a simple implementation of an iterative method: examples using MOST, surface renewal, Penman-Monteith reference evaporation and the psychrometric equation. Abstract, Combined Congress 2010, South African Society for Horticultural Sciences, Weed Science Society, Crop Production Society and Soil Science Society of South Africa.

This work, as a supplement to various chapters (specifically Chapters 4, 5, 6, 7, and 10) is my own work using data from various sources, including data I collected when we first used the surface renewal and surface-layer scintillometer methods. Data from other sources for use in estimating grass reference evaporation and wet bulb is acknowledged.
[Appendix for Chapters 4, 5, 6, 7 and 10]

Signed: …..  ……

Date: 30 March 2010

ACKNOWLEDGEMENTS

A number of special acknowledgements deserve specific mention:

Meryl A. Savage for her support through the many years that the reported research encompasses;

Jothimala Manickum for her administrative and technical support over the last fifteen years;

Professor Colin S. Everson of the Council for Scientific and Industrial Research (CSIR) for the research cooperation from the early 1990 under-the-mountain lysimeter days;

the masters and PhD students, who so willingly took ideas and tested them through their field experimentation, but in particular Michael G. Abraha, Michael G. Mengistu and Eltayeb S. Nile;

the anonymous reviewers of the various papers and the efforts of the Editors/Sub-editors of Agricultural and Forest Meteorology, Journal of Hydrology, Journal of Hydrometeorology, South African Journal of Science and Water SA;

the various agencies for funding and in particular the South African Water Research Commission (WRC) and the University of KwaZulu-Natal (UKZN);

the many colleagues from WRC, CSIR, UKZN and other universities and research institutions for assistance over the years in many different ways;

the staff from the various UKZN workshops who assisted: Electronics Centre, Mechanical Instruments, Howard College/Westville Workshops. In particular, Mr Guy M. Dewar assisted in many different ways and the Howard College/Westville staff hosted our annual fine-very-fine-wire thermocouple welding days. The support of other UKZN technical staff is also acknowledged.

Chapter 2 (Selected methods for estimating the sensible heat flux component of the surface energy balance: surface-layer scintillometry) The financial support from the University of KwaZulu-Natal, the Water Research Commission (WRC project K1335) and the National Research Foundation is acknowledged. Support of the WRC project team and Steering Committee members and the owner and workers of Bellevue Farm, where the field research work for the WRC project was conducted, is gratefully acknowledged. This work was rewritten following an early submission to S. Afr. J. Sci. by Dr G.O. Odhiambo.

Chapter 2a (Selected methods for estimating the sensible heat flux component of the surface energy balance: surface renewal) Funding from the University of KwaZulu-Natal, CSIR, and Water Research Commission (part of projects K1335 and K1567) for this study is gratefully acknowledged.

Chapter 3 (Infrared calibration of net radiometers and infrared thermometers)
Funding from the WRC through projects K349 and K1335, University of KwaZulu-Natal, the South African National Research Foundation (NRF) and the United States Council for the International Exchange of Scholars for a Fulbright grant is gratefully acknowledged. Dr Gaylon S. Campbell (Decagon, Pullman, Washington, USA) contributed to some of the early impetus of this work. Mr Guy M. Dewar of the Electronics Centre (UKZN) ably assisted with the electronics for heater stirrer and lighting control of the large radiator and Mr Roelie Hendriks of the Mechanical Instruments Workshops assisted with the water bath and pump. The manuscript benefitted from comments from the anonymous reviewers and the Associate Editor of Agricultural and Forest Meteorology.

Chapter 4 (Estimation of evaporation using a dual-beam surface layer scintillometer and component energy balance measurements)
Funding from the WRC and the contribution of the members of the Steering Committee and the project team is gratefully acknowledged. Additional funding in the latter stages of the project from the NRF is also gratefully acknowledged. The project was only possible with the cooperation of the following: George Odhiambo, Michael Mengistu, Peter Dovey, Jothi Manickum; UKZN for part-payment of the surface layer scintillometer equipment; owner Mr S.J. Hilcove and farm manager Mr H. Ovenstone and workers of the Bellevue farm site used for this research; Mr Vivek Naiken of the CSIR for assistance with Fig. 4.1. This work benefitted from comments from the anonymous reviewers from Agricultural and Forest Meteorology.

Chapter 5 (Sensible heat flux by surface layer scintillometry and eddy covariance over a mixed grassland community as affected by Bowen ratio and MOST formulations for unstable conditions)
Financial support from the WRC, UKZN and the NRF is acknowledged. The assistance received from the WRC Steering Committee and project team members is gratefully acknowledged. Our gratitude also goes to the owner Mr S.J. Hilcove and farm manager Mr H. Ovenstone and workers of the Bellevue farm where this study was carried out. The manuscript benefited from the valuable comments of the reviewers.

Chapter 6 (Measurement of grassland evaporation using a surface-layer scintillometer)
The financing of the project by the WRC through projects K349 and K1335 and the contribution of the members of the two WRC Steering Committees is gratefully acknowledged. Additional funding in the latter stages of the WRC K1335 scintillometer project from the NRF is also gratefully acknowledged.

The CSIR kindly provided the open-path EC system. The project was only possible with the cooperation of the following: owner Mr S.J. Hilcove and farm manager Mr H. Ovenstone of the Bellevue farm site used for this research; Ms Jothimala Manickum (Agrometeorology) of the School of Environmental Sciences, UKZN for her assistance, and Mr Peter N Dovey for part of the technical support required for this project.

Chapter 7 (Sensible heat flux estimation using temperature variance above various canopies for unstable conditions)
The financing of the Bellevue scintillometer project, conducted at the grassland site, by the Water Research Commission and the contribution of the members of the Steering Committee is gratefully acknowledged. This work was only possible with the cooperation of the following: owner Mr S.J. Hilcove, farm manager Mr H. Ovenstone of the Bellevue farm site used for this research, the Agrometeorology postgraduate students involved (Dr George O. Odhiambo, Mr Michael G. Mengistu), Ms Jody Manickum (Agrometeorology) of the School of Environmental Sciences, University of KwaZulu-Natal for her assistance, Mr Peter N. Dovey for part of the technical support required for the scintillometer project and project team members from the CSIR (Drs Colin S. Everson and Caren Jarmain and others); Dr Monique Y. Leclerc of the University of Georgia, Griffin, USA who provided the pine canopy EC data, Mr Gator Howerton for collecting the field data and Drs Anand Karipot and Tara Prabha who provided assistance with some of the Fortran programming for analyzing the eddy covariance data; the Hluhluwe work was only possible through assistance from Hluhluwe staff, Michael Mengistu and assistance in the field from the CSIR team (Drs Colin Everson and Caren Jarmain, Mr Alistair Clulow and others). Michael G. Abraha provided some insight into this work using data from another project but these results are not reported on here.

Chapter 8 (Bowen ratio evaporation measurement in a remote montane grassland: Data integrity and fluxes)
Funding from the WRC through projects K349 and K1335, UKZN, the NRF, and the CSIR which also provided technical support and infrastructure is gratefully acknowledged. The Department of Water Affairs and Forestry are also thanked for their initial funding of the project. The technical support of G. Molefe and K. Hudson, and the two WRC Steering Committees, was invaluable.

Chapter 9 (Placement height and "footprints" of eddy covariance sensors above a short turfgrass surface)
Texas A & M University and the United States Council for the International Exchange of Scholars for a Fulbright grant provided financial support for this research. Use of two of the EC systems from Dr W.A. Dugas, Blackland Research Centre, Texas Agricultural Experiment Station, Temple, Texas is gratefully acknowledged. The comments from anonymous reviewers for Agricultural and Forest Meteorology are gratefully acknowledged. Use of EC systems from Dr C.S. Everson of the CSIR for the spectral analysis of the Pietermaritzburg placement height research is gratefully acknowledged.

Chapter 10 (Open water evaporation estimation for a small shallow reservoir in winter using surface renewal)
We acknowledge the staff of the Department of Water Affairs and Forestry offices at Midmar for allowing the use of their facilities for this work. This work would not have been possible without the technical support from Mr E.S. Nile and Mrs J. Manickum, (UKZN) and Mr A.D. Clulow, Professor

C.S. Everson and Dr C. Jarmain (CSIR). Funding for this research from the UKZN, CSIR, and WRC as part of projects K1335 and K1567 is gratefully acknowledged.

Appendix (Flux estimation using a simple implementation of an iterative method: examples using MOST, surface renewal, Penman-Monteith reference evaporation and the psychrometric equation).

The weather station data for Pretoria for the ETo and wet bulb calculations were provided by the South African Weather Service, Pretoria, South Africa and that for Kaalrug by the South African Sugar Research Institute. We acknowledge financial support from the UKZN, CSIR, and WRC as part of projects K349, K1335 and K1567. Thanks to my postgraduates for pestering me to work on these procedures.

Genesis 1: 1 In the beginning God created the heaven and the earth. And the earth was without form, and void; and darkness was upon the face of the deep. And the Spirit of God moved upon the face of the waters.

ABSTRACT

The focus of the research is on investigations of various methods for obtaining sensible heat flux (H) for estimating evaporation. The key for this approach is the application of the shortened energy balance equation, and in the case of methods based on the Monin-Obukhov similarity theory (MOST), such as surface-layer scintillometry and temperature variance with adjusted for stability using air temperature skewness, and surface renewal (SR), the iterative procedures. The application of the shortened energy balance requires that errors associated with measurement of net irradiance (R_{net}) and soil heat flux (S) are kept to a minimum. To this end, methodology for the calibration of net radiometers for both the infrared and short wave irradiances receive attention. A field study attempts to quantify the error in soil heat flux measurement for a mesic grassland. A standard, convenient and accurate method for calibrating net radiometers would assist in unravelling reasons for the perplexing lack of surface energy balance closure when employing the eddy covariance (EC) flux estimation method as well as improve on the accuracy of the energy balance residual method for estimating evaporation. A relatively inexpensive, accurate and quick laboratory method, based on physical theory, for non-steady radiative conditions above a large water-heated or water-cooled radiator containing circulated water, with surface-embedded thermocouples is used to obtain reproducible net radiometer calibration factors for the infrared waveband for a wide range in net irradiance. When applied, the method would reduce error in the most important term of the shortened energy balance and assist in energy balance closure aspects of EC measurements. The SLS method, reliant on MOST, is used for estimating areally-averaged H for a mesic grassland for a 30-month period. Comparisons with EC measurements feature prominently in this unique study. These comparisons include using different MOST procedures and the influence of the Bowen ratio on SLS measurements of H is investigated. Furthermore, since there are reports in the literature that the EC method may underestimate H and/or latent energy flux (LE), resulting in the shortened energy balance not being closed, effort is devoted to this aspect. Other methods used for comparison purposes are the traditional Bowen ratio energy balance (BREB), SR, TV and ETo (grass reference) methods. The TV and SLS and/or EC measurements of H are compared above three contrasting canopy surfaces. It is shown that other high frequency air temperature-based methods, for example, for the first time the TV method with adjustment for skewness, may pave the way for evaporation stations from which real-time and sub-hourly estimates may be obtained relatively inexpensively. Another area of research that receives attention is the placement height of EC instruments above short-canopy surfaces and a spectral analysis of the vertical wind speed and sonic temperature measurements for close-canopy placement heights. The SR method is used to estimate, for the first time, open-water evaporation. The ideal SR method applied above canopies is the most inexpensive micrometeorological method for estimating H, but the SR weighting factor α needs to be determined using EC and for this reason, the TV method with adjustment for skewness was investigated. Finally, a unique implementation of SR uses an iterative method for calculating H. A similar iterative procedure is applied for MOST and ETo calculations.

EXTENDED ABSTRACT

The 1998 Republic of South Africa National Water Act refers to the possible prescription, by government, of methods for making a volumetric determination of water for purposes of water allocation and charges in the case of activities resulting in stream flow reduction. Given this scenario and the demand on water resources it is important to consider how evaporation, one of the main components of the water balance, and of the energy balance, is to be measured or estimated with reliable accuracy and precision. Determination of reliable and representative evaporation data is an important aspect of atmospheric research with respect to applications in agriculture, catchment hydrology and the environmental sciences, not only in South Africa. Long-term measurements of evaporation at different time scales and from different climate regions are not yet readily available.

Nature and scope

This work focuses on the measurement of sensible heat flux (H) and estimation of evaporation through the use of the shortened energy balance. Included in the shortened energy balance are the sensible and soil heat fluxes, net irradiance and the latent energy flux (LE). Evaporation is calculated, from the latent energy flux estimated as a residual of the energy balance, thereby forcing energy balance closure, by measurement of net irradiance and soil heat flux as well as H using surface-layer scintillometer (SLS), eddy covariance (EC), Bowen ratio energy balance (BREB), surface renewal (SR) and temperature variance (TV) methods. All of these methods are essentially point-based methods except for the SLS path-weighted method which is also used for comparison.

Key significant/technological questions

Key questions that existed prior to the commencement of the research included: would it be possible to use integrative methods for which flux measurements represent a large area? Also, can the method of estimating evaporation using the shortened energy balance be applied to different surfaces? At the commencement of this research in the 1990s, only the BREB and EC micrometeorological methods had been used with some measure of success in a montane grassland. However, there were many aspects of uncertainty in these comparative measurements. For both EC and BREB methods, particularly for fetch-limited sites such as those usually available in topographically variable KwaZulu-Natal, the fetch to measurement height ratio for representative measurements was a key uncertainty. In the case of the BREB method, practical aspects such as the measurement heights for the two levels and theoretical aspects in terms of correctly defining data exclusion for when the BREB method fails. In the case of the EC measurements, trial and error was used to initially determine measurement frequency, the averaging period and the placement height. At that time, it was not possible to store the high frequency EC data so almost a decade had to pass before the technology improved to make this possible. Furthermore, the EC equipment could not be left unattended without sensor damage by rain or dew. This limited the use of EC considerably. Other questions emanated from this work: would it be possible to use high frequency air temperature data to obtain H and together with the measurements of net irradiance and soil heat flux, estimate evaporation using the simplified energy balance; would it be possible to answer the questions surrounding placement height, fetch, measurement frequency, the uncertainties in the implementation of MOST, the contribution of net irradiance measurements to the overall error in estimating evaporation, but more importantly, could a less expensive method for estimating H be found?

Research objectives

The overarching objective of the research is the investigation of micrometeorological methods for measuring *H* for calculating *LE* and hence evaporation using the shortened energy balance. To this end, a number of broad objectives are listed:

literature review: at the commencement of this investigation, there was no review on SLS methodology and SR methodology. Understanding the literature for these two areas of research was key in mapping research progress;

theoretical investigations: a number of theoretical investigations were necessary during the study. These included understanding MOST, and its application, EC and BREB theory, footprint analysis and theoretical development for the correction of sonic temperature for water vapour pressure, atmospheric pressure and the Bowen ratio. These were important issues that guided the research as it progressed;

calibration studies: early on in the investigations, the importance of the role of net irradiance measurements was realised. To this end, net radiometer calibration studies were key in understanding the components of the shortened energy balance. Other calibration studies improved the understanding of the BREB method;

field studies: these played a central role in the investigations and allowed a number of key questions to be answered from which further questions emerged. Some field studies were undertaken to answer specific questions, such as the EC placement height and the SR open water studies, but other studies such as the Cathedral Peak BREB and Bellevue SLS studies were used to gather data which served to answer a number of key questions. An objective of this research was to use the SLS method, previously untested in South Africa, to obtain measurements of areally averaged *H* and compare with measurements using the BREB and EC methods and also to estimate evaporation from the additional measurements of net irradiance and soil heat flux. A method chosen for preliminary measurement comparisons was the relatively new SR method, also previously untested in South Africa, for measuring *H*. The TV method, which relies on MOST was also tested. The SR and TV methods are the least expensive of the methods used and are both based on high frequency air temperature measurements;

analysis of data integrity and validity: a huge amount of data were collected in the various investigations. Analysis and definition of valid data was an extremely important aspect of the research for BREB, EC, SLS, SR and TV methods for estimating *H*. The protocols for inclusion of valid data and exclusion of suspect or invalid data were defined with care;

inter-comparison methods/studies: the benefit of the long-term studies, such as the Cathedral Peak BREB and Bellevue SLS studies, were key in that after the installation of the initial equipment, more and more equipment and methods were used and applied thereby allowing comparisons among the various estimation methods.

Literature reviews

The SLS and SR methods for estimating *H* are reviewed. The former method relies on the Monin-Obukhov similarity theory (MOST) for which homogeneous conditions in the inertial layer is assumed. The SR method is not based on MOST and may be used in the inertial and roughness layers. The relatively recently developed scintillometry method, with a focus on the dual-beam SLS, allows boundary-layer atmospheric turbulence, surface sensible heat and momentum flux to be estimated in real-time. Much of the previous research using the scintillometer method has involved the large aperture scintillometer method, with only a few studies using the SLS method. The SLS method has been mainly used by agrometeorologists, hydrologists and micrometeorologists for atmospheric

stability and surface energy balance studies to obtain estimates of sensible heat from which evaporation estimates representing areas of one hectare or larger are possible. Other applications include the use of the SLS method in obtaining crucial input parameters for atmospheric dispersion and turbulence models. The SLS method relies upon optical scintillation of a horizontal laser beam between transmitter and receiver for a separation distance typically between 50 and 250 m caused by refractive index inhomogeneities in the atmosphere that arise from turbulence fluctuations in air temperature and to a much lesser extent the fluctuations in water vapour pressure. Measurements of SLS beam transmission allow turbulence of the atmosphere to be determined, from which sub-hourly, real-time and *in situ* path-weighted fluxes of sensible heat and momentum may be calculated by application of MOST. Unlike the EC method for which corrections for flow distortion and coordinate rotation are applied, no corrections to the SLS measurements, apart from a correction for water vapour pressure, are applied. Also, path-weighted SLS estimates over the propagation path are obtained. The SLS method also offers high temporal measurement resolution and usually greater spatial coverage compared to EC, BREB, SR and other sensible heat measurement methods. Applying the shortened surface energy balance, measurements of net irradiance and soil heat as well as SLS estimates of sensible heat allows path-weighted evaporation from the surface to be estimated. Research applications involving the use of the SLS method, as well as the theory on which the method is based, are presented.

Inexpensive methods for estimating H are of considerable interest. If such a method could be found, for short canopies, latent energy flux could be estimated using a shortened surface energy balance from measurements of sensible and soil heat flux and the net irradiance at the surface. To this end, the SR method was investigated. The SR method for estimating sensible heat, latent energy, and other scalar fluxes has the advantage over other micrometeorological methods since the method requires only measurement of the scalar of interest at one point and the method may be applied close to the canopy surface, thereby reducing fetch requirements. The SR analysis for estimating H from canopies involves high frequency air temperature measurements (typically 2 to 10 Hz) using unshielded and naturally-ventilated 25- to 75-μm diameter fine-wire thermocouples. The SR method is based on the premise that a parcel of air connected to the surface, after it has been enriched or depleted, is renewed by an air parcel from above. There are two SR analysis approaches: the ideal SR analysis approach which presumes a constant α factor; a set of SR approaches that avoid the use of the α calibration factor. The weighting factor α depends on measurement height, canopy structure and stability conditions since it depends on the capability of the highest frequency eddies to mix the scalar within the air parcels renewed by coherent structures. A combination approach using SR and either similarity theory, that requires friction velocity or wind speed measurements, or dissipation theory, have also been used to estimate H. The combination SR and dissipation method only requires high frequency air temperature data and may be considered not to require calibration. The ideal SR and combination SR/dissipation approaches are the least expensive micrometeorological methods for estimating H and also LE if one forces closure of the surface energy balance. However application of SR analysis using slow dataloggers require some expertise since high frequency air temperature data are not usually stored with the slower dataloggers. Some structure functions can be stored for post-processing and determination of ramp amplitude and ramp period, but the appropriate time lags have to be chosen *a priori*. Fortunately, modern dataloggers avoid this problem and complex SR analysis approaches can now be applied. However, routinely applications using the ideal SR analysis approach with slow dataloggers may be of interest since it is a very affordable method.

Net radiometer calibration investigation

The estimation of evaporation as a residual using the shortened energy balance is critically depended on the net irradiance. A standard, convenient and accurate method for calibrating net radiometers would assist in unravelling reasons for the perplexing lack of surface energy balance closure as well as improving on the accuracy of the energy balance residual method for estimating evaporation. A relatively inexpensive, accurate and quick laboratory method for non-steady radiative conditions above a large water-heated or water-cooled radiator containing circulated water, with surface-embedded thermocouples, was used to obtain reproducible net radiometer calibration factors for the infrared waveband for a wide range in net irradiance. Infrared calibration factors for two-component, four-component, miniature polyethylene, polyethylene-domed (with and without ventilation) and domeless net radiometers were obtained. A method was also used for the shortwave calibration of net radiometers by placement of a net radiometer adjacent to a standard shortwave radiometer with both instruments placed above the radiator. Measurements from heated-needle anemometers demonstrated that thermally induced wind speed was not a significant factor in the infrared calibrations. Furthermore, the temperature gradient across the radiator was fairly uniform at any time. For the infrared calibrations, the two- and four-component net radiometers yielded average root mean square errors (RMSE) of 0.88 and 0.97 W m^{-2} respectively compared to 0.92 W m^{-2} for the polyethylene-domed net radiometers, 2.59 W m^{-2} for four domeless units and 2.27 W m^{-2} for a polyethylene-domed miniature net radiometer. Theory presented and collected measurements allowed the net radiometer infrared calibration factor to be determined for cases when the infrared irradiance from the environment was not constant. For the broadband domeless net radiometers used, the shortwave and infrared calibration factors were within 6.5 % of each other and yet 24.3 % different for some of the polyethylene-domed instruments. The use of ventilators, for polyethylene-domed net radiometers, resulted in more variable data and larger-than-expected infrared calibration factors. The most consistent infrared calibrations for the domed net radiometers were obtained using an air-conditioned laboratory. The radiator method also provides a convenient method for calibrating a number of infrared thermometers (IRTs) simultaneously for a wide temperature range. Different regression procedures for the non-linear calibration relationships, for IRTs with and without a body temperature sensor, were applied to obtain estimates of the radiator surface temperature. The residuals between the average radiator surface temperature and the corresponding IRT target temperature measurements were within 0.15 ^{o}C for all IRT types except for a handheld IRT unit which was within 0.2 ^{o}C. The radiator method used allows net radiometers to be calibrated for both infrared and shortwave under near-identical laboratory conditions, as well as IRTs to be calibrated, and is relatively simple to set up and operate.

Bellevue long-term field investigation using SLS, BREB and EC methods

In spite of the usefulness of scintillometry, the idea of routine and long-term measurements using scintillometry has in general not been achieved. A dual-beam SLS, for the estimation of H for a path length of 101 m, was used in a mixed grassland community in the eastern seaboard of South Africa for 30 months. Measurements also included BREB and EC estimates of H. Acceptable SLS data between 06h00 and 18h00, judged by the percent of error-free 1-kHz data exceeding 25 % and an inner scale of turbulence exceeding 2 mm, showed little seasonal variation and was consistently high –between 86.7 % and 94.8 %. An analysis of the various MOST empirical dimensionless stability functions used for estimating H from the SLS measurements showed percent differences in H that varied from -30 to 28 % for neutral to unstable conditions respectively and for stable continuous conditions the differences in H were within 60 W m^{-2} with much larger differences for stable sporadic conditions. The good

agreement in measurements of H over an extended period for the SLS, BREB and EC methods demonstrates the applicability and robustness of the SLS method and the associated MOST empirical functions used for estimating H for a range of canopy heights, stability conditions and diurnal and seasonal weather conditions. Furthermore, there was no evidence for an underestimation in EC sensible heat compared to SLS and BR measurements, which implies that any lack of energy balance closure points to possible latent energy EC underestimation or due to energy fluxes not included in the shortened energy balance if the net irradiance and soil heat flux components are correct. A sensitivity analysis was used to determine the relative importance of the SLS data inputs of air temperature, atmospheric pressure, beam path length and beam height on H estimates. Worst-case errors in air temperature, atmospheric pressure, beam path length and beam height resulted in errors in H within 1.0, 1.3, 3.0 and 4.0 % respectively. Overall, the worst-case total percent error in SLS-estimated H is within 5.3 % and the typical percent error is within 3.9 %. Accounting for the error in net irradiance and soil heat flux measurements, the seasonal variation in the error in daily evaporation estimated as a residual of the energy balance is generally less than 0.2 mm (0.49 MJ m^{-2}) in winter when the daily evaporation was about 1 mm (2.45 MJ m^{-2}) and typically less than 0.4 mm (0.98 MJ m^{-2}) when the evaporation exceeded 4 mm (9.8 MJ m^{-2}). Soil heat flux density measurements can contribute significantly to the overall error.

The SLS measurement of H is dependent on the Bowen ratio (β). Measurements of H_{SLS} were compared with those obtained using EC for a wide range of β. A comparison of the SLS-measured structure parameter of air temperature C_T^2 corrected for β and that uncorrected was carried out at a mixed community grassland site, with the results showing good correspondence but with a slight bias indicating that not correcting SLS measurements of C_T^2 for β would also result in a slight bias in H. Eddy covariance estimates of sensible heat flux (H_{EC}), obtained using averaging periods between 1 and 120 min and compared with SLS measurements, demonstrated that short-time averaging periods resulted in H_{EC} underestimated. The EC measurements for 60- and 120-min averaging periods were sometimes inconsistent with SLS measurements. A sensitivity analysis indicates that both the EC and SLS measurements of H are influenced by β. For $0 < \beta < 0.2$, the correction to H_{SLS} amounts to more than 10 % compared to more than 20 % for H_{EC} although the magnitude of the differences are small. A comparison of H_{EC} and H_{SLS} measurements for 0.1-intervals of β, for β between 0 and 4.3 shows reasonable correspondence for $\beta > 1$. For $0 < \beta < 1$, the H_{SLS} (y) *vs* H_{EC} (x) scatterplot linear regression slope decreased from 1.25 to close to 1 for β increasing from 0 to 1. A comparison between β-corrected H_{EC} and H_{SLS} measurements – the latter computed using various empirical stability functions used by MOST – shows significant differences compared to H_{EC} ranging from almost 20 % overestimation for some methods to 20 % underestimation for others. Long-term use of the recommended MOST stability functions for the SLS method is shown to result in reasonable correspondence between SLS and H_{EC} for a wide range in atmospheric conditions, stability, and sensible heat magnitude.

From H estimates using SLS and measurements of soil heat flux and net irradiance for the grassland site, evaporation rates were calculated as a residual of the shortened energy balance equation and compared with grass reference evaporation rates (ETo). Inconsistent hourly ETo values occur in the late afternoon due to the incorrect assumption that the soil heat flux is 10 % of net irradiance. The SLS estimates of H and the estimates of evaporation rate as a residual compared favourably with those obtained using the BREB and EC methods for cloudless days, cloudy days and days with variable cloud. On many days, the diurnal variation in H_{SLS} was asymmetrical, peaking before noon.

Sensible heat flux estimation using temperature variance above various canopies

The TV method for the free convective range of turbulence was used for estimating *H*, one of the important terms of the shortened energy balance equation, from three contrasting canopies for mainly unstable conditions. The TV method involves high frequency (10 Hz) air temperature measurements using a fine-wire thermocouple at various levels for various canopy types. MOST for unstable conditions was applied for estimating *H*. The direction of the flux was determined from the sign of a third order air temperature structure function. The main advantage of the TV method is that it is inexpensive compared to most methods and that the friction velocity is not required when estimating *H*. Daytime estimates of *H* were compared with estimates obtained using SLS and/or EC estimates of the same. The skewness of air temperature was included in the analysis to extend the *H* estimates to include both the free and forced convective turbulence ranges. The comparisons between *H* for the TV method and one or both of the SLS and the EC methods were quite good for the three canopy types: grassland (slope of 1.1088 and RMSE of 21.1 W m^{-2}), pine forest (slope of 0.9915 and RMSE = 20.4 W m^{-2}) and for the chromolaena site (slope of 1.030 and RMSE = 22.7 W m^{-2} for the SLS and a slope of 1.0338 and RMSE = 30.0 W m^{-2} for the EC method). Given the theoretical limitation of the TV method, it performed remarkably well against much more expensive SLS and EC methods. The requirement for 10 Hz air temperature data for the TV method was investigated by comparing *H* calculated from 10-Hz and for 2-Hz data sets. The agreement in *H* for these two data sets was very good. The implication of this result is that the requirement for high frequency data may be relaxed somewhat. The TV method for estimating *H* shows promise as an inexpensive method for providing real-time estimates at sub-hourly intervals. The method has the additional advantage of much reduced data processing and electrical power requirements compared to the SLS and EC methods.

Cathedral Peak long-term field investigation using mainly the BREB method

It has been argued that the BREB method is obsolete. However, BREB measurements are still of interest since the method is less expensive than EC and scintillometry and there is reduced operator skill required with fewer corrections to the data applied. Furthermore, the method will remain of interest until the issue of lack of closure of eddy covariance measurements is resolved. Evaporation measurements using two BREB systems in a remote high altitude montane grassland catchment of the Drakensberg Mountains, Cathedral Peak, South Africa are also reported on. Various methods of data verification and rejection of inaccurate measured air temperature and water vapour pressure gradients are examined. A theoretical analysis, based on the equivalent temperature, results in data rejection procedures using the measurement of the air temperature profile difference. Data rejection is necessary whenever the β approaches -1, resulting in extremely inaccurate and impossibly large positive or negative sensible heat and latent energy fluxes. Using the shortened energy balance, it is shown that when the β approaches the limit of -1, for which the available energy flux approaches 0 W m^{-2}, conditions are pseudoadiabatic and isobaric and that such conditions can be depicted by the wet-bulb temperature isolines of the psychrometric chart. Disregarding evaporation estimates for which the Bowen ratio values are between arbitrarily chosen values remedies the problem to some extent. With this method, daily total evaporation may be reasonable but 20-min values unreasonable during mainly early morning and late afternoon periods. A more sensitive and dynamic approach is used to prevent BREB data from being excluded unnecessarily and to prevent rogue values escaping detection. Once the rejection procedures were applied, the 20-min BREB latent energy flux estimates compared well with measurements from a weighing lysimeter adjacent the site. Three methods were used to estimate the exchange coefficient K which allowed flux estimation for when BREB data are invalid or lacking. One method involved calculating K from wind speed only and the second method was based on the

MOST-dependent temperature-variance method for which the 20-min standard deviation of 1-Hz air temperature data were used. From independent measurements of H and LE, a time-invariant exchange coefficient K was also determined from measurements of the air temperature profile difference. These methods were used when there were invalid water vapour pressure data due to condensation in the hoses or problems with the cooled dew point mirror or when the fine-wire thermocouples were damaged or when there were unreliable estimates of the air temperature gradient. The time-invariant value for K used in one of the methods, 0.239 m^2 s^{-1}, was confirmed for a mixed grassland catchment using independent EC and SLS measurements of H and BREB measurements of the air temperature profile difference.

EC placement height field investigation

The EC method is often regarded as the standard method for obtaining scalar fluxes such as *H*. Insufficient attention has been devoted to how close to vegetated surfaces EC sensors may be placed without the measured scalar flux being significantly different from that further from the surface, but still within the equilibrium boundary layer. Variation in measured *H* with sensor height above short turfgrass during mainly unstable conditions was investigated using the EC method. The data showed that EC-measured *H* at 0.25 and 0.38 m above the turfgrass were 15 and 10 % lower, respectively, than that at the 1.00-m height. There was no statistical difference in the EC-measured *H* at 0.50, 1.00 and 1.25 m. These placement heights corresponded to fetch-to-height ratios from 520:1 to 95:1. Calculations based on fetch showed that the lowest four heights were within the equilibrium layer whereas the heights at or greater than 1.25 m were above the equilibrium layer. The greater *H* measurements above the 1.25-m height, compared to the lower heights, were probably from advected *H* from nearby tar roads and buildings. Measurements of atmospheric stability were obtained by calculating the ratio of height *z* above surface to the Obukhov length. Most measurements were obtained under unstable conditions when mixed convection prevailed. Our measurements show that it is possible for EC sensors to be placed as low as 0.50 m above the surface, during unstable periods, without significant difference from the *H* measurements at a height of 1.00 m. Data were obtained with a pan filled with soil placed 0.27 m below the fine-wire thermocouple of an EC system placed 1.00 m above surface. These data demonstrated that the reduction in the sensible heat was not due to acoustic reflections from that surface. Possibly, the reduction was due to small-sized eddies near the surface being contained between the sonic separation distance. An analysis of "footprints" shows that, at least 90 % of the measured *H* at a height of 0.5 m was from our experimental site, decreasing to less than 70 % at the 1.5-m height. Calculations showed that the fetch requirement for micrometeorological measurements above a forest canopy was more stringent than for grassland canopy. Sensor placement at the 0.5-m height would result in little reduction, as did occur at heights less than 0.50 m, in the covariance between vertical wind speed fluctuation and air temperature fluctuation due to small-sized eddies being contained between the separation distance of the sonic anemometer transducers. We speculate that measurements closer than 0.5 m to the surface differed from those at 1.00 m due to small-sized eddies near the surface being contained between the sonic separation distance and therefore not completely detected by the sonic anemometer. A power spectrum analysis for 10-Hz vertical wind speed for decreasing measurement heights demonstrate a drop-off of measurements from the -5/3 Kolmogorov law for the inertial sub-range for the lower frequencies. The drop-off was not noticeable for sonic temperature.

Open water evaporation investigation using SR and EC methods

As an application of the SR and EC methods for estimating H, measurements were obtained above open water. To date, the SR method has not been used above open water. Evaporation is one of the main components of the energy and water balance of reservoir water behind dams and is a major component of water loss. The small magnitude of H during winter makes it difficult to test the reliability of the H estimates obtained using instruments and sensors mounted above the water surface using the SR, renewal model and EC methods. Measurements in winter of H for the small and shallow reservoir of Midmar Dam, KwaZulu-Natal, South Africa were made using EC and SR and a renewal model method that uses the average cubic air temperature structure function. Latent energy flux was estimated as a residual of the energy balance using additional measurements of net irradiance R_n above the water surface and the water-stored heat flux. For heights of 1.0, 1.3, 1.9 and 2.5 m above the water surface, H_{SR} was estimated using two air temperature time lags r of 0.4 and 0.8 s of the 10-Hz measurements. The SR method depends on a weighting factor α which represents the capability of the atmospheric turbulence to mix the scalar, within the air parcel to be renewed. The factor α was determined for each measurement height and time lag from the slope of a linear regression relationship forced through the origin of H_{EC} values on the y-axis *vs.* H_{SR} or renewal model H on the x-axis. All α values obtained using the renewal model method were not statistically different from that obtained using the SR method for z = 1.0 m for both time lags. Using a calibration dataset, an average α value for the 1.0- and 1.3-m heights of 0.198 for r = 0.4 s and 0.245 for r = 0.8 s for the SR and renewal model methods was obtained. The 30-min H_{SR}, renewal model and H_{EC} estimates were often the smallest component of the energy balance (generally -40 to 40 W m^{-2}) and compared reasonably well for the validation dataset. The heat storage flux G was larger in magnitude (0 to 200 W m^{-2}) compared to the H. The SR, renewal model and EC latent energy fluxes, each calculated as residuals of the energy balance, were almost the same in magnitude as the available energy flux $R_n - G$ due to the relatively small magnitude of the H during the winter measurement period. The daily evaporation ranged between 1.0 and 3.9 mm.

Development of simple iterative procedures for MOST, SR and ETo methods for flux estimation

Surface renewal and MOST methods require complex iterative procedures for estimating H from which evaporation is calculated from net irradiance and soil heat flux. Also, for example, the Penman-Monteith grass-reference evaporation method requires the saturation water vapour pressure *vs* temperature slope at canopy temperature and specific latent energy of vaporisation requires the wet bulb, both unknown temperatures. A single-cell spreadsheet iterative method is described. For the SR method, the air temperature ramp and period and H for the averaging period is calculated in a single-cell for stable and unstable conditions. The roots of a third-order polynomial in ramp amplitude, dependent on the second-, third- and fifth-order air temperature structure functions obtained for each averaging period, were efficiently determined by the iterative procedure with the result of the polynomial varying between -0.015 and 0.01. For SR measurements in a mesic grassland for a two-week period for stable conditions, α values for H were obtained less than 40 % of the time compared to in excess of 95 % for unstable conditions. This is a weakness of the SR method. Using three months of 2-min SLS data, the spreadsheet procedure agreed well with the online estimates of H. Large negative differences occurred for large values for the structure parameter of refractive index, corresponding to large H. These outlier points represent less than 1 % of the dataset. For ETo, for short grass, an iterative procedure is required since the slope of the saturation water vapour pressure *vs* temperature relationship, theoretically, is that slope between the grass surface temperature and the air temperature. The Penman approximation of this slope was to replace the grass surface temperature

with the wet bulb temperature. The iterative procedure showed differences between ETo with and without iteration. Maximum differences for Kaalrug, South Africa ranged between -0.9 and 0.4 mm compared to -0.5 to 0.3 mm for Pretoria. The aerodynamic term of ETo was more affected by not using the iterative procedure with the largest ETo differences occurring under large water vapour pressure deficit conditions. An iterative procedure was also used to estimate wet bulb temperature, used in estimating open-water evaporation, and compared with an approximation by Penman for the wet bulb based on air temperature, dew point temperature, the psychrometric constant and the slope of the saturation water vapour pressure *vs* temperature relationship evaluated at the average of the two temperatures. Generally, the Penman estimate of wet bulb overestimated and increasingly so with decreasing dew point (increasing air temperature) with the largest overestimation being as much as 4.6 ^{o}C at negative dew points with differences of 0.5 ^{o}C occurring for more than a third of the dataset. The iterative procedure is quick, accurate and convenient, easy to repeat following changes to equations or data and allows easy manipulation and allow convenient visual inspection of data and graphics compared to other methods involving programming.

Concluding remarks

The nagging question about the appropriateness of the shortened energy balance equation and its use for estimating evaporation remain. To this end, there is some evidence in the literature that as convective conditions are approached, the energy balance closure significantly worsens. The reasons need to be investigated further. This aspect is important and impacts on all of the methods used to estimate measurements of H for which LE is calculated using the simplified energy balance. Further research in this area would necessitate investigating low-frequency H transport. An approach, that includes flux contributions from large organised turbulent structures, would be to apply spatial averaging instead of temporal averaging for the calculation of fluxes that contribute to vertical transport. Also, since the TV, SLS and SR methods all process a single signal – the temperature fluctuations – through optical and/or digital filters to produce a heat flux, further research is needed to determine which filter works best.

Measurement of sensible heat flux for estimating evaporation

TABLE OF CONTENTS

LIST OF FIGURES

LIST OF TABLES

1 INTRODUCTION: JUSTIFICATIONS, AIMS AND CHAPTER STRUCTURE[1]

1.1 Abstract

The estimation of evaporation presents challenges due its temporal and spatial nature – temporal due to seasonal changes as a result of changes in precipitation and vegetation during each year, and year-to-year, and spatial due to the influence of topography, soils, altitude, land management and the like. There is an increased need for timely information on ground-based measured evaporation over time and space as more and more remote sensing techniques are becoming available at improved resolution, decreased cost, more frequently and over larger areas. One of the justifications for this work is the reference, in the 1998 Republic of South Africa Water Act, to the possible prescription by the Minister, of methods for making a volumetric determination of water for purposes of water allocation and charges in the case of activities that result in stream flow reduction. Also, given the demand on water resources and the potential and/or real impact of global warming and/or climate change, it is important to consider how evaporation is to be measured or estimated with reliable accuracy and precision over time and space. Currently there is no single accepted method that is reliable and results in adequate resolution that can provide accurate temporal and spatial evaporation measurements or modelling estimates of evaporation. The focus of this work is on the measurement of sensible heat flux for estimation of evaporation using micrometeorological measurement methods. An objective of this work is the use of the surface-layer scintillometer (SLS) method, previously untested in South Africa, to estimate areally-averaged sensible heat flux over a mesic grassland and comparisons with measurements obtained using the eddy covariance (EC) method. The SLS methodology for evaporation estimation relies on the energy balance and in particular relies on the measurement of the net irradiance, defined by net short wave and net long wave irradiances, and the soil heat flux and depends on the Monin-Obukhov similarity theory for determining sensible heat flux. Other evaporation methods used for comparison purposes either with SLS or EC estimates also include the traditional Bowen ratio energy balance and the surface renewal and temperature variance methods, the latter two also previously untested in South Africa. This research, within the area of hydrometeorology, micrometeorology, biometeorology and environmental physics, will contribute to water resources assessment, management and sustainable utilisation in South Africa, by improving the methodologies for monitoring evaporation from both land and water surfaces, possibly resulting in a standard for evaporation measurement by which other methods will be judged. An important aspect of the work is research on inexpensive methods for estimating evaporation and in one case, in real-time. The rationale for the research together with key questions that existed prior to the commencement of the research and broad objectives of the research in relation to the key questions are presented. A summary structure of the work on a chapter-by-chapter basis is outlined.

1.2 Rationale for the research (nature and scope)

The 1998 Republic of South Africa National Water Act states that the Minister may make regulations: "requiring that any water use be registered" (p 19). Furthermore, the Minister may also prescribe "...methods for making a volumetric determination of water to be ascribed to a stream flow reduction activity for purposes of water use allocation and the imposition of charges" (p 20).

[1] Based on Savage et al. (1997, 2004)

The Water Research Commission, South Africa in 2004 called for solicited research project proposals refining tools for evaporation monitoring in support of water resource management, stating that: "This (the Act) makes it important to know (a) the degree of accuracy/precision that can be achieved when measuring or estimating evaporation using currently available methods, including those computational methods built into hydrological and agrohydrological models, and (b) how closely these values come to meeting requirements of IWRM (Integrated Water Resource Management) within the context of the Water Act. There are also other compelling water-resource related reasons for being able to monitor evaporation with sufficient confidence in the accuracy and precision of the measurements/estimates." Given the reference in the Water Act to the possible prescription, by the Minister, of methods for making a volumetric determination of water for purposes of water allocation and charges in the case of activities that result in stream flow reduction and given the demand on water resources and the potential and/or real impact of global warming and/or climate change, it is important to consider how evaporation, one of the main components of the water balance, is to be measured or estimated routinely with reliable accuracy and precision.

The need for increased food and timber production has led to dramatic increases in irrigated and forestry lands in South Africa. Agriculture and forestry faces increased competition for water by industries, municipalities and other groups. This ever-growing demand for water makes it imperative that water resource management procedures and policies are wisely implemented and improved. The accurate assessment of evaporation is essential if this is to be done.

So, what is the standard or benchmark for evaporation measurement or estimation? This important and fundamental question needs to be addressed to achieve the ideal of accurate and reliable evaporation data. Although this investigation on the surface-layer scintillometer (SLS), and other methods for estimating evaporation, will also necessarily focus on the more fundamental aspects of micrometeorological research, advances in this field may have direct benefits to water resources assessments and management processes. Examples of areas not easily addressed using the more traditional evaporation measurement techniques include amongst others: measurement of evaporation in riparian zones; determination of open water evaporation from rivers and dams (both large and small); effluent water management from saline dams in the mining environment; measurement of evaporation from slimes tailings; water use of trees and crops in agro-forestry trials; remote sensing applications; determination of baseline evaporation from natural communities (e.g. indigenous forests); irrigation research.

Since John Dalton first introduced the mass transport equation for evaporation estimation, and Penman researched the potential evaporation formulation, numerous methods for estimating or measuring evaporation have been developed. Currently, there is no single accepted method, capable of providing both spatial and temporal measurements and estimates of evaporation, which is reliable and has adequate resolution.

The shortened energy balance equation allows evaporation to be estimated if sensible heat flux, net irradiance and soil heat flux are measured. If the net irradiance and soil heat flux can be reliably measured, then it is possible to calculate evaporation from measurement of sensible heat flux assuming that energy balance closure exists. The emphasis of the research is therefore on methods for

measuring sensible heat flux and furthermore the development and use of inexpensive methods that would then allow evaporation estimation in space and time.

South African researchers have had good success with the heat pulse velocity (HPV) (Dye et al., 1992, Dye and Olbricht, 1993) and energy balance techniques (Savage et al., 1997). The HPV technique for estimating sap flow is based on using heat as a tracer for the flow of sap in the stem of plants. Needles and a heater probe are inserted into the stem of the plant and a pulse of heat is applied at regular intervals of time. The rate of heat movement is related to the sap flow. However, the HPV technique is suited only to mono-specific stands of trees, is problematic when scaling from single trees to whole stands and is a destructive technique – trees must be felled to calculate sapwood areas and wound size. The lack of wound size information at the time of measurement makes calculations of transpiration only possible at the end of an experiment. The stem steady state heat energy balance technique for determining sap flow has also received attention in South Africa (Savage et al., 1993, 2000; Lightbody et al., 1994) but is not highlighted here. Sap flow measurements take no account of soil evaporation.

The Bowen ratio energy balance (BREB) method on the other hand, is well-suited to mixed species communities such as in a mesic grassland. The BREB method is a traditional method for the estimation of evaporation using measurements of profile differences in air temperature and water vapour pressure above the canopy, surface net irradiance and soil heat flux. The technique assumes that the coefficients of energy exchange between the surface and the atmosphere for sensible heat – heat transferred from the atmosphere to a surface, or vice versa, that results in a temperature change – and latent energy are identical. The method therefore requires no correction for atmospheric stability. The BREB method is limited by constraints imposed by both fetch distances and measurement height. Fetch refers to the upwind distance of traverse across a uniformly rough surface such as a forest or a grassland surface from the instrument location until there is a discontinuous change in surface roughness. The fetch often depends on the wind direction (unless the shape of the uniformly rough surface is circular). Thus, the BREB method is not suited to narrow strips (e.g. riparian zones, wetlands etc.), where fetch distances are short, or above tall vegetation where there are small gradients of air temperature and water vapour pressure (caused by the increased wind turbulence above tall canopies). These gradients may be outside the measurement resolution of the sensors particularly when placed above forest canopies. The method is critically dependent on a cooled dew point mirror sensor that is prone to bias, requires almost weekly adjustment and periodically and inexplicably occasionally ices up resulting in unacceptable data. In areas prone to advection, errors arise with the use of the BREB method since the assumption of similarity between the exchange coefficients for sensible heat (H) and latent energy flux (LE) is not valid.

In recent years, direct measurements of turbulent fluxes have been achieved by eddy covariance (EC) measurements in KwaZulu-Natal and Texas (Monnik et al., 1995; Savage et al., 1995a, b). A drawback of EC measurements is that they, like BREB measurements, are point measurements although both sets of measurements may represent a fairly large upwind area depending on the atmospheric stability. However, the application of the EC method is sometimes problematic. The necessary sensors for vertical wind speed, air temperature and water vapour pressure must respond very quickly (frequency of 5 Hz or greater) and at the same time must not show noticeable drift. This makes them delicate, expensive and in some cases difficult to calibrate. However, more serious is that

airflow distortions by the sensor, mast, etc., as well as horizontal misalignments may cause measurement errors. In addition, there are technical problems because temporal co-spectra, measured at a fixed local sensor, extend to very low frequencies. To achieve acceptable significance often demands averaging periods of several tens of minutes. Such long averaging periods reduce the temporal resolution and conflict with the requirement of atmospheric stationarity within the averaging period.

Because of these and other theoretical and practical difficulties, alternative and/or complementary flux measurement methods have been sought. Recent investigations have demonstrated the potential of using a scintillometer to measure areally averaged sensible heat flux densities. A scintillometer measures the intensity fluctuations of visible or infrared radiation after propagation over the plant canopy of interest. The fluctuations are caused by interference after the radiation has been scattered by inhomogeneities in the refractive index of the air, the latter caused by turbulent fluctuations of air temperature and humidity. In contrast to BREB and EC measurements, scintillometers provide path-averaged results. Surface-layer scintillometers have beam path lengths between about 50 and 250 m and large aperture scintillometers (LAS) usually operate over 500 m and 3 km or even up to 10 km for BLS (boundary layer scintillometer) systems. For all three types of scintillometer systems, measurement of the net irradiance and soil heat flux terms of the energy balance is required to estimate evaporation as a residual term of the energy balance equation.

The reported research supports water resources assessment, management and sustainable utilisation in South Africa, by improving the methodologies for monitoring evaporation from both land and water surfaces, possibly resulting in a standard for evaporation measurement by which other methods will be judged.

1.2.1 The physical processes of evaporation and transpiration

Evaporation is a physical process for which a liquid or a solid substance is transformed to a gas. In meteorology, evaporation is usually restricted to the change of liquid to gas/vapour without little change in temperature. Sublimation is used to describe the change from solid to gas. In the case of the evaporation of water, large amounts of energy are required. The process of evaporation for the most part is invisible. However, in times of drought, for example, water managers can see the depleting water levels in dams and rivers. On the other hand, evaporation is a necessary process that provides us with an inhabitable earth.

The evaporation of water exists everywhere in the hydrological cycle, from rain, land and water surfaces and from vegetation in the form of transpiration. When water evaporates from a surface, there is a removal of energy. Thus, evaporation is a cooling process. Whilst part of this energy remains latent in the atmosphere, it is released when water vapour condenses. This is an ongoing process as the average tenure of a water vapour molecule in the atmosphere is about nine days.

Thus water vapour is an energy carrier, and energy must be available to cause the water to evaporate. In terms of energy flux, the magnitude of the flux is dictacted by the gradient in water vapour pressure between the surface and the overlying atmosphere. That part of energy flux from a surface which produces a temperature change is often referred to as sensible heat to distinguish it from latent energy. The word "latent" is derived from the Latin word *lateo* meaning hidden and is used to

describe the evaporation process since there is little temperature change during the evaporation process even though a cooling effect at the surface is evident. Also, the process of evaporation is usually invisible. At 25 ^{o}C, 1 kg of water will remove about 2.44 MJ of energy from the evaporating surface if all the water evaporates. Sources of energy in the soil-plant-atmosphere system include:

sun (solar energy) during the day and long wave or terrestrial radiant energy at night;
heat energy carried into the area by wind (advected energy);
heat energy stored by vegetation and in land masses;
heat energy stored in water bodies.

The most important of these energy sources is usually solar energy, but advected energy may on occasion be considerable.

1.2.2 Evaporation measurement methods

Most often, a water balance approach is used for the estimation of evaporation. The disadvantages in this approach (Slatyer, 1967) include the low level of measurement accuracy and the difficulties of determining total evaporation during rainy periods. However, even with careful measurements, it is difficult to detect daily soil water changes to within 2 mm of water. This magnitude of error makes it unsuited for estimating daily total evaporation for many locations and times of the year.

1.2.2.1 Lysimetry

Weighing lysimeters have been used for decades to estimate evaporative loss from large containers, filled with soil, water and other chemicals and whole plants. The containers are weighed at regular time intervals to calculate evaporation. Improved instrumentation allows water loss from such containers to be measured for very short time intervals and longer from minutes to days or longer.

Lysimeters are regarded as the standard for evaporation measurement although they may require extensive engineering logistics to ensure accurate measurement and also require adequate drainage mechanisms at their base. Also, lysimetric methods are non-portable, expensive and destructive in the sense that usually a relatively large volume of disturbed or sometimes undisturbed soil is placed in a container usually of metal construction. Their lack of spatial scale and their high cost serve as a justification for the quest for alternative accurate evaporation measurement methods. Furthermore, after long dry periods, the measured evaporation for the lysimeter may not match that outside the non-permeable lysimeter walls.

If evaporation could be measured using above-canopy methods, they would be more portable than lysimetric methods. However, such measurement methods have not been fully researched. The height placement of sensors above surfaces, in relation to the fetch distance, is important.

1.2.2.2 Transpiration

Transpiration may be measured directly using a variety of methods. Two of these, the heat pulse velocity method (Dye et al., 1992) and a stem steady state heat energy balance method (Savage et al., 2000), formed the basis of previous research.

1.2.2.3 Micrometeorological methods

Above-surface flux measurement methods are complex. Estimates of sensible heat and latent energy flux, for example, at the canopy surface are affected by a dynamic atmosphere changing in character in time and three-dimensional space, in turn affected by radiation and the variable gaseous constituents. Over an extensive uniform stand of level vegetation, fluxes of water vapour are constant with height in the lowest parts of the turbulent boundary layer. Exchange fluxes between the canopy and the air flowing over it can be determined by measuring vertical fluxes, representative of surface fluxes, in this part of the boundary layer provided there is adequate fetch. To measure evaporation above a grassland surface, adequate fetch would ensure that the measured evaporation is not influenced by evaporation from adjacent non-grassland areas.

Five methods of determining fluxes, above a uniform stand of vegetation, from micrometeorological measurements in the boundary layer were used in this research. Two of the methods are regarded as traditional methods and the other three largely untested or in the experimental phases.

The direct method, known as the EC method (Swinbank, 1951; Verma et al., 1992) requires simultaneous and rapid measurements of vertical wind speed and air temperature for the determination of sensible heat flux (Fig. 1.1a). The covariance between these two measurements is a direct measure of the sensible heat flux at the point of measurement. Most often, a single sensor, a sonic anemometer is used for measurement of both the vertical wind speed and air temperature at high frequency and estimation of sensible heat flux.

The BREB method (Bowen, 1926; Sverdrup, 1943), an indirect method of determining fluxes (Fig. 1.1d), relies on the measurement of mean air temperatures and water vapour pressures and their gradients in the atmosphere as well as the net irradiance and soil heat flux terms of the energy balance.

The surface renewal (SR) method (Snyder et al., 1996) involves high frequency air temperature measurement (Fig. 1.1b) and considering air temperature ramps (positive or negative) consisting of periods during which there is no change in air temperature with time and then ramping periods for which there is an air temperature ramp. Positive ramps occur for unstable conditions and negative ramps for stable conditions. The amplitude of the ramps and the time taken for them is estimated from the high frequency record of air temperature and the sensible heat flux calculated from the amplitude and the times. The method is still in the experimental phase (Castellví, 2007).

The temperature variance (TV) method used is based on the method of Tillman (1972) and uses the same sensors and measurements used by SR. The implementation of the method requires the Monin-Obukhov similarity theory (MOST) which refers to a surface-layer over an extensive flat and homogeneous surface.

The SLS method (Fig. 1.1c, f) is intensively investigated in this research. It is a micrometeorological method since turbulent fluctuations in air temperature affect the transmission of the scintillometer beam.

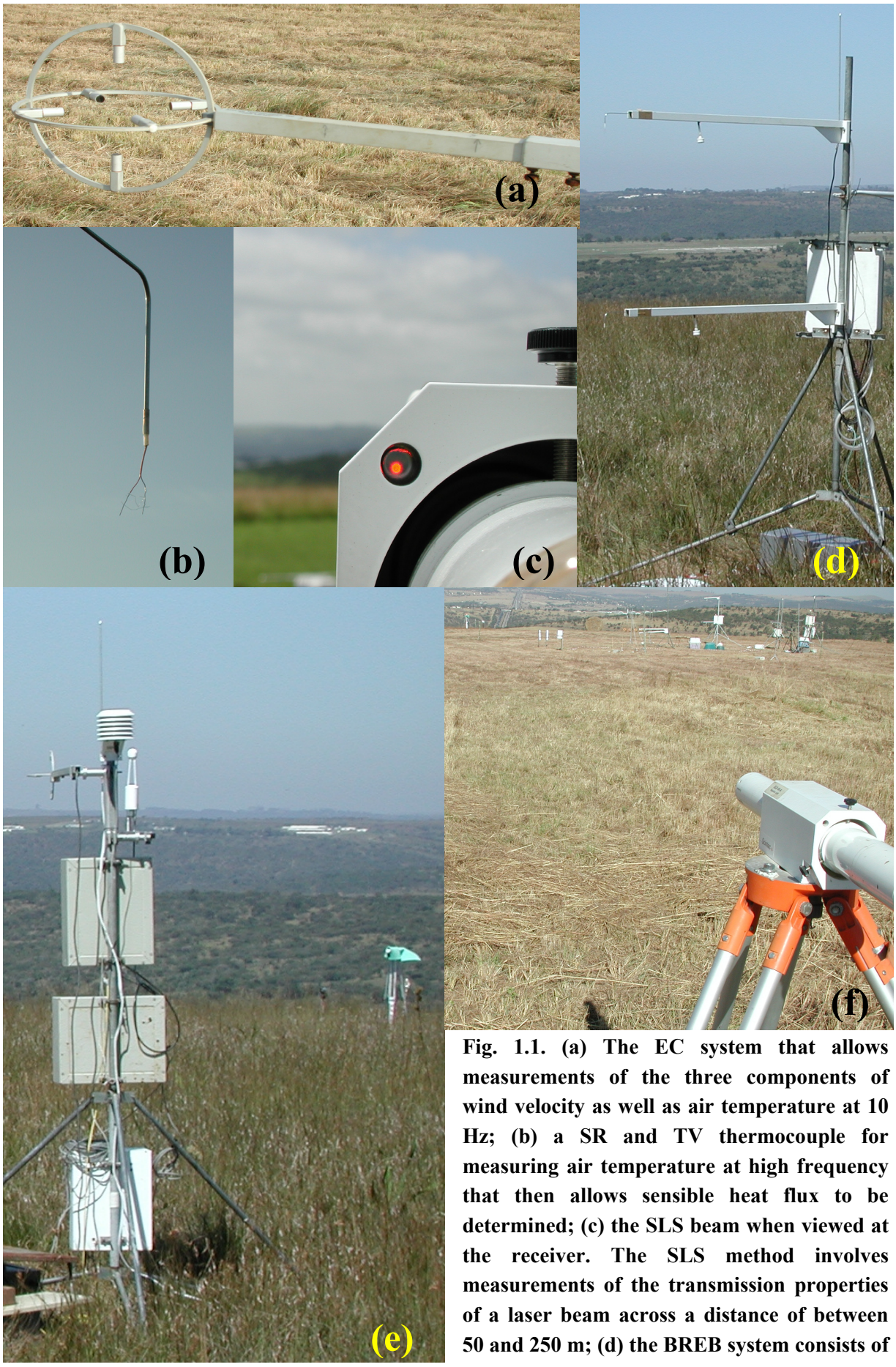

Fig. 1.1. (a) The EC system that allows measurements of the three components of wind velocity as well as air temperature at 10 Hz; (b) a SR and TV thermocouple for measuring air temperature at high frequency that then allows sensible heat flux to be determined; (c) the SLS beam when viewed at the receiver. The SLS method involves measurements of the transmission properties of a laser beam across a distance of between 50 and 250 m; (d) the BREB system consists of

a pair of air temperature and water vapour pressure measurements, net irradiance and soil heat flux; (e) the EC open path system showing the open path sensor (white, upper right of the mast); (f) the SLS receiver (bottom right) and the transmitter is shown at the top left corner. Also barely in view at the top is the BREB equipment as well as the EC sonic anemometer.

The emphasis in the research documented here is on the use of the SLS method for evaporation estimation largely based on measurements of sensible heat flux and the application of the energy balance equation. These estimates however need to be compared against other methods in order that the accuracy of the SLS measurements may be ascertained.

1.2.2.4 Surface-layer scintillometry

Scintillometry depends on the application of MOST. A SLS consists of a transmitter and a receiver unit separated by between 50 and 250 m with a laser beam between the transmitter and receiver. In the case of the commercially-available dual-beam SLS used, two parallel and displaced beams with orthogonal polarizations are used (Thiermann and Grassl, 1992). The receiver unit measures the radiation intensity fluctuations at 1 kHz, caused by atmospheric refractive scattering of turbulent eddies in the path of the SLS beam. The so-called inner scale of refractive index fluctuations (l_o) is calculated from the beam path length and the variances of the logarithm of the amplitude of the two beams and the structure parameter of refractive index fluctuations C_n^2 is calculated from the covariance of the logarithm of the amplitude fluctuations between the two beams. Using an iterative method, and applying MOST, sensible heat flux may be calculated from inputs of air temperature, atmospheric pressure, beam path length and the SLS beam height above the zero plane displacement height. The latent energy flux is then estimated as a residual using the shortened energy balance equation and measurements of net irradiance and soil heat flux.

1.2.3 Nature and scope of study

There are few methods that allow evaporation to be measured directly. The exception is the EC method which is expensive and its estimates require many corrections and uncertainty in terms of the measurement frequency to be used as well as the averaging period for the flux estimates. The nature and scope of the research here therefore focuses on indirect methods of obtaining evaporation by measuring the sensible heat flux and other components of the surface energy balance. The use of methods for measuring sensible heat flux include the traditional methods such as EC and BREB methods and the less expensive SR and TV methods. These methods are all essentially point-based methods so the SLS path-weighted method is also used for comparison.

1.2.4 Key significant/technological questions existing prior to the commencement of the research

In the 1990s, prior to undertaking the research described here, there was no agreement on a single accepted method for the estimation of evaporation. In particular in South Africa, but also elsewhere, scant attention had been devoted to micrometeorological methods for estimating evaporation. At the time, many of the measurements of evaporation, but also photosynthetic rates, were at the leaf level using mainly porometer methods. Water balance methods were also common as was the crop factor method for estimating evaporation from weather station data. Would it be possible to use integrative

methods for which flux measurements represent a large area? Also, can the method of estimating evaporation using the shortened energy balance be applied to different surfaces? At the commencement of this research, only the BREB and EC micrometeorological methods had been used with some measure of success in a montane grassland. However, there were many aspects of uncertainty in these comparative measurements. For both EC and BREB methods, particularly for fetch-limited sites such as commonly available in topographically variable KwaZulu-Natal, the fetch to measurement height ratio for representative measurements was a key uncertainty. In the case of the BREB method, practical aspects such as the measurement heights for the two levels and theoretical aspects in terms of correctly defining data exclusion for when the BREB method fails. In the case of the EC measurements, trial and error was used to initially determine measurement frequency, the averaging period and the placement height. At that time, it was not possible to store the high frequency EC data so almost a decade had to pass before the technology improved to make this possible. Furthermore, the EC equipment could not be left unattended without sensor damage by rain or dew. This limited the use of EC considerably. Other questions emanated from this work: would it be possible to use high frequency air temperature data to obtain H and together with the measurements of net irradiance and soil heat flux, estimate evaporation using the simplified energy balance?

Many theoretical and practical questions remained unanswered from this early work. After the initial BREB study in a montane grassland together with some preliminary EC measurements, the initial idea was to first attempt to answer the unanswered question about a calibration standard for net irradiance measurements. Following on this research, the work commenced on determining the impact of placement height on EC measurements for a short grassland surface – similar in some respects to a placement height study by Heilman et al. (1989) for the BREB method. Further experience in the use of the EC method was obtained by the vineyard micrometeorological research (Heilman et al., 1994, 1996) but this work is not further reported on here. At the time, plant-based measurements were in vogue and so the stem steady state heat energy balance method was explored as a possibility – the method, while good, did not allow accurate scaling from individual plant to plant canopy.

Increasingly, concerns were raised with EC measurements of H and LE since the sum of these did not balance the difference between net irradiance and soil heat flux as they should if all terms had been measured accurately and all terms of the energy balance were accounted for.

The 2000s saw the use of scintillometry being applied for the estimation of optical beam path-weighted sensible heat flux. This method, although expensive, showed promise and could assist in answering some of the uncertainties with respect to the BREB and EC methods. There were however challenges since the use of scintillometry required a solid understanding of the Monin-Obukhov similarity theory (MOST). Key decisions had to made: should the EC method be further pursued or should the emphasis of the research be on scintillometry? The answer to this question led to unique measurements in a mesic grassland (Bellevue) site for which there were simultaneous measurements of H using BREB, EC and SLS methods for an extended period of time. This had never being attempted elsewhere. Other methods such as SR and TV followed. The emphasis of the research reported here is based mainly on measurements from the Bellevue site. Would it now be possible to answer the questions surrounding placement height, fetch, measurement frequency, the uncertainties in the implementation of MOST, the contribution of net irradiance measurements to the overall error in

estimating evaporation, but more importantly, could a less expensive method for estimating sensible heat flux be found?

Stemming from this research, application to various other surfaces, Chromolaena in 2006 and an open water surface in 2007 followed as well by simple iterative solutions for MOST and surface renewal estimates of sensible heat flux.

The nagging question about the appropriateness of the shortened energy balance equation and its use for estimating evaporation remained.

1.2.5 Brief site and methodology description

Field measurements were conducted during the period 1990 to 2007 at various research sites (Fig. 1.2), each described in more detail in the respective chapters. Studies include:

an investigation of the BREB method at the montane grassland site of Catchment VI of the Cathedral Peak Forestry Research Station, in the foothills of the Drakensberg, KwaZulu-Natal, South Africa at 29.00°S, 29.25°E, at an altitude of 1935 m. The catchment has a predominantly north-facing aspect and average slope of about 15^{o}. It is 0.677 km^2 (68 ha) in area and varies in altitude from 1847 to 2076 m;

an investigation of the placement height of EC systems for measuring sensible heat above a turf grass surface in College Station adjacent the Texas Agricultural Engineering Workshop, Texas A & M University, College Station, Texas, USA (altitude of 100 m, latitude 30^{o}30'N and longitude of 96^{o}W). The research area was flat and 1.6 ha in area, consisting of Bermuda grass;

a Pine (*Pinus elliottii*) canopy in Florida, reporting on the TV method using EC sonic temperature data collected by the research group of Professor M.Y. Leclerc, Laboratory for Environmental and Atmospheric Physics, University of Georgia, Griffin, Georgia, USA. This AmeriFlux site is part of a managed slash pine plantation adjoining the Austin-Cary Memorial Forest of the University of Florida, Gainesville, Florida, USA (29^{o}44'N, 8^{o}09'W). The topography is uniformly flat;

an open and mesic grassland and summer rainfall site in the Hay Paddock area neighbouring Ashburton and close to the suburb of Bellevue of Pietermaritzburg, South Africa (29°38'S, 30°26'E) with an altitude of 671.3 m. Scintillometer (SLS) measurements were conducted from January 2003 to June 2005. During winter, there is frequent dewfall but frost hardly ever occurs. Management practices at the research site include mowing (normally in April each year) and burning (in August when firebreaks are established, and in October). The average slope of the study site was 1^{o}15' to the SE. Beyond the study site and to the south and SW, the site was exposed and the slope increased. The site adjacent to the mesic grassland site used had similar vegetation with the occasional *Acacia* tree. To the NW of the study area, there is a residential area and tall trees. The SLS and EC measurements were performed over a period of 30 months apart for when there was data memory loss, SLS beam misalignments, SLS beam saturation problems, mist, site management operations (–burning

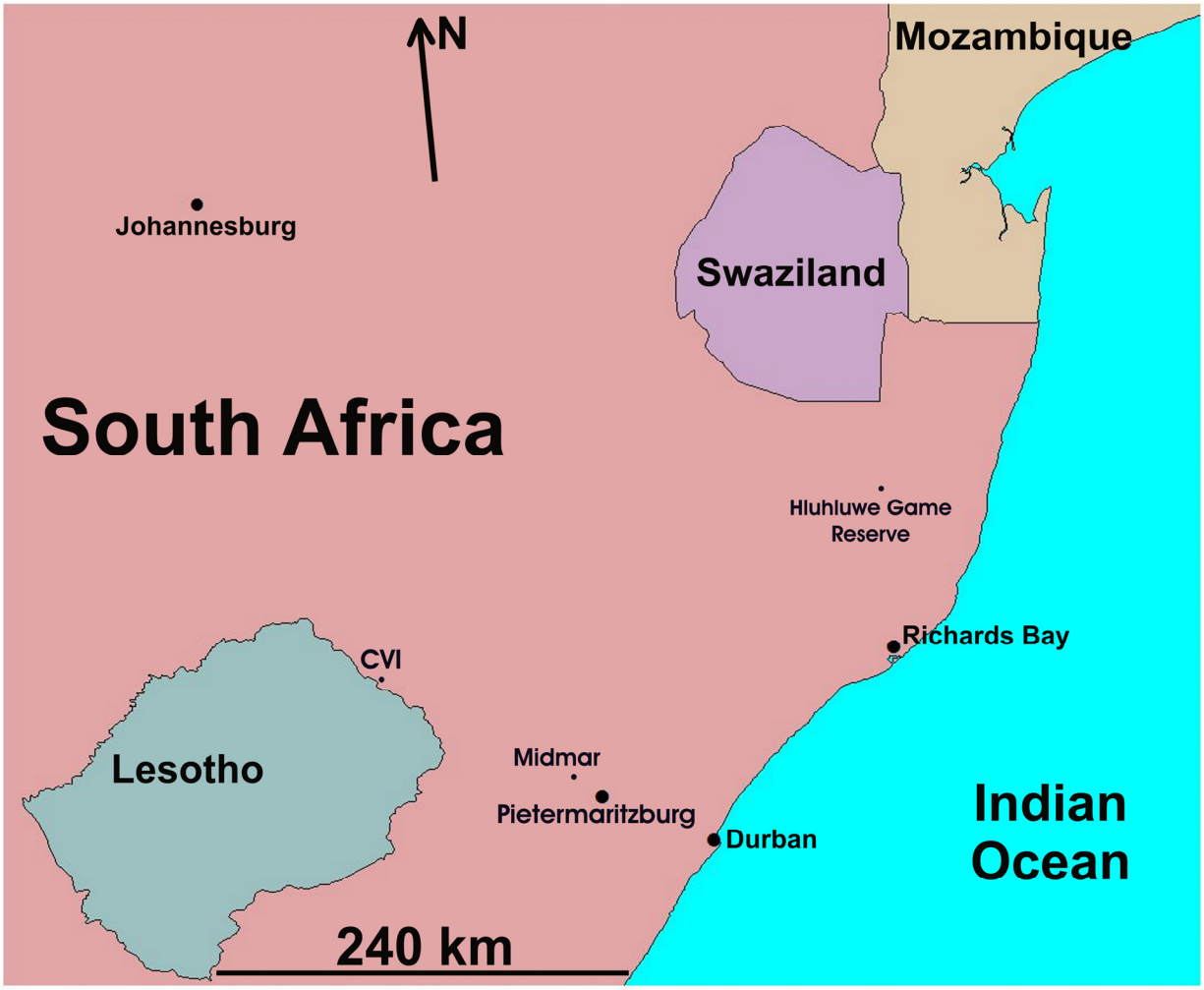

Fig. 1.2. A map showing the location of the study sites in KwaZulu-Natal, South Africa. The Bellevue (29°38'S, 30°26'E) mesic grassland SLS and Midmar Dam open water SR (29°30'S, 30°10'E) sites are close to Pietermaritzburg. The Catchment VI, Cathedral Peak (29.00°S, 29.25°E) montane grassland BREB site is close to Lesotho. The site for *Chromolaena odorata* TV research (28°08'S, 32°17'E) is within the Hluhluwe Game Reserve. The repeat placement height EC study was in a flat tufted grass area, mainly *Themeda traindrox* L. in Pietermaritzburg (28°35'S, 30°26'E)

and mowing), rainfall, power problems, interruptions due to an accidental fire, accidental cutting of cables and finally theft of the SLS transmitter. The BREB measurements commenced in December 2003 and continued for seven months apart from periods when there were data interruptions mainly due to humidity sensor problems and condensation in the hoses;

a *Chromolaena odorata* site, part of the Hluhluwe Game Reserve, in northern KwaZulu-Natal (altitude of 91 m, latitude of 28°08'S, longitude of 32°17'E). In this study, the SLS and TV methods were used to estimate H from which evaporation was estimated using measurements of the other components of the shortened energy balance. This research was part of a WRC research project led by Dr C. Jarmain of the CSIR;

and a study of evaporation for open water at Midmar Dam, near Howick in the midlands of KwaZulu-Natal, South Africa (29°30'S, 30°10'E, elevation 985 m). In this study, also part of the previously mentioned WRC project, the SR and EC methods were used to estimate H from which evaporation was estimated using measurements of the other components of the shortened energy balance.

Participation in other BREB and other micrometeorological studies were also key to the research conducted above. These investigations have been published but are not included as part of this reporting (Savage et al., 1993, 2000; Heilman et al., 1994, 1996; McInnes et al., 1994).

1.3 Broad objectives of the research related to the key questions

The overarching objective of the research is the investigation of micrometeorological methods for measuring sensible heat flux H for calculating the latent energy flux LE (or λE) and hence evaporation using the shortened energy balance. To this end, a number of broad objectives are listed:

literature review: at the commencement of this investigation, there was no review on SLS methodology and SR methodology. Understanding the literature for these two areas of research was key in mapping research progress;

theoretical investigations: a number of theoretical investigations were necessary during the study. These included understanding MOST, and its application, EC and BREB theory, footprint analysis and theoretical development for the correction of sonic temperature for water vapour pressure, atmospheric pressure and the Bowen ratio. These were important issues that guided the research as it progressed;

calibration studies: early on in the investigations, the importance of the role of net irradiance measurements was realised. To this end, net radiometer calibration studies were key in understanding the components of the shortened energy balance. Other calibration studies improved the understanding of the BREB method;

field studies: these played a central role in the investigations and allowed a number of key questions to be answered. Some field studies were undertaken to answer specific questions, such as the EC placement height and SR open water studies, but other studies such as the Cathedral Peak BREB and Bellevue SLS studies were used to gather data which served to answer a number of key questions. An objective of this research was to use the SLS method, previously untested in South Africa, to obtain measurements of areally averaged sensible heat flux and compare with measurements using the BREB and EC methods and also to estimate evaporation from the additional measurements of net irradiance and soil heat flux. A method chosen for preliminary measurement comparisons was the relatively new SR method, also previously untested in South Africa, for measuring sensible heat flux. The TV method, which relies on MOST was also tested. The SR and TV methods are the least expensive of the methods used and are both based on high frequency air temperature measurements;

analysis of data integrity and validity: a huge amount of data were collected in the various investigations. Analysis and definition of valid data was an extremely important aspect of the research

for BREB, EC, SLS, SR and TV methods for estimating sensible heat flux. The protocols for inclusion of valid data and exclusion of suspect or invalid data were defined with care;

inter-comparison methods/studies: the benefit of the long-term studies, such as the Cathedral Peak BREB and Bellevue SLS studies, were key in that after the installation of the initial equipment, more and more equipment and methods could be used and applied thereby allowing comparisons among the various estimation methods.

1.4 Specific chapter objectives

More specific objectives for each chapter are:

to review the literature concerning the SLS and SR methods for measuring sensible heat flux;

to describe an accurate, relatively quick, convenient, relatively inexpensive and repeatable non-steady laboratory method, based on established physical theory, for infrared calibration of various types of net radiometers and calibration of IRTs placed above a radiator, for a wide range in infrared irradiance and surface temperature respectively. An additional aim included specifying a laboratory method using a standard pyranometer and the same radiator for the shortwave calibration of net radiometers. Striving for a standard, convenient and accurate method for calibrating net radiometers would assist in unravelling reasons for the perplexing lack of surface energy balance closure as well as improving on the accuracy of the energy balance residual method for estimating evaporation;

to make recommendations on the feasibility, to provide guidelines for the use, and to specify the limitations of the SLS method for the estimation of areally-averaged H. This entailed the use of the SLS method and other energy balance measurements for the estimation of evaporation, and an assessment of its error, for a mesic grassland for an extended period of time. The methodology for the measurement of H and the subsequent estimation of LE is presented. A sensitivity analysis is used to determine the order of importance of the input parameters for the SLS method. Additional objectives include an analysis of the impact of various MOST methods used on the SLS-estimated H as well as a comparison of LE estimated as a residual of the energy balance using measurements of sensible heat flux from SLS, BREB and EC methods and measurements of net irradiance and soil heat flux. The comparisons of H for the SLS, EC and BREB methods would assist in assessing if any of the methods underestimate. This has significance in terms of energy balance closure;

to evaluate the performance of the SLS method for measuring H for different Bowen ratio values and various MOST formulations for unstable conditions for a mesic grassland against the widely-used EC method. A secondary objective is to evaluate the performance of the SLS and EC methods and in particular the estimation of H using different averaging periods;

to evaluate the performance of the TV method for a wide range of canopies, including the application of air temperature skewness to sensible heat flux estimates for both free and forced convective turbulence ranges;

to make recommendations on the feasibility, to provide guidelines for the use, and to specify the limitations of the BREB method for the estimation of evaporation. This research uses the BREB

method to collect accurate and reliable evaporation measurements as part of a larger long-term study of the total evaporation in grassland systems but in particular in a remote montane grassland. The treatment of BREB data, including data rejection procedures, is emphasized. An additional aim included the estimation of H in the absence of either air temperature or water vapour pressure gradients. To this end, the use of an exchange coefficient, calculated in different ways for estimating H and LE, is investigated;

to assess how close to canopy surfaces measurements may be obtained, EC measurements are obtained using four EC systems placed at eight different heights above a short grassland surface of limited fetch (less than 200 m) with measurements at or below 2 m. The effect of placement height on measurements of H is investigated and using these measurements calculated, for different placement heights for grassland and forest canopies, the fraction of H emanating from within an adjacent upwind area - the footprint of the measurements;

to test the SR method, and the renewal model method for estimating H, over open water surfaces. For this purpose, H measurements are obtained with the SR and renewal model methods and calibrated against EC measurements. This also involved an evaluation of the performance of the SR and renewal model methods for estimating H, and LE as a residual of the energy balance, above an open water surface. The range of H is small and this presented an added difficulty in testing the reliability of these two air temperature based methods above open water, during periods of low H, and comparisons with EC measurements

to describe the implementation of a spreadsheet-based iterative procedure for flux estimation using micrometeorologial examples using MOST, surface renewal and Penman-Monteith grass reference evaporation.

1.5 Structure of thesis

A review of SLS and SR methods for measuring sensible heat flux is presented in Chapter 2, in two parts.

The issue of energy balance closure when using the shortened energy balance equation is a central theme to many of the chapters. Assuming that the shortened energy balance equation contains all the necessary terms, the first question involves the calibration of net radiometers. Chapter 3 discusses the important issue of net radiometer calibration. A relatively inexpensive, accurate and quick laboratory method for non-steady radiative conditions above a large water-heated or water-cooled radiator containing circulated water, with surface-embedded thermocouples, is used to obtain reproducible net radiometer calibration factors for the infrared waveband for a wide range in net irradiance. Infrared calibration factors for two-component, four-component, miniature polyethylene, polyethylene-domed (with and without ventilation) and domeless net radiometers were obtained. A method was also used for the shortwave calibration of net radiometers by placement of a net radiometer adjacent to a standard shortwave radiometer with both instruments placed above the radiator.

Chapter 4 is devoted solely to the SLS method but also addresses the possible underestimation of H as measured by EC and therefore lack of energy balance closure. A dual-beam SLS is used to

estimate sensible heat flux H for a path length of 101 m in a mesic grassland in the eastern seaboard of South Africa for 30 months. Measurements include EC and BREB estimates of H. This chapter also assesses the use of the various MOST semi-empirical functions used to calculate H and also discusses the error in evaporation due to errors in H, net irradiance and soil heat flux.

In Chapter 5, measurements of SLS sensible heat flux are compared with those obtained using EC for a wide range of Bowen ratio (β). Eddy covariance estimates of H are obtained using averaging periods between 1 and 120 min and compared with scintillometer measurements. A sensitivity analysis is used to investigate the influence of β on EC and SLS measurements of H.

Procedures for checking SLS data integrity in real-time are highlighted in Chapter 6 as are the post-data collection rejection procedures. Evaporation rates calculated as a residual of the shortened energy balance equation from SLS measurements are compared with grass reference evaporation rates ETo. The shape of the diurnal variation in SLS H is briefly investigated.

In Chapter 7 the temperature variance method, including adjustment for skewness, is applied to three contrasting surfaces: mesic grassland, chromolaena and pine forest.

Chapter 8 is concerned with the BREB method. Evaporation measurements using two BREB systems in a remote high altitude montane grassland catchment of the Drakensberg Mountains, Cathedral Peak, South Africa are compared. Various methods of data verification and rejection of inaccurate measured air temperature and water vapour pressure gradients are examined. A theoretical analysis, based on the equivalent temperature, is used to develop data rejection procedures. The thermodynamics of events for which β approaches the limit of -1 is examined. Various methods were used to estimate the exchange coefficient K which allowed flux estimation for when BREB data are invalid or lacking.

Chapter 9 deals with the effect of placement height above short turf grass during mainly unstable conditions on EC measurements of H. Field experiments are conducted to determine the effect on fluxes for heights as low as 0.50 m above the surface, during unstable periods. A "footprint" analysis is undertaken.

Measurements in winter of H for the small and shallow reservoir of Midmar Dam, KwaZulu-Natal, South Africa form the basis of Chapter 10. The SR method, a renewal model method that uses the average cubic air temperature structure function and eddy covariance (EC) together with water temperature measurements and net irradiance are used to estimate open water evaporation.

The final chapter, Chapter 11, attempts to integrate the work as well as provide conclusions and document the original contributions of this research.

An Appendix to the thesis deals with spreadsheet-based iterative procedures used for the SR, SLS and grass reference evaporation methods for estimating or calculating sensible heat flux and ETo.

1.6 References

Bowen, I.S., 1926. The ratio of heat losses by conduction and by evaporation from any water surface. Phys. Rev. 27, 779–787.

Castellví, F., 2007. The estimation of latent heat flux: a reflection for the future. Tethys 4, 19–26.

Dye, P.J., Olbricht, B.W., 1993. Estimating transpiration from six year old Eucalyptus grandis trees: development of a canopy conductance model and comparison with independent sap flux measurements. Plant, Cell Environ. 16, 45–53.

Dye, P.J., Olbricht, B.W., Poulter, A.G., 1992. The influence of growth rings in Pinus patula on heat pulse velocity measurement. J. Exp. Bot. 42, 867–870.

Heilman, J.L., Brittin, C.L. and Neale, C.M.U., 1989. Fetch requirements for Bowen ratio measurements of latent and sensible heat fluxes. Agric. For. Meteorol. 44, 261–273.

Heilman, J.L., McInnes, K.J., Gesch, R.W., Lascano, R.J. and Savage, M.J., 1996. Effects of trellising on the energy balance of a vineyard. Agric. For. Meteorol. 81, 79–93.

Heilman, J.L., McInnes, K.J., Savage, M.J., Gesch, R.W. and Lascano, R.J., 1994. Soil and canopy energy balances in a west Texas vineyard. Agric. For. Meteorol. 71, 99–114.

Lightbody, K.E., Savage M.J., Graham, A.D.N., 1994. In situ measurement of sap flow rate in lateral roots and stems of Eucalyptus grandis using a steady state heat energy balance technique. J. S. Afr. Soc. Horticultural Sciences 4, 1–7.

McInnes, K.J., Heilman, J.L., Savage, M.J., 1994. Aerodynamic conductances along a bare ridge furrow tilled soil surface. Agric. For. Meteorol. 68, 119–131.

Monnik, K.A., Savage, M.J., Everson, C.S., 1995. Comparison of eddy correlation estimates of evaporation with Bowen ratio and equilibrium evaporation. Proc. S. Afr. Irrig. Symp. 167–171.

Savage, M.J., Everson, C.S., Metelerkamp, B.R., 1995a. Evaporation measurement comparisons and advective influences using Bowen ratio, lysimetric and eddy correlation methods. Proc. S. Afr. Irrig. Symp. 160–166.

Savage, M.J., Everson, C.S., Metelerkamp, B.R., 1997. Evaporation measurement above vegetated surfaces using micrometeorological techniques. Water Research Commission Report No. 349/1/97, p248, Pretoria, South Africa, ISBN 1–86845–363–4.

Savage, M.J., Everson, C.S., Odhiambo, G.O., Mengistu M.G., Jarmain, C., 2004. Theory and practice of evaporation measurement, with special focus on surface layer scintillometry as an operational tool for the estimation of spatially averaged evaporation. Water Research Commission Report No. 1335/1/04, p204, Pretoria, South Africa, ISBN 1–77005–247–X.

Savage, M.J., Graham, A.D.N., Lightbody, K.E., 2000. An investigation of the stem steady state heat energy balance technique in determining water use by trees. Water Research Commission Report No. 348/1/00, p181, Pretoria, South Africa, ISBN 1–86845–617–X.

Savage, M.J., Graham, A.D.N., Lightbody, K.E., 1993. Use of a stem steady state heat energy balance technique for the in situ measurement of transpiration in Eucalyptus grandis: Theory and errors. J. S. Afr. Soc. Horticultural Sciences 3, 46–51.

Savage, M.J., McInnes, K.J., Heilman, J.L., 1995b. Placement height of eddy correlation sensors above a short grassland surface. Agric. For. Meteorol. 74, 195–204.

Slayter, R.O., 1967. Plant Water Relationships. Academic Press, London.

Snyder, R.L., Spano, D., Paw U, K.T., 1996. Surface renewal analysis for sensible heat and latent heat flux density. Boundary-Layer Meteorol. 77, 249–266.

South African National Water Act, 1998. Republic of South Africa Government Gazette, 26th August, 1998, Act 36, number 19182,

www.info.gov.za/gazette/acts/view/downloadfileaction?id=70693 accessed on 30th March 2010, 101 pp.

Sverdrup, H.U., 1943. On the ratio between heat conduction from the sea surface and the heat used for evaporation. Ann. N. Y. Acad. Sci. 68, 81–88.

Swinbank, W.C., 1951. The measurement of vertical transfer of heat and water vapor by eddies in the lower atmosphere. J. Meteorol. 8(3): 135–145.

Thiermann, V., Grassl, H., 1992. The measurement of turbulent surface-layer fluxes by use of bichromatic scintillation. Boundary-Layer Meteorol. 58, 367–389.

Tillman, J.E., 1972. The indirect determination of stability, heat and momentum fluxes in the atmospheric boundary layer from simple scalar variable during dry unstable conditions. J. Appl. Meteorol. 11, 783–792.

Verma, S.B., Ullman, F.G., Billesbach, D., Clement, R.J., Kim, J., 1992. Eddy correlation measurements of methane flux in a northern peatland ecosystem. Boundary Layer Meteorol. 58: 289–304.

2 SELECTED METHODS FOR ESTIMATING THE SENSIBLE HEAT FLUX COMPONENT OF THE SURFACE ENERGY BALANCE: SURFACE-LAYER SCINTILLOMETRY[1]

2.1 Abstract

The relatively recently developed scintillometry method, with a focus on the dual-beam surface-layer scintillometer (SLS), allows boundary layer atmospheric turbulence, surface sensible heat and momentum flux to be estimated in real-time. Much of the previous research using the scintillometer method has involved the large aperture scintillometer method, with only a few studies using the SLS method. The SLS method has been mainly used by agrometeorologists, hydrologists and micrometeorologists for atmospheric stability and surface energy balance studies to obtain estimates of sensible heat from which evaporation estimates representing areas of one hectare or larger are possible. Other applications include the use of the SLS method in obtaining crucial input parameters for atmospheric dispersion and turbulence models. The SLS method relies upon optical scintillation of a horizontal laser beam between transmitter and receiver for a separation distance typically between 50 and 250 m caused by refractive index inhomogeneities in the atmosphere that arise from turbulence fluctuations in air temperature and to a much lesser extent the fluctuations in water vapour pressure. Measurements of SLS beam transmission allow turbulence of the atmosphere to be determined, from which sub-hourly, real-time and *in situ* path-weighted fluxes of sensible heat and momentum may be calculated by application of the Monin-Obukhov similarity theory. Unlike the eddy covariance (EC) method for which corrections for flow distortion and coordinate rotation are applied, no corrections to the SLS measurements, apart from a correction for water vapour pressure, are applied. Also, path-weighted SLS estimates over the propagation path are obtained. The SLS method also offers high temporal measurement resolution and usually greater spatial coverage compared to EC, Bowen ratio energy balance, surface renewal and other sensible heat measurement methods. Applying the shortened surface energy balance, measurements of net irradiance and soil heat as well as SLS estimates of sensible heat allows path-weighted evaporation from the surface to be estimated. Research applications involving the use of the SLS method, as well as the theory on which the method is based, are presented.

2.2 Introduction

Measurements of turbulent fluxes such as sensible heat, latent energy and momentum flux, are useful to many applications in agrometeorology, hydrology, micrometeorology, environmental studies and agriculture and forestry, and the demand for reliable information of the components of the energy and water balances of land (and water) surfaces on a large spatial scale such as watershed or river-basin scales is increasing.[1]

Increased demand for water, increased human impact on water resources (both negative and positive) and the potential medium-to longer-term natural and anthropogenic impacts of climate change on water resources necessitate continued research on measurement technologies involving not only surface energy flux exchanges but also evaporation estimation: The 1998 Republic of South

[1] Based on Savage *et al.*[3] and Odhiambo and Savage[80]

Africa National Water Act[2] refers to the possible prescription, by government, of methods for making a volumetric determination of water for purposes of water allocation and charges in the case of activities resulting in stream flow reduction. Given this scenario and the demand on water resources it is important to consider how evaporation, one of the main components of the water balance, is to be measured or estimated with reliable accuracy and precision. Determination of reliable and representative evaporation data is an important issue of atmospheric research with respect to applications in agriculture, catchment hydrology and the environmental sciences, not only in South Africa. Long-term measurements of evaporation at different time scales and from different climate regions are not yet readily available.[3,4]

For an idealised atmospheric boundary layer, which is in equilibrium, the shortened energy balance at the surface is given by the (vertical) one-dimensional energy balance equation:[5]

$$R_{net} = LE + H + S \tag{2.1}$$

where R_{net} is the net irradiance, LE the latent energy flux , H the sensible heat flux and S the soil heat flux. All terms are in W m^{-2}. In the shortened energy balance, advection and canopy-stored sensible heat and latent energy, for example, are neglected. For most relatively short or sparse canopies, the canopy-stored terms are negligible but for taller and fully-covered canopies, they may need to be measured and included in Eq. (2.1). The presence of advection is a difficulty but can be associated with windy sites with abrupt changes in roughness and/or management – for example, a change from an untilled dry area to a crop-irrigated humid area. The correctness of the energy balance assumption may be checked by measuring R_{net} using net radiometers placed above the surface and by measuring soil temperature and soil heat flux at a depth to obtain S. Alternatively, eddy covariance[6] (EC) measurements may be used to obtain H and LE or LE could be measured using weighing lysimeters. Instead of measuring both LE and H, H may be measured and LE calculated from the shortened energy balance (Eq. (2.1)). The latter method, essentially a residual method, is based on the assumption that Eq. (2.1) is valid. In certain instances, other methods when used to estimate LE are accurate and reliable but some are unsuitable or provide only rough approximations of LE.[3,7,8] Because of the difficulties experienced with the various measurement techniques, most of which may only represent small areas, alternative methods have been sought in recent years for the reliable estimation of H and LE. Direct measurements of turbulent fluxes such as H and LE, components of the shortened energy balance (Eq. (2.1)), are usually obtained by EC, which is considered the standard for H and LE measurement and involves the use of measurements from EC instruments mounted on an instrumentation mast.

This work focuses on scintillometry, surface-layer scintillometry in particular, for the estimation of H from which LE may also be estimated. A scintillometer is an optical instrument that consists of a radiation source (transmitter) and a receiver which consists of a highly-sensitive detector and a data acquisition system that can register the intensity of fluctuations of the radiation after propagation through a turbulent medium, to deduce various meteorological parameters.[9,10] A beam of radiation is transmitted over a path and the fluctuations in the radiation intensity at the receiver are analysed to give the variations in the refractive index along the path and, as a result, the turbulent characteristics of the atmosphere. Interest in using optical propagation measurements to infer turbulence information is more recent than the many other methods used for measuring H and LE, with Wesley[11] being one of

the first to attempt to derive estimates of *H* using an optical method, although the first scintillometer measurements were made earlier by Tatarskii[12]. Much of the appeal of optical techniques is derived from the opportunity for spatial averaging and the requirement of only very short averaging periods of the order of a minute or longer to give statistically-reliable measurements.[13]

Numerous methods, including the dual-beam surface-layer scintillometer (SLS) operating over hundreds of metres and the large aperture scintillometer (LAS) and extra-large aperture scintillometer (XLAS) methods, the latter two operating over kilometres, for estimating or measuring turbulent kinetic flux densities *H*, and momentum τ (Pa) (Table 2.2 of the Appendix to Chapter 2) from which *LE* may also be estimated using Eq. (2.1) have been developed and tested over many decades.[3,7] Table 2.1 of the Appendix to Chapter 2 summarises the various meteorological parameters estimated or required by the scintillometer method.

The SLS, LAS and XLAS measurements of *H* allow for the estimation of spatial evaporation *LE* from a surface if R_{net} and *S* are also measured (Eq. (2.1)). Besides some of the technical limitations related to the required horizontal homogeneity of the surface layer, measurement methods for determining *H* such as EC, Bowen ratio energy balance (BREB),[3,8,14-16] surface renewal (SR),[17-20] and others are also very expensive if used at multiple points or locations for wider areas since that would require a number of such units.[10,21]

The scintillometer method has been applied and tested by several authors[1,3,4,9,10,21-23] and studies carried out in the past have revealed that the scintillometer method is an attractive alternative to the commonly-used measurement methods such as EC, for the estimation of *H* and τ. In most of these studies, the scintillometer measurements of *H* showed good agreement with *H* obtained using the EC method.

Many of the methods for estimating *H* also allow estimates of other fluxes and meteorological parameters. Table 2.2 of the Appendix to Chapter 2 lists some of the meteorological parameters, and other parameters, determined using the various measurement methods already mentioned.

There has been extensive attention devoted to EC and BREB methods with much less attention devoted to the more recent SR and scintillometer methods. For the three scintillometer methods, more attention has been devoted to the LAS method with significantly less attention devoted to the SLS method. The progress of optical scintillation has been reviewed by Hill[9]; Andreas, [24] who collected papers on turbulence in a refractive medium and Green[25] who provided a review of the scintillation method 'from a pragmatic perspective'. Aside from these reviews, which concentrate on the LAS method, little attention has been devoted to SLS.

2.3 Scintillometry and the role of the refractive index structure constant

The refractive index structure constant, C_n^2 ($m^{-2/3}$), pioneered by Tatarskii[12] and others, is a parameter used to describe the strength of atmospheric turbulence and is central to optical scintillometry. Related to C_n^2 is the structure parameter for air temperature C_T^2 ($K^2\ m^{-2/3}$) (Table 2.1, Appendix to Chapter 2). The parameters C_n^2 and C_T^2 are key in scintillometry for characterising the intensity of the turbulent fluctuations of the atmospheric refractive index and of air temperature respectively. The refractive index fluctuations cause scattering of radiation due to inhomogeneities of the refractive index of air,

the latter caused by turbulent fluctuations of air temperature and, to a lesser extent, atmospheric humidity.[9,10]

When electromagnetic radiation propagates through the atmosphere, it is distorted by a number of processes that can influence its characteristics, for example, its intensity (or amplitude), polarisation and phase. The constituent gases and particles in the atmosphere cause scattering and absorption of the radiation beam, attenuating it and reducing its energy.

Atmospheric turbulence produces small fluctuations in the refractive index of air through the influence of associated changes in air temperature. Although the magnitude of the individual fluctuations is very small, the cumulative effect in propagation along an atmospheric path may be very significant.[26] The turbulence-induced fluctuations in the refractive index produce a phase distortion of the wave front.[27] The movement of small eddies through the path of a beam therefore causes random deflections and interference between different portions of the beam wave front.[9] This causes the beam spot to constantly change pattern like the boiling effect of water. A small detector would measure intensity fluctuations or scintillations.

Scintillation in science is usually treated as a disturbance especially in optical communications and astronomical observations (Tatarskii[12]; cited by Tatarskii[27,28]), but it has also been recognised that scintillation can be used to characterise atmospheric turbulence[29] and to measure cross-wind.[28]

An important mechanism that influences the propagation of electromagnetic radiation, as mentioned above, is due to the small fluctuations of the refractive index of air stemming from air temperature-induced fluctuations. These turbulent refractive index fluctuations of the atmosphere lead, for example, to transmitted beam intensity fluctuations and are known as scintillations.[9] Some examples that clearly show the distortion of wave propagation by the turbulent atmosphere, which can be seen regularly, are the twinkling of stars, image dancing and image blurring above hot surfaces as seen in a mirage. The refractive index of air is a function of air temperature and to a lesser degree the water vapour pressure of air. As eddies transport both *H* and *LE*, their refractive index fluctuates and this results in scintillations.[9]

The smallest diameter of the spectrum of eddy sizes in the SLS beam path is denoted l_o (mm) (Table 2.1, Appendix to Chapter 2). If the parameters C_n^2 and l_o are measured and the level of the line of sight above ground and beam path length are approximately known, then *H* and τ can be determined using the Monin-Obukhov similarity theory (MOST)[30] discussed briefly in the Appendix to Chapter 2.

2.4 Types of scintillometers

The estimation of *H* and τ over large and heterogeneous surfaces usually cannot be fulfilled without deploying a network of several surface flux measurement systems.[10] The SLS may be used to estimate sensible heat *H* and momentum τ flux densities (Table 2.2, Appendix to Chapter 2) over a path distance. The SLS system consists of two laser beams and either two or four detectors.[10] The typical wavelength of the SLS beams is 670 nm with a small displacement of 2.7 mm. The recommended path length of the SLS is typically between 50 and 250 m although distances up to 350 m have been used.[31] The LAS and XLAS units are designed for measuring only C_n^2 over horizontal path lengths typically from 0.25 to 4.5 km (LAS) and 1 to 8 km (XLAS) and employ a near infrared beam wavelength with

additional horizontal wind speed measurements required for the estimation of H and τ using an iterative procedure – discussed in an Appendix to the thesis – and MOST. The signal processing unit of the SLS measures C_n^2 (Table 2.2, Appendix to Chapter 2) and using MOST,[30] allows H and τ to be estimated without the need for wind speed measurements. The beam height for a SLS unit is typically 1 m, for a homogeneous surface, and depending on the atmospheric turbulence the typical path length is 100 m. As is the case for LAS and XLAS units, an iterative procedure is required for the estimation of H for both stable and unstable atmospheric conditions. The SLS unit, due to the use of two beams, also allows τ to be estimated. This is also the case for the multiple-beam LAS unit but not the case for the LAS and XLAS single-beam units.

The scintillometer method depends on MOST to link measurements in the dissipation or inertial sub-range of turbulent frequencies to the entire range of eddy sizes contributing to turbulent transport.[10,32,33] Large eddies adjust only slowly to changing surface conditions and therefore reflect terrain and surface features well upstream of the measurement position.[34,35]

For the different types of scintillometers, besides the path length and beam wavelength differences, there are differences in the aperture size of the receiver compared to the Fresnel (pronounced Fray-nel, without the s) zone F, defined by $F = \sqrt{\lambda \times L_{beam}}$, where λ is the wavelength of the transmitter beam and L_{beam} the beam path length. The most optically-active eddies have sizes of the order of the Fresnel zone.[10] The SLS has a small receiver aperture, is dual-beam and has a receiver aperture size less than F whereas the LAS units have a receiver with an aperture size greater than F.[1] The XLAS units have a much larger receiver aperture size, nearly twice that of LAS, and are used for surface-layer turbulence measurements over longer distances of up to 10 km.[33] The C_n^2 measurements obtained with the LAS or XLAS units, beam height and beam path length and standard meteorological observations (air temperature, horizontal wind speed and atmospheric pressure) are used to derive H,[25] although with multiple-beam LAS measurements, C_n^2 and cross-wind are also obtained directly by the instrument.36 Multiple-beam LAS units such as the so-called boundary layer scintillometer,[36] unlike single-beam LAS units, optically measure atmospheric turbulence, H and cross-wind over spatial scales up to 5 km and give time series outputs of C_n^2, C_T^2, H, τ and cross-wind.

With the SLS method, a transmitter emits two highly parallel and differentially polarised laser beams over a known distance and beam height.[10,32,33] The radiation from the laser is scattered by refractive index inhomogeneities in the air which are caused by turbulent fluctuations in air temperature. At the receiver, the two beams reach two separate detectors. From the magnitude and the correlation of the intensity modulations, C_n^2 and the inner scale length of refractive index fluctuation l_o are derived.[10,37] The idea behind the use of the SLS method is based upon consideration that C_n^2, measured directly by the scintillometer can be related to C_T^2, which is then used to derive H and the friction velocity u_*, a wind speed scaling parameter from which the momentum flux τ is estimated (Table 2.2, Appendix to Chapter 2).

2.5 Advantages of SLS

Scintillometry, and SLS in particular, offers several advantages over EC and other more conventional methods of measuring H. The advantages include[38-40] the fact that flow distortion effects[38] are minimised by scintillometry, due to intensity fluctuations being path-weighted in a parabolic manner with a maximum at midway between the transmitter and the receiver and tapering to zero at either end

of the optical path.[10] Furthermore, unlike the EC method, there are no corrections, such as EC coordinate rotation corrections, [41] that need to be applied; path-weighted estimates over the propagation path are obtained, reducing the averaging period of the SLS method which boosts spatial representivity of the method.[10] As a result, the SLS method offers high temporal resolution and usually greater spatial coverage as compared to other measurement methods such as EC, BREB and SR. Source areas for the scintillometer-measured flux are generally larger than those for the EC method, so that at low heights over inhomogeneous terrain, the SLS method offers advantages; as pointed out by Odhiambo and Savage,[42] there has been no general agreement for the averaging period for EC measurements of *H*. Our work in a mesic grassland, using simultaneous SLS and EC measurements of *H* showed that, when using an averaging period of 2 min, the EC fluxes tended to be overestimated with the EC 60- and 120-min averages sometimes differing significantly from the SLS fluxes. Depending on source characteristics and measurement height, path-averaging up to several hundred metres for the SLS method offers possibilities for validating remote-sensing estimates of *H*. Remote-sensing measurement comparisons with LAS turbulent fluxes[43,44] and aerodynamic surface temperature estimates[45] have already proved promising. Compared to EC and BREB measurements of *H*, SLS measurements may be obtained at heights closer to the surface – this would be particularly useful when there is limited fetch available such as is often the case for riparian strips or small-area agricultural crops; since the small-scale eddies adjust quickly to the local terrain, it might appear that the SLS method may allow some relief from general fetch restrictions on micrometeorological measurements compared to, for example the BREB method, and thus provides averaging over horizontally inhomogeneous terrain. Compared to the other methods the SLS method further quantifies the micro-environment through the following parameters obtained by its use: the dissipation rate of turbulent kinetic energy parameter ε ,[10] Obukhov length *L* for quantifying atmospheric stability and friction velocity u_* (Table 2.2, Appendix to Chapter 2). The scintillometer method allows for *H* and τ to be estimated in real-time from which real-time estimates of *LE* are also possible. This aspect has however not been the focus of the many scintillometer studies conducted thus far; no absolute instrument calibration is required for the SLS, LAS and XLAS methods for estimating *H* whereas sensor calibration is required for the EC and BREB methods.

In the case of the SLS method, the last-mentioned advantage arises because the quantity measured is the variance of the logarithm of the amplitude of the radiation, at the receiver position, so that any multiplicative calibration factors cancel and constant terms are removed by band-pass filtering at scintillation frequencies.[10]

There is, therefore, an innate attractiveness about using optical scintillation to obtain turbulence information over target specific scales[9,33] as well as *H* from which *LE* may be determined using Eq. (2.1).

2.6 Disadvantages, assumptions and requirements of SLS

Scintillometry has the following disadvantages: MOST, discussed later, is assumed to apply in order to derive the fluxes[9,10] and the beam height and zero-plane displacement *d* [46] (Table 2.2, Appendix to Chapter 2) need to be known due to the flux estimates being dependent on these heights via MOST.

Another disadvantage is that the direction of *H* cannot be determined by any of the scintillometer types and so accurate air temperature difference measurements corresponding to two

vertical heights are often used to obtain this flux direction. The SLS equipment, including other scintillometer units, are also comparatively expensive but have been extremely useful for comparison purposes with EC, BREB and other estimates of H,[3,4] including determining the most appropriate averaging period for EC measurements.[42] A practical disadvantage, particularly for tall forest canopies, is that two positions/instrument towers are required[40] – one for the transmitter unit and one for the receiver.

By comparison with the SLS method, the EC method, based on fewer assumptions, requires many quality control corrections,[47,48] often necessitating calculation of the fluxes after the data-collection period. While there are more EC corrections for EC estimates of LE and carbon fluxes, corrections to EC-determined H and τ are still required.[41,49] However, many of these EC corrections have been the debate of recent research[41,48] and besides the BREB profile method and the SLS, LAS and XLAS methods, there are few other methods that can be used to check the corrected EC H and τ fluxes. It should however be re-emphasised that the single-beam LAS and XLAS units require independent (horizontal) wind speed measurements for the estimation of H and τ.

Other necessary assumptions of scintillometry are that the turbulent field through which the beam passes is isotropic and that the scintillations are weak.[28] Due to the assumption that the SLS beam is weakly scattered, the SLS method suffers from the problem of saturation when scintillations are not weak and hence measurements are usually limited to a maximum of 250 m between the transmitter and receiver units unless the power supply settings are altered. Corrections for saturation applied to XLAS measurements gave satisfying comparisons with EC estimates of H.[50]

A requirement of the SLS method is the need to know whether the SLS beam is in the roughness sub-layer (in which case the effective height of the sensor is the height above ground level z) or in the overlying inertial layer (in which case the effective height is determined as $z-d$ where d is the zero-plane displacement).[51] The separating height between the roughness sub-layer and the inertial layer is typically $5h_{canopy}/3$ [51] where h_{canopy} is the canopy height. As mentioned previously, the height specified directly affects the MOST calculations used for all scintillometer types.

2.7 Application of SLS

Most of the studies carried out using the scintillometer method for measurement of H have used LAS units with only a few of these studies involving use of the SLS method. These studies indicate that scintillometer measurements, can be adopted for reliable routine H and τ measurements.[9,21-23] Once H has been estimated using the SLS method, LE can be estimated from the shortened form of the energy balance using Eq. (2.1) as a residual, as long as R_{net} and S are also measured. Measurement of H is therefore very important and the SLS, being an instrument that can allow larger spatial measurement of H as opposed to EC (and other methods) measurements of H, is very useful in this regard.

In spite of the usefulness of scintillometry, the idea of routine and long-term measurements using scintillometry has in general not been achieved. There are however a few exceptions: using a LAS, Beyrich *et al.*[52] reported on results of one-year continuous measurements over a heterogeneous surface. In Table 2.1, fuller details of the studies involving use of the SLS are shown. Apart from the work of *S*avage *et al.*[3,61] *S*avage,[4] Odhiambo and *S*avage,[42] and Nakaya *et al.*[62] only short-term studies have been undertaken using the SLS method. Two SLS studies were conducted above a forest

canopy,[40,62] two in an urban environment,[55,58] one above wheat,[39] one above snow-covered ice[31] and the remaining studies above short vegetation,[10] mainly grassland.[3,4,32,33,42,53,61,63] In all of these studies, the spatially-integrating nature of the SLS measurements was an important feature of the work.

Anandakumar[39] carried out a study which was designed to compare the SLS estimates of *H* over a wheat canopy with the widely-used EC method to obtain an understanding of the performance of the SLS method and confirmed the good agreement between *H* obtained by EC and SLS methods.

A similar study carried out by Green *et al.*[53] over grassland for a period of two months confirmed an improved correlation between EC and SLS estimates of *H* observed for wind directions parallel to the scintillometer beam path compared to when the prevailing wind direction was traverse to the beam path.

Work by Weiss[56] showed that the SLS method is applicable to derive line-averaged *H* over various types of terrain and for different atmospheric conditions giving good temporal resolution. The findings from the same study carried out over different surfaces, ranging from flat terrain to alpine valley, also show that an inclined SLS propagation path does not impair the accuracy of *H* derived by SLS for all fetch and stability conditions.

Thiermann and Grassl[10] showed that 10-min averages of *H* between 10h00 to 18h00 appear more scattered due to short-term variations of turbulence along the beam path (Table 2.1). Thiermann[37] carried out a study to compare SLS-determined *H* and l_o with his model calculations based on wind speed and solar irradiance measurements using five- and ten-min averages of *H* for a 100-m beam path length at a height of 1.9 m. The model calculations agreed with the SLS measurements.

Findings by de Bruin *et al.*,[32] using the SLS method, indicated that the friction velocity u_* is overestimated when u_* is less than ~ 0.2 m s^{-1} (for very stable or unstable cases) and underestimated at high wind speed (or under near neutral conditions). This could imply that the SLS measurements of l_o, a direct measure for the dissipation rate of turbulent kinetic energy ε, are biased, resulting in biased *H*.

The SLS method has also been used for studying the turbulence flux above rough urban surfaces. In a study conducted by Kanda *et al.*[55] in a densely built-up residential neighbourhood in Tokyo, Japan, the EC and SLS methods were employed for the estimation of *H*. The SLS measurements of *H* obtained at a height 3.5 times the average building height agreed well with those obtained using the EC method.

Noting that turbulence can limit the angular resolution of an electro-optical imaging system operating over large distances, significantly degrading such systems, Hutt[54] compared modelled and SLS-measured values of C_n^2 and l_o over a period of two months in summer. The night-time comparisons were poorer compared to those for the day-time unstable periods. The model, based on that of Thiermann and Grassl,[10] and invoking MOST, required relatively simple meteorological measurements and can be used to optimise the performance of electro-optical systems susceptible to scintillation, beam wander and image distortion caused by optical turbulence. In one of the few cases

of the use of a single-beam SLS, Wasiczko[59] performed measurements in both weak and strong turbulence conditions in order to improve the quality of strong turbulence theory and models.

From SLS measurements above snow-covered sea ice, Andreas *et al.*[31] considered how to average scintillometer measurements of C_n^2 and l_o from which H and u_* are estimated. They contest the assumption that H and τ can be measured using path-averaging instruments, such as the SLS, with shorter averaging times than the typical times of 30 to 60 min used for EC measurements. They claim that short-term flux averages are only possible for quasi-stationary time series and that assuming that MOST similarity functions derived from 30- to 60-min averages is equally valid, when applied to short time averages, is unjustified.

In South Africa, Savage *et al.*[3] and Savage[4] focused on the SLS method for estimating H and LE and compared their estimates with EC, BREB and SR estimates of H. Their studies were conducted in a mesic grassland for a period of over 30 months and the study by Odhiambo[63] over 12 months.

2.8 Scintillometry theory and determination of *H*

Since the 1950s many scientists have conducted theoretical studies to explain the scintillation phenomenon.[12,64-66] Several different theoretical approaches have been proposed to describe the propagation of electromagnetic radiation in a turbulent medium. In some approaches, the turbulent eddies are visualised as a collection of concave and convex lenses which focus and defocus the beam resulting in scintillations.[9] In others, diffractional effects are taken into account. In the 1960s with the invention of the laser, experimental studies were conducted to validate the proposed propagation models.[12,28]

Owing to the success of the models that are able to relate the propagation statistics of electromagnetic radiation with the turbulent patterns of the atmosphere, it is today possible to measure and quantify the turbulent characteristics of the atmosphere over large horizontal distances using the scintillometer method as a ground-based remote sensing method.[26] The minimum path length for the SLS method should be 50 m since at path lengths less than this, the measured l_o would often be less than the recommended value of 3.5 mm for this path length making the instrument susceptible to measurement errors.[67]

The algorithm for the SLS method, based on MOST, is summarised in Fig. 2.1. Transmitted radiation measurements are at a frequency of 1 kHz with variances of the logarithm of beam amplitudes, and covariances, for at least one-min periods determined. By determining both the variances of the logarithm of the amplitude of the respective SLS beam radiation, for both beams, and the covariance, C_n^2 and l_o may be determined.[9,10,66,67] At optical wavelengths, compared to water vapour pressure fluctuations, the influence of air temperature fluctuations on the radiation measurements at the receiver dominates. The structure parameter of temperature C_T^2 can be deduced from the C_n^2 measurements.[9,27] Assuming little error in the measurement of atmospheric pressure P (Pa) and air temperature T (K), the spatially averaged C_T^2 is related to C_n^2:[68]

$$C_T^2 = C_n^2 \cdot \left(\frac{T^2}{\gamma P}\right)^2 \cdot \left(1 + \frac{0.03}{\beta}\right)^{-2} \tag{2.2}$$

where γ = 7.89 × 10^{-7} K Pa^{-1} and $\beta = H / LE$ is the Bowen ratio which may be incorporated as a humidity correction such that C_T^2 decreases with increasing evaporation rate (Fig. 2.1), provided air temperature and atmospheric humidity fluctuations are strongly correlated[68] and consistent with MOST. The correction for β for uncorrelated air temperature and humidity fluctuations is negligible. As noted by Savage[4], the term in Eq. (2.2) involving β is often ignored with the justification being that for land studies the fluctuations of refractive index caused by humidity are one order of magnitude smaller than those caused by air temperature fluctuations.[10] Furthermore, when C_T^2 is used to estimate *H*, the correction for water vapour pressure fluctuations is small.[69] This conclusion was based on the fact that for small $|\beta|$, the correction for *H* is large but $|H|$ is small and yet for large $|\beta|$, the correction is small (with possibly little impact on the estimated energy balance components). A similar humidity correction applies to EC measurement of *H*: the relative percentage error in SLS estimates of *H* are less than $3/\beta$ compared to $6/\beta$ for EC estimates of *H* due to the effect of humidity on the speed of sound.[70]

Sensible heat flux *H* is then determined iteratively from the Obukhov stability length L (Fig. 2.2, and also refer to the Appendix to Chapter 2) from which the MOST semi-empirical functions $f(\zeta)$ and $g(\zeta)$ are calculated which in turn allow the determination of the temperature scale of turbulence T_* (Table 2.2 of the Appendix to Chapter 2) and the friction velocity u_*. Application of the energy balance through the use of Eq. (2.1) then allows evaporation *LE* to be calculated. Of particular note is the fact that the algorithm used by SLS for obtaining *H* and τ (Fig. 2.1) applies to both the unstable and stable cases but that the algorithm does not allow for the determination of the sign of *H*. Additional estimates from the SLS algorithm include the vertical air temperature and refractive index gradients dT/dz and dn/dz respectively as well as Φ_n (Fig. 2.1), the latter corresponding to the spectrum of refractive index inhomogeneities caused by the interaction between air temperature and the refractive index of air (Appendix to Chapter 2).

2.9 Conclusions

Surface-layer scintillometers, operating over hundreds of metres, together with the application of MOST, may be used to estimate sensible heat *H* and momentum fluxes τ in real-time. The method has successfully been used above snow-covered ice, urban environs, grasslands, agricultural crops and forest canopies. The scintillometer method is a relatively new method for the estimation of *H* and τ and has recently been applied in agrometeorological and hydrological research in South Africa. Large and extra large aperture scintillometers operate over kilometer distances. The SLS studies indicate that the scintillometer measurements can be adopted for reliable routine *H* and τ measurements over larger heterogeneous areas.

The scintillometer method has several advantages over other methods representative of smaller areas: flow distortion effects are minimised due to intensity fluctuations being path-weighted in a parabolic manner with a maximum at midway and tapering to zero at either end of the optical path; averaging over the propagation path, reducing the averaging period which boosts spatial representivity of the method; depending on source characteristics and measurement height, path-averaging is possible up to several hundred metres, a range which offers possibilities for validating remote sensing estimates of *H*; and no absolute instrument calibration is required. Furthermore, unlike the EC method, for which many corrections are required, there are few corrections necessary for the SLS method. However, the SLS method assumes that MOST is valid.

Increased demand for water, increased human impact on water resources and the potential medium- and long-term impacts of climate change on water resources demands continued research on measurement technologies involving surface flux exchanges and in particular on evaporation estimation.

2.10 Acknowledgements

The financial support from the University of KwaZulu-Natal, the Water Research Commission (WRC project K1335) and the National Research Foundation is acknowledged. Support of the WRC project team and Steering Committee members and the owner and workers of Bellevue Farm, where the field research work for the WRC project was conducted, is gratefully acknowledged. This work was rewritten following an early submission to S. Afr. J. Sci. by Dr G.O. Odhiambo.

2.11 References

1. Meijninger, W.M.L., Hartogensis, O.K., Kohsiek, W., Hoedjes, J.C.B., Zuurbier, R.M. and de Bruin, H.A.R. (2002). Determination of area-averaged sensible heat fluxes with large aperture scintillometer over a heterogeneous surface-Flevoland field experiment. Boundary-Layer Meteorol. 101, 37–62.
2. South African National Water Act (1998). Republic of South Africa Government Gazette, 26th August, 1998, Act 36, number 19182, www.info.gov.za/gazette/acts/view/downloadfileaction?id=70693
3. Savage, M.J., Everson, C.S., Odhiambo, G.O., Mengistu, M.G. and Jarmain, C. (2004). Theory and Practice of Evapotranspiration Measurement, With Special Focus on Surface Layer Scintillometer (SLS) as an Operational Tool for the Estimation of Spatially-Averaged Evaporation. Water Research Commission Report No. 1335/1/04. ISBN 1-77005-247-X. Water Research Commission, Pretoria, Republic of South Africa, 204 pp.
4. Savage, M.J. (2009). Estimation of evaporation using a dual-beam surface layer scintillometer. Agric. For. Meteorol. 149, 501–517.
5. Thom, A.S. (1975). Momentum, mass and heat exchange in plant communities. In: Vegetation and the Atmosphere. Vol. 1. Principles, ed. J.L. Monteith, pp 57-109. Academic Press, London, UK.
6. Swinbank, W.C. (1951). The measurement of vertical transfer of heat and water vapour by eddies in the lower atmosphere. J. Meteorol. 8, 135–145.
7. Drexler, J.Z., Snyder, R.L., Spano, D. and Paw U, K.T. (2004). A review of models and micrometeorological methods used to estimate wetland evapotranspiration. Hydrol. Process. 18, 2071–2101.
8. Savage, M.J., Everson, C.S. and Metelerkamp, B.R. (1997). Evaporation Measurement Above Vegetated Surfaces Using Micrometeorological Techniques. Water Research Commission Report No. 349/1/97, ISBN 1-86845-363-4, 227 pp. Water Research Commission, Pretoria, Republic of South Africa.
9. Hill, R.J. (1992). Review of optical scintillation methods of measuring the refractive index spectrum, inner scale and surface fluxes. Waves Random Media 2, 179–201.
10. Thiermann, V. and Grassl, H. (1992). The measurement of turbulent surface-layer fluxes by use of bichromatic scintillation. Boundary-Layer Meteorol. 58, 367–389.
11. Wesley, M.L. (1976). A comparison of two optical methods for measuring line averages of thermal exchanges above warm water surfaces. J. Appl. Meteorol. 15, 1177–1188.

12. Tatarskii, V.I. (1983). Wave Propagation in a Turbulent Medium, pp 285, Dover Publications. New York. Translated Version.
13. Wyngaard, J.C. and Clifford, S.F. (1978). Estimating momentum, heat and moisture fluxes from structure parameters. J. Atmos. Sci. 35, 1204–1211.
14. Bowen, I.S. (1926). The ratio of heat losses by conduction and by evaporation from any water surface. Phys. Rev. 27, 779–787.
15. Sverdrup, H.U. (1943). On the ratio between heat conduction from the sea surface and the heat used for evaporation. Ann. N. Y. Acad. Sci. 68, 81–88.
16. Tanner, B.D., Greene, J.P. and Bingham, G.E. (1987). A Bowen ratio design for long term measurements. Am. Soc. Agric. Eng. Tech. Paper no. 87–2503, Am. Soc. Agric. Eng., St. Joseph, MI.
17. Paw U, K.T., Snyder, R.L., Spano, D. and Su, H.B. (2005). Surface renewal estimates of scalar exchange. In Micrometeorology in Agricultural Systems Agronomy Monograph no. 47, eds Hatfield, J.L. and Baker, J.M., pp. 455–483, Amer. Soc. Agron., Madison, USA.
18. Castellví, F. (2004). Combining surface renewal analysis and similarity theory: A new approach for estimating sensible heat flux. Water Resour. Res. 40, W05201, doi:10.1029/2003WR002677.
19. Castellví, F., Martínez-Cob, A. and Pérez-Coveta, O. (2006). Estimating sensible and latent heat fluxes over rice using surface renewal. Agric. For. Meteorol. 139, 164–169.
20. Mengistu, M.G. (2008). Heat and energy exchange above different surfaces using surface renewal, pp 148. PhD thesis, University of KwaZulu-Natal, South Africa.
21. de Bruin, H.A.R., van den Hurk, B.J.J.M. and Kohsiek, W. (1995). The scintillation method tested over dry vineyard area. Boundary-Layer Meteorol. 76, 25–40.
22. Kohsiek, W. (1985). A comparison between line-averaged observation of C_n^2 from scintillation of a CO_2 laser beam and time averaged in situ observations. J. Clim. Appl. Meteorol. 24, 102–109.
23. Hill, R.J., Ochs, J.R. and Wilson, J.J. (1992). Measuring surface layer fluxes of heat and momentum using optical scintillation. Boundary-Layer Meteorol. 58, 391–408.
24. Andreas, E.L. (ed.) (1990). Selected Papers on Turbulence in a Refractive Medium, 693 pp. SPIE Milestones Series, 25. Society of Photo-Optical Instrumentation Engineers, Bellingham WA, USA.
25. Green, A.E. (2001). The practical application of scintillometers in determining the surface fluxes of heat, moisture and momentum, pp 177. Doctoral thesis, Wageningen University, Holland. ISBN 90-5808- 336-5.
26. Andreas, E.L. (1989). Two-wavelength method of measuring path-averaged turbulent surface heat fluxes. J. Atmos. Ocean. Technol. 6, 280–292.
27. Böckem, B., Flach, P., Weiss, A. and Hennes, M. (2000). Refraction influence analysis and investigations on automated elimination of refraction effects on geodetic measurements. In 16th IMEKO World Congress, pp 6, IMEKO, Vienna, Austria.
28. Tatarskii, V.I. (1993). Review of scintillation phenomena. In Wave Propagation in Random Media (Scintillation), eds V.I. Tatarskii, A. Ishimaru and V.U. Zavorotny, co-published by SPIE-International Society for Optical Engineering and Institute of Physics Publishing. Bellingham, Washington, USA.
29. Daoo, V.J., Panchal, N.S., Faby, S. and Venkat, R.J. (2004). Scintillometric measurements of daytime atmospheric turbulent heat and momentum fluxes and their application to atmospheric evaluation. Exper. Therm. Fluid Sc. 28, 337–354.
30. Monin, A.S. and Obukhov, A.M. (1954). Basic laws of turbulent mixing in the atmosphere near the ground. Akad. Nauk. 24, 163–187.

31. Andreas, E.L., Fairall, C.W., Persson, P.O.G. and Guest, P.S. (2003). Probability distributions for the inner scale and the refractive index structure parameter and their implications for flux averaging. J. Appl. Meteorol. 42, 1316–1329.
32. de Bruin, H.A.R., Meijninger, W.M.L., Smedman, A.S. and Magnusson, M. (2002). Displaced-beam small aperture scintillometer test. Part I: the WINTEX data–set. Boundary-Layer Meteorol. 105, 129–148.
33. Hartogensis, O.K., de Bruin, H.A.R. and van de Wiel, B.J.H. (2002). Displaced-beam small aperture scintillometer test. Part II: Cases-99 stable boundary-layer experiment. Boundary-Layer Meteorol. 105, 149–176.
34. Højstrup, J. (1981). A simple model for the adjustment of velocity spectra in unstable conditions downstream of an abrupt change in roughness and heat flux. Boundary-Layer Meteorol. 21, 341–356.
35. Panofsky, H.A. and Dutton, J.A. (1984). Atmospheric Turbulence, Models and Methods for Engineering Applications. John Wiley and Sons, New York, USA.
36. Scintec (2007). Scintec Boundary Layer Scintillometer User Manual. pp 70. Scintec Atmosphärenmessetechnik, Tübingen, Germany.
37. Thiermann, V. (1992). A displaced-beam scintillometer for line-averaged measurements of surface layer turbulence. In Tenth Symposium on Turbulence and Diffusion, pp 244-247, American Meteorological Society, Portland, Oregon, USA.
38. Wyngaard, J.C. (1981). The effects of probe-induced flow distortion on atmospheric turbulence measurements. J. Appl. Meteorol. 20, 784–794.
39. Anandakumar, K. (1999). Sensible heat flux over a wheat canopy: optical scintillometer measurements and surface renewal analysis estimations. Agric. For. Meteorol. 96, 145–156.
40. Nakaya, K., Chieko, S., Takuya K., Hideshi, I. and Shinji, Y. (2006). Application of a displaced-beam small aperture scintillometer to a deciduous forest under unstable atmospheric conditions. Agric. For. Meteorol. 136, 45–55.
41. Finnigan, J.J., Clement, R., Malhi, Y., Leuning, R. and Cleugh, H.A. (2003). A re-evaluation of long-term flux measurement techniques, Part I: Averaging and coordinate rotation. Boundary-Layer Meteorol., 107, 1–48.
42. Odhiambo, G.O. and Savage, M.J. (2009). Surface layer scintillometer and eddy covariance sensible heat flux comparisons for a mixed grassland community as affected by Bowen ratio and MOST formulations. J. Hydrometeorol. 10, 479–492.
43. Bange, I., Beyrich, F. and Engelbart, D.A.M. (2002). Airborne measurements of turbulent fluxes during LITFASS-98: Comparison with ground measurements and remote sensing in a case study. Theor. App. Climatol. 73, 35–51.
44. Marx, A., Kunstmann, H., Schüttemeyer, D. and Moene, A.F. (2008). Uncertainty analysis for satellite derived sensible heat fluxes and scintillometer measurements over Savannah environment and comparison to mesoscale meteorological simulation results. Agric. For. Meteorol. 148, 656–667.
45. Min, W.B., Chen, Z.M., Sun, L.S., Gao, W.L., Luo, X.L., Yang, T.R., Pu, J., Huang, C.L. and Yang, X.R. (2004). A scheme for pixel-scale aerodynamic surface temperature over hilly land. Adv. Atmos. Sciences 21, 125–131.
46. Brutsaert, W.H. (1982). Evaporation into the Atmosphere. pp 299, Reidel, Dordrecht, Holland.
47. Ham, J.M. and Heilman, J.L. (2003). Experimental test of density and energy-balance corrections on carbon dioxide flux as measured using open-path eddy covariance. Agron. J. 95, 1393–1403.

48. Mauder, M., Foken, T., Clement, R., Elbers, J.A., Eugster, W., Grünwald, T., Heusinkveld, B. and Kolle, O. (2008). Quality control of CarboEurope flux data – Part II: Inter-comparison of eddy-covariance software. Biogeosciences. 5, 451–462
49. Foken, T. (2008). The energy balance closure problem - An overview. Ecol. Appl. 18, 1351–1367.
50. Kohsiek, W., Meijninger, W.M.L., de Bruin H.A.R. and Beyrich, F. (2006). Saturation of the large aperture scintillometer. Boundary-Layer Meteorol. 121, 111–126.
51. Sellers, P.J. and Mintz, Y. (1986). A simple biosphere model (SiB) for use within general circulation models. J. Atmos. Sci. 43, 505–530.
52. Beyrich, F., de Bruin, H.A.R., Meijninger, W.M.L., Schipper, J.W. and Lohse, H. (2002). Results from one-year continuous operation of a large aperture scintillometer over a heterogeneous land surface. Boundary-Layer Meteorol. 105, 85–97.
53. Green, A.E., McAneney, K.J. and Astill, M.S. (1994). Surface-layer scintillation measurements of daytime sensible and momentum fluxes. Boundary-Layer Meteorol. 68, 357–373.
54. Hutt, D.L. (1999). Modeling and measurements of atmospheric optical turbulence over land. Opt. Engin. 38, 1288–1295.
55. Kanda, M., Moriwaki, R., Roth, M. and Oke, T.R. (2002). Area-averaged sensible heat flux and a new method to determine zero-plane displacement length over an urban surface using scintillometry. Boundary-Layer Meteorol. 105, 177–193.
56. Weiss, A. (2002). Determination of thermal stratification and turbulence of the atmospheric surface layer over various types of terrain by optical scintillometry, pp 152. PhD thesis, Swiss Federal Institute of Technology, Switzerland.
57. Weiss, A.I., Hennes, M. and Rotach M.W. (2001). Derivation of refractive index and temperature gradients from optical scintillometry to correct atmospherically induced errors for highly precise geodetic measurements. Surv. Geophys. 22, 589–596.
58. Salmond, J.A., Roth, M., Oke, T.R., Satyanarayana, A.N.V., Vogt, R. and Christen, A. (2003). Comparison of turbulent fluxes from roof top versus street canyon locations using scintillometers and eddy covariance techniques. In Fifth International Conference on Urban Climate, pp 4, Int. Assoc. Urban. Clim. and WMO, Lodz, Poland.
59. Wasiczko, L.M. (2004). Techniques to mitigate the effects of atmospheric turbulence on free space optical communication links. pp 135. PhD thesis, University of Maryland, USA.
60. Göckede, M., Markkanen, T., Mauder, M., Arnold, K., Leps, J-P. and Foken, T. (2005). Validation of footprint models using natural tracer measurements from a field experiment Agric. For. Meteorol. 135, 314–325.
61. Savage, M.J., Odhiambo, G.O., Mengistu, M.G., Everson, C.S. and Jarmain, C. (2005). Theory and practice of evapotranspiration measurement, with special focus on surface layer scintillometer as an operational tool for the estimation of spatially-averaged evaporation. In 12th South African National Chapter of the International Association for Hydrological Sciences Symposium. Eskom Convention Centre, Midrand, Republic of South Africa, pp 9.
62. Nakaya, K., Chieko, S., Takuya, K., Hideshi, I. and Shinji, Y. (2007). Spatial averaging effect on local flux measurement using a displaced-beam small aperture scintillometer above the forest canopy. Agric. For. Meteorol. 145, 97–109
63. Odhiambo, G.O. (2008). Long-term measurements of spatially averaged sensible heat flux for a mixed grassland community using surface layer scintillometer, pp 151. PhD thesis, University of KwaZulu-Natal, South Africa.
64. Jenkins, F. and White, H. (1976). Fundamentals of Optics. pp768. McGraw-Hill, New York, USA.

65. Hill, R.J. and Lataitis, R.J. (1989). Effect of refractive dispersion on the bichromatic correlation of irradiances for atmospheric scintillation. Appl. Opt. 28, 4121–4125.
66. Hill, R.J. (1997). Algorithms for obtaining atmospheric surface-layer fluxes from scintillation measurements. J. Atmos. Oceanic Tech. 14, 456–467.
67. Scintec (2006). Surface Layer Scintillometer, SLS20/SLS20-A/SLS40/SLS40-A. User's Manual. pp 100. Scintec Atmosphärenmessetechnik, Tübingen, Germany.
68. Wesely, M.L. (1976). The combined effect of temperature and humidity on the refractive index. J. Appl. Meteorol. 15, 43–49.
69. Moene, A.F. (2003). Effects of water vapour on the structure parameter of the refractive index for near-infrared radiation. Boundary-Layer Meteorol. 107, 635–653.
70. Schotanus, P., Nieuwstadt, F.T.M. and de Bruin, H.A.R. (1983). Temperature measurement with a sonic anemometer and its application to heat and moisture fluctuations. Boundary-Layer Meteorol. 26, 81–93.
71. Kolmogorov, A.N. (1941). The local structure of turbulence in compressible turbulence for very large Reynolds numbers. Dokl. Akad. Nauk. SSSR 30, 301–305.
72. de Bruin, H.A.R., Kohsiek ,W. and van den Hurk, B.J.J.M. (1993). A verification of some methods to determine the flux of momentum, sensible heat and water vapour using standard deviation and structure parameter of scalar meteorological quantities. Boundary-Layer Meteorol. 63, 231–257.
73. Kaimal, J.C. and Finnigan, J.J. (1994). Atmospheric Boundary Layer Flows: Their Structure and Measurement. Oxford University Press, New York.
74. Meijninger, W.M.L. (2003). Surface fluxes over natural landscapes using scintillometry, pp. 164. Ph.D. thesis, Wageningen University, Netherlands.
75. Tennekes, H. and Lumley, J.L. (1972). A First Course in Turbulence, pp. 390. MIT Press, Cambridge.
76. Hill, R.J. and Clifford, S.F. (1978). Modified spectrum of atmospheric temperature fluctuations and its application to optical propagation. J. Opt. Soc. Am. 68, 330–342.
77. Wang, T., Ochs, G.R. and Clifford, S.F. (1978). A saturation-resistant optical scintillometer to measure C_n^2. J. Opt. Soc. Am. 68, 892–899.
78. McAneney, K.J., Green, A.E. and Astill, M.S. (1995). Large-aperture scintillometry: the homogeneous case. Agric. For. Meteorol. 76, 149–162.
79. Lawrence, R.S. and Strohbehn, J.W. (1970). A survey of clear-air propagation effects relevant to optical communications. Proc. Itau 58, 1523–1545.
80. Odhiambo, G.O. and Savage, M.J. (2009). Surface layer scintillometry for estimating the sensible heat flux component of the surface energy balance. S. Afr. J. Sci. 105, 208–216.
81. Mengistu, M.G. and Savage, M.J. (2010). Open water evaporation for a small shallow dam in winter using surface renewal and eddy covariance methods. J. Hydrol. 380, 27–35.
82. Savage, M.J. (2009). Evaporation estimation method and system. Provisional Patent Application Number 2009/06090 filed 2 September 2009. Invention assigned to University of KwaZulu-Natal, South Africa.

Table 2.1. A summary of the various investigations using surface-layer scintillometry.

Reference	Measurement distance	Surface on which study was done	Duration of study	Measurement height (m)	Comments/main findings
Thiermann[37]	100 m	Not mentioned	One day	1.90 m above ground	With the SLS one can obtain path averaged turbulent flux with much higher temporal resolution than obtained using the EC method. Comparison of *H* values measured by SLS show good agreement with EC *H* measured values.
Thiermann and Grassl[10]	120 m	Stubble field surrounded by flat and agriculturally-used terrain	One week	2 m above ground level	Results of one- and 10-min averages between 10h00 to 18h00 show more scatter due to short-term variations of turbulence along beam path.
Green *et al.*[53]	100 m	Horizontally homogenous pasture sward well supplied with water Sparse thyme canopy in a semi-arid environment	First experiment done for one month and second one for another one month	1.2 and 1.5 m above ground level	Excellent agreement obtained between the flux measured by SLS with those measured by EC system. Friction velocities obtained using EC and SLS methods agreed within 2 % over the range 0 to 0.9 m s^{-1}.
Anandakumar[39]	70 m	Wheat canopy (average wheat crop height = 0.9 m)	One month	1.4 m above surface (0.5 m above wheat crop)	Estimated *H* measured by SLS was in good correspondence with SR-measured estimates, with the SLS ones showing smoother variations.
Hutt[54]	185 m	Level grass field	Two months	1.8 m	Beam perpendicular to prevailing winds Measured and modelled l_o in good agreement for unstable atmospheric conditions

Reference	Measurement distance	Surface on which study was done	Duration of study	Measurement height (m)	Comments/main findings
de Bruin *et al.*[32]	117 m	Old dead grass	Ten days	2.15 m above ground level	Random errors in the SLS measurements of *H* are small compared to scatter found with two EC systems. Assuming that the hot-film system used yields the 'true' flux measurements, the SLS overestimated u_* for $u_* < 0.2$ m s^{-1} and underestimated u_* at high wind speeds. The derived *H* appears to be less sensitive to errors in l_o and C_T^2 because errors in these quantities tend to cancel out.
Hartogensis *et al.*[33]	112 m	Grassland	One month	2.45 m above ground level	There is good agreement between dissipation rate of kinetic energy ε measured by SLS and those measured by EC method for mainly stable conditions. A proposed revision of beam displacement, but not for general application is used, to improve results for u_* measured by SLS.
Kanda *et al.*[55]	250 m	Densely built-up neighbourhood in Tokyo	Two days	3.5 m above building heights (16 and 32 m above ground level)	SLS-derived *H* obtained at height 3.5 times the building height agree well with those obtained using EC technique. Source area for SLS flux is larger than for the EC sensors, so that at low heights over inhomogeneous terrain SLS offers advantages.
Weiss[56] and Weiss *et al.*[57]	Varied on the various measurement days	Varied from homogeneous and flat terrain to flat non-homogenous terrain in an alpine valley	Three months and 12 days	1.1 m above the ground level	The SLS method is applicable to deriving line-averaged refraction correction values over various types of terrain and for different atmospheric conditions with good temporal resolution.

Reference	Measurement distance	Surface on which study was done	Duration of study	Measurement height (m)	Comments/main findings
	between 76 to 77 m				
Andreas *et al*.[31]	300 to 350 m	Snow-covered sea ice	Periods during 1998	2.60 to 2.88 m	Used 1-min SLS measurements of C_n^2 and l_o to investigate possible time-averaging benefits.
Salmond *et al.* [58]	116 m 171 m	Urban roughness sub-layer	Seventeen days	15.1 m and 19.3 m above street level	Good correlation between *H* measured by EC and SLS methods, although the increased spatial averaging of turbulent eddies in the SLS flux results in a smoother diurnal cycle compared to EC flux. SLS is shown to be an appropriate tool for the measurement of *H* in the urban roughness sub-layer with careful determination of *d* and the use of urban forms of MOST.
Daoo *et al.*[29]	Approximately 100 m	Homogeneous and even surface	Four days	1.2 m above soil	Obtained 2-min measurements of *H* and u_*. Obtained limited comparisons of *H* for SLS, surface energy balance and SODAR methods.
Wasiczko[59]	863 m	Grass and urban pavements	Four-hour window data collection periods	Transmitter and receiver at 14 and 12 m above ground respectively	Single-beam laser scintillometer measurements of C_n^2 and l_o obtained to investigate the impact of atmospheric turbulence on free space optical communication links
Göckede *et al*.[60]	86 and 140 m	Ploughed field	Three days	Not stated	SLS measurements of *H* were used to evaluate the performance of footprint models
Savage *et al.*[3,61] and Savage[4]	50 and 101 m	Mesic grassland with canopy height varying	More than two years	1.5 and 1.68 m above	20-min measurements of *H* by SLS, EC, BREB and SR methods were in good agreement most of the times,

Reference	Measurement distance	Surface on which study was done	Duration of study	Measurement height (m)	Comments/main findings
		between 0.2 m to 1.3 m		ground level	especially for cloudless days. SLS- and EC-measured *H* compares closely/agree well. There was no evidence of consistent underestimation of *H* by EC method compared to SLS method. Beam height above $d + z_0$ needs to be known accurately as the error in beam height contributes the most to the overall error in SLS measurements of *H*.
Nakaya *et al.*[40]	86 m	Deciduous forest canopy	Six months	10 m above the forest canopy (28 m above the ground level)	Greater values of dissipation rates of turbulent kinetic energy ε (Appendix to Chapter 2, Table 2.2) by SLS compared to EC were measured under the atmospheric unstable conditions with weak wind or under strong wind conditions. The dissipation rates by EC indicated greater values than by SLS under atmospheric neutral and weak wind conditions. SLS method tended to overestimate *H* compared to EC, and did not indicate a clear relationship to the wind direction. This overestimation in *H* by the SLS method tended to close the energy balance.
Nakaya *et al.*[62]	86 m	Deciduous forest canopy	June to Nov 2002, 2003	10 m above the forest canopy (28 m above the ground level)	The lack of energy balance closure for the EC measurements changed depending on the difference between ε for the SLS and EC measurement systems. The SLS system measured a more spatially-averaged turbulence signal compared to that using the EC method.
Odhiambo and Savage[42]	100 m	Mesic grassland	12 months	1.68 m	Investigated the influence of MOST formulations and the influence of the Bowen ratio on *H*.

Reference	Meas-urement distance	Surface on which study was done	Duration of study	Measure-ment height (m)	Comments/main findings
					Compared *H* estimated using SLS and EC methods using different averaging periods.

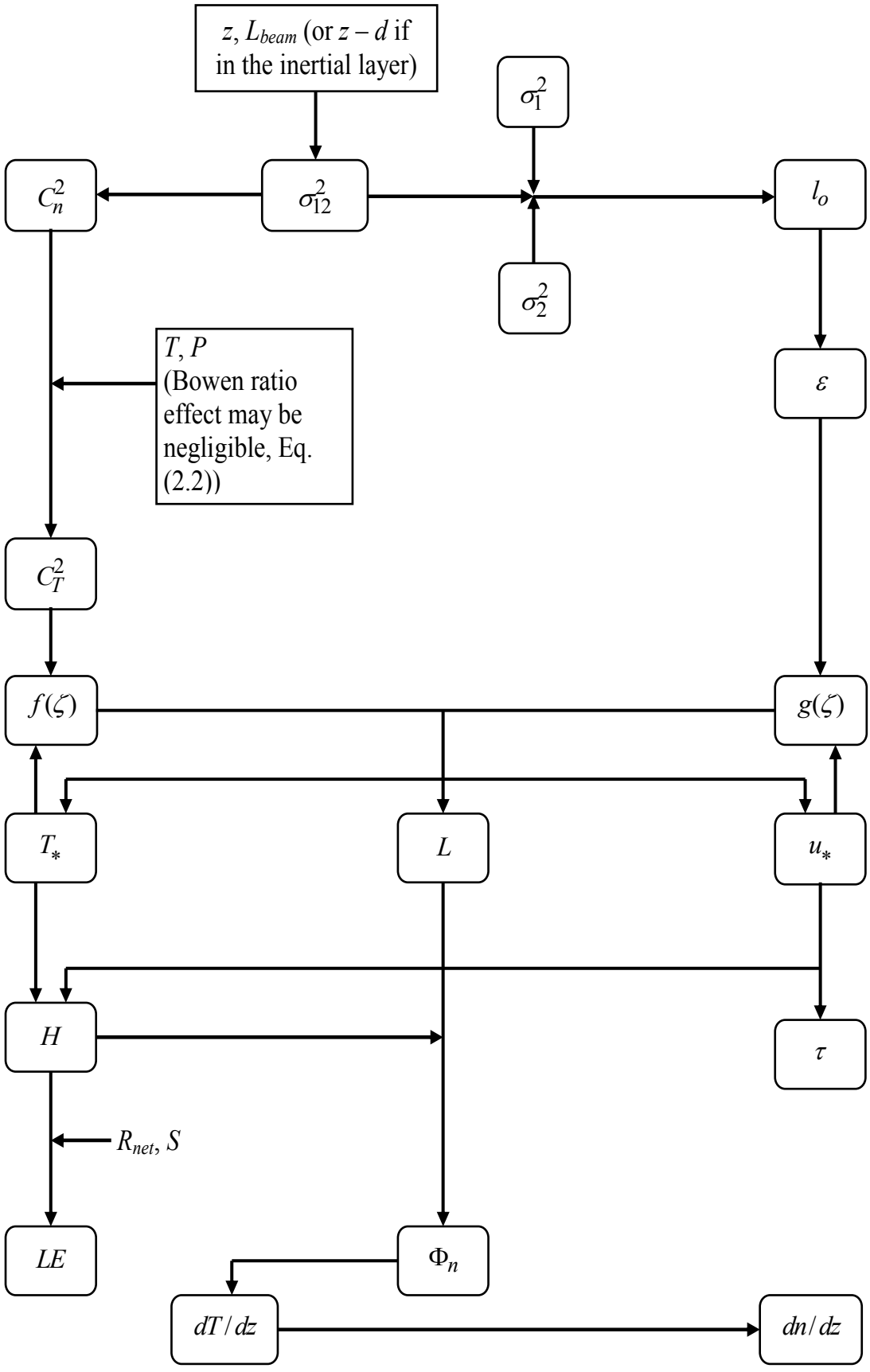

Fig. 2.1. The algorithm Hill[66] used for the various estimates obtained using the SLS method based on weak scattering theory and measurements of the variances of the logarithm of the

amplitude of the transmitted radiation σ_1^2 and σ_2^2, for beam 1 and beam 2 respectively, covariance σ_{12}^2, inputs of beam height above the zero-plane displacement height, beam path length L_{beam}, air temperature T and atmospheric pressure P (based on Weiss[56] and modified by Savage *et al.*[3] to reflect the role of single-detector variances σ_1^2 and σ_2^2 and that T_* and u_* are required to calculate $f(\zeta)$ and $g(\zeta)$).

2.12 Appendix to Chapter 2

2.12.1 Monin-Obukhov similarity theory (MOST) and application to surface-layer scintillometry

The atmospheric surface layer is also known as the constant flux layer because under the assumption of steady-state and horizontal homogeneous conditions, the vertical turbulent flux is nearly constant with height, with variations of less than 10 %.[71]

Unlike the EC and BREB methods, which do not invoke MOST, empirical MOST relations are used to convert the scintillometer measurements of the C_n^2 and l_o into H and τ.[33] Validity of MOST and the determination of the effective measurement height therefore dominate the applicability of flux calculation from optically-determined C_n^2 and l_o.

Dissipation rate of the turbulent kinetic energy ε ($m^2\ s^{-3}$) can be deduced from l_o and the definition of Kolmogorov[71] scale η:

$$\eta = l_o \left(\frac{12\,\beta_1}{\mathrm{Pr}} \right)^{-\frac{3}{4}} = \left(\frac{\nu^3}{\varepsilon} \right)^{\frac{1}{4}} \tag{2.3}$$

or

$$\varepsilon = \nu^3 [\frac{7.4}{l_o}]^4 \tag{2.4}$$

where β_1 is the Obukhov-Corrsin constant (= 0.86), Pr the Prandtl number (= 0.72) and ν the kinematic viscosity of air ($m^2\ s^{-1}$):[67]

$$\nu = [1.718 + 0.0049(T - 273.15)] \times 10^{-5} / \rho \tag{2.5}$$

where T is the air temperature (K) and ρ the density of air (kg m^{-3}).

The application of MOST to surface-layer scintillometer measurements adopted by Thiermann and Grassl[10] is followed in which a simultaneous optically-measured inner scale length l_o is related to the dissipation rate of turbulent kinetic energy ε and one assumes that ε obeys MOST. A fixed C_T^2 and l_o then corresponds to a set of values for H and τ. According to MOST, for a constant flux, the structure of turbulence is determined by the following scaling parameters (Table 2.1):[30]

$$u_* = \sqrt{\tau / \rho} \tag{2.6}$$

$$T_* = \frac{H}{\rho c_p u_*} \tag{2.7}$$

where c_p is the specific heat capacity of air at constant pressure (J kg^{-1} K^{-1}).

According to MOST, C_T^2 and ε are made dimensionless by respectively scaling them with the temperature scale T_* and friction velocity u_*, are universal functions of the stability parameter $\zeta = (z - d) / L$ with the Obukhov length L defined by:

$$L = -\frac{T}{k\,g}\frac{\rho\, c_p}{H}\cdot u_*^3 \tag{2.8}$$

where k is the von Kármán constant (0.41) and g the acceleration due to gravity (9.81 m s^{-2})[6]. From MOST:

$$f(\zeta) = \frac{C_T^2\,(z-d)^{2/3}}{T_*^2} \tag{2.9}$$

and

$$g(\zeta) = \frac{\varepsilon\, k\,(z-d)}{u_*^3}\cdot \tag{2.10}$$

Various forms for the stability functions, $f(\zeta)$ and $g(\zeta)$, have been proposed: Thiermann and Grassl[10], Hill *et al.*,[23] Wyngaard[38] and de Bruin *et al.*[72] and others. The functions used for stable and unstable conditions as proposed by Thiermann and Grassl[10] and which are used to derive *H* by the Scintec[67] SLSRUN software developed for the SLS used, were found adequate.[4]

Thiermann and Grassl[10] give the following semi-empirical expressions for $f(\zeta)$ and $g(\zeta)$:

for $\zeta > 0$ (stable condition)

$$f(\zeta) = C_T^2\,(z-d)^{2/3}\,T_*^{-2} = 4\beta_1\left(1 - 7\,\zeta + 20\,\zeta^2\right)^{-1/3} \tag{2.11}$$

and

$$g(\zeta) = \varepsilon\, k(z-d)\,u_*^{-3} = \left(1 - 4\,\zeta + 16\,\zeta^2\right)^{-1/2} \tag{2.12}$$

and for $\zeta < 0$ (unstable condition)

$$f(\zeta) = C_T^2\,(z-d)^{2/3}\,T_*^{-2} = 4\beta_1\left(1 - 7\,\zeta + 75\,\zeta^2\right)^{-1/3} \tag{2.13}$$

$$g(\zeta) = \varepsilon\, k\,(z-d)\,u_*^{-3} = \left(1 - 3\,\zeta\right)^{-1} - \zeta, \tag{2.14}$$

where $\beta_1 = 0.86$ is the Obukhov-Corrsin constant.

Hill *et al.*,[23] on the other hand, proposed that for unstable atmospheric conditions for which $\zeta < 0$:

$$f(\zeta) = C_T^2\,(z-d)^{2/3}\,T_*^{-2} = 8.1\left(1 + 15\,\zeta\right)^{-1/3}. \tag{2.15}$$

Eqs (2.11) and (2.12) for stable conditions and (2.13) and (2.14) for unstable conditions can be solved for *H* and τ using a numerical iterative scheme – discussed in an Appendix to the thesis – to obtain u_* and T_* using the definition of *L* (Eq. 2.8). Sensible heat flux *H* and momentum flux τ are finally obtained from Eqs (2.6) and (2.7).

2.12.2 Scintillometry and the role of the refractive index structure constant

The graph of the refractive index spectrum is shown in Fig. 2.1[73]. According to Kolmogorov[71], in the inertial sub-range, energy neither enters the system nor is dissipated. It is merely transferred at rate ε where ε is the dissipation rate of turbulent kinetic energy ($m^2\ s^{-3}$) (Table 2.1) from smaller wave numbers to larger wave numbers, where it is dissipated. As a result, the three-dimensional spectral density function, $\Phi_n(\kappa)$, where κ is the wave number $\kappa = 2\pi / l$ associated with the spectrum of eddies of size l, would depend on the viscous dissipation rate ε and the turbulent spatial wave number κ only.

Kolmogorov's first hypothesis[71,92] applies in the range determined by the inequality $l_o << 1\ \text{m} < \mu$ (called the equilibrium range), where μ is called the Kolmogorov microscale (Fig. 2.1). The Kolmogorov microscale defines the size of eddies dissipating the kinetic energy. The second hypothesis is for sufficiently large Reynolds numbers. The sub-range defined by $\eta < 1\ \text{m} << \Lambda$, is called the inertial sub-range, where Λ is the outer scale length and is approximately equal to the scintillometer measurement height and η is the Taylor microscale (which marks where the viscous effect becomes significant) and is dominated by inertial forces whose actions redistribute the energy across the turbulent spectrum (Fig. 2.1).

2.12.3 Scintillometry theory and determination of H

The energy spectrum of turbulence (Fig. 2.1), representing the scale of turbulence from the so-called energy-containing range through to the inertial sub-range of turbulence to the dissipation range,[74] may be defined through the use of a wave number for turbulence. The turbulent wave number κ (m^{-1}) range is defined by the corresponding range in eddy size values experienced in the atmosphere with the spectrum of wave number occurring due to the numerous eddies of variable size.[74] These eddy sizes are indicative of the turbulence regime of the atmosphere and may impact on the transmission of electromagnetic radiation.

The variance of the natural logarithm of the intensity incident at the receiver is related to C_n^2 defined as:[9]

$$C_n^2 = \frac{\overline{(n(r_1) - n(r_2))^2}}{r_{12}^{2/3}} \tag{2.16}$$

where $n(r)$ is the refractive index at location r and r_{12} (m) is a distance that is between two length scales r_1 and r_2 characteristic of the turbulence.[75] The changes in the refractive index of air caused by air temperature fluctuations are usually random functions in both time and space. Thus, turbulence intensity of the refractive index of air $n(r,t)$ can only be determined by the average of certain quantities, such as C_n^2. Assuming the random process generating the changes in refractive index is isotropic, then $C_n^2(r) = C_n^2 \cdot |r|$.[28,76]

The distance between the transmitter and the receiver can range from tens to thousands of metres depending on the type of instrument. Different types of radiation sources can be used. The beam wavelength for the different scintillometer types is also different, with the LAS and XLAS having a beam wavelength of 930 nm, within 5 nm. The displaced-beam surface-layer scintillometer, the SLS, emits two parallel and differently polarised laser beams with the separating distance, d_{SLS}.

The commercial SLS unit, the SLS40-A uses a class 3a type laser at a wavelength λ of 670 nm which is similar to that of an ordinary laser pointer, a beam displacement distance, d_{SLS} of 2.7 mm and a detector diameter, D_{SLS} of 2.5 mm. With this instrument the beam of one source is split into two parallel, displaced beams with orthogonal polarizations. By determining both the variances of the logarithm of the amplitude of the two beams, σ_1^2 and σ_2^2 and the covariance of the two beams, σ_{12}^2, l_o and C_n^2 can be obtained.[67] At the receiver usually located 50 to 250 metres away from the transmitter, the two beams reach two separate detectors. The SLS set up is shown (Photo 2.1) with a close-up of the transmitter, receiver, junction box and signal processing unit of the SLS (Photo 2.2).

The covariance of the logarithm of the amplitude of the received radiation is given by:[10]

$$\sigma_{12}^2 = 4\pi^2 K^2 \int_{r=0}^{L_{beam}} \int_{\kappa=0}^{\infty} \kappa \, \Phi_n(\kappa) J_o(\kappa d_{SLS}) \cdot \sin^2\left[\frac{\kappa^2 \cdot r \cdot (L_{beam} - r)}{2K L_{beam}}\right] \cdot \left[\frac{4J_1^2(\kappa D_{SLS} r / (2L_{beam}))}{(\kappa D_{SLS} r / 2L_{beam})^2}\right] d\kappa \, dr \tag{2.17}$$

Eq. (2.17) is valid for $\sigma_{12}^2 < 0.3$, corresponding to weak scattering. If the scattering is not weak, then the measured σ_{12}^2 is less than that determined from Eq. (2.17) and saturation is said to occur.[77] Due to this fact, the maximum path length for the SLS is usually limited to 250 m. To overcome the saturation problem, which limits the SLS measurements to a beam path distance of 250 m, the beam path length should be decreased or beam height position increased.[3,61] Otherwise a LAS would be the option for obtaining *H* over longer path lengths, e.g. of up to 5 to 10 km.[78]

The functional dependence of the covariance σ_{12}^2 in Eq. (2.17) includes two wave numbers – the optical wave number *K* (m^{-1}) for the SLS beam where $K = 2\pi / \lambda$ where λ = 670 nm for the SLS and wave number defined as $\kappa = 2\pi / l$ corresponding to the spectrum of eddy sizes that the beam encounters where l is eddy size. The functional dependence of Eq. (2.17) also includes the function $\Phi_n(\kappa)$ corresponding to the three-dimensional spectrum of refractive index inhomogeneities caused by the interaction of changes in air temperature with refractive index, SLS beam displacement distance d_{SLS}, two Bessel functions J_0 and J_1 of the first kind, *r* the distance along the beam measured from the transmitter with L_{beam} corresponding to the beam path length, and D_{SLS} the aperture diameter of the scintillometer detectors. As presented by Lawrence and Strohbehn[79] and pointed out by Thiermann and Grassl[10], substituting d_{SLS} = 0 m corresponding to a single beam into Eq. (2.15), provides the expression for the variances σ_1^2 and σ_2^2 at each of the single detector pair.

Table 2.2. Summary of meteorological parameters estimated or required by the various measurement methods and MOST.

Parameter	Symbol (unit)	Description
Refractive index structure parameter	C_n^2 (m $^{-2/3}$)	Spatial statistics used as a measure of the path-averaged strength of refractive turbulence, or simply a measure of the fluctuations in refractive index of air caused mainly by air temperature variations
Momentum flux	τ (Pa)	The turbulent horizontal wind stress in the surface boundary layer
Bowen ratio	β (no unit)	The ratio of sensible heat flux to that of latent energy flux
Structure function parameter of temperature	C_T^2 (K^2 m $^{-2/3}$)	A measure of the structure of air temperature fluctuations (determined from C_n^2)
Dissipation rate of turbulent kinetic energy	ε (m^2 s^{-3})	Refers to the rate of change in turbulent kinetic energy (TKE) per unit mass of fluid, due to viscous effects
Fresnel zone	F (m)	$F = \sqrt{\lambda \times L_{beam}}$, where λ is the wavelength of the transmitter beam and L_{beam} the beam path length. The most optically-active eddies have sizes of the order of the Fresnel zone
Inner scale length	l_o (mm)	The smallest diameter of the occurring eddies
Friction velocity	u_* (m s^{-1})	A basic wind speed scaling parameter equal to the square root of τ / ρ where ρ is the air density
Obukhov length	L (m)	The height above the zero-plane displacement height d at which free convection dominates over forced convection
Zero-plane displacement height	d (m)	A height scale in turbulent flow over roughness elements such as vegetation above the ground at which zero wind speed is achieved as a result of the flow obstacles. It is generally approximated as 2/3 of the average height of the obstacles. The displacement height represents the mean height where momentum is absorbed by the canopy
Temperature scale of turbulence	T_* (K)	A term for the temperature that an air parcel at a height would potentially have if brought adiabatically (i.e. without thermal contact with the surrounding air) to a given height, i.e. the effective temperature of air parcel after removing the heat of the parcel associated solely with compression

Table 2.3. Meteorological parameters determined for selected different methods.

	Meteorological parameters						
Method used for determination of meteorological parameter	H	u_*	ε	τ	$LE_{\text{residual}} = R_{net} - H - S$	LE	**CO_2 flux (F_c)**
LAS or XLAS	✓	-	-	-	+	-	-
SLS or multi-beam LAS	✓	✓	✓	✓	+	-	-
1-Dimensional EC	✓	-	-	-	+	-	-
3-Dimensional EC	✓	✓	-	✓	+	-	-
CO_2 sensor and 3-D sonic (EC)	✓	✓	-	✓	-	-	✓
H_2O sensor and 3-D sonic (EC)	✓	✓	-	✓	+	✓	-
BR	✓	-	-	-	✓	✓	✓
SR (high frequency air temperature measurements)	✓	-	-	-	+	-	-
SR (high frequency specific humidity measurements)	-	-	-	-	-	✓	-

✓ Meteorological parameter that can be measured using the method

- Meteorological parameter that cannot be measured or determined using the method

+ Meteorological parameter can be estimated if net irradiance R_{net} and soil heat flux S are known

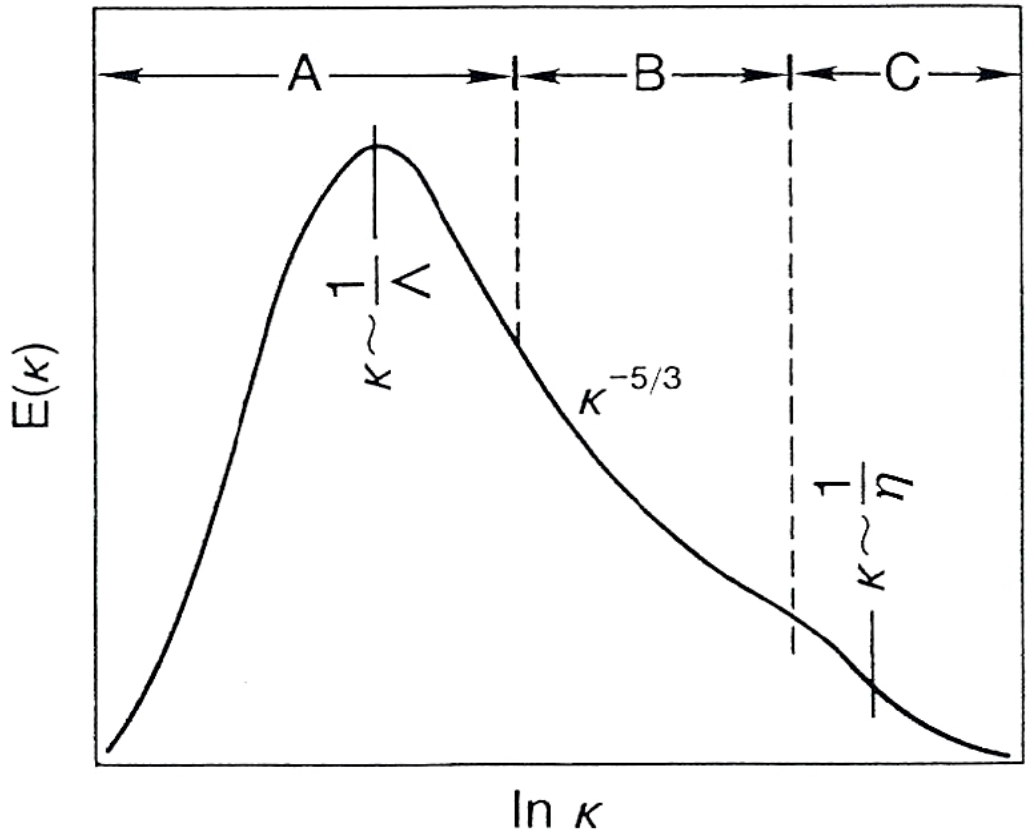

Fig. 2.2. The energy spectrum $E(\kappa)$ associated with turbulence for a range of wave numbers κ for the various boundary layer flows (taken from Kaimal and Finnigan[73]): A corresponds to regions of energy production, B to the inertial sub-range of turbulence and C to the dissipation range where kinetic energy is converted to internal energy acting to raise the temperature of the fluid. The integral length scale of turbulence is denoted Λ and η denotes the Kolmogorov[71] microscale of length.

Photo 2.1. The surface-layer scintillometer set up showing the transmitter (far) and receiver (near) for the initial field-work for a path length of 50 m. The colour version of the bottom photo shows the beam at the transmitter position.

Photo 2.2. The SLS (top left) transmitter, (top right) receiver with the laser in view through the alignment hole, (bottom left) a below-front view of the receiver, (middle right) the switch box and (bottom right) the signal processing unit.

2a SELECTED METHODS FOR ESTIMATING THE SENSIBLE HEAT FLUX COMPONENT OF THE SURFACE ENERGY BALANCE: SURFACE RENEWAL[1]

2a.1 Abstract

For short canopies, latent energy flux may be estimated using a shortened surface energy balance from measurements of sensible and soil heat flux and the net irradiance at the surface. The surface renewal (SR) method for estimating sensible heat, latent energy, and other scalar fluxes has the advantage over other micrometeorological methods since the method requires only measurement of the scalar of interest at one point and the method may be applied close to the canopy surface, thereby reducing fetch requirements. The SR analysis for estimating sensible heat flux from canopies involves high frequency air temperature measurements (typically 2 to 10 Hz) using unshielded and naturally-ventilated 25- to 75-μm diameter fine-wire thermocouples. The SR method is based on the premise that a parcel of air connected to the surface, after it has been enriched or depleted, is renewed by an air parcel from above. There are two SR analysis approaches: the ideal SR analysis approach which presumes a constant α factor; a set of SR approaches that avoid the use of the α calibration factor. The weighting factor α depends on measurement height, canopy structure and stability conditions since it depends on the capability of the highest frequency eddies to mix the scalar within the air parcels renewed by coherent structures. A combination approach using SR and either similarity theory, that requires friction velocity or wind speed measurements, or dissipation theory have also been used to estimate H. The combination SR and dissipation method only requires high frequency air temperature data and may be considered not to require calibration. The ideal SR and combination SR/dissipation approaches are the least expensive micrometeorological methods for estimating sensible heat flux and also latent energy flux if one forces closure of the surface energy balance. However application of SR analysis using slow dataloggers require some expertise since high frequency air temperature data are not usually stored with the slower dataloggers. Some structure functions can be stored for post-processing and determination of ramp amplitude and ramp period, but the appropriate time lags have to be chosen *a priori*. Fortunately, modern dataloggers avoid this problem and complex SR analysis approaches can now be applied. However, routine applications using the ideal SR analysis approach with slow dataloggers may be of interest since it is a very affordable method.

Keywords:

surface energy balance

sensible heat flux

latent energy flux

evaporation

2a.2 Introduction

Accurate and routine measurement of latent energy flux λE is crucial in micrometeorology, agriculture and water resources management. In spite of this need, routine evaporation estimates over temporal and spatial scales are not yet readily available (Bezuidenhout et al., 2006; Jarmain et al., 2009). The

[1] Based on Savage et al. (2004) and Mengistu and Savage (2010)

latent energy flux may be estimated using a variety of techniques, including weighing lysimetry, soil water monitoring, and micrometeorological methods. Lysimeters are too expensive and mainly used in agriculture. Soil water monitoring is labour intensive and is often inaccurate depending on appropriate spatial sampling, choice of method and equipment reliability. Micrometeorological methods for estimating scalar fluxes, such as eddy covariance, Bowen ratio energy balance, surface renewal, flux variance, and optical scintillation methods, do not disturb the microenvironment and they minimize sampling problems by integrating fluxes over a large area. The eddy covariance (EC) method directly measures the turbulence, but it is stringent (Drexler et al., 2004), and requires many post-processing corrections, favourable wind directions, careful sensor positioning and alignment. The Bowen ratio energy balance (BREB) and the flux variance methods are limited by constraints imposed by extensive fetch requirements with the latter based on Monin-Obukhov similarity theory (MOST) which refers to an atmospheric layer over an extensive flat and homogeneous surface. The surface layer consists of a roughness sub-layer adjacent to the surface and an inertial sub-layer above that. MOST applies to the inertial sub-layer. The scintillation method provides path-averaged estimates of sensible heat flux (see e.g. Hill, 1992; Hill et al., 1992; Thiermann and Grassl, 1992; Green et al., 1994; de Bruin et al., 1995; Anandakumar, 1999; Meijninger and de Bruin, 2000; Savage et al., 2004; Savage, 2009; Savage et al., 2010). A scintillometer is a device that optically measures the intensity fluctuations of visible or infrared radiation, caused by interference due to inhomogeneities of the refractive index of air along the path of propagation (Hill, 1992). In contrast to point measurements, displaced-beam scintillometers combined with MOST provide path-averaged measurements of sensible heat and momentum fluxes over distances between 50 and 250 m (Thiermann and Grassl, 1992) although distances up to 350 m have been used (Savage, 2009). Nevertheless, the cost of the scintillometer is high. Despite the availability of different methods for estimating λE directly or indirectly (i.e. by forcing closure of the energy balance), based on the assumptions made, accuracy, simplicity, spatial representation, robustness, fetch requirements, and cost, each method has advantages and disadvantages. Thus the search for methods integrating most of the advantages and avoiding most of the disadvantages is a matter of intensive research.

2a.3 Radiation and energy balances: the shortened energy balance method

Solar radiation is a significant source of energy available at the earth's surface used for heating the air and soil, evaporating water, and driving photosynthesis within the earth-atmosphere system (Campbell and Diak, 2005). Net irradiance is the difference between the sum of all incoming and sum of all outgoing irradiances at the earth's surface (Arya, 2001). For a smooth, horizontal, homogeneous, and extensive surface, net irradiance R_n is the sum of the incoming shortwave I_s and infrared L_d irradiances, less the reflected shortwave $r \cdot I_s$ and emitted infrared L_u irradiances:

$$R_n = I_s - r \cdot I_s + L_d - L_u \,. \tag{2a.1}$$

Net irradiance, typically expressed in W m^{-2}, is the major source of energy flux for heating and cooling at the surface of the earth and is one of the major components of the surface energy balance.

To reduce the cost in estimating λE, micrometeorological methods for estimating sensible heat flux are combined with the energy balance equation. The shortened energy balance equation for a short and flat surface is expressed as:

$$R_n = G + H + \lambda E \tag{2a.2}$$

where R_n is the net irradiance, G the soil heat flux, and H the sensible heat flux where advection is assumed to be negligible. The energy flux associated with photosynthesis and respiration, and energy flux stored in plant canopies are usually small compared with the other terms (Thom, 1975).

2a.4 Historical development of the surface renewal method

Surface renewal (*SR*) theory was originally developed in the field of chemical engineering by Higbie (1935) to investigate interfacial heat transfer between a liquid and a gas and the SR analysis to estimate scalar exchange in the vegetation-atmosphere interface was originally conceived as a simple 'transilient' theory (Stull, 1984) that is Lagrangian in nature and based on the scalar conservation equation (Paw U et al., 1995; Castellví, 2009). This theory arises from the concept that turbulent exchange can be described as the exchange of air parcels from one known height to another, with weighting factors assigned to the fraction of exchange to one height from each of many other heights (Paw U et al., 2005). Scalars such as air temperature, water vapour pressure, carbon dioxide concentration, for which SR theory could be applied, would have relevance in biometeorology.

Several studies have reported on the use of the SR analysis for estimating *H* above different surfaces in the past decade. The original SR method as used by Snyder et al. (1996) must be calibrated against another standard method, such as the EC method. Currently, the most used SR analysis approaches are: an ideal SR analysis equation that only requires the temporal trace of the scalar as input (Snyder et al., 1996; Chen et al., 1997a) and the other SR analysis equations that require the temporal trace of the scalar and friction velocity as inputs (Chen et al., 1997b; Castellví et al., 2002; Castellví, 2004). Combination approaches, for example using SR/similarity and SR/dissipation methods have also been used, by Castellví (2004) and Castellví and Snyder (2009a) respectively. The SR/similarity combination method requires calibration and also wind speed measurements whereas Castelví and Snyder (2009a) showed that the SR/dissipation method requires only the air temperature trace measurements.

Surface renewal analysis is a relatively new, low cost, attractive and simple method for estimating scalar fluxes (Paw U et al., 1995; Snyder et al*.,* 1996; Spano et al*.,* 1997a, b, 2000; Savage et al., 2004; Paw U et al*.,* 2005; Castellví et al*.,* 2006a, 2008; Castellví, 2007). For estimating sensible heat flux, high frequency air temperature measured at a point in the flow using unshielded and naturally-ventilated fine-wire thermocouples is required as an input for the ideal SR approach and the SR combination approaches. The low cost of the method allows for replication of the method in field trials (Snyder et al., 2008).

The SR analysis is based on the premise that an air parcel from above sweeps to the surface and replaces a parcel that has been enriched (depleted) of scalar during its contact with the sources (sinks). Therefore the air parcel is ejected from the canopy scalar into the atmosphere. Coherent structures (Fig. 2a.1) are responsible for transport of momentum, heat and other scalar quantities (Raupach et al., 1989, 1996; Qui et al., 1995). Temperature traces, typically between 2 and 10 Hz often exhibit organized coherent structures which resemble ramp events (Bergström and Högström, 1989; Gao et al., 1989; Shaw et al., 1989; Paw U et al., 1992). The analysis of the observed ramp events in temperature traces is required to estimate H (Paw U et al., 1992). The use of air temperature structure

functions was suggested by van Atta (1977) and Chen et al. (1997b). Low-pass filtering techniques (Paw U et al., 1995; Katul et al., 1996), and other techniques such as wavelet transforms have also been used to extract the air temperature ramp amplitude and ramp period. The ideal SR analysis equation (Snyder et al., 1996) only requires the trace as an input. Therefore, for estimation of *H*, only air temperature measurements are required but the method requires calibration against a standard method such as eddy covariance.

Chen et al. (1997b) presented a new third-order structure function for estimating *H* that uses the zero plane displacement and friction velocity as inputs. Castellví et al. (2002) proposed a new method that combined SR analysis and similarity theory. Castellví (2004) explained the companion method presented by Castellví et al. (2002) and derived a new method that is exempt for calibration. However, unlike the ideal SR analysis, the methods proposed by Chen et al. (1997a) and Castellví (2004) also require wind speed measurements. Using a result from Hsieh and Katul (1997) concerning the dissipation method which is based on turbulent kinetic energy, scalar variance and MOST, Castellví and Snyder (2009a) used a combination SR/dissipation method which appears to be exempt from calibration requiring only measurements at frequencies between 4 and 10 Hz.

If λE is obtained as the residual of the shortened energy balance equation (Eq. (2a.2)), H estimated using SR analysis is convenient since it operates either in the roughness or the inertial sub-layers and it is relatively inexpensive. In the next section, the most commonly-used SR approach will be described in detail.

2a.5 Ideal surface renewal analysis model based on an air temperature structure function analysis

Paw U et al. (1995) expressed H as the change in heat energy content of air with time across a unit horizontal area:

$$H = \alpha \rho c_p \frac{dT}{dt}\frac{V}{A}, \tag{2a.3}$$

where α is a weighting factor (regression coefficient fit to the above equation when H is measured independently using a standard method such as EC), ρ the density of air (kg m^{-3}), c_p the specific heat capacity of air (J kg^{-1} K^{-1}), dT/dt the rate of change in air temperature (^{o}C s^{-1}) and V/A the volume of air per unit horizontal area. If the air temperature measurement is taken at canopy height, then V/A (which is equal to the vertical distance) will be the canopy height (h). High frequency air temperature data are measured at a fixed point and hence the use of Eq. (2a.3) assumes that dT/dt is approximately equal to $\partial T/\partial t$ and internal advection is negligible (Paw U and Brunet, 1991; Paw U et al., 1995). This assumed proportional relationship between the advective term $\partial T/\partial t$ and the total derivative dT/dt has been discussed in detail by Paw U et al. (1995). However, this assumption may not be correct under all conditions. For example, the assumption may be invalid when there is strong local advection and under high wind shear close to the canopy top of low vegetation and soil surface (Snyder et al., 1996). Low-pass filtering techniques were used by Paw U et al. (1995) to smooth the high frequency air temperature data to remove the internal advection and to determine H. However, the filtering technique is cumbersome, due to the necessity of choosing filtering functions and use of numerical methods to identify scalar increases or decreases (Paw U et al., 2005).

When high frequency air temperature measurements are taken at a point at or above the canopy top, ramps are observed (Fig. 2a.1) in the air temperature traces. These air temperature ramps are characterized by an amplitude a (^{o}C), a ramp period L_r (s) where the change in air temperature with time occurs, and a quiescent period L_q (s) for which there is no change in air temperature with time (Snyder et al., 1996, 1997).

The total ramp duration τ (s) is the sum of ramp period L_r and quiescent period L_q (Fig. 2a.2). The amplitude a is positive when the atmosphere is unstable and (the sign of H is positive) and a is negative for stable atmospheres (H is negative).

For estimating H , Paw U et al. (1995) simplified and modified the SR analysis by substituting dT/dt in Eq. (2a.3) by a/τ (^{o}C s^{-1}) for the average rate of change in air temperature for the total ramp period:

$$H = \alpha \rho c_p \frac{a}{L_r + L_q} z , \tag{2a.4}$$

where α is a weighting factor accounting for the spatially-averaged (vertical) air temperature derivative from the bottom to the top of the air parcel (a correction factor for unequal heating or cooling below the sensor). The weighting factor α depends on z (which is the measurement height), canopy structure and atmospheric stability conditions. According to Castellví and Snyder (2009a), the factor α is a measure of the capability of the turbulence to mix the scalar within the air parcel to be renewed. Also in the factor α, one may include other aspects such as thermocouple size and the frequency available to determine the ramp parameters (Snyder et al., 1996; Spano et al., 1997a, b, 2000; Paw U et al., 2005). Generally, for near-neutral conditions, α = 0.5 as shown over mixed deciduous forest, Walnut orchard, and maize canopies (Table 2a.1) for measurements taken at canopy height (Paw U et al., 1995). For a short turf grass (0.1-m tall), excellent estimates of H were obtained using α = 1, when the measurements are taken in the inertial sub-layer for mainly unstable conditions (Snyder et al., 1996).

Snyder et al. (1996) used structure functions of air temperature and the analysis technique of van Atta (1977) to estimate the amplitude a and the ramp period $\tau = L_r + L_q$ as shown in Fig. 2a.2. The structure function value $S^n(r)$ is calculated for each averaging period, typically sub-hourly, from high frequency air temperature measurements at frequency f (Hz) using the relation

$$S^n(r) = \frac{1}{m-j} \sum_{i=1+j}^{m} (T_i - T_{i-j})^n , \tag{2a.5}$$

where m is the number of data points in the averaging period, n is the power of the function, j is the number of time lags between data points corresponding to a time lag (s) $r = j/f$ and T_i is the ith temperature sample. Van Atta (1977) suggested that τ must be much less than r , typically $\tau > 10\,r$, or otherwise the structure function theory is invalid. Snyder et al. (2007) used the condition that $\tau > 5\,r$ and imposed an upper limit for τ of 600 s.

The van Atta (1977) method involves estimating the mean value for amplitude a during the time interval by solving the following equation for real roots:

$$a^3 + pa + q = 0 \tag{2a.6}$$

where

$$p = 10S^2(r) - \frac{S^5(r)}{S^3(r)} \tag{2a.7}$$

and

$$q = 10S^3(r)\,. \tag{2a.8}$$

The ramp period τ is calculated using

$$\tau = -\frac{a^3 r}{S^3(r)}\,. \tag{2a.9}$$

The disadvantage of using a fixed α (Eq. (2a.4)) is that the ideal SR method measurements of H must be calibrated using EC estimates. Slow dataloggers are limited and the weighting factor α depends on the time lag used (Snyder et al., 1996; Zapata and Martínez-Cob, 2001). The size of the air temperature sensor affects the amplitude a and the ramp period τ, and hence α. The sensor time constant represents the time it takes for the sensor to respond to 63.2 % of a step change in temperature. For a 75-µm diameter sensor for example, the time constant is 50 ms for low air flow (Medtherm, 2007). Therefore, the use of 75-µm diameter sensors, in general, is adequate for air temperature measurements for the SR method. The α values for various surfaces using different time lags r and sensor sizes are shown in Table 2a.1, for unstable atmospheric conditions.

Once the weighting factor α is determined for a particular canopy, it is stable and does not change from site to site regardless of the weather conditions (Drexler et al., 2004) unless there are considerable changes in vegetation canopy structure (Paw U et al., 1995; Snyder et al., 1996; Spano et al. 2000). The parameter α increases to some extent with increase in temperature sensor size and this can cause a problem related to sensitivity of the SR model to slower response scalar sensors (Paw U et al., 2005).

2a.6 Surface renewal analysis using a ramp model with finite microfront period

Chen et al. (1997a) proposed a more realistic ramp model, which takes into consideration a finite microfront period L_f instead of a sharp decrease in air temperature (Fig. 2a.3), and assumes an insignificant quiescent period L_q to avoid numerical complexity. The quiescent period exists, but when the model takes into account the quiescent period between the microfront and formation of the next ramp, there were no significant changes in the sensible heat flux estimates.

Because very high frequencies are required to determine L_f, the approach estimates the amplitude a and total ramp duration $\tau = L_r + L_f$, from fluctuations of high frequency air temperature measurements using a cubic temperature structure function as:

$$\frac{a}{\tau^{1/3}} = -\gamma \left(\frac{S^3_{(r_m)}}{r_m} \right)^{1/3}, \tag{2a.10}$$

where $S^3_{(r_m)}$ is the third order of the structure function for temperature, r_m the sampling time lag at which $-(S^3_{(r)}/r)^{1/3}$ is a maximum, and γ a coefficient which corrects for the difference between $a/\tau^{1/3}$ and the maximum value of $-(S^3_{(r)}/r)^{1/3}$.

Raupach et al. (1989) predicted that for canopies $1/\tau$ should scale with maximum wind shear (du/dz at $z = h$, where u is the mean wind speed and h the canopy height). In the canopy and roughness sub-layer, transport of momentum and scalar fluxes are dominated by eddies of length scale comparable to h, while in the inertial sub-layer, dominant eddies scale with $z - d$, where d is zero-plane displacement height (Raupach et al., 1996; Chen et al., 1997b).

Chen et al. (1997b) scaled $1/\tau$ as follows,

$$\frac{1}{\tau} = \begin{cases} \beta \dfrac{u_*}{h}, & 0.2h < z \le h + 2(h-d), \\ \beta \dfrac{u_*}{z-d}, & z > h + 2(h-d) \text{ or } z \le 0.2h, \end{cases} \tag{2a.11}$$

where β is an empirical coefficient and u_* the friction velocity (m s^{-1}). Following Sellers et al. (1986), the roughness sub-layer is assumed to be between $z = h$ and $z = h + 2(h-d)$. The layer adjacent to the soil within canopies ($z \le 0.2h$) is treated the same as the inertial sub-layer, with appropriate u_* and d for the soil or canopy understory (Lee and Black, 1993).

Chen et al. (1997b) recommended that for routine application of the finite microfront SR model, only the maximum of $-(S^3_{(r)}/r)^{1/3}$ is required from high frequency air temperature data. According to the model, H is proportional to $z/h^{2/3}$ in the roughness sub-layer and proportional to $z/(z-d)^{2/3}$ in the inertial sub-layer. Substituting expressions for a and τ from Eqs (2a.10) and (2a.11) into Eq. (4) to obtain H yields,

$$H = \begin{cases} -\alpha\beta^{2/3}\gamma\rho c_p \left(\dfrac{S^3_{(r_m)}}{r_m}\right)^{1/3} u_*^{2/3} \dfrac{z}{h^{2/3}}, & 0.2h < z \le h + 2(h-d), \\ -\alpha\beta^{2/3}\gamma\rho c_p \left(\dfrac{S^3_{(r_m)}}{r_m}\right)^{1/3} u_*^{2/3} \dfrac{z}{(z-d)^{2/3}}, & z > h + 2(h-d) \text{ or } z \le 0.2h. \end{cases} \tag{2a.12}$$

The empirical combined coefficient $\alpha\beta^{2/3}\gamma$ is a common factor in both roughness and inertial sub-layers. Chen et al. (1997b) found a roughly constant value of 0.4 for the combined coefficient $\alpha\beta^{2/3}\gamma$ (Table 2a.2), in their experiments on Douglas-fir forest, bare soil, and straw mulch.

Sensible heat flux may be estimated from the average cubic temperature structure function (using high frequency air temperature data) and measured or estimated friction velocity within the canopy and roughness sub-layers and inertial sub-layer, using this model for stable and unstable conditions. The approach does not require calibration but additional measurement of horizontal wind speed is needed and slow dataloggers may be limited in determining the third-order air temperature structure function.

2a.7 Combined surface renewal analysis model and similarity theory

Castellví et al. (2002) proposed an SR analysis model based on a turbulent diffusion approach (similarity theory), to estimate H using high-frequency air temperature data, friction velocity, and similarity formulae. Similarity theory describes H as:

$$H = \rho c_p K_h \frac{dT}{dz} \tag{2a.13}$$

where K_h is the turbulent transfer coefficient ($m^2\ s^{-1}$) or eddy diffusivity for H, T the average air temperature (K) during the measurement time, and z the height above the surface (m). Invoking Eq. (2a.4) for the ideal SR model (Paw U et al., 1995), the variable αz represents the "effective eddy size" responsible for the air parcel renewal (Castellví et al., 2002; Castellví, 2004). Since ramp-like structures (characterized by amplitude a and total ramp duration τ) contribute to vertical transport, Castellví et al. (2002) proposed the following relationship:

$$\frac{a}{\alpha z} \propto \frac{\partial T}{\partial z} = \beta \frac{a}{z}, \quad \text{for the roughness sub-layer} \tag{2a.14}$$

$$\frac{a}{\alpha z} \propto \frac{\partial T}{\partial z} = \beta \frac{a}{z-d}, \quad \text{for the inertial sub-layer}$$

where β is a scale or link parameter (not to be confused with β in Eq. (2a.11)), and d the zero-plane displacement height – the latter normally taken as $2h/3$ where h is the canopy height. When measurements are taken well above the canopy top in the inertial sub-layer, MOST can be used to express K_h as follows:

$$K_h = k u_* (z-d) / \phi_h(\zeta) \tag{2a.15}$$

where k is the von Kármán constant (0.41) and $\phi_h(\zeta)$ the stability function for sensible heat flux where $\zeta = (z-d)/L$ is a dimensionless buoyancy (stability) parameter and L is the Obukhov length (m):

$$L = \frac{T}{k\,g} \frac{\rho c_p u_*^3}{(H + 0.61 c_p T E)}.$$

Following Businger et al. (1971), the stability function $\phi_h(\zeta)$ is

$$\text{unstable} \quad \phi_h(\zeta) = 0.74 \Big/ \sqrt{1-9\zeta}$$

$$\text{neutral} \quad \phi_h(\zeta) = 0.74 \tag{2a.16}$$

$$\text{stable} \quad \phi_h(\zeta) = 0.74 + 4.7\zeta\ .$$

Castellví et al. (2002) proposed the following relationship to estimate H in the inertial and roughness sub-layers by combining Eqs (2a.14) to (2a.16) to yield

$$H = \begin{cases} \rho c_p \beta_2 a u_*, & \text{roughness sub-layer} \\ \rho c_p \beta_1 a u_* / \phi_h(\zeta), & \text{inertial sub-layer} \end{cases} \tag{2a.17}$$

where the amplitude β_1 is a scale parameter for the inertial sub-layer, β_2 a scale parameter for the roughness sub-layer, and a is determined using the van Atta (1977) approach with u_* and ζ determined by iteration[2]. Castellví et al. (2002) found β_1 values ranging from 0.10 to 0.15 and β_2 values ranging from 0.23 to 0.33 above grass, wheat, and grapevine canopies for measurements taken in inertial and roughness sub-layers.

Castellví (2004) derived the following relationship for estimating the weighting factor α in Eq. (2a.4) for measurements above the canopy:

$$\alpha = \begin{cases} \left(\frac{k}{\pi} \frac{(z-d)}{z^2} \frac{\tau u_*}{\phi_h(\zeta)} \right)^{1/2}, & z - d > z^* \\ \left(\frac{k}{\pi} \frac{z^*}{z^2} \frac{\tau u_*}{\phi_h(\zeta)} \right)^{1/2}, & h \le z - d \le z^* \end{cases} \tag{2a.18}$$

where z^* is the roughness sub-layer depth.

Combining Eqs (2a.4) and (2a.18), Castellví (2004) proposed the following expression for estimating sensible heat flux:

$$H = \begin{cases} \rho c_p \left(\frac{a}{\tau^{1/2}} \right) \left(\frac{k(z-d)}{\pi} \right)^{1/2} \left(\frac{u_*}{\phi_h(\zeta)} \right)^{1/2}, & z - d > z^* \\ \rho c_p \left(\frac{a}{\tau^{1/2}} \right) \left(\frac{k z^*}{\pi} \right)^{1/2} \left(\frac{u_*}{\phi_h(\zeta)} \right)^{1/2}, & h \le z - d \le z^*. \end{cases} \tag{2a.19}$$

Equation (2a.19) is valid when measurements are made over homogeneous canopies but good performance has been observed over heterogeneous canopies (Castellví et al., 2006b). In particular, however, the relationship is exempt from calibration regardless of the stability conditions (Castellví, 2004). Also by combining Eqs (2a.18), (2a.19), and invoking the relationship between the ramp period and amplitude (Eq. (2a.10)) from the microfront model, Castellví (2004)[3] derived the following relationship to estimate sensible heat flux:

---

[2] Iterative procedures are key in micrometeorology and biophysics. The Appendix is devoted to selected examples of iterative procedures used in the topic of the thesis, namely SR, MOST and other iterative procedures

[3] Similar relationships are presented by Castellví and Martínez-Cob (2005) but there is a misprint in their Eqs (5) and (6) which contains $k(z-d)^{4/5}$ instead of the correct term $\left(k(z-d)\right)^{4/5}$

$$H=\begin{cases}\rho c_p\left(\dfrac{g}{T}\right)^{1/5}\dfrac{\left(k(z-d)\right)^{4/5}}{\pi^{3/5}}\left(-\gamma^3\dfrac{S^3_{(r_m)}}{r_m}\right)^{3/5}\dfrac{1}{a^{3/5}}\left(\dfrac{1}{-\zeta\,\phi^3{}_h(\zeta)}\right)^{1/5}, & z-d>z^*\\ \rho c_p\left(\dfrac{g}{T}\right)^{1/5}k^{4/5}\left(\dfrac{z^*}{\pi}\right)^{3/5}z^{1/5}\left(-\gamma^3\dfrac{S^3_{(r_m)}}{r_m}\right)^{3/5}\dfrac{1}{a^{3/5}}\left(\dfrac{1}{-\zeta\,\phi^3{}_h(\zeta)}\right)^{1/5}, & h\le z-d\le z^*.\end{cases}$$

(2a.20)

Equation (2a.20) depends on the stability parameter ζ, and hence wind speed measurements are also required as an input. If one uses slow dataloggers, the method is not totally exempt from calibration because of parameter γ (Castellví, 2004; Castellví and Martínez-Cob, 2005). However, γ varies by less than 25 % with respect to unity for different canopies (Chen et al., 1997b). Equation (2a.20) performed well using γ = 1.1 (Table 2a.2) for measurements taken at different heights above the canopy (Castellví and Martínez-Cob, 2005). The function $\left(-\zeta\,\phi^3{}_h(\zeta)\right)^{-1/5}$ in Eq. (2a.20) can be set to approximately 2.4 for the stability range $-3\le\zeta\le-0.03$, with a relative error of less than 8.5 % and can be expressed as (Castellví, 2004):

$$H=\begin{cases}2.4\rho c_p\left(\dfrac{g}{T}\right)^{1/5}\dfrac{\left(k(z-d)\right)^{4/5}}{\pi^{3/5}}\left(-\gamma^3\dfrac{S^3_{(r_m)}}{r_m}\right)^{3/5}\dfrac{1}{a^{3/5}}, & z-d>z^*\\ 2.4\rho c_p\left(\dfrac{g}{T}\right)^{1/5}k^{4/5}\left(\dfrac{z^*}{\pi}\right)^{3/5}z^{1/5}\left(-\gamma^3\dfrac{S^3_{(r_m)}}{r_m}\right)^{3/5}\dfrac{1}{a^{3/5}}, & h\le z-d\le z^*\end{cases}. \qquad \text{(2a.21)}$$

Equation (2a.21) holds under slightly unstable conditions, is valid in both the roughness and inertial sub-layers, only requires air temperature data as an input, and may be considered exempt from calibration (Castellví, 2004) since β_1 in Eq. (2a.17), approximately 0.1, is appropriate under unstable conditions over a variety of canopies. For both roughness and inertial layers, Castellví (2004) found that the value of 0.1 was robust with height.

The main advantage of this SR analysis combination approach therefore is that it is not sensitive to measurement height, and furthermore that it is based on the fact that vertical velocity of the mean eddies responsible for the renewal process has been properly scaled for the corresponding amplitude of the air temperature of the mean ramp events (Castellví et al., 2002).

2a.8 Combined surface renewal analysis model and dissipation theory

An analysis of combining the SR method with dissipation theory was presented by Castellví and Snyder (2009a). For the dissipation method, the normalised dissipation rate for scalar *s* can be expressed as

$$\Phi_s(\zeta)=\frac{k(z-d)}{u_*\,s_*^2}\varepsilon_s \qquad \text{(2a.22)}$$

where s_* is the scalar surface scale and ε_s is the mean dissipation rate for scalar s where

$$u_* s_* = \left(\frac{k(z-d)u_*}{\Phi_s(\zeta)\varepsilon_s} \right)^{\frac{1}{2}}. \tag{2a.23}$$

Using a result of Hsieh and Katul (1997), which involved combining dimensional analysis and the traditional dissipation method, Castellví and Snyder (2009a) showed that

$$u_* s_* = \frac{1.66}{\pi}(z-d)\frac{a_s^2}{\tau_s \sigma_s} \tag{2a.24}$$

where σ_s is the scalar standard deviation. For sensible heat flux, then

$$\alpha = \frac{1.66}{\pi}\frac{(z-d)}{z}\frac{a}{\sigma_T}. \tag{2a.25}$$

They note that the new dissipation-SR analysis, based on Eq. (2a.24), does not require ε_s as an input and does not depend on stability nor on any similarity relationships. Furthermore, for sensible heat flux, only air temperature at frequencies between 4 and 10 Hz are required. They contend that the constant 1.66 does not depend on height. Further research on this aspect is required.

2a.9 Application of the SR method

Most-often, crop coefficients are obtained using lysimeters to measure the evaporation and simultaneously, short-grass (or tall-crop) reference is calculated from weather data. Using SR to estimate sensible heat flux, from which evaporation was calculated using measurements of net irradiance and soil heat flux, Snyder and O'Connell (2007) obtained crop coefficients of microsprinkled-irrigated citrus for four years. A similar method for estimating irrigated pasture evaporation was applied by Snyder et al. (2008) for eight months. For a two-year period, Hanson et al. (2007) used the SR method and other measurements in a water-short area (Eq. (2a.2)) to investigate the effect of deficit irrigation of alfalfa on the yield and evaporation. The performance of an ecosystem evaporation model was investigated using SR measurements of sensible heat flux at a wetlands site (Spano et al., 2009). Bare-soil evaporation was modelled using a coupled heat, water vapour and liquid water flux model and the modelled estimates compared with that using the SR method and energy balance measurements (Eq. (2a.2)) (Bittelli et al., 2008).

Noting that that the BREB method is not recommended for locations influenced by regional advection, and using the SR-similarity combination approach, Castellví and Snyder (2009b) used SR analysis to estimate sensible heat flux over two growing rice fields under regional advection.

Of particular relevance to studies for which there are fetch limitations, Paw U et al. (1995) demonstrated that for short canopies, there was an indication that the SR method was not sensitive to inadequate fetch. They also concluded that the SR method decreased in accuracy as height above the (maize) canopy increased.

The SR method has also been applied to flux estimates of latent energy and carbon dioxide (Castellví et al., 2008). In this investigation, surface energy balance closure over rangeland grass, using SR measurements of H and λE, by application of Eq. (2a.18), was investigated and compared

with EC closure. The EC method consistently underestimated the available energy flux ($R_n - G$ of Eq. (2a.2)) by about 10 % whereas the SR closure was always good.

For measurements in a peach orchard and using the SR/similarity theory combination method (Eq. (2a.19)), Castellví and Snyder (2009c) found that for unstable cases, H_{SR} underestimated by about 7 % and as a result, the sign of the ramp amplitude a was not in agreement with the sign of H_{EC}. They concluded that their experiment demonstrated the potential of SR as a method applicable at any height above the canopy surface for estimating H.

2a.10 Recommendations for future research

The SR method is relatively new and quite simple (Paw et al., 1995; Snyder et al., 1996; Spano et al., 2000). The advantages of the SR method over other micrometeorological methods are the relatively low cost, easy installation and maintenance, apparently that the method is less dependent on fetch since it is based on the theory of short-term heat transfer between a surface and that it operates in the roughness and inertial sub-layers. The ideal SR method is the most inexpensive micrometeorological method for estimating sensible heat flux, but the SR weighting factor α needs to be determined using a standard method such as eddy covariance method. At least two calibrations are recommended: one for night-time and one for day-time conditions to better account for stability conditions. In South Africa, the SR method has been evaluated by Savage et al. (2004), Mengistu (2008) and Nile (2010) for a wide range of canopies and above water (Mengistu and Savage, 2010). Savage (2007) suggested that high frequency air temperature-based methods may pave the way for evaporation stations from which real-time and sub-hourly estimates may be obtained relatively inexpensively.

The SR method has mostly been used for estimating sensible heat flux over different surfaces, and the latent energy flux obtained as a residual of the energy balance (Eq. (2a.2)). The latter provides the most inexpensive procedure to estimate latent energy flux (Drexler et al., 2004).

The SR analysis can be applied to other scalars such as water vapour pressure, carbon dioxide concentration, and other gas concentrations. However, there has been little research on the application of the SR analysis to estimate the flux of other scalars. Currently there are very few published works detailing the application of SR analysis to determine latent energy flux (Katul et al., 1996; Castellví et al., 2008) and only two for carbon dioxide (Spano et al. 2002; Castellví et al., 2008). Therefore, further studies should focus on the use of the SR method to estimate fluxes of water vapour, carbon dioxide, and other scalars. Also, the SR method applied here does not allow real-time estimation of sensible heat flux and further research on this aspect would be valuable for long-term monitoring. The SR methods that are exempt from calibration need to be applied to other surfaces to confirm their applicability over a wide range of atmospheric and surface conditions.

2a.11 Acknowledgements

Funding from the University of KwaZulu-Natal, CSIR, and Water Research Commission (part of projects K1335 and K1567) for this study is gratefully acknowledged.

2a.12 References

ANANDAKUMAR K (1999) Sensible heat flux over a wheat canopy: optical scintillometer measurements and surface renewal analysis estimations. *Agric. For. Meteorol.* **96** 145-156.

ARYA SP (2001) *Introduction to Micrometeorology*. (2nd edn.) Academic Press. London, UK. 420 pp.

BERGSTRÖM H and HÖGSTRÖM U (1989) Turbulent exchange above a pine forest: II. Organized structures. *Boundary-Layer Meteorol.* **49** 231–263.

BEZUIDENHOUT CN, LECLER NL, GERS C and LYNE PWL (2006) Regional based estimates of water use for commercial sugar-cane in South Africa. Water SA **32** 219–222.

BITTELLI M, VENTURA F, CAMPBELL GS, SNYDER RL, GALLEGATI F and PISA PR (2008) Coupling of heat, water vapor, and liquid water fluxes to compute evaporation in bare soils. *J. Hydrol*. **362** 191–205.

BUSINGER JA, WYNGAARD JC, IZUMI I and BRADLEY EF (1971) Flux profile relationships in the atmospheric surface layer. *J. Atmos. Sci.* **28** 181–189.

CAMPBELL GS and DIAK GR (2005) Net and thermal radiation estimation and measurement. In: HATFIELD JL, BAKER JM (eds.) *Micrometeorology in Agricultural Systems. Agronomy Monograph* No. 47. pp. 59–92.

CASTELLVÍ F (2004) Combining surface renewal analysis and similarity theory: a new approach for estimating sensible heat flux. *Water Resour. Res*. 40, W05201, 1-20.

CASTELLVÍ F (2007) The estimation of latent heat flux: a reflection for the future. *Tethys* **4** 19–26.

CASTELLVÍ F (2009) Some advance on the comprehension of SR analysis for estimating the flux of a scalar. *Geophys. Res. Abstr.* **11** EGU2009-2251-1.

CASTELLVÍ F and MARTÍNEZ-COB A (2005) Estimating sensible heat flux using surface renewal analysis and flux variance method: A case study over olive trees at Sastago (NE of Spain). *Water Resour. Res.* **41** W09422, 1–10.

CASTELLVÍ F and SNYDER RL (2009a) Combining the dissipation method and surface renewal analysis to estimate scalar fluxes from the time traces over rangeland grass near Ione (California). *Hydrol. Process.* **23** 842–857.

CASTELLVÍ F and SNYDER RL (2009b). On the performance of surface renewal analysis to estimate sensible heat flux over two growing rice fields under the influence of regional advection. *J. Hydrol*. **375** 546–553.

CASTELLVÍ F and SNYDER RL (2009c). Sensible heat flux estimates using surface renewal analysis A study case over a peach orchard. *Agric. For. Meteorol.* **149** 1397–1402.

CASTELLVÍ F, MARTÍNEZ-COB A and PEREZ-COVETA O (2006a) Estimating sensible and latent heat fluxes over rice using surface renewal. *Agric. For. Meteorol.* **139** 164–169.

CASTELLVÍ F, PEREZ PJ and IBAÑEZ M (2002) A method based on high frequency temperature measurements to estimate sensible heat flux avoiding the height dependence. *Water Resour. Res.* **38 (6)** WR000486–20, 1–10.

CASTELLVÍ F, SNYDER RL and BALDOCCHI DD (2008) Surface energy-balance closure over rangeland grass using the eddy covariance method and surface renewal analysis. *Agric. For. Meteorol.* **148** 1147–1160.

CASTELLVÍ F, SNYDER RL, BALDOCCHI DD and MARTÍNEZ-COB A (2006b) A comparison of new and existing equations for estimating sensible heat flux using surface renewal and similarity concepts. *Water Resour. Res.* **42** W08406, 1–18.

CHEN W, NOVAK MD, BLACK TA and LEE X (1997a) Coherent eddies and temperature structure functions for three contrasting surfaces. Part I: Ramp model with finite micro front time. *Boundary-Layer Meteorol.* **84** 99–123.

CHEN W, NOVAK MD, BLACK TA and LEE X (1997b) Coherent eddies and temperature structure functions for three contrasting surfaces. Part II: Renewal model for sensible heat flux. *Boundary-Layer Meteorol.* **84** 125–147.

DE BRUIN HAR, VAN DEN HURK BJJM and KOHSIEK W (1995) The scintillation method tested over dry vine yard area. *Boundary-Layer Meteorol.* **76** 25–40.

DREXLER JZ, SNYDER RL, SPANO D and PAW U KT (2004) A review of models and micrometeorological methods used to estimate wetland evapotranspiration. *Hydrol. Process.* **18** 2071–2101.

DUCE P, SPANO D and SNYDER RL (1998) Effect of different fine-wire thermocouple design on high frequency temperature measurement. In: *AMS Proc. 23rd Conf. Agric. For. Meteorol*. 2–6 Nov. Albuquerque, NM. pp. 146–147.

DUCE P, SPANO D, SNYDER RL and PAW U KT (1997) Surface renewal estimates of evapotranspiration. Short canopies. *Acta Hort.* **449** 57–62.

GAO W, SHAW RH and PAW U KT (1989) Observation of organized structure in turbulent flow within and above a forest canopy. *Boundary-Layer Meteorol.* **47** 349–377.

GREEN AE, MCANENEY KJ and ASTILL MS (1994) Surface layer scintillation measurements of daytime heat and momentum fluxes. *Boundary-Layer Meteorol.* **68** 357–373.

HANSON B, PUTNAM D and SNYDER R (2007) Deficit irrigation of alfalfa as a strategy for providing water for water-short areas. *Agric. Water Manage*. **93** 73–80.

HIGBIE R (1935) The rate of absorption of a pure gas into a still liquid during short periods of exposure. *Trans. Amer. Inst. Chem. Eng.* **31** 365–388.

HILL RJ (1992) Review of optical scintillation methods of measuring the refractive-index spectrum, inner scale and surface fluxes. *Waves Random Media* **2** 179–201.

HILL RJ, OCHS JR and WILSON JJ (1992) Measuring surface layer fluxes of heat and momentum using optical scintillation. *Boundary-Layer Meteorol.* **58** 391–408.

HSIEH C-I and KATUL GG (1997) Dissipation methods, Taylor's hypothesis, and stability correction functions in the atmospheric surface layer. *J. Geophys. Res.* **102** 16391–16405.

JARMAIN C, EVERSON CS, SAVAGE MJ, MENGISTU MG, CLULOW AD and GUSH MB 2009. Refining tools for evaporation monitoring in support of water resources management. Water Research Commission Report No. 1567. Water Research Commission, Pretoria, South Africa. ISBN 978–1–77005–798–2. p137.

KATUL GG, HSIEH C-I, OREN R, ELLSWORTH D and PHILIPS N (1996) Latent and sensible heat flux predictions from a uniform pine forest using surface renewal and flux variance methods. *Boundary-Layer Meteorol.* **80** 249–282.

LEE X and BLACK TA (1993) Atmospheric turbulence within and above a Douglas-Fir stand. Part I: Statistical properties of the velocity field. *Boundary-Layer Meteorol.* **64** 149–174.

MEDTHERM CORP (2007) Fine wire thermocouple probes for measuring transient gas temperature. URL: http://www.dr-kubelik.de/infomaterial/TCFW%20Brochure%20B112.pdf (Accessed, March 30, 2010).

MEIJNINGER WML and DE BRUIN HAR (2000) The sensible heat fluxes over irrigated areas in western Turkey determined with a large aperture scintillometer. *J. Hydrol.* **229** 42–49.

MENGISTU MG (2008) Heat and energy exchange above different surfaces using surface renewal. Ph.D. thesis, University of KwaZulu-Natal, pp. 151.

MENGISTU MG and SAVAGE MJ (2010) Open water evaporation estimation for a small shallow reservoir in winter using surface renewal. *J. Hydrol.* **380** 27–35.

MENGISTU MG and SAVAGE MJ (2010) Surface renewal method for estimating sensible heat flux. *Water SA* 36, 9-17.

NILE ES (2010) Sensible heat flux estimation for unstable conditions for sugarcane using temperature variance and surface renewal. Ph.D. thesis, University of KwaZulu-Natal, pp. 171.

PAW U KT and BRUNET Y (1991) A surface renewal measure of sensible heat flux density. *Proc. 20th Conf. Agric. For. Meteorol*, 10–13 September, Salt Lake City, UT. American Meteorological Society, Boston, MA. pp. 52–53.

PAW U KT, BRUNET Y, COLLINEAU S, SHAW RH, MAITANI T, QUI J and HIPPS L (1992) On coherent structure in turbulence within and above agricultural plant canopies. *Agric. For. Meteorol.* **61** 55–68.

PAW U KT, QUI J, SU HB, WATANABE T and BRUNET Y (1995) Surface renewal analysis: a new method to obtain scalar fluxes. *Agric. For. Meteorol.* **74** 119–137.

PAW U KT, SNYDER RL, SPANO D and SU HB (2005) Surface renewal estimates of scalar exchange. In: Hatfield JL and Baker JM (eds.) *Micrometeorology in Agricultural Systems. Agronomy Monograph* No. 47, Amer. Soc. Agron., Madison, USA. pp. 455–483.

QUI J, PAW U KT and SHAW RH (1995) Pseudo-wavelet analysis of turbulence patterns in three vegetation layers. *Boundary-Layer Meteorol.* **72** 177–204.

RAUPACH MR, FINNIGAN JJ and BRUNET Y (1989) Coherent eddies in vegetation canopies. In: Proc. 4th Australasian Conf. on Heat and Mass Transfer, Christchurch, New Zealand, May 9–12. Bergell House, New York. pp 75–90.

RAUPACH MR, FINNIGAN JJ and BRUNET Y (1996) Coherent eddies in vegetation canopies: The mixing-layer analogy. *Boundary-Layer Meteorol.* **78** 351–382.

SAVAGE MJ (2007) Sensible heat estimation using a high frequency temperature-based method above various canopies. *Proc*. 13th S. *Afr. Nat. Chap.* of the Int. *Assoc. Hydro. Sci.* (SANCIAHS) Symp. 6–7 September, Cape Town, Republic of South Africa.

SAVAGE MJ (2009) Estimation of evaporation using a dual-beam surface layer scintillometer and component energy balance measurements. *Agric. For. Meteorol.* **149** 501–517.

SAVAGE MJ, EVERSON CS, ODHIAMBO GO, MENGISTU MG and JARMAIN C (2004) Theory and Practice of Evapotranspiration Measurement, with Special Focus on SLS as an Operational Tool for the Estimation of Spatially-Averaged Evaporation. WRC Report No. 1335/1/04. Water Research Commission, Pretoria, South Africa. ISBN 1–77005–247–X. p204.

SAVAGE MJ, ODHIAMBO GO, MENGISTU MG, EVERSON CS, JARMAIN C (2010) Measurement of grassland evaporation using a surface-layer scintillometer. Water SA **36** 9-17.

SELLERS PJ, MINTZ Y, SUD YC and DALCHER A (1986) A simple biosphere model (SiB) for use within general circulation models. *J. Atmos. Sci.* **43** 505–531.

SHAW RH, PAW U KT and GAO W (1989) Detection of temperature ramps and flow structures at deciduous forest site. *Agric. For. Meteorol.* **47** 123–138.

SIMMONS LJ, WANG J, SAMMIS TW and MILLER DR (2007). An evaluation of two inexpensive energy-balance techniques for measuring water use in flood-irrigated pecans. *Agric. Water Manage*. **88** 181−191.

SNYDER RL, ANDERSON FE, SPANO D, DUCE P, PAW U KT and RUSSO AE (2007). An Excel application program to compute surface renewal estimates of sensible heat flux from the 2nd, 3rd and 5th moments of a structure function using high frequency temperature data and to compute ET and crop coefficients using energy balance. University of California, Davis, California.

SNYDER RL and O'CONNELL NV (2007). Crop coefficients for microsprinkler-irrigated clean-cultivated, mature citrus in an arid climate. *J. Irrig. Drain. Engin*. **133** 43–52.

SNYDER RL, SPANO D, DUCE P and PAW U KT (1997) Surface renewal estimates of evapotranspiration. Theory. *Acta Hort.* **449** 49–55.

SNYDER RL, SPANO D and PAW U KT (1996) Surface renewal analysis for sensible heat and latent heat flux density. *Boundary-Layer Meteorol.* **77** 249–266.

SNYDER RL, SPANO D, DUCE P, PAW U KT and RIVERA M (2008) Surface renewal estimation of pasture evapotranspiration. *J. Irrig. Drain. Engin.* **134** 716–721.

SPANO D, DUCE P, SNYDER RL and PAW U KT (1997a) Surface renewal estimates of evapotranspiration: tall canopies. *Acta Hort.* **449** 63–68.

SPANO D, SNYDER RL, DUCE P and PAW U KT (1997b) Surface renewal analysis for sensible heat flux density using structure functions. *Agric. For. Meteorol.* **86** 259–271.

SPANO D, SNYDER RL, DUCE P and PAW U KT (2000) Estimating sensible and latent heat flux densities from grape vine canopies using surface renewal. *Agric. For. Meteorol.* **104** 171–183.

SPANO D, SNYDER RL, DUCE P, PAW KT and FALK M (2002) Surface renewal determination of scalar fluxes over an old-growth forest. *Am. Meteorol. Soc.* **104** 171–183.

SPANO D, SNYDER RL, SIRCA C and DUCE P (2009) ECOWAT – a model for ecosystem evapotranspiration estimation. *Agric. For. Meteorol.* **149** 1584–1596.

STULL RB (1984) Transilient turbulence theory: 1. The concept of eddy-mixing across finite distances. *J. Atmos. Sci.* **41** 3351–3367.

THIERMANN V and GRASSL H (1992) The measurement of turbulent surface-layer fluxes by use of bichromatic scintillation. *Boundary-Layer Meteorol.* **58** 367–389.

THOM AS (1975) Momentum, mass and heat exchange in plant communities. In: MONTEITH JL (eds.) *Vegetation and the Atmosphere. Principles*. Academic Press. London, UK. **Vol. 1**. pp 57–109.

VAN ATTA CW (1977) Effect of coherent structures on structure functions of temperature in the atmospheric boundary layer. *Arch. Mech.* **29** 161–171.

ZAPATA N and MARTÍNEZ-COB A (2001) Estimation of sensible and latent heat flux from natural sparse vegetation surface using surface renewal. *J. Hydrol*. **254** 215–228.

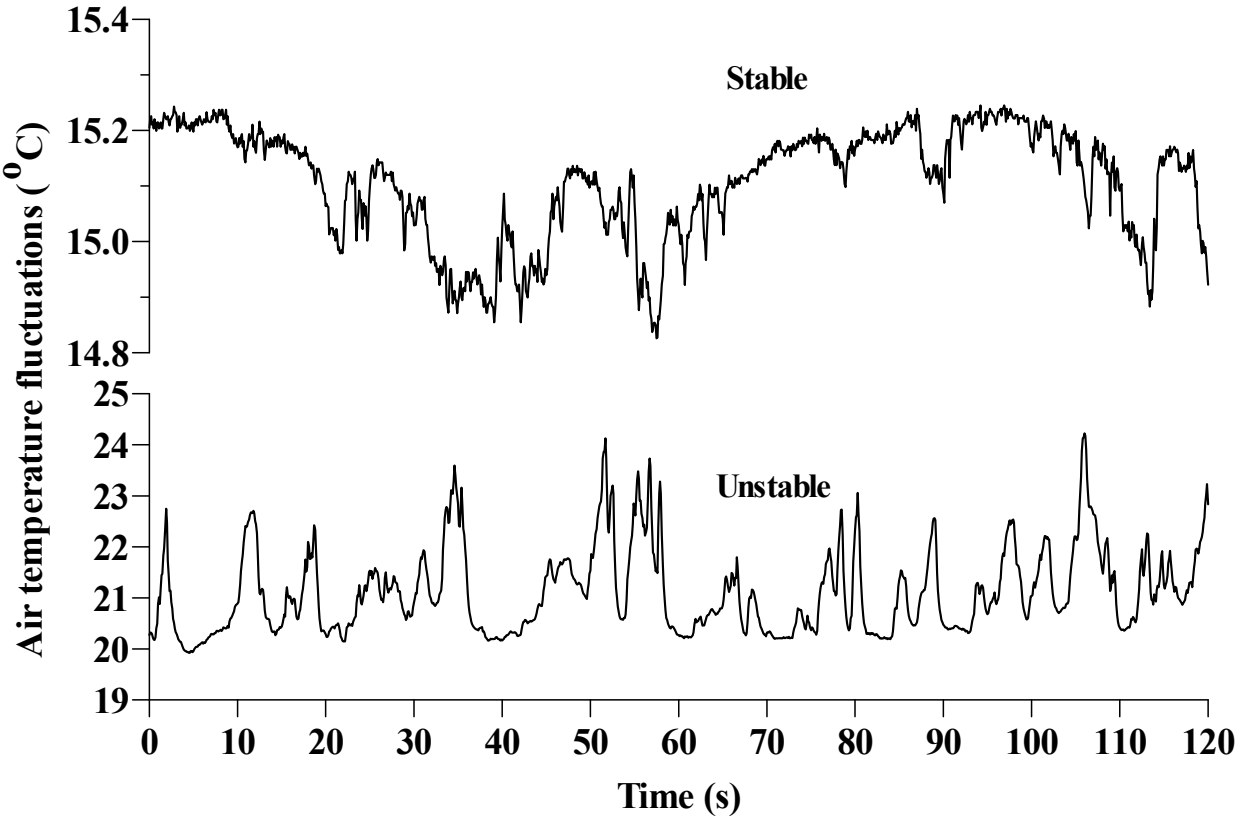

Fig. 2a.1. Air temperature ramps observed in a sample of 120 s of 10 Hz air temperature traces. The measurements were taken at 0.5 m above grass (0.3 m tall) for unstable (10h00) and stable conditions (01h00), in the Bellevue area neighbouring Ashburton and close to Pietermaritzburg, South Africa for day of year 321 (2003).

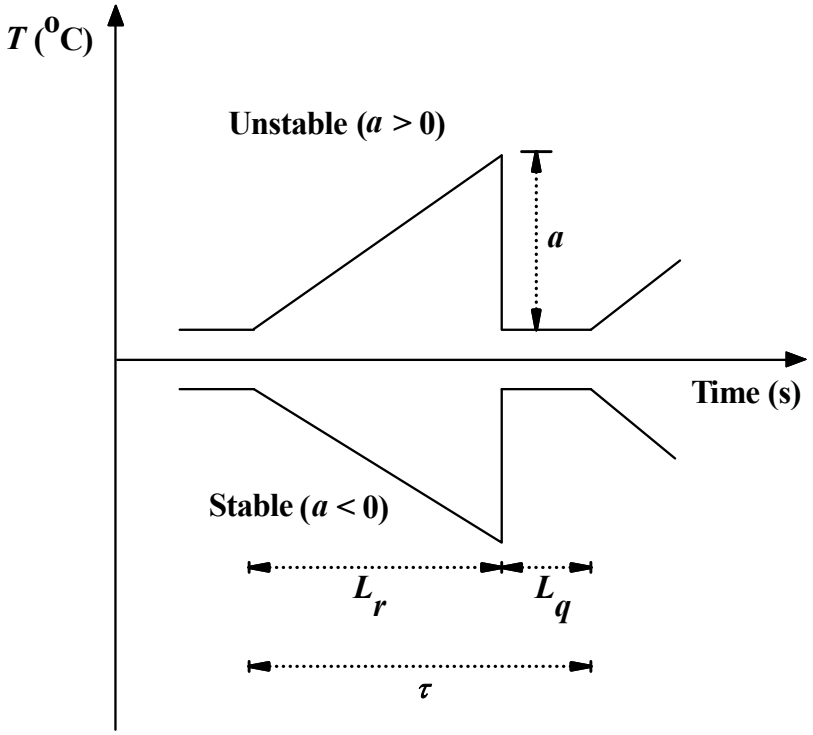

Fig. 2a.2. An ideal surface renewal analysis ramp model, assuming a sharp instantaneous drop in air temperature with amplitude $a > 0$ for unstable and $a < 0$ for stable atmospheric conditions. The ramp period is L_r and L_q the quiescent time period with $\tau = L_r + L_q$ the total ramp period (inverse ramp frequency).

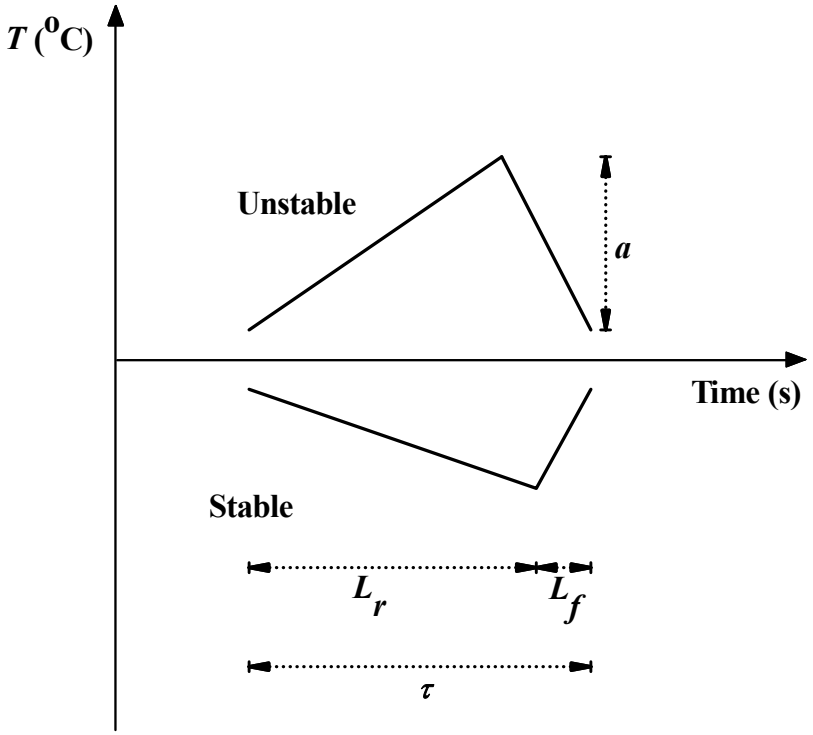

Fig. 2a.3. Surface renewal analysis ramp model which assumes a finite microfront time, where a is the air temperature amplitude, L_r is the ramp period, L_f is the microfront period, and τ is the total ramp period.

Table 2a.1. The weighting factor α for a range of surfaces using different time lags and sensor sizes during unstable conditions. The slope of the regression of H estimated using the SR method *vs* H obtained using a standard method (eddy covariance) yields α for linear fits forced through the origin.

Surface	Canopy height (m)	Height above canopy (m)	Sensor size (μm)	Sampling frequency (Hz)	Time lag *r* (s)	α	Authors
Bare-soil	0.00	-	12.7	8	0.25	0.90	Duce et al. (1998)
Bare-soil	0.00	-	25.4	8	0.25	1.04	Duce et al. (1998)
Bare-soil	0.00	-	76.2	8	0.25	1.88	Duce et al. (1998)
Bare-soil	0.00	0.03	25.0	10	0.10	0.69	Chen et al. (1997b)
Endorreic salty lagoon	0.00	0.90	76.2	8	0.75	1.00	Zapata and Martínez-Cob (2001)
Open water	0.00	1.0, 1.3, 1.9, 2.6	75	10	0.4, 0.8	0.2, 0.25	Mengistu and Savage (2010)
Mulch	0.05	0.09	25.0	10	0.10	0.51	Chen et al. (1997b)
Grass (alta fescue)	0.10	0.35	76.2	8	0.75	1.00	Snyder et al. (1996)

Surface	Canopy height (m)	Height above canopy (m)	Sensor size (μm)	Sampling frequency (Hz)	Time lag *r* (s)	α	Authors
Grass (alta fescue)	0.10	0.30	76.2	8	0.25	0.97	Duce et al. (1997)
Irrigated pasture (tall fescue)	0.08 to 0.12	0.75 (0.6)	75	4	0.25, 0.5	0.35 (0.4)	Snyder et al. (2008)
Wheat	0.70	0.30	76.2	8	0.50	1.00	Duce et al. (1997)
Sorghum	0.70	0.30	76.2	8	0.75	1.02	Duce et al. (1997)
Wheat	0.90	0.50	25.4	16	0.30	1.00	Anandakumar (1999)
Sugarcane	> 1 m	0.2, 0.5, 0.75, 1.5	75	10	0.4, 0.8	0.55 to 0.66	Nile (2010)
Sparse grape vine	2.20	0.00	76.2	8	0.50	0.87	Spano et al. (1997b)
Maize	2.60	0.00	12.5	10	0.10	0.50	Paw U et al. (1995)
Peach orchard	3.95	1.55	Sonic temperature	10	Several	0.95	Castellví and Snyder (2009)
Citrus	4 to 4.5	0 to 0.5	76.2	4	0.5, 1.0	0.227	Snyder and O'Connell (2007)

Surface	**Canopy height (m)**	**Height above canopy (m)**	**Sensor size (μ m)**	**Sampling frequency (Hz)**	**Time lag *r* (s)**	α	**Authors**
Avocado	5.20	0.00	76.2	8	0.50	0.59	Spano et al. (1997b)
Flood-irrigation pecan	12.8	-3.7, 0	-	4	1.0	1.1 ($z = d$), 0.5 ($z = h$)	Simmons et al. (2007)
Douglas-fir forest	16.70	6.30	25.0	2	0.50	0.52	Chen et al. (1997b)
Mixed deciduous forest	18.00	0.00	12.5	10	0.10	0.50	Paw U et al. (1995)

Table 2a.2. Average coefficients α, β, γ, and the combined coefficient $\alpha\beta^{2/3}\gamma$, for Douglas-fir forest, straw mulch, and bare soil (Chen et al., 1997b).

Canopy	α	β	γ	$\alpha\beta^{2/3}\gamma$
Douglas-fir forest	0.527	0.795	1.001	0.418
Straw mulch	0.511	0.538	1.175	0.397
Bare soil	0.691	0.398	1.104	0.413

3 INFRARED CALIBRATION OF NET RADIOMETERS AND INFRARED THERMOMETERS[1]

3.1 Abstract

A standard, convenient and accurate method for calibrating net radiometers would assist in unravelling reasons for the perplexing lack of surface energy balance closure as well as improving on the accuracy of the energy balance residual method for estimating evaporation. A relatively inexpensive, accurate and quick laboratory method for non-steady radiative conditions above a large water-heated or water-cooled radiator containing circulated water, with surface-embedded thermocouples, was used to obtain reproducible net radiometer calibration factors for the infrared waveband for a wide range in net irradiance. Infrared calibration factors for two-component, four-component, miniature polyethylene, polyethylene-domed (with and without ventilation) and domeless net radiometers were obtained. A method was also used for the shortwave calibration of net radiometers by placement of a net radiometer adjacent to a standard shortwave radiometer with both instruments placed above the radiator. Measurements from heated-needle anemometers demonstrated that thermally induced wind speed was not a significant factor in the infrared calibrations. Furthermore, the temperature gradient across the radiator was fairly uniform at any time. For the infrared calibrations, the two- and four-component net radiometers yielded average root mean square errors of 0.88 and 0.97 W m^{-2} respectively compared to 0.92 W m^{-2} for the polyethylene-domed net radiometers, 2.59 W m^{-2} for four domeless units and 2.27 W m^{-2} for a polyethylene-domed miniature net radiometer. Theory presented and collected measurements allowed the net radiometer infrared calibration factor to be determined for cases when the infrared irradiance from the environment was not constant. For the broadband domeless net radiometers used, the shortwave and infrared calibration factors were within 6.5 % of each other and yet 24.3 % different for some of the polyethylene-domed instruments. The use of ventilators, for polyethylene-domed net radiometers, resulted in more variable data and larger-than-expected infrared calibration factors. The most consistent infrared calibrations for the domed net radiometers were obtained using an air-conditioned laboratory. The radiator method also provides a convenient method for calibrating a number of infrared thermometers (IRTs) simultaneously for a wide temperature range. Different regression procedures for the non-linear calibration relationships, for IRTs with and without a body temperature sensor, were applied to obtain estimates of the radiator surface temperature. The residuals between the average radiator surface temperature and the corresponding IRT target temperature measurements were within 0.15 ^{o}C for all IRT types except for a handheld IRT unit which was within 0.2 ^{o}C. The radiator method used allows net radiometers to be calibrated for both infrared and shortwave under near-identical laboratory conditions, as well as IRTs to be calibrated, and is relatively simple to set up and operate.

Keywords:

Net radiometer calibration

Infrared thermometer calibration

Energy balance closure

Net radiation

---

[1] Based on Savage et al. (1997, 2004) and Savage and Heilman (2009)

3.2 Introduction

Net irradiance measurements are an essential part of surface energy balance investigations and especially so when estimating latent energy flux, as a residual of the energy balance using measurements of net irradiance R_{net} (W m^{-2}) and sensible and soil heat flux, or when investigating closure of the energy balance. Often, the weakest aspect of energy balance investigations is the lack of or unknown accuracy of the R_{net} measurements caused by the absence of or non-reliable infrared calibration and in some cases unreliable or incorrect shortwave calibration measurements. From personal communications we know that other workers arrived at similar conclusions for their R_{net} measurements. Invariably, the calibration factor(s) specified by the manufacturer is used (for example, Brotzge and Duchon, 2000; Sridhar and Elliott, 2002; Cobos and Baker, 2003), for many years or until a recalibration or instrument intercomparison, together with the measured net radiometer voltage(s) to obtain R_{net}.

Eddy covariance measurements of sensible heat H and latent energy LE flux densities are cross-checked by calculating the so-called closure of the energy balance. For closure to exist, the sum of the terms of the shortened energy balance usually ignoring canopy-stored heat, viz., net irradiance R_{net}, H, LE and soil heat flux S, is zero (Stannard et al., 1994; Twine et al., 2000; Lamaud et al., 2001; Wilson et al., 2002; Baker, 2003; Brotzge and Crawford, 2003; Ham and Heilman, 2003). Invariably however, $H + LE < -R_{net} - S$ and closure is said not to be achieved and

$$c = (H + LE) / (-R_{net} - S) \tag{3.1}$$

is less than 1. An additional complication here is the effect of the neglect of the usually unknown sensible heat and latent energy advection components on the energy balance and also on closure (Lee et al., 2004).

Using the residual energy balance approach, H is measured using the eddy covariance, scintillometer (Savage, 2009), surface renewal (Castellví, 2004; Mengistu and Savage, 2009) or temperature variance (Prueger and Kustas, 2005; Chapter 7) methods and LE calculated as a residual from the shortened form of the energy balance, using R_{net} and S measurements. Furthermore, R_{net} measurements play an important role in the Bowen ratio method (Savage et al., 2009). For all these situations, the R_{net} (and S) measurements are crucial and a standard method for the calibration of net radiometers would be an important contribution towards unravelling the uncertainties surrounding the lack of energy balance closure and also in reducing the error in estimating the residual term of the energy balance LE. Some workers have suggested that the extent of closure at FLUXNET sites probably result from bias errors in net irradiance measurements of up to 15 % (Wilson et al., 2002). However, Liu et al. (2006) for example, noted that a lack of closure of the energy balance of 10 % or more (for which $c \leq 0.9$) at eddy flux sites is not uncommon and that the causes for the lack of energy balance closure for which c < 1 still remain unclear. Furthermore, the influence of advection in these studies is uncertain. In the case of the Bowen ratio and residual energy balance methods for estimating LE, closure is by definition satisfied and therefore c = 1. The residual energy balance, eddy covariance and Bowen ratio methods however are critically dependent on the measured R_{net} when estimating LE or for checking for closure for when LE is measured directly using eddy covariance.

Shuttleworth (1991) and Brotzge and Duchon (2000) describe R_{net} as one of the most difficult micrometeorological variables to measure accurately and Cobos and Baker (2003) state that despite efforts to develop accurate and cost-effective instrumentation for R_{net} measurements, there is still no widely accepted best field-measurement method. Calibration of a net radiometer, domed or domeless (Brotzge and Duchon, 2000; Cobos and Baker, 2003), may involve the use of a standard radiometer for a shortwave calibration procedure or involves a net radiometer intercomparison. Laboratory/field instrument comparisons of net radiometers or pyrgeometers are rare – some examples of such include the work by Halldin and Lindroth (1992), Philipona et al. (1998), Reda et al. (2002) and Blonquist et al. (2009).

A common field method for calibrating net radiometers for shortwave is the "occulting" or "shading" (Idso, 1974) or partial shading (Fritschen and Fritschen, 2007) method. Fritschen and Fritschen (2007) however advocate the use of a translucent shade procedure to avoid negative R_{net} values during shading, indicative of net infrared irradiance magnitudes exceeding the net shortwave irradiance. The change in the net radiometer voltage between unshaded and (partially) shaded conditions is a measure of the known change in shortwave irradiance recorded by the pyranometer or pyrheliometer standard, measurements from the latter adjusted for the solar elevation, allowing a calibration factor for the net radiometer to be determined. When the sun/shade calibration method is used:

1) the net radiometer should not be positioned too close to the canopy or soil surface since the net radiometer shadow may alter the net irradiance (short-wave and infrared components) received from the ground;

2) the accuracy of the net irradiance measurements will be no more accurate than the short-wave irradiance measurements using the solar radiation standard or sub-standard sensor;

3) the calibration factor obtained is that for the net radiometer voltage response to short-wave irradiance and does not indicate the net radiometer voltage response to infrared irradiance. The sun/shade method assumes no change in the net infrared irradiance during the shaded and unshaded measurements and between pairs of these measurements. The only way to check the similarity of the net radiometer voltage response to short-wave and infrared irradiance is to also perform a calibration, usually indoors, of the net radiometer for infrared irradiance (wavelengths greater than 3 μm) (Idso, 1974) or to infer an infrared irradiance calibration factor by intercomparison with a pyrgeometer or component net radiometer;

4) the *in situ* sun/shade calibration method is fraught with the problems of a non-static radiation source - the sun - causing the shaded and unshaded radiometer voltage measurements to be performed at different times;

5) the shaded net radiometer and shaded pyranometer or pyrheliometer measurements using the sensor standard may be subject to error, caused by the shading itself, and involve the use of an expensive solar radiometer standard.

In the FIFE micrometeorological investigation (Kanemasu et al., 1987; Field et al., 1992; Nie et al., 1992), five participating groups measured a midday R_{net} of between 300 and 530 W m^{-2} – more than a 75 % variation. Field et al. (1992) noted 5 to 7 % relative differences in R_{net} for side-by-side sun/shade shortwave calibrations for instruments of the same manufacture and R_{net} measurement differences of 10 to 15 % between instruments of different manufacture. Fritschen and Fritschen (2007) commented that these field comparisons used outdated net radiometers with old calibration factors. Brotzge and Duchon (2000) found R_{net} measurement differences that parallel those found by Field et al. (1992) and Halldin and Lindroth (1992) and Tanner and Greene (1989) found a 16 % difference in daytime net irradiance between different net radiometers using calibration factors supplied by the manufacturers.

Ohmura et al. (1998) noted that due to the lack of a well-accepted standard (and method) for infrared irradiance, none of the pyrgeometers or net radiometers can be regarded as correct or incorrect. To date, there is no international agreement for the calibration procedure and choice of a radiation standard for pyrgeometers (Kohsiek et al., 2007) and treatment of the data. The World Meteorological Organisation has a classification system for pyranometers, e.g. primary standard, secondary standard, etc., but not for net radiometers. Most net radiometer "calibrations" are therefore performed in the field by comparing measurements from one net radiometer against those from another (for example, Brotzge and Duchon (2000) and Blonquist et al. (2009)); in one case, a round-robin pyrgeometer calibration experiment was undertaken (Philipona et al., 1998). In the round-robin experiment, differences of up to 20 % from the median instrument responsivity were obtained by the various participating specialist laboratories. In another case, an unexpected shift was noted in the time series of infrared data, following a change in the calibration procedures for field instruments (Stoffel, 2005).

Duchon and Wilk (1994) also demonstrated significant day-time and night-time R_{net} measurement differences for instruments of different manufacture. The large differences in H and LE estimates in the FIFE investigation were attributed mainly to the calibration factor used for the R_{net} measurements and partly to the measurements of S. Kustas et al. (1998) found inconsistent differences in R_{net} measured using different instrument models, indicating that there was no possibility of removing bias between the instruments for all conditions. They emphasised the need for calibration procedures for accurate measurements over a range of surface conditions. Twine et al. (2000) report typical errors of 3 % in net solar irradiance and 15 % in net infrared irradiance and report a case of factory calibration errors causing a 15 % underestimation in net irradiance. For the almost cloudless conditions of the EBEX-2000 experiment, the error in R_{net} was estimated at within 25 W m^{-2} during the day (typically within 5 %) and within 10 W m^{-2} at night (typically within 20 %) (Kohsiek et al., 2007). Halldin and Lindroth (1992), using a four-component net radiometer, found for reference and individual instruments relative differences in R_{net} between 6 and 20 % and commented: "(data) support a general scepticism toward the calibration factors given by the manufacturers" and cautioned that it seems mandatory to have a standard established for the infrared calibration of net radiometers and pyrgeometers. They also quote a comment from Kondratyev (1970) that measurement accuracy (in net irradiance) cannot be increased in the absence of a standard net radiometer.

Vogt et al. (1996) discussed sources of error in net irradiance field measurement, including sensor levelling, calibration drift, dome transmissivity, sensor wavelength response, unequal losses of

energy via convection and infrared emission between upper and lower sensors of the instrument under high solar irradiance.

Polyethylene-domed net radiometers should be recalibrated every six months when the domes are replaced – Brotzge and Duchon (2000) noted domes degrading after a few months of exposure and Cobos and Baker (2003) found dome degradation over three months. This again justifies the need for a convenient and inexpensive method for regular net radiometer calibration. Furthermore, should a standard infrared radiation source be found, it could possibly also be used as a standard for calibrating (far) infrared thermometers.

In the case of two- or four-component net radiometers, the shortwave calibration may be performed using standard pyranometers or sub-standard pyranometers calibrated against a standard without resorting to the shading or partial shading method. In such cases, the shortwave calibration may result in accurate estimation of the net shortwave irradiance but the net infrared irradiance is then measured without calibration. For domed net radiometers, Fritschen and Fritschen (2007) advocate laboratory methods with steady-state radiative conditions, as opposed to outdoor calibrations, using ventilated net radiometers for shortwave and infrared calibrations. Ventilation is not often used – for example, most of the participating laboratories in the round-robin pyrgeometer calibration experiment (Philipona et al., 1998) did not use instrument ventilation.

Cook and Holdridge (2006) found that the source of R_{net} measurement differences between two instrument models was mostly in the infrared, not the shortwave, for their side-by-side field comparisons. They noted that the transmittance of polyethylene is weak for wavelengths of strongest infrared transmission by water vapour and speculate that there may be a systematic water vapour dependent error for the infrared for polyethylene-domed net radiometers.

A common calibration method for pyrgeometers, as judged by the protocols of the participating groups in the round-robin pyrgeometer calibration experiment, involves the use of blackbody cones or cylinder cavities (Philipona et al., 1998). Idso (1971) and Campbell and Diak (2005) used a large-area blackbody radiator of known temperature to calibrate domed net radiometers for the infrared.

Huband and Monteith (1986) and Campbell and Norman (1990) discuss limitations on precision and accuracy for surface temperature measurements using radiometric thermometers, suggesting values of 0.4 K for precision and 1.0 K for accuracy. Barber and Brown (1978) used a blackbody surface for the calibration of infrared thermometers (IRTs). Their unit could display the blackbody surface temperature but temperature control was not possible. Sadler and van Bavel (1982) devised a method, modified by Ham (1990), for the calibration of IRTs using a blackbody calibration chamber. Amiro et al. (1983) and Kalma and Alksnis (1988) describe the use and calibration of IRTs. Baker et al. (2001) used a continuously calibrated infrared system using a blackbody cavity, the temperature of which was controlled by a Peltier block and measured using thermocouples. Pinnock and Bugbee (undated) used a copper plate sprayed with flat black paint to calibrate their IRTs. Most published methods only allow for single-unit IRT calibrations and are also not suitable for the infrared calibration of net radiometers. Water-cone IRT calibrators are convenient (Bugbee et al., undated), and inexpensive, but may result in water condensation on the IRT window area and maintenance of the water-cone during the entire heating and/or cooling calibration period is often not possible.

The aim of this work is to describe an accurate, relatively quick, convenient, relatively inexpensive and repeatable non-steady laboratory method, based on established physical theory, for infrared calibration of various types of net radiometers and calibration of IRTs placed above a radiator, for a wide range in infrared irradiance and surface temperature respectively. A laboratory method using a standard pyranometer and the same radiator for the shortwave calibration of net radiometers is also presented and used. This shortwave calibration method avoids the problems in the field associated with the sun/shade calibration technique previously described and also allows comparisons for the same instrument of the calibration factors for both shortwave and infrared under near-identical laboratory conditions. In the case of the IRT calibration method, a number of IRTs may be calibrated simultaneously, the problems of the water-cone calibration method are avoided and the method is applied to non-linear IRT calibration relationships.

3.3 Theory

Suppose that a net radiometer to be calibrated is placed directly above the centre of a circular radiator of radius r and area A. From radiation geometry, the net radiometer view factor F for the circular radiator positioned at a vertical distance d away from the nearest net radiometer sensing element is given by:

$$F = \sin^2 \beta = r^2 / (r^2 + d^2) = A / (A + \pi d^2), \tag{3.2}$$

where β is the angle between the vertical and the line from the sensor to the edge of the circular radiator. If a sufficiently large rectangular radiator with area A is used, the radiator radius r may be estimated with sufficient accuracy as $\sqrt{A/\pi}$.

The upward infrared irradiance $L_{u\,rad}$ (W m^{-2}) from the radiator, at uniform surface temperature T_{rad} (K), is therefore:

$$L_{u\,rad} = F \varepsilon_{rad} \sigma T_{rad}^4, \tag{3.3}$$

where ε_{rad} is the radiator infrared emissivity and $\sigma = 5.6704 \times 10^{-8}$ W m^{-2} K^{-4} is the Stefan-Boltzmann constant. If the radiator infrared reflectivity is $\rho_{l\,rad}$, then using Kirchhoff's Law, $\rho_{l\,rad} = 1 - \varepsilon_{rad}$ and:

$$L_{u\,rad} = F \varepsilon_{rad} \sigma T_{rad}^4 + F\,(1 - \varepsilon_{rad})\, L_{d\,surr}, \tag{3.4}$$

where $L_{d\,surr}$ is the downward infrared irradiance from the surrounds. The net infrared irradiance L_{net} measured by a net radiometer suspended above the centre of the radiator a distance d away would however also include from the surrounds the downward and the upward infrared irradiances $L_{d\,surr}$ and $(1 - F)\, L_{u\,surr}$ respectively and hence:

$$L_{net} = -F \varepsilon_{rad} \sigma T_{rad}^4 - F\,(1 - \varepsilon_{rad}) L_{d\,surr} + L_{d\,surr} - (1 - F)\, L_{u\,surr}. \tag{3.5}$$

Eq. (3.5) may be simplified for a radiator for which $\varepsilon_{rad} \approx 1$ and therefore the second term on the right-hand side could be neglected. The net infrared irradiance may be varied by altering T_{rad} and maintaining constant or measuring the other infrared components of Eq. (3.5).

The net irradiance R_{net} above the radiator surface at the net radiometer position is therefore:

$$R_{net} = -F\,\varepsilon_{rad}\sigma T_{rad}^4 - F\,(1-\varepsilon_{rad})\,L_{d\,surr} + L_{d\,surr} - (1-F)\,L_{u\,surr} + I_s(1-\rho_{s\,rad}) \tag{3.6}$$

where I_s is the shortwave irradiance and $\rho_{s\,rad}$ is the shortwave reflection coefficient of the radiator surface. The measured R_{net} is calculated from the measured net radiometer voltage V_{net} and the net radiometer calibration factor k (W m^{-2} mV^{-1}) by using:

$$R_{net} = k\,V_{net}\,. \tag{3.7}$$

For some net radiometers and two-component net radiometers, two calibration factors for the same sensor are specified, one for positive R_{net} and one for negative R_{net} for the former, and for two-component instruments, calibration factors k_s and k_l for net shortwave and net infrared irradiances respectively. Using these factors for two-component net radiometers, the net irradiance $\hat{R}_{net\,2-comp}$ is estimated using the voltages for shortwave ($V_{net\,s}$) and infrared ($V_{net\,l}$) as:

$$\hat{R}_{net\,2-comp} = k_s\,V_{net\,s} + k_l\,V_{net\,l}\,. \tag{3.8}$$

Campbell and Diak (2005) show that the product of dome transmittance and sensor plate absorptance must be equal for both shortwave and infrared for the calibration factors for the two wavebands to match.

Assuming that $L_{d\,surr}$ and $L_{u\,surr}$ are constant during the infrared calibration period and that I_s and $\rho_{s\,rad}I_s$ are also constant or negligible and that $1-\varepsilon_{rad} \approx 0$, using Eq. (3.6) and (3.7),

$$\partial(F\,\sigma T_{rad}^4)\,/\,\partial V_{net} = -k_l\,. \tag{3.9}$$

Varying T_{rad} and measuring the corresponding net radiometer voltage V_{net} will calibrate the net radiometer for the infrared assuming F is known or almost 1 (Eq. (3.2)).

If it is necessary to account for the infrared irradiance from the surrounds due to changing surrounding temperature T_{surr} during the calibration period, and assuming that in magnitude $L_{u\,surr} \approx L_{d\,surr} \approx \sigma T_{surr}^4$, then using Eq. (3.6) and (3.7),

$$\partial(F\,\sigma T_{rad}^4 - F\,L_{d\,surr})\,/\,\partial V_{net} = -k_l\,. \tag{3.10}$$

If the upward radiator infrared irradiance $F\sigma T_{rad}^4$ is calculated from independent T_{rad} surface temperature measurements and the known view factor F (Eq. (3.2)), measurement of the corresponding net radiometer voltage will calibrate the net radiometer for infrared irradiance using Eq. (3.10). It is assumed here that $\varepsilon_{rad} \approx 1$ and that, as previously mentioned, the infrared irradiance from the surrounds - $L_{u\,surr}$ and $L_{d\,surr}$ - are of approximately equal magnitude and I_s and $\rho_{s\,rad}\,I_s$ are constant for the calibration period or negligibly small (Eq. (3.6)).

Using the method described, it is also possible to calibrate two- and four-component net radiometers for the infrared using the radiator method (Eq. (3.6)) by applying Eq. (3.9) and ensuring that the associated underlying assumptions are met and if not, then by applying Eq. (3.10) to account for small changes in temperature of the surrounds.

If a shortwave irradiance source is suspended above a near-perfect radiator with a net radiometer placed close to the latter, the changes in net radiometer voltage will correspond only to the changes in the incident shortwave irradiance with the reflected amount from the radiator constant or negligible (Eq. (3.6)). For broadband net radiometers, it may be necessary to correct for any temperature changes of the radiator surface and the surrounds during the shortwave calibration since the shortwave source may alter these temperatures and hence alter $L_{u\,rad}$ and $L_{d\,surr}$. However, corrections for such changes in the infrared conditions may be applied using F and measurements of T_{rad} and T_{surr} (Eq. (3.6)).

If the radiator has a surface temperature T_{rad} and an infrared emissivity ε_{rad} and an infrared thermometer (IRT) registers a temperature of T_{IRT} (K) for the radiator, then:

$$\sigma T_{IRT}^4 = \varepsilon_{rad}\,\sigma T_{rad}^4 + (1-\varepsilon_{rad})\,\sigma T_{surr}^4 . \tag{3.11}$$

Hence, by rearrangement of Eq. (3.11):

$$\varepsilon_{rad} = (T_{IRT}^4 - T_{surr}^4) / (T_{rad}^4 - T_{surr}^4) . \tag{3.12}$$

If the surrounds are imperfect radiators with unknown temperature, then ε_{rad} can only be estimated and then with least error if $T_{rad} \approx T_{surr}$ and in that case, $\varepsilon_{rad} = T_{IRT}^4 / T_{rad}^4$. If $T_{IRT} = T_{rad}$, then ε_{rad} = 1 (Eq. (3.12)).

From an analysis of data for the laboratory calibration of IRTs using the radiator with surface-embedded thermocouples, an approach which is similar but not identical to that of Kalma and Alksnis (1988) was used: the non-linear relationship between the corrected target temperature of an IRT, T_{CTT} (K), T_{IRT} and the body temperature of the sensor T_{SB} (K) is expressed empirically by:

$$\sigma T_{CTT}^4 = c_1 \sigma T_{IRT}^4 + c_2 \sigma T_{SB}^4 + c_3 T_{IRT} + c_4 T_{SB} + c_5 . \tag{3.13}$$

The second to last term on the right-hand side of Eq. (3.13) involving T_{SB}, not included by Kalma and Alksnis (1988), improves the regression analysis. Furthermore, their method did not include the first term to fourth order involving T_{IRT} and the empirical constants c_1, c_2, c_3, c_4 and c_5. Corresponding measurements of the radiator surface temperature from the embedded thermocouples, taken as $T_{CTT} = T_{rad}$, and IRT estimates of the radiator surface T_{IRT} and its body temperature T_{SB} allow the empirical constants of Eq. (3.13) to be determined by linear regression, thereby calibrating the IRT.

3.4 Materials and methods

3.4.1 Calibration equipment and materials

3.4.1.1 Infrared calibration of net radiometers

A large-size truck radiator (0.710 m by 0.481 m – for which the averaged F = 0.9869 for d = 65 mm – and 50 mm thick) was used for the initial experiments. The vertical distance d was measured from the centre of the radiator to the centre of the lower net radiometer sensor. A larger radiator (0.800 m by 0.675 m – for which F = 0.9916 for d = 65 mm – and 34 mm thick) was manufactured and used at another location for subsequent calibrations (Fig. 3.1, top). In both cases, the radiators were electrically grounded. The radiator was placed on a thick (37 mm) polystyrene base covered with aluminium foil that had been painted matt black. Matt black paint (Sprayon, Bedford Heights, Ohio, USA – industrial acrylic enamel flat black number 03725, emissivity listed as 0.95 at 25 ^{o}C) was applied to the surface of the radiator although as mentioned by Campbell and Diak (2005), the colour of the radiator surface is not important for (infrared) calibrations. Furthermore, the multiple cavity reflections would result in a radiator emissivity greater than 0.95. The cavities of both radiators used were triangular-shaped when viewed from above (Fig. 3.1, bottom left) with a depth to aperture ratio of 5 in the one direction and a ratio of 20 in the perpendicular direction for the smaller radiator and respective ratios of 4 and 11 for the larger radiator.

A number of 24-gauge copper-constantan thermocouples (model PR-T-24, Omega Engineering Inc., Stamford, Connecticut, USA) were used to measure the surface temperature of the radiator (Fig. 3.1, bottom right) as well as the temperature of the water pumped into and out of the radiator.

For the infrared calibrations using the smaller radiator, the surface temperature of the radiator was measured at five locations. The thermocouples were pushed through from the bottom of the radiator, with the radiator in the horizontal position, to the top. The 5-mm tip end of the thermocouple was bent to form an "L" shape. The thermocouple was then soldered on to the radiator surface so as to be flush with the radiator surface (Fig. 3.1, bottom left). Electrical checks confirmed that there were no electrical ground loops – the paint of the radiator prevented electrical contact between the radiator metal and the thermocouples. Each thermocouple was about 50 mm away from the nearest other thermocouple with the complete array in the shape of a large plus sign centred on the centre position of the radiator. For the larger radiator there were nine thermocouples also arranged in the shape of a large plus sign (Fig. 3.1, bottom right). Each thermocouple was also sprayed with matt black paint. These important procedures minimised temperature differences between the cavities of the radiator and the thermocouples. A single electrically insulated thermocouple was also used to measure the temperature of the circulated water in the well of the heater stirrer and water bath. Insulated thermocouples were used to measure the inlet and outlet water temperatures to check for temperature gradients across opposite corners of the radiator (Fig. 3.1, top). The polystyrene base ensured that radiative cooling from the radiator surface was uniform across the radiator and mostly from the topside. For non-controlled cooling-cycle infrared calibrations, these procedures also lessened the rate of temperature reduction after the heater circuit was switched off. For the larger radiator, a water pump and a water-well stirrer was used to ensure rapid water flow and to minimise radiator surface temperature gradients. It was important to ensure that the radiator contained as little air as possible – air instead of water increased the variability of the radiator surface temperatures slightly.

All openings into the radiator were sealed with silicon sealant, apart from an inlet and an outlet opening, to prevent water leaks (Fig. 3.1, top). The radiator was placed horizontally on a trolley, for ease of transport, and positioned in the centre of the laboratory. The inlet opening of the radiator was connected using plastic hoses to the outlet of the water-well with the radiator outlet connected to the inlet of a heater stirrer. Short and thermally-insulated water hoses were used to ensure rapid water circulation between the water-well and the radiator, to minimise temperature gradients across the radiator surface and to reduce the rate of heating (or cooling) of the radiator surface. A 30-W water pump (Fig. 3.1, top) with a rated and maximum capacity of 16 and 30 l min^{-1} respectively was used to circulate the water into the radiator from the water bath (Haake Gebruder, Berlin, Germany, type FE number 67236 distributed by PolyScience Corp., Evanston, Illinois, USA) and back to the water bath.

For the smaller radiator, a Campbell Scientific 21X datalogger (Logan, Utah, USA) was used to perform slow differential radiator temperature measurements, and in subsequent calibrations using the larger radiator, a Campbell CR3000 datalogger was used. The datalogger earth was always electrically grounded to the radiator and in turn firmly connected to earth.

The radiator surface temperature measurements were cross-checked, showing excellent agreement, against that measured using two Fenwal thermistors (model UUA32J4 with 0.2 ^{o}C interchangeability and equivalent to 192-222LET A01, Honeywell, Golden Valley, Minnesota, USA) embedded so as to be flush with the surface of the radiator: slope = 1.0025 $\pm$ 0.0002, adjusted coefficient of determination r^2 = 0.9999, root mean square error (*RMSE*) = 0.12 ^{o}C for surface temperatures between 1.2 and 51.7 ^{o}C. A prior calibration of the thermocouple temperature measurements against a mercury-in-glass thermometer registering the temperature of stirred water in the water bath was also used as an independent check of the accuracy of the thermocouple temperatures.

Changes in radiator infrared irradiance were non-steady and by design fairly similar for heating and cooling cycles but more importantly slow – less than 1.6 W m^{-2} min^{-1} and averaging 1.0 W m^{-2} min^{-1} for both radiators used for radiator surface temperatures less than 55 ^{o}C. These slow rates ensured that the time response of the net radiometer voltage did not result in a significant non-correspondence between net radiometer voltage and radiator surface temperature. For surface temperatures greater than 55 ^{o}C, the rate of irradiance change for non-controlled cooling exceeded 5 and 2 W m^{-2} min^{-1} for the smaller and larger radiators respectively. These rates were considered too large for accurate calibrations and therefore routinely the datalogger-controlled heating was limited to 55 ^{o}C. Other checks were performed to ensure that the influence of instrument time response was small. Fritschen and Gay (1979, p41) present an analysis for dealing with instrument time response, for which in this case the net radiometer voltage asymptotically approaches the voltage corresponding to the actual R_{net}. A ramp change in the net infrared irradiance was assumed and the net radiometer voltages were corrected for their instrument time response – around 30 s for domed instruments and less than 20 s for domeless instruments. The influence of the polyethylene-domed net radiometer time response was investigated further by collecting data for the same net radiometer infrared calibration run in two ways, one for which heating was applied at a rate of 0.5 ^{o}C every 2 min and the second for a heating rate of 1 ^{o}C every 1 min.

3.4.1.2 Shortwave calibration of net radiometers

Laboratory shortwave calibrations were performed using six 50-W AC halogen lamps directed at the centre of the radiator, more than 600 mm away, with a lamp attached to a matt-black wooden dowel rod at each corner of the radiator and a lamp at the middle positions of the radiator widths. The intensity of all lamps was altered using a 0 to 10-V noise-suppressed DC-controlled dimmer (model K8064, Velleman Components NV, Gavere, Belgium) that was controlled by a 0 to 5-VDC signal from a datalogger. Field shortwave calibrations of six polyethylene-domed net radiometers were performed following the shading method of Idso (1971) for which voltage measurements from a standard pyranometer and each net radiometer before and after shading were obtained.

3.4.2 Net radiometer calibration procedures

A typical cycle of laboratory infrared calibration measurements was as follows: ice was added to the stirred water in the water–well and after melting, a single net radiometer was placed at the centre of the radiator at a typical distance of 65 mm from the surface of the radiator. After an equilibrium period of 5 min, measurements commenced and the temperature of the heater stirrer was slowly increased under datalogger control at a rate of 0.5 ^{o}C every 2 min from close to 0 to about 55 ^{o}C taking 2 h for the smaller radiator and 3.5 h for the larger radiator. Placement of the radiometer closer than 45 mm from the radiator caused too great a heating of the radiometer dome, or cooling when ice was used, and slightly more variable voltage measurements. Since the temperature of the net radiometer housing may affect the infrared values, particularly for large four-component instruments, care needs to be exercised to ensure that housing temperature changes do not affect calibrations. Before reaching 55 ^{o}C, the water circulation was continued and the heater circuit of the heater stirrer controlled to allow pulsed heating so as to maintain cooling at the same rate of 0.5 ^{o}C every 2 min. This rate was maintained unless the natural cooling rate was less than 0.5 ^{o}C every 2 min in which case the pulsed heating was not applied. A datalogger was programmed to perform slow (16.67-ms integration time) differential temperature measurements of the radiator thermocouples and differential net radiometer voltage measurements. Measurements were performed every 1 s with the average and the standard deviation of these measurements over a one-minute period being recorded for the early calibrations and every 15 s for later calibrations. Measurements were continued after the end of the heating cycle for an additional period of about 2 h for the smaller radiator and an additional 4 h for the larger radiator at which time the water temperature had decreased to close to the ambient temperature of the laboratory.

The surface temperature of the radiator (T_{rad}) was calculated as the average of the temperatures measured using the embedded thermocouples. No correction was applied to these temperature measurements. For each net radiometer, a plot of $L_{u\,rad}$ on the y-axis *vs* the measured net radiometer voltage on the x-axis, the former calculated from $F\sigma T_{rad}^4$ (Eq. (3.8)), was performed and the slope magnitude calculated to yield the instrument calibration factor for the infrared (using the known value for F and assuming that $\varepsilon_{rad} \approx 1$ due to the cavity-like structure of the radiator). In cases where the downward infrared irradiance was estimated using temperature measurements from a set of averaging thermocouples affixed to the roof of the laboratory (at four positions), or from infrared thermometer measurements or from $L_{d\,surr}$ measurements using the CNR 1 four-component net radiometer, the slope magnitude of a plot of $F\sigma T_{rad}^4 - F\,L_{d\,surr}$ *vs* V_{net} (see Eq. (3.10)) yielded the infrared calibration factor for the net radiometer.

In some cases, for test purposes, the infrared calibration procedure was repeated for the same net radiometer some days later or repeated with the net radiometer inverted, another net radiometer chosen or another laboratory used for the infrared calibration. For some of the calibrations, laboratory lights were left on or half on and in other calibrations, the lights were switched off. In some cases, windows were darkened to reduce the possible influence of outside shortwave irradiance on measurements. In all cases, the air-conditioning setting in the laboratories was not altered but any possible influence was monitored using roof-attached thermocouples. For selected net radiometers, the calibration was repeated many times but most radiometers were calibrated at least twice.

For some of the net radiometer infrared calibrations, a number of additional experiments were conducted: (a) fine-wire type-T thermocouples were attached to the inside of the domes of the polyethylene-domed net radiometers during calibration runs. Measurements included the radiator surface temperature, laboratory roof temperature, upper and lower dome temperatures and air temperature as well as the net radiometer voltage; (b) the possible influence of instrument time response was investigated. In addition to calibrations for a heating rate of 0.5 ^{o}C every 2 min, some heating cycle calibrations were repeated using a heating rate of 1 ^{o}C every 1 min with the 1-s net radiometer voltage and radiator and laboratory roof temperatures averaged 0, 15, 30 and 45 s after the applied heating. Normal regressions were applied using Eq. (3.9) to obtain the infrared calibration factor for each time period after heating; (c) to investigate the vertical (or horizontal) wind speed magnitudes above the radiator for selected heating- and cooling-cycle calibration runs, three heated-needle anemometers (model SNA22 originally from SoilTronics, Burlington, Washington State, USA: 40 mm in length and 0.7 mm in diameter) positioned horizontally and in some cases vertically above the radiator were used. The needle anemometers were individually field-calibrated against the vertical wind speed measured using a three-dimensional sonic anemometer (model SWS-211/3V, Applied Technologies, Boulder, Colorado, USA) – typical regression statistics: slope = 1.030 ± 0.070, r^2 = 0.974, *RMSE* = 0.107 m s^{-1}, n = 727 for wind speed varying between 0.08 and 3.2 m s^{-1}; (d) the sensor-radiator distance d for selected net radiometer infrared calibrations was varied from 45 to 110 mm, particularly for a four-component net radiometer; (e) for selected polyethylene-domed net radiometers, small fans were used to pass air across both the upper and lower domes in an attempt to equalise the dome temperatures with minimal disturbance to the surface temperatures of the radiator. The ventilation system was similar to that used by Fritschen and Fritschen (2007).

For the laboratory shortwave calibrations, domeless, polyethylene-domed, miniature and two-component net radiometers were used. A datalogger-controlled light dimmer was used to alter the shortwave irradiance every 7 min. The 15-s voltage measurements from the standard pyranometer and an adjacent net radiometer were made in the last 2 min of the 7-min period. The instruments were placed at the centre of the radiator. The sensors were always maintained at a vertical distance of 70 mm above the radiator for the shortwave calibrations. During these calibrations, the radiator temperature was maintained at room temperature using circulating water and the laboratory roof, air and radiator temperatures were measured. The near isothermal conditions ensured a net infrared irradiance of near 0 W m^{-2}. Near isothermality was easily achieved by performing measurements within an hour. Measurements made using a pair of pyranometers, one inverted, demonstrated that the shortwave reflection coefficient of the radiator was less than 0.5 % and this radiation balance component was therefore neglected and not measured during the shortwave calibrations.

3.4.3 Calibration procedures for infrared thermometers

The procedures for the laboratory calibration of twenty-one IRTs were similar to the net radiometer infrared calibrations. The IRTs were placed directly above the centre of the radiator at a distance of 0.97 m from the radiator for the 4° field-of-view units and 0.2 to 0.4 m for the others. These distances accommodated for the wider field of view than that specified by the manufacturers, as mentioned by Bugbee et al. (undated). Once the temperature of the radiator had decreased from a high value (65 to 80 °C) to room temperature, water at near 0 °C was used to decrease the radiator surface temperature to below 15 °C. Measurements were collected as the system slowly equilibrated back to room temperature. Unlike the net radiometer calibrations for which only one sensor at a time was calibrated, many IRTs were calibrated simultaneously since for these calibrations, the radiation balance components were not required.

Measurements of R_{net} and T_{rad}, the latter using the IRTs, were slightly more variable when T_{rad} was at or below the dewpoint temperature of the laboratory air. The resultant condensation of water on the radiator surface could not easily be avoided for laboratories without air-conditioning. However, judging from the calibration data, the condensation event did not significantly affect the calibration calculations.

3.4.4 Calibration instruments

Twelve Radiation and Energy Balance Systems (Seattle, Washington, USA) (six Q*6 and six Q*7) polyethylene-domed net radiometers, two thin polyethylene-domed Middleton Instruments (Carter-Scott Design, Brunswick, Victoria, Australia) net radiometers, a Middleton miniature polyethylene-domed net radiometer, four Kipp and Zonen (Delft, The Netherlands) NR LITE domeless net radiometers, a two-component CNR 2 and a four-component CNR 1 net radiometer (Kipp and Zonen) were used for the net radiometer calibration tests. All net radiometers were in a new condition at the time of calibration apart from the Middleton instruments. For the laboratory shortwave calibrations of the net radiometers, a Kipp and Zonen CM 11 pyranometer was used as the standard and measurements confirmed using a CMP 3 pyranometer. An Eppley model 60 standard radiometer (The Eppley Laboratory Inc., Newport, Rhode Island, USA) was used for the field shortwave calibrations of the six domed REBS Q*6 net radiometers. The Q*6 net radiometer instruments were designed to have equal infrared and shortwave responsivity by the addition of white paint on the sensor surface (Vogt et al., 1996). The Q*7 net radiometers were supplied with one calibration factor for positive net irradiance and one for negative.

For the two- and four-component net radiometers, two and four voltages were measured respectively. For the former instrument, the two calibration factors k_s and k_l supplied with the instrument were used for net shortwave and net infrared irradiance respectively to calculate $\hat{R}_{net\,2-comp}$ (Eq. (3.8)). In the case of the four-component net radiometer, the internal temperature of the instrument was also measured (YSI thermistor 44032, Yellow Springs, Ohio, USA) and used for estimating R_{net} according to normal recommendations.

For the calibrations of the IRTs, with emissivity set to 1.0 if applicable, the following IRTs were used: Apogee models IRTS-P and IRR-P (Apogee Instruments, Logan, Utah, USA), Everest Interscience Inc. (Tucson, Arizona, USA) IRT models (4000ALCS, 40004-A, 4004AL and hand-held

110) and Omega model OS36SM-K-80F. All calibrations were performed at least twice. The Everest IRTs had no body temperature sensor. For the Omega IRTs, the sensors were inserted into an aluminium housing and a type-K thermocouple added to measure the sensor body temperature inside the housing.

A possible source of error in the calibration method used for both net radiometers and IRTs is the assumption that the radiator cavity emissivity is equal to 1. Heinisch (1972) showed that a matt-black painted right-regular cylindrical cavity with a depth to aperture ratio greater than 2 has an emissivity greater than 0.9915. Bedford (1972) showed that the critical ratio was 10 for spherical cavities. Based on this, the assumption of an emissivity of near unity for the two radiators used is a good one. Using a pair of IRTs, one directed at the radiator and another directed at the laboratory roof, using a calibrated IRT, it was possible to estimate ε_{rad} for the radiator (Eq. (3.12)). The upward facing IRT was used to measure T_{surr} and this estimate was compared with the temperature estimate of $[L_{d\,surr} / (F\,\sigma)]^{1/4}$ calculated from the y-intercept using Eq. (3.9) from polyethylene-domed net radiometer calibration data.

3.5 Results and discussion

3.5.1 Thermal conditions, instrument time response and convective radiator conditions

The non-steady infrared laboratory calibration method for a net radiometer is based on the premise that temperature gradients across the radiator are small but at the same time gradual increments (or decrements) in T_{rad} with time are imposed and that convective influences on net irradiance measurements are small. A measure of the thermal gradients across the radiator was obtained from the standard deviation of all measured radiator surface temperatures. Another measure of the gradients was the temperature difference between the outlet and inlet water temperatures over a distance of about 0.95 m for the larger radiator. For a typical infrared calibration, the standard deviation of all radiator temperatures for each time period for an infrared calibration was less than 0.08 ^{o}C and the 15-s averaged outlet and inlet temperature difference was less than 0.06 ^{o}C in magnitude at any time with the largest magnitude difference occurring at the greatest radiator temperatures (Fig. 3.2). These standard deviations and temperature differences are small, justifying the assumption of constant temperature across the radiator at a given time.

The influence of net radiometer time response was investigated using the correction method of Fritschen and Gay (1979). The correction applied to polyethylene-domed net radiometer voltages due to the instrument 30-s time response, resulted in calibration slopes that were within 0.7 % of the uncorrected slopes when using 15-s averages. For 60-s averages, the difference in corrected and uncorrected slopes was even smaller. To further determine if the instrument time response affected the results, net radiometer calibrations for a heating cycle at a temperature increase rate of 1 ^{o}C every 1 min were performed for a Q*7 polyethylene-domed net radiometer (instrument 2 in Table 3.1 with a manufacturer's negative R_{net} calibration factor of 10.75) using voltage averages 0, 15, 30 and 45 s after a 1 ^{o}C heating. The calculated infrared calibration factors (k_l, W m^{-2} mV^{-1}), based on Eq. (3.9), were 11.52 for all 15-s averages, 11.52 for data 0 s after heating increment, 11.50 for 15 s after heating, 11.49 for 30 s after heating and 11.50 for 45 s after heating. Therefore, for the slow rate of radiator heating used, the 15-s measurement averages were not impaired by the time response of the instrument. The calibration statistics for a Q*7 domed net radiometer for which the voltage

measurements were corrected, and not corrected, for instrument time response are shown in Table 3.1 (instruments 9 and 10). For the worst case differences, there was less than a 0.7 % difference in the calculated infrared calibration factors for when the correction was applied compared to when it was not applied.

The issue of the possible influence of thermally driven vertical convection, causing more variable net radiometer voltages and therefore unreliable infrared calibrations, was investigated. Heated-needle anemometer wind speeds, measured near the centre of the radiator, showed that vertical and horizontal wind speeds were less than 0.62 m s^{-1} at all times. Vertical wind speeds gradually increased from around 0.3 to 0.62 m s^{-1} with increase in T_{rad} from 0 to 55 ^{o}C followed by a slow decrease to around 0.3 m s^{-1} as the radiator was allowed to cool to room temperature (Fig. 3.2). The wind speed correction for the maximum wind speed of 0.62 m s^{-1} using the correction function recommended by the manufacturer of the polyethylene-domed units is 0.9986 and 1.007 for the domeless units and therefore based on these corrections the influence of thermally generated wind speed does not affect the infrared calibration results significantly.

During an infrared calibration of a polyethylene-domed net radiometer (Fig. 3.3a), the increase in the lower dome temperature with time mirrored the increase in vertical wind speed, with the lower dome increasing in temperature by about 18 ^{o}C with an increase in air temperature of about 10 ^{o}C (Fig. 3.3b). Also shown in Figs. 3.3a and b by the vertical arrow for the net radiometer voltage V_{net} = 0 mV, are the nearly equal radiator surface, laboratory roof, air, lower and upper dome temperatures at 15 ^{o}C although there is a slight time lag in the dome temperatures. This equality is good affirmation of the correct functioning of the infrared calibration system.

3.5.2 Infrared calibration of net radiometers

For a cooling-cycle infrared calibration, the change in T_{rad} and also the magnitude of $L_{u\,rad}$ calculated from $L_{u\,rad} = F\sigma T_{rad}^4$ and the corresponding standard deviation in radiator temperature, as a function of net radiometer voltage for a Q*7 polyethylene-domed net radiometer, is shown (Fig. 3.4). The greatest radiator temperature standard deviations generally occurred at low and at high radiator temperatures.

Only data points for which T_{rad} was less than 55 ^{o}C were included in the regression analysis for the $F\sigma T_{rad}^4$ *vs* V_{net} plots. Strictly, these calibration plots should have $F\sigma T_{rad}^4$ as the independent variable on the x-axis. However, given the high r^2, it is immaterial except that as shown in Fig. 3.4, the *RMSE* of the irradiance is conveniently shown, the slope is the calibration factor (W m^{-2} mV^{-1}) and the equation intercept corresponds to $L_{d\,surr}$.

Care needs to be exercised to ensure that the downward infrared irradiance $L_{d\,surr}$ is not influenced significantly by the elevated temperature of the radiator or the lowered temperatures when ice or cold water is used, particularly in small laboratories. If the temperature of the surrounds T_{surr} is elevated and then decreases as the radiator cools, there may be a non-linear relationship between $F\sigma T_{rad}^4$ and net radiometer voltage V_{net}. In such cases Eq. (3.10), which requires measurement of T_{surr}, could be applied as opposed to Eq. (3.9). Care also needs to be exercised to ensure that changes in shortwave irradiance do not significantly influence the infrared calibrations. Most of the calibrations were in darkened laboratories or performed overnight.

The infrared calibration data for two domeless net radiometers are shown (Fig. 3.5), the calibrations performed on different days. The confidence belts of Fig. 3.5 represent those for a single predicted value at the 99 % level of confidence. Dashed lines, offset by 5 W m^{-2} for greater clarity, correspond to slope magnitudes equal to the calibration factors supplied with the instrument (shown in square brackets after the calibration regression equations). There is a 7.0 % difference in the slopes for these two net radiometers. The difference in the intercepts would be due to the different laboratory wall and ceiling temperatures for the two days. The one calibration was performed in a laboratory with the lights switched off. Extraneous light from outside the building was visible. In the other calibration, the laboratory lights were switched off and the room was completely darkened. The shortwave irradiance measured using a thermopile pyranometer was less than 1 W m^{-2}. For these two domeless net radiometer infrared calibrations, the calibration slope magnitudes agreed quite well with the manufacturers' shortwave calibration factor for calibrations performed some two to three months previously under windless and clear-sky outdoor conditions (Table 3.1, second-last column). The intercepts were different (Fig. 3.5 and Table 3.1, 7th column marked intercept), and consistent with $L_{d\,surr}$ calculated from the laboratory roof temperatures. For a net radiometer placed above the radiator for which $L_{u\,rad}$ is calculated using Eq. (3.4), it is therefore possible to separate the upward and downward infrared irradiance components of R_{net} by equating the y-intercept of Fig. 3.5 to $L_{d\,surr}$ (Eq. (3.6)).

In early calibration tests using Q*6 polyethylene-domed instruments in which T_{rad} was allowed to exceed 80 °C, a plot of $F\sigma T_{rad}^4$ *vs* V_{net} for the first 10 °C yielded a greater $L_{d\,surr}$ intercept than the intercept value for the next 10 °C. These differing intercept values were due to increased temperatures of the environs due to the heated radiator causing increased $L_{d\,surr}$ values, possibly due to the temperature difference between the upper and lower domes particularly during a heating calibration cycle and possibly also due to net radiometer time constant limitations. However, the measured vertical convection currents were shown to be less than 0.62 m s^{-1} for T_{rad} less than 55 °C, and therefore of minor influence and the time constant limitations have been shown to be minor. The data of Fig. 3.3b show the upper and lower dome temperatures. The dome temperatures were measured using fine-wire thermocouples attached to the dome sides nearest the sensor. From these data, the infrared irradiance from dome to sensor may be calculated. For the heating cycle calibrations, assuming a dome emissivity of 0.06 (Fritschen and Fristschen, 2007), the net flux difference from dome to sensor ranged from -1.8 to 3.5 W m^{-2} for radiator temperatures increasing from 0 to 55 °C – the upper dome increasing from 18 to 26 °C and the lower dome increasing from 12 to 35 °C. For cooling-cycle calibrations, the difference between the dome to sensor fluxes for upper and lower domes decreased from 3.5 W m^{-2} at 55 °C to 1.8 W m^{-2} at room temperature – the upper dome decreasing from 26 to 19 °C and the lower dome decreasing from 35 to 23 °C. For most of the time, the infrared flux difference was almost constant at 1.8 W m^{-2} since both upper and lower domes tended to cool at similar rates. To also check that their influence was small, we repeated some of the domed calibrations with and without ventilation. For the ventilated calibrations, small fans were used to pass air across both the upper and lower domes with minimal disturbance to the surface temperatures of the radiator. The calibration slopes associated with dome ventilation (Table 3.1, net radiometer 2, runs 8, 9, 12, 13) were significantly greater in magnitude than the negative R_{net} calibration factor supplied by the manufacturer and greater than those for no ventilation but with the ventilator in place (runs 10, 11, 14 to 17) and greater than those for when the ventilator was not used (runs 1 to 7 in laboratory 3 and runs 18, 19 in laboratory 4). It would appear that the placement of a ventilator alongside the net

radiometer results in a change in the calibration slope presumably due to its influence on the infrared components of the radiation balance and was therefore not used routinely.

The infrared calibrations and recalibrations of the polyethylene-domed net radiometers were repeatable (e.g. net radiometer 2 of Table 3.1, Fig. 3.4) and reasonably consistent. Side-by-side calibration for a pair of net radiometers at a time gave slightly more variable calibration data (data not shown) and is therefore not recommended.

The domeless (instruments 4 to 7) and miniature polyethylene-domed (instrument 3) net radiometer infrared calibration data (Figs. 6a and b), for heating and heating/cooling cycles respectively, were more variable compared to their polyethylene-domed counterparts (average *RMSE* = 2.59 W m^{-2} and 2.27 W m^{-2} respectively for all calibration runs) compared to 0.50 W m^{-2} (Table 3.1) for the polyethylene-domed net radiometer 2 of Fig. 3.4 (and an average of 0.99 W m^{-2} for calibration runs shown in Table 3.1 but excluding the ventilation runs). Presumably the polyethylene-domed net radiometers are less sensitive to convective exchanges between the surface of the net radiometer and the surrounding atmosphere, due to greater time constants and the protection provided by the domes, than the domeless and miniature polyethylene-domed net radiometers. In the case of Fig. 3.6b, for the miniature polyethylene-domed net radiometer, Eq. (3.10) which accounts for the influence of any changes in the surrounding temperature on the measurements, was applied. As expected, compared to the application of Eq. (3.9), the slope magnitude was similar – within 0.9 % of that obtained by applying Eq. (3.10) (calibration data not shown). This confirms the assumption that the surrounding infrared irradiance contribution to the radiation balance is reasonably constant during the calibration. The calibration for a domeless net radiometer inverted yielded a very similar calibration slope magnitude (Table 3.1, instrument 4) with slopes within 0.7 % of the manufacturer's calibration factor obtained six months previously using a shortwave calibration for the upper surface.

The most consistent infrared calibrations for the domed net radiometers were obtained using an air-conditioned laboratory for which the lights remained on (Table 3.1, instrument 10). For these calibrations, the *RMSE* was less than 1 W m^{-2} and the difference in calibration factors for day- and night-time calibrations were less than 1 %. For these calibrations, the roof temperature and laboratory air temperatures were measured, the former using an infrared thermometer. The roof temperature was (21.92 ± 0.06) ^{o}C. Both the upper and lower sensors of this net radiometer were marked due to use in the field when the domes were cracked. Both upper and lower sensors were brushed repeatedly with distilled water, very dilute liquid soap and again repeated brushing with distilled water. There were still slight visual marks on both upper and lower sensors. The infrared calibration factor for instrument 10 prior to field use was similar to that of the manufacturer (average of 11.52 W m^{-2} mV^{-1} compared to 11.8 W m^{-2} mV^{-1} respectively, Table 3.1, runs 1 to 3) compared to 12.75 W m^{-2} mV^{-1} after field use (Table 3.1, run 4).

The two-component net radiometer infrared calibrations were very consistent apart from runs 1, 2 and 3 (Table 3.1, instrument 8) with an average *RMSE* of 0.88 W m^{-2}, similar to the average of 0.92 W m^{-2} for the polyethylene-domed net radiometers even when inverted. For the two-component calibrations, the instrument net irradiance was regressed against $L_{u\,rad} - F\,L_{d\,surr}$ (Eq. (3.10)).

A four-component net radiometer (instrument 9) was used to check the assumptions of Eq. (3.10) and the sensitivity of the calculated sensor infrared calibration factor to the sensor-radiator distance *d* (Eq. (3.2)). As was the case with the two-component net radiometer, the instrument net irradiance was regressed against $L_{u\,rad} - F\,L_{d\,surr}$. Varying the sensor-radiator distance from 45 mm to 110 mm resulted in a very small change in calibration slope with no obvious relationship between *d* and the calibration slope if the calibration for *d* = 110 mm is excluded. However, the manufacturers estimate of R_{net} underestimates the measured R_{net} (average slope of 0.96). For a distance of 110 mm, the slope of the regression relationship is 0.993 with a *RMSE* lower than the average for the other distances. Possibly therefore, for larger instruments, the distance away from the radiator should be increased but this decreases *F*. For these calibrations, the $L_{d\,surr}$ values were within 0.2 % between the beginning and end of the measurements (data not shown). The measured downward infrared irradiance was within 0.7 % of that estimated using the roof-affixed thermocouples. The $\rho_{s\,rad}\,I_s$ values (Eq. (3.6)) were negative at times, typical of thermopile sensors exposed to low shortwave irradiance (Reda et al., 2005) but this did not affect the calibration results since both the $\rho_{s\,rad}\,I_s$ and I_s values were reasonably constant for the calibration period.

The repeatability of the infrared calibration measurements was also demonstrated by the twelve repeat calibrations of the four-component net radiometer, once in the inverted position, showing a relative variation in the slopes from the mean between -2.2 and 3.3 % (Table 3.1). The two- and four-component net radiometers generally exhibited the smallest *RMSE* values (Table 3.1). Generally, calibration data collected by cooling as opposed to radiator heating exhibited smaller *RMSE* values particularly calibration under datalogger control with a slow incremental change in infrared irradiance of about 1 W m^{-2} min^{-1}.

3.5.3 Shortwave calibration of net radiometers

Calibrations for domeless net radiometers demonstrated differences between shortwave and infrared calibration factors k_s and k_l with an average ratio of $k_s / k_l = 0.94$ for domeless instruments 5 and 6 (Table 3.1). For instrument 5, the k_s values were consistently less than that of the manufacturer's value by about 7 % compared to 1 % for instrument 6.

For the Q*6 net radiometers, for which the manufacturer matched the positive and negative R_{net} calibration factors (Vogt et al., 1996), the infrared calibration slopes agreed remarkably well with the manufacturer's calibration performed some two to three months previously in a chamber using a quartz-iodine lamp and shortwave irradiance measurements performed outdoors under windless and cloudless conditions using a standard shortwave pyranometer (Table 3.1, instrument 1). Compared to the domeless net radiometers, there is a greater inequality between k_s and k_l for the Q*7 polyethylene-domed instrument (Table 3.1, domed-radiometer 2 calibration runs 20 (S) to 27 (S) with and without correction for infrared irradiance from the surrounds) with $k_s / k_l = 0.76$. Similarly, there is inequality between k_s and k_l for the miniature polyethylene-domed net radiometer (instrument 3) for which $k_s / k_l = 0.87$. A ratio of $k_s / k_l < 1$ for polyethylene-domed net radiometers is consistent with the findings of Cook and Holdridge (2006) that transmittance of polyethylene is weaker for wavelengths of strongest infrared transmission by water vapour.

For the two-component net radiometer, the value of k_s was consistent the manufacturer's value (Table 3.1, instrument 8) - percentage difference of 2.3 %. Unlike the shortwave calibration data of

Table 3.1 for which a range of shortwave irradiance values was used in obtaining the calibration factor, the manufacturer's value was obtained for a shortwave irradiance of about 500 W m^{-2} two to three months previously under a metal-halide lamp, 1.1 m vertically above the sensor.

3.5.4 Calibration of infrared thermometers

A typical calibration relationship for an IRT using a cooling cycle is shown (Fig. 3.7). The non-linear calibration relationship for the various IRTs showed a marked variation between different sensors (Table 3.2). In the case of IRT 1 (Table 3.2), the deviation between the actual radiator surface temperature measured using the embedded thermocouples (T_{rad}, °C in this case) of the radiator and the IRT estimate of the same (T_{IRT}, °C) decreased to -1.5 °C at T_{rad} = 60 °C compared to about -0.2 °C for IRT 2 (run 2). All but two of the IRTs, including the Apogee and Omega IRTs, exhibited a plateau as shown in the $T_{rad} - T_{IRT}$ *vs* T_{rad} curves (Fig. 3.7). In one case, for IRT 2, second calibration, the shape of $T_{rad} - T_{IRT}$ *vs* T_{rad} was parabolic with a maximum of 0.6 °C at 30 to 40 °C and a minimum of -0.4 °C at 70 °C. The Everest IRTs tended to underestimate T_{rad}, for temperatures less than 40 °C, by differing amounts.

The hand-held IRT model 110 had an almost linear $T_{rad} - T_{IRT}$ *vs* T_{rad} relationship (Fig. 3.8). For this IRT, $T_{rad} - T_{IRT}$ was 0 °C at 20 °C increasing almost linearly to 6 °C at 70 °C. The hand-held IRT (model 110) was calibrated twice for temperatures ranging between 15 and 70 °C: once with ten calibration points (Table 3.2, run 1) and once with nearly 1000 data points (run 2). There was no significant difference in the slope or intercept of the calibration relationship for the two calibrations (Table 3.2). This hand-held IRT had the greatest temperature bias for all IRTs tested, underestimating radiator temperature at 50 °C by 3 °C and overestimating by 1 °C at 15 °C (Fig. 3.8).

For the IRTs without a body temperature sensor, fitting a cubic polynomial to the residual $T_{rad} - T_{IRT}$ as a function of T_{IRT} (instead of T_{rad} as shown in Figs. 3.7 and 3.8) allows an estimate of the radiator surface temperature $\hat{T}_{rad}$ to be calculated:

$$\hat{T}_{rad} = T_{IRT} + (a_0 + a_1 T_{IRT} + a_2 T_{IRT}^2 + a_3 T_{IRT}^3) \,. \tag{3.14}$$

The residual plot after this procedure is shown in Fig. 3.9. The Everest IRTs (Figs. 3.9a and b) had no body temperature sensor (Eq. (3.14) applied) and for the other sensors (c, d, e), a body temperature correction was applied (Eq. (3.13)). Using this procedure, for the hand-held IRT, the estimate of radiator temperature for this procedure applied three times to further minimise the residuals is within 0.2 °C of actual for temperatures between 5 and 55 °C without the need for any correction for IRT body temperature (Table 3.3).

The analysis of the calibration data for IRTs with a body temperature sensor was different (Figs. 3.9c to e). From collected data of the actual target temperature, obtained using the average of all thermocouples embedded in the surface of the radiator ($T_{CTT} = T_{rad}$), T_{IRT} (K), and the infrared sensor body temperature (T_{SB}, K), the coefficients c_1 to c_5 of Eq. (3.13) were determined using linear regression. From this regression, the residual $T_{rad} - T_{IRT}$ was plotted as a function of T_{IRT} (°C) (Figs. 3.9c to e). For most of the IRTs used, the residuals were within 0.15 °C for temperatures between 4 and 60 °C. The approach used can be applied to different makes of IRTs, allows for the inclusion of the sensor body temperature T_{SB} and improves on the method used by Kalma and Alksnis (1988).

The evaporation of condensed water, caused by the radiator temperatures being less than the atmospheric dewpoint, resulted in a temporary decrease in $T_{rad} - T_{IRT}$ (Figs. 3.9c to e) – data were excluded for this event.

In view of the differences between different model IRTs, the non-linear nature of the calibration relationship and the differences between IRTs of the same model, it is important to calibrate such units prior to and after use and especially so for surface temperatures exceeding 35 ^{o}C.

3.5.5 Radiator emissivity

Although near unity, there is a non-linear variation in the estimated ε_{rad} *vs* T_{rad} relationship (Fig. 3.7) and the estimate is affected by the event corresponding to the addition of cold water. This calculation for ε_{rad} assumes no error in the IRT estimate of the temperature of the surroundings at all temperatures. The non-linear shape would imply that the shape of the upward infrared irradiance *vs* net radiometer voltage calibration relationships (Eq. (3.9) and (3.10)) would also be non-linear. No such gradual curvature in the net radiometer calibration relationship was observed for the temperature range 55 to near 0 ^{o}C (Figs. 3.4 to 3.6).

3.6 Summary and conclusions

Energy balance closure investigations and estimates of evaporation as a residual term of the energy balance are critically dependent on R_{net}. In spite of the importance of R_{net}, there is still no widely accepted best field-measurement method, associated calibration method and data treatment. Some workers have suggested that the extent of energy balance closure between FLUXNET sites is probably the result in bias errors in R_{net} with biases of up to 15 % noted. Laboratory procedures for the non-steady infrared calibration of net radiometers using a water-heated or cooled radiator using circulated water and calibrated surface-embedded thermocouples and a method for shortwave calibration of net radiometers are presented and tested. Calibration for various types of net radiometers included polyethylene-domed, miniature polyethylene-domed, domeless, two-component and four-component net radiometers. Calibration factors obtained for the polyethylene-domed net radiometers were repeatable and reasonably consistent with the manufacturers' calibration factor. Calibration tests included measurements of upper and lower dome, air, radiator surface and laboratory roof temperatures, net radiometer voltage(s) as well as the thermally driven vertical and horizontal wind speed above the radiator. Routine calibrations included measurement of radiator and laboratory roof temperatures and net radiometer voltage(s). The calibration method is reasonably quick, convenient, datalogger-controlled and relatively inexpensive in that apart from a datalogger, a heater stirrer and an inexpensive radiator, no additional equipment is required. The most consistent infrared calibrations for the domed net radiometers were obtained using an air-conditioned laboratory for which the laboratory roof temperature was constant to within 0.06 ^{o}C. The shortwave calibrations showed consistent calibration factors for the different runs that were in reasonable agreement with the manufacturer values.

The same radiator may also be used for the calibration of IRTs. A statistical procedure minimised for a wide range in temperature, the temperature residual between the radiator surface temperature and the IRT estimate of the radiator surface temperature. The residuals were within

0.15 ^{o}C for all makes and models of IRT sensors used apart from a hand-held IRT which was within 0.2 ^{o}C.

The radiator method for calibrating net radiometers for infrared and shortwave, and IRTs, is relatively simple to set up and operate and requires no specialised equipment apart from the data collection equipment. Accurate and reproducible calibrations are achievable.

3.7 Acknowledgements

Funding from the Water Research Commission (South Africa) through projects K349 and K1335, University of KwaZulu-Natal, the South African National Research Foundation and the United States Council for the International Exchange of Scholars for a Fulbright grant is gratefully acknowledged. Dr Gaylon S. Campbell (Decagon, Pullman, Washington, USA) contributed to some of the early impetus of this work. Mr Guy M. Dewar of the Electronics Centre of the University of KwaZulu-Natal ably assisted with the electronics for heater stirrer and lighting control of the large radiator and Mr Roelie Hendriks of the Mechanical Instruments Workshops assisted with the water bath and pump. The manuscript benefitted from comments from the anonymous reviewers and the Associate Editor of Agricultural and Forest Meteorology.

3.8 References

Amiro, B.D., Thurtell, G.W., Gillespie, T.J., 1983. A small infra red thermometer for measuring leaf temperature in leaf chambers. J. Exp. Bot. 34, 1569–1576.

Baker, J.M., 2003. Recalcitrant problems in environmental instrumentation. Agron. J. 95, 1404–1407.

Baker, J.M., Norman, J.M., Kano, A., 2001. A new approach to infra red thermometry. Agric. Forest Meteorol. 108, 281–292.

Barber, R., Brown, M.E., 1978. Calibration methods and standards for infra red thermometers. Instrument Soc. Am. Trans. 17, 63–69.

Bedford, R.E., 1972. Effective emissivities of blackbodies - a review. In: H.H. Plumb (Ed). Temperature - Its Measurement and Control in Science and Industry, vol. 4, no.1, Instrum. Soc. Am., Pittsburg, Pa, USA, pp. 425–434.

Blonquist, J.M., Tanner, B.D., Bugbee, B., 2009. Evaluation of measurement accuracy and comparison of two new and three traditional net radiometers. Agric. Forest Meteorol. 149, 1709–1721.

Brotzge, J.A., Crawford, K.C., 2003. Examination of the surface energy budget: A comparison of eddy correlation and Bowen ratio measurement systems. Forest Hydrometeorol. 4, 160–178.

Brotzge, J.A., Duchon, C.E., 2000. A field comparison among a domeless net radiometer, two 4-component net radiometers, and a domed net radiometer. J. Atmos. Ocean. Technol. 17, 1569–1582.

Bugbee, B., Droter, M., Monje, O., Tanner, B., undated. Evaluation and modification of commercial infra-red tranducers for leaf temperature measurement, 8 pp. http://www.apogee-inst.com/irt_manu.htm (accessed 30.03.10).

Campbell, G.S., Diak, G.R., 2005. Net and thermal radiation estimation and measurement. In: Hatfield, J.L., Baker, J.M. (Eds), Micrometeorology in Agricultural Systems by ASA Monogr. 47. ASA, CSSA and SSSA, Madison, Wisconsin, USA, pp. 59–92.

Campbell, G.S., Norman, J.M., 1990. Estimation of plant water status from canopy temperature: an analysis of the inverse problem. P 255–271. In Applications of Remote Sensing in Agriculture by M.D. Steven and J.A. Clark, ed. Butterworths, London.

Castellví, F., 2004. Combining surface renewal analysis and similarity theory: a new approach for estimating sensible heat flux. Water Resour. Res. 40, W05201, doi:10.1029/2003WR002677.

Cobos, D.R., Baker, J.M., 2003. Evaluation and modification of a domeless net radiometer. Agron. J. 95, 177–183.

Cook, D.R., Holdridge, D.J., 2006. EBBR-SIRS net radiation difference: an evaluation. In: Proceedings of the Sixteenth ARM Science Team Meeting, Albuquerque, New Mexico, USA, March 27 to 31, p. 10.

Duchon, C.E., Wilk, G.E., 1994. Field comparisons of direct and component measurements of net radiation under clear skies. J. Appl. Meteorol. 33, 245–251.

Field, R.T., Fritschen, L.J., Kanemasu, E.T., Smith, E.A., Stewart, J.B., Verma, S.B., Kustas, W.P., 1992. Calibration, comparison, and correction of net radiation instruments used during FIFE. J. Geophys. Res. 97 (D17), 18681–18695.

Fritschen, L.J., Fritschen, C.L., 2007. Calibration of shielded net radiometers. Agron. J. 99, 297–303.

Fritschen, L.J., Gay, L.W., 1979. Environmental Instrumentation. Springer-Verlag, London.

Halldin, S., Lindroth, A., 1992. Errors in net radiometry: comparison and evaluation of six radiometer designs. J. Atmos. Ocean. Technol. 9, 762–783.

Ham, J.M., 1990. Soil water evaporation and transpiration from a row crop at partial cover. Ph. D. Dissertation, Texas A & M University, College Station, USA. 109 pp.

Ham, J.M., Heilman, J.L., 2003. Experimental test of density and energy-balance corrections on carbon dioxide flux as measured using open-path eddy covariance. Agron. J. 95, 1393–1403.

Heinisch, R.P., 1972. The emittance of blackbody cavities. In: H.H. Plumb (Ed). Temperature - Its Measurement and Control in Science and Industry, vol. 4, no. 1, Proc. Instrum. Soc. Am., Pittsburgh, Pa, USA, pp. 435–447.

Huband, N.D.S., Monteith, J.L., 1986. Radiative surface temperature and energy balance of a wheat canopy. I. Comparison of radiative and aerodynamic canopy temperature. Boundary-Layer Meteorol. 36, 1–17.

Idso, S.B., 1971. A simple technique for the calibration of long-wave radiation probes. Agric. Meteorol. 8, 235–243.

Idso, S.B., 1974. The calibration and use of net radiometers. Adv. Agron. 26, 261–275.

Kalma, J.D., Alksnis, H., 1988. Calibration of small infra-red surface temperature transducers. Agric. Forest Meteorol. 43, 93–98.

Kanemasu, E.T., Asrar, G., Nie, D., Watts, D., Fritschen, L., Gay, L., Weaver, H., Stannard, D., Tanner, B., Tanner, M., Greene J., 1987. Inter- and intra-sensor comparisons among Bowen ratio and eddy correlation instruments. In: Proceedings of the International Symposium on Flow and Transport in the Natural Environment: Advances and Applications. Poster Abstract, p. 11.

Kohsiek, W., Liebethal, C., Foken, T., Vogt, R., Oncley, S.P., Bernhofer, C., de Bruin, H.A.R., 2007. The Energy Balance Experiment EBEX-2000. Part III. Behaviour and quality of the radiation measurements. Boundary-Layer Meteorol. 123, 55–75.

Kondratyev, K.Ya., 1970. Global atmospheric research programme (GARP) and radiation factors of weather and climate. Radiation Including Satellite Techniques. WMO Tech. Note No. 104. WMO-No. 248.TP.136, Secretariat of the World Meteorological Organization, Geneva. Xxiii-xxxii.

Kustas, W.P., Prueger, J.H., Hipps, L.E., Hatfield, J.L, Meek, D., 1998. Inconsistencies in net radiation estimates from use of several models of instruments in a desert environment. Agric. Forest Meteorol. 90, 257–263.

Lamaud, E., Ogee J., Brunet, Y., Berbigier, P., 2001. Validation of eddy flux measurements above the understorey of a pine forest. Agric. Forest Meteorol. 106, 187–203.

Lee, X., Yu, Q., Sun, X., Liu, J., Min, Q., Liu, Y., Zhang, X., 2004. Micrometeorological fluxes under the influence of regional and local advection: a revisit. Agric. Forest Meteorol. 122, 111–124

Liu, H., Randerson, J.T., Lindfors, J., Massman, W.J., Foken, T., 2006. Consequences of incomplete surface energy balance closure for CO2 fluxes from open-path CO2/H2O infrared gas analysers. Boundary-Layer Meteorol. 120, 65–85.

Mengistu, M.G., Savage, M.J., 2010. Open water evaporation estimation for a small shallow reservoir in winter using surface renewal. J. Hydrol. 380, 27–35.

Nie, D., Kanemasu, E.T., Fritschen, L.J., Weaver, H.L., Smith, E.A., Verma, S.B., Field, R.T., Kustas, W.P., Stewart J.B., 1992. An intercomparison of surface energy flux measurement systems used during FIFE 1987. J. Geophys. Res. 97, 18715–18724.

Ohmura, A., Dutton, E.G., Forgan, B., Fröhlich, C., Gilgen, H., Hegner, H., Heimo, A., König-Langlo, G., McArthur, B., Müller, G., Philipona, R., Pinker, R., Whitlock, C.H., Dehne, K., Wild, M., 1998. Baseline Surface Radiation Network (BSRN/WCRP): New precision radiometry for climate research. Bull. Amer. Meteor. Soc. 79, 2115–2136.

Philipona, R., Fröhlich, C., Dehne, K., DeLuisi, J., Augustine, J., Dutton, E., Nelson, D., Forgan, B., Novotny, P., Hickey, J., Love, S.P., Bender, S., McArthur, B., Ohmura, A., Seymour, J.H., Foot, J.S., Shiobara, M.,Valero, F.P.J., Strawa, A.W., 1998. The Baseline Surface Radiation Network pyrgeometer round-robin calibration experiment. J. Atmos. Ocean. Technol. 15, 687–696.

Pinnock, D.R., Bugbee, B., undated. A simple test to evaluate the calibration stability and accuracy of infrared thermocouple sensors. http://www.apogee-inst.com/pdf_files/IR_onepagerCPL.pdf (accessed 30.03.10), 1 p.

Prueger, J.H., Kustas, W.P., 2005. Aerodynamic methods for estimating turbulent fluxes. P 387–416. In Micrometeorology in Agricultural Systems by J.L. Hatfield and J.M. Baker, ed. ASA Monogr. 47. ASA, CSSA and SSSA, Madison, Wisconsin, USA.

Reda, I., Hickey, J.R., Sto1el, T., Myers, D., 2002. Pyrgeometer calibration at the National Renewable Energy Laboratory (NREL). J. Atmos. Solar-Terres. Phy. 64, 1623–1629.

Reda, I., Hickey, J.R., Long, C., Myers, D., Stoffel, T., Wilcox, S., Michalsky, J.J., Dutton, E.G., Nelson, D., 2005. Using a blackbody to calculate net longwave responsivity of shortwave solar pyranometers to correct for their thermal offset error during outdoor calibration using the component sum method. J. Atmos. Ocean. Technol. 22, 1531–1540.

Sadler, E.J., van Bavel, C.H.M., 1982. A simple method to calibrate an infra red thermometer. Agron. J. 74, 1096–1098.

Savage, M.J., 2009. Estimation of evaporation using a dual-beam surface layer scintillometer and component energy balance measurements. Agric. Forest Meteorol. 149, 501–517.

Savage, M.J., Everson, C.S., Metelerkamp, B.R., 1997. Evaporation measurement above vegetated surfaces using micrometeorological techniques. Water Research Commission Report No. 349/1/97, p248, Pretoria, South Africa, ISBN 1–86845–363–4.

Savage, M.J., Everson, C.S., Metelerkamp, B.R., 2009. Bowen ratio evaporation measurement in emote montane grassland: Data integrity and fluxes. J. Hydrol. 376, 249–260.

Savage, M.J., Everson, C.S., Odhiambo, G.O., Mengistu M.G., Jarmain, C., 2004. Theory and practice of evaporation measurement, with special focus on surface layer scintillometry as an operational tool for the estimation of spatially averaged evaporation. Water Research Commission Report No. 1335/1/04, p204, Pretoria, South Africa, ISBN 1–77005–247–X.

Savage, M.J., Heilman, J.L., 2009. Infrared calibration of net radiometers and infra red thermometers. Agric. For. Meteorol. 149, 1279–1293.

Shuttleworth, W.J., 1991. Insight from large-scale observational studies of land/atmosphere interactions. Surv. Geophy. 12, 3–20.

Sridhar, V., Elliott, R.L., 2002. On the development of a simple downwelling longwave radiation scheme. Agric. Forest Meteorol. 112, 237–243.

Stannard, D.I., Blanford, J.H., Kustas, W.P., Nichols, W.D., Amer, S.A., Schmugge, T.J., Welze, M.A., 1994. Interpretation of surface flux measurements in heterogeneous terrain during the Monsoon '90 experiment. Water Resour. Res. 30, 1227–1239.

Stoffel, T., 2005. ARM pyrgeometer calibrations and field measurements: information regarding the data restriction notice. National Renewable Energy Laboratory Report DOE/SC-ARM/P-05-011, 37 pp. www.arm.gov/publications/programdocs/doe-sc-arm-p-05-011.pdf (accessed 30.03.10).

Tanner, B.D., Greene, J.P., 1989. Measurement of sensible heat and water vapor fluxes using eddy correlation methods. Campbell Scientific, Inc. Logan, Utah. Final report prepared for U.S. Army Proving Grounds. Dugway, Utah, USA.

Twine, T.E., Kustas, W.P., Norman, J.M., Cook, D.R., Houser, P.R., Meyers, T.P., Prueger, J.H., Starks, P.J., 2000. Correcting eddy covariance flux underestimates over a grassland. Agric. Forest Meteorol. 103, 279–300.

Vogt, R., Bernhofer, C., Gay, L.W., Jaeger, L., Parlow, E., 1996. The available energy over a Scots pine plantation: What's up for partitioning? Theor. Appl. Clim. 53, 23–31.

Willmott, C.J., 1981. On the validation of models. Phys. Geogr. 2, 184–194.

Wilson, K., Goldstein, A., Falge, E., Aubinet, M., Baldocchi, D., Berbigier, P., Bernhofer, C., Ceulemans, R., Dolman, H., Field, C., Grelle, A., Ibrom, A., Law, B.E., Kowalski, A., Meyers, T., Moncrieff, J., Monson, R., Oechel, W., Tenhunen, J., Valentini, R., Verma, S., 2002. Energy balance closure at FLUXNET sites. Agric. Forest Meteorol. 113, 223–243.

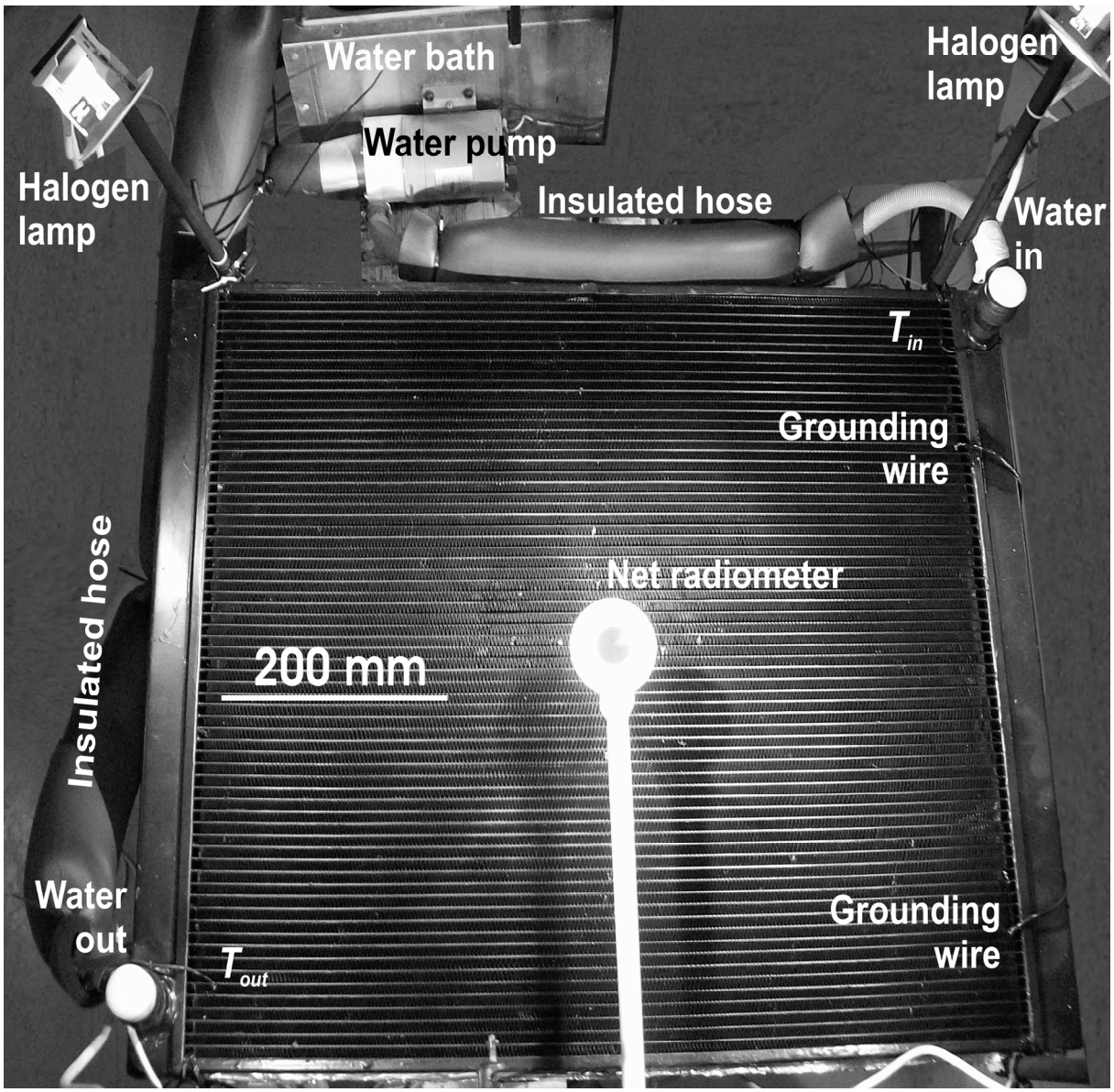
Water bath
Halogen lamp
Water pump
Halogen lamp
Insulated hose
Water in
T_{in}
Grounding wire
Insulated hose
Net radiometer
200 mm
Water out
T_{out}
Grounding wire

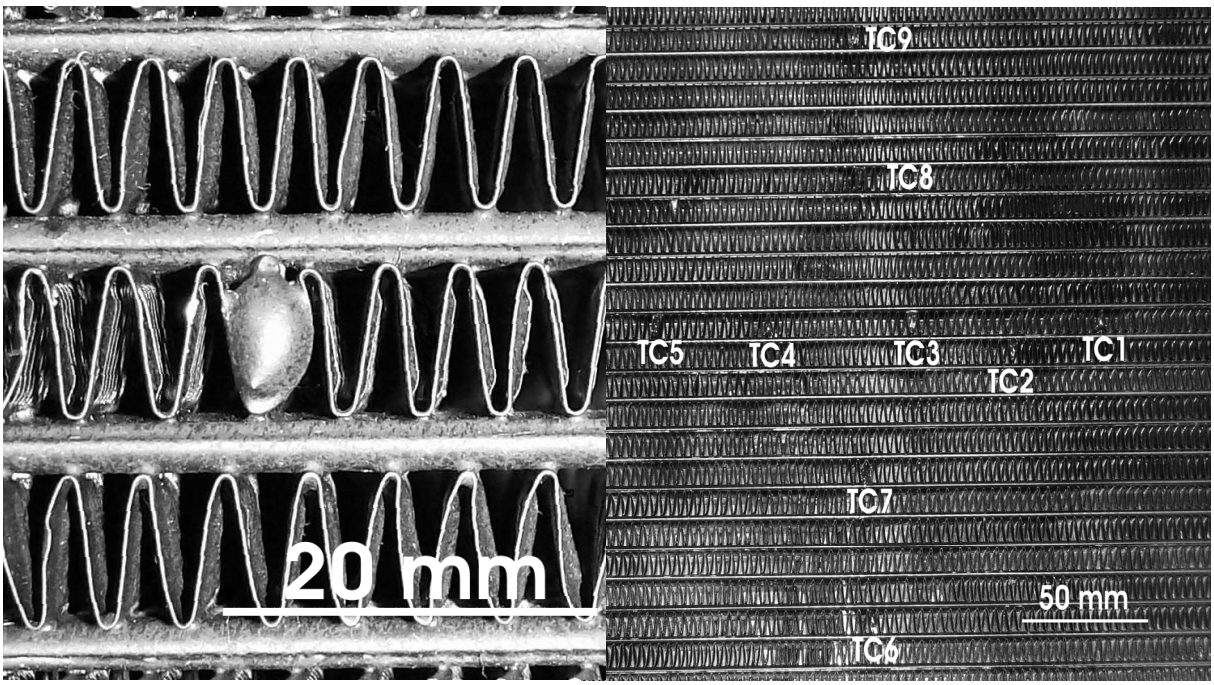
20 mm
TC9
TC8
TC5
TC4
TC3
TC2
TC1
TC7
50 mm
TC6

Fig. 3.1. The large radiator system: (a) top: the radiator, a net radiometer, insulated hoses, grounding wires, water pump, water bath and outlet and inlet TCs and some of the halogen lamps, the latter for shortwave calibrations; (b) bottom left: close-up of radiator cavities and a single TC; (c) bottom right: the array of surface-mounted thermocouples and the radiator cavities. Not shown are the two TCs for measuring outlet and inlet water temperatures.

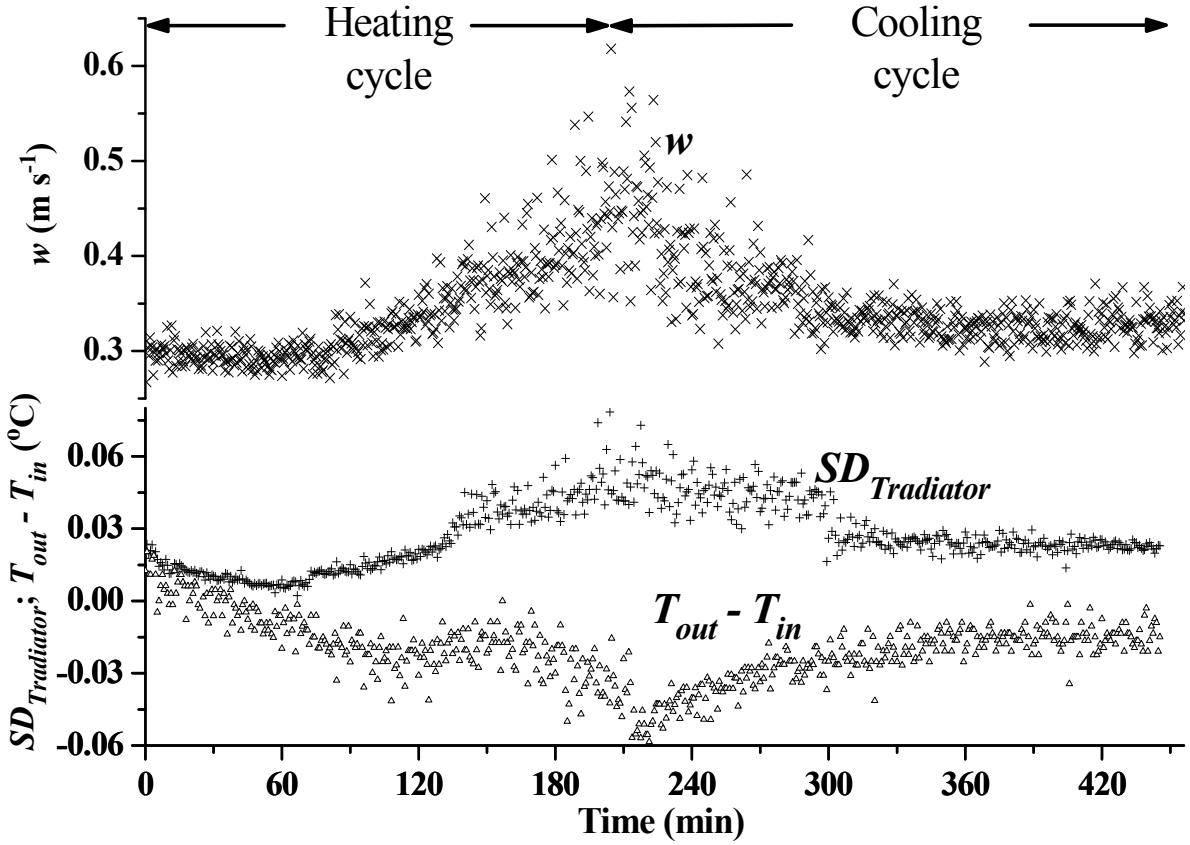

Fig. 3.2. Conditions during a polyethylene-domed infrared net radiometer calibration: temporal variation in the standard deviation of the radiator surface temperatures SD_{Trad}, temperature difference between water out of and into the radiator ($T_{out} - T_{in}$) and temporal variation in vertical wind speed *w*.

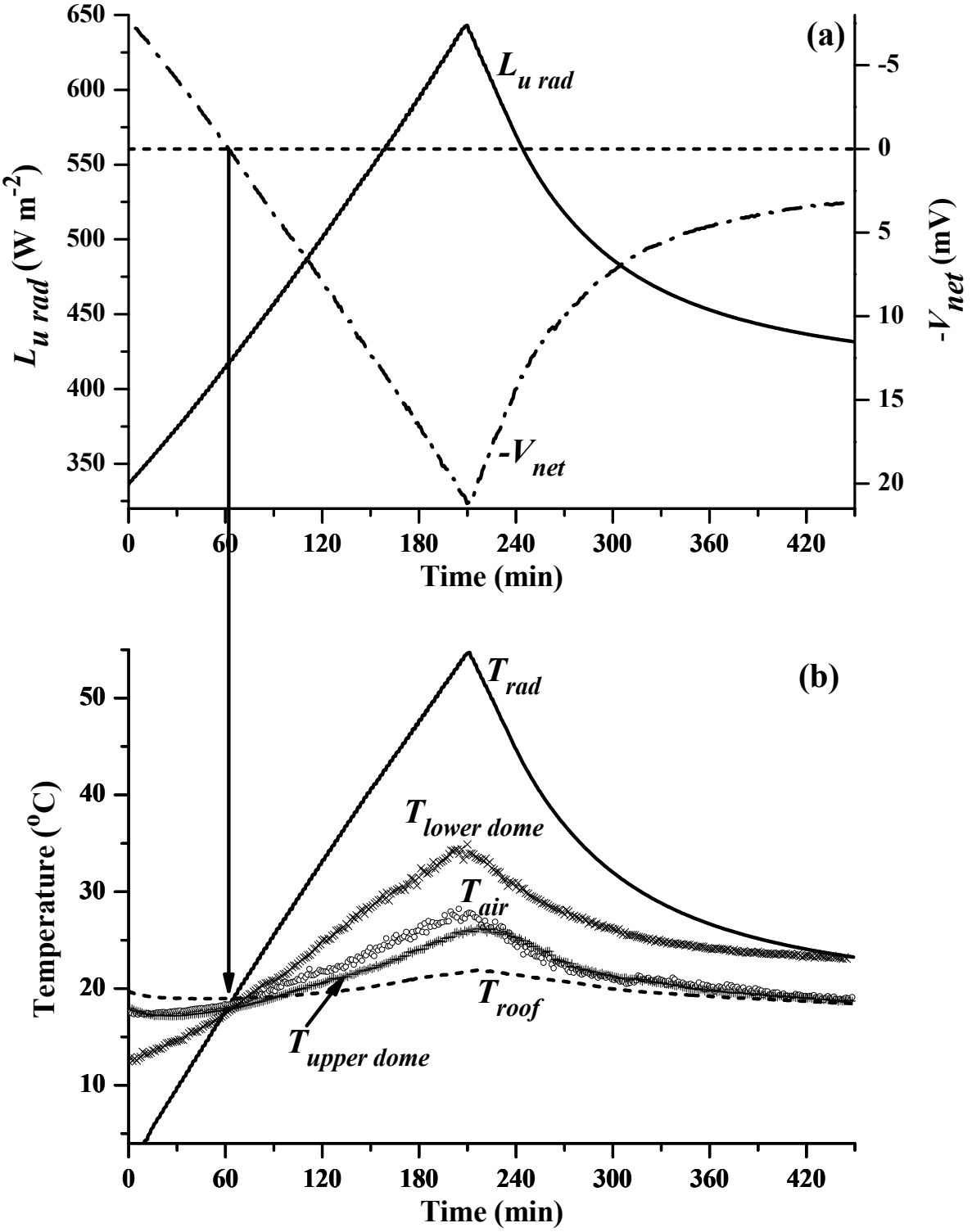

Fig. 3.3. Conditions during a polyethylene-domed net radiometer infrared calibration for a heating cycle followed by a cooling cycle: (a) temporal variation in net radiometer voltage plotted as $-V_{net}$ and $L_{u\,rad}$; (b) temporal variation in upper and lower dome temperatures, radiator surface, air and laboratory roof temperatures.

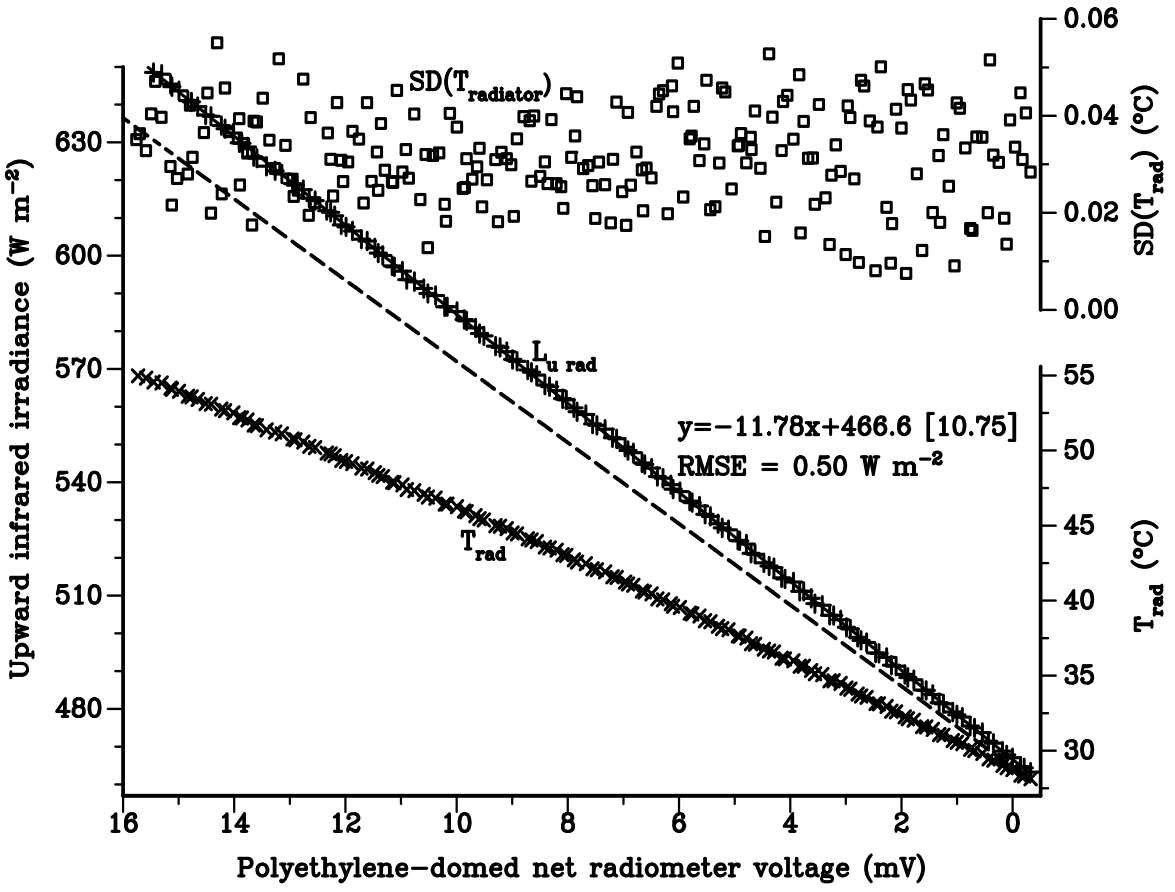

Fig. 3.4. A plot of the upward infrared irradiance $L_{u\,rad}$ (left hand y-axis, W m^{-2}) estimated from $F\sigma T_{rad}^4$ for a heating cycle, the radiator surface temperature T_{rad} (bottom right-hand y-axis, ^{o}C) and the standard deviation of the radiator surface temperature (top right hand y-axis, ^{o}C) as a function of the net radiometer voltage (mV) for Q*7 net radiometer number 2 (run 4). The dashed line has a slope magnitude equal to the calibration factor supplied with the instrument (shown in square brackets after the calibration regression equation).

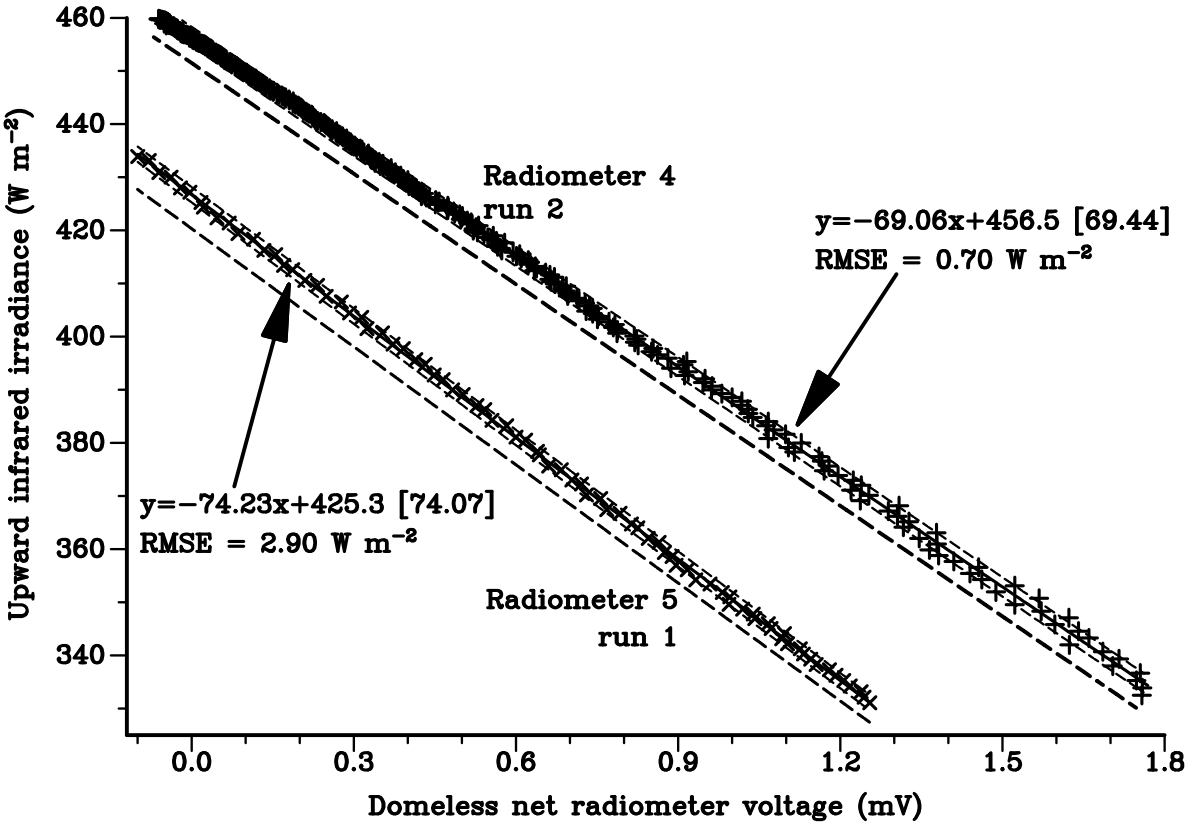

Fig. 3.5. A plot of the upward infrared irradiance $L_{u\,rad}$ (W m^{-2}) as a function of the net radiometer voltage (mV) for net radiometer numbers 4 and 5 (domeless instruments) for a heating cycle. The dashed lines, offset by 5 W m^{-2}, have a slope magnitude equal to that supplied by the manufacturer.

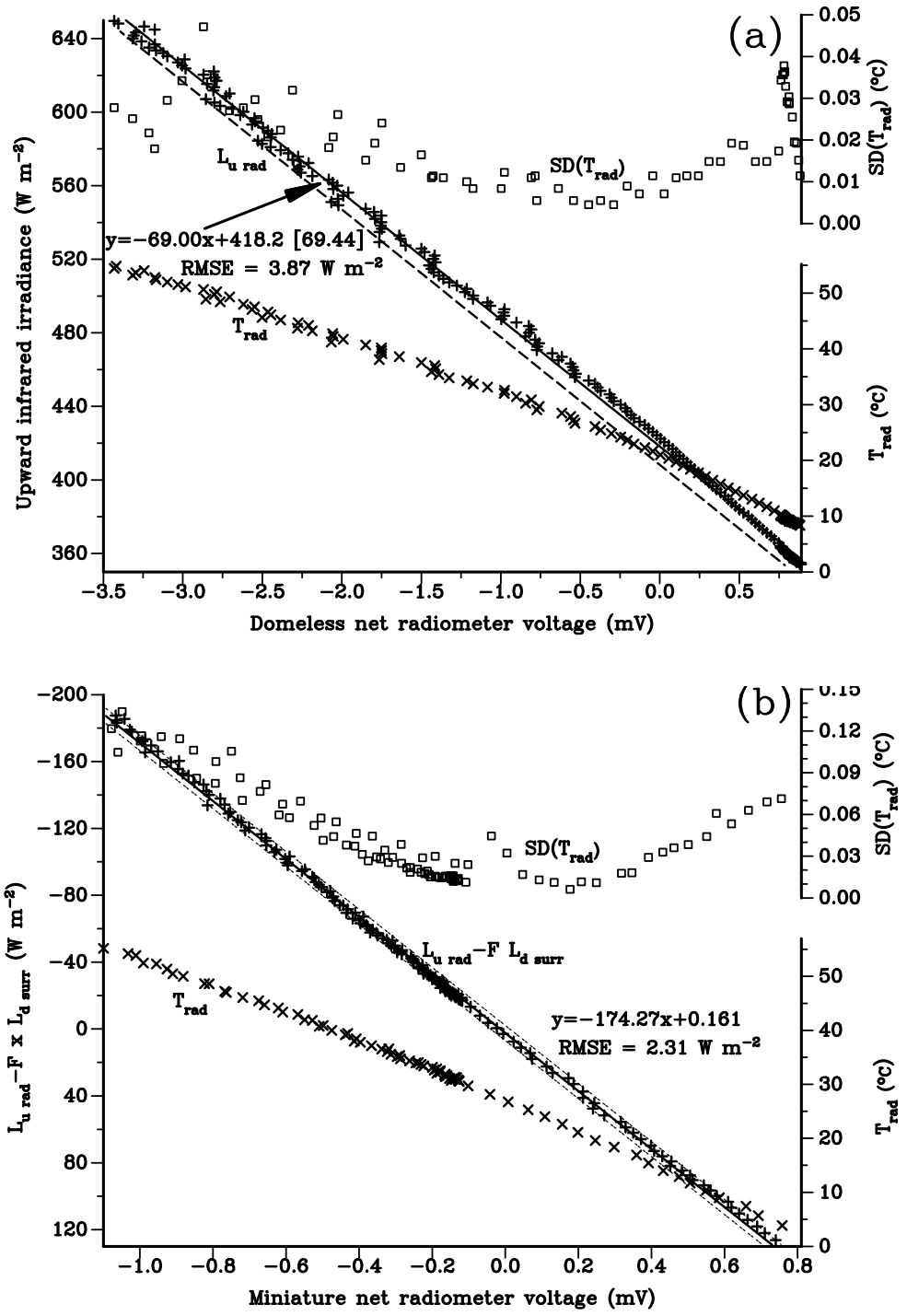

Fig. 3.6. (a) A plot of the upward infrared irradiance (W m^{-2}) as a function of the net radiometer voltage (mV) for net radiometer number 4 (domeless, run 3, heating cycle) – the dashed line, offset by 10 W m^{-2}, corresponds to a slope magnitude equal to that supplied with the instrument; (b) a plot of the upward infrared irradiance minus $F\ L_{d\ surr}$ (W m^{-2}) as a function of the net radiometer voltage (mV) for net radiometer number 3 (miniature polyethylene-domed, run 5, heating and cooling cycles).

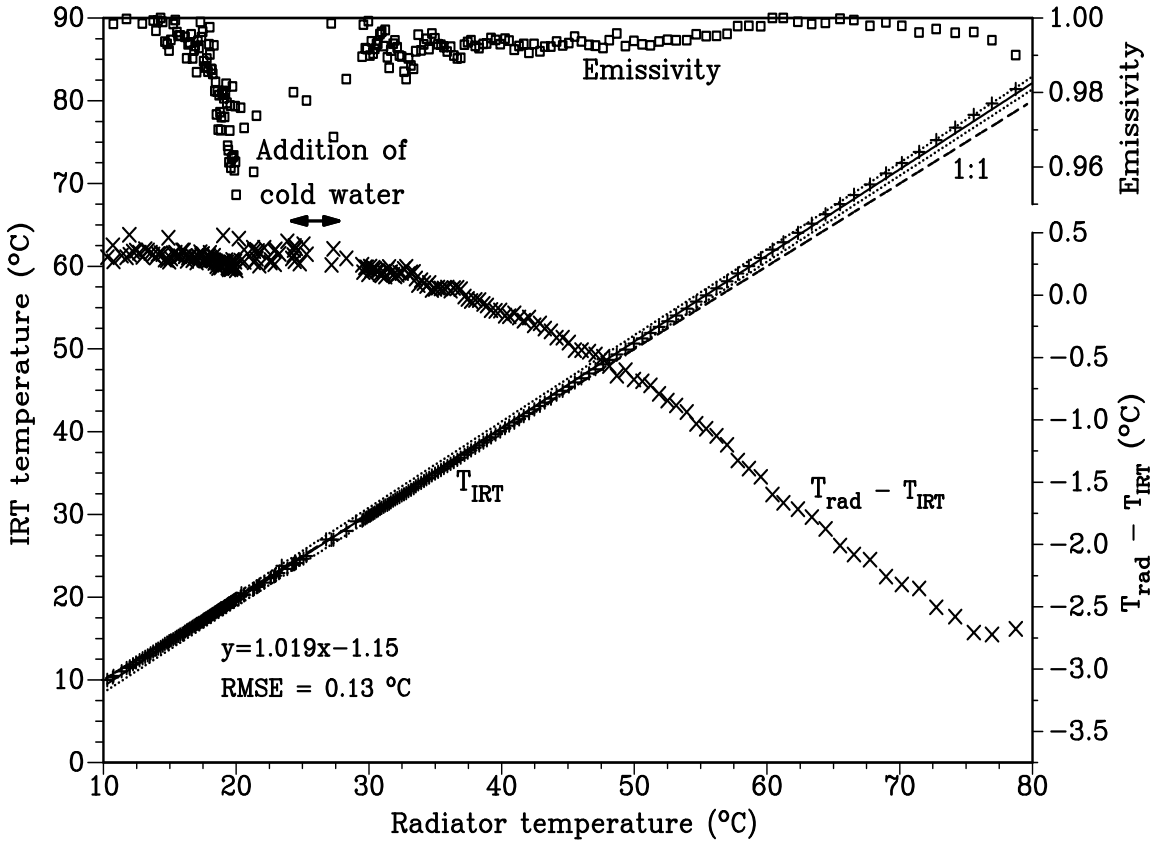

Fig. 3.7. A plot of the IRT (number 2, run 2) temperature (left hand y-axis, °C), the temperature difference between radiator surface and IRT temperatures (bottom right hand y-axis, °C), and calculated emissivity of the radiator (top right hand y-axis, unitless).

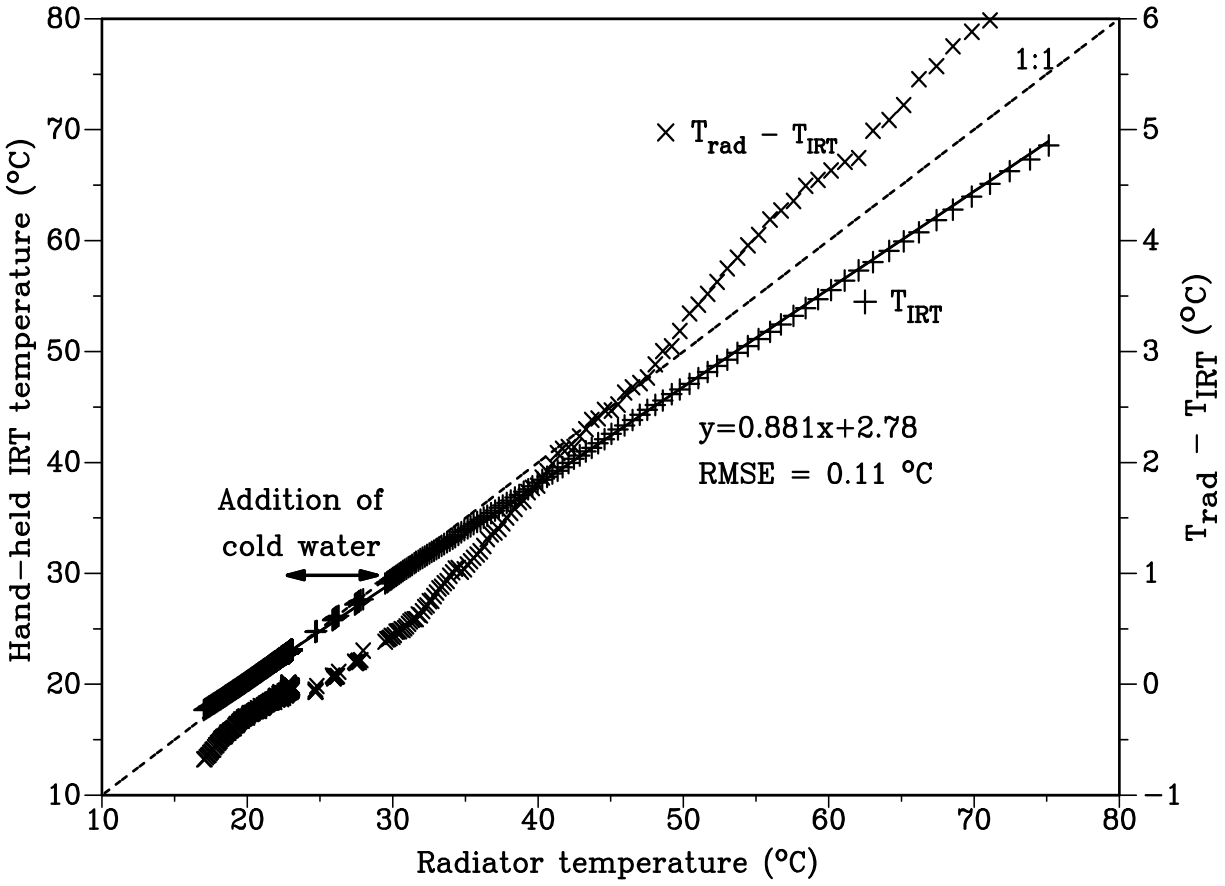

Fig. 3.8. A plot of the IRT (hand-held model 110) temperature (left hand y-axis, °C) and the temperature difference between radiator surface and IRT temperatures (right hand y-axis, °C).

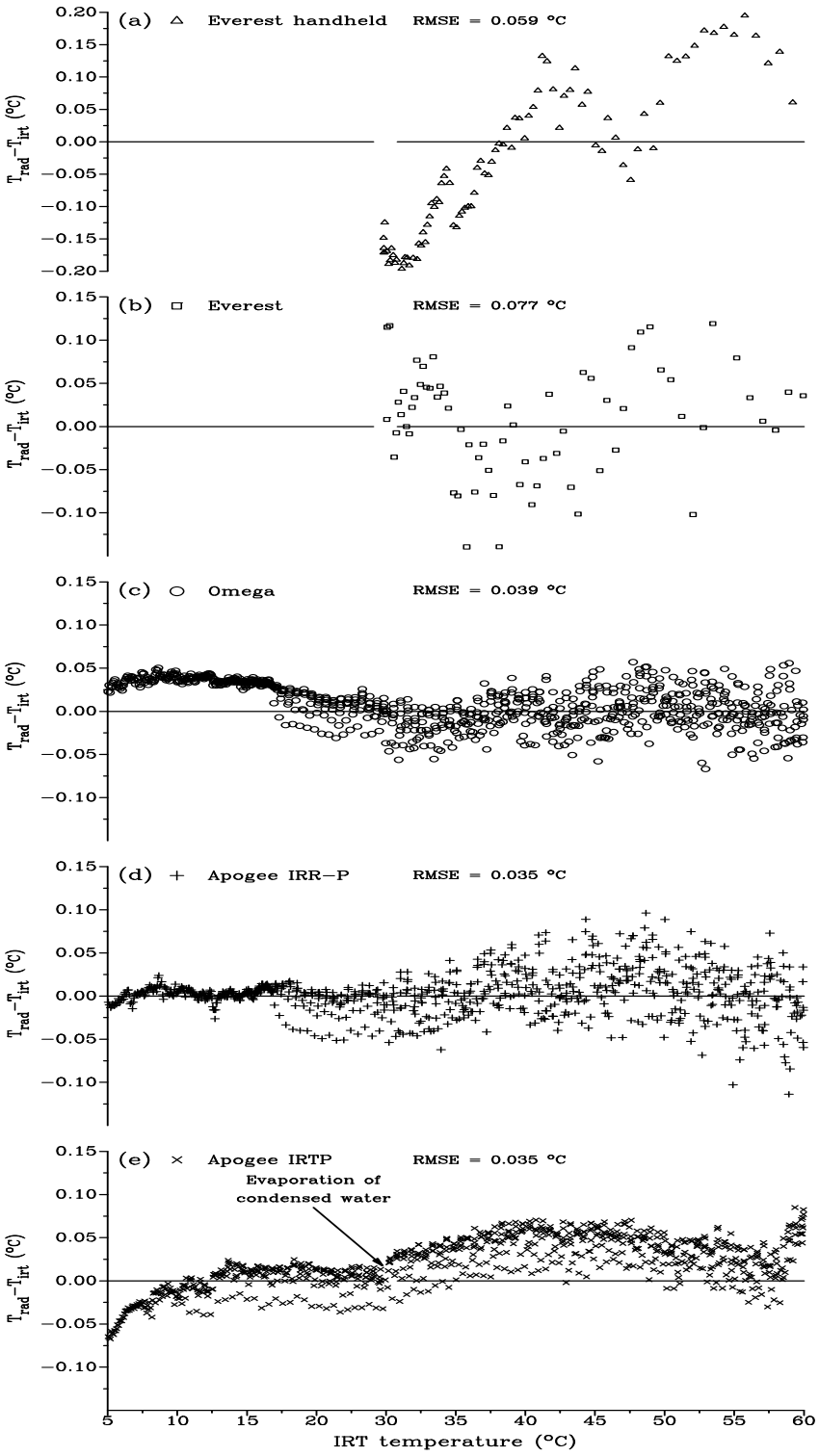

Fig. 3.9. A plot of the radiator surface and IRT temperature residuals for selected IRT sensors. The five horizontal lines correspond to a residual of 0 °C.

Table 3.1. Details and statistical results for selected net radiometer infrared (I) and shortwave (S) calibrations. The outdoor calibrations for the domed net radiometers, last column, were performed using the field shortwave sun/shade technique.

Manufacturer	Radiometer number	Calibration number	Laboratory number (cooling phase, C; heating, H), *d* (mm)†	Equation used	*n*	Intercept (W m^{-2})	$SE_{intecept}$ (W m^{-2}) ††	Slope magnitude (W m^{-2} mV^{-1})	SE_{slope} (W m^{-2} mV^{-1})	r^2	*RMSE* (W m^{-2})	Manufacturers shortwave (S) and/or infrared (I) calibration factor (W m^{-2} mV^{-1})	Field shortwave calibration factor (W m^{-2} mV^{-1})
REBS	1 Polyethylene-domed Q*6	1 (I)	2 (C)	8	77	435.2	0.16	13.86	0.035	0.9995	0.84	13.7 (S and I)	13.59
		2 (I)	2 (C)		246	432.9	0.09	13.82	0.019	0.9995	1.32		
	1	1	2 (C)		77	427.2	0.16	13.60	0.035	0.9995	0.83	13.7 (S)	13.59
		2	2 (C)		246	425.0	0.09	13.56	0.019	0.9995	1.30		
	2	1	1 (C)		106	415.5	0.16	13.88	0.019	0.9998	0.94	14.0 (S)	14.84
	2 (Figs 3.2, 3.5)		1 (C)		125	414.2	0.11	13.96	0.014	0.9999	0.81		
	3	1	1 (C)		117	412.8	0.15	14.10	0.017	0.9998	0.98	14.1 (S)	14.94
		2	1 (C)		114	413.2	0.13	14.05	0.017	0.9998	0.80		
	4	1	2 (C)		436	423.5	0.02	14.02	0.016	0.9994	0.25	14.1 (S)	14.56
		2	1 (C)		103	415.4	0.33	14.10	0.038	0.9993	1.86		
		3	1 (C)		81	418.6	0.27	14.12	0.029	0.9997	1.22		
	5	1	1 (C)		93	429.4	0.23	12.44	0.023	0.9997	1.12	12.7 (S)	13.82
		2	2 (C)		197	428.2	0.11	12.66	0.017	0.9997	1.05		
		3	2 (C)		202	427.7	0.06	12.65	0.015	0.9997	0.58		
		4	2 (C)		216	427.5	0.02	12.55	0.013	0.9998	1.09		
	6	1	2 (C)		216	427.5	0.02	12.91	0.012	0.9998	0.95	12.9 (S)	13.70
	7	1	2 (C)		252	424.6	0.07	12.93	0.010	0.9999	0.87	12.8 (S)	13.57
	8 Polyethylene-domed Q*7	1 (I)	3 (H), 55	8	907	459.5	0.04	11.61	0.004	0.9999	1.17	8.89 (positive	
		2 (I)	3 (C), 55		940	459.7	0.06	11.61	0.009	0.9994	1.15	R_{net}),	
		3 (I)	3 (H), 50		857	457.6	0.03	11.52	0.004	0.9999	0.91	10.75 (negative	

Manufacturer	Radiometer number	Calibration number	Laboratory number (cooling phase, C; heating, H), *d* (mm)†	Equation used	*n*	Intercept (W m^{-2})	$SE_{intecept}$ (W m^{-2}) ††	Slope magnitude (W m^{-2} mV^{-1})	SE_{slope} (W m^{-2} mV^{-1})	r^2	*RMSE* (W m^{-2})	Manufacturers shortwave (S) and/or infrared (I) calibration factor (W m^{-2} mV^{-1})	Field shortwave calibration factor (W m^{-2} mV^{-1})
		4 (Fig. 3.4) (I)	3 (H), 50		446	466.6	0.05	11.78	0.005	0.9999	0.50	R_{net})	
		5 (I)	3 (C), 57		1008	475.9	0.02	11.58	0.004	0.9999	0.44		
		6 (I)	3 (C), 57		959	472.4	0.05	11.71	0.008	0.9996	0.90		
		7 (I)	3 (C), 57		959	468.2	0.03	11.54	0.005	0.9998	0.62		
		8 (I)	4 (H, V)†††, 61		1038	430.9	0.05	13.15	0.009	0.9996	1.43		
		9 (I)	4 (C, V), 61		990	427.5	0.08	13.74	0.010	0.9995	1.09		
		10 (I)	4 (H, U) ††††, 61		227	432.4	0.17	11.25	0.031	0.9983	2.38		
		11 (I)	4 (C, U), 61		189	427.3	0.20	11.98	0.035	0.9984	1.13		
		12 (I)	4 (H, V), 62		840	418.0	0.06	13.33	0.008	0.9997	1.55		
		13 (I)	4 (C, V), 62		958	416.5	0.01	13.66	0.011	0.9994	1.37		
		14 (I)	4 (H, U), 61		198	436.8	0.22	11.73	0.024	0.9992	2.86		
		15 (I)	4 (C, U), 61		223	429.1	0.21	12.45	0.028	0.9989	1.69		
		16 (I)	4 (H, U), 60		856	418.2	0.10	11.69	0.010	0.9994	2.45		
		17 (I)	4 (C, U), 60		901	416.6	0.04	12.11	0.006	0.9987	0.64		
		18 (I)	4 (H), 63		842	409.3	0.08	11.75	0.008	0.9996	2.01		
		19 (I)	4 (C), 63		958	409.0	0.07	11.99	0.008	0.9996	1.13		
		20 (S)	4, 57	7	72	19.2	0.29	8.66	0.014	0.9998	1.18		
	IR correction	21 (S)				-0.4	0.24	8.97	0.012	0.9999	0.99		
		22 (S)	4, 75		45	10.0	0.35	8.75	0.012	0.9999	1.15		
	IR correction	23 (S)				-2.0	0.82	8.99	0.027	0.9996	2.70		
		24 (S)	4, 70		69	23.5	0.17	8.91	0.011	0.9999	1.20		
	IR correction	25 (S)				-4.4	0.21	8.92	0.013	0.9998	1.49		
		26 (S)	4, 60		18	4.1	0.33	8.86	0.017	0.9999	0.99		
	IR correction	27 (S)			18	12.7	0.20	8.70	0.010	1.0000	0.59		
	9 Polyethylene-domed Q*7	1 (I)	5 (H, $V_{corrected,}$ A†††††), 53.5	8	871	423.8	0.05	11.50	0.005	0.9998	1.30	8.98 (positive R_{net}), 11.01 (negative R_{net})	
		1 (I)	5 (H, $V_{uncorrected,}$ A), 53.5		871	424.6	0.05	11.50	0.005	0.9998	1.28		
		1 (I)	5, (C, $V_{corrected,}$ A), 53.5		944	425.6	0.04	11.31	0.006	0.9998	0.82		
		1 (I)	5, (C, $V_{uncorrected,}$ A), 53.5		944	425.7	0.04	11.23	0.005	0.9998	0.71		

Manufacturer	Radiometer number	Calibration number	Laboratory number (cooling phase, C; heating, H), *d* (mm)†	Equation used	*n*	Intercept (W m^{-2})	$SE_{intecept}$ (W m^{-2}) ††	Slope magnitude (W m^{-2} mV^{-1})	SE_{slope} (W m^{-2} mV^{-1})	r^2	*RMSE* (W m^{-2})	Manufacturers shortwave (S) and/or infrared (I) calibration factor (W m^{-2} mV^{-1})	Field shortwave calibration factor (W m^{-2} mV^{-1})
		1 (I)	5, (H, C, $V_{corrected,}$ A), 53.5		1815	424.4	0.04	11.45	0.004	0.9997	1.26		
		1 (I)	5, (H, C, $V_{uncorrected,}$ A), 53.5		1815	424.6	0.04	11.43	0.005	0.9997	1.33		
	IR correction	2 (S)	5										
	10 Polyethylene-domed Q*7 (calibrations 1 to 3 were before instrument field use and 4, 5 after field use during which the sensor was marked slightly following dome damage during an intense rainfall)	1 (I)	5 (C, $V_{corrected}$), 60.0		941	460.2	0.07	11.71	0.010	0.9994	1.21	9.40 (positive R_{net}), 11.80 (negative R_{net})	
		2 (I)	5 (C, $V_{corrected}$), 50.0		959	458.9	0.04	11.49	0.006	0.9997	0.79		
		3 (I)	5 (C, $V_{corrected}$), 50.0		960	473.3	0.02	11.36	0.003	0.9999	0.39		
		4 (I)	5 (H, $V_{corrected,}$ A/c, night), 60.1	8	840	423.8	0.04	12.84	0.005	0.9999	1.13		
		4 (I)	5 (H, $V_{uncorrected,}$ A/c, night), 60.1		840	424.6	0.04	12.85	0.005	0.9999	1.00		
		4 (I)	5, (C, $V_{corrected,}$ A/c, night), 60.1		960	425.3	0.05	12.66	0.007	0.9997	1.00		
		4 (I)	5, (C, $V_{uncorrected,}$ A/c, night), 60.1		960	425.3	0.05	12.59	0.007	0.9997	0.94		
		4 (I)	5, (H, C, $V_{corrected,}$ A/c, night), 60.1		1800	424.3	0.04	12.79	0.005	0.9998	1.20		
		4 (I)	5, (H, C, $V_{uncorrected,}$ A/c, night), 60.1		1800	424.6	0.04	12.76	0.005	0.9997	1.25		
		5 (I)	5 (H, $V_{corrected,}$ A/c, day), 60.1		871	424.6	0.04	12.84	0.005	0.9999	1.14		
		5 (I)	5 (H, $V_{uncorrected,}$ A/c, day), 60.1		871	425.3	0.04	12.85	0.005	0.9999	1.01		
		5 (I)	5, (C, $V_{corrected,}$ A/c, day), 60.1		960	424.7	0.06	12.77	0.008	0.9997	1.05		
		5 (I)	5, (C, $V_{uncorrected,}$ A/c, day), 60.1		960	424.8	0.05	12.69	0.007	0.9997	0.97		

Manufacturer	Radiometer number	Calibration number	Laboratory number (cooling phase, C; heating, H), *d* (mm)†	Equation used	*n*	Intercept (W m^{-2})	$SE_{intecept}$ (W m^{-2}) ††	Slope magnitude (W m^{-2} mV^{-1})	SE_{slope} (W m^{-2} mV^{-1})	r^2	*RMSE* (W m^{-2})	Manufacturers shortwave (S) and/or infrared (I) calibration factor (W m^{-2} mV^{-1})	Field shortwave calibration factor (W m^{-2} mV^{-1})
		5 (I)	5, (H, C, $V_{corrected,}$ A/c, day), 60.1		1831	424.6	0.03	12.82	0.004	0.9998	1.12		
		5 (I)	5, (H, C, $V_{uncorrected,}$ A/c, day), 60.1		1831	424.9	0.04	12.79	0.005	0.9997	1.28		
		6 (S)	5, 60	7	47	0	0	9.33	0.030	0.9779	0.94		
Middleton	11 Miniature polyethylene-domed	1 (I)	3 (H, C), 46	9	1795	0.226	0.063	175.46	0.123	0.9991	2.34	Unknown	
		2 (I)	3 (H, C), 46		1823	0.952	0.067	175.14	0.131	0.9990	2.53		
		3 (I)	3 (H, C), 46		1835	-1.138	0.058	176.29	0.115	0.9992	2.22		
		4 (I)	3 (H, C), 46		1813	1.154	0.053	175.70	0.104	0.9994	1.97		
		5 (Fig. 3.6b) (I)	3 (H, C), 46		1821	0.161	0.061	174.27	0.121	0.9991	2.31		
		6 (S)	4, 68	7	18	16.03	0.926	153.06	0.745	0.9996	2.92		
Kipp and Zonen	12 Domeless NR LITE, 12th June 2005 vintage	1 (I)	3 (H), 53.5	8	273	417.6	0.22	69.18	0.121	0.9992	3.19	69.44 (S) Upper surface	
		2 (Fig. 3.5) (I)	3 (H), 50		1473	456.5	0.03	69.06	0.039	0.9995	0.70		
		3 (Fig. 3.6a) (I)	3 (H), 50, sensor inverted		212	418.2	0.31	69.00	0.187	0.9985	3.87		
	13 29th May 2008 vintage	1 (Fig. 3.5) (I)	4 (H), 59	8	809	425.3	0.12	74.23	0.082	0.9990	2.90	74.07 (S) Upper surface	
		2 (I)	4 (C), 59		959	426.5	0.17	74.29	0.131	0.9970	2.80		
		3 (S)	4, 60	7	15	20.4	1.03	69.85	0.370	0.9996	2.93		
		4 (S)	4, 60		18	24.3	0.65	69.66	0.248	0.9998	1.97		
		5 (S)	4, 60		24	19.88	0.71	69.97	0.291	0.9996	2.45		
		6 (S)	4, 60		18	24.29	0.65	69.66	0.248	0.9998	1.97		
		7 (S)	5, 53.5		32	12.55	0.64	69.18	0.228	0.9997	2.94		
	14 29th May 2008 vintage IR correction	1 (I)	4 (H), 57	8	824	419.7	0.08	77.72	0.055	0.9996	1.89	74.63 (S) Upper surface	
		2 (I)	4 (C), 57		423	421.8	0.37	79.11	0.215	0.9968	2.55		
		3 (S)	4, 60	7	15	-8.46	1.03	72.52	0.308	0.9997	2.32		
		3 (S)	4, 60		15	16.42	0.45	73.54	0.142	0.9999	1.04		
		4 (S)	4, 60		114	16.3	0.42	74.51	0.159	0.9995	2.92		
	IR correction	4 (S)	4, 60		114	-24.1	0.19	74.43	0.067	0.9999	1.23		
	15 14th October	1 (I)	4 (H), 63	8	856	418.6	0.11	70.25	0.066	0.9993	2.86	70.92 (S) Upper surface	
		2 (I)	4 (C), 63		960	423.7	0.14	71.31	0.097	0.9982	2.29		

Manufacturer	Radiometer number	Calibration number	Laboratory number (cooling phase, C; heating, H), *d* (mm)†	Equation used	*n*	Intercept (W m^{-2})	$SE_{intecept}$ (W m^{-2}) ††	Slope magnitude (W m^{-2} mV^{-1})	SE_{slope} (W m^{-2} mV^{-1})	r^2	*RMSE* (W m^{-2})	Manufacturers shortwave (S) and/or infrared (I) calibration factor (W m^{-2} mV^{-1})	Field shortwave calibration factor (W m^{-2} mV^{-1})
	2008 vintage	1 (I)	4 (H), 63	8	886	413.5	0.12	70.86	0.079	0.9989	2.87		
		2 (I)	4 (C), 63		918	419.7	0.16	70.15	0.127	0.9970	2.56		
	16 Two-component CNR 2	1 (I)	3 (C), 48	9	959	-3.50	0.022	1.035	0.000	0.9999	0.42	66.62 (S), 79.30 (I)	
		2 (I)	3 (H), 83		1044	-0.50	0.027	1.039	0.000	0.9999	0.86		
		3 (I)	3 (C), 83		949	0.52	0.013	1.032	0.000	0.9999	0.23		
		4 (I)	3 (H), 50		2180	1.97	0.035	1.006	0.001	0.9984	1.39		
		5 (I)	3 (H), 50		1037	0.53	0.087	1.014	0.001	0.9981	1.74		
		6 (I)	4 (H), 63.5		846	-4.46	0.034	1.000	0.000	0.9999	0.80		
		7 (I)	4 (C), 63.5		958	-2.70	0.027	0.992	0.000	0.9999	0.45		
		8 (I)	4 (H), 67.5, sensor inverted		849	0.34	0.049	1.003	0.000	0.9998	1.18		
		9 (S)	4	7	61	0.146	0.690	65.34	0.31	0.9986	2.79		
		10 (S)	4		46	0.776	0.335	65.39	0.15	0.9998	1.69		
		11 (S)	4, sensor inverted		32	-3.43	0.434	65.27	0.14	0.9999	1.89		
		12 (S)	4, sensor inverted		32	-0.63	0.375	64.46	0.12	0.9999	1.66		
	17 Four-component CNR 1	1 (I)	3 (H), 45	9	762	-3.89	0.074	0.959	0.001	0.9992	0.93	82.304 (I)	
		2 (I)	3 (H), 65		1536	-1.55	0.047	0.940	0.001	0.9989	1.25		
		3 (I)	3 (H), 80		1773	0.45	0.019	0.963	0.000	0.9997	0.61		
		4 (I)	3 (H), 110		509	-4.24	0.059	0.993	0.001	0.9996	0.49		
		5 (I)	3(H), 70		1423	1.19	0.034	0.957	0.001	0.9995	0.94		
		6 (I)	3(H), 70		1120	-2.37	0.043	0.954	0.001	0.9995	1.27		
		7 (I)	3(C), 70		930	0.18	0.044	0.982	0.001	0.9997	0.83		
		8 (I)	3(natural H), 70		1562	0.40	0.016	0.952	0.000	0.9998	0.51		
		9 (I)	3 (H, C), 70		770	-2.82	0.067	0.959	0.001	0.9998	1.02		
			3 (H), 70		145	-1.70	0.276	0.963	0.002	0.9996	1.58		
		10 (I)	3 (H), 70		1396	-1.75	0.033	0.960	0.001	0.9994	0.91		

Manufacturer	Radiometer number	Calibration number	Laboratory number (cooling phase, C; heating, H), *d* (mm)†	Equation used	*n*	Intercept (W m^{-2})	$SE_{intecept}$ (W m^{-2}) ††	Slope magnitude (W m^{-2} mV^{-1})	SE_{slope} (W m^{-2} mV^{-1})	r^2	*RMSE* (W m^{-2})	Manufacturers shortwave (S) and/or infrared (I) calibration factor (W m^{-2} mV^{-1})	Field shortwave calibration factor (W m^{-2} mV^{-1})
		11 (I)	3 (H, C), 70		1102	-4.43	0.067	0.961	0.001	0.9995	1.41		
			3 (H), 70		114	-2.22	0.101	0.967	0.001	0.9999	0.64		
		12 (I)	3 (H), 70, inverted		136	-5.00	0.108	0.951	0.002	0.9997	1.25		

† Infrared calibration data were obtained for cooling (C) and heating (H) phase. In some cases, the data for both radiator heating and radiator cooling (indicated by H, C) were combined

†† *SE*: standard error; r^2: coefficient of determination; *RMSE*: root mean square error

††† V: calibration performed using ventilation of upper and lower domes

†††† U: calibration with the ventilator in place but the fans off

††††† A/c: air-conditioned laboratory set at 20 ^{o}C with lights on during the day and the night for which normal linear regression statistics were applied by correcting ($V_{corrected}$) and not correcting net radiometer voltages ($V_{uncorrected}$) for sensor time response

Table 3.2. Details and statistical results of the selected IRT laboratory calibrations.

Model and number	Calibration number	Maximum, minimum radiator temperatures (°C)	*n*	Intercept (°C)	$SE_{intercept}$ (°C)	Slope	SE_{slope}	r^2	*RMSE* (°C)	$\frac{MSE_{unsystematic}}{MSE_{total}}$ †	$\frac{MSE_{systematic}}{MSE_{total}}$
Everest Model 4000ALCS 1	1	10.29, 81.7	233	-1.18	0.03	1.041	0.001	0.9997	0.29	0.15	0.85
	2	20.55, 84.10	144	-1.19	0.06	1.039	0.002	0.9996	0.32	0.22	0.78
	3	24.09, 83.10	189	-1.35	0.05	1.043	0.001	0.9998	0.23	0.11	0.89
	4	2.89, 83.10	521	-0.44	0.03	1.022	0.001	0.9995	0.31	0.50	0.50
2	1 (Fig. 3.9)	27.68, 74.97	99	-1.50	0.05	1.020	0.001	0.9999	0.14	0.01	0.99
	2 (Fig. 3.7)	26.64, 69.58	131	-1.15	0.04	1.019	0.001	0.9999	0.13	0.07	0.93
3	1	20.55, 84.10	144	-0.38	0.05	1.000	0.001	0.9997	0.27	0.28	0.72
	2	24.09, 83.10	189	-0.35	0.00	1.000	0.001	0.9997	0.23	0.23	0.77
	3	2.89, 83.10	521	0.26	0.02	1.000	0.001	0.9997	0.24	0.48	0.52
4	1	17.00, 75.13	970	0.00	0.01	0.999	0.001	0.9999	0.13	0.02	0.98
5	1	17.00, 75.13	970	-1.16	0.01	1.042	0.000	0.9998	0.11	0.11	0.89
6	1	17.00, 75.13	970	-1.48	0.01	1.061	0.000	0.9998	0.11	0.05	0.95
Everest Model 110 (hand-held) 7	1	20.33, 81.7	10	2.89	0.11	0.880	0.002	1.0000	0.17	0.00	1.00
	2 (Figs. 3.8, 3.9)	17.00, 75.13	970	2.78	0.01	0.881	0.000	0.9997	0.11	0.01	0.99
Apogee IRTP 8	1	1.04, 60.11	933	-0.07	0.05	1.036	0.002	0.9981	0.78	0.28	0.72
9	1 (Fig. 3.9)	4.35, 60.13	959	-1.33	0.05	1.086	0.002	0.9982	0.76	0.13	0.87
	2	0.88, 60.00	952	-0.71	0.06	1.070	0.002	0.9975	0.93	0.19	0.81
	3	1.04, 60.11	933	-0.76	0.06	1.070	0.002	0.9977	0.88	0.18	0.82
IRR-P 10	1 (Fig. 3.9)	4.57, 60.13	958	-0.99	0.06	1.063	0.002	0.9980	0.77	0.22	0.78

Model and number	Calibration number	Maximum, minimum radiator temperatures (°C)	*n*	Intercept (°C)	$SE_{intercept}$ (°C)	Slope	SE_{slope}	r^2	*RMSE* (°C)	$\frac{MSE_{unsystematic}}{MSE_{total}}$ †	$\frac{MSE_{systematic}}{MSE_{total}}$
	2	0.88, 60.00	952	-0.27	0.06	1.047	0.002	0.9972	0.96	0.31	0.69
	3	1.04, 60.11	933	-0.55	0.06	1.053	0.002	0.9976	0.88	0.27	0.73
Omega 11	1 (Fig. 3.9)	4.35, 60.13	959	-0.98	0.06	1.077	0.002	0.9974	0.89	0.17	0.83
	2	0.88, 60.00	952	-0.24	0.07	1.059	0.002	0.9965	1.10	0.25	0.75
	3	1.04, 60.11	933	-0.45	0.07	1.063	0.002	0.9969	1.01	0.22	0.78

† $MSE_{total} = MSE_{systematic} + MSE_{unsystematic}$; $MSE_{systematic} = \sum_{i=1}^{n} (\hat{y}_i - x_i)^2 / n$; $MSE_{unsystematic} = \sum_{i=1}^{n} (y_i - \hat{y}_i)^2 / n$

Table 3.3. The statistical results of the hand-held IRT laboratory calibration with and without application of the statistical method used to reduce the residuals (n = 970 and $r^2 > 0.9997$ for all datasets).

Statistical parameters	Without application of Eq. (3.14)	Application of Eq. (3.14)	Reapplication of Eq. (3.14)	Third application of Eq. (3.14)
Slope	0.881	0.986	0.998	1.001
SE_{slope}	0.0005	0.0003	0.0003	0.0003
Intercept (^{o}C)	2.78	0.33	0.04	-0.02
RMSE (^{o}C)	0.11	0.07	0.06	0.06
Mean bias error (^{o}C)	-0.184	-0.093	-0.019	0.005
Mean absolute error (^{o}C)	0.307	0.096	0.050	0.041
d–index (Willmott, 1981)	0.9958	0.9999	1.0000	1.0000

4 ESTIMATION OF EVAPORATION USING A DUAL-BEAM SURFACE-LAYER SCINTILLOMETER AND COMPONENT ENERGY BALANCE MEASUREMENTS[1]

4.1 Abstract

A dual-beam surface-layer scintillometer (SLS), for the estimation of sensible heat flux *H* for a path length of 101 m, was used in a mesic grassland in the eastern seaboard of South Africa for 30 months. Measurements also included eddy covariance (EC) and Bowen ratio (BREB) estimates of *H*. Acceptable SLS data between 06h00 and 18h00, judged by the percent of error-free 1-kHz data exceeding 25 % and an inner scale of turbulence exceeding 2 mm, showed little seasonal variation and was consistently high - between 86.7 % and 94.8 %. An analysis of the various Monin-Obukhov similarity theory (MOST) empirical dimensionless stability functions used for estimating *H* from the SLS measurements showed percent differences in *H* that varied from -30 to 28 % for neutral to unstable conditions respectively and for stable continuous conditions the differences in *H* were within 60 W m^{-2} with much larger differences for stable sporadic conditions. The good agreement in measurements of *H* over an extended period for the SLS, BREB and EC methods demonstrates the applicability and robustness of the SLS method and the associated MOST empirical functions used for estimating *H* for a range of canopy heights, stability conditions and diurnal and seasonal weather conditions. Furthermore, there was no evidence for an underestimation in EC sensible heat compared to SLS and BREB measurements, which implies that any lack of energy balance closure points to possible latent energy EC underestimation or due to energy fluxes not included in the shortened energy balance if the net irradiance and soil heat flux components are correct. A sensitivity analysis was used to determine the relative importance of the SLS data inputs of air temperature, atmospheric pressure, beam path length and beam height on *H* estimates. Worst-case errors in air temperature, atmospheric pressure, beam path length and beam height resulted in errors in *H* within 1.0, 1.3, 3.0 and 4.0 % respectively. Overall, the worst-case total percent error in SLS-estimated *H* is within 5.3 % and the typical percent error is within 3.9 %. Accounting for the error in net irradiance and soil heat flux measurements, the seasonal variation in the error in daily evaporation estimated as a residual of the energy balance is generally less than 0.2 mm (0.49 MJ m^{-2}) in winter when the daily evaporation was about 1 mm (2.45 MJ m^{-2}) and typically less than 0.4 mm (0.98 MJ m^{-2}) when the evaporation exceeded 4 mm (9.8 MJ m^{-2}). Soil heat flux measurements can contribute significantly to the overall error.

Keywords:

Surface-layer scintillometry

Evaporation estimation

Dual-beam scintillometer

Surface energy balance

Bowen ratio

Eddy covariance

MOST

[1] Based on Savage et al. (2004) and Savage (2009)

Closure

4.2 Introduction

The 1998 Republic of South Africa National Water Act refers to the possible prescription, by government, of methods for making a volumetric determination of water for purposes of water allocation and charges in the case of activities resulting in stream flow reduction. Given this scenario and the demand on water resources it is important to consider how evaporation, one of the main components of the water balance, and of the energy balance, is to be measured or estimated with reliable accuracy and precision. Determination of reliable and representative evaporation data is an important issue of atmospheric research with respect to applications in agriculture, catchment hydrology and the environmental sciences, not only in South Africa. Long-term measurements of evaporation at different time scales and from different climate regions are not yet readily available. Drexler et al. (2004) noted that very few evaporation estimation methods work well for an hourly time-step, and in some cases, do not work well even for a daily time-step. The Bowen ratio (BREB) (Bowen, 1926; Sverdrup, 1943) and eddy covariance (EC) (Swinbank, 1951) methods, used for obtaining measures of sensible heat and latent energy flux above the surface, are the more popular research methods for estimating evaporation. The flux measurements represent a footprint area in both methods. Both BREB and EC systems are portable systems that can be used to collect unattended flux measurements, for reasonably long periods of time (Savage et al., 1997).

The surface-layer scintillometer (SLS) method, based on Monin-Obukhov similarity theory (MOST), is attractive since it allows for the estimation of path-weighted sensible heat flux H (W m^{-2}) [and momentum flux] over distances of between 50 and 250 m (Thiermann and Grassl, 1992) for turbulent conditions for which there is weak scattering of the SLS beam although Andreas et al. (2003) used their unit over distances of 300 to 350 m above snow-covered sea ice. Lidar (light detection and ranging) methods (Eichinger et al., 2006) also use MOST and yield, typically over distances of kilometers, spatially-integrated estimates of H but the equipment is very expensive. The frequency of SLS measurements is 1 kHz compared to typical frequencies of 125 Hz for boundary-layer scintillometer measurements if crosswind measurements are included, typically 10 Hz for EC measurements and 1 Hz for BREB and large aperture scintillometer measurements. For SLS flux measurements, the averaging period used has been as short as 1 or 2 min (Thiermann and Grassl, 1992) if the transverse wind speed is not too low although Andreas et al. (2003) found that such short periods would only be reliable for quasi-stationary time series. The rationale for short flux-averaging times for the SLS method is given by Andreas et al. (2003): compared to point-measurements, there are many more turbulent eddies per unit time for a path-averaging sensor such as the SLS. The commonly-used averaging period for BREB measurements is 20 min, with one documented case of 5 min, and for EC flux measurements it is 30 min and tending to longer times for taller vegetation (Sun et al., 2006). For EC measurements, Foken et al. (2006) and Sun et al. (2006), both using an Ogive analysis, report on the influence of the EC averaging time interval on energy balance closure and flux estimates respectively. For a relatively short crop – wheat – Sun et al. (2006) found that biases in H and LE became very small when the averaging period was 5 min or longer.

Green et al. (1997) found that EC and scintillometer data-scatter for crosspath winds was similar. There was a tighter regression for down-path winds. Sensible heat flux for a wheat canopy

was measured by Anandakumar (1999) using SLS, EC, and surface renewal (Castellví, 2004) methods for one month to investigate the influence of cloud shadows on 1-min temporal SLS data collected. Anandakumar (1999) found that H, averaged over 20 min for the various methods, were in good correspondence with the SLS measurements (H_{SLS}) showing a smoother variation. Weiss (2002) used the SLS method for window periods in homogeneous and flat terrain to flat, non-homogeneous terrain to slanted, non-homogeneous terrain. There was satisfactory accuracy for the H_{SLS} measurements. However, many of the studies employing the SLS method have been very short in duration – in some cases for a few days and in other cases for a couple of months. There have been no studies that we are aware of involving simultaneous comparisons of the SLS, BREB and EC methods and comparisons of the flux estimates and none that have used the SLS method for an extended period of time.

Most of the studies undertaken agree that the SLS method is a useful, robust and accurate method for obtaining a path-weighted estimate for H for beam path lengths between 50 and 250 m and in one documented case, up to 350 m. A limitation of the SLS method is that of saturation under conditions of strong turbulence, necessitating using shorter beam path lengths and higher beam heights.

The MOST-dependent SLS approach has a number of advantages over, for instance, BREB and EC methods: the SLS method appears to be applicable for short time intervals; the method is robust resulting in path-weighted estimates of H and momentum flux ; measurements may be made close to the surface; unlike the EC method, no corrections are applied to the SLS data, other than a small correction for the influence of water vapour pressure on beam transmission, through the Bowen ratio.

Measurements of $H = H_{SLS}$ together with net irradiance (R_{net}) and soil heat flux (S) measurements are used to determine the evaporation from the latent energy flux (LE) calculated as a residual using the shortened surface energy balance equation. This type of application has rarely been reported in the scientific literature.

In the work reported here, the SLS and EC data collected for a grassland site in South Africa span a period of thirty months, with simultaneous BREB data collected for more than seven months. The objective of this work is the use of the SLS method and other energy balance measurements for the estimation of evaporation, and an assessment of its error, for a mesic grassland for an extended period of time. The methodology for the measurement of H and the subsequent estimation of LE is presented. A sensitivity analysis is used to determine the order of importance of the input parameters for the SLS method. Additional objectives include an analysis of the impact of various MOST methods used on the SLS-estimated H as well as a comparison of LE estimated as a residual of the energy balance using measurements of H from SLS, BREB and EC methods and measurements of R_{net} and S.

4.3 Theory

The shortened surface energy balance for a flat and extensive surface

$$R_{net} + LE + H + S = 0 \tag{4.1}$$

allows *LE* to be determined from measurements of R_{net}, *H* and *S*. All terms are in W m^{-2}. In this shortened energy balance, terms such as advection (sensible and latent) and canopy-stored heat are not taken into account. SLS measurements, with the use of MOST, allow for the estimation of *H* and the momentum flux since the friction velocity u_* is also estimated from which *LE* is estimated from measurements of R_{net} and *S*. The SLS method relies on the determination of the covariance of the logarithm of the amplitude of radiation intensity (B_{12}) received from two radiation sources of orthogonal polarisations and known wavelength, distance apart for a known propagation path length in the horizontal (Thiermann and Grassl, 1992) and known vertical placement height of the beam relative to the zero-plane displacement height. The radiation measurements are at a very high frequency (1 kHz) and the covariances and other computed values determined over periods of the order of minutes. The method is only valid for weak scattering, corresponding to $B_{12} < 0.3$ (Lawrence and Strohbehn, 1970). Otherwise, saturation is said to occur, for which the measured covariance B_{12} is less than that predicted. From measurements of B_{12}, and B_1 and B_2, which correspond to voltage variances measured at the individual photodiode detectors for each beam, the correlation coefficient $r = B_{12} / (B_1 \cdot B_2)^{1/2}$ for the measured transmitted photodiode voltage signals for the two beams may be calculated. This correlation coefficient is a function of the inner scale of refractive index fluctuations l_o (mm) and the beam path length (Thiermann and Grassl, 1992). Hence l_o is determined from the single detector variances B_1 and B_2 and *r*.

De Bruin et al. (2002) and Hartogensis et al. (2002) indicated possible problems with the SLS instrument with the method underestimating u_* for near-neutral conditions and overestimating u_* for stable or unstable conditions. De Bruin et al. (2002) noted however that the errors they identified tend to cancel out when evaluating H_{SLS}. For mainly stable conditions, Hartogensis et al. (2002) found that l_o is sensitive to even slight changes in the distance d_{beam} between the displaced beams and that recalculation of the data following an adjustment of d_{beam} from 2.7 mm to 2.6 mm removed an overestimation in u_* for small u_* and an underestimation in u_* for large u_*. They suggested their adjustment as a working hypothesis for their measurements, but not as a general solution. However, Nakaya et al. (2006), even by recalculating u_* through adjustment of d_{beam} by 0.1 mm to 2.6 mm, found no grounds to conclude that u_* underestimation occurs because of systematic errors of the SLS instrument.

For the dissipation range of turbulence, the structure parameter of refractive index C_n^2 (m$^{-2/3}$) is calculated from the B_{12}, B_1 and B_2 measurements at the receiver position. The parameter C_n^2 provides the linkage between radiation transmission and atmospheric turbulence via the optical properties of the atmosphere. For the dissipation range, a function describing the decay of the refractive index fluctuations is used for calculating C_n^2 (Thiermann and Grassl, 1992). This function, proposed by Hill and Clifford (1978), includes the spectral "bump" in the dissipation range reported by Champagne et al. (1977) and Williams and Paulson (1977).

The structure parameter of temperature C_T^2 (K^2 m$^{-2/3}$), a measure of air temperature fluctuations, can be calculated from C_n^2 via

$$C_T^2 = C_n^2 \cdot (\frac{T^2}{a\,P})^2 \cdot (1 + (\frac{0.03}{\beta})^2)^{-1} \tag{4.2}$$

assuming no correlation between water vapour pressure and air temperature fluctuations, or via

$$C_T^2 = C_n^2 \cdot (\frac{T^2}{a\,P})^2 \cdot (1 + \frac{0.03}{\beta})^{-2} \tag{4.3}$$

assuming a perfect correlation (Wesely, 1976a; Moene, 2003) where T is the air temperature (K), a = 0.789 × 10^{-3} K kPa^{-1} at 670 nm, P is the atmospheric pressure (kPa) and β the Bowen ratio. Since the extent of the correlation mentioned is generally not known when measurements are made, the exact contribution of humidity fluctuations via β on C_T^2 is usually unknown. Many authors have ignored the term in Eq. (4.2) or (4.3) involving β. Andreas et al. (2003), for example, ignored the humidity correction and Thiermann and Grassl (1992) justified the neglect over land on the basis that the fluctuations of refractive index caused by humidity are one order of magnitude smaller than those caused by air temperature fluctuations. Also, Moene (2003) concluded that when C_T^2 is used to estimate H, the correction for water vapour pressure fluctuations is small. This conclusion was based on the fact that for small $|\beta|$, the correction for H is large but $|H|$ is small and yet for large $|\beta|$, the correction is small [with possibly little impact on the estimated energy balance components]. Furthermore, for the more significant correction, Eq. (4.3), the relative percent error in H_{SLS} for such neglect is less than $3/\beta$ compared to $6/\beta$ for H_{EC} due to the effect of humidity on the speed of sound (Schotanus et al., 1983).

The dissipation rate of the turbulent kinetic energy ε (referred to as TKE in the literature, m^2 s^{-3}) is estimated using SLS measurements of l_o using the Hill and Clifford (1978) relationship for the dissipation range for which

$$\varepsilon = \nu^3 (\frac{7.4}{l_o})^4 \tag{4.4}$$

where ν (m^2 s^{-1}) is the kinematic viscosity of air. The constant 7.4 is derived from $(12\beta_1 / \mathrm{Pr})^{3/4} = 7.37$ where β_1 = 0.86 is the Obukhov-Corrsin constant and Pr = 0.72 is the Prandtl number. Some authors define β_1 = 3.47 for which $(3\beta_1 / \mathrm{Pr})^{3/4} = 7.41$.

Invoking MOST, the temperature scaling parameter T_* (K) is given by

$$T_* = C_T \cdot (z-d)^{1/3} \cdot [f(\zeta)]^{-1/2} \tag{4.5}$$

where C_T is determined from measurements of C_n^2 and from T and P (Eq. (4.2) or (4.3) or equivalent), measurement height z (m) and the zero-plane displacement d (m) where $\zeta = \frac{z-d}{L}$ is the argument of the MOST semi-empirical and dimensionless function $f(\zeta)$ where L is the Obukhov stability length

$$L = \frac{T}{k\,g}\frac{\rho c_p u_*^3}{H} \text{ or equivalently } L = -\frac{T}{k\,g}\frac{u_*^2}{T_*} \tag{4.6}$$

where k is the von Kármán constant (0.41), g the acceleration of gravity (m s^{-2}), ρ the density of air (kg m^{-3}) and c_p the specific heat capacity of air at constant pressure (J kg^{-1} K^{-1}). Also from MOST,

$$u_* = \varepsilon^{1/3} \cdot [k \cdot (z-d)]^{1/3} \cdot [g(\zeta)]^{-1/3} \tag{4.7}$$

where ε is obtained using Eq. (4.4) from ν and l_o, the latter estimated from measurements of B_{12}, B_1 and B_2, and where $g(\zeta)$ is the second MOST empirical and dimensionless function.

Different forms of the MOST functions $f(\zeta)$ and/or $g(\zeta)$ have been used by various authors (for example Wyngaard et al., 1971; Wesely, 1976b; Andreas, 1988; Hill et al., 1992; Thiermann and Grassl, 1992; de Bruin et al., 1993) and the functions have different forms for stable ($\zeta \geq 0$) and unstable ($\zeta < 0$) conditions (Table 4.1). These functions allow T_* and u_* to be estimated (Eqs (4.5) and (4.7) respectively) from which H is then determined using

$$H = -\rho c_p u_* T_* . \tag{4.8}$$

Measurements of C_n^2 and ε and use of the MOST functions $f(\zeta)$ and $g(\zeta)$ respectively, allow T_* and u_* to be determined by iteratively varying L (Eq. 4.6) obtained by combining Eqs (4.5) and (4.7). Sensible heat flux $H = H_{SLS}$ is then calculated using Eq. (4.8). These calculations also require knowledge of T, P, z, and d (Eqs (4.2) to (4.7)). The shortened form of the energy balance is then used to determine LE (Eq. (4.1)). The iterative procedure is discussed in an Appendix to the thesis.

In summary, SLS measurements allow for the determination of H_{SLS} using MOST, relying on the determination of the structure parameter for refractive index fluctuations C_n^2 from which T_* is estimated and from measurements of the inner scale of refractive index fluctuations l_o from which u_* is calculated. This is in contrast with large aperture scintillometers that allow determination of C_n^2 with u_* estimated from additional horizontal wind speed or EC measurements.

4.4 Materials and methods

4.4.1 Site details

Surface-layer scintillometer measurements were conducted from January 2003 to June 2005 above an open, mesic grassland and summer rainfall site in the Hay Paddock area neighbouring Ashburton and close to the suburb of Bellevue of Pietermaritzburg, South Africa (29°38'S, 30°26'E) with an altitude of 671.3 m (Fig. 4.1a). The long-term annual rainfall for Pietermaritzburg (South African Weather Service data) is 928 mm (58 years of data) and the mean daily minimum and maximum air temperatures are 12.3 and 24.8 ^{o}C respectively. During winter, there is frequent dewfall but frost hardly ever occurs. Management practices at the research site include mowing (normally in April each year) and burning (in August when firebreaks are established, and in October). Due to the low rainfall in 2004, no burning was carried out prior to November 2004.

The average slope of the study site was 1^{o} 15' to the SE. The minimum fetch distance for the site in the prevailing SE wind direction was 135 m for the EC system and 90 and 138 m for the SLS transmitter and receiver respectively (Fig. 4.1b). The minimum fetch for the occasional winds from the NW was 80 m for the EC system and 122 and 50 m for the SLS transmitter and SLS receiver respectively. Beyond these distances and to the south and SW, the site was exposed and the slope increased. The site adjacent to the mesic grassland site used had similar vegetation with the occasional *Acacia* tree. To the NW of the study area, there was a residential area and tall trees (Fig. 4.1b). The SLS and EC measurements were performed over a period of 30 months except for when there was data memory loss, SLS beam misalignments, SLS beam saturation problems, mist, site management

operations (– burning and mowing), rainfall, power problems, interruptions due to an accidental fire, accidental cutting of cables and finally theft of the SLS transmitter. The BREB measurements commenced in December 2003 and continued for seven months except for periods when there were data interruptions mainly due to humidity sensor problems and condensation in the hoses.

4.4.2 Instrumentation details

For comparison purposes, different measurement systems were used for measuring H (Fig. 4.1b): SLS, BREB and EC systems including an energy balance (EB) system for the measurement of R_{net} and S using Q*7 and HFT-3 sensors respectively (REBS, Seattle, Washington, USA) for determining evaporation as a residual of the energy balance (Eq. (4.1)). The three net radiometers used were calibrated against a known infrared irradiance using a heated plate to minimise net irradiance measurement error and standardise the R_{net} measurements. Other measurements were provided by an automatic weather station system. The averaging periods used in the field for the various measurement systems varied but subsequent to field data collection, the data were recomputed to yield 20-min estimates of the energy balance components, apart from the BREB 20-min estimates which already contained 20-min estimates of H.

A BREB system, modified after the 023A system of Campbell Scientific Inc. (Logan, Utah, USA) with sensors connected to a Campbell 21X datalogger operating at 1 Hz, was used to measure air temperature and water vapour pressure profile differences between heights of 1.55 and 2.96 m above the soil surface. A single HMP45C Vaisala air temperature and relative humidity sensor was sealed in a chamber with air drawn into the chamber from one of the two heights every 2 min past the sensor and then vented to the atmosphere. Every 1 s, for the last 80 s of each 2-min period for each height in turn, the airstream atmospheric water vapour pressure was calculated from the air temperature measured using a type-E thermocouple in close proximity to the humidity sensor and from the HMP45C relative humidity measurement. On occasion, the water vapour pressure estimates were confirmed with measurements from a cooled dewpoint mirror (Dew10, General Eastern Corp., Watertown, Massachusetts, USA). The air temperature difference between the two heights was measured using a pair of naturally-ventilated, unshielded and parallel fine-wire 75-μm type-E thermocouples, one at each height. These air temperature differences were confirmed with measurements from another pair of fine-wire thermocouples located about 10 meters away (Fig. 4.1b).

Over the 30-month period, three different EC systems were used. Initially, for a few months, a one-dimensional sonic anemometer (path length of 100 mm) and a fine-wire (12.5 μm) thermocouple (Campbell model CA-27) connected to a 21X datalogger operating at 10 Hz were used to obtain real-time covariances between vertical wind speed and air temperature. In February 2004, this EC system was replaced by a three-dimensional sonic anemometer (model SWS-211/3V and digital to analogue converter SA-4, Applied Technologies, Boulder, Colorado, USA – path length of 100 mm) and connected to a Campbell 23X datalogger operating at 10 Hz. The EC systems were maintained at a height of 1.5 m above the soil surface and 2.12 m in summer. Sonic temperature corrections for humidity were performed. Real-time covariances between vertical wind speed and corrected sonic temperature were stored in the memory of the datalogger. The lack of online processing using a computer at the field site was due to security issues which also prevented storage of high frequency sonic anemometer data. In April 2004, a second three-dimensional sonic anemometer (RM Young ultrasonic, model 81000, Traverse City, Michigan, USA – path length of 150 mm) was added with

both sonics connected to a Campbell CR5000 datalogger. The ultrasonic anemometer data were also sampled at a frequency of 10 Hz (average of two measurements every 10 Hz) and data processed online in the datalogger and stored on a PC card, together with the high frequency data, for further analysis. Post-data collection corrections applied to the 10-Hz EC data were similar to those of Oncley et al. (2007) and included an averaging coordinate rotation procedure (Kaimal and Finnigan, 1994) to remove the effects of instrument tilt and air flow irregularities. Other EC corrections for this system included wake and crosswind corrections. Detrending or filtering the data was not applied since this is ineffective in reducing non-stationarity (Cava et al., 2008) and not appropriate since it acts as a high-pass filter (Finnigan et al., 2003; Mauder et al., 2007). The common physical "constants" used for calculating H make a difference (Savage et al., 1997; Mauder et al., 2007) and therefore the same "constants" (temperature- and humidity-dependent) were used for the SLS, BREB and EC methods for each time period.

The choice of an averaging period of 20 min for data from the different measurement systems, particularly for the EC measurements, was arrived at by performing an ensemble block time-averaging procedure (Finnigan et al., 2003; Sun et al., 2006) that involved obtaining coordinate-rotated H_{EC} values for 2, 20 and 60 min averaging periods. These estimates were then used to obtain a relative flux ratio by normalising all H_{EC} estimates with that for the 60-min period. The results of this analysis for the period 19th April to 25th May 2004, data not shown, confirm the adequacy of the 20-min H_{EC} data – a linear regression analysis of $H_{EC\ (3\ x\ 20\ min)}$ (y-axis) and $H_{EC\ (1\ h)}$ (x-axis) yielded a slope of 0.9716, y-intercept of -1.1 W m^{-2} and r^2 = 0.9782 for n = 579.

To further check the quality of the EC data, 20-min measurements of H_{EC} during periods of the latter half of 2004 were compared for the two makes of 3-D sonic anemometers placed a few meters apart: slope of 1.0142 (slope SE = 0.0017), r^2 = 0.9646, root mean square error (*RMSE*) of 16.7 W m^{-2} and n = 12993. Furthermore, the RM Young three-dimensional sonic anemometer model used showed good agreement with an independent reference system for estimates of H_{EC} (Mauder et al., 2007). Their finding and the empirical confirmation above ensure the correctness of our H_{EC} measurements, obtained by averaging measurements from all 3-D sonics.

4.4.3 Surface-layer scintillometer

A dual-beam surface-layer scintillometer (model SLS40-A, Scintec Atmospärenmessetechnik, Tübingen, Germany), referred to as the SLS system, was used to measure H_{SLS} every 2 min (Thiermann and Grassl, 1992). As mentioned previously, post-data collection, a recomputation of the data was performed to yield 20-min estimates of H_{SLS}. A beam path length of 101 m (Fig. 4.1b) for the duration of the study was used except for January 2003 when the path length was 50 m. The scintillometer beam was positioned at a height of between 1.5 and 1.65 m above the soil surface for the duration of the study except for a period when changes in beam height on H_{SLS} were investigated.

The beam height was referenced to $d + z_o$ where d is the zero-plane displacement and z_o the roughness length. Using the neutral wind profile equation, this height was assumed to be $d + z_o$ where $d \approx 0.67h$ and $z_o \approx 0.1h$ (Brutsaert, 1982; Mölder, 1997). Canopy height for the duration of the study is shown in Fig. 4.2. Vegetation height, averaged over the beam path length, varied seasonally but was always less than 1.13 m. Canopy height was measured at various times during the study and on each occasion was measured every 5 m of the direct line between transmitter and receiver. These heights

were weighted according to a path-weighting function used for the log-amplitude variances (Thiermann and Grassl, 1992) which was then normalised so as to have an area under the curve of 1. Of note is that the weighting process favours effective beam heights midway between the transmitter and receiver units with vegetation height near the transmitter and receiver carrying little weight.

The SLS measurements were not possible if condensation or mist affected the passage of the laser beam through the boundary layer, particularly during the night-time. Also, cobwebs or dirt covering the SLS windows reduce the voltage signal. Cleaning was achieved using a cotton bud to remove the cobwebs and distilled water to remove dirt on the window. High wind or rain may affect SLS alignment. Rain events loosen the soil with the result that the tripod stands may move their positions.

Saturation of the voltage signals, which results in low measured voltages under conditions of strong turbulence (Gracheva et al., 1974), invalidate the assumption of weak scattering (Lawrence and Strohbehn, 1970) upon which the SLS method depends. The manufacturer recommends that should saturation occur frequently, then the effective beam height should be increased and/or the beam path length decreased. In the unlikely event that following these procedures the voltage signals are still too low, then the voltage range setting needs to be altered. Signal saturation generally resulted in smaller than expected B_{12} estimates and therefore smaller than expected r (signal correlation coefficient) values, smaller l_o values, greater ε values and finally greater than expected H_{SLS} magnitudes. A cut-off of l_o = 2 mm is recommended for path lengths of 100 m or greater (Scintec, 2006) and therefore H_{SLS} values corresponding to l_o < 2 mm were excluded.

The percent of "acceptable" 2-min H_{SLS} measurements for the day-time hours (taken as 06h00 to 18h00) showed little seasonal variation and was consistently high – between 86.7 % and 94.8 % for the period Jan 2003 to August 2004 used for analysis (data not shown).

4.4.4 Estimation of latent energy flux

The latent energy flux LE is calculated as a residual using the energy balance from measurements of R_{net}, S and H_{SLS} (or H_{EC}) using the shortened form of the surface energy balance (Eq. (4.1)). Soil heat flux , during the day-time, is often the smallest term in magnitude. However, for time scales of less than a day, the importance of S cannot be ignored especially for short vegetation such as grassland.

Net irradiance was measured using three collocated net radiometers placed 2 m above the soil surface. The procedures for estimating soil heat flux estimates were similar to those recommended by Liebethal et al. (2005). Estimates were obtained from the average of measurements of soil heat flux $\overline{F_{plate}}$ (W m^{-2}) at a depth of 80 mm (using five soil heat flux plates) and the average stored heat flux $\overline{F_{stored}}$ (W m^{-2}) above the plates:

$$\overline{S} = \overline{F_{plate}} + \overline{F_{stored}} \,. \tag{4.9}$$

The stored heat flux $\overline{F_{stored}}$ was estimated from measurements of the average soil temperature difference (between 20 and 60 mm) from one period to another, the depth of soil, and the volumetric soil water content assuming a dry-soil specific heat capacity of 837 J kg^{-1} ^{o}C^{-1} and a soil bulk density of 1200 kg m^{-3}. Five sets of type-E averaging thermocouples were used for the soil temperature

measurements. A Campbell CR7X data logger was used for these measurements for much of 2003 and after the accidental fire a Campbell 23X data logger, including measurements of the volumetric soil water content in the first 50 mm of the surface using a frequency domain reflectometer (ThetaProbe, model ML2x, Delta-T Devices, Cambridge, UK) and a Campbell CS615 soil reflectometer.

4.5 Results and discussion

4.5.1 MOST analysis

For the SLS method, the estimation of sensible heat flux H using Eq. (4.8) is based on MOST which requires the use of semi-empirical formulations $f(\zeta)$ for the estimation of the temperature scale of turbulence T_* (Eq. (4.5)) and $g(\zeta)$ for the estimate of friction velocity u_* (Eq. (4.7)). Various methods of MOST for estimating H for unstable and stable conditions were investigated (Table 4.1): Wyngaard et al. (1971), Wesely (1976b), Andreas (1988), Hill et al. (1992) [derived from a refitting of the Wyngaard et al. (1971) MOST function coefficients], Thiermann (1990) and Thiermann and Grassl (1992), de Bruin et al. (1993), Edson and Fairall (1998) and Frederickson et al. (2000). Using an iterative procedure, H, denoted H_{SLS} in this case, was obtained using Eqs (4.2) to (4.8) using SLS measurements of ε and C_n^2 and the Thiermann and Grassl (1992) form for $f(\zeta)$ and $g(\zeta)$ (Table 4.1). In some cases only $f(\zeta)$ was available from published works and not $g(\zeta)$ (Table 4.1) – in such cases, the $g(\zeta)$ function of Thiermann and Grassl (1992) was used. Comparisons were made between H_{SLS} and between H estimated, using the various MOST functions listed in Table 4.1 using the same ε and C_n^2 SLS measurements, and comparisons also made with the EC measurements of H (H_{EC}). The MOST measurement comparisons using the SLS measurements were performed for each month and typical results are shown for January 2004 in Fig. 4.3 for unstable conditions and in Fig. 4.4 for stable conditions. Clearly, there are large differences in H for both unstable and stable conditions between the different MOST methods. While it may be possible to analytically calculate, using Eqs (4.5), (4.7) and (4.8), the relative differences and differences between H_{SLS} obtained using the Thiermann and Grassl (1992) MOST functions and H using any other MOST functions without any measurements of C_n^2 and ε, the plots shown in Figs 4.3 and 4.4 give more information: the plots show the actual variation of differences and relative differences in 20-min estimates of H from measurements of C_n^2 and ε as a function of ζ corresponding to a wide range of actual field stability conditions experienced at the site.

In particular for unstable conditions, the percent differences $100\times(H - H_{SLS})/H_{SLS}$ range between -30 % and 28 % depending on the method used (Fig. 4.3g). The curves of Figs 4.3g and 4.4e, using measurements of C_n^2 and ε, represent a comparison between the different MOST empirical stability functions and their effect on H: the stability function used for the particular MOST method to estimate H is represented on the x-axis via $-\zeta$ or ζ respectively, and the other functions on the y-axis via the percent relative difference in H for the particular MOST method, compared to H_{SLS}. For unstable conditions, the difference $H - H_{SLS}$ for the various MOST methods is within 60 W m^{-2} for the Hill et al. (1992) formulation (Fig. 4.3d). The maximum difference for the Wyngaard et al. (1971) (Fig. 4.3a) and de Bruin et al. (1993) (Fig. 4.3e) formulations is about 100 W m^{-2}, about 125 W m^{-2} for the Wesely (1976b) (Fig. 4.3b) and about 40 W m^{-2} for the Edson and Fairall (1998) (Fig. 4.3f) formulations. The Edson and Fairall (1998) formulation produced the lowest percent relative difference for neutral and convectively unstable conditions (Fig. 4.3g). Even slight changes in the constants used in the $f(\zeta)$ function may cause significant percent difference relative to H_{SLS} – for

example, just changing $f(\zeta) = 4.9(1-7\zeta)^{-2/3}$ as used by Wyngaard (1973) to $f(\zeta) = 4.9(1-6.1\zeta)^{-2/3}$ as used by Andreas (1988) to account for a change in k from 0.35 to 0.4 shows significant differences for $-\zeta > 0.1$ (Fig. 4.3g).

For the stable case, the percent relative difference for the various MOST methods (Table 4.1, stable case) increased significantly towards and within the stable sporadic region (Fig. 4.4e) since in this region the H_{SLS} values were small in magnitude. For stable continuous conditions, the differences in H were within 60 W m^{-2} with much larger differences for stable sporadic conditions. The differences between the Wyngaard et al. (1971), Wyngaard (1973) and Andreas (1988) MOST methods were very small. The Frederickson et al. (2000) MOST method produced the lowest percent relative differences for all stable conditions (Figs 4.4d, e).

For both summer (typically January) and winter (July) and day-time (mainly unstable), the MOST function used by Thiermann and Grassl (1992) resulted in H_{SLS} estimates that are in good agreement with H_{EC} (Table 4.2) with the lowest mean absolute difference (*MAD*), root mean square difference (*RMSD*) and slope values for the H_{EC} (x) *vs* H_{SLS} (y) comparisons closer to 1 compared to the other MOST methods. For stable (mainly night-time) conditions, *MAD* for the SLS method was the smallest but there was a large variation in the slope of the H_{EC} *vs* H_{SLS} relationship. The agreement between H_{SLS} and H_{EC}, particularly for unstable conditions, justified the continued use of the Thiermann and Grassl (1992) MOST functions used by the SLS method. For January all MOST methods overestimated H for unstable conditions compared to H_{EC} (negative $H_{SLS} - H_{EC}$, both fluxes negative for unstable conditions). This was usually the case for July (Table 4.2), and the other months analysed (data not shown).

4.5.2 Error analysis for SLS sensible heat

Aside from investigating the errors associated with the use of a particular form of the MOST semi-empirical functions $f(\zeta)$ and $g(\zeta)$, a sensitivity analysis was conducted to determine the relative importance of the data input errors in determining H_{SLS}. Errors in the input data affect the real-time measurements displayed and these inputs would also affect post-data recalculations. For the purposes of the sensitivity analysis calculations, data for 23rd February 2003, a relatively cloudless day, were used.

Each of the four data inputs of air temperature, atmospheric pressure, beam path length and beam height were varied from below to above a "normal" value. The following were used for the normal values:

measured air temperature $T_{correct}$, for each averaging period. The air temperature $T_{correct}$ was calculated from the average of all available measurements of air temperature;

the estimated atmospheric pressure $P_{correct}$ based on the measured air temperature, altitude and the measured water vapour pressure;

the measured beam path length $L_{beam\ correct}$ of 101 m;

the beam height $h_{beam\ correct}$ above $d + z_o$, estimated as 1.04 m for example, using:

$$h_{beam\,correct} = z_{beam} - 0.77h \tag{4.10}$$

using a typical beam height z_{beam} = 1.68 m and h = 0.83 m (Fig. 4.2).

For each data input, a fractional error is calculated. For example, the fractional error associated with beam height, $\varepsilon_{h_{beam}}$, is given by:

$$\varepsilon_{h_{beam}} = (h_{beam} - h_{beam\,correct}) / h_{beam\,correct} \,. \tag{4.11}$$

The effect of each fractional error for the SLS method, corresponding to errors in T_{air}, P, L_{beam} and h_{beam} on H was calculated and converted into a fractional error based on the actual H_{SLS} for each period. From the collected data with at worst $\varepsilon_{L_{beam}}$ varying between -0.02 and 0.02, $\varepsilon_{H\,L_{beam}}$ varied between -0.030 and 0.030 (Fig. 4.5).

The overall fractional error in H_{SLS} was then calculated using:

$$\varepsilon_H = \sqrt{\varepsilon_{H\,T_{air}}^2 + \varepsilon_{H\,P}^2 + \varepsilon_{H\,L_{beam}}^2 + \varepsilon_{H\,h_{beam}}^2} \tag{4.12}$$

with worst-case values ∓ 0.01 for $\varepsilon_{H\,T_{air}}$, ± 0.013 for $\varepsilon_{H\,P}$, ∓ 0.030 for $\varepsilon_{H\,L_{beam}}$ and ± 0.040 for $\varepsilon_{H\,h_{beam}}$. Overall, therefore, the worst-case total error $\varepsilon_H = \pm 0.053$ with typical fractional errors in H_{SLS} due to input errors amounting to ± 0.039.

4.5.3 Energy balance measurements and evaporation comparisons

Evaporation was estimated from H obtained using the SLS and EC methods and measurements of R_{net} and S (Eq. (4.1)). The BREB measurements provided important additional comparisons. The agreement between LE_{SLS}, LE_{BR} and LE_{EC} estimates of evaporation is generally good (Fig. 4.6, 2004 data). Typical days chosen for the comparison range from almost completely cloudless (Fig. 4.6b, e) to cloudless for part of the day (Fig. 4.6a, c, f) and a day with variable cloud (Fig. 4.6d). The SLS measurements are more smooth than the LE_{BR} and LE_{EC} measurements due to the path-weighting nature of the SLS measurements compared to the point measurements for EC and BREB, although measurements from the latter two methods do also have areal representation (Schmid and Oke, 1990; Stannard, 1997). On some days, the agreement between the methods is much better than on others. There were periods, infrequent, when the SLS method was unable to yield sufficiently accurate H_{SLS} or there was loss of data due to the condition that l_o should be greater than 2 mm. There were also periods when LE_{EC} was significantly greater than LE_{SLS} or LE_{BR} (e.g., Fig. 4.6a, d, e, f) particularly in the early morning hours. This is also evident in Fig. 4.7 (lower panel graphs, 2004 data). In some cases, LE_{EC} showed excursions from positive values (condensation) to sudden negative values (e.g., Fig. 4.6f). During this period, the standard deviation of the sonic temperature and the vertical wind speed was much larger than expected (data not shown). Wind direction shifts in the morning times occurred more frequently than for the afternoon times. For example on 17th March in Fig. 4.6e, the direction varied from being parallel to perpendicular to the beam from one measurement period to the next. These direction shifts seemed to affect LE_{EC} but not LE_{SLS}. High wind speed did not seem to play an obvious role in these comparisons with 8th January (Fig. 4.6b) experiencing horizontal wind speeds in excess of 4.3 m s^{-1} with good comparisons between the different methods. This was not the case for

low wind speeds: on the 21st March (Fig. 4.6f) low wind speeds were experienced, corresponding to less atmospheric mixing, and the *LE* agreement was significantly worse.

There is much literature establishing the robustness of the BREB method for estimating evaporation at a sub-hourly scale. There have however been few studies comparing LE_{SLS} with LE_{BR} or indeed LE_{EC} with LE_{BR} and even fewer that make such comparisons for extended periods of time. For these comparisons, all of the *H* data shown in Figs 4.6 and 4.7 for each method were included in an extended set of data and standard linear regression analyses performed.

There is good agreement between 20-min LE_{SLS} and LE_{EC} estimates (Fig. 4.8a) and also between LE_{BR} and LE_{EC} (Fig. 4.8b). The data covers the period for which the BREB equipment was available – the first seven months of 2004. Overall for this period which encompassed a wide range of weather and stability conditions, the SLS method fared better than the BREB method when both were compared with the EC method as indicated by a reduced mean square error, and r^2 and slope values closer to 1. We have therefore shown that H_{SLS} used together with R_{net} and *S* and the shortened energy balance equation to estimate LE_{SLS} compares very well with LE_{EC} and by inference from Fig. 4.8b with LE_{BR}.

It is recognised here that common variable, namely R_{net} and *S*, are used in both *x* and *y* data in these plots. This criticism could be avoided throu8gh the use of independent measurements of R_{net} and *S* used to determine LE_{SLS}, LE_{BR} and LE_{EC}. The independent measurements of R_{net} and *S* would, presumably, be highly correlated.

The other observation from the data of Figs 4.7 to 4.8 concerns the use of empirical MOST relationships (SLS method, listed in Table 4.1) and other methods that do not directly invoke MOST (BREB and EC methods). For the BREB method, however, a reviewer pointed out that at least the Reynolds analogy is necessary. Also, with the assumption that the exchange coefficients for H_{BR} and LE_{BR} are equal, stability dependence of the BREB method is removed. This is true only when the gradients and fluxes are in local equilibrium, circumstances for which MOST is valid. For this mesic grassland site, the good agreement between H_{SLS} and with H_{BR} and H_{EC} illustrate the applicability of MOST as applied to the SLS method for a range of canopy heights, stability conditions and diurnal and seasonal weather conditions. This further reinforces the robustness of the SLS method for estimating *H*.

For days with the Bowen ratio $\beta > 1$ (Fig. 4.7a), the agreement between LE_{SLS} and LE_{EC} appears as good for days with $\beta < 1$ (Fig. 4.7b) in spite of the neglect of the humidity fluctuations on C_T^2 (Eq. (4.2) or (4.3)), as suggested by Moene (2003), even when β is significantly less than 1. These comparisons demonstrate that the SLS method can be used with confidence for the estimation of evaporation.

The top panes of Fig. 4.7 show the diurnal variation in ζ and the footprint peak x_{peak} (m). The range of day-time stability conditions cover neutral, unstable and convectively unstable conditions for which the sensible heat comparisons are in good agreement. The footprint peak positions x_{peak} from the centre of the SLS beam, calculated using an Eulerian-Lagrangian approach (Hsieh et al., 2000) range from a few metres for convectively unstable conditions to a few tens of metres for neutral conditions.

The SLS footprint has a greater source area than the BREB and EC footprints but for this site, the vegetation was reasonably uniform near the centre of the beam. The SLS beam centre has the greatest weighting for the H_{SLS} measurements.

The debate on a possible lack of energy balance closure (Stannard et al., 1994; Anthoni et al., 1999; Wilson et al., 2002; Foken et al., 2006), viz., that $-(H_{EC} + LE_{EC}) < R_{net} + S$, where LE_{EC} is independently measured from the covariance between the vertical wind speed and water vapour concentration, deserves comment. We have shown that there is good agreement between H_{SLS} *vs* H_{EC} and H_{BR} *vs* H_{EC} (the former also demonstrated by the data of Table 4.2). Therefore, if there is any underestimation in the magnitude of either H_{EC} or the directly-measured LE_{EC}, this could be due to the underestimation in the LE_{EC} magnitude – for if not we would have found significant underestimation in H_{EC} compared to H_{SLS} or compared to H_{BR}. Alternatively, the lack of closure could be due to energy fluxes not included in the shortened energy balance. This finding assumes that the R_{net} and S measurements are not the cause for a lack of closure. A reviewer could not follow the argument, based on the demonstrated good agreement between H_{SLS}, H_{BR} and H_{EC}, which excludes a possible underestimation in H_{SLS}. The reviewer suggests that a possible underestimation is not a difficulty of MOST but it could also be a difficulty of the EC method which assumes that all parts of the turbulent fluxes are observable during the measurement period. We used differing averaging periods – 2, 20 and 60 min – for the EC data to demonstrate that this was not the case for our 10-Hz EC data apart from periods less than 10 min (data not shown; Odhiambo and Savage, 2009). However, while the EC method does not directly depend on MOST for estimating H_{EC}, the form of the empirical MOST functions $f(\zeta)$ and $g(\zeta)$ were determined based on direct comparisons of H_{EC} with the MOST-determined H using the SLS method (Thiermann, 1990). Since the H_{EC} estimates were obtained for an unknown energy balance closure condition, Kohsiek et al. (2002) suggests that the EC method is non-standard! Furthermore, as pointed out by Andreas et al. (2003), SLS flux estimates use similarity functions derived from long averaging periods, claiming that there is no evidence that MOST is also valid for 1- to 10-min laser scintillometer fluxes. More importantly though as far as the present study is concerned is that strictly, the EC and SLS methods are not independent – their dependence is due to the fact that the MOST functions used with the SLS method were developed with the use of EC data and then using stability functions derived from long-averaging periods. This would apply to any method that uses MOST for which the semi-empirical MOST functions derived were based on EC measurements.

4.5.4 Error analysis for estimated evaporation

Since LE is estimated from R_{net}, H and S (Eq. (4.1)), the error in R_{net} and S measurements needs to be considered. The fractional errors in R_{net} and S are due to calibration errors and errors associated with field measurements, including the influence of spatial variation differences. It is assumed that the R_{net} errors due to dirt or damaged domes or levelling are negligible (Payero et al., 2003). While the errors associated with calibration are known at the time when calibration is performed against an accurate and standard reference or method for R_{net} or S, the error may change with time after calibration in an unknown fashion. Furthermore, the errors associated with field measurement of S are dependent on the measurement errors associated with a change in soil temperature (for the 20 to 60 mm depth) from one measurement period to another, the errors in measuring the placement depths and the consequence of this error as it affects the measured soil temperature, the error in measuring the soil heat flux at the plate placement depth and the error in the measurement of the soil water content. The spatial

variability in S is affected by soil and vegetation cover variability and varies as canopy height changes seasonally. To obtain a more reliable spatial average, many measurements over a larger area, typically several tens of square metres, of soil heat flux at plate depth and many measurements of soil temperature would be required. Compared to S measurements, R_{net} measurements represent a much larger area, and are therefore more spatially representative.

Angus and Watts (1984) used the following for error in R_{net} and S measurements:

$$\sigma_{R_{net}} = \pm 0.025 R_{net} \tag{4.13}$$

and

$$\sigma_S = \pm 0.2 S \,. \tag{4.14}$$

In the latter case, they included a calibration error of 5 % for the soil heat flux plates. The overall error of 20 % of S was used to take into account spatial variability and sampling problems inherent with these soil sensors, as well as errors in the determination of stored heat energy from the change in soil temperature, the soil bulk and the soil specific heat capacity. Other workers, for example Ham and Heilman (2003) working in a forest site, give typical errors for $R_{net} + S$ as 5 to 10 % compared to within 4 % using the Angus and Watts (1984) β-independent calculation. Based on 20-min R_{net} measurements for the first 200 days of 2004 using the three net radiometers, $\sigma_{R_{net}} / R_{net}$ averaged 0.026, close to the value of 0.025 used by Angus and Watts (1984), increasing from less than 0.01 in summer to less than 0.06 in winter. The gradual increase in $\sigma_{R_{net}} / R_{net}$ towards winter is partly due to the reduction in R_{net} as winter approaches (from a daily R_{net} of close to 20 MJ m^{-2} in summer to around 5 MJ m^{-2} in winter). Decreased cloudiness and increased patchiness in the vegetation in winter also contributed to the increase in $\sigma_{R_{net}} / R_{net}$ to 0.06. Using five independent measurements of S for our mesic grassland site, for day-time periods when 20-min measurements of S exceeded 35 W m^{-2} in magnitude, σ_S / S varied between 0.10 and 0.50. Weighting σ_S / S for R_{net} resulted in daily averaged values of between 0.05 and 0.27 with an average of 0.203 (for the period February to April 2003) compared to the value of 0.2 used by Angus and Watts (1984) (Eq. (4.14)).

In the case of the SLS method, the estimation of evaporation is based on H_{SLS} and the other energy balance components. Besides errors in the input data affecting H_{SLS} and errors due to the use of the MOST empirical functions or errors due to the inappropriateness of MOST, the estimation of LE using Eq. (4.1) using H_{SLS}, results in additional errors. Based on the results of Section 4.2 for the error in H_{SLS}, the final overall worst-case standard deviation in LE measurement to LE ratio is given by:

$$\frac{\sigma_{LE}}{LE} = \sqrt{\frac{(0.025 R_{net})^2 + (0.2S)^2 + (0.053 H_{SLS})^2}{LE^2}} \,. \tag{4.15}$$

Combining the first two terms of Eq. (4.15) by assuming that $S \approx 0.05 R_{net}$ for daytime and fairly dry conditions, Angus and Watts (1984) reduced the first two terms inside the square root to $0.037^2 \cdot (1+\beta)^2$. Hence:

$$100 \cdot \sigma_{LE} / LE = (13.69 + 27.38\beta + 41.78\beta^2)^{1/2} \,. \tag{4.16}$$

This relationship demonstrates the point that as conditions become drier, corresponding to increasing β, $100 \cdot \sigma_{LE} / LE$ increases almost linearly in β with the last term on the right hand side dominating. The absolute error σ_{LE} does not vary much for β between 0 and 2 and is typically 20 W m^{-2} for $H + LE$ = 500 W m^{-2} and typically 8 W m^{-2} for $H + LE$ = 200 W m^{-2}.

The component worst-case error terms of the energy balance are shown in Fig. 4.9 for two cloudless days, one in summer (Fig. 4.9a) and one in winter (Fig. 4.9b). The diurnal variation of the error terms occurs since, for example, σ_{LE} depends on $\sigma_{R_{net}}$, σ_H and σ_S which in turn depend on R_{net}, H and S respectively, with each of R_{net}, H and S having a diurnal variation. Also of particular note, is that while the overall standard deviation in LE is similar for the two days, the component error values are different. The values for σ_H and $\sigma_{R_{net}}$ are greater in summer. However, as mentioned previously, due to the greater amount of plant material covering the soil in summer, σ_S values are smaller in summer (Fig. 4.9a) than in winter (Fig. 4.9b). In brackets in the upper left legend of Fig. 4.9 is the daily evaporation equivalent for each error component calculated by summing the error values for the 06h00 to 18h00 period and converting them to mm units.

The seasonal variation in LE for selected mainly cloudless days is shown in Fig. 4.10 (bottom). The evaporation totals shown in Fig. 4.10 (bottom) are calculated from the SLS total for the period 06h00 and 18h00. The seasonal variation in daily σ_{LE} in mm, shown in Fig. 4.10 (middle), was typically 0.2 mm (0.49 MJ m^{-2}) in winter when the daily evaporation was around 1 mm (2.45 MJ m^{-2}) and typically 0.4 mm (0.98 MJ m^{-2}) when daily evaporation exceeded 4 mm (9.8 MJ m^{-2}) in summer. The coefficient of variation in LE, expressed as a fraction (Fig. 4.10, top), is therefore typically 0.25 in winter and a minimum of 0.05 in summer. This confirms the result using Eq. (4.16) that greater errors occur for drier conditions. The contribution of error in S in the overall energy balance may dominate, particularly in winter.

4.6 Conclusions

A MOST analysis using various empirical functions and surface-layer scintillometer (SLS) measurements demonstrated a large variation in the estimated sensible heat flux H (a relative error from -30 to 28 % for unstable conditions for the various functions used). The relative error in sensible heat H for stable conditions for the various empirical functions was much greater, particularly for stability approaching stable continuous and stable sporadic stability conditions. The MOST empirical functions used with the SLS method resulted in the smallest root mean square difference relative to eddy covariance measurements H_{EC}. The H_{SLS} estimates were in good long-term agreement with H_{BR} (Bowen ratio) and H_{EC}. The implication of these findings in terms of energy balance closure is that there appears to be no underestimation in H_{EC} compared to H_{SLS} and H_{BR} measurements. The good agreement between the various estimates of H resulted in good agreements between LE_{SLS}, LE_{BR} and LE_{EC} estimated by application of the shortened energy balance.

The estimate of $d + z_o$ has the largest influence on H_{SLS}, and therefore on LE_{SLS}, apart from the errors in net irradiance R_{net} and soil heat flux S when evaporation LE_{SLS} is calculated as a residual from the shortened energy balance equation. Assuming the applicability of MOST, the worst-case errors in air temperature, atmospheric pressure, beam path length and beam height resulted in fractional errors in H of ∓ 0.01, ± 0.013, ∓ 0.030 and ± 0.040 respectively. The worst-case total fractional error in H_{SLS} is ± 0.053 and the typical fractional error amounted to ± 0.039.

The seasonal variation in the error in LE_{SLS} is generally less than 0.2 mm day^{-1} (equivalent to 0.49 MJ m^{-2}) in winter when the daily evaporation rate was around 1 mm day^{-1} (2.45 MJ m^{-2}) and typically less than 0.4 mm day^{-1} (0.98 MJ m^{-2}) when the evaporation rate generally exceeded 4 mm day^{-1} (9.8 MJ m^{-2}). If R_{net} is measured correctly, then available heat depends on S. If H_{SLS} (or H_{BR}, or H_{EC}) have relatively small errors, then the error in S is important for the estimation of LE as a residual from the shortened energy balance.

In this study, the SLS method has proved to be very useful in obtaining long-term estimates of H, useful as a method for cross-checking against other methods such as EC and BREB and useful in indicating no apparent underestimation in H_{EC} as might be expected if there was a lack of closure of the energy balance.

4.7 Acknowledgements

Funding from the South African Water Research Commission and the contribution of the members of the Steering Committee and the project team is gratefully acknowledged. Additional funding in the latter stages of the project from the National Research Foundation is also gratefully acknowledged. The project was only possible with the cooperation of the following: George Odhiambo, Michael Mengistu, Peter Dovey, Jothi Manickum; the University of KwaZulu-Natal for part-payment of the surface layer scintillometer equipment; owner Mr S.J. Hilcove and farm manager Mr H. Ovenstone and workers of the Bellevue farm site used for this research; Mr Vivek Naiken of the CSIR for assistance with Fig. 4.1. This work benefitted from comments from the anonymous reviewers from Agricultural and Forest Meteorology.

4.8 References

Anandakumar, K., 1999. Sensible heat flux over a wheat canopy: optical scintillometer measurements and surface renewal analysis estimates. Agric. For. Meteorol. 96, 145–156.

Andreas, E.L., 1988. Estimation of C_n^2 over snow and seas ice for meteorological data. J. Opt. Soc. Am. 5, 481–495.

Andreas, E.L., Fairall, C.W., Persson, P.O.G., Guest, P.S., 2003. Probability distributions for the inner scale and the refractive index structure parameter and their implications for flux averaging. J. Appl. Meteorol. 42, 1316–1329.

Angus, D.E., Watts, P.J., 1984. Evapotranspiration: how good is the Bowen ratio method? Agric. Water Mgt 8, 133–150.

Anthoni, P.M., Law, B.E., Unsworth, M.H., 1999. Carbon and water vapor exchange of an open-canopied ponderosa pine ecosystem. Agric. For. Meteorol. 95, 151–168.

Bowen, I.S., 1926. The ratio of heat losses by conduction and by evaporation from any water surface. Phys. Rev. 27, 779–787.

Brutsaert, W.H., 1982. Evaporation into the Atmosphere. Reidel, Dordrecht, Holland, 299 pp.

Castellví, F., 2004. Combining surface renewal analysis and similarity theory: A new approach for estimating sensible heat flux. Water Resour. Res. 40, W05201, doi:10.1029/2003WR002677.

Cava, D., Contini, D., Donateo, A., Martano, P., 2008. Analysis of short-term closure of the surface energy balance above short vegetation. Agric. For. Meteorol. 148, 82–93.

Champagne, F.H., Friehe, C.A., La Rue, J.C., Wyngaard, J.C., 1977. Flux measurements, flux estimation techniques, and fine scale turbulence measurements in the unstable surface layer over land. J. Atmos. Sci. 34, 515–530.

de Bruin, H.A.R., Kohsiek, W., van den Hurk, B.J.J.M., 1993. A verification of some methods to determine the fluxes of momentum, sensible heat, and water vapour using standard deviation and structure parameter of scalar meteorological quantities. Boundary-Layer Meteorol. 63, 231–257.

de Bruin, H.A.R., Meijninger, W.M.L., Smedman, A.S., Magnusson, M., 2002. Displaced-beam small aperture scintillometer test. Part I: the WINTEX data-set. Boundary-Layer Meteorol. 105, 129–148.

Drexler, J.Z., Snyder, R.L., Spano, D., Paw U, K.T., 2004. A review of models and micrometeorological methods used to estimate wetland evapotranspiration. Hydro. Proc. 18, 2071–2101.

Edson, J.B., Fairall, C.W., 1998. Similarity relationships in the marine atmospheric surface layer for terms in the TKE and scalar variance budgets. J. Atmos. Sci. 55, 2311–2328.

Eichinger, W.E., Holder, H.E., Cooper, D.I., Hipps, L.E., Knight, R., Kustas, W.P., Nichols, J., Prueger, J.H., 2006. Lidar measurement of boundary layer evolution to determine sensible heat fluxes. J. Hydrometeorol. 6, 840–853.

Finnigan, J.J., Clement, R., Malhi, Y., Leuning, R., Cleugh, H.A., 2003. A re-evaluation of long-term flux measurement techniques Part I: averaging and coordinate rotation Boundary-Layer Meteorol. 107, 1–48.

Foken, T., Wimmer, F., Mauder, M., Thomas, C., Liebethal, C., 2006. Some aspects of the energy balance closure problem. Atmos. Chem. Phys. 6, 4395–4402.

Frederickson, P.A., Davidson, K.L., Zeisse, C.R., Bendall, C.S., 2000. Estimating the refractive index structure parameter (Cn2) over the ocean using bulk methods. J. Appl. Meteorol. 39, 1770–1783.

Frenzen, P., Vogel, C.A., 1992. The turbulent kinetic energy budget in the atmospheric surface layer: A review and an experimental reexamination in the field. Boundary-Layer Meteorol. 60, 49–76.

Gracheva, M.E., Gurvich, A.S., Lomadze, S.O., Pokasov, V.I., Khrupin, A.S., 1974. Probability distribution of strong fluctuations of light intensity in the atmosphere. Radiophysics Quantum Electronics 17, 83–87.

Green, A.E., McAneney, K.J., Lagouarde, J.-P., 1997. Sensible heat and momentum flux measurements with an optical inner scale meter. Agric. For. Meteorol. 85, 259–267.

Ham, J.M., Heilman, J.L., 2003. Experimental test of density and energy-balance corrections on carbon dioxide flux as measured using open-path eddy covariance. Agron. J. 95, 1393–1403.

Hartogensis, O.K., de Bruin, H.A.R., van de Wiel, B.J.H., 2002. Displaced-beam small aperture scintillometer test. Part II: CASES-99 stable boundary layer experiment. Boundary-Layer Meteorol. 105, 149–176.

Hill, R.J., Clifford, S.F., 1978. Modified spectrum of atmospheric temperature fluctuations and its application to optical propagation. J. Opt. Soc. Am. 68, 1201–1211.

Hill, R.J., Ochs, G.R., Wilson, J.J., 1992. Measuring surface-layer fluxes of heat and momentum using optical scintillation. Boundary-Layer Meteorol. 58, 391–408.

Hsieh, C-I., Katul, G., Chi, T-W., 2000. An approximate analytical model for footprint estimation of scalar fluxes in thermally stratified atmospheric flows. Adv. Water Resour. 23, 765–772.

Kaimal, J.C., Finnigan, J.J., 1994. Atmospheric Boundary Layer Flows, Their Structure and Measurement. Oxford University Press, New York, 289 pp.

Kohsiek, W., Meijninger, W.M.L., Moene, A.F., Heusinkveld, B.G., Hartogensis, O.K., Hillen, W.C.A.M., de Bruin, H.A.R., 2002. An extra large aperture scintillometer for long range applications. Boundary-Layer Meteorol. 105, 119–127.

Lawrence, R.S., Strohbehn, J.W., 1970. A survey of clear-air propagation effects relevant to optical communications. Proc. IEEE 58, 1523–1545.

Liebethal, C., Huwe, B., Foken, T., 2005. Sensitivity analysis for two ground heat flux calculation approaches. Agric. For. Meteorol. 132, 253–262.

Mauder, M., Oncley, S.P., Vogt, R., Weidinger, T., Ribeiro, L., Bernhofer, C., Foken, T., Kohsiek, W., de Bruin, H.A.R., Liu., H., 2007. The energy balance experiment EBEX-2000. Part II: Intercomparison of eddy-covariance sensors and post-field data processing methods. Boundary-Layer Meteorol. 123, 29–54.

Moene, A.F., 2003. Effects of water vapour on the structure parameter of the refractive index for near-infrared radiation. Boundary-Layer Meteorol. 107, 635–653.

Mölder, M., 1997. Parameterization of exchange processes over a barley field. Boundary-Layer Meteorol. 84, 341–361.

Nakaya, K., Suzuki, C., Kobayashi, T., Ikeda, H., Yasuike, S., 2006. Application of a displaced-beam small aperture scintillometer to a deciduous forest under unstable atmospheric conditions. Agric. For. Meteorol. 136, 45–55.

Odhiambo, G.O., Savage, M.J., 2009. Sensible heat flux by surface layer scintillometry and eddy covariance over a mixed grassland community as affected by Bowen ratio and MOST formulations for unstable conditions. J. Hydrometeorol. 10, 479–492.

Oncley, S.P., Foken, T., Vogt, R., Kohsiek, W., de Bruin, H.A.R., Bernhofer, C., Christen, A., van Gorsel, E., Grantz, D., Feigenwinter, C., Lehner, I., Liebethal, C., Liu, H., Mauder, M., Pitacco, A., Ribeiro, L., Weidinger, T., 2007. The energy balance experiment EBEX-2000. Part I: overview and energy balance. Boundary-Layer Meteorol. 123, 1–28.

Payero, J.O., Neale, C.M.U., Wright, J.L., Allen, R.G., 2003. Guidelines for validating Bowen ratio data. Trans ASCE 46, 1051–1060.

Savage, M.J., 2009. Estimation of evaporation using a dual-beam surface layer scintillometer and component energy balance measurements. Agric. For. Meteorol. 149, 501–517.

Savage, M.J., Everson, C.S., Metelerkamp, B.R., 1997. Evaporation measurement above vegetated surfaces using micrometeorological techniques. South African Water Research Commission Report No. 349/1/97, Pretoria, South Africa, 248 pp., ISBN 1–86845–363–4.

Savage, M.J., Odhiambo, G.O., Mengistu, M.G., Jarmain, C., 2004. Theory and practice of evapotranspiration measurement, with special focus on surface layer scintillometer (SLS) as an operational tool for the estimation of spatially-averaged evaporation. Water Research Commission (WRC) Report No. 1335/1/04. WRC, Pretoria, Republic of South Africa, 204 pp., ISBN 1-77005-247-X.

Schmid, H.P., Oke, T.R., 1990. A model to estimate the source area contributing to turbulent exchange in the surface layer over patchy terrain. Q. J. R. Meteorol. Soc. 116, 965-988.

Schotanus, P., Nieuwstadt, F.T.M., de Bruin, H.A.R., 1983. Temperature measurement with a sonic anemometer and its application to heat and moisture fluctuations. Boundary-Layer Meteorol. 26, 81–93.

Scientific Programming Enterprises, 1999. Plotit for Windows 95/NT, Version 3.20k. Haslett, Michigan, USA.

Scintec, 2006. Scintec Surface Layer Scintillometer SLS20/SLS40 SLS20-A/SLS40-A User Manual (including OEBMS1). Scintec Atmosphärenmesstechnik AG, Tübingen, Germany, 105 pp.

South African National Water Act, 1998. Republic of South Africa Government Gazette, 26th August, 1998, Act 36, number 19182, www.info.gov.za/gazette/acts/view/downloadfileaction?id=70693 accessed on 30th March 2010, 101 pp.

Stannard, D.I., 1997. A theoretically based determination of Bowen-ratio fetch requirements. Boundary-Layer Meteorol. 83, 375–406.

Stannard, D.I., Blanford, J.H., Kustas, W.P., Nichols, W.D., Amer, S.A., Schmugge, T.J., Weltz, M.A., 1994. Interpretation of surface flux measurements in heterogeneous terrain during the Monsoon ’90 experiment. Water Resour. Res. 30, 1227–1239.

Sun, X.-M., Zhu, Z.-L., Wen, X.-F., Yuan, G.-F., Yu, G.-R. 2006. The impact of averaging period on eddy fluxes observed at ChinaFLUX sites. Agric. For. Meteorol. 137, 188–193.

Sverdrup, H.U., 1943. On the ratio between heat conduction from the sea surface and the heat used for evaporation. Ann. N. Y. Acad. Sci. 68, 81–88.

Swinbank, W.C., 1951. The measurement of vertical transfer of heat and water vapour by eddies in the lower atmosphere. J. Met. 8, 135–145.

Thiermann, V., 1990. Optische messung turbulenter flüsse und vorhersage der optischen turbulenz aus einfachen grenzschichtparametern. Ph.D. dissertation, University of Hamburg, 96 pp.

Thiermann, V., Grassl, H., 1992. The measurement of turbulent surface-layer fluxes by use of bichromatic scintillation. Boundary-Layer Meteorol. 58, 367–389.

Weiss, A.I., 2002. Determination of thermal stratification and turbulence of the atmospheric surface layer over various types of terrain by optical scintillometry. Diss. D. Nat. Sci., Swiss Federal Institute of Technology, Zurich, Switzerland, 157 pp.

Wesely, M.L., 1976a. The combined effect of temperature and humidity on the refractive index. J. Appl. Meteorol. 15, 43–49.

Wesely, M.L., 1976b. A comparison of two optical methods for measuring line averages of thermal exchanges above warm water surfaces. J. Appl. Meteorol. 15, 1177–1188.

Williams, R.M., Paulson, C.A., 1977. Microscale temperature and velocity spectra in the atmospheric boundary layer. J. Fluid Mech. 83, 547–567.

Wilson, K., Goldstein, A., Falge, E., Aubinet, M., Baldocchi, D., Berbigier, P., Bernhofer, C., Ceulemans, R., Dolman, H., Field, C., Grelle, A., Ibrom, A., Law, B.E., Kowalski, A., Meyers, T., Moncrieff, J., Monson, R., Oechel, W., Tenhunen, J., Valentini R., Verma, S., 2002. Energy balance closure at FLUXNET sites. Agric. For. Meteorol. 113, 223–243.

Wyngaard, J.C., 1973. On surface-layer turbulence. Workshop on Micrometeorology, D.A. Haugen, Ed., Am. Meteorol. Soc., 101–149.

Wyngaard, J.C., Izumi, Y., Collins, S.A., 1971. Behaviour of the refractive index structure parameter near the ground. J. Opt. Soc. Am. 61, 1646–1650.

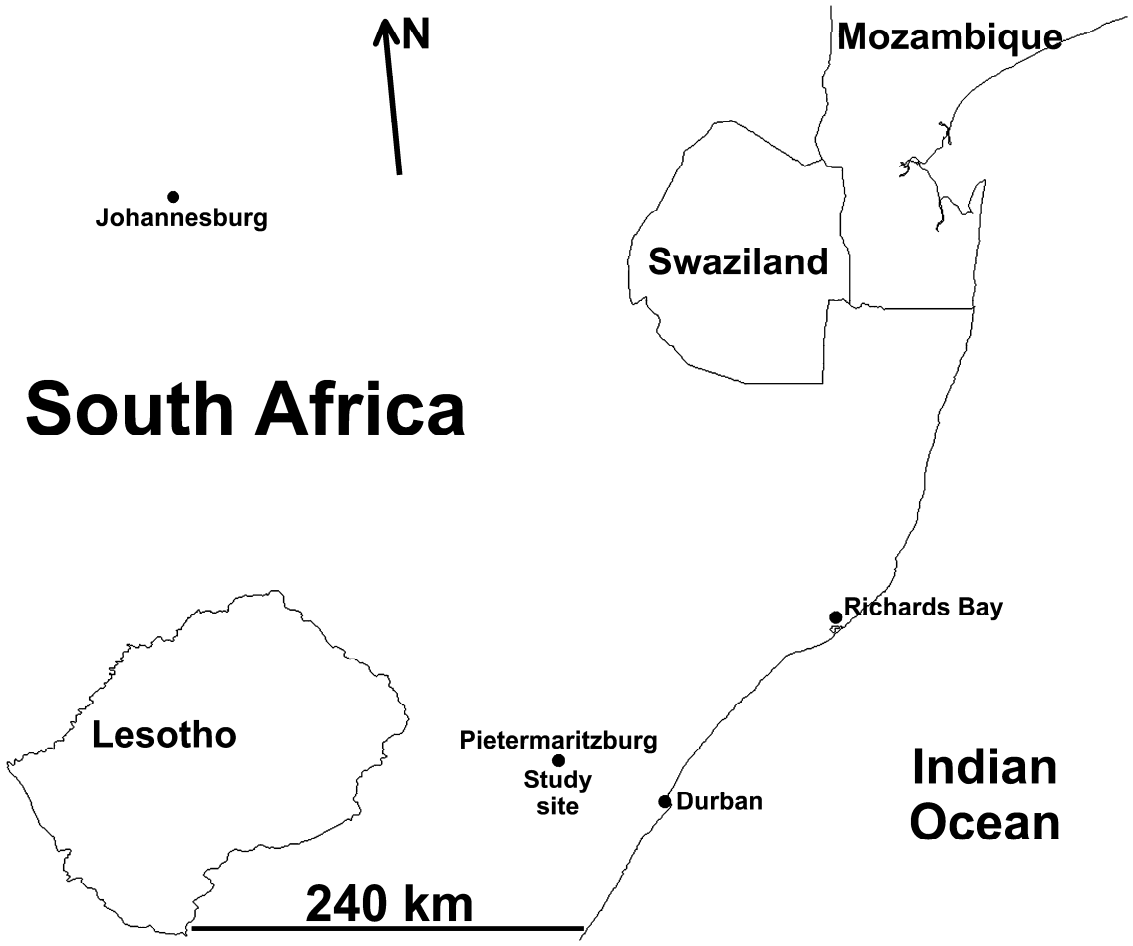

Fig. 4.1. Top: A map showing the location of the Bellevue study site close to Pietermaritzburg, KwaZulu-Natal, South Africa.

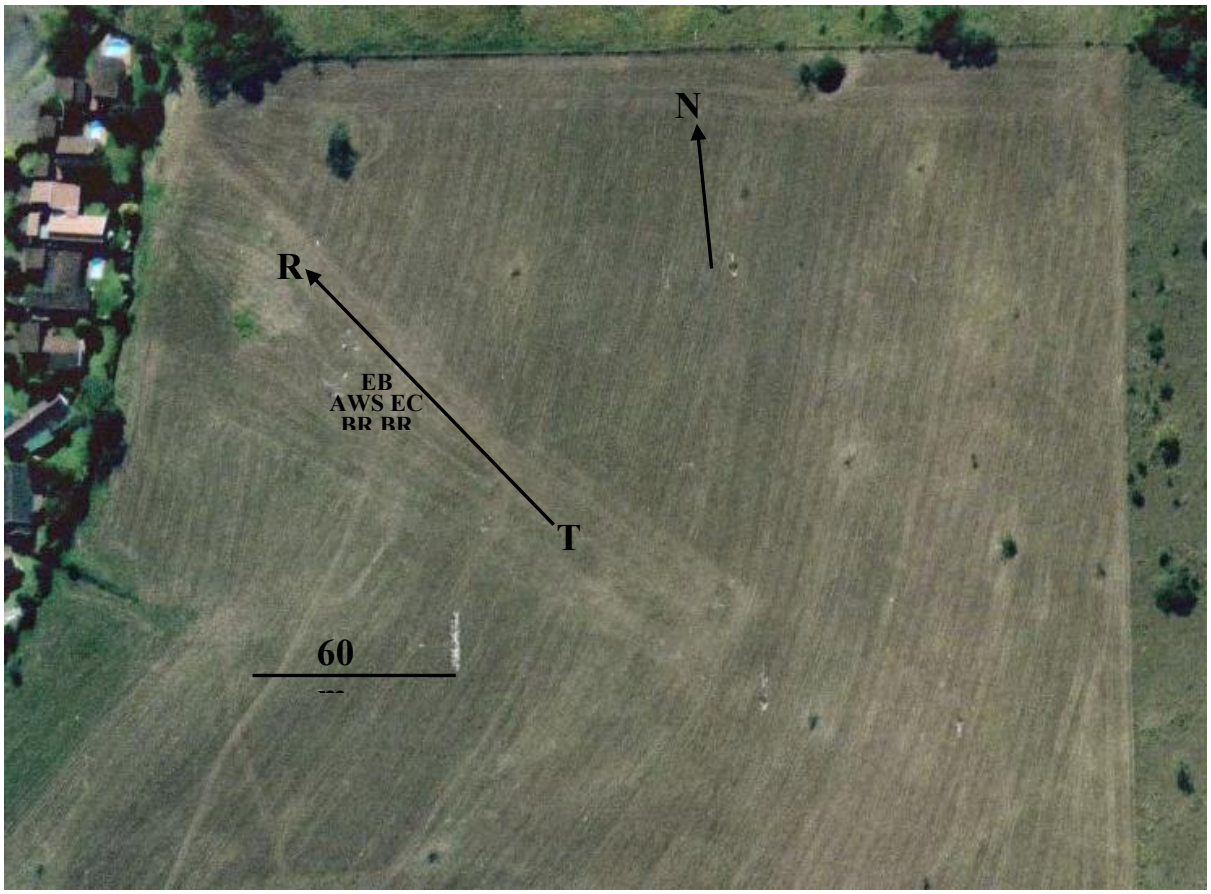

Fig. 4.1. Bottom: an aerial view of the study site following an autumn (April) mow. The SLS transmitter and receiver positions are indicated by T and R, respectively (beam path length of 101 m), BR for the BREB systems, EC for the eddy covariance systems, EB for the energy balance system (net irradiance, soil heat flux, soil water content, soil temperature), and AWS for the automatic weather station system.

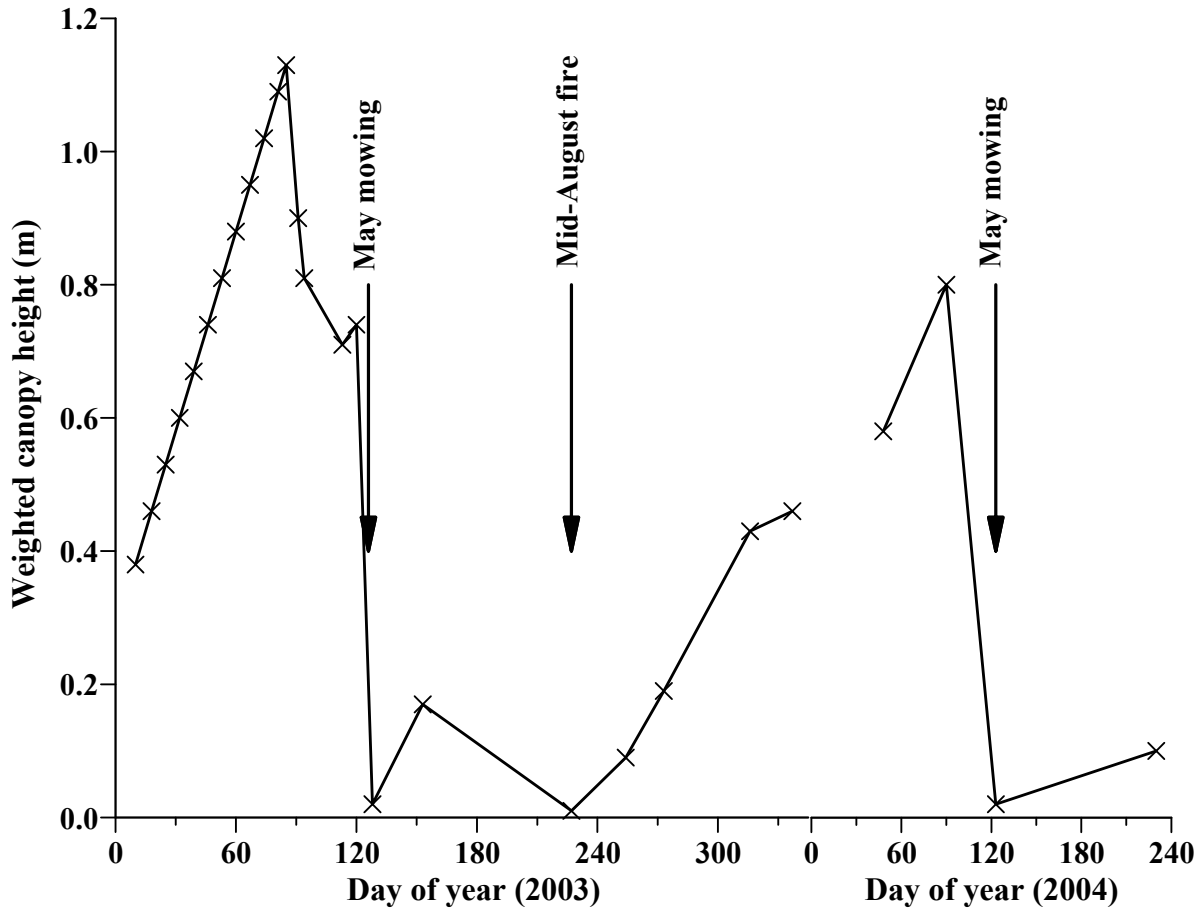

Fig. 4.2. The seasonal march of the path-weighted canopy height, for a path length of 101 m and an inner scale of turbulence l_o = 4 mm, for 600 days of the study. Events such as the two mowings and the fire are indicated.

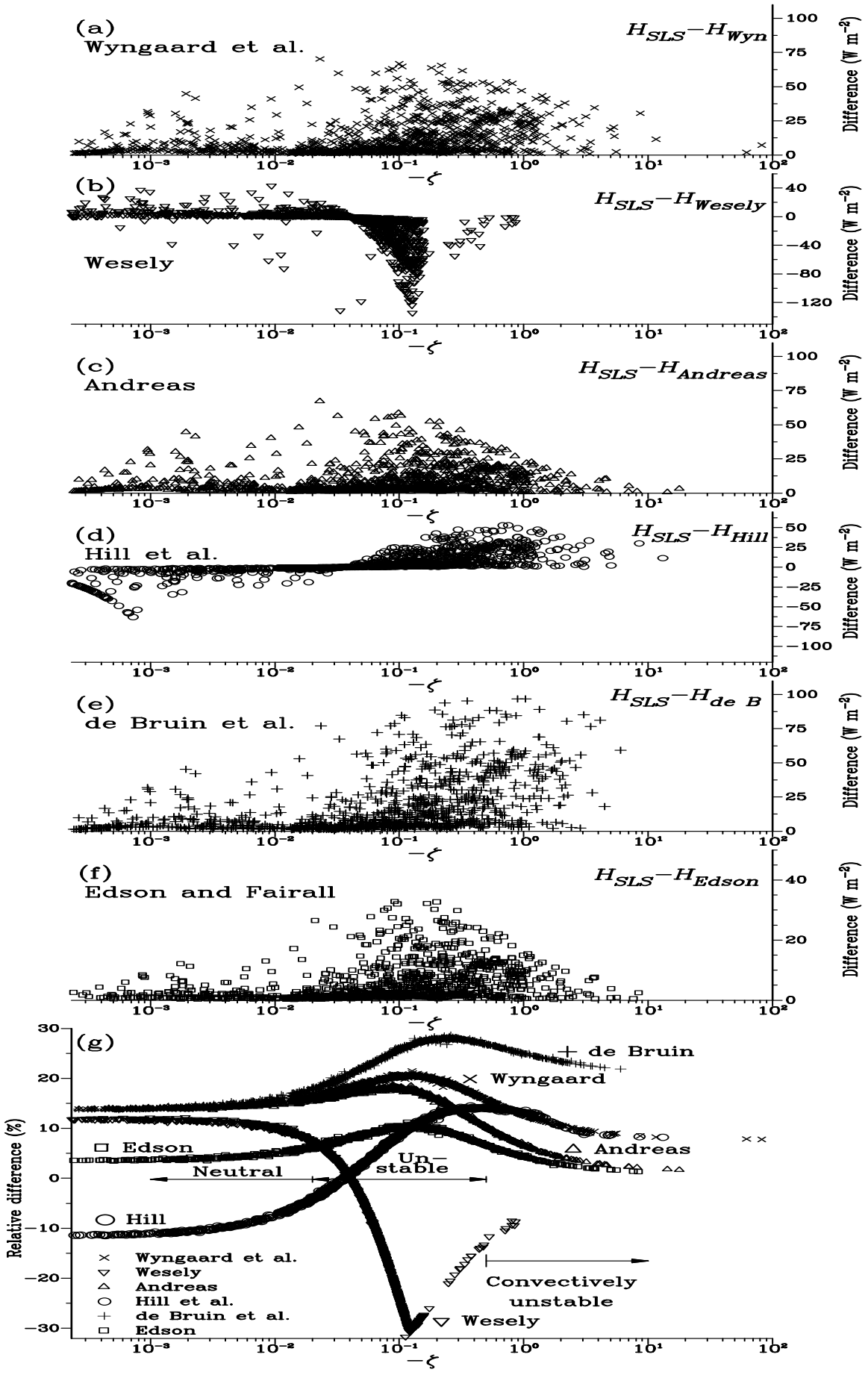
(a)
Wyngaard et al.
$H_{SLS}-H_{Wyn}$
(b)
Wesely
$H_{SLS}-H_{Wesely}$
(c)
Andreas
$H_{SLS}-H_{Andreas}$
(d)
Hill et al.
$H_{SLS}-H_{Hill}$
(e)
de Bruin et al.
$H_{SLS}-H_{de\ B}$
(f)
Edson and Fairall
$H_{SLS}-H_{Edson}$
Difference (W m^{-2})
$-\zeta$
(g)
Relative difference (%)
de Bruin
Wyngaard
Andreas
Edson
Hill
Neutral
Un–
stable
Convectively
unstable
Wesely
Wyngaard et al.
Wesely
Andreas
Hill et al.
de Bruin et al.
Edson

Fig. 4.3. The variation as a function of $-\zeta$, for unstable conditions for January 2004, in the difference between H_{SLS} and that estimated using selected MOST methods (shown in Table 4.1): (a) Wyngaard et al. (1971) method; (b) Wesely (1976b) method; (c) Andreas (1988) method; (d) Hill et al. (1992) method; (e) de Bruin et al. (1993) method; (f) Edson and Fairall (1998) method; and in (g) the percent difference $100\times(H - H_{SLS})/H_{SLS}$ for H estimated using the various MOST methods specified. The range of $-\zeta$ for the convectively unstable, unstable and neutral conditions is indicated. The y-axis scale for (a) to (f) are not the same.

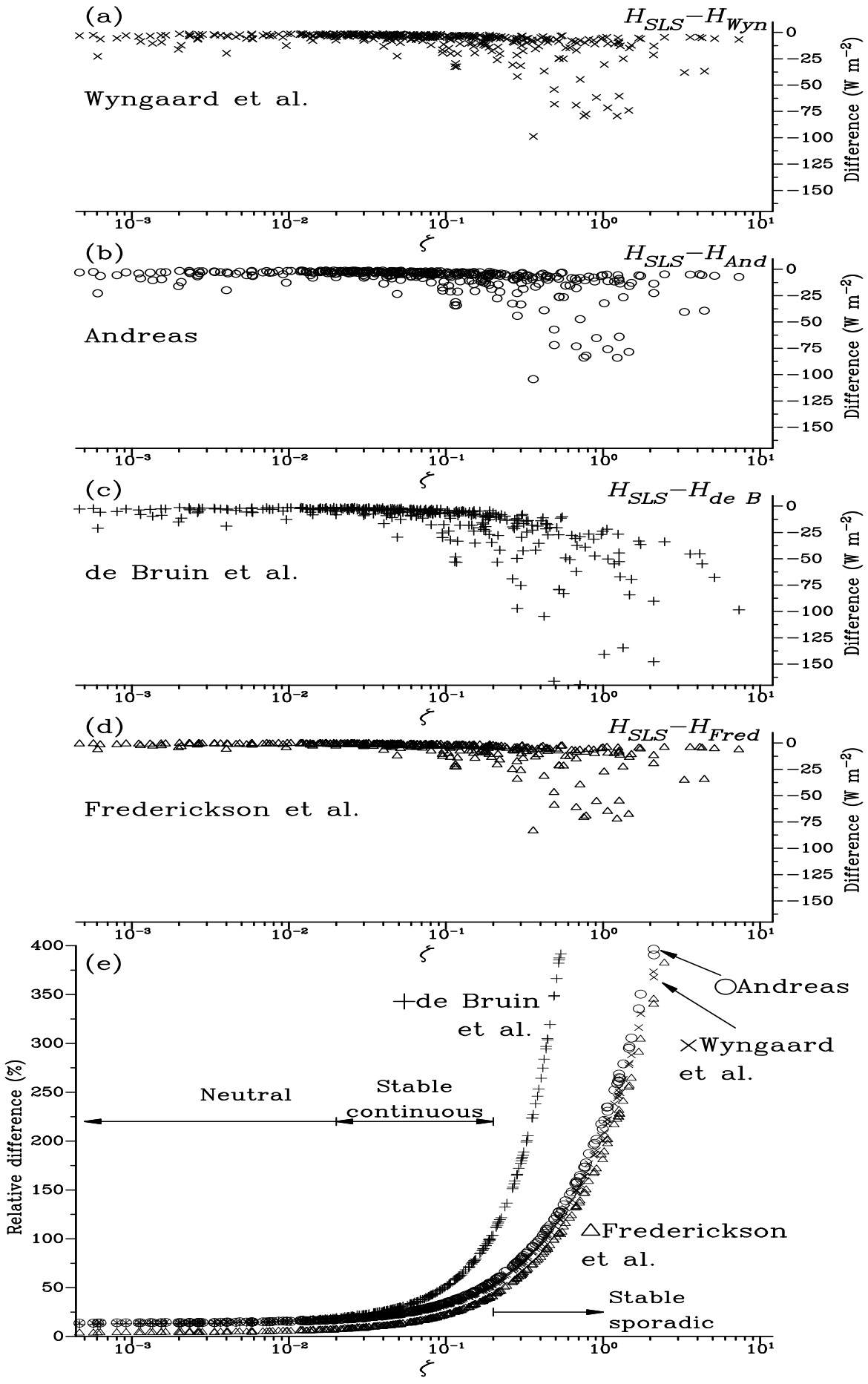
(a)
$H_{SLS}-H_{Wyn}$
Wyngaard et al.
(b)
$H_{SLS}-H_{And}$
Andreas
(c)
$H_{SLS}-H_{de\ B}$
de Bruin et al.
(d)
$H_{SLS}-H_{Fred}$
Frederickson et al.
Difference (W m^{-2})
0
−25
−50
−75
−100
−125
−150
10^{-3}
10^{-2}
10^{-1}
10^{0}
10^{1}
ζ
(e)
Relative difference (%)
400
350
300
250
200
150
100
50
0
+de Bruin et al.
○Andreas
×Wyngaard et al.
△Frederickson et al.
Neutral
Stable continuous
Stable sporadic

Fig. 4.4. The variation as a function of ζ, for stable conditions for January 2004, in the difference between H_{SLS} and that estimated using selected MOST methods (shown in Table 4.1): (a) Wyngaard et al. (1971) method; (b) Andreas (1988) method; (c) de Bruin et al. (1993) method; (d) Frederickson et al. (2000) method; and in (e) the percent difference $100 \times (H - H_{SLS}) / H_{SLS}$ for H estimated using the various MOST methods specified. The range of ζ for the neutral, stable continuous and stable sporadic conditions is indicated.

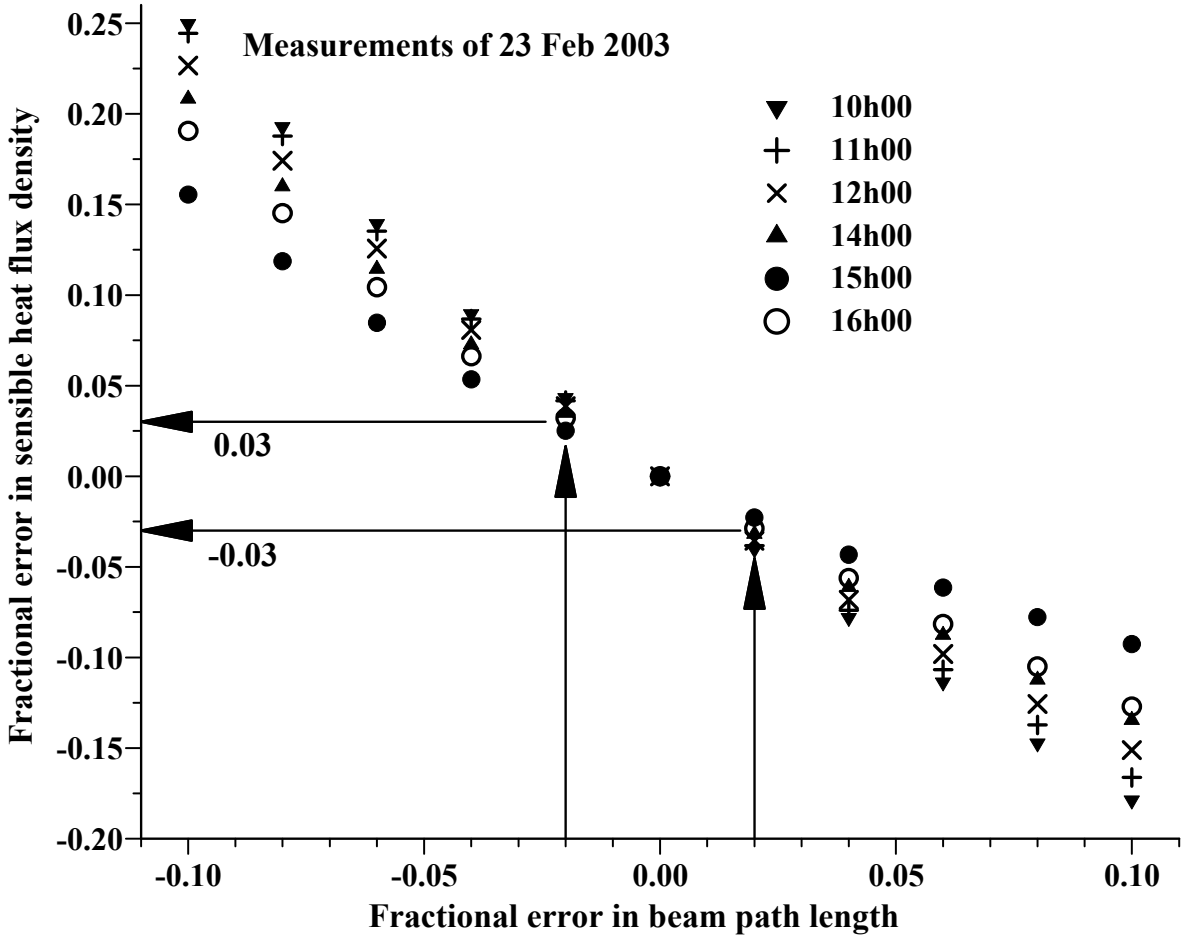

Fig. 4.5. The results of the sensitivity analysis for the 23rd February 2003 for the effect of worst-case fractional error in beam path length (from 2 % below 101 m to 2 % above) on the fractional error in H_{SLS}.

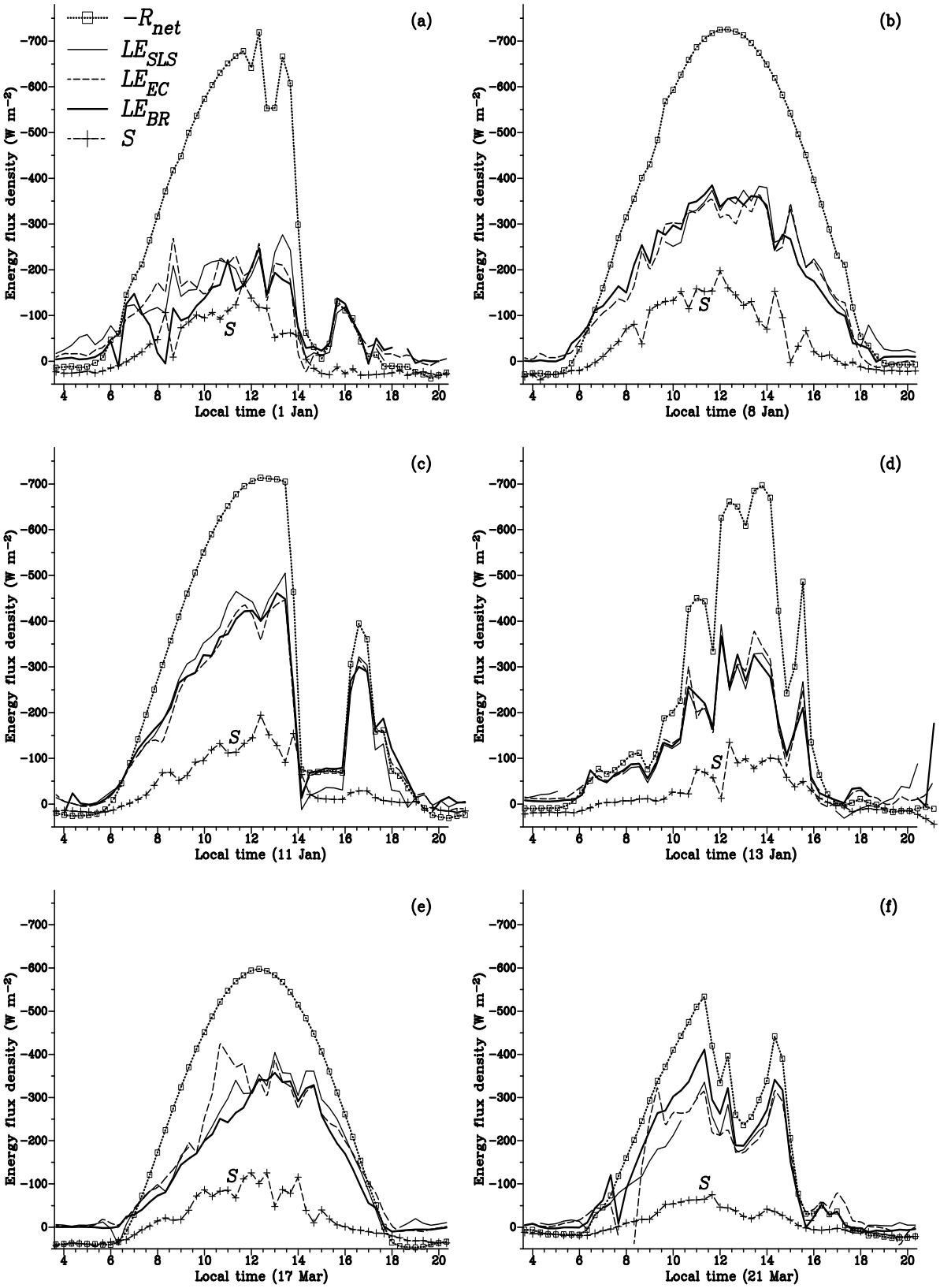

Fig. 4.6. The components of the energy balance for the mesic grassland for selected days in 2004. Each point represents a 20-min period.

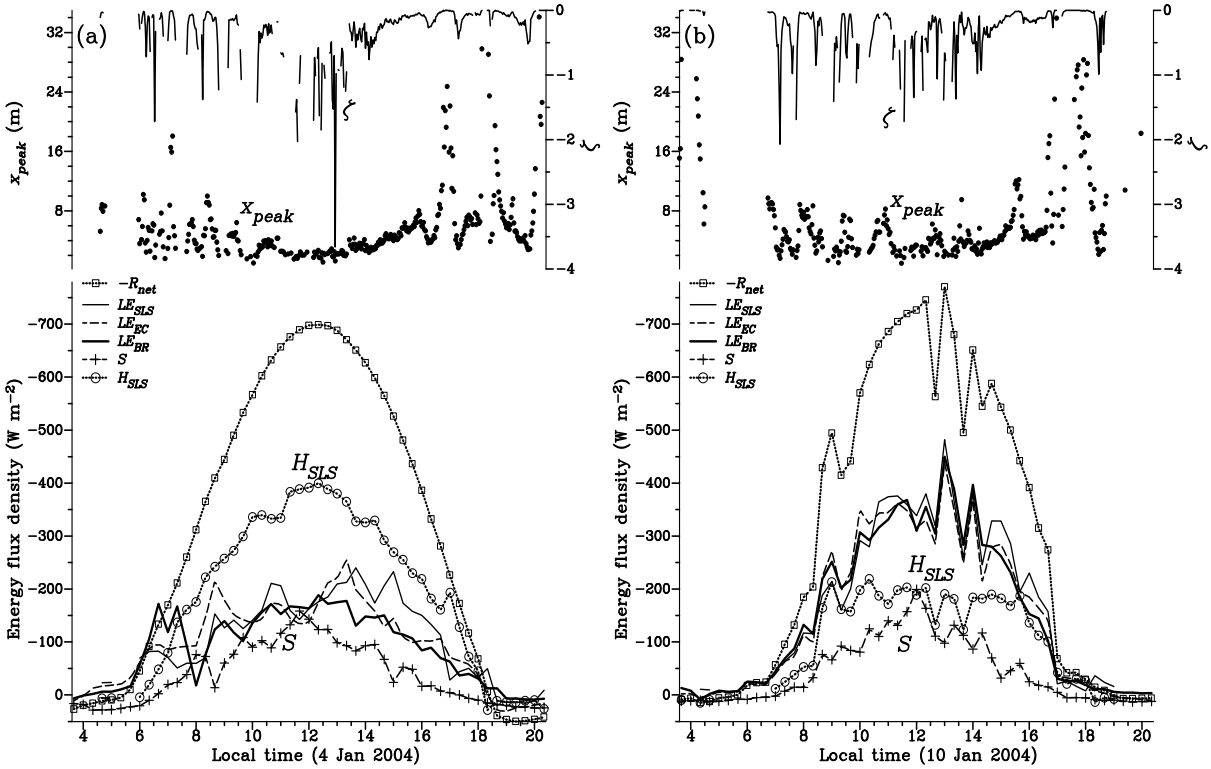

Fig. 4.7. The components of the energy balance (- left-hand y-axis) and net irradiance (right-hand y-axis) for (a) 4th January 2004 [left] and (b) 10th January 2004 [right]. Each point represents a 20-min period. The upper graphs show the variation in the peak of the footprint x_{peak} (left-hand y-axis, dots) and ζ (right-hand y-axis, line).

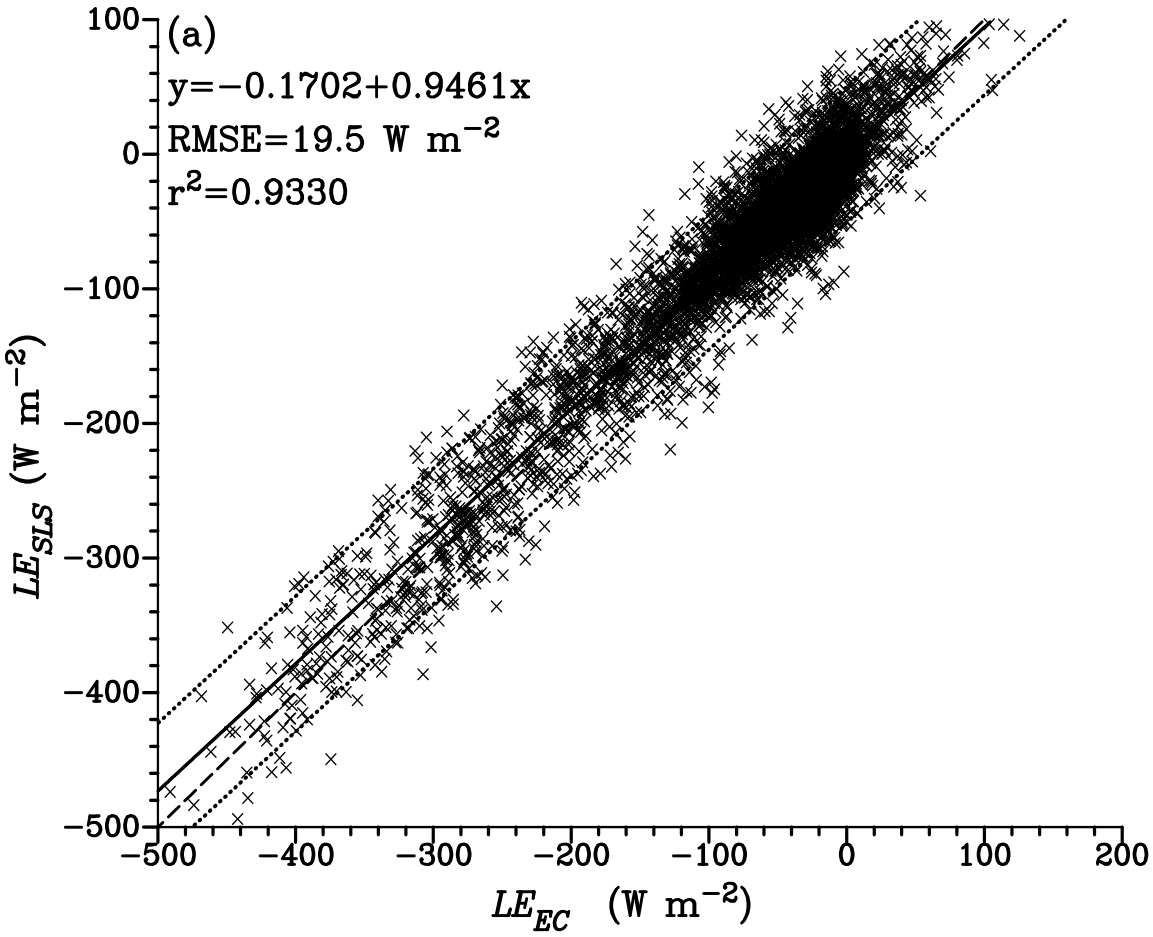
(a)
y=−0.1702+0.9461x
RMSE=19.5 W m^{-2}
r^2=0.9330
LE_{SLS} (W m^{-2})
LE_{EC} (W m^{-2})
100
0
−100
−200
−300
−400
−500
−500
−400
−300
−200
−100
0
100
200

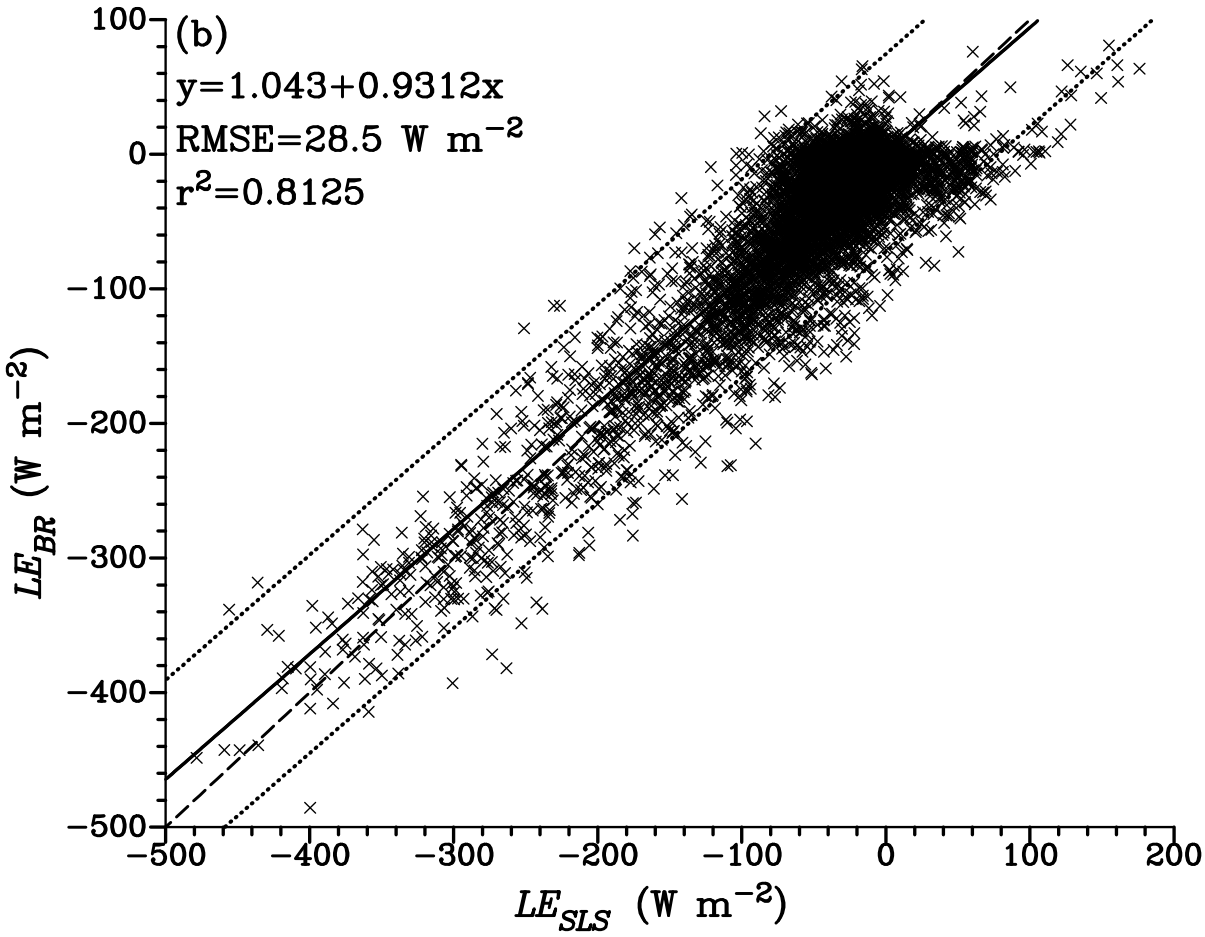

Fig. 4.8. Comparison, for January to July 2004 (20-min data), between (a) LE_{SLS} and LE_{EC} and (b) LE_{BR} and LE_{SLS}. The solid line is the regression line, the dashed line the 1:1 relationship and the dotted curves the 99 % prediction belts for a single predicted *y* value are also shown.

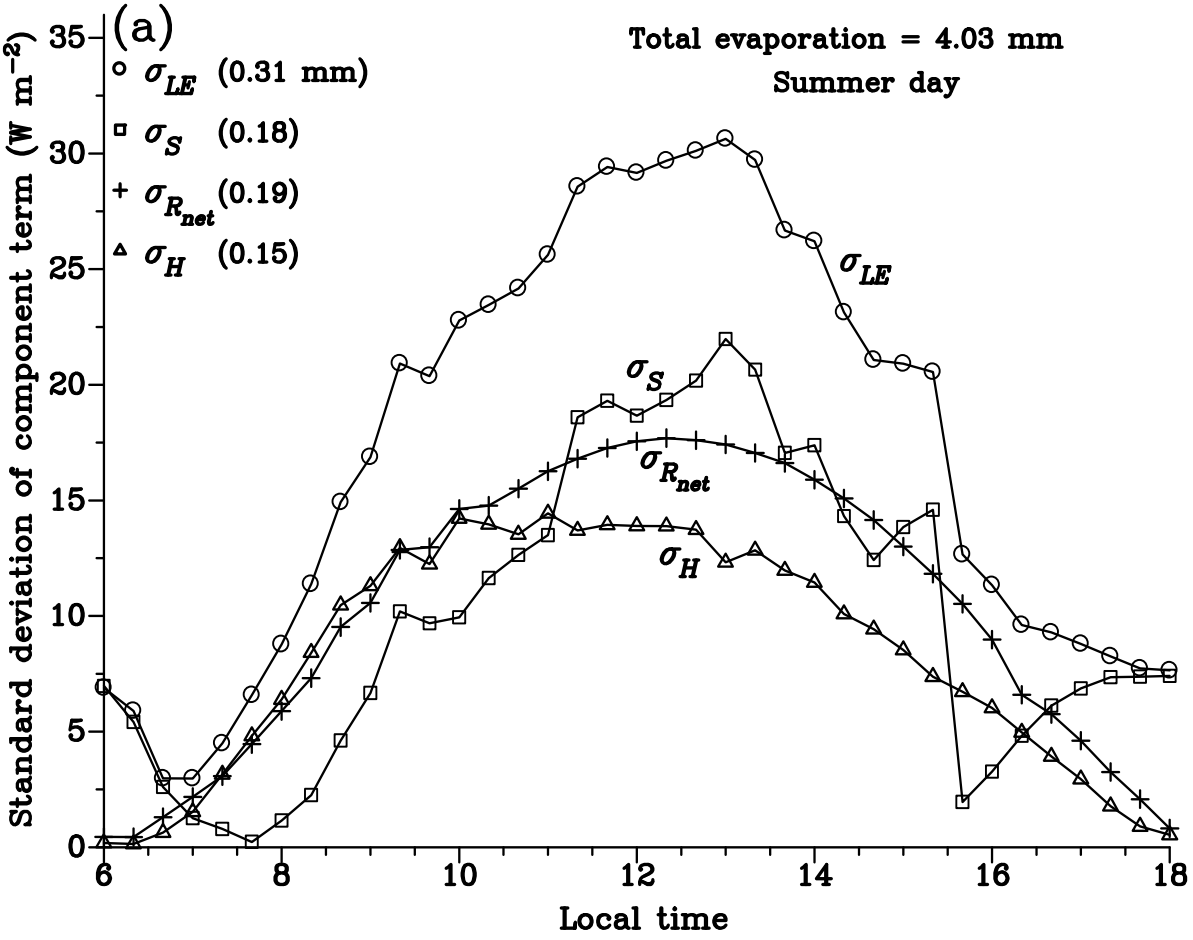
(a)
Total evaporation = 4.03 mm
Summer day
σLE (0.31 mm)
σS (0.18)
σRnet (0.19)
σH (0.15)
σLE
σS
σRnet
σH
Standard deviation of component term (W m−2)
Local time
0
5
10
15
20
25
30
35
6
8
10
12
14
16
18

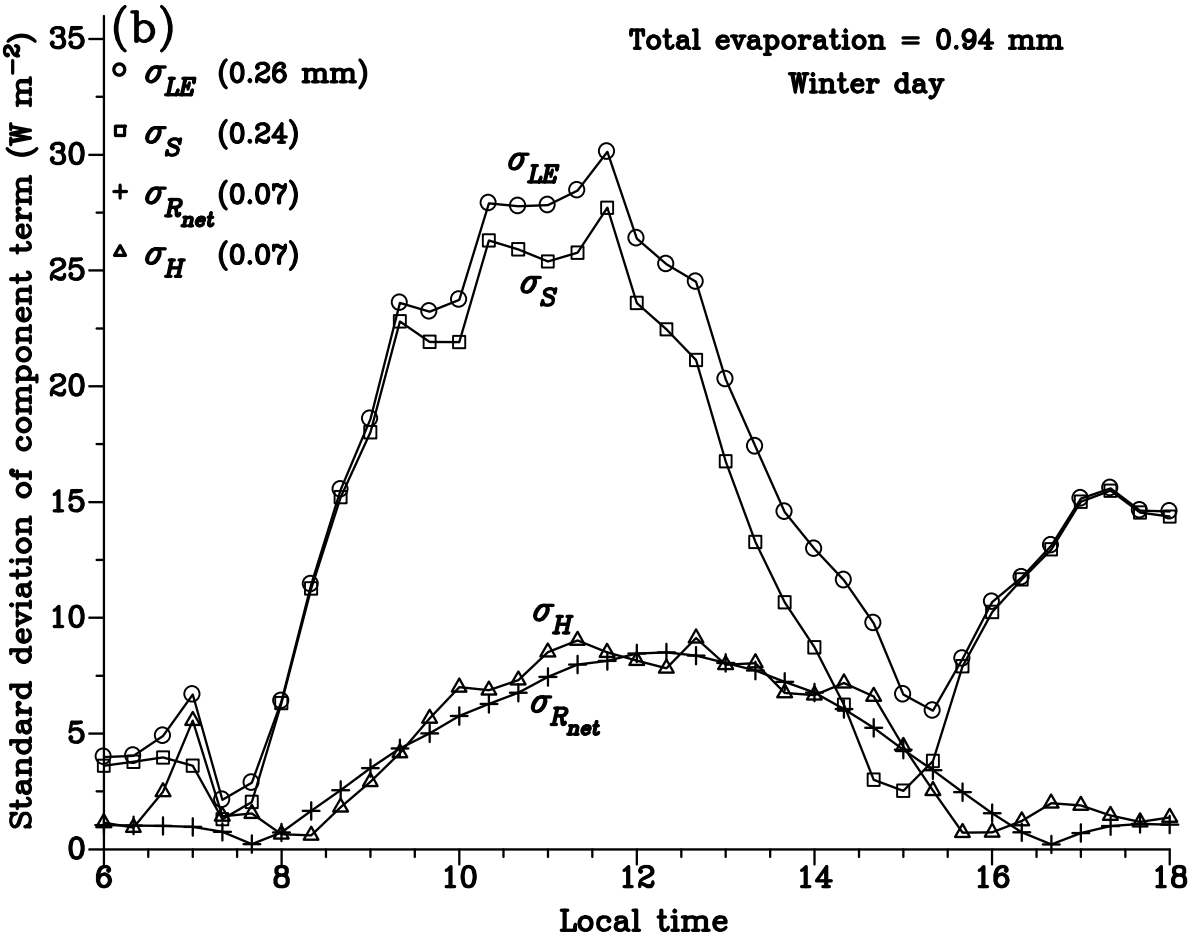

Fig. 4.9. The diurnal variation in the calculated component error terms (20-min data) of the energy balance for (a) a summer day (day 53, 2003) and (b) a winter day (day 188, 2003). In brackets, upper left for each graph, is the total error amount for the day for each component, converted into mm units. The worst-case error amount is used for H_{SLS}.

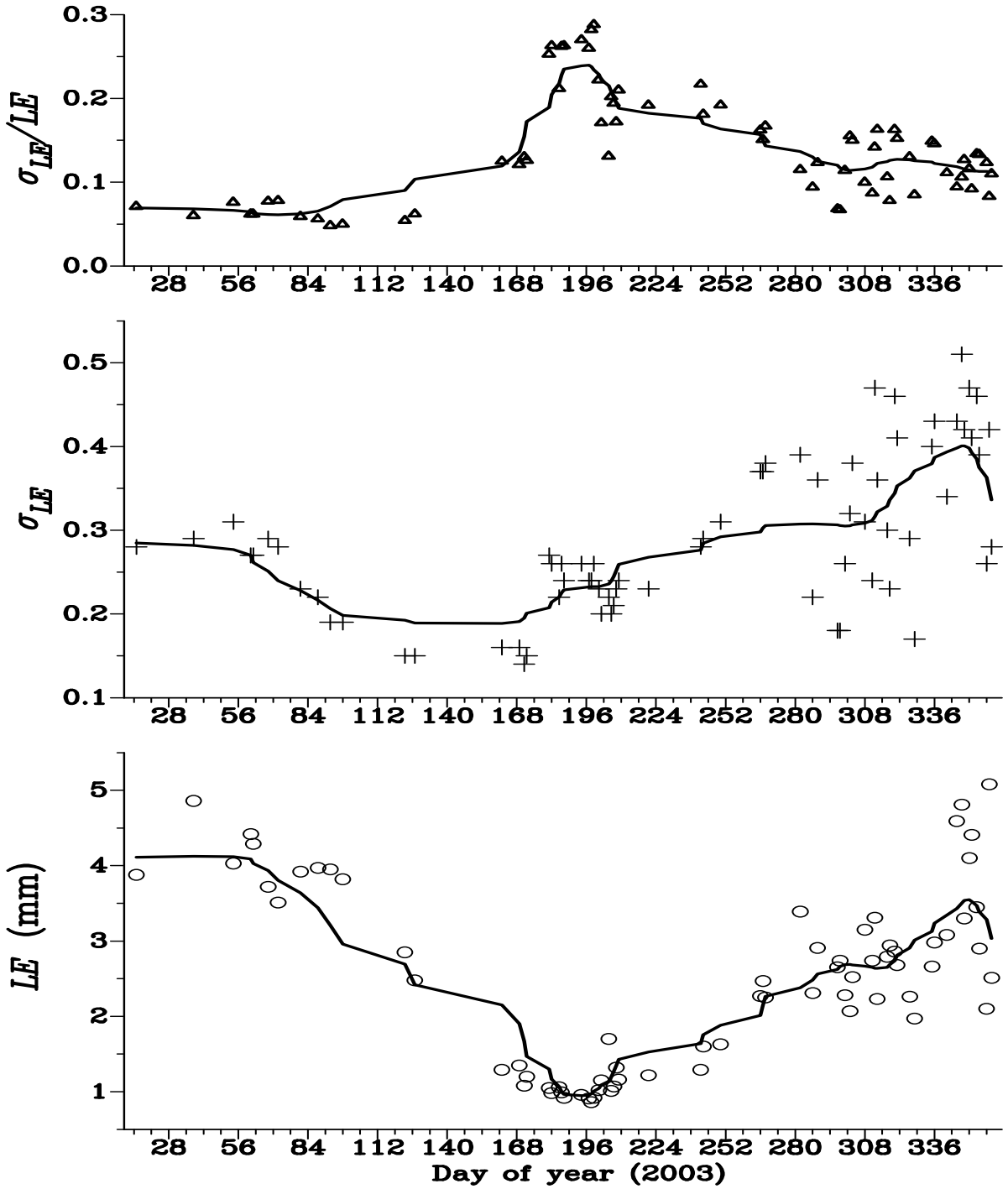

Fig. 4.10. Seasonal variation in daily evaporation LE_{SLS} (mm) (bottom), σ_{LE} (mm) (middle) and fractional error in evaporation (σ_{LE}/LE) (top) for 2003 for selected relatively cloudless days. The smooth curves were created by smoothing the *y* values in *x*, *y* data using a smoothing factor of 0.4 (Scientific Programming Enterprises, 1999). The worst-case error amount used for H_{SLS} is used to determine σ_{LE}.

Table 4.1. Comparisons between the various MOST empirical functions $f(\zeta)$ and $g(\zeta)$ used for estimating T_* and u_* for unstable and stable conditions.

Author	Empirical relationship(s)
Unstable case ($\zeta < 0$)	
Wyngaard et al. (1971), Wyngaard (1973)	$f(\zeta) = 4.9\,(1-7\zeta)^{-2/3}$; $g(\zeta) = [1+0.5\,(-\zeta)^{2/3}]^{3/2}$
Wesely (1976b)	$f(\zeta) = (1+0.45(1.5+\zeta)+0.01(1.5+\zeta)^{10})^2$ (typically for $-1.0<\zeta<-0.05$)
Andreas (1988)	$f(\zeta) = 4.9(1-6.1\zeta)^{-2/3}$; $g(\zeta) = [1+0.46\,(-\zeta)^{2/3}]^{3/2}$
Thiermann (1990)[2]	$f(\zeta) = 6.34\,(1-7\zeta+75\zeta^2)^{-1/3}$ (for $\zeta > -4.5$); $g(\zeta) = (1-3\zeta)^{-1} - \zeta$
Frenzen and Vogel (1992)	$g(\zeta) = (1.0-15.1\zeta)^{-1/3} - \zeta - 0.16$
Hill et al. (1992)	$f(\zeta) = 8.1\,(1-15\zeta)^{-2/3}$
Thiermann and Grassl (1992)	$f(\zeta) = 6.23\,(1-7\zeta+75\zeta^2)^{-1/3}$; $g(\zeta) = (1-3\zeta)^{-1} - \zeta$
de Bruin et al. (1993)	$f(\zeta) = 4.9\,(1-9\zeta)^{-2/3}$
Edson and Fairall (1998)	$f(\zeta) = 5.92\,(1-8\zeta)^{-2/3}$
Stable case ($\zeta \geq 0$)	
Wyngaard et al. (1971)	$f(\zeta) = 4.9\,(1+2.75\zeta)$; $g(\zeta) = 1+5\zeta$
Wyngaard (1973)	$f(\zeta) = 4.9\,(1+2.4\zeta)$
Andreas (1988)	$f(\zeta) = 4.9\,(1+2.2\zeta)$
Thiermann (1990)	$f(\zeta) = 6.34\,(1+7\zeta+20\zeta^2)^{1/3}$ (for $0<\zeta<4$); $g(\zeta) = (1+4\zeta+16\zeta^2)^{1/2}$
Frenzen and Vogel (1992)	$g(\zeta) = 0.84+5.0\zeta$ (for $0.0<\zeta<0.2$)
Thiermann and Grassl (1992)	$f(\zeta) = 6.23\,(1+7\zeta+20\zeta^2)^{1/3}$; $g(\zeta) = (1+4\zeta+16\zeta^2)^{1/2}$
de Bruin et al. (1993)	$f(\zeta) = 4.9$
Frederickson et al. (2000)	$f(\zeta) = 5.9\,(1+2.4\zeta)$

[2] The coefficient 6.34 is obtained from $4\beta_1 / k^{2/3}$ where β_1 = 0.86 is the Obukhov-Corrsin constant and k = 0.4. Thiermann and Grassl (1992) used k = 0.41 for which $4\beta_1 / k^{2/3}$ = 6.23

Table 4.2. Comparisons between the various MOST methods used for estimating sensible heat *H* for the SLS method for day-time (mainly unstable) and night-time (mainly stable) conditions, relative to the corresponding EC measurement, for the selected months January and July 2004.

	20-min data for January 2004 for unstable conditions					20-min data for July 2004 for unstable conditions				
	SLS	Wyngaard	de Bruin	Hill	Andreas	SLS	Wyngaard	de Bruin	Hill	Andreas
MAD	23.64	33.17	39.72	28.19	30.32	18.58	32.50	41.75	26.78	29.00
RMSD	32.58	44.79	53.49	38.64	41.14	24.66	40.39	50.99	34.75	36.36
95 % slope	(1.000, 1.038)	(1.133, 1.175)	(1.231, 1.275)	(1.118, 1.157)	(1.083, 1.124)	(0.938, 0.987)	(1.089, 1.145)	(1.052, 1.108)	(1.177, 1.238)	(1.041, 1.096)

	20-min data for January 2004 for stable conditions			20-min data for July 2004 for stable conditions		
	SLS	Wyngaard	de Bruin	SLS	Wyngaard	de Bruin
MAD	13.27	16.01	21.35	10.16	11.48	26.15
RMSD	18.24	19.44	24.82	14.70	18.13	32.03
95 % slope	(0.479, 1.042)	(0.781, 1.355)	(0.727, 1.664)	(0.479, 1.041)	(0.781, 1.356)	(0.727, 1.667)

Wyngaard: sensible heat estimated using the MOST method of Wyngaard et al. (1971); **de Bruin**: sensible heat estimated using the MOST method of de Bruin et al. (1993); **Hill**: sensible heat estimated using the MOST method of Hill et al. (1992); **Andreas**: sensible heat estimated using the MOST method of Andreas (1988)

MAD: mean absolute difference (W m^{-2}); *RMSD*: root mean square difference (W m^{-2}); **95 % slope**: 95 % confidence for the slope of measured (SLS) sensible heat (y) and EC sensible heat (x) (W m^{-2})

5 SENSIBLE HEAT FLUX BY SURFACE-LAYER SCINTILLOMETRY AND EDDY COVARIANCE OVER A MESIC GRASSLAND AS AFFECTED BY BOWEN RATIO AND MOST FORMULATIONS FOR UNSTABLE CONDITIONS[1]

5.1 Abstract

Measurements of sensible heat flux for an extended period for unstable conditions using surface-layer scintillometry (SLS) and eddy covariance (EC) and supplemented by Bowen ratio measurements for a mesic grassland community on the eastern seaboard of South Africa are presented. Measurements of SLS sensible heat flux were compared with those obtained using EC for a wide range of Bowen ratio (β). Also presented is an analysis of the different forms of the Monin-Obukhov similarity (MOST) functions used in micrometeorology and suggested by various authors, done by comparing EC sensible heat and that measured by SLS through the use of an iterative determination of Monin-Obukhov parameters. A comparison of the SLS-measured structure parameter of air temperature C_T^2 corrected for β and that uncorrected was carried out, with the results showing good correspondence but with a slight bias indicating that not correcting SLS measurements of C_T^2 for β would also result in a slight bias in H. Eddy covariance estimates of sensible heat flux (H_{EC}), obtained using averaging periods between 1 and 120 min and compared with scintillometer measurements, demonstrated that short-time averaging periods resulted in H_{EC} underestimated. The EC measurements for 60- and 120-min averaging periods were sometimes inconsistent with SLS measurements. A sensitivity analysis indicates that both the EC and SLS measurements of H are influenced by β. For $0 < \beta < 0.2$, the correction to H_{SLS} amounts to more than 10 % compared to more than 20 % for H_{EC} although the magnitude of the differences are small. A comparison of H_{EC} and H_{SLS} measurements for 0.1-intervals of β, for β between 0 and 4.3 shows reasonable correspondence for $\beta > 1$. For $0 < \beta < 1$, the H_{SLS} (y) *vs* H_{EC} (x) scatterplot linear regression slope decreased from 1.25 to close to 1 for β increasing from 0 to 1. A comparison between β-corrected H_{EC} and H_{SLS} measurements – the latter computed using various empirical stability functions used by MOST – shows significant differences compared to H_{EC} ranging from almost 20 % overestimation for some methods to 20 % underestimation for others. Long-term use of the recommended MOST stability functions for the SLS method is shown to result in reasonable correspondence between SLS and EC sensible heat flux for a wide range in atmospheric conditions, stability, and sensible heat magnitude.

5.2 Introduction

The 1998 Republic of South Africa National Water Act suggests a possible prescription for water allocation and charges for different land uses, making it even more crucial to consider how evaporation, which is one of the main components of the water balance, is to be measured or estimated routinely with reliable accuracy and precision (Savage, 2009).

Reliable estimation of energy fluxes from a surface is also important for understanding atmospheric boundary layer stability, regional water balance, irrigation needs, and weather forecasting as well as to generally address a growing list of environmental issues that range from defining the local water balance to accounting for land-atmosphere interactions in support of climate modelling. Several methods can be used to measure or estimate surface fluxes, such as sensible heat and latent

[1] Based on Odhiambo and Savage (2009)

energy (Savage et al., 1997). Development and testing of methods for estimating energy fluxes that are reliable and simple to apply are important aspects of micrometeorological research. Methods such as the Bowen ratio energy balance (BREB) and eddy covariance (EC) methods have been widely used in micrometeorological research. Other methods, for example, the scintillometer approach, involve measurement of the sensible heat flux from which evaporation can be estimated from measurement of net irradiance and soil heat flux and application of the shortened energy balance equation (Savage, 2009).

In the recent past scintillometry, which appears to offer greater spatial coverage than other conventional micrometeorological methods, is becoming popular (de Bruin, 2002) for applications such as surface energy balance studies, especially given that this method can be used for evapotranspiration studies covering large heterogeneous areas (Meijninger et al., 2002). Compared to EC and BREB methods for flux estimation, the large aperture scintillometer (LAS) method in boundary layer physics is simple and provides spatially averaged fluxes at scales of the order of several kilometres depending on the aperture size and type of beam used (Green et al., 1997). Measurements of LAS sensible heat flux can be used to validate and/or calibrate satellite estimates of sensible heat and latent energy fluxes over large areas (for example Watts et al., 2002). Surface-layer scintillometry (SLS) is complementary to LAS in that sensible heat flux measurements between 50 and 350 m for the former are possible. An advantage of the SLS method is that besides sensible heat, estimates of momentum flux are also possible. The measurement height of both LAS and SLS instruments may be altered to achieve measurements representative of larger areas than conventional flux measurement systems. Furthermore, unlike other flux measurement systems, SLS flux measurements may be obtained close to the surface using low-beam heights and therefore smaller associated footprint area, and employ averaging times as short as 1 min (Thiermann, 1990; de Bruin, 2002). The SLS used in the current study has a limitation of saturation for which the signal variance no longer increases linearly with the refractive index structure parameter C_n^2 as the refractive turbulence increases above a certain threshold. The problem of saturation limits the use of the SLS to a distance of about 350 m. For a path length less than 50 m, the inner scale length may often be less than the recommended minimum of 2 mm making the instrument susceptible to measurement errors (Scintec, 2006).

The estimates of SLS-derived sensible heat flux are dependent on the Monin-Obukhov Similarity Theory (MOST) through the particular formulations of the MOST semi-empirical functions used and also on the Bowen ratio. Some studies have found that the sensible heat flux measured by scintillometer methods needs to be corrected for the Bowen ratio (Green and Hayashi, 1998; Meijninger and de Bruin, 2000). Green and Hayashi (1998), for example, used a LAS above a paddy field, with its large evaporation. They suggest the need for a water vapour pressure correction for scintillometer sensible heat flux estimates under small Bowen ratio conditions. It is assumed that the scintillometer-derived sensible heat fluxes require correction for small Bowen ratios (de Wekker, 1996) and this view for the SLS is endorsed by Nakaya et al. (2006).

In this paper, the performance of the SLS method for measuring sensible heat flux for different Bowen ratios and various MOST formulations for unstable conditions for a grassland site is evaluated against the widely-used EC method. A secondary objective is to evaluate the performance of the SLS

and EC methods and in particular the estimation of sensible heat flux *H* using different averaging periods.

5.3 Theoretical background

A brief review of the various methods used in this study (BREB, EC and SLS) is presented.

5.3.1 Bowen ratio energy balance (BREB) method

The BREB method is an indirect method for estimating sensible and latent energy fluxes. The Bowen ratio β is estimated from vertical gradients of air temperature $\Delta T / \Delta z$ and water vapour pressure $\Delta e / \Delta z$ where ΔT and Δe are the vertical differences in air temperature and water vapour pressure respectively. The Bowen ratio is calculated as:

$$\beta = \frac{H}{LE} = \gamma \frac{\Delta T / \Delta z}{\Delta e / \Delta z} \tag{5.1}$$

(Sverdrup, 1943) where *L* is the specific latent heat of vapourisation (J kg^{-1}), *E* the mass flux of water vapour (kg s^{-1} m^{-2}) and γ the psychrometric constant (Pa K^{-1}). The method assumes that the eddy diffusivities for heat and water vapour respectively are equal and therefore any stability dependence is removed. The vertical gradients in air temperature and water vapour pressure are measured by air temperature and humidity sensors mounted at two different heights above ground level or a single humidity sensor that alternately measures the air stream humidity between the two heights.

5.3.2 Eddy covariance – sensible heat flux

The EC method is a direct method based on the covariance between vertical wind speed and sonic virtual temperature which by definition corresponds to the product of vertical wind speed fluctuations (w') and sonic virtual temperature fluctuations (T_s') yielding the sensible heat flux H_s (W m^{-2}):

$$H_s = -\rho_a c_p \overline{w' T_s'} \tag{5.2}$$

where ρ_a is the density of air (kg m^{-3}), c_p the specific heat capacity for air at constant pressure (J kg^{-1} K^{-1}) and $w'T_s'$ the covariance between w and T_s for a specified time period. Eq. (5.2) needs adjustment in order to obtain the actual sensible heat flux by eddy covariance (H_{EC}) since the sonic anemometer measures the sonic virtual temperature T_s (K) (Schotanus et al., 1983; Kaimal and Gaynor, 1991) and not the air temperature T_a (K). Furthermore, the volumetric heat capacity of air, $\rho_a c_p$ needs to include dry-air and moist-air influences. Ignoring the vertical pressure flux and cross-wind influences with the latter influences normally accounted for by internal 3-D sonic processing (Loescher et al., 2005) and assuming that the sonic path length is correct, but including correction to the sonic virtual temperature and moist-air influences, H_{EC} is obtained using:

$$H_{EC} = H_s \cdot \frac{\overline{T_a}}{\overline{T_s}} \cdot \left(1 + \frac{0.515 \rho_a c_p R \overline{T_a}^2}{L \cdot m_d \cdot (\overline{P} + 0.32\overline{e}) \cdot \beta} \right)^{-1} \tag{5.3}$$

where *R* is the Universal gas constant (J mol^{-1} K^{-1}), m_d the molecular mass of dry air (g mol^{-1}), $\overline{P}$ the average atmospheric pressure (kPa) and $\overline{e}$ the average water vapour pressure (kPa) and where

$\overline{T_a} / \overline{T_s} = (1 + 0.32\bar{e} / \overline{P})^{-1}$ (Schotanus et al., 1983). For a temperature range of 0 to 45 °C and an atmospheric pressure range of 80 to 100 kPa, Eq. (5.3) may be simplified with good accuracy to:

$$H_{EC} = H_s \cdot \left(1 + \frac{0.322\bar{e}}{\overline{P}} + \frac{10^{-3} \cdot (0.722\overline{P} - 0.399\bar{e})}{\beta} \right)^{-1} . \tag{5.4}$$

The EC method requires an adequate fetch. A fetch to height ratio of 100:1 is usually considered adequate but a greater fetch is desirable (Kaimal and Finnigan, 1994). The distribution of eddy size contributing to vertical transport creates a range of frequencies important to EC measurements. The EC sensors must therefore be sufficiently responsive to frequencies at the high end of the range such as 10 Hz, while the covariance averaging time must be long enough to include frequencies at the low end such as of the order of 0.01 Hz or less (Kaimal and Finnigan, 1994). There has been no general agreement for the EC averaging period for sensible heat flux. A 30- or 60-min period is commonly used. Sun et al. (2006) found that shorter averaging periods were possible for shorter canopies.

The main advantage of the EC method is that it offers the most direct and independent measurements of sensible heat and latent energy fluxes that is possible with micrometeorological methods without invoking MOST. No assumptions are made about the land surface properties such as aerodynamic roughness, zero-plane displacement or measurement height, and no corrections for atmospheric stability are necessary. Furthermore, unlike the SLS method, the sign of the fluxes are automatically assigned through the covariances.

5.3.3 Surface-layer scintillometer method

A surface-layer scintillometer (SLS) consists of a dual-beam laser transmitter and a receiver separated by between 50 and 350 m. The SLS measures intensity fluctuations from a beam, or 'amount' of scintillations after propagation through a turbulent medium. The amount of scintillation is expressed through the refractive index structure parameter of air (C_n^2, $m^{-2/3}$) which is a representation of the turbulent strength of the atmosphere (Chehbouni et al., 1999). The turbulent strength of the boundary-layer describes its ability to transport scalars, such as sensible heat, latent energy and other species (gases etc.). It is assumed that these intensity fluctuations are caused by inhomogeneities in refractive index resulting from the turbulent eddy motions along the beam path. These eddy motions (turbulence) are generated by fluctuations in air temperature and atmospheric humidity (Thiermann, 1990). Since fluctuations in air temperature and humidity cause changes in the refractive index of air and hence C_n^2, the measured C_n^2 is directly related to the turbulent structure parameter of air temperature C_T^2 (Thiermann, 1990). For visible to near-infrared wavelengths used for the wavelength of the scintillometer beam, fluctuations in air temperature are primarily responsible for atmospheric scintillation, with humidity fluctuations playing only a minor role (Green et al., 1994). In this wavelength region (visible for SLS and infrared for LAS) the spatially-averaged C_n^2 measured directly by the SLS is related to C_T^2 ($K^2\ m^{-2/3}$) as follows, provided air temperature and atmospheric humidity fluctuations are strongly correlated (Wesely, 1976) and consistent with MOST:

$$C_T^2 = C_n^2 \cdot \left(\frac{T^2}{\gamma P} \right)^2 \cdot \left(1 + \frac{0.03}{\beta} \right)^{-2} \tag{5.5}$$

where T is the absolute air temperature (K) and γ = 7.89 × 10^{-7} K Pa^{-1} at 670 nm. When there is no correlation between the fluctuations in air temperature and water vapour pressure:

$$C_T^2 = C_n^2 \cdot \left(\frac{T^2}{\gamma P}\right)^2 \cdot \left(1+\left(\frac{0.03}{\beta}\right)^2\right)^{-1} . \quad (5.6)$$

The square root of the last bracketed term in Eqs (5.5) and (5.6), viz. $(1+0.03/\beta)^{-1}$ and $(1+(0.03/\beta)^2)^{-0.5}$ respectively, are correction factors for the effect of humidity on the SLS measurement of *H*. The influence of β on C_T^2 via Eq. (5.6) is much reduced compared to Eq. (5.5). de Wekker (1996), who used a LAS for areally-averaged measurements of sensible heat over complex terrain, has shown that the Bowen ratio correction can be neglected when $\beta > 0.6$. This could also mean that the *H* values determined by the SLS method should be corrected for $|\beta| \leq 0.6$, especially for humid areas since neglecting the Bowen ratio (or humidity) influence would impair the accuracy of the SLS-derived *H* values (Weiss, 2002). However the contribution of humidity-related scintillations is much smaller than temperature-related scintillations, i.e. the laser (used in SLS) is primarily sensitive to temperature-related scintillations (Thiermann, 1990). When the surface conditions are dry, *H* is larger than LE resulting in large β values (> 3) and the correction term in Eqs (5.5) and (5.6) approaches 1.

One of the ways for assessing the accuracy of measured surface fluxes so as to increase the confidence in measurements (Twine et al., 2000) is through comparison of the agreement in measurements obtained by two micrometeorological methods used at the same time period and location. Agreement between two independent methods for measuring surface fluxes would therefore increase confidence in both approaches so a comparison of *H* measured by SLS and EC is of paramount importance. The SLS yields an areally-averaged estimate of *H* because it is derived from line-averaged values of C_T^2 and the dissipation rate of turbulent kinetic energy ε, and MOST parameters. Both EC, and SLS, measurements of sensible heat would have footprint representativity (Schmid, 1994) that depends on measurement height and the stability condition of the boundary-layer. A distinct advantage of SLS is that it provides better sampling than EC of the spatial variability of turbulent eddies and flux measurements (Thiermann, 1990; Nakaya et al., 2006, 2007).

5.3.4 Estimation of sensible heat flux using different forms of MOST stability functions

According to MOST, C_n^2 and the dissipation rate of turbulent kinetic energy ε ($m^2 s^{-3}$), made dimensionless by respectively scaling them with the temperature scale T_* and friction velocity u_*, are also universal functions of the stability parameter $\zeta = (z-d)/L$ where z is the height above the soil surface (m), d the zero-plane displacement (m) with the Obukhov length L (m) defined as:

$$L = \frac{T_a}{k\,g} \cdot \frac{\rho_a\, c_p}{H} \cdot u_*^3 \quad (5.7)$$

where *k* is the von Kármán constant (0.41) and *g* the acceleration of gravity ($m s^{-2}$). Hence, from MOST,

$$f(\zeta) = \frac{C_T^2 \cdot (z-d)^{2/3}}{T_*^2} \quad (5.8)$$

$$g(\zeta) = \frac{\varepsilon\, k\,(z-d)}{u_*^3} \quad (5.9)$$

where T_* is the temperature-scaling parameter (K) defined as:

$$T_* = -H / (\rho_a \, c_p u_*) . \tag{5.10}$$

Based on different datasets, various semi-empirical forms for the MOST stability functions $f(\zeta)$ and $g(\zeta)$ have been used and are summarised by Cain et al. (2001) and Savage (2009). An iterative scheme is used to solve Eqs (5.7) and (5.8) for T_* from SLS measurements of C_T^2 and using an empirical MOST function $f(\zeta)$ to compute H_{SLS}, if estimates of u_* are available. Friction velocity u_* however is obtained from Eqs (5.7) and (5.9) using SLS measurements of ε, the empirical function $g(\zeta)$ and an iterative procedure, from which H_{SLS} is calculated using Eq. (5.10). The iterative procedure is discussed in an Appendix to the thesis.

The empirical functional dependence of $f(\zeta)$ for unstable conditions is:

$$f(\zeta) = C_{T1} \cdot (1 - C_{T2})^{-2/3} \tag{5.11}$$

where constant C_{T1} = 4.9 and C_{T2} is given as 7 by Wyngaard et al. (1971), 6.1 by Andreas (1988) and 9 by de Bruin et al. (1993). Edson and Fairall (1988) used C_{T1} = 5.92 and C_{T2} = 8 and Hill et al. (1992) used C_{T1} = 8.1 and C_{T2} = 15. Wesely (1976) used

$$f(\zeta) = (1 + 0.45 \cdot (1.5 + \zeta) + 0.01 \cdot (1.5 + \zeta)^{10})^2 \tag{5.12}$$

for $-1 < \zeta < -0.05$. Thiermann (1990) on the other hand proposed:

$$f(\zeta) = 6.23 \cdot (1 - 7\zeta + 75\zeta^2)^{-1/3} . \tag{5.13}$$

For $g(\zeta)$, Andreas (1988) used

$$g(\zeta) = (1 + 0.46 \cdot (-\zeta)^{2/3})^{3/2} , \tag{5.14}$$

Thiermann (1990) used

$$g(\zeta) = (1 - 3\zeta)^{-1} - \zeta \tag{5.15}$$

and Wyngaard et al. (1971) used:

$$g(\zeta) = (1 + 0.5(-\zeta)^{2/3})^{3/2} . \tag{5.16}$$

5.4 Experimental details

5.4.1 Study area

Field measurements were carried out from January to December 2004 over an open, mesic grassland site in Ashburton (30°27'E, 29°40'S) close to Pietemaritzburg in KwaZulu-Natal, South Africa (Fig. 5.1), at an altitude of 671.3 m. KwaZulu-Natal, on the eastern seaboard of South Africa (Fig. 5.1), is bordered by the warm Indian Ocean to the east and the high escarpment of the Drakensberg Mountains

to the west. The climate is sub-tropical and humid with summer rainfall. Occasional frosts occur in winter. The surface above which the SLS was installed was nearly flat over a distance of 135 m along the prevailing S-E wind direction, with a downward slope of 1°15' to the S-E (Savage et al., 2004). To the north-west/west of the study site, 90 m away, was a residential area with tall trees but wind was seldom from this direction.

5.4.2 Data collection and analysis

Data collected using the BREB method included air temperature, measured at 1.55 and 2.96 m using 75-µm type-E bare and unshielded thermocouples; water vapour pressure, measured using a cooled dew point mirror; net irradiance, measured using four net radiometers (model Q*7 REBS, Seattle, Washington, USA); soil heat flux, measured using HFT-3 (REBS) soil heat flux plates, at a soil depth of 0.08 m and a system of parallel thermocouples at soil depths of 0.02 and 0.06 m used to calculate soil heat flux stored above the soil heat flux plate; volumetric soil water content measured using a frequency domain reflectometer (ThetaProbe model ML2x, Delta-T Devices, Cambridge, UK) and a Campbell Scientific (Logan, Utah, USA) CS615 soil reflectometer with the sensors inserted so as to measure in the first 0.06 m.

An EC system was mounted at a height of 2.12 m about midway along the scintillometer beam path. The EC setup provided H_s and u_* and the wind speed and wind direction data. The details of the EC methodology (Savage et al., 2004; Savage, 2009) are summarized here for completeness. The EC setup initially consisted of a three-dimensional sonic anemometer (SWS-211/3V, Applied Technologies, Boulder, Colorado, USA) with a 100-mm sonic path length. A Campbell 23X datalogger was used to record sonic temperature and the three wind velocity components at a frequency of 10 Hz, after which the covariance between vertical wind speed and sonic temperature for an averaging period of 20 min was used to calculate $H = H_s$ (Eq. (5.2)). Early in 2004, another 3D sonic anemometer with a 150-mm path length was used (RM Young ultrasonic model 81000, Traverse City, Michigan, USA) using a datalogger sampling at a frequency of 10 Hz with the sonic outputting the average of two measurements every 10 Hz. The EC instruments were within metres of each other with both pointing to the prevailing south-easterly wind direction. A Campbell CR5000 datalogger sampling at a frequency of 10 Hz was used with the raw and preliminary processed data stored for further analysis. Corrections applied to EC data (Oncley et al., 2007) included an averaging coordinate rotation procedure (Kaimal and Finnigan, 1994) for removing instrument tilt and air flow irregularity effects, and wake and crosswind corrections and the correction for $\overline{e}$, $\overline{P}$ and β (Eq. (5.4)). Detrending or filtering the data has been found to be ineffective in reducing non-stationarity (Cava et al., 2008) and acts as a high-pass filter (Finnigan et al., 2003; Mauder et al., 2007) and was not applied. Routine checks of the data from the two sonics confirmed the quality of the collected EC data.

A dual-beam surface-layer scintillometer (SLS40-A, Scintec Atmosphärenmessetechnik, Tübingen, Germany) was placed at a height of about 1.68 m above the soil surface with a path length between the transmitter and receiver units of 101 m. Beam alignment, which is crucial to SLS use, ensured that the laser beam from the transmitter pointed directly to the receiver. Initial alignment ensured that the beam was located through the alignment hole of the SLS receiver unit. The use of two-way radios, one person at the SLS receiver and the other at the transmitter, was necessary to reduce time taken for alignment. After the initial alignment, final alignment was done using the SLSRUN software from Scintec. Input values of air temperature, atmospheric pressure, beam path

length and effective height (which is the beam height above the soil surface minus $d + z_o$ where zo is the surface roughness length) were entered into the SLSRUN program before commencement of measurements. The canopy height h along the beam path length was measured using a tape measure and *d* estimated as 0.66 *h* and z_o as 0.1 *h*. For each site visit, the following were checked: Error Free Data (EFD) which should be greater than 25 %; the inner scale length l_o which should be greater than 2 mm for the beam path distance of 101 m since if l_o falls out of this range, the instrument is susceptible to measurement errors; beam distance, which should be greater than 80 % and the signal strength, which should range between 700 and 1400 units for both beams and both channel detectors. The beam distance refers to the distance of the beam from the central position and is given in percent of the possible scan range. Zero percent means that the beam is in the centre while values close to 100 % mean that the beam reached the outer area of the scan cone. To account for future drifts, a manual re-alignment should be performed if the beam distance approaches values of 80 % or greater (Scintec, 2006). The SLSRUN program automatically rejects the data if EFD < 25 %, l_o < 2 mm, the beam is cut by raindrops, insects, or the beam is misaligned. Uncorrected online measurements of *H* were obtained using the SLS method from which 2-, 20- and 60-min averages were calculated for comparison with EC sensible heat.

5.5 Results and discussion

5.5.1 Comparison of C_T^2 measured by SLS and C_T^2 corrected for β

Assuming that there is no error in air temperature T and atmospheric pressure P, and that air temperature and humidity fluctuations are strongly correlated, C_T^2 is a function of C_n^2, T, P and Bowen ratio β (Eqs 5.5 or 5.6) where C_n^2 is calculated from the covariance of the logarithm of the amplitude of radiation intensity and the voltage variances measured at the individual photodiode detectors for each beam (Thiermann and Grassl, 1992). Measured C_T^2 values corrected for β (Eq. (5.5)) were compared with the measured C_T^2 values. This was done to check for any significant differences between the C_T^2 corrected for β and the uncorrected C_T^2 values measured directly by SLS. The β value was obtained by dividing the 20-min sensible heat flux and latent energy flux obtained using the BREB method and/or using the average *H* from the SLS and EC measurements divided by the estimated latent heat flux as a residual of the energy balance. In Fig. 5.2, a scatterplot of the β-corrected and measured C_T^2 is shown for DOY 116 to 180 and 274 to 340 (2004). The correspondence between C_T^2 and C_T^2 corrected for β is reasonable but a slight bias is evident (slope of 0.910), that may impact on the estimated H_{SLS} through the influence of C_T on T_* (Eq. (5.8)). The dashed line in Fig. 5.2 is the 1:1 relationship and the dotted curves are the 99 % confidence bands for a single predicted y value. The slight bias is noticeable under highly turbulent conditions with large C_T^2, usually at midday. The bias was also consistent throughout the different seasons, both warm summer and cold winter seasons, prompting further comparisons of H_{SLS} with H_{EC}.

5.5.2 SLS and EC averaging periods

The SLS method allows use of very short averaging periods, as short as 1 min. In our case, a 2-min period yielded consistent $H_{SLS2\ min}$ measurements from one period to another under cloudless weather conditions and together with $H_{SLS20\ min}$ measurements were used as the basis for all comparisons with H_{EC}. Using the method of Thiermann (1990), a variation of less than 8 % in H_{SLS} could be expected for a path length of 100 m, a 2-min averaging period and a wind speed of at least 0.5 m s^{-1}. The averaging

period used for EC measurements is an important aspect of EC data processing (Loescher et al., 2005; Wolf et al., 2008) and may be arrived at by comparing EC fluxes for various averaging periods (Sun et al., 2006). In this study, we were able to do this but unlike other studies also compare the EC and SLS estimates of *H*. For the EC measurements the ensemble block averaging method (Finnigan et al., 2003; Sun et al., 2006) was applied. This method has been shown by Sun et al. (2006) to produce similar results to the Ogive method. The method involved obtaining β-corrected (Eq. (5.4)) and coordinate-rotated H_{EC} values for 2-, 20- and 60-min averaging periods, and others. These estimates were then used to compare with β-corrected H_{SLS} [Eqs (5.5) and (5.6)] – either 2-, 20- or 60-min fluxes. Comparisons were made between $H_{EC10x2\ min}$ and $H_{EC20\ min}$ and between $H_{EC3x20\ min}$ and $H_{EC60\ min}$. Diurnal comparisons are shown of H_{EC} for 24th May 2004, for which the Bowen ratio weighted for the available energy was 2.5, as an example, for various selected averaging periods between 1 and 120 min (Fig. 5.3). The shorter averaging periods result in much more scatter in H_{EC} with a tendency to underestimate compared to the 2-min H_{SLS} measurements. For a 10-min averaging period, the EC measurements are in reasonable agreement with $H_{SLS2\ min}$ (Fig. 5.3f) with less scatter between H_{EC} and $H_{SLS2\ min}$ for averaging periods of 20 and 30 min (Figs 5.3c, d). Somewhat inconsistent H_{EC} fluxes are obtained for 60- and 120-min averaging periods (Figs 5.3a, b). On the basis of these results, repeated for many days (data not shown), an EC averaging period of 20 min was used.

As a further test of the 20-min averaging period but for an extended experimental period, the results of this analysis for the period 19th April to 25th May 2004, are also shown (Fig. 5.4). There is good agreement between $H_{EC10x2\ min}$ and $H_{EC20\ min}$ (Fig. 5.4a) and $H_{EC3x20\ min}$ and $H_{EC60\ min}$ (Fig. 5.4b). The comparisons of H_{EC} with the H_{SLS} measurements (Figs 5.4c to f) show greater root mean square (RMSE) compared to Figs 5.4a and b for the EC comparisons. As was confirmed by the data of Fig. 5.3, the $H_{EC2\ min}$ data underestimated with $H_{EC10x2\ min}$ (y) *vs* $H_{SLS20\ min}$ (x) yielding a slope of 0.8882 compared to a slope of 0.9856 for the $H_{EC20\ min}$ (y) vs $H_{SLS20\ min}$ (x) comparison. The largest RMSE was noted for the $H_{EC3x20\ min}$ (y) *vs* $H_{SLS60\ min}$ (x) and $H_{EC60\ min}$ (y) vs $H_{SLS60\ min}$ (x) comparisons. As a consequence, the 99 % confidence belts for a single predicted y value are much wider than for Figs 5.4a, b and Figs 5.4c, d.

Theoretically, the averaging period for H_{EC} measurements is given by $64 \cdot (z-d)/(E^2 U)$ (Sreenivasan et al., 1978) where E is the flux measurement fractional error and U the horizontal wind speed. Assuming $z-d$ = 2 m, E = 0.1 and U = 2 m s^{-1}, a theoretical averaging period of 6400 s = 1.78 h results. The empirical results from the H_{EC} *vs* H_{EC} and H_{EC} *vs* H_{SLS} comparisons (Fig. 5.4) demonstrate that 20-min averaging periods, in spite of being significantly less than the theoretical estimate, still yield reasonable flux comparisons for the Bellevue grassland site. The $H_{EC20\ min}$ estimates provide good comparisons with $H_{SLS2\ min}$ (Fig. 5.3) and $H_{SLS20\ min}$ (Fig. 5.4d) and therefore H_{EC} estimates based on a 20-min averaging period were used for the remainder of the study.

5.5.3 Comparison of SLS- and EC-measured sensible heat flux

In this section, the β-corrected *H* values obtained by the EC and SLS methods for different Bowen ratio values covering different seasons of the year are compared. This was done to capture periods of rainfall and high humidity and also dry seasons when Bowen ratio values are expected to be different. Statistical analyses of *H* measured by both EC and SLS methods are compared for 0.1-increments of β for January to July 2004 corresponding to the period for which the Bowen ratio equipment was available.

Both the EC and SLS methods are humidity dependent through the Bowen ratio β. For the SLS method, the dependence is determined using Eq. (5.5) assuming strong correlation between air temperature and water vapour pressure. For the EC method, the dependence is more complex, via Eq. (5.3), or in more simplified form, Eq. (5.4).

A sensitivity analysis, based on Eqs (5.5) and (5.6), of the influence of β on H measurements by the SLS method indicates that, for $0 < \beta < 1$, there is an increased influence of β on H measurements. In Fig. 5.5, the fractional relative difference resulting from not correcting H measured by the EC and SLS methods is shown. The correction to the EC measurements of H for the humidity dependence of the speed of sound on sonic temperature (Eq. (5.4)) is similar in shape to the correction for the SLS measurements (Fig. 5.5). For $0 < \beta < 0.3$, the percent difference in H for both EC and SLS is greater than 10 % in magnitude through the use of Eqs (5.4) and (5.5) respectively. The correction for H_{EC} is mainly dependent on β and to a much lesser extent on atmospheric pressure and water vapour pressure, as indicated by the lower and upper curves obtained using Eq. (5.4) for atmospheric pressures of 80 and 100 kPa respectively (Fig. 5.5). Meijninger and de Bruin (2000) reported that the scintillometer sensible heat flux depends on β and that a variation of β from 0.3 to 1 causes a variation in the sensible heat flux by about 15 %, although their argument is based on expected or roughly-approximated β values and not what was actually measured at the same site where the sensible heat flux measurements were obtained. In their study, they used a LAS for measurements of sensible heat flux over irrigated areas.

Some studies have found that sensible heat flux measured by scintillometry needs to be corrected for β (Green and Hayashi, 1998; Meijninger and de Bruin, 2000). Green and Hayashi (1998), for example, used a LAS above a rice paddy field, with a highly evaporating surface. They suggest the need for some correction for water vapour pressure to scintillometer estimates of H for $|\beta| < 1$. However, even in their case, the difference between corrected and uncorrected H was about 5 % at most. Both EC and SLS estimates of H are somewhat similarly affected by the Bowen ratio correction and this tends to mask the need for correction for β for the SLS method.

The paired SLS and EC sensible heat flux dataset was separated according to β, the latter in 0.1 increments. This ensured that there were at least 100 data points for each interval within $0 < \beta < 1.5$. The mean value for β for the study period was 0.365 for all β with β being between 0.4 and 0.5 for most paired flux measurements. If only events for which $\beta > 0$ are included, the mean value for β is 0.519. A scatterplot of the difference between β-corrected H_{EC} and H_{SLS} and β is shown (Fig. 5.6). This plot proved particularly useful in providing clues for subsequent data analysis. The difference $H_{EC} - H_{SLS}$ shows an increased magnitude as β increases from 0 to around 0.5 followed by a decrease in $|H_{EC} - H_{SLS}|$ as β increases further.

The frequency distribution for β is shown in Fig. 5.7a. More than a third of the dataset corresponded to $0 < \beta < 1$. Linear regressions between H_{SLS} (y) and H_{EC} (x) corresponding to each Bowen ratio increment interval yielded slope and adjusted coefficient of determination (r^2) values (shown in Figs 7b and c respectively). The slope of the H_{SLS} (y) and H_{EC} (x) scatterplot for H_{SLS} uncorrected for β decreases from 1.75 to around 1 for β increasing from 0 to 1. This is in contrast to the corresponding slope for H_{SLS} corrected for β using Eq. (5.5) decreasing from 1.25 to just below 1.

Generally, for $0 < \beta < 1$, the adjusted r^2 is less than 0.9 (Fig. 5.7c) with the coefficient of variation of the mean H_{SLS} and H_{EC} greater than 60 % (Fig. 5.7d).

The correction for β on H_{SLS} is based on the assumption that there is strong correlation between humidity and air temperature using Eq. (5.5) as opposed to the less influential Eq. (5.6) for when there is no correlation. Ludi et al. (2005) demonstrated that the correlation coefficient between air temperature and humidity, designated r_{Tq}, increased from 0 to around 0.7 for β increasing from 0 to 1. We therefore reprocessed the data so that Eq. (5.6) was applied for when $0 < \beta < 0.5$ and otherwise Eq. (5.5) was applied (Figs 5.7 b and c, data indicated by crosses). This latter procedure reduced the slope of the H_{SLS} (y) *vs* H_{EC} (x) regressions slightly for $0 < \beta < 0.5$ compared to the slopes using uncorrected data but not the adjusted r^2 (Figs 5.7 b and c respectively). While the β-corrected H_{SLS} measurements using Eq. (5.5) gave the best agreement with H_{EC} based on data collected over a long period, there is still an overestimation in H_{SLS} relative to H_{EC} for $0 < \beta < 0.5$ and it is not possible using just these two datasets to determine which sensible heat flux is in fact correct. However, the magnitude of the SLS and EC sensible heat flux differences is small for $0 < \beta < 0.5$ (Fig. 5.6) – average of $H_{SLS} - H_{EC}$ for the full data period is 12.1 W m^{-2}.

Considering that the SLS and EC methods are independent flux-measuring methods relying on such different physical principles, with the SLS method providing an integrated value of H over the beam path which in the present study was 101 m, and the EC method whose measurements may have a different spatial representativity (Schmid, 1994), the agreement in H obtained by the two methods can be considered reasonable. In particular, there does not appear to be underestimation in H_{EC}, compared to H_{SLS}, as may occur if the energy balance is not closed. However, in spite of the corrections for β, the greatest discrepancy between H_{SLS} and H_{EC} occurs when $0 < \beta < 1$ which corresponds to small magnitude H and/or relatively large magnitude latent heat flux.

Other studies carried out before (for example Thiermann 1990, Thiermann and Grassl, 1992; Green et al., 1994; Savage, 2009) have found close agreement between the SLS and EC H measurements, the latter considered as the standard method for surface energy flux measurements. The study by Thiermann and Grassl (1992) was carried out in a stubble field surrounded by flat and agriculturally-used terrain. For a thyme canopy in a semi-arid environment and a pasture sward well supplied with water, Green et al. (1994) found that there was very close agreement between the H values measured by EC and SLS with no correction of SLS data for β applied. Perfect agreement in measurements of H by the two methods is not possible due to the fact that the SLS and EC measurements represent different footprint areas. However, there may also be differences in H due to the SLS method being dependent on MOST and the EC method not.

5.5.4 Analysis of sensible heat flux using different forms of the MOST stability functions

In this section, results of the analysis of the H values calculated using the various MOST stability functions are presented. Cain et al. (2001), and others, had difficulty in determining which of the scaling (stability) functions, $f(\zeta)$ for example, is more accurate. In our case, long-term SLS and EC measurements supplemented by Bowen ratio measurements were used to pursue this aspect. The estimates of H_{SLS}, corrected for β (Eq. (5.5)) through the actual β estimates used previously, using the various MOST functions were determined from the measurements of C_T^2 and ε for DOY 1 to 210. In cases when only $f(\zeta)$ was available from published works, the $g(\zeta)$ function of Thiermann (1990)

was used. All measurements were then compared with H_{EC}, also corrected for β. The results of the analysis (Fig. 5.8), for selected MOST functions $f(\zeta)$ and $g(\zeta)$, show that relative to H_{EC}, H_{SLS} estimates are greater than H_{EC} by 20 % for some of the MOST methods and underestimated by almost 20 % for others. The results for the Andreas (1988) MOST functions were similar to those for Edson and Fairall (1998). The MOST method of Thiermann (1990) for determining H_{SLS} recommended for use with the SLS, tested in this study for an extended period and a wide range of atmospheric and stability conditions compared reasonably well with H_{EC} (slope = 0.9701, adjusted r^2 = 0.9016, RMSE = 25.43 W m^{-2}). The scatter of the data was greater for most of the other methods. Clearly however, the SLS method yields reasonable estimates of H compared to H_{EC}.

5.6 Conclusions

A comparison of the SLS-measured C_T^2 and that corrected for β showed good correspondence, but with a slight bias indicating that sensible heat flux may need correction for β. The averaging period used for EC sensible heat flux measurements was investigated using an ensemble block averaging method with the computed fluxes compared with those for the SLS method. For SLS fluxes using an averaging period of 2 min, the EC fluxes tended to be underestimated and the 60- and 120-min periods sometime resulted in fluxes that differed from SLS. Reasonable flux comparisons resulted from using a 20-min averaging period. A sensitivity analysis showed that the influence of β on SLS and EC sensible heat flux results in a change of more than 10 % for $\beta < 0.6$. The analysis also showed that the EC method is more significantly influenced by β than SLS especially for $0 < \beta < 0.5$. Comparison of the sensible heat flux measured using SLS and EC methods for $\beta > 1$ show reasonably good correspondence but there is a bias for $0 < \beta < 1$, in spite of the correction for β on SLS and EC sensible heat flux measurements. The SLS and EC agreement was more variable with bias for $0 < \beta < 1$ with the slope increasing from 0.978 for β close to 1 to 1.25 for $0 < \beta < 0.1$. Unlike the EC measurements, SLS-measured sensible heat values require only a small correction for $\beta > 1$. Long-term and continuous sensible heat flux measurements using SLS were in reasonable agreement with β-corrected measurements using the EC method which is considered the standard method for surface turbulence flux measurements. A comparison of the various methods for computing the empirical stability functions used by MOST showed a significant difference in H with differences ranging from 20 % greater than EC measurements to almost 20 % below. The recommended function resulted in estimates of H which corresponded much more closely to EC measurements.

5.7 Acknowledgements

Financial support from the Water Research Commission (WRC), the University of KwaZulu-Natal and the National Research Foundation is acknowledged. The assistance received from the WRC Steering Committee and project team members is gratefully acknowledged. Our gratitude also goes to the owner Mr S. J. Hilcove and farm manager Mr H. Ovenstone and workers of the Bellevue farm where this study was carried out. The manuscript benefited from the valuable comments of the reviewers.

5.8 References

Andreas, E. L., 1988: Estimation of C_n^2 over snow and seas ice for meteorological data. J. Opt. Soc. Amer. 5, 481–495.

Cain, J. D., P. T. W. Rosier, W. M. L. Meijninger, and H. A. R. de Bruin, 2001: Spatially averaged sensible heat fluxes measured over barley. Agric. For. Meteor. 107, 307–322.

Cava, D., D. Contini, A. Donateo, and P. Martano, 2008: Analysis of short-term closure of the surface energy balance above short vegetation. Agric. For. Meteor. 148, 82–93.

Chehbouni, A., Y. H. Kerr, C. Watts, O. Hartogensis, D. Goodrich, R. Scott, J. Schieldge, K. Lee, W. J. Shuttleworth, G. Dedieu, G., and H. A. R. de Bruin, 1999: Estimation of area-averaged sensible heat flux using large-aperture scintillometer during the Semi-Arid Land-Surface-Atmosphere (SALSA) experiment. Water Res. Res. 35, 2505–2511.

de Bruin, H. A. R., 2002: Introduction: renaissance of scintillometry. Boundary-Layer Meteor. 105, 1–4.

de Bruin, H. A. R., W. Kohsiek, and B. J. J. M. van den Hurk, 1993: A verification of some methods to determine the fluxes of momentum, sensible heat and water vapour using standard deviation and structure parameter of scalar meteorological quantities. Boundary-Layer Meteor. 63, 231–257.

de Wekker, S. F. J., 1996: The estimation of areally-averaged sensible heat fluxes over complex terrain with a large-aperture scintillometer. MSc Thesis. Department of Meteorology, Wageningen University. Wageningen, Netherlands, 172 pp.

Edson, J. B., and C. W. Fairall, 1998: Similarity relationships in the marine atmospheric surface layer for terms in the TKE and scalar variance budgets. J. Atmos. Sci. 55, 2311–2328.

Finnigan, J. J., R. Clement, Y. Malhi, R. Leuning, and H. A. Cleugh, 2003: A re-evaluation of long-term flux measurement techniques Part I: averaging and coordinate rotation Boundary-Layer Meteor. 107, 1–48.

Green, A. E., and Y. Hayashi, 1998: Using the scintillometer over a rice paddy. Jap. J. Agric. Meteor. 54, 225–231.

Green, A. E., K. J. McAneney, and M. S. Astill, 1994: Surface-layer scintillation measurements of daytime sensible heat and momentum fluxes. Boundary-Layer Meteor. 68, 357–373.

Green, A. E., K. J. McAneney, and J. P. Lagouarde, 1997: Sensible heat and momentum flux measurement with an optical inner scale meter. Agric. For. Meteor. 85, 259–297.

Hill, R. J., G. R. Ochs, and J. J. Wilson, 1992: Measuring surface-layer fluxes of heat and momentum using optical scintillation. Boundary-Layer Meteor. 58, 391–408.

Kaimal, J. C., and J. J. Finnigan, 1994: Atmospheric Boundary Layer Flows, Their Structure and Measurement. Oxford University Press. Oxford, UK.

Kaimal, J. C., and J. E. Gaynor, 1991: Another look at sonic anemometry. Boundary-Layer Meteor. 56, 401–410.

Loescher, H. W., T. Ocheltree, B. Tanner, E. Swiatek, B. Dano, J. Wong, G. Zimmerman, J. Campbell, C. Stock, L. Jacobsen, Y. Shiga, J. Kollas, J. Liburdy, and B. E. Law, 2005: Comparison of temperature and wind statistics in contrasting environments among different sonic anemometer–thermometers. Agric. For. Meteor. 133, 119–139.

Ludi, A., F. Beyrich, and C. Matzler, 2005: Determination of the turbulent temperature–humidity correlation from scintillometric measurements. Boundary-Layer Meteor. 117, 525–550.

Mauder, M., S. P. Oncley, R. Vogt, T. Weidinger, L. Ribeiro, C. Bernhofer, T. Foken, W. Kohsiek, H. A. R. de Bruin, and H. Liu, 2007: The energy balance experiment EBEX-2000. Part II: Intercomparison of eddy-covariance sensors and post-field data processing methods. Boundary-Layer Meteor. 123, 29–54.

Meijninger, W. M. L., and H. A. R. de Bruin, 2000: The sensible heat fluxes over irrigated areas in Western Turkey determined with a large aperture scintillometer. J. Hydro. 229, 42–49.

Meijninger, W. M. L., O. K. Hartogensis, W. Kohsiek, J. C. B. Hoedjes, R. M. Zuurbier, and H. A. R. de Bruin, 2002: Determination of area-averaged sensible heat fluxes with large aperture scintillometer over a heterogeneous surface-Flevoland field experiment. Boundary-Layer Meteor. 101, 37–62.

Nakaya, K., S. Chieko, K. Takuya, I. Hideshi, and Y. Shinji, 2006: Application of a displaced-beam small aperture scintillometer to a deciduous forest under unstable atmospheric conditions. Agric. For. Meteor. 136, 45–55.

Nakaya, K., S. Chieko, K. Takuya, I. Hideshi, and Y. Shinji, 2007: Spatial averaging effect on local flux measurement using a displaced-beam small aperture scintillometer above the forest canopy. Agric. For. Meteor. 145, 97–109.

National Amendment Water Act (Chapter 36) 1998: Department of Water Affairs and Forestry, Ministry of Environmental Affairs and Tourism. Pretoria, Republic of South Africa.

Odhiambo, G. O. and M. J. Savage, M.J., 2009: Sensible heat flux by surface layer scintillometry and eddy covariance over a mixed grassland community as affected by Bowen ratio and MOST formulations for unstable conditions. J. Hydrometeorol. 10, 479–492.

Oncley, S. P., T. Foken, R. Vogt, W. Kohsiek, H. A. R. de Bruin, C. Bernhofer, A. Christen, E. van Gorsel, D. Grantz, C. Feigenwinter, I. Lehner, C. Liebethal, H. Liu, M. Mauder, A. Pitacco, L. Ribeiro, and T. Weidinger, 2007: The energy balance experiment EBEX-2000. Part I: overview and energy balance. Boundary-Layer Meteor. 123, 1–28.

Savage, M. J., 2009: Estimation of evaporation using a dual-beam surface layer scintillometer. Agric. For. Meteor. 149, 501–517.

Savage, M. J., C. S. Everson, and B. R. Metelerkamp, 1997: Evaporation measurement above vegetated surfaces using micrometeorological techniques. Water Research Commission (WRC) Report No. 349/1/97, ISBN 1-86845-363-4. WRC, Pretoria, Republic of South Africa, 227 pp.

Savage, M. J., C. S. Everson, G. O. Odhiambo, M. G. Mengistu, and C. Jarmain, 2004: Theory and practice of evapotranspiration measurement, with special focus on surface layer scintillometer (SLS) as an operational tool for the estimation of spatially-averaged evaporation. Water Research Commission (WRC) Report No. 1335/1/04. ISBN 1-77005-247-X. WRC, Pretoria, Republic of South Africa, 204 pp.

Schmid, H. P., 1994: Source areas for scalars and scalar fluxes. Boundary-Layer Meteor. 67, 293–318.

Schotanus, P., F. T. M. Nieuwstadt, and H. A. R. de Bruin, 1983: Temperature measurement with a sonic anemometer and its application to heat and moisture fluctuations. Boundary-Layer Meteor. 26, 81–93.

Scintec, 2006: Scintec Surface Layer Scintillometer SLS20/SLS40 SLS20-A/SLS40-A User Manual (including OEBMS1). Scintec Atmosphärenmesstechnik AG, Tübingen, Germany, 105 pp.

Sreenivasan, K. R., A. J. Chambers, R. A. and Antonia, 1978: Accuracy of moments of velocity and scalar fluctuations in the atmospheric surface. Boundary-Layer Meteor. 14, 341–359.

Sun, X. -M., Z. -L. Zhu, X. -F. Wen, G. -F. Yuan, and G. -R. Yu, 2006: The impact of averaging period on eddy fluxes observed at ChinaFLUX sites. Agric. For. Meteor. 137, 188–193.

Sverdrup, H. U., 1943: On the ratio between heat conduction from the sea surface and the heat used for evaporation. Ann. N. Y. Acad. Sci. 68, 81–88.

Thiermann, V., 1990. Optische messung turbulenter flüsse und vorhersage der optischen turbulenz aus einfachen grenzschichtparametern. PhD Thesis, University of Hamburg, 96 pp.

Thiermann, V., and H. Grassl, 1992: The measurement of turbulent surface-layer fluxes by use of bichromatic scintillation. Boundary-Layer Meteor. 58, 367–389.

Twine, T. E., W. P. Kustas, J. M. Norman, D. R. Cook, P. R. Houser, T. P. Meyers, J. H. Prueger, and P. J. Starks, 2000: Correcting eddy covariance flux underestimates over grassland. Agric. For. Meteor. 103, 279–300.

Watts, C. J., A. Chehbouni, J. C. Rodriguez, Y. H. Kerr, O. Hartogensis, and H. A. R. de Bruin, 2002: Comparison of sensible heat flux estimates using AVHRR with scintillometer measurements over semi-arid grassland in northwest Mexico. Agric. For. Meteor. 105, 81–89.

Weiss, A., 2002: Determination of thermal stratification and turbulence of the atmospheric surface layer over various types of terrain by optical scintillometry. PhD Thesis. Swiss Federal Institute of Technology, Zurich, Switzerland, 152 pp.

Wesely, M. L., 1976: The combined effect of temperature and humidity on the refractive index. J. Appl. Meteor. 15, 43–49.

Wolf, A., N. Saliendra, K. Akshalov, D. A. Johnson, and E. Laca, 2008: Effects of different eddy covariance correction schemes on energy balance closure and comparisons with the modified Bowen ratio system. Agric. For. Meteor. 148, 942–952.

Wyngaard, J. C., Y. Izumi, and S. A. Collins, 1971: Behaviour of the refractive index structure parameter near the ground. J. Opt. Soc. Amer. 61, 1646–1650.

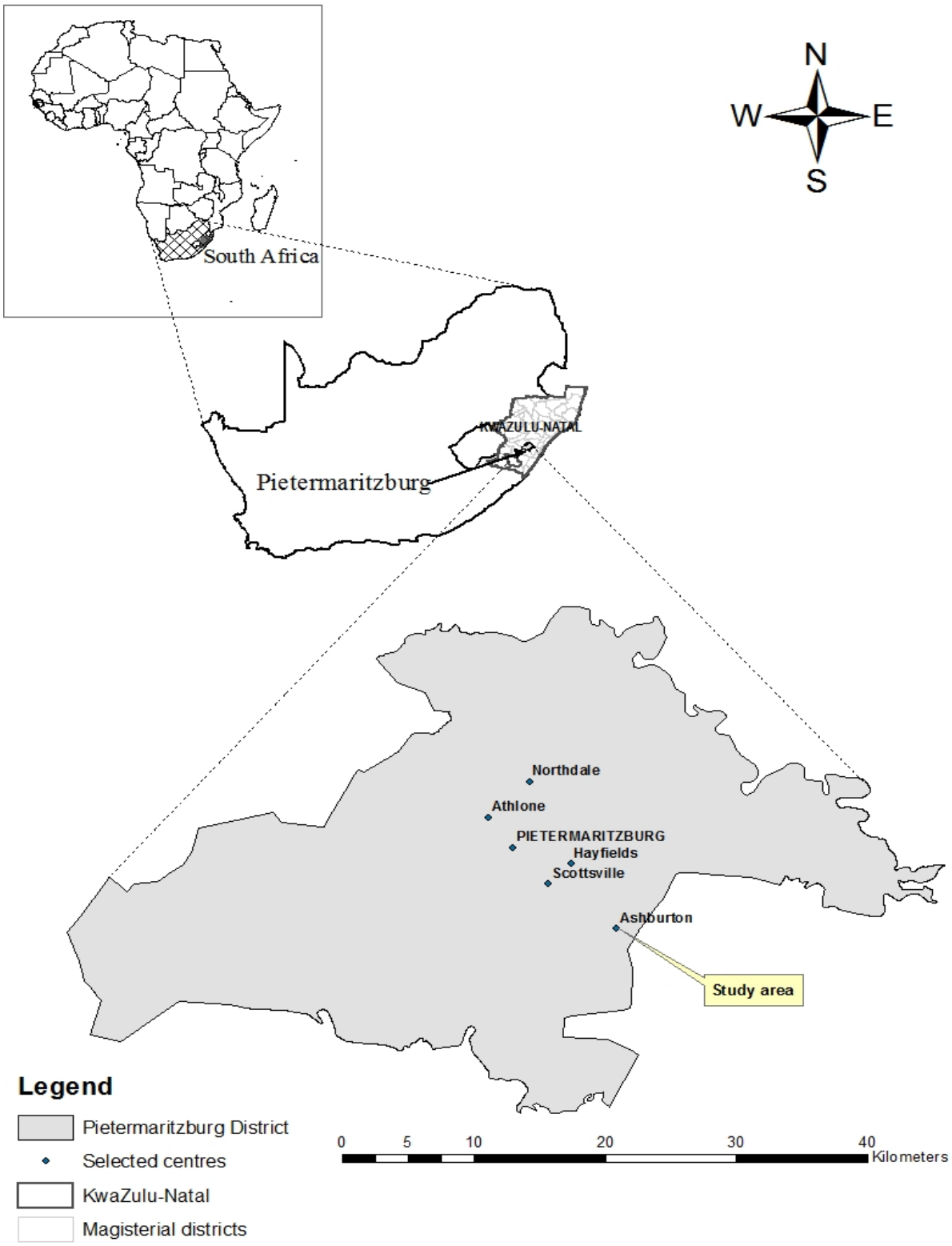

Fig. 5.1. A map showing the location of the study area. The scale is for the Pietermaritzburg district (where the study area is located).

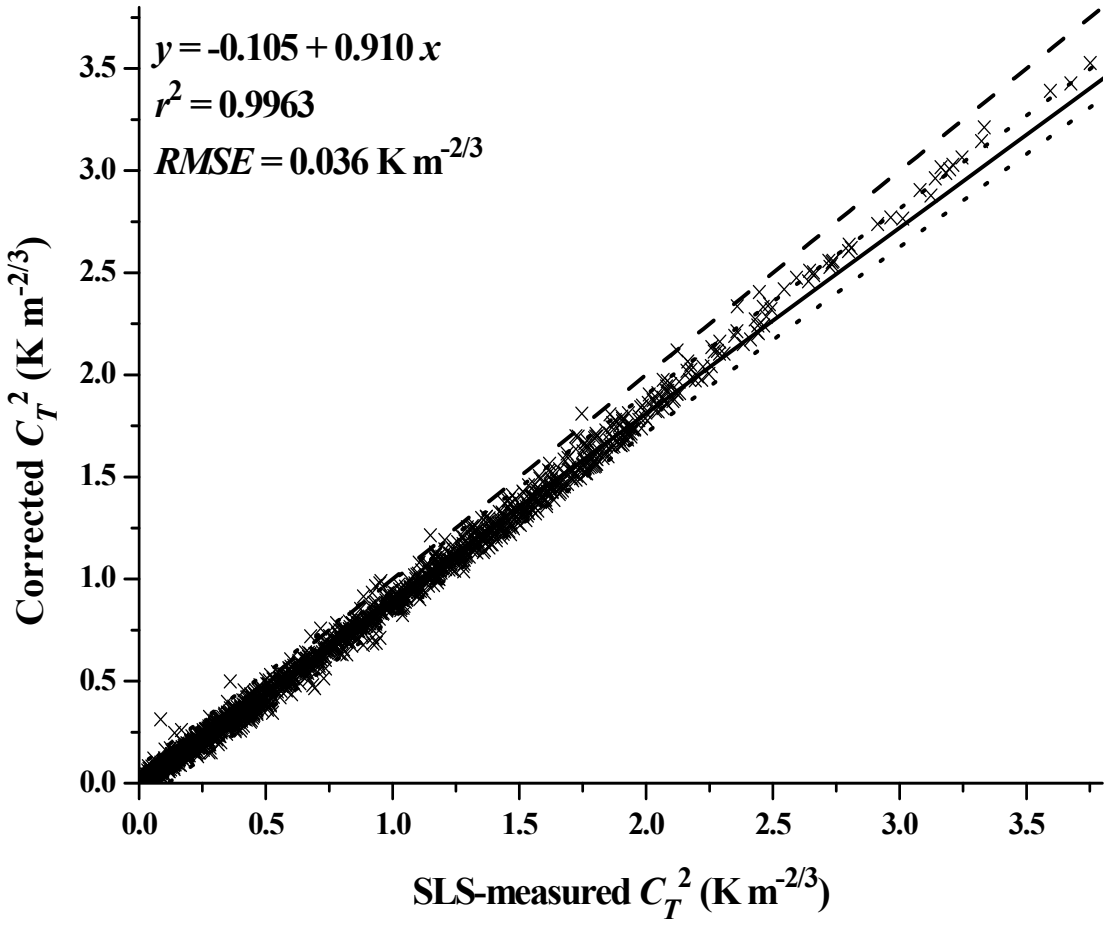

Fig. 5.2. A scatterplot of 20-min SLS-measured C_T^2 *vs* that corrected for β for DOY 116 to 181 (April to June 2004) and 274 to 340 (October to November).

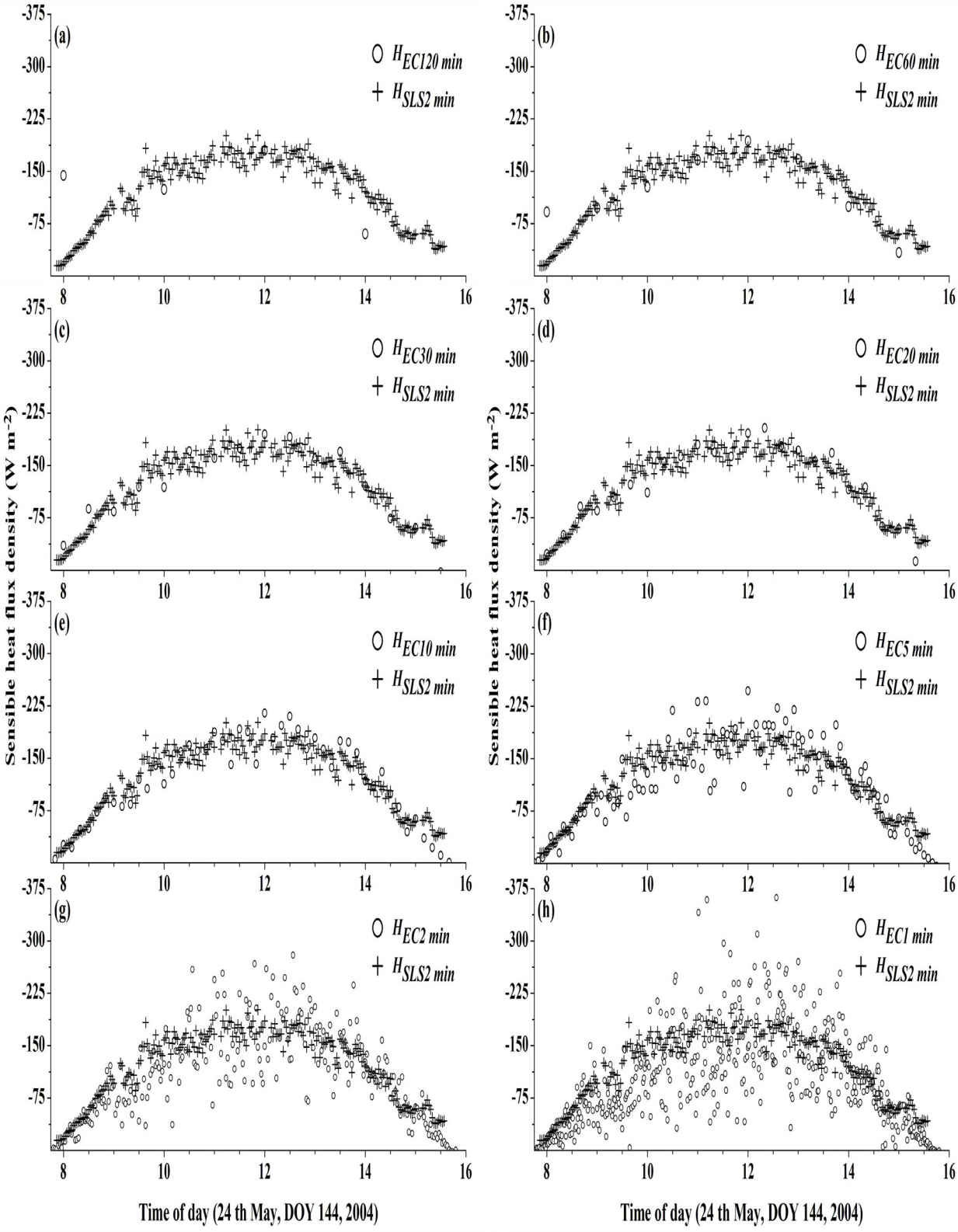

Fig. 5.3. Diurnal variation in estimated *H* using SLS and EC methods for 24th May, 2004 for various EC averaging periods, (a) 120 min; (b) 60 min; (c) 30 min; (d) 20 min; (e) 10 min; (f) 5 min; (g) 2 min and (h) 1 min, and in all panels H_{SLS} with an averaging period of 2 min is shown for comparison.

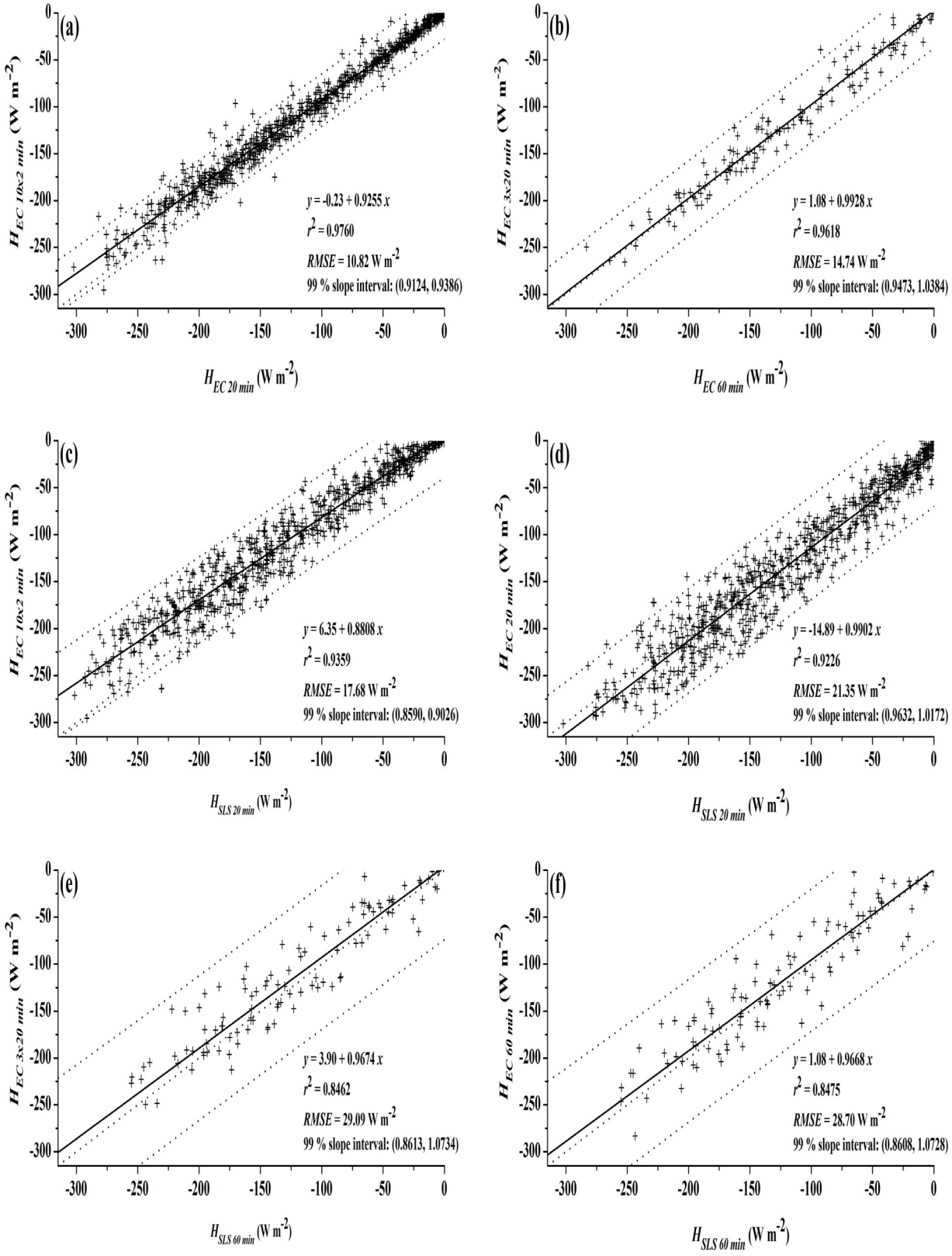

Fig. 5.4. Scatterplots for the period 19th April to 25th May 2004 of the estimates of β-corrected *H* for SLS and EC methods for various averaging periods: (a) $H_{EC10x2\ min}$ (*y*) *vs* $H_{EC20\ min}$ (*x*); (b) $H_{EC3x20\ min}$ (*y*) *vs* $H_{EC60\ min}$; (c) $H_{EC10x2\ min}$ (*y*) *vs* $H_{SLS20\ min}$ (*x*); (d) $H_{EC20\ min}$ (*y*) *vs* $H_{SLS20\ min}$ (*x*); (e) $H_{EC3x20\ min}$ (*y*) *vs* $H_{SLS60\ min}$ (*x*); (f) $H_{EC60\ min}$ (*y*) *vs* $H_{SLS60\ min}$ (*x*).

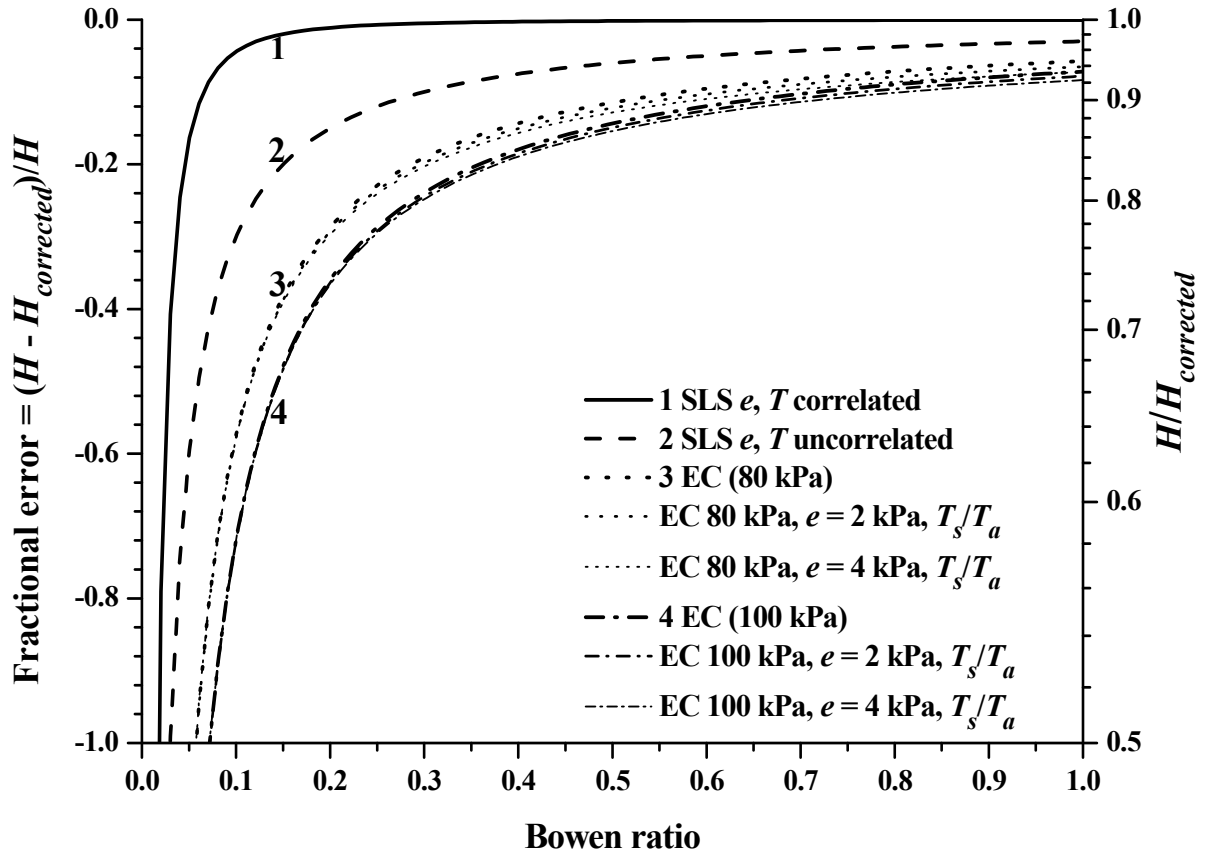

Fig. 5.5. Relative difference between *H* and $H_{corrected}$ for both EC and SLS methods as affected by the Bowen ratio. For curve 1, it is assumed that e and T are correlated whereas for curve 2, *e* and *T* are uncorrelated. Curve 3 is for the EC method for an atmospheric pressure of 80 kPa compared to 100 kPa for curve 4. The other EC curves include the correction of the sonic virtual temperature to air temperature (Eq. (5.4)). The right-hand y-axis is scaled according to $H/H_{corrected}$.

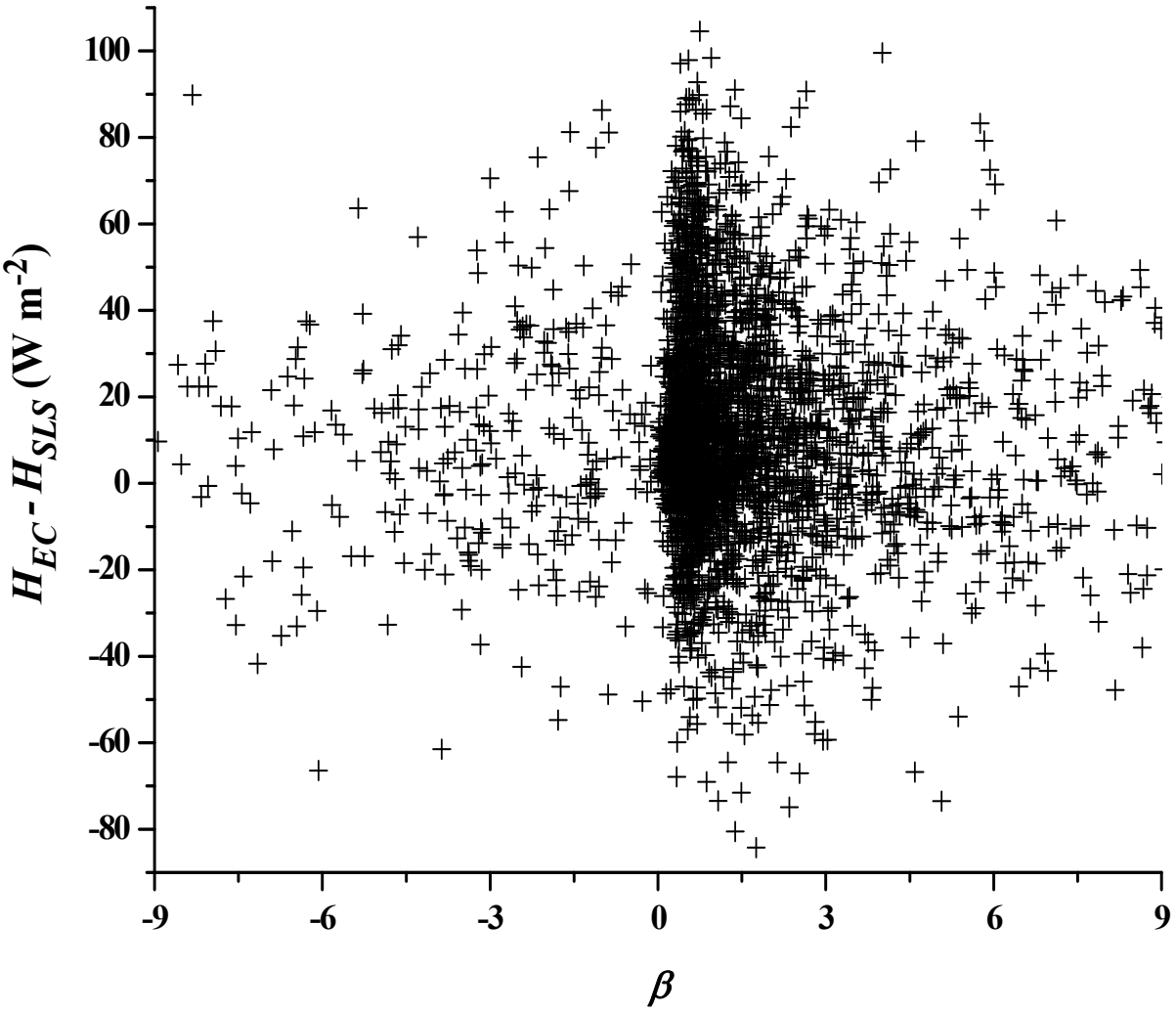

Fig. 5.6. A scatterplot of the 20-min differences in H_{EC} and H_{SLS} *vs* β for January to July 2004.

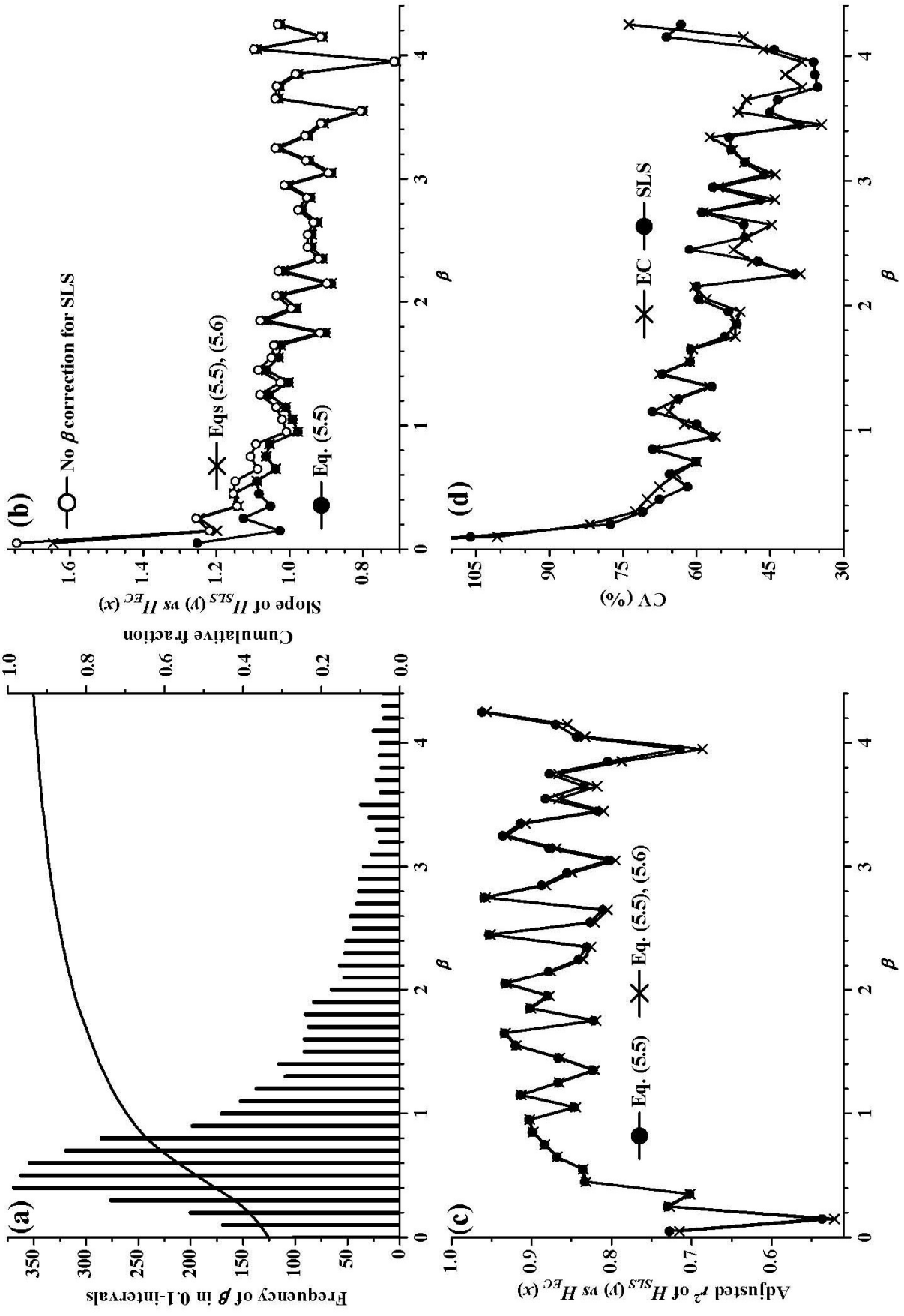
(a)
Frequency of β in 0.1-intervals
Cumulative fraction
(b)
No β correction for SLS
Eqs (5.5), (5.6)
Eq. (5.5)
Slope of H_{SLS} (y) vs H_{EC} (x)
(c)
Eq. (5.5)
Eq. (5.5), (5.6)
Adjusted r^2 of H_{SLS} (y) vs H_{EC} (x)
(d)
EC
SLS
CV (%)
β

Fig. 5.7. The results for the period January to July of the influence of β, in 0.1-increments, on the H_{SLS} (y) and H_{EC} (x) measurement comparisons: (a) the histogram and cumulative fraction of β; (b) the slope of the H_{SLS} and H_{EC} comparisons; (c) the adjusted slope of the H_{SLS} and H_{EC} comparison; (d) the coefficient of variation for H_{SLS} and H_{EC}.

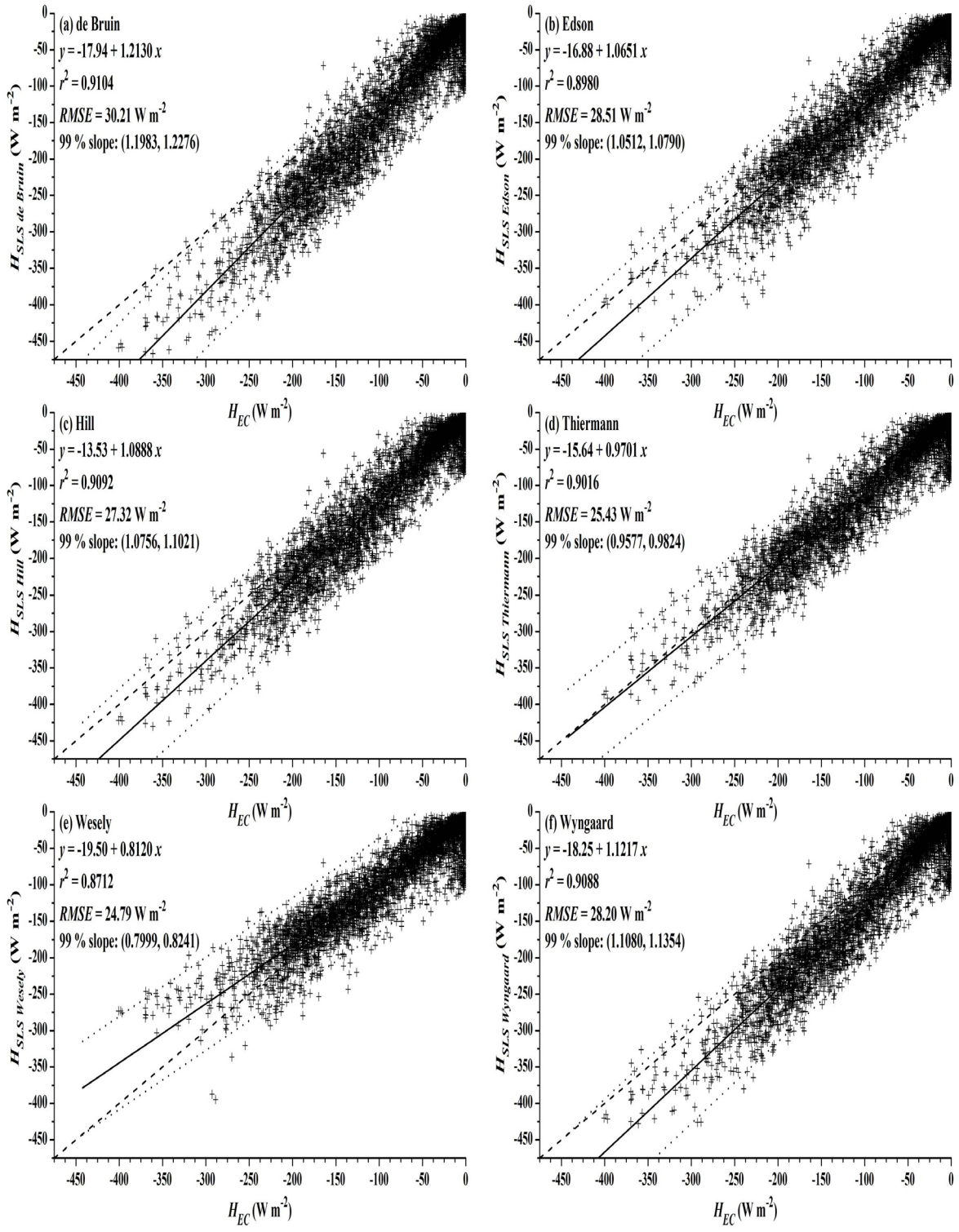

Fig. 5.8. The results for the period January to July of the 20-min comparisons between H_{SLS} and H_{EC} with the SLS estimates estimated using selected MOST methods: (a) de Bruin et al. (1993); (b) Edson and Fairall (1988); (c) Hill et al. (1991); (d) Thiermann (1990); (e) Wesely (1976) and (f) Wyngaard et al. (1971).

6 MEASUREMENT OF GRASSLAND EVAPORATION USING A SURFACE-LAYER SCINTILLOMETER[1]

6.1 Abstract

A dual-beam surface-layer scintillometer (SLS) was used to estimate sensible heat flux (*H*) every 2 min for a path length of either 50 or 101 m, for more than 30 months in a mesic grassland in eastern South Africa. The SLS method relies on Monin-Obukhov similarity theory, the correlation between the laser beam signal amplitude variances and the covariance of the logarithm of the beam signal amplitude measured using two laser detectors. Procedures for checking SLS data integrity in real-time are highlighted as are the post-data collection rejection procedures. From the *H* estimates using SLS and measurements of soil heat flux and net irradiance, evaporation rates were calculated as a residual of the shortened energy balance equation and compared with grass reference evaporation rates (ETo). Inconsistent hourly ETo values occur in the late afternoon due to the incorrect assumption that the soil heat flux is 10 % of net irradiance. The SLS estimates of *H* and the estimates of evaporation rate as a residual compared favourably with those obtained using the Bowen ratio and eddy covariance methods for cloudless days, cloudy days and days with variable cloud. There was no evidence for the eddy covariance measurements of *H* being underestimated in comparison to the Bowen ratio and SLS measurements. On many days, the diurnal variation in SLS *H* was asymmetrical, peaking before noon.

Keywords:

Energy balance

Bowen ratio

Eddy covariance

Grass reference evaporation

Rejection criteria

6.2 Introduction

The possible prescription by government of methods for making a volumetric determination of water, for purposes of water allocation and charges in the case of activities resulting in stream flow reduction, is stated in the 1998 Republic of South Africa National Water Act. It is therefore important to consider how evaporation, and evaporation rate, can be measured or estimated routinely, with reliable accuracy and precision (Savage et al., 2004; Savage, 2009), for a range of land surface types. Determination of reliable and representative evaporation data using land-based instrumentation is an important issue of atmospheric research with respect to applications in agriculture, applied environmental sciences, hydrology and micrometeorology and has particular value in validating remotely-sensed evaporation estimates. Long-term measurements of evaporation at different time scales and from different climate regions are not yet readily available (Jarmain et al., 2009).

Point (single-level), profile and path-weighted atmospheric measurements have been used to estimate sensible heat flux *H*. Profile measurements consist of measurements at two vertical positions

[1] Based on Savage et al. (2010)

above the surface in question and are used in the Bowen ratio (BR) method. Sensible heat flux is driven by vertical temperature differences between the canopy or soil surface and overlying air. By contrast, latent energy flux *LE* – from which evaporation rate may be calculated – is driven by vertical water vapour pressure differences between just above the canopy or soil surface and that of overlying air. Point measurements of $H = H_{EC}$ and $LE = LE_{EC}$ are obtained by eddy covariance (EC) and path-weighted measurements of $H = H_{SLS}$ by scintillometry. All of these flux measurements have footprint representation. The flux footprint refers to the relative contribution of upwind surface sources to *H*, or *LE*, measured at a height above the canopy surface. Sensible heat flux *H* and latent energy flux *LE* are important components of the shortened energy balance. For a flat extensive surface, the shortened energy balance which neglects some terms – advection and canopy-stored heat fluxes for example – is expressed as:

$$R_{net} + H + LE + S = 0 \tag{6.1}$$

where R_{net} is the net irradiance, L □ 2.43 MJ kg^{-1} the specific latent energy of vaporisation, E the evaporation (mass) flux (kg s^{-1} m^{-2}, equivalent to mm s^{-1}) and S the soil heat flux. Hence *LE* may be estimated as a residual using measurements of the terms on the right hand side of:

$$LE = -R_{net} - H - S\,. \tag{6.2}$$

There have been reports in the literature of a lack of energy balance closure when using EC to measure both H_{EC} and LE_{EC} directly (Twine et al., 2000; Wilson et al., 2002). Lack of closure usually results in $|H_{EC} + LE_{EC}| < R_{net} + S$. Since a comparison between two methods such as BREB and EC does not identify the correct method for measurement of *H* and/or *LE*, there is a need for a third method, such as the surface-layer scintillometry (SLS), especially in view of the alleged lack of closure using EC flux measurements.

Commonly, evaporation rate is estimated from grass reference evaporation rate ETo at an automatic weather station (AWS) using the Penman-Monteith approach (Allen et al., 1998; 2006), based on daily or hourly point atmospheric measurements at a single level of solar irradiance, air temperature, water vapour pressure and wind speed. In addition, a crop factor is used as a multiplying factor for ETo to obtain the actual evaporation rate. The crop factor effectively distinguishes the vegetation under consideration from a grass reference crop. The dual crop factor approach uses one crop factor for the soil surface and another for vegetation.

A scintillometer is used to measure path-weighted *H*. The instrument measures the intensity fluctuations of visible or infrared radiation after propagation above the plant canopy of interest. It optically measures a parameter associated with refractive index fluctuations of air C_n^2, caused by air temperature fluctuations that represent the atmospheric turbulence structure. The sensible heat flux, *H*, may be estimated using the empirically-based Monin-Obukhov similarity theory (MOST). SLS instruments operate over horizontal distances between 50 and 350 m. Large aperture scintillometers (LAS) operate over typical distances between 250 m and up to 3 km. Typically, for areas of between about 0.25 and 5 ha, the SLS would be appropriate and the LAS for areas larger than about 6 ha.

The objective of this work is to contrast various methods used for estimating evaporation rate as a residual of the shortened energy balance. Practical aspects of the use of the SLS method for the estimation of evaporation rate for a mesic grassland are presented. Grass reference evaporation rate ETo measurements are also presented for comparison. Comparisons are made between H obtained using the various methods to investigate whether H estimates using the EC method are underestimated, as is implied by the lack of closure when using EC measurements. The methodology for the measurement of $H = H_{SLS}$ and the subsequent estimation of $LE = LE_{SLS}$ is presented. A comparison is made between BREB, EC and SLS methods of estimating H and LE. Also, procedures and definition for rejection of out-of-range and bad or "doubtful" SLS data are presented.

6.3 Energy balance aspects, evaporation methods, energy balance closure and measurement footprint

There are many methods used for estimating evaporation rate. As mentioned by Drexler et al. (2004) in their review, very few evaporation estimation methods work well for an hourly time-step, and in some cases, do not work well even for a daily time-step. Virtually all of the methods, except for EC, from which direct measurements of H_{EC} and LE_{EC} at a point are obtained, rely on a theoretical framework and certain assumptions or approximations for arriving at an expression for LE, in terms of other measurable quantities. Many methods invoke use of a shortened surface energy balance (Eq. (6.1)) that allows LE to be estimated indirectly.

Weighing lysimeters are large containers, filled with soil, water, other chemicals and entire plant(s). The weighing lysimeter method allows for a direct measurement of the rate of total water loss from a vegetated surface (soil evaporation plus transpiration plus wet-canopy evaporation), and is often regarded as the standard method for measuring LE (Aboukhaled et al., 1982). Weight measurements are made at regular time intervals. The weight difference per unit time difference divided by the density of water and divided by the cross-sectional area of the lysimeter yields the evaporation rate in mm h^{-1} or mm day^{-1}. Lysimeters allow the water loss rate from such containers to be measured for very short time intervals and longer, from hours to days or longer. The disadvantages of the lysimetric method include: cost, destructive nature of the measurements in the sense that a relatively large volume of disturbed or sometimes undisturbed soil is placed in a container usually of metal construction, which isolates the lysimeter soil from neighbouring soil, and the non-portable nature of the measurement method. Also, the representation, or the so-called footprint, of the evaporation rate measurement is localised to the cross-sectional area of the lysimeter, although evaporation rate is also influenced by atmospheric events not confined to this area. Much less expensive is the microlysimetric method, but the surface area is an order of magnitude less than a large weighing lysimeter and it is still a destructive method, still isolated from neighbouring soil, and often not able to contain whole plants and therefore used for measuring only soil evaporation rate over short periods.

Given the limitations of the lysimetric method, the search for an alternative standard for evaporation rate estimation has been the focus of many studies for several decades. Methods such as EC involve measurement, typically at a frequency of 10 Hz, of two atmospheric variables, vertical wind speed and water vapour pressure, from which LE_{EC} is calculated directly by eddy covariance following many corrections. Similarly, using eddy covariance, H_{EC} is calculated from the covariance of vertical wind speed and air temperature measurements over a specified time interval – usually

hourly or sub-hourly. The BREB method involves up to eight measurements, usually at a frequency of 1 Hz, of atmospheric and energy balance components, and a theoretical framework and assumptions to estimate H_{BR} and LE_{BR} (Savage et al., 2004). Empirical methods, or the Penman-Monteith approach, are used to estimate grass reference evaporation rate, ETo, which uses the crop factor approach to calculate evaporation rate. The more portable and much less invasive BREB and EC methods, compared to the use of a lysimeter, are more popular research methods for the estimation of evaporation rate and can be used to collect unattended measurements for extended periods of time. These methods were the focus of previous research reports (Savage et al., 1997, 2004; Jarmain et al., 2009). The EC and BREB methods essentially yield point estimates of H and LE although these flux estimates are influenced by events upwind of the point of measurement. The extent of the footprint area of influence on the flux measurement, using both BREB and EC methods has received attention. For example, Stannard (1997) investigated the footprint of BREB flux measurements and Savage et al. (1995; 1996) investigated the footprint of EC flux measurements. Agreement between BREB, EC, and SLS flux measurements of H, for example, may be dependent on the footprint of H, which in turn depends on sensor height and atmospheric stability condition.

Some literature reports on the inadequacy of the EC method for the direct estimation of LE (Wilson et al., 2002; Ham and Heilman, 2003) resulting in $|H_{EC} + LE_{EC}| < R_{net} + S$ (Twine et al., 2000). An alternative approach to using a full EC system for measuring H_{EC} and LE_{EC} is to measure H_{EC} only, and to estimate LE as a residual of the shortened energy balance from simultaneous measurements of R_{net}, S and $H = H_{EC}$ using Eq. (6.2).

The frequency of SLS measurements is typically 1 kHz, 125 Hz for boundary-layer scintillometer measurements for which the path length is up to 10 km, compared to 1 Hz for BREB measurements and 10 Hz for EC measurements. Because of the high frequency of the SLS measurements, the averaging period for H_{SLS} can be as short as 1 or 2 min compared to the commonly-used 20 min for BREB and 30 min for EC averaging periods (Savage, 2009).

The SLS method appears to be a useful, robust and accurate method for obtaining a path-weighted estimate for $H = H_{SLS}$. However, many of the studies employing the SLS method have been very short in duration – in some cases just for a few days as mentioned by Odhiambo and Savage (2009b) and in other cases for a couple of months – and have not in detail compared the SLS method with BREB and EC measurement methods.

6.4 Materials and methods

6.4.1 Site details

Field EC and SLS measurements were conducted during the period January 2003 to June 2005 in the Hay Paddock area, neighbouring Ashburton and close to Pietermaritzburg, South Africa (29°38' S, 30°26' E) with an altitude of 671.3 m. This is a natural grassland site dominated by *Diheropogon amplectens*, *Themeda triandra*, *Tristachya leucothrix* and *Cymbopogon excavatus*. The soils are derived from Dwyka Tillite with a typical soil profile consisting of a loam A horizon (0–0.3 m) overlying clay B1 and B2 horizons extending to 1 m. The site experiences summer rainfall and has an average slope of 1°15' to the SE and a minimum fetch distance in the prevailing S-E wind direction of 135 m for the EC system (Fig. 6.1). The SLS system, consisting of a transmitter and a receiver, had

respective fetch distances of 90 and 138 m for the 101-m path length. The minimum fetch for the next-most dominant winds from the N-W is 117 m for the EC system and 146 and 114 m for the SLS transmitter and SLS receiver respectively. Fetch distances from the middle position of the beam was 118 m for S-E winds and 130 m for N-W winds; vegetation height at this position has the greatest influence on the calculated beam-weighted vegetation height used in the SLS computations. Beyond these distances and to the south, the site is exposed and the slope increases. Adjacent to the site was natural grassland and occasional trees, with the exception of the north-west side of the study area which is residential with some trees. The grass growth is seasonal and this seasonality affects the partitioning of $-R_{net} - S$ into H and LE. There were occasional power problems and interruptions due to the accidental fire in August 2004 and accidental cutting of cables. The BREB measurements commenced in December 2003.

6.4.2 Grass reference evaporation estimation

The procedures for estimating sub-daily grass reference evaporation rate, ETo, are described by Allen et al. (2006). The calculations were performed in a spreadsheet with ETo estimated every 2 minutes using these procedures, from AWS measurements of solar irradiance, air temperature, water vapour pressure and wind speed. While the AWS system was available at the site, ETo estimates were based on the AWS data. After the AWS system was removed, measurements from the same model of sensors were used to calculate ETo, except that for solar irradiance, a Kipp and Zonen (Delft, The Netherlands) CM3 thermopile sensor was used. For some of the time, horizontal wind speed from the three-D sonic anemometer was used. Water vapour pressure was measured using a Vaisala CS500 (Helsinki, Finland) air temperature and relative humidity sensor from the AWS system, or using one of the following humidity sensors: another CS500, a Vaisala HMP35C or HMP45C air temperature and relative humidity sensor or a cooled dew point hygrometer (model Dew-10, General Eastern Corp., Watertown, Massachusetts, USA). An iterative procedure, discussed in an Appendix to the thesis, is used to calculate ETo.

6.4.3 Surface-layer scintillometer measurements

A dual-beam surface-layer scintillometer (model SLS40-A, Scintec Atmospärenmessetechnik, Tübingen, Germany) (Thiermann, 1992; Thiermann and Grassl, 1992), was used to estimate $H = H_{SLS}$. The beam distance of the SLS was 50 m for the initial experiments and later changed to 101 m. The beam heights were 1 and 1.6 m above the soil surface. Different path lengths would need to be used for different experimental areas. The objective for the use of the two path lengths was to test the reliability of the SLS method for the shortest possible and for an average path length. The SLS40-A receiver has four detectors, with two of the detectors used for automatic identification of, and correction for, transmitter vibration by the software used for analysis. In other words, the SLS40-A dual-beam system and its four detectors enable the separation, and correction for, the intensity fluctuations caused by beam movement. There are two detectors per beam. The SLS employs a diode laser source with an output wavelength of 670 nm and 1-mW mean output power (2-mW peak). The beam displacement and detector separation distances are 2.5 mm each, with a detector diameter of 2.7 mm. The correlation between the transmitted laser beam signal variances and the covariance of the logarithm of the beam signal amplitude is measured using the two detectors. Software, together with the instrument, allows on-line measurements at a frequency of 1 kHz and subsequent calculation every 1 or 2 min (Thiermann and Grassl, 1992) of the structure parameter for refractive index fluctuations

(C_n^2, $m^{-2/3}$), structure parameter for temperature (C_T^2, $K^2\ m^{-2/3}$), the inner scale of turbulence l_o (mm), turbulent kinetic energy dissipation rate (ε, $m^2\ s^{-3}$), sensible heat flux (H, $W\ m^{-2}$), momentum flux (τ, Pa) and the Obukhov length (L, m). Monin-Obukhov similarity theory (MOST) is assumed. The methodology for calculating the 2-, 20- or 30-min H_{SLS}, using MOST, is described by Odhiambo and Savage (2009a) and Savage (2009). This involves an iterative procedure, discussed in an Appendix to the thesis. The direction of H_{SLS} was determined from the sign of the profile air temperature gradient. Data rejection or filtering procedures were applied in a spreadsheet to the 2-min values of $H = H_{SLS}$. Sensible heat flux values were rejected, blanks were created or data recalculated:

data were rejected if the percentage of 1 kHz error-free data (EFD) was less than or equal to 25 %, most-often due to misty conditions;

data were rejected for $l_o \leq 2$ mm for the 101-m path length or $l_o \leq 3.5$ mm for the 50-m path length (Scintec, 2006). So-called saturation of the transmitted SLS signal (Lawrence and Strohbehn, 1970; Gracheva et al., 1974) generally resulted in smaller-than-expected estimates for the covariance of the logarithm of the amplitude of the radiation intensity for the two beams, and, therefore, smaller-than-expected signal correlation coefficient values for the two beams, smaller l_o values and greater-than-expected H_{SLS} magnitudes;

for missing data, designated by zeros, a blank cell was used for H_{SLS}.

6.4.4 Bowen ratio measurements

Two BREB systems (based on the Campbell 023A system, Campbell Scientific Inc., Logan, Utah, USA) and connected to a Campbell 21X datalogger, were used to measure water vapour pressure and air temperature profile differences between heights of 1.55 and 2.96 m above the soil surface. The BREB water vapour pressure profile measurements were obtained using one or more of the following sensors placed in a humidity sensor chamber: a HMP45C Vaisala air temperature and relative humidity sensor, a cooled mirror Dew-10 hygrometer, a CS500 Vaisala air temperature and relative humidity sensor. A pump was used to alternately switch the flow of air every 2 min, from one measurement height to another, to the chamber and return to the atmosphere.

Air temperature was measured at two levels using unshielded and naturally-ventilated 75-μm type-E thermocouples. At each level, a parallel combination of thermocouples was used. Extra insulation was used to cover the thermocouple connectors at the thermocouple joins. Extra precautions were taken to cover and thermally insulate the point at which the thermocouple wires were connected to the datalogger. The thermocouples were regularly inspected for damage, cleanliness, insects and cobwebs. The BREB data exclusion procedures, mainly associated with a Bowen ratio approaching –1 but also due to condensation events, are described by Savage et al. (2009).

For measuring the remaining components of the energy balance, three net radiometers (model Q*7, REBS, Seattle, Washington, USA) within a few metres of each other were used to measure R_{net}. The net radiometers were calibrated according to the procedures of Savage and Heilman (2009). Placement height was 2 m above the soil surface. Seven soil heat flux plates (model HFT-3, REBS) were used to measure soil heat flux at a depth of 80 mm and a system of parallel thermocouples at depths of 20 and 60 mm was used to calculate the soil heat flux stored above the plates (Tanner,

1960). Volumetric soil water content in the first 60 mm of the surface was measured using a frequency domain reflectometer (ThetaProbe, model ML2x, Delta-T Devices, Cambridge, UK) and a Campbell 615 soil reflectometer. Most of these sensors were connected to a Campbell CR7X datalogger and transferred to a CR23X datalogger after the 2003 accidental fire. The net radiometers and soil heat flux plates and other EC sensors were positioned approximately midway between the transmitter and receiver units of the SLS. Measurements were every 1 s and averages obtained every 2 min. These in turn were used to calculate 20-min averages for the BREB calculations.

6.4.5 Eddy covariance measurements

Adjacent to the AWS, a three-dimensional sonic anemometer (SWS-211/3V, Applied Technologies, Boulder, Colorado, USA), referred to as the EC system, was used to measure $H = H_{EC}$ at a height of 1.45 m above the soil surface. Later in the study, the EC measurement height was increased to 2.12 m above the soil surface to correspond to the average height of the BREB levels. This three-D anemometer, with a 100-mm sonic path length, was connected to a Applied Technologies digital-to-analogue SA-4 converter which was then connected to a Campbell 21X datalogger. Measurements of the three components of wind velocity, u, v, w in the x, y and z directions, respectively, and sonic temperature, T, were performed every 0.1 s (frequency of 10 Hz). Following the accidental fire, the 21X datalogger was replaced by a CR23X datalogger and a replacement three-D sonic anemometer was used (same model). The sonic anemometer measurements were processed on-line and the 2-min covariance between w and T (for determining $H = H_{EC}$) and the covariance between w and the horizontal wind speed $U = (u^2 + v^2)^{1/2}$ (for determining momentum flux) were calculated using ρ = 1.12 kg m^{-3} and c_p = 1033 J kg^{-1} K^{-1}. The 2-min averages of u, v, w and sonic temperature, T, and wind direction, $\theta = \arctan(v/u)$, were also stored. Coordinate rotations for the EC data (Kaimal and Finnigan, 1994) were not performed for the initial study using a field computer due to security concerns and the lack of equipment to store the 10-Hz EC data. For the initial measurements, for which the SLS beam path length was 50 m, w and T were sampled every 0.2 s using a Campbell CA27 one-D sonic anemometer and 25-μm fine-wire thermocouple, respectively, and data processed using a Campbell 21X datalogger. Two-min averages, standard deviations and covariances were stored for further data analysis. Data rejection rules for the EC measurements were fairly simple: sometimes, usually whenever there was condensation, covariances of -99999 were excluded. Missing values, and also periods when incorrect sonic temperatures approaching 50 ^{o}C were recorded, were excluded and not used to calculate $H = H_{EC}$. These incorrect values were caused by dirt on the sonic transducers, faulty transducers or sonic beam interruptions. Night-time EC measurements were often unreliable due to condensation or mist affecting the acoustic signal.

Calibration of the EC system and its replacement was performed by placing the three-D system in a box for which each component of the wind speed was 0 m s^{-1}. Air temperature and relative humidity, required for accurate speed of sound estimation (from which the sonic temperature is calculated), were independently measured using averaging thermocouples and a Vaisala CS500 air temperature and relative humidity sensor placed inside the box.

For a limited period, a fast-responding open-path infrared analyser for water vapour pressure and carbon dioxide concentration (model LI-7500, LI-COR Inc., Lincoln, Nebraska, USA) and a second Applied Technologies three-D sonic anemometer (model SATI/3V) with a sonic path length of

150 mm were used to calculate the following fluxes using the EC technique: H_{EC}, LE_{EC}, momentum, and carbon dioxide.

6.5 Results and discussion

6.5.1 Rejection criteria for the exclusion of out-of-range and "bad" or doubtful SLS data

For positive dT/dz values, adjusted for the dry adiabatic lapse rate, where dT/dz is the profile air temperature gradient measured using BREB thermocouples, corresponding to unstable atmospheric conditions, EFD > 25 % and l_o > 2 mm for the 101-m path length and non-blank H_{SLS} values, $-H_{day}$ is displayed in the cell. For stable atmospheric conditions, corresponding to negative dT/dz adjusted values, and EFD > 25 %, and l_o > 2 mm, $-H_{night}$ is displayed in the cell. For periods when the BREB equipment was not available, the sign of H_{SLS} was made equal to that of H_{EC}. If both BREB and EC measurements were unavailable, it was assumed that unstable conditions prevailed between 06h00 and 18h00 (usually corresponding to R_{net} > 0 W m^{-2}) and stable conditions otherwise.

6.5.2 Percentage of acceptable SLS data

For the period January 2003 to August 2004 there was little seasonal variation in the percentage of "acceptable" 2-min H_{SLS} measurements for the day-time hours (taken as 06h00 to 18h00) and the percentage was consistently high – between 86.7 and 94.8 % (Fig. 6.2a). The night-time variation in the percentage had a more pronounced seasonal pattern, with the lowest percentage acceptable measurements occurring between January and March in summer of each year (Fig. 6.2b). The lower night-time percentage values were due to the effects of dew and mist. These events also affected EC and BREB data.

The average percentage of the reliable 1-kHz data, denoted Nok%, varied between 62 and 85 % (Fig. 6.2c) for the period 06h00 to 18h00 and between 33 to 73 % for the night-time (Fig. 6.2d). These data demonstrate the reliability of the SLS method for obtaining long-term H_{SLS} measurements and other micrometeorological parameters. The lowest Nok% was, during the summer rainfall period (September to March), due to the influence of rain and mist events on beam transmission.

6.5.3 Flux comparisons

The averaging periods for the various measurement systems are 2 min for energy balance, ETo and SLS systems, 20 min for the BREB system and 30 min for the open-path EC system. The 2-min H values are easily scaled to 20 min, 30 min and daily time intervals but scaling from longer to shorter times is not possible. For EC measurements, 2- and 20-min averaging periods were used.

The EC technique is often regarded as the standard for flux measurements, against which all comparisons of H are usually made. However, there is currently no agreement on the averaging period for EC measurements (Sun et al., 2006; Odhiambo and Savage, 2009a). Initially, in January/February 2003, H_{EC} measurements were at intervals of 20 min using the CA27 EC system consisting of a one-D sonic anemometer and a fine-wire thermocouple. A field experiment using two EC systems was conducted with one system performing the covariance between w and T every 20 min and the second system every 2 min. The calculated 2-min $H = H_{EC}$ values were then averaged over 20 min and compared with H_{EC} determined using a 20-min time averaging period (Fig. 6.3). The correspondence

is good (slope of 0.9689 and root mean square error (RMSE) of 9.67 W m^{-2}) and this partly justifies using the 20-min time period for the EC method.

The diurnal variation of the surface energy balance components for day of year 81, 2003, as a typical example, is shown with LE_{SLS} estimated as a residual, in this case every 2 min, using Eq. (6.2) from H_{SLS}, R_{net} and S (Fig. 6.4). The agreement between H_{SLS} (2 min) and H_{EC} (20 min) is good in spite of the SLS yielding path-weighted measurements, the very different principles of operation, different footprints for the EC and SLS measurements, and the different measurement heights. The 2-min EC point measurements of H_{EC}, data not shown, exhibit a marked variation from one measurement period to the next whereas there is a much-reduced variation in the corresponding path-weighted H_{SLS} measurements (Odhiambo and Savage, 2009a). Very occasionally, the H_{SLS} measurements are impacted on by l_o approaching the critical value of 2 mm. Such an occurrence is indicated by the arrow (at 12h48 for example) in Fig. 6.4. The 2-min ETo estimates are also shown and for some of the time (late afternoon) exceeded R_{net}. This is unexpected, although it should be noted that R_{net} used for estimating ETo is based on solar irradiance measurements and an estimate of the surface reflection coefficient (0.23) and S estimated as 0.1 of R_{net}, the latter clearly not the case in the late afternoon (Fig. 6.4). The ratio of LE_{SLS} to ETo was quite stable during the day, peaking at 0.8 at 08h00 and at 16h00, with a minimum of about 0.67 at noon and averaging 0.73 for day-time hours with a standard deviation of 0.06. The R_{net} measurements are symmetrical around noon whereas S is generally asymmetrical with a peak after the noon period due to the conductive lag of the soil measurements. Measurements of H_{SLS} are also asymmetrical with a peak before noon with the result that the LE_{SLS} (residual) estimates (Eq. 6.2) are roughly symmetrical around noon. The correspondence in H between the EC and SLS measurement methods is improved on most days under conditions when there is reduced turbulence, particularly on uniformly cloudy days, and times before 10h00 and after 14h00 (data not shown).

The asymmetrical diurnal trend in H_{SLS} is shown in Fig. 6.5, more clearly on some days than on others. Also shown in Fig. 6.5 is the reasonable agreement between H_{EC} and H_{SLS} for a number of near-cloudless days. The H_{EC} estimates were every 20 min and H_{SLS} every 2 min, as previously mentioned, since the 2-min H_{EC} measurements showed considerable variation. There is no evidence in Fig. 6.5 for a consistent underestimation of H_{EC} compared to H_{SLS} over an extended period of time. Furthermore, there is no evidence to indicate that the effective (path-weighted) beam height input was incorrect (Cain et al., 2001). An incorrect input would have caused a consistent overestimation or underestimation in H_{SLS} compared to H_{EC}: the results of an error analysis showed that a fractional error in the beam height of 5 % would result in a fractional error of 4 % in H_{SLS} (Savage, 2009).

Comparisons between the BREB, EC and SLS methods for estimating H are shown (Fig. 6.6) for a three-day period (4 to 6 June, 2004) of variable weather conditions. Sky conditions varied from cloudless, to scattered cloud, and with completely overcast conditions on the 5 June. In spite of these contrasting weather conditions, the SLS path-averaging method showed reasonable agreement with H_{EC} point measurements (20-min values), with BREB and/or EC methods overestimating for some of the time on day of year 178 and 180. Both H_{EC} and H_{BR} measurements showed spikes in their variation but there was no evidence of this for the H_{SLS} measurements. The spikes occur when there are sudden changes in microclimatic conditions, particularly R_{net} (Fig. 6.6). The SLS path-weighted method tends

to average such spikes over the beam path length. Of particular note is the rather unexpected agreement in measurements for all methods during the night (stable conditions).

A regression comparison between daily (accumulated 20-min) evaporation values for the BREB and SLS methods is shown for a period of 187 days (1 Jan to 5 July, 2004) in Fig. 6.7a. It is recognised here that common variable, namely R_{net} and S, are used in both x and y data in these plots. This criticism could be avoided throu8gh the use of independent measurements of R_{net} and S used to determine LE_{SLS}, LE_{BR} and LE_{EC}. The independent measurements of R_{net} and S would, presumably, be highly correlated. The impact of errors in R_{net} and S on LE estimated as a residual using Eq. (6.2) has been reported on by Savage (2009) and will therefore not be repeated here. The agreement between daily LE_{SLS} (mm) and LE_{BR} (mm) was fair, with a slope of 0.842 mm mm^{-1} (standard error of slope SE = 0.037 mm mm^{-1}) and correlation coefficient R = 0.871. The wide bands represent the 95 % confidence belts for a single predicted y value and the narrower ones that for the population mean. Much of the variability can be attributed to the BREB method, for which condensation in the hoses and mixing bottles, particularly in the early-morning hours and/or rain periods, invalidated measurements for many hours and longer when unchecked.

The regression comparison between daily (accumulated 20-min) LE values for the EC and SLS methods for the same time period showed much less scatter (Fig. 6.7b). The slope value of 0.874 mm mm^{-1} (SE = 0.020 mm mm^{-1}) and R = 0.960 are indicative of the good comparison between measurements for the two methods. Much of the variability can be attributed to the differences between H_{EC} point-estimates and H_{SLS} path-weighted estimates, although both fluxes have footprint representation. The footprint area for each of the fluxes from BREB, EC and SLS methods is different and varies according to wind direction, measurement height, stability parameters, friction velocity and H. The fetch distances for the different measurement methods were not the same, and this too would have contributed to the measurement differences in H and LE in Fig. 6.6 and in Figs. 6.7 (a), (b) respectively.

All three measurement methods are affected by mist, dew, rainfall and other events that affect the complete transmission of either the EC sonic beam or the SLS laser beam. In the case of the BREB measurements, as mentioned previously, condensation on sensors or inside the hoses and mixing bottles affects the accuracy of the air temperature and water vapour pressure profile measurements adversely. Furthermore, the upper domes of the net radiometer(s) are often covered with droplets of water during such conditions and during rain events, invalidating the R_{net} measurements and therefore invalidating LE calculated as a residual and also LE_{BR}.

The agreement between estimates of LE obtained using the independent open-path EC system and that estimated using $LE_{SLS} = -R_{net} - S - H_{SLS}$ was poor (data not shown). The reason(s) for this poor agreement needs to be explored further. It would appear however that the problem related to the lack of energy balance closure using direct measurements of H_{EC} and LE_{EC} may be due to the direct measurement LE_{EC}, given that H_{EC} compares well with H_{SLS} and assuming that R_{net} and S are measured correctly.

6.6 Conclusions

Three methods for estimating point (EC and BREB) and path-weighted (SLS) sensible heat flux, each with a very different theoretical basis or formulation, showed reasonable agreement for a variety of wind and weather conditions and different canopy heights, for a mesic grassland site for which the grass canopy growth was seasonal, with evaporation rates being a maximum in summer and a minimum in winter. The measurements of the energy balance components allowed evaporation rate to be estimated using the shortened energy balance and AWS measurements allowed grass reference evaporation rate (ETo) estimates. Inconsistent late-afternoon ETo estimates, greater than the net irradiance R_{net}, occurred due to the incorrect assumption that soil heat flux is 10 % of R_{net}. The BREB sensible heat flux and evaporation rate measurements were more variable than those obtained using the EC and SLS methods. The BREB method was adversely affected, on occasion for days, by condensation events due to liquid water on sensors, in hoses and in mixing bottles. We conclude that the SLS method is a robust method allowing long-term and continuous evaporation rate measurements that represent a larger measurement footprint than may be the case for the BREB and EC methods. There was no evidence for the underestimation in sensible heat flux by the EC method, as has been suggested in the literature.

6.7 Acknowledgements

The financing of the project by the Water Research Commission (WRC) through projects K349 and K1335 and the contribution of the members of the two WRC Steering Committees is gratefully acknowledged. Additional funding in the latter stages of the WRC K1335 scintillometer project from the National Research Foundation is also gratefully acknowledged. The CSIR kindly provided the open-path EC system. The project was only possible with the cooperation of the following: owner Mr SJ Hilcove and farm manager Mr H Ovenstone of the Bellevue farm site used for this research; Ms Jody Manickum (Agrometeorology) of the School of Environmental Sciences, University of KwaZulu-Natal for her assistance, and Mr Peter N Dovey for part of the technical support required for this project.

6.8 References

ABOUKHALED A, ALFARO A and SMITH M (1982) Lysimeters. Food and Agriculture Organization of the United Nations, Rome, Italy. 68 pp.

ALLEN RG, PEREIRA LS, RAES D and SMITH M (1998) Crop evapotranspiration - Guidelines for computing crop water requirements - FAO Irrigation and drainage paper 56. Food and Agriculture Organization of the United Nations, Rome, Italy. 315 pp.

ALLEN RG, PRUITT WO, WRIGHT JL, HOWELL TA, VENTURA F, SNYDER R, ITENFISU D, STEDUTO P, BERENGENA J, YRISARRY JB, SMITH M, PEREIRA LS, RAES D, PERRIER A, ALVES I, WALTER I and ELLIOTT R (2006) A recommendation on standardized surface resistance for hourly calculation of reference ETo by the FAO56 Penman-Monteith method. *Agric. Water Manage.* **81** 1–22.

CAIN JD, ROSIER PTW, MEIJNINGER W and DE BRUIN HAR (2001) Spatially averaged sensible heat fluxes measured over barley. *Agric. Forest Meteorol.* **107** 307–322.

DREXLER JZ, SNYDER RL, SPANO D and PAW U KT (2004) A review of models and micrometeorological methods used to estimate wetland evapotranspiration. *Hydrol. Process.* **18** 2071–2101.

GRACHEVA ME, GURVICH AS, LOMADZE SO, POKASOV VI and KHRUPIN AS (1974) Probability distribution of strong fluctuations of light intensity in the atmosphere. *Radiophys. Quantum Electron.* **17** 83–87.

HAM JM and HEILMAN JL (2003) Experimental test of density and energy-balance corrections on carbon dioxide flux as measured using open-path eddy covariance. *Agron. J.* **95** 1393–1403.

JARMAIN C, EVERSON CS, SAVAGE MJ, MENGISTU MG, CLULOW AD, WALKER S and GUSH MB (2009) Refining Tools for Evaporation Monitoring in Support of Water Resources Management. WRC Report No. 1567, Water Research Commission, Pretoria, South Africa, ISBN 978–1–77005–798–2. 137 pp.

KAIMAL JC and FINNIGAN JJ (1994) Atmospheric Boundary Layer Flows, Their Structure and Measurement. Oxford University Press, New York. 289 pp.

LAWRENCE RS and STROHBEHN JW (1970) A survey of clear-air propagation effects relevant to optical communications. *Proc. IEEE* **58** 1523–1545.

ODHIAMBO GO and SAVAGE MJ (2009a) Surface layer scintillometer and eddy covariance sensible heat flux comparisons for a mixed grassland community as affected by Bowen ratio and MOST formulations. *J. Hydrometeorol*. **10** 479–492.

ODHIAMBO GO and SAVAGE MJ (2009b) Surface layer scintillometry for estimating the sensible heat flux component of the surface energy balance. *S. Afr. J. Sci*. **105** 208–216.

SAVAGE MJ (2009) Estimation of evaporation using a dual-beam surface layer scintillometer and component energy balance measurements. *Agric. Forest Meteorol*. **149** 501–517.

SAVAGE MJ, EVERSON CS and METELERKAMP BR (1997) Evaporation Measurement Above Vegetated Surfaces Using Micrometeorological Techniques. WRC Report No. 349, Water Research Commission, Pretoria, South Africa, ISBN 1–86845–363–4. 248 pp,

SAVAGE MJ, EVERSON CS and METELERKAMP BR (2009) Bowen ratio evaporation measurement in a remote montane grassland: Data integrity and fluxes. *J. Hydrol.* **376** 249–260.

SAVAGE MJ, EVERSON CS, ODHIAMBO GO, MENGISTU MG and JARMAIN C (2004) Theory and Practice of Evapotranspiration Measurement, With Special Focus on SLS as an Operational Tool for the Estimation of Spatially-Averaged Evaporation. WRC Report No. 1335, Water Research Commission, Pretoria, South Africa, ISBN 1–77005–247–X. 204 pp.

SAVAGE MJ and HEILMAN JL (2009) Infrared calibration of net radiometers and infra red thermometers. *Agric. Forest Meteorol.* **149** 1279–1293.

SAVAGE MJ, HEILMAN JL, MCINNES KJ and GESCH RW (1995) Placement height of eddy correlation sensors above a short grassland surface. *Agric. Forest Meteorol.* **74** 195–204.

SAVAGE MJ, MCINNES KJ and HEILMAN JL (1996) The "footprints" of eddy correlation sensible heat flux density, and other micrometeorological measurements. *S. Afr. J. Sci.* **92** 137–142.

SAVAGE MJ, ODHIAMBO GO, MENGISTU MG, EVERSON CS and JARMAIN C (2010) Measurement of grassland evaporation using a surface-layer scintillometer. *Water SA* 36, 9–17.

SCINTEC (2006) Scintec Surface Layer Scintillometer SLS20/SLS40 SLS20-A/SLS40-A User Manual (including OEBMS1). Scintec Atmosphärenmesstechnik AG, Tübingen, Germany. 105 pp.

STANNARD DI (1997) A theoretically based determination of Bowen-ratio fetch requirements. *Boundary-Layer Meteorol.* **83** 375–406.

SUN X-M, ZHU Z-L, WEN X-F, YUAN G-F and YU G-R (2006) The impact of averaging period on eddy fluxes observed at ChinaFLUX sites. *Agric. Forest Meteorol.* **137** 188–193.

TANNER CB (1960) Energy balance approach to evapotranspiration from crops. *Soil Sci. Proc. Amer.* **24** 1–9.

THIERMANN V (1992) A displaced-beam scintillometer for line-averaged measurements of surface layer turbulence. *10th Symposium on Turbulence and Diffusion*. Portland, Oregon, USA.

THIERMANN V and GRASSL H (1992) The measurement of turbulent surface-layer fluxes by use of bichromatic scintillation. *Boundary-Layer Meteorol.* **58** 367–389.

TWINE TE, KUSTAS WP, NORMAN JM, COOK DR, HOUSER PR, MEYERS TP, PRUEGER JH, STARKS PJ and WESELY ML (2000) Correcting eddy-covariance flux underestimates over a grassland. *Agric. Forest Meteorol.* **103** 279–300.

WILSON K, GOLDSTEIN A, FALGE E, AUBINET M, BALDOCCHI D, BERBIGIER P, BERNHOFER C, CEULEMANS R, DOLMAN H, FIELD C, GRELLE A, IBROM A, LAW BE, KOWALSKI A, MEYERS T, MONCRIEFF J, MONSON R, OECHEL W, TENHUNEN J, VALENTINI R and VERMA S (2002) Energy balance closure at FLUXNET sites. *Agric. Forest Meteorol.* **113** 223–243.

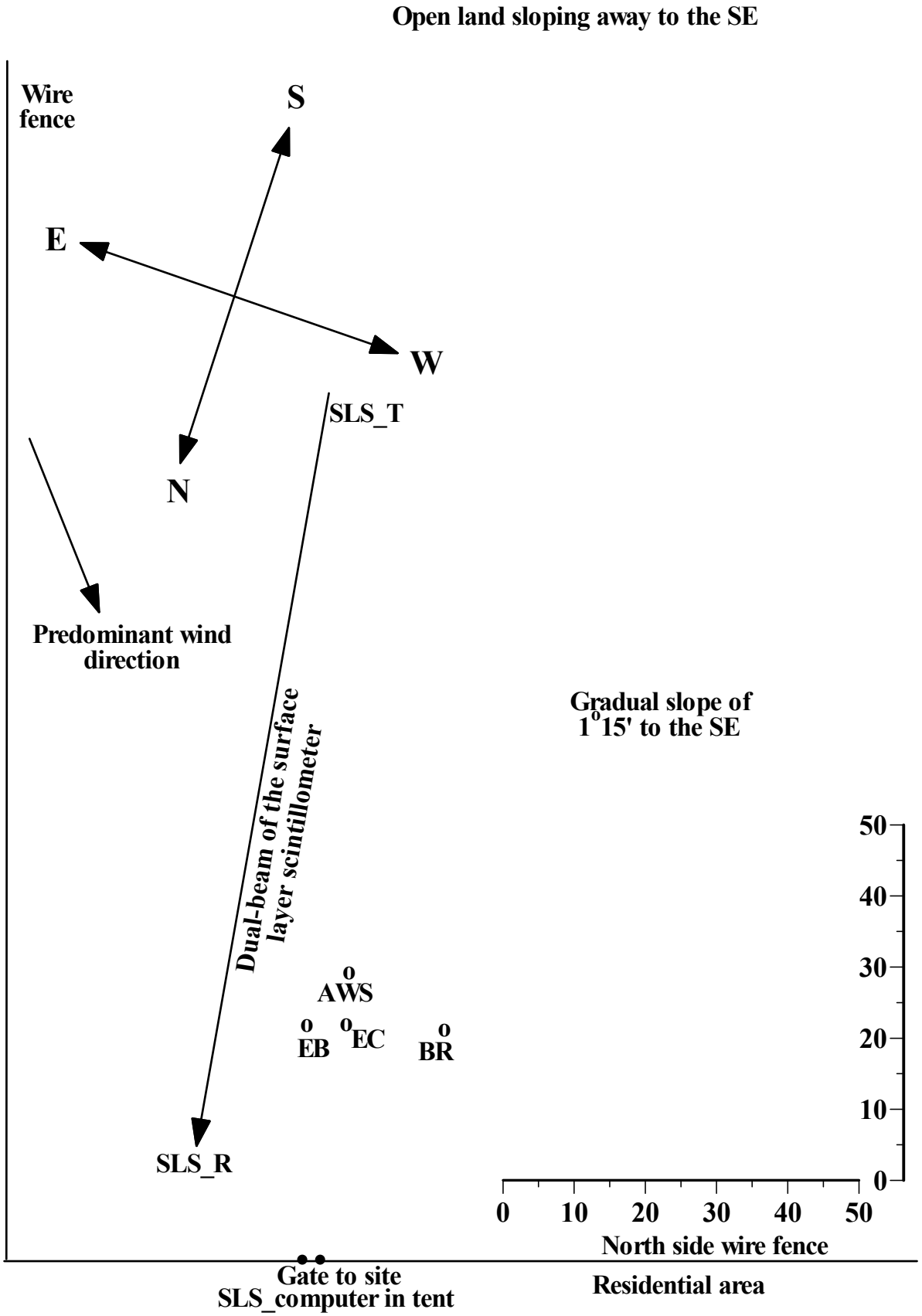
Open land sloping away to the SE
Wire fence
S
E
W
N
SLS_T
Predominant wind direction
Dual-beam of the surface layer scintillometer
Gradual slope of 1°15' to the SE
AWS
EB
EC
BR
SLS_R
50
40
30
20
10
0
0 10 20 30 40 50
North side wire fence
Gate to site
SLS_computer in tent
Residential area

Fig. 6.1. Schematic of the research site and instrumentation placement. The diagram is approximately to scale (metres). The SLS transmitter and receiver positions are indicated by SLS_T, SLS_R; the EC system is indicated by EC; the energy balance system (net irradiance, soil heat flux, soil water content, soil temperature, fine-wire thermocouples for air temperature profile measurements) is indicated by EB; the BREB system is indicated by BREB; the automatic weather station system is indicated by AWS.

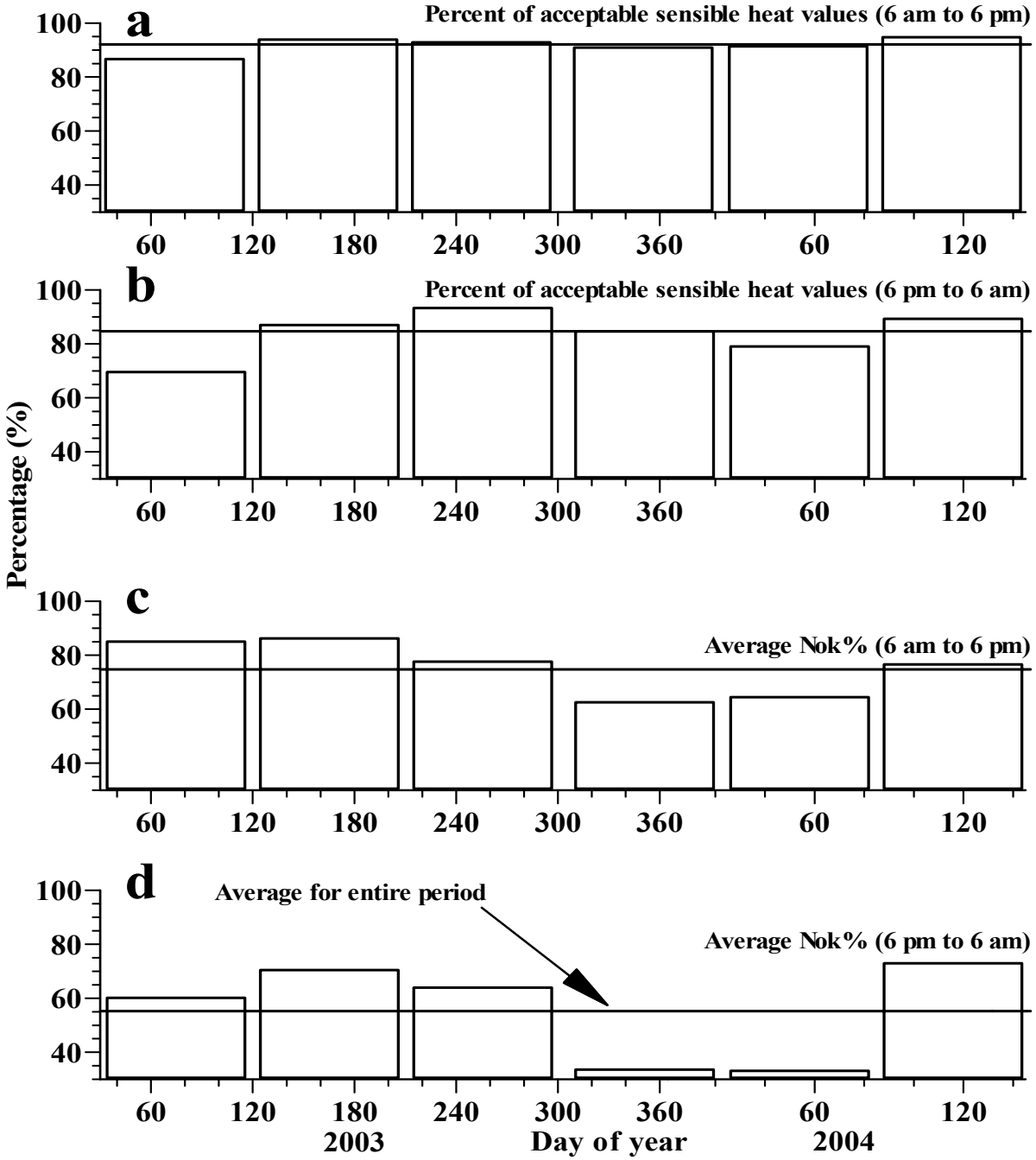

Fig. 6.2. Temporal variation, for an 18-month period, in: (a) and (b) percent of acceptable 2-min SLS sensible heat flux measurements for the 06h00 to 18h00 period and for the 18h00 to 06h00 periods respectively; (c) and (d) the average 2-min SLS Nok% values for the 06h00 to 18h00 period and for the 18h00 to 06h00 periods respectively. The horizontal line is the average for the entire period: 92 % for (a), 85 % for (b), 75 % for (c) and 55 % for (d).

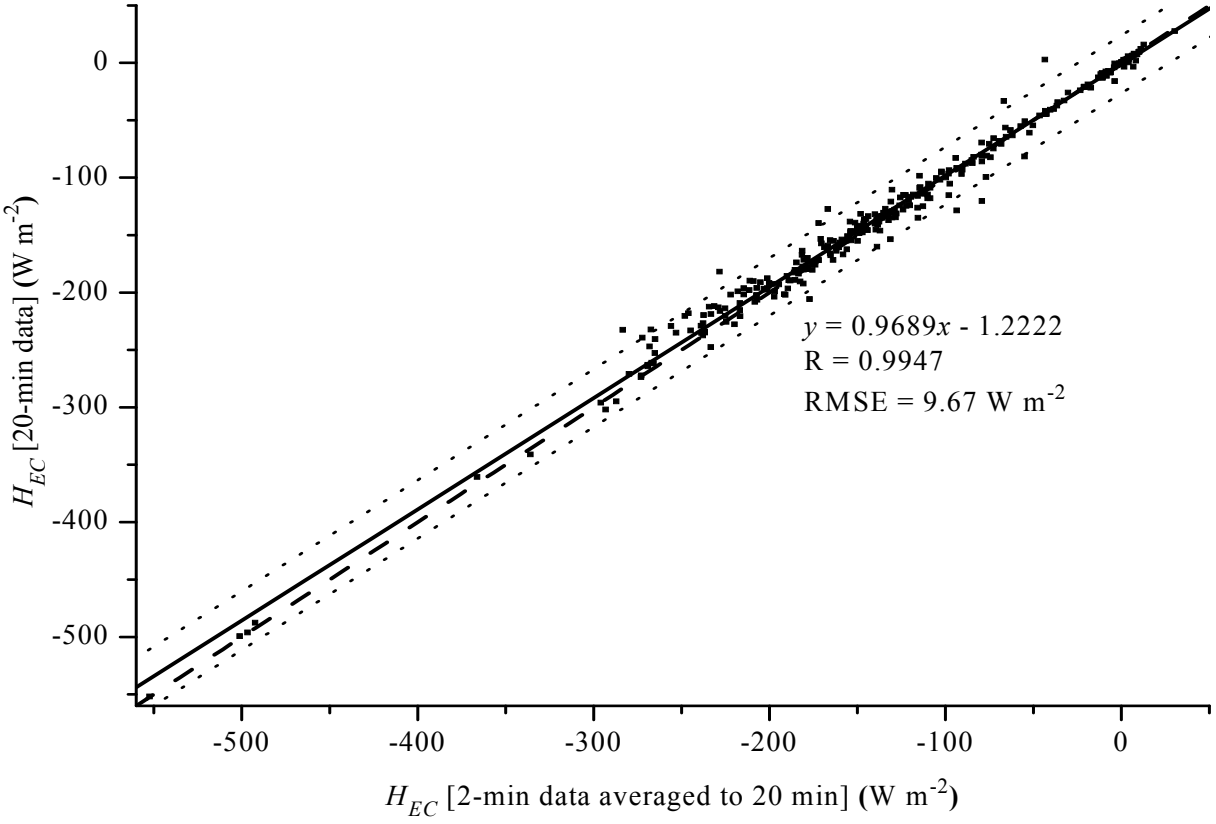

Fig. 6.3. A comparison between H_{EC} (CA27 system) measurements, using 20-min and 2-min averaging periods with the latter then averaged to 20 min, for two weeks in January/February 2003. The solid line is the linear regression line, the dashed line the 1:1 line and the dotted curves correspond to the 99 % confidence bands for a single predicted y value.

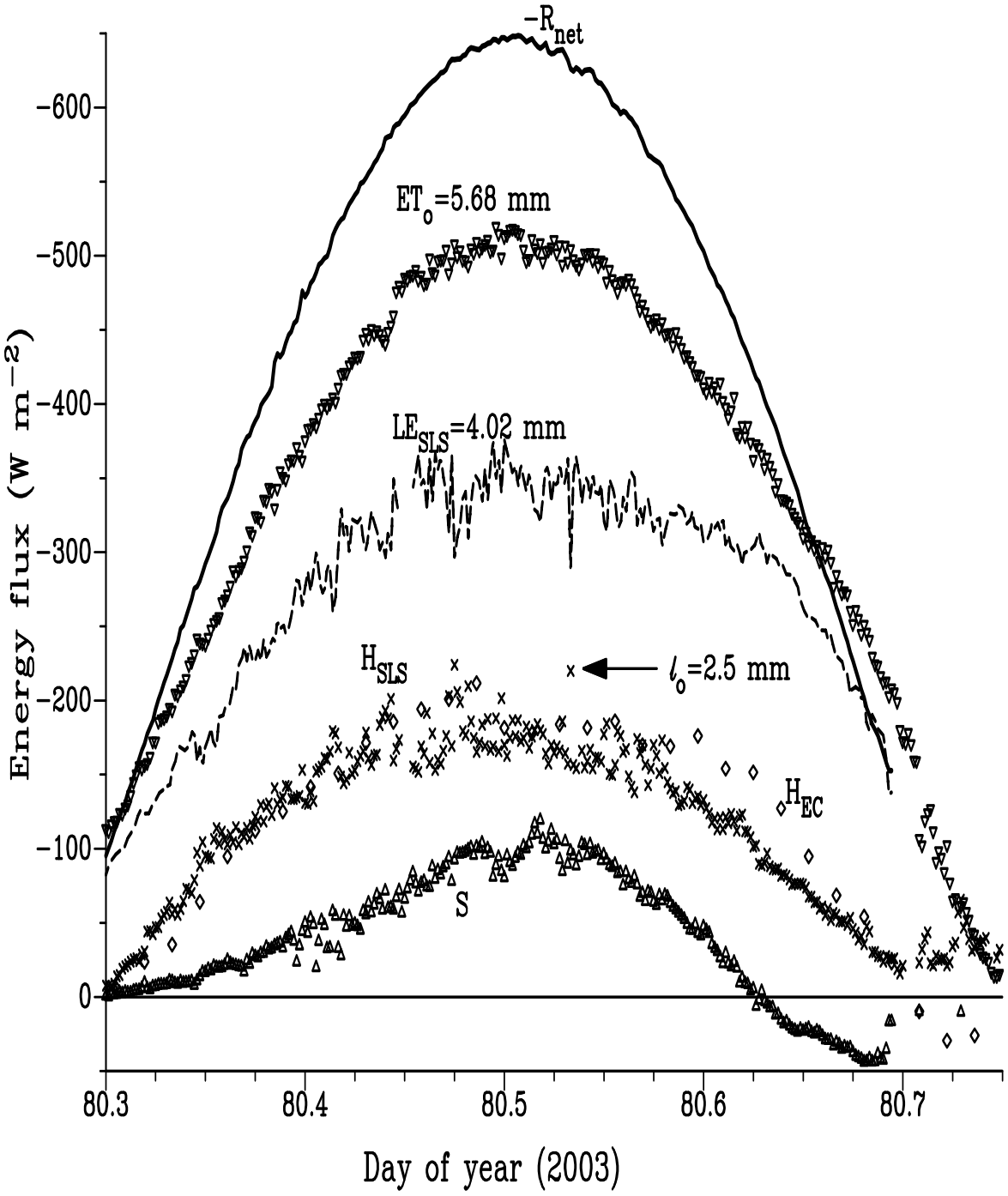

Fig. 6.4. Diurnal variation in the energy balance components for day of year 81, 2003. For comparison, the grass reference evaporation rate ETo and H for both SLS (2-min) and EC (20-min) methods are included. The ETo and LE_{SLS} daily totals (mm) are indicated above the respective evaporation curves.

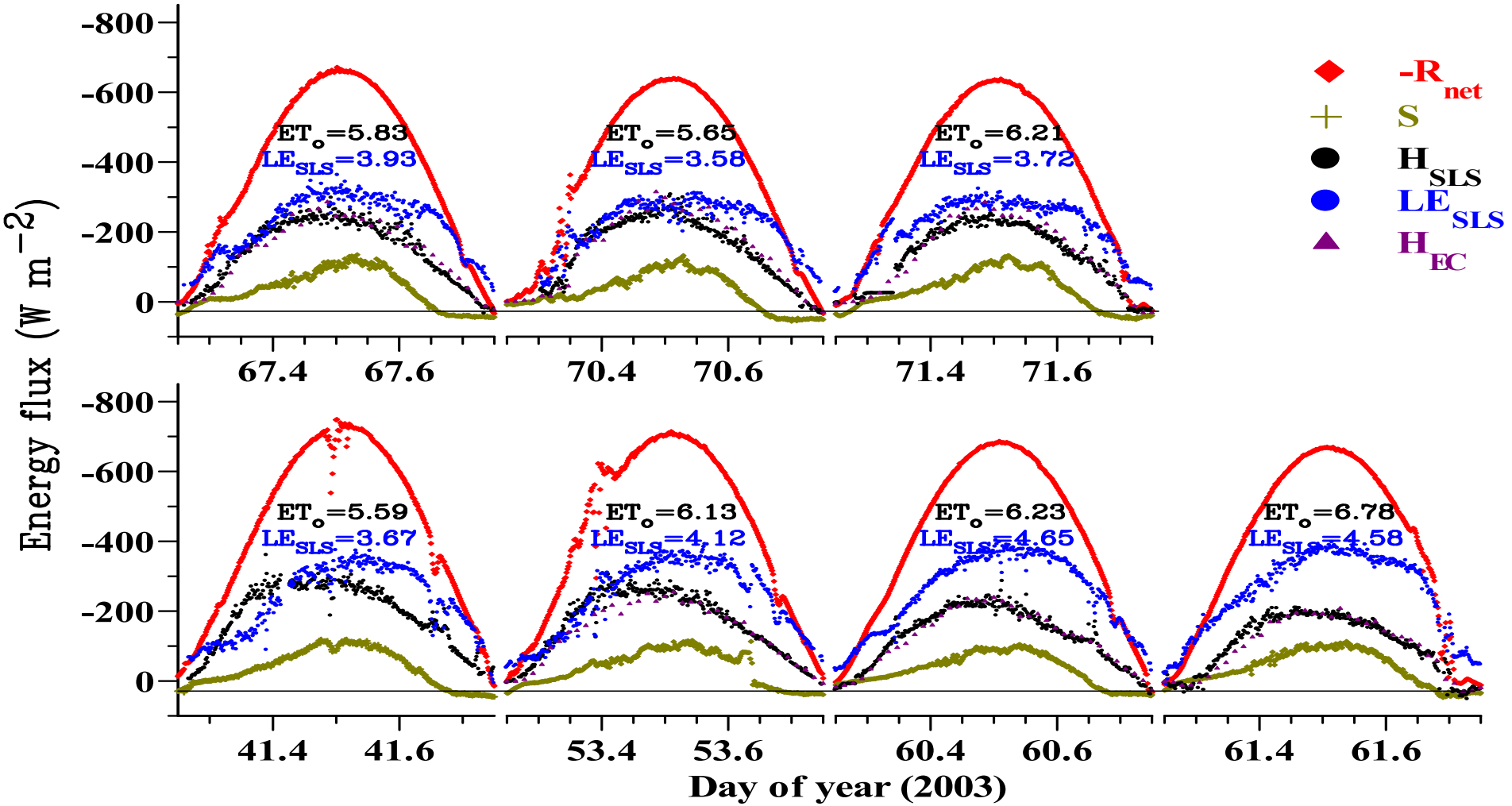

Fig. 6.5. Diurnal variation in the energy balance components for various selected near-cloudless days (2003) with *H* for both EC and SLS methods included. The residual of the energy balance, LE_{SLS} is estimated from H_{SLS}, R_{net} and *S* with the daily total LE_{SLS} and ETo in mm shown for each day.

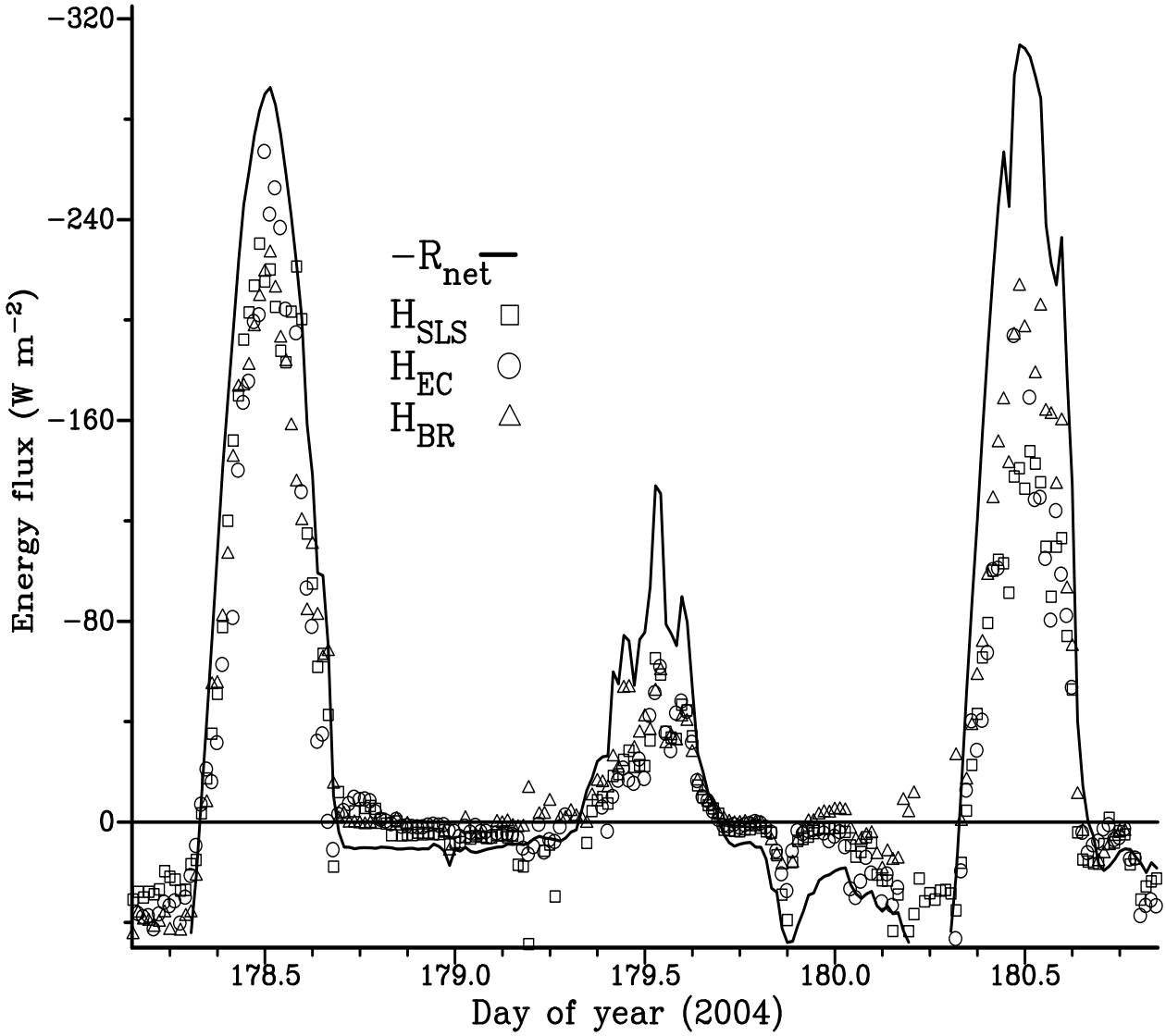

Fig. 6.6 Diurnal variation in $-R_{net}$ and comparisons between the three methods (BR, EC and SLS) for estimating *H* for a three-day period (4 to 6 June, 2004).

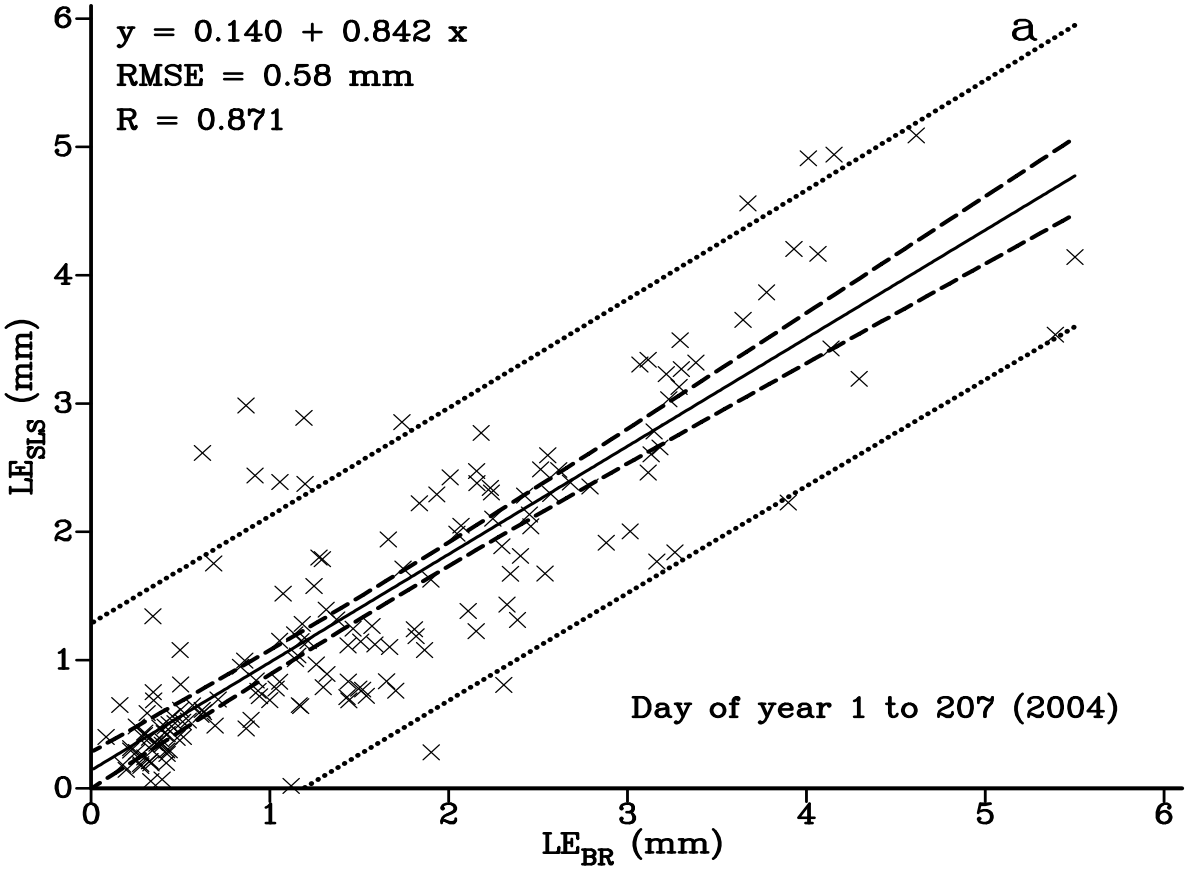
y = 0.140 + 0.842 x
RMSE = 0.58 mm
R = 0.871
a
Day of year 1 to 207 (2004)
LE_SLS (mm)
LE_BR (mm)
0
1
2
3
4
5
6

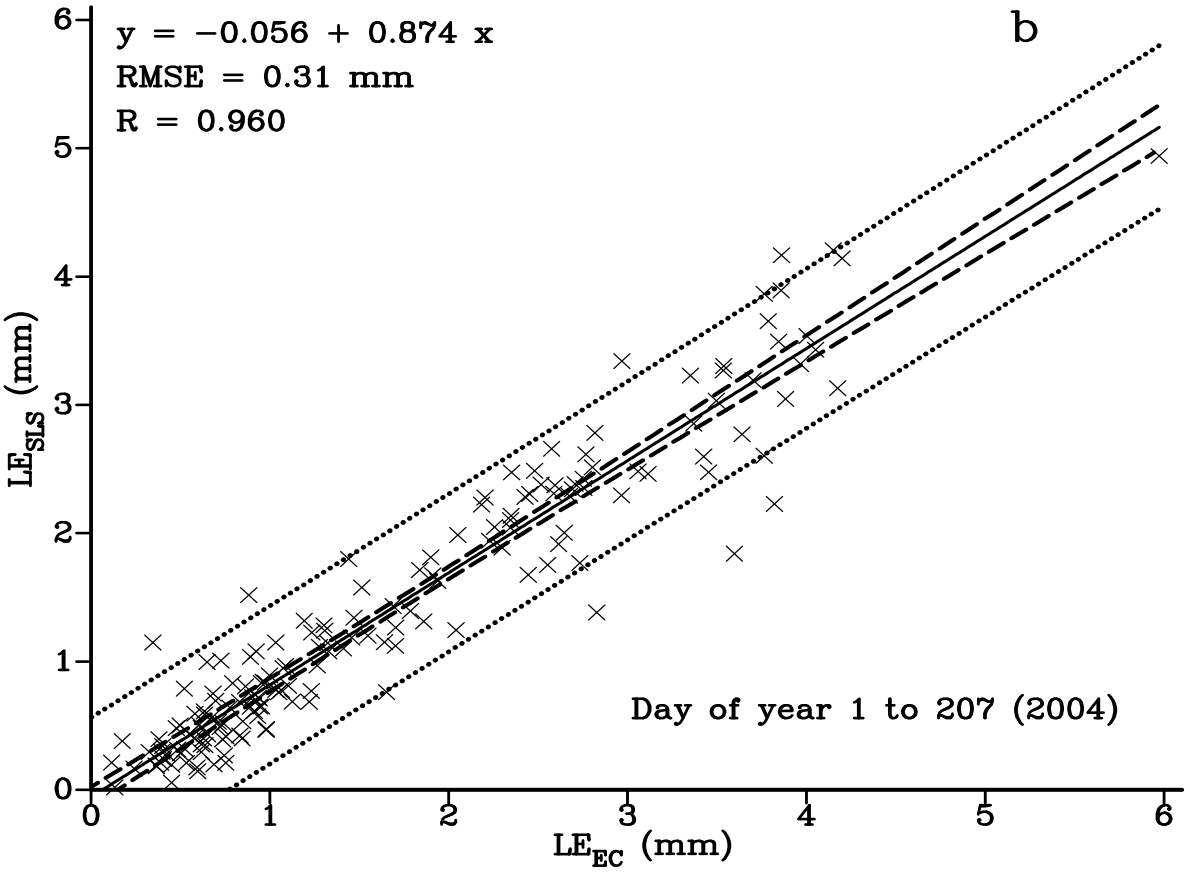
y = −0.056 + 0.874 x
RMSE = 0.31 mm
R = 0.960
b
Day of year 1 to 207 (2004)
LE_SLS (mm)
LE_EC (mm)
0
1
2
3
4
5
6

Fig. 6.7. (a) Comparisons, for the mesic grassland community, between daily LE measurements in mm (taken from the period day of year 1 Jan to 5 July, 2004) for the BREB and SLS systems; (b) measurement comparisons for the EC and SLS systems. The solid line in both cases is the regression line. The wide bands (dotted) represent the 95 % confidence belts for a single predicted value and the narrower ones (dashed) that for the population mean.

7 SENSIBLE HEAT FLUX ESTIMATION USING TEMPERATURE VARIANCE ABOVE VARIOUS CANOPIES FOR UNSTABLE CONDITIONS[1]

7.1 Abstract

The temperature variance (TV) method for the free convective range of turbulence was used for estimating sensible heat flux, one of the important terms of the shortened energy balance equation, from three contrasting canopies for mainly unstable conditions. The TV method involves high frequency (10 Hz) air temperature measurements using a fine-wire thermocouple at various levels for various canopy types. Monin-Obukhov similarity theory for unstable conditions was applied for sensible heat flux estimation. The direction of the flux was determined from the sign of a third-order air temperature structure function. The main advantage of the TV method is that it is inexpensive compared to most methods and that the friction velocity is not required when estimating sensible heat flux. Daytime estimates of sensible heat flux were compared with estimates obtained using a surface-layer scintillometer (SLS) and/or eddy covariance (EC) estimates of the same. The skewness of air temperature was included in the analysis to extend the sensible heat flux estimates to include both the free and forced convective turbulence ranges. The comparisons between sensible heat flux for the TV method and one or both of the SLS and the EC methods were quite good for the three canopy types: grassland (slope of 1.1088 and root mean square error (RMSE) of 21.1 W m^{-2}), pine forest (slope of 0.9915 and RMSE = 20.4 W m^{-2}) and for the *Chromolaena odorata* site (slope of 1.030 and RMSE = 22.7 W m^{-2} for the SLS and a slope of 1.0338 and RMSE = 30.0 W m^{-2} for the EC method). Given the theoretical limitation of the TV method, it performed remarkably well against much more expensive SLS and EC methods. The requirement for 10-Hz air temperature data for the TV method was investigated by comparing sensible heat flux calculated from 10 Hz and for 2-Hz datasets. The agreement in sensible heat flux for these two datasets was very good. The implication of this result is that the requirement for high frequency data may be relaxed somewhat. The TV method for estimating sensible heat flux shows promise as an inexpensive method for providing real-time estimates at sub-hourly intervals. The method has the additional advantage of much reduced data processing and electrical power requirements compared to the SLS and EC methods. The method appears to be calibration-free.

Keywords

temperature variance

evaporation measurement

scintillometer

eddy covariance

7.2 Introduction

The field-measurement of total evaporation sensible heat flux is of paramount importance in determining the water use of vegetation. In general, evaporation studies are limited due to the high

[1] Based on Savage (2007) and Savage (2009a, b)

cost of instrumentation and sensors, instrumentation battery power requirements and the difficulty in obtaining real-time measurements in, for example, remote areas. Furthermore, many micrometeorological measurement methods require site homogeneity and adequate fetch and application of the Monin-Obukhov similarity theory (MOST). Different measurement methods for estimating evaporation have been reviewed by Drexler et al. (2004) and Savage et al. (1997, 2004). A commonly-used method for estimating evaporation is through the use of the shortened energy balance equation

$$R_{net} + LE + H + S = 0 \tag{7.1}$$

where R_{net} is the net irradiance, LE is latent energy flux (evaporation) where L is the specific latent heat of vapourisation (L = 2.442 MJ kg^{-1}), H the sensible heat flux and S the soil heat flux (all in W m^{-2}). Rearranging, LE is estimated using:

$$LE = - R_{net} - H - S \tag{7.2}$$

from measurements of R_{net}, H and S. Sensible heat flux H may be estimated using a number of different methods, most of which require expensive equipment with power requirements that necessitate frequent site visits. Such power requirements impose severe limitations on the use of such equipment for remote sites. In addition, high frequency measurements are often necessary. Measurement methods for R_{net} and S are almost standard but methods for estimating H range in complexity and cost. A commonly-used standard for estimating H is through the use of a three-dimensional sonic anemometer and the collection of high frequency data of the three components of wind velocity and the sonic temperature, the latter being a good estimate of air temperature. The focus of this work investigates an inexpensive method for estimating H that involves high frequency measurements of air temperature at a single point.

We report on estimates of H using an air temperature variance (TV) method (Tillman 1972), also referred to as the flux variance method (Wesson et al., 2001), but usually when the scalar flux is not sensible heat flux – such as latent energy and carbon dioxide fluxes. The TV method for estimating H, first mooted by Tillman (1972) for mainly dry and convectively unstable atmospheric conditions is an inexpensive method involving high frequency air temperature measurements at a single height above the canopy. Van Dijk et al. (2004) used the TV method to estimate H for a maize and cassava cropping system, Hsieh et al. (1996) used the method above a short grassland surface, Unland et al. (1996) used the method in a semi-arid desert site and Albertson et al. (1995) used the method above a crusted sand surface in an arid region. Hsieh et al. (2008) used the temperature variance method for estimating sensible heat flux and the flux variance method for estimating latent energy and carbon dioxide fluxes.

Kustas et al. (1994) used a TV method, for unstable conditions based on MOST, for estimating H based on the work of Tillman (1972). Kustas et al. (1994) used empirical constants and knowledge of the friction velocity for estimating H. They cautioned that the TV method should always be calibrated with measurements from other flux measurement systems. They calculated the friction velocity using MOST, either from the standard deviation of the vertical wind speed or from the measured wind speed.

The applicability of the TV method however, is much less established over heterogeneous canopies (Sugita and Kawakubo, 2001), for locations with limited fetch and within the roughness sublayer. Furthermore, comparisons with the surface-layer scintillometer (SLS) (Thiermann and Grassl, 1992) method of estimating *H*, for example, are extremely rare. Many of the studies employing the so-called TV method of Tillman (1972) used the air temperature variance for the free convective turbulence range but exclude his extension to also include forced convection. This extension requires estimates of the air temperature skewness which is not normally computed from the real-time measurements.

In this study, the focus is on the measurement of *H* using the inexpensive TV method, including fetch-limiting conditions and possibly just within the roughness sublayer of turbulence, and the subsequent estimation of total evaporation using R_{net} and S components of the shortened energy balance (Eq. (7.2)). Also, TV sensible heat flux (H_{TV}) and latent energy (LE_{TV}) was compared with those estimates from the SLS path-averaging method (H_{SLS} and LE_{SLS}). The influence of sensor measurement height, measurement frequency and inclusion of the skewness of temperature to include free and forced convective turbulence influences on *H* measurements was also investigated.

7.3 Theory

Evaporation measurements using a weighing lysimeter are usually regarded as the standard measurements against which all other evaporation (latent energy) measurements or estimates are compared. In spite of this standard, the use of lysimeters is often fraught with complications that may impact on measurement accuracy. The main limitation of their use is the cost and complex engineering involved and the non-portable nature of measurements that represent a small area of the experimental site. Furthermore, after long dry periods, the measured evaporation for the lysimeter may not match that outside the non-permeable lysimeter walls.

For a short, horizontal and extensive surface, net irradiance R_{net} is the sum of the incoming short and infra red irradiances, less the reflected short wave and emitted infra red irradiances. The net irradiance also appears as a term in the energy balance equation (Eq. (7.1)). For a short and flat surface, the use of the shortened form of the energy balance equation ignores advection (both *H* and latent energy forms) and the photosynthetic flux and canopy-stored heat flux are considered negligible (Thom, 1975) compared to the other energy balance components. So the important terms of the energy balance are the R_{net}, H, LE and S if advection is negligible (Eq. (7.1)). Due to its complex nature, advection is usually not routinely accounted for when using methods to estimate surface *H* and latent energy flux densities.

The surface renewal (SR) method for estimating *H* is relatively new and quite simple (Paw et al., 1995; Snyder et al., 1996; Spano et al., 2000; Castellví, 2004). In terms of sensor measurement requirements, the earlier TV method of Tillman (1972) is similar to the SR method. Both methods allow *H* to be estimated from high frequency measurements of air temperature at a single level at or above a plant canopy using an unshielded and naturally ventilated fine-wire thermocouple. Frequency of measurement for the SR method is typically 4 to 10 Hz and post-measurement calculations are used to estimate *H*.

For a wide range of atmospheric stability conditions at height z above flat and short homogeneous vegetated surfaces, using the MOST semi-empirical relationships, Wyngaard et al. (1971) showed that:

$$\sigma_T / T_* = C_1 \left(-z / L\right)^{-1/3} \text{ for } z / L < 0 \tag{7.3}$$

where σ_T is the temporal standard deviation in air temperature (K) over a time period (typically 30 min) where σ_T^2 is the variance in air temperature, T_* the turbulent scale for temperature (K), C_1 an empirical constant (typically between 0.9 and 1.1), where z (m) is the measurement height above soil surface of the air temperature sensor (m) and

$$L = \frac{\overline{T}}{k\,g} \cdot \frac{\rho\, c_p}{H} \cdot u_*^3 \tag{7.4}$$

is the Obukhov stability length (m) [negative during unstable daytime conditions if the convention of Eq. (7.1) is used] where $\overline{T}$ (K) is the mean air temperature, k the von Kármán constant (0.41), g the acceleration of gravity (typically 9.7968 m s^{-2}), ρ the density of air (typically 1.14 kg m^{-3}), c_p the specific heat capacity of air at constant pressure (typically 1011 J kg^{-1} K^{-1}) and u_* the friction velocity (m s^{-1}) and where the H is given by:

$$H = -\rho\, c_p\, u_*\, T_* . \tag{7.5}$$

The condition in Eq. (7.3), that $z / L < 0$, corresponds to unstable atmospheric conditions. Furthermore, due to the semi-empirical nature of MOST, the form of Eq. (7.3) is not unique. Various forms of Eq. (7.3) require, for example, knowledge of the friction velocity as demonstrated by Kustas et al. (1994). The form presented in Eq. (7.3) is based on the original version used by Wyngaard et al. (1971) and Tillman (1972) and has the advantage that friction velocity is not required and that the flux can be computed in real-time from σ_T.

Combining Eqs (7.3), (7.4) and (7.5) and solving for H, for a homogeneous vegetated surface, as is required by Eq. (7.3), results in:

$$H_{TV} = -\,\rho\, c_p\, (\sigma_T / C_1)^{3/2} (k\, g\, z / \overline{T})^{1/2} \tag{7.6}$$

for the free convective range of turbulence. The TV method, defined by the use of Eq. (7.6), assumes a horizontally homogeneous atmospheric surface layer and that the MOST applies (Tillman, 1972). He indicated that Eq. (7.6), the free convection approximation, should be valid for $0.05 << -z / L < 60$. Tillman (1972) used k = 0.35 compared to the now more generally-accepted value of 0.41. Furthermore, he used the constant C_1 = 0.95 to describe the free convection range of turbulence. He mentioned that other research had reported a variation in C_1 from 0.9 to 1.1. Taking into account the change in the von Kármán constant k from 0.35 to 0.41 and a change from the Tillman (1972) C_1 value from 0.95 to 1.0, for which 1.0 is the average of the limits of the 0.9 to 1.1 range, we get:

$$H_{TV} = -\,0.9978\,\rho\, c_p\, (\sigma_T / C_1)^{3/2} (k\, g\, z / \overline{T})^{1/2} \tag{7.7}$$

where $0.9978 = (1.0 / 0.95)^{3/2} \cdot (0.35 / 0.41)^{1/2}$ where now in Eq. (7.7), C_1 = 1.0 and k = 0.41. For stable conditions, a different factor for C_1 is used in Eq. (7.7) (de Bruin et al., 1993).

In this study, we therefore used Eq. (7.7) for estimating *H* for unstable conditions using the TV method with C_1 = 1.0 and k = 0.41. Tillman (1972) extended his method, for the free convection range (Eq. (7.7)) to encompass the free and forced convective turbulent ranges through the use of the air temperature skewness S_T. Of particular note is that the friction velocity is not required in Eqs (7.6) or (7.7), nor is there any apparent need for empirically adjusting the *H* estimates for vegetation type as is required for the SR method through the use of the so-called α value: α = 0.5 for coniferous forests, orchards and maize when the sensor is at canopy level. For short grass, α = 1 for a sensor height of about 1 m (Paw U et al., 1995).

Tillman (1972) extended the method, for the free convection range (Eq. (7.7)) to encompass the free and forced convective turbulent ranges through the use of the air temperature skewness S_T. Skewness involves the sum over a time interval of the cube of the air temperature deviation from the mean:

$$S_T = (1 / \sigma_T^3) \, \Sigma (T_i - \overline{T})^3 / n \tag{7.8}$$

where T_i is the i th sample air temperature measurement and n the number of air temperature samples within the given time period. This extension results in:

$$H_{TV S_T} = -0.993 \, \rho c_p \, (\sigma_T^3 \, k \, g \, z / \overline{T})^{0.5} \times f(S_T) \tag{7.9}$$

where

$$f(S_T) = \frac{(0.0549 + 0.0137 \exp(4.39 \, S_T))^{0.5}}{(0.0137 \exp(4.39 \, S_T))^{0.5}} . \tag{7.10}$$

Eq. (7.9) was found to be valid for the range $0.03 < -z / L < 60$.

A skewness value of 0 occurs when, within an averaging time interval, the distribution of temperature is symmetric with respect to the average temperature. Positive skewness occurs when the mode for the averaging period is greater than the average temperature and negative skewness occurs when the mode is less than the average. Typical skewness values range between 0 and 1 for which unstable conditions. The functional dependence of $f(S_T)$ on S_T is shown in Fig. 7.1. For $S_T > 0.83$, the adjustment for skewness using Eqs (7.9) and (7.10) results in less than a 5 % adjustment to *H*.

As is the case with other applications of MOST, the flux direction is not determined. The direction of *H* may be determined using the sign of the amplitude of air temperature ramps using the surface renewal (SR) method. For SR the ramping period τ is calculated using:

$$\tau = -\frac{a^3 \, r}{S_r^3} \tag{7.11}$$

where the air temperature structure function is defined as:

$$S_r^n(r) = \frac{1}{m-j} \sum_{i=1+j}^{m} (T_i - T_{i-j})^n , \tag{7.12}$$

where n is the order of the air temperature structure function[2] for which n = 2, 3 and 5 for SR analyses, m the number of data points measured at frequency f in Hz in the averaging time interval, T_i the ith air temperature sample measurement, and j the number of lags between measurements corresponding to an air temperature time lag $r = j/f$ (s). As pointed out if the Appendix to the thesis, by definition, τ in Eq. (7.11) is positive. For unstable conditions, $a > 0$ ^{o}C and therefore $a^3 r > 0$ and therefore the negative sign on the right-hand side of Eq. (7.11) forces $S_r^3 < 0$. Similarly, for stable conditions $a < 0$ ^{o}C which forces $S_r^3 > 0$. Hence, for unstable conditions,

$$H_{TV\,S_T} = \frac{S_r^3}{|S_r^3|} \rho c_p (\sigma_T^3 k g z / \overline{T})^{0.5} \times f(S_T) . \tag{7.13}$$

Structure functions and MOST are the basis for scintillometry (Hill, 1997). Structure functions can be defined for air temperature, water vapour pressure, refractive index of air, wind speed, etc. For example, the time-average of the air temperature deviations squared, termed the air temperature structure function is defined as:

$$D_T(r) = \overline{[T(r,t) - T(0,t)]^2} \tag{7.14}$$

where the entire right hand side of the equation is time-averaged, $T(0,t)$ denotes the air temperature at reference position 0 at time t and $T(r,t)$ denotes the air temperature at position r from the reference point temperature measurement $T(0,t)$. Therefore both $T(r,t)$ and $T(0,t)$ are measured at the same time t but the measurements are separated spatially by distance r. In the case of Eq. (7.14), it is the average deviation squared for two measurements of air temperature at slightly different positions with both measurements performed at the same time. For spacing r in the inertial range of turbulence, millimetres to tens of millimetres, Obukhov (1949) showed that:

$$D_T(r) = C_T^2 r^{2/3} \tag{7.15}$$

where C_T^2 is termed the structure parameter of air temperature.

Another structure function, the spectral amplitude of the refractive index fluctuations C_n^2 is referred to as the structure function constant or simply the structure constant which is in turn determined from C_n^2. Since the refractive index fluctuations are most often affected by air temperature fluctuations and less by fluctuations in atmospheric humidity, C_n^2 is often interpreted as a measure of the structure parameter of air temperature (Thiermann and Grassl, 1992). It may also be interpreted as a measure of the strength of the refractive turbulence (Green, 2001). A scintillometer, depending on its type, allows determination of a number of micrometeorological parameters but in particular C_n^2. Under certain conditions, in particular under conditions of weak scattering of the scintillometer beam, and using certain measurement methods or assumptions, H may be derived from C_n^2 using MOST. As with the TV method, knowledge of the net irradiance and soil heat flux allows the latent energy flux

[2] The use of an exponent in the air temperature function is functional notation and does not mean that, for example, S^3 is S multiplied itself multiplied by itself

LE to be estimated as a residual using the energy balance (Eq. (7.2)). A full understanding of scintillometry requires knowledge in electronics, optics, wave propagation theory, data logging and micrometeorology. Andreas (1990) presents a collection of selected key papers on wave propagation and atmospheric turbulence. A comprehensive review describing the background, progress and future trends in optical scintillation is described by Hill (1992). The scintillometry method is dependent on algorithms, based on MOST, for determining atmospheric surface-layer fluxes. A detailed description of these algorithms is described by Hill (1997).

Essentially, a scintillometer consists of a source of light of known wavelength usually directed over some horizontal distance to a receiver. The light beam needs to be collimated –that is, the light rays need to be parallel. For the SLS system, for example, the changes in the intensity and the phase of the light beam is detected at the receiver position some known horizontal distance from the transmitter. These changes result from the atmospheric temperature perturbations causing changes in air density that refract the light beam. The key to the implementation of the surface-layer scintillometer (SLS) method (Thiermann and Grassl, 1992) is the interaction between eddy size, beam distance, beam wavelength and aperture diameter and for some of the estimates, effective beam height, air temperature and atmospheric pressure. The estimated *H* requires the friction velocity measurement or an estimate of same. The small aperture SLS system is sensitive to eddies with diameters corresponding to the inertial sub-range, defined by Raupach and Legg (1984), containing larger eddies or to the so-called dissipation sub-range of turbulence containing smaller eddies. In the case of eddies in and close to the dissipation range, the measured variances do not only depend on C_T^2 but also on the inner scale of turbulence l_o. For the SLS system employed in this study, a dual-beam laser method, two detectors are used. The inner scale l_o of refractive index fluctuations is calculated from the correlation of the light intensities at two detectors. Only once l_o is known, can the structure parameter of refractive index fluctuations C_n^2 be calculated from the variances of the intensity from the two beams.

A comparison of the theoretical aspects of the TV, SLS and SR methods deserves attention. The TV method (Eq. (7.7)), relies on the standard deviation in the air temperature σ_T over a typical period of 30 minutes:

$$\sigma_T = \sqrt{\Sigma(T - \overline{T})^2 / (n-1)} \tag{7.16}$$

where T is the air temperature at an instant in time, $\overline{T}$ is the mean air temperature for the 30-min period for example where, for a temperature measurement interval of 100 ms, n = 18000 for the 30-min time period and where the summation is performed over 18000 data points. A comparison between Eqs (7.14) and (7.16) is most revealing. The SLS method (Eq. (7.14)) relies on a comparison of air temperature at two positions separated by distance r but at the same time. The measurements at two positions necessitate the use of a dual-beam system. The TV method relies on a comparison between air temperature and its time-averaged mean, all measurements performed at the same position (Eq. (7.16)). As is the case for the SLS method, the TV method cannot distinguish between stable and unstable atmospheric conditions since the standard deviation is always positive. However, the sign of S_r^3 can reveal the direction of the *H* (Eq. (7.13)). The SR method uses an analysis of the air temperature structure functions, of order 2, 3 and 5, to determine *H*.

As such, the TV, SLS and SR methods all process a single signal – the temperature fluctuations – through optical and/or digital filters to produce a heat flux. Which filter works best is still an open question.

7.4 Materials and methods

Measurements were collected for three different canopy types. In some cases, measurements were at a single height only and in other cases, a number of different measurement heights were used. At each site, the use of a three-dimensional sonic anemometer allowed for the estimation of *H*. At two of the sites, the SLS method for estimating *H* was used. At each site, *H* was estimated using the TV method using either the sonic air temperature data or the measured air temperature obtained using an unshielded and naturally-ventilated fine-wire chromel-constantan thermocouple.

7.4.1 Site details

7.4.1.1 Chromolaena site

Measurements were conducted above *Chromolaena odorata* within the Hluhluwe Game Reserve in northern KwaZulu-Natal as part of a CSIR evaporation measurement project funded by the WRC (project leader Dr C. Jarmain, CSIR). For the TV measurements, unshielded and naturally-ventilated fine-wire chromel-constantan thermocouples were used. Each thermocouple unit consisted of a pair of 75-µm thermocouples in parallel. Each thermocouple extended a distance of 0.68 m from its support arm. Four separate units were used, placed at heights of 2.3, 2.9, 2.9 and 3.6 m above the soil surface. The vegetation height was 2.4 m on average. The thermocouples were connected to a Campbell Scientific CR5000 datalogger (Campbell Scientific, Logan, USA). Thermocouple measurements were done differentially with a settling time of 0.1 ms and an integration time of 0.1 ms with a measurement interval of 100 ms (corresponding to a measurement frequency of 10 Hz). The raw data were stored on a 1 Gbyte PC card. Subsequently, from the data stored on the card, 30-min means and standard deviations of the air temperature were calculated using Split (part of LoggerNet (version 3.2.2) available from Campbell Scientific). Since neither the TV nor the SLS methods could determine the sign of the flux, the sign of *H* was determined from that of S_r^3. The influence of temperature measurement intervals from 100 to 1000 ms, corresponding to frequencies from 10 to 1 Hz respectively, on the *H* calculated were investigated. The beam of the transmitter was aligned 30^o west of magnetic north which meant that wind directions of 330 or 150^o were perpendicular to the beam and wind directions of 240 or 60^o were parallel to the beam. Two three-dimensional ultrasonic anemometers (model 81000, RM Young, Traverse City, Michigan, USA) were used for sonic temperature and EC estimates of *H*.

7.4.1.2 Pine forest site

Eddy covariance measurements of *H* were also obtained in a managed slash pine canopy (*Pinus elliottii* L.) near the Austin Cary Memorial Forest of the University of Florida, Gainesville, USA. The closed forest canopy had an average height of 9.8 m. The instrumentation tower contained five Campbell Scientific CSAT3 three-dimensional sonic anemometers. A Campbell CR9000 datalogger was used for data collection at a frequency of 10 Hz. The raw data were stored on memory cards and subsequently processed using a Fortran programme. The measurement heights for the different systems were as follows: 14.02, 10.05, 7.83, 6.09 and 3.96 m, representing 1.4 *h*, 1.0 *h*, 0.8 *h*, 0.6 *h*

and 0.4 *h* where *h* is the canopy height. The data for this experiment was provided by Dr M.Y. Leclerc from the University of Georgia, USA. In this experiment, the sonic temperature was used for the air temperature.

7.4.1.3 Grassland site

We report on field measurements conducted above an open mesic grassland summer rainfall site near the Bellevue area neighbouring Ashburton and close to Pietermaritzburg, South Africa (29°38'S, 30°26'E) with an altitude of 671.3 m. The average slope of the study site is 1°15' to the SE.

Three methods were used to measure *H*: SLS method, EC method and the TV method. A dual-beam SLS system (model SLS40-A, Scintec Atmospärenmessetechnik, Tübingen, Germany) (Thiermann, 1992; Thiermann and Grassl, 1992), was used to estimate the *H* every one min or two min based on voltage measurements, corresponding to laser beam transmission, at a frequency of 1000 Hz for a beam distance of 90 m and a beam height of 3.0 m above the soil surface. The 1-min or 2-min measurements were subsequently averaged to 30 min. The SLS40-A receiver has four detectors with two of the detectors used for automatic identification of and correction for transmitter vibration by the software used for analysis. In other words, the SLS40-A dual-beam system and its four detectors enable the separation and correction for the intensity fluctuations caused by beam movement. There are two detectors per beam. The SLS employs a diode laser source with an output wavelength of 670 nm and 1 mW mean output power (2 mW peak). The beam displacement and detector separation distances are 2.5 mm each, with a detector diameter of 2.7 mm. Software together with the instrument allows on-line measurements at a frequency of 1000 Hz and subsequent calculation every 1 min of the structure parameter for refractive index fluctuations (C_n^2, $m^{-2/3}$), structure parameter for temperature (C_T^2, $K^2\ m^{-2/3}$), the inner scale of turbulence l_o (mm) as indicated by the inner scale of refractive index fluctuations, kinetic energy dissipation rate (ε, $m^2\ s^{-3}$), sensible heat flux (*H*, $W\ m^{-2}$), momentum flux (τ, Pa) and the Monin-Obukhov length (*L*, m). MOST is assumed. The signal processing unit of the SLS40-A was connected to a computer.

Adjacent to an automatic weather station, a three-dimensional sonic anemometer (SWS-211/3V, Applied Technologies, Boulder, USA), referred to as the ECAT system was used as an EC system to measure the *H* at a height of 2.12 m above the soil surface. This anemometer, with a 100-mm sonic path length, was connected to a digital to analogue converter that then connected to a CR5000 datalogger. Measurements of the three components of wind velocity, *u*, *v*, *w* in the x, y and z directions respectively and sonic temperature *T* were performed every 0.1 s (frequency of 10 Hz). The sonic anemometer measurements were processed on-line and the two-min covariance between *w* and *T* (for determining *H* using c_p = 1136.3 J m^{-3} K^{-1} and ρ = 1.12 kg m^{-3}) and the covariance between w and the horizontal wind speed $U = (u^2 + v^2)^{0.5}$ (for determining momentum flux τ and hence the friction velocity u_* (Eq. (7.4)) were calculated). The two-minute averages of *u*, *v*, *w* and sonic temperature *T* and wind direction $\theta = \arctan(v/u)$ were also stored. Data rejection rules were fairly simple: sometimes, usually whenever there was condensation, covariances of -99999 were excluded. Missing values and also periods when incorrect sonic temperatures approaching 50 °C were also used to exclude *H* data. These incorrect values were caused by dirt on the sonic transducers or faulty transducers. Night-time EC measurements were often unreliable due to condensation or mist affecting the acoustic signal.

Calibration of the ECAT system and its replacement was performed by placing the 3D system in a box for which each component of the wind speed was 0 m s^{-1}. The air temperature and relative humidity, required for accurate speed of sound estimation (from which the sonic temperature is calculated), was independently measured using averaging thermocouples and a Vaisala CS500 air temperature and relative humidity sensor placed inside the box.

The minimum fetch distance for the site in the prevailing S-E wind direction is 135 m for the EC system and 90 and 138 m for the SLS transmitter and receiver respectively. The minimum fetch for the next-most dominant winds from the N-W is 117 m for the EC system and 146 and 114 m for the SLS transmitter and SLS receiver respectively. Beyond these distances and to the south, the site is exposed and the slope increases and the site adjacent is mesic grassland with occasional trees. To the north-west of the study area, there is a residential area and tall trees.

7.5 Results and discussion

Most of the measurements for the three sites were within the roughness sub-layer as opposed to the inertial layer and measurements were therefore referenced to the soil surface. The roughness sub-layer is assumed to extend from canopy height h to roughly 5 h/3 (Sellers et al., 1986). Shear-induced turbulence is strongly influenced by canopy features such as the uneven height of plants and the spacing of plants (Mahrt, 2000). The thickness of the roughness sublayer is proportional to the degree of roughness and heterogeneity at the canopy surface. The inertial sublayer is the layer above the roughness sublayer and represents the top portion of the surface layer, and is the layer where fluxes are approximately constant. In the case of pine canopy experiment, the reported measurements were at 14.02 and 10.05 m compared to a canopy height of almost 10 m.

7.5.1 Chromolaena site

For the Chromolaena site, H_{SLS}, H_{EC} and H_{TV} estimates were obtained. There was reasonable agreement between all methods (Figs 7.2a, b) but the error mean square was greater than for the grassland and pine canopy sites, probably due to the limited fetch for the Chromolaena site. The RMSE values were much greater for the TV *vs* EC comparison (Fig. 7.2a) compared to the TV *vs* SLS comparison. This is mainly due to the path-averaging capability of the SLS method compared to point measurements for the EC method.

Evaporation estimates, using the shortened energy balance (Eq. (7.2)) using the SLS and TV sensible heat estimates, show good agreement (Fig. 7.2c). In this figure, the available energy flux shown is the sum of the R_{net} and S.

For all locations of this study, the high frequency measurements consisted of measurements every 100 ms (corresponding to a measurement frequency of 10 Hz). The 100-ms dataset was used to create a 500-ms dataset by deleting four out of five data lines and then recomputing the 2-min H estimate for the TV method. The 2-min values were then averaged to 30-min. The good agreement in H using the 100- and 500-ms datasets (Fig. 7.2d) is an indication that it may be possible to use 500-ms measurements corresponding to a frequency of 2 Hz compared to the 10 Hz generally used. The significance of this result is that it may be possible to use less-expensive – slower – dataloggers for the TV method.

7.5.2 Pine canopy site

In this experiment, the sonic temperature was used together with Eq. (7.7) to obtain the TV estimate of *H*. For some days (e.g., day of year 251, Fig. 7.3a), the TV method overestimated slightly *H* compared to the EC method but for other days (e.g., day of year 255, Fig. 7.3b), there was a slight underestimation. A comparison between the half-hourly *H* estimates for the TV and EC methods for the 14.02-m height (Fig. 7.3c) showed a slope of 0.992 and a root mean square error of 20.4 W m^{-2} (compared to 30.04 W m^{-2}) for the Chromolaena site (Fig. 7.2a). Of note though is the greater variability in the pine canopy measurements as the magnitude of *H* increased (Fig. 7.3c). The agreement between H_{EC} and H_{TV} estimates for the 10.06-m height is also quite reasonable (Fig. 7.3c). There was good agreement in σ_T for the 14.02- and 10.05-m heights (Fig. 7.3d) in spite of the fact that there were inconsistent differences in skewness.

7.5.3 Grassland site

The diurnal variation in *H*, estimated using the eddy covariance (EC) and temperature variance (TV) methods, is shown for a five-day period (Fig. 7.4a). Also shown is the TV-estimated *H* adjusted for skewness. The TV method overestimates compared to the H_{EC} (Fig. 7.4b) by about 10 %. The data depicted is for the period 2 nd May to 15 th May and from 21 st June to 9 th July 2004. The sensible heat flux adjusted for skewness resulted in a consistent bias compared to the H_{EC} and H_{TV} estimates. The reason for this needs to be investigated further. The consistency of the thermocouple σ_T values were cross-checked by comparing with σ_T values obtained from the sonic temperature. There was good agreement on some days (e.g., day of year 122 in Fig. 7.4c) compared to consistent differences on day of year 173 (Fig. 7.4d) when *H* was much greater in magnitude. The differences in skewness obtained from the thermocouple and sonic temperature measurements are however much more variable with inconsistent differences (Figs 7.4c, d). This inconsistency may explain the greater variability in *H* adjusted for skewness.

In summary, for this grassland site the TV method provides reasonable estimates of *H* compared to the EC estimate. Since the correspondence between EC and SLS estimates of *H* has been established (Savage et al., 2004; Savage, 2009a), the TV estimate would also show agreement with the SLS estimates.

7.6 Conclusions

The temperature variance (TV) method for estimating *H* relies on the application of MOST and assumes that free convection dominates. The requirements of the method include high frequency measurements of air temperature. In this work, we have found reasonable comparisons between H_{EC}, H_{SLS} and H_{TV} for a range of canopy surfaces: grassland, pine canopy and chromolaena canopy. The importance of this result is that the TV method for estimating *H* is inexpensive and allows for real-time estimation at sub-hourly time intervals. A pair of fine-wire thermocouples not only allows for cross-checking of measurements but also the direction of *H* can be determined from the sign of S_r^3. If the other components of the shortened energy balance are also measured, namely the net irradiance and the soil heat flux, then the latent energy (evaporation) can be calculated.

7.7 Acknowledgements

The financing of the (scintillometer) project, conducted at the grassland site, by the Water Research Commission and the contribution of the members of the Steering Committee is gratefully acknowledged. This work was only possible with the cooperation of the following: owner Mr S.J. Hilcove, farm manager Mr H. Ovenstone of the Bellevue farm site used for this research, the Agrometeorology postgraduate students involved (Dr George O. Odhiambo, Mr Michael G. Mengistu), Ms Jody Manickum (Agrometeorology) of the School of Environmental Sciences, University of KwaZulu-Natal for her assistance, Mr Peter N. Dovey for part of the technical support required for the scintillometer project and project team members from the CSIR (Drs Colin S. Everson and Caren Jarmain and others); Dr Monique Y. Leclerc of the University of Georgia, Griffin, USA who provided the pine canopy eddy covariance data, Mr Gator Howerton for collecting the field data and Drs Anand Karipot and Tara Prabha who provided assistance with some of the Fortran programming for analyzing the eddy covariance data; the Hluhluwe work was only possible through assistance from Hluhluwe staff, Michael Mengistu and assistance in the field from the CSIR team (Drs Colin Everson and Caren Jarmain, Mr Alistair Clulow and others). Michael G. Abraha provided some insight into this work using data from another project but these results are not reported on here.

7.8 References

Albertson, J.D., Parlange, M.B., Katul, G.G., Chu, C.-R., Stricker, H., 1995. Sensible heat flux from arid regions: a simple flux-variance method. Water Resour. Res. 31, 969–973.

Andreas, E.L. (ed.), 1990. Selected Papers on Turbulence in a Refractive Medium. SPIE Milestones Series, 25. Society of Photo-Optical Instrumentation Engineers, Bellingham WA, USA. 693 pp.

Castellví, F., 2004. Combining surface renewal analysis and similarity theory: A new approach for estimating sensible heat flux. Water Resour. Res. 40, W05201 doi:10.1029/2003WR002677 1–20

de Bruin, H.A.R., Kohsiek, W., van den Hurk, B.J.J.M., 1993. A verification of some methods to determine the fluxes of momentum, sensible heat and water vapour using standard deviation and structure parameter of scalar meteorological quantities. Boundary-Layer Meteorol. 63, 231–257.

Drexler, J.Z., Snyder, R.L., Spano, D., Paw U, K.T., 2004. A review of models and micrometeorological methods used to estimate wetland evapotranspiration. Hydrological Processes. 18, 2071–2101.

Green, A.E., 2001. The practical application of scintillometers in determining the surface fluxes of heat, moisture and momentum. Doctoral Thesis, Wageningen University, Holland. ISBN 90–5808–336–5. Pp 177.

Hill, R.J., 1992. Review of optical scintillation methods of measuring the refractive index spectrum, inner scale and surface fluxes. Waves Random Media 2, 179–201.

Hill, R.J., 1997. Algorithms for obtaining atmospheric surface-layer fluxes from scintillation measurements. J. Atmos. Oceanic Tech. 14, 456–467.

Hsieh, C-I., Katul, G.G., Schieldge, J., Sigmond, J., Knoerr, K.R., 1996. Estimation of momentum and heat fluxes using dissipation and flux-variance methods in the unstable surface layer. Water Resour. Res. 32, 2453–2462.

Hsieh, C-I., Lai, M-C., Hsia, Y-J., Chang, T-J., 2008. Estimation of sensible heat, water vapour and CO2 fluxes using the flux-variance method. Int. J. Biometeorol. 52, 21–533.

Kustas, W.P., Blanford, J.H., Stannard, D.I., Douglas, C.S.T., Nichols, W.D., Weltz, M.A., 1994. Local energy flux estimates for unstable conditions using variance data in semiarid rangelands. Water Resour. Res. 30, 1351–1361.

Mahrt, L., 2000. Surface heterogeneity and vertical structure of the boundary layer. Boundary-Layer Meteorol. 96, 33–62.

Obukhov, A.M., 1949. Structure of the temperature field in turbulent flow. Izv. Akad. Nauk, SSSR, Ser. Geogr. i Geofiz. 13 58–69.

Paw U, K.T., Qiu, J., Su, H.B., Watanabe, T., Brunet, Y., 1995. Surface renewal analysis: a new method to obtain scalar fluxes without velocity data. Agric. Forest Meteorol. 74, 119–137.

Raupach, M.R., Legg, B.J., 1984. The uses and limitations of flux gradient relationships in micrometeorology. In: Sharma, M.L. (Ed.) Evapotransipration from Plant Communities. Elsevier, Amsterdam.

Savage, M.J., 2007. Sensible heat estimation using a high frequency temperature-based method above various canopies. Proc. 13th S. Afr. Nat. Comm. Int. Assoc. of Hydro. Sci. (SANCIAHS) Symp, Sept 6–7, Cape Town, Republic of South Africa.

Savage, M.J., 2009a. Estimation of evaporation using a dual-beam surface layer scintillometer and component energy balance measurements. Agric. Forest Meteorol. 149, 501–517.

Savage, M.J., 2009b. Evaporation estimation method and system. Provisional Patent Application Number 2009/06090 filed 2 September 2009. Invention assigned to University of KwaZulu-Natal, South Africa.

Savage, M.J., Everson, C.S., Metelerkamp, B.R., 1997. Evaporation measurement above vegetated surfaces using micrometeorological techniques. Water Research Commission Report No. 349/1/97, p248, ISBN 1–86845–363–4.

Savage, M.J., Everson, C.S. Odhiambo, G.O. Mengistu, M.G., Jarmain, C., 2004. Theory and practice of evaporation measurement, with special focus on surface layer scintillometry as an operational tool for the estimation of spatially averaged evaporation. Water Research Commission Report No. 1335/1/04, p204, ISBN 1–77005–247–X.

Sellers, P.J., Mintz, Y., Sud, Y.C., Dalcher, A., 1986. A simple biosphere modeil (SiB) for use within general circulation models. J. Atmos. Sci. 43, 505–531.

Snyder, R.L., Spano, D., Paw U, K.T., 1996. Surface renewal analysis for sensible and latent heat flux density. Boundary-Layer Meteorol. 77, 249–266.

Spano, D., Snyder, R.L., Duce, P., Paw U, K.T., 2000. Estimating sensible and latent heat flux densities from grapevine canopies using surface renewal. Agric. For. Meteorol. 104, 171–183.

Sugita, M., Kawakubo, N., 2001. Surface and mixed-layer variance methods to estimate regional sensible heat flux at the surface. Boundary-Layer Meteorol. 106, 117–145.

Thiermann, V., 1992. A displaced-beam scintillometer for line-averaged measurements of surface layer turbulence. 10th Symposium on turbulence and diffusion. Portland, Oregon, USA.

Thiermann, V., Grassl, H., 1992. The measurement of turbulent surface-layer fluxes by use of bichromatic scintillation. Boundary-Layer Meteorol. 58, 367–389.

Thom, A.S., 1975. Momentum, mass and heat exchange in plant communities. In: Monteith JL (ed.) Vegetation and the Atmosphere. Vol. 1. Principles pp 57-109. Academic Press. London, UK.

Tillman, J.E., 1972. The indirect determination of stability, heat and momentum fluxes in the atmospheric boundary layer from simple scalar variable during dry unstable conditions. J. Appl. Meteorol. 11, 783–792.

Unland, H.E., Houser, P.R., Shuttleworth, W.J., Yang, Z-L., 1996. Surface flux measurement and modeling at a semi-arid Sonoran Desert site. Agric. Forest Meteorol. 82, 119–153.

Van Dijk, A.I.J.M., Bruijnzeel, L.A.S., Schellekens, J., 2004. Micrometeorology and water use of mixed crops in upland West Java, Indonesia. Agric. Forest Meteorol. 124, 31–49.

Wesson, K.H., Katul, G., Lai, C.T., 2001. Sensible heat flux estimation by flux variance and half-order time derivative methods. Water Resour. Res. 37, 2333–2343.

Wyngaard, J.C., Cote, O.R., Izumi, Y., 1971. Local free convection, similarity and the budgets of shear stress and heat flux. J. Atmos. Sci. 7, 1171–1182.

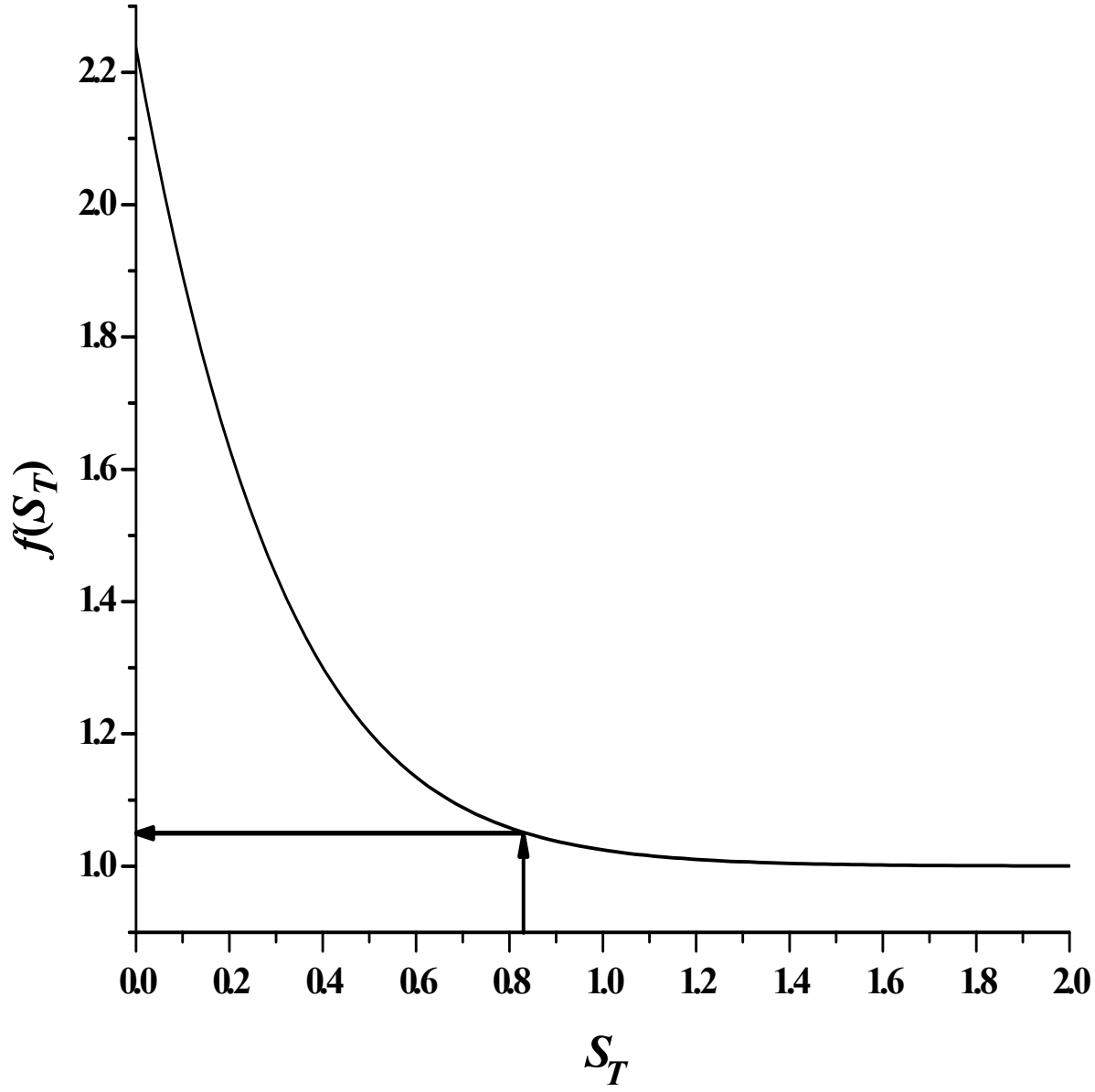

Fig. 7.1. The functional dependence of $f(S_T)$ on air temperature skewness S_T (Eq. (7.10)) showing that for skewness values $S_T > 0.83$, $f(S_T) < 1.05$.

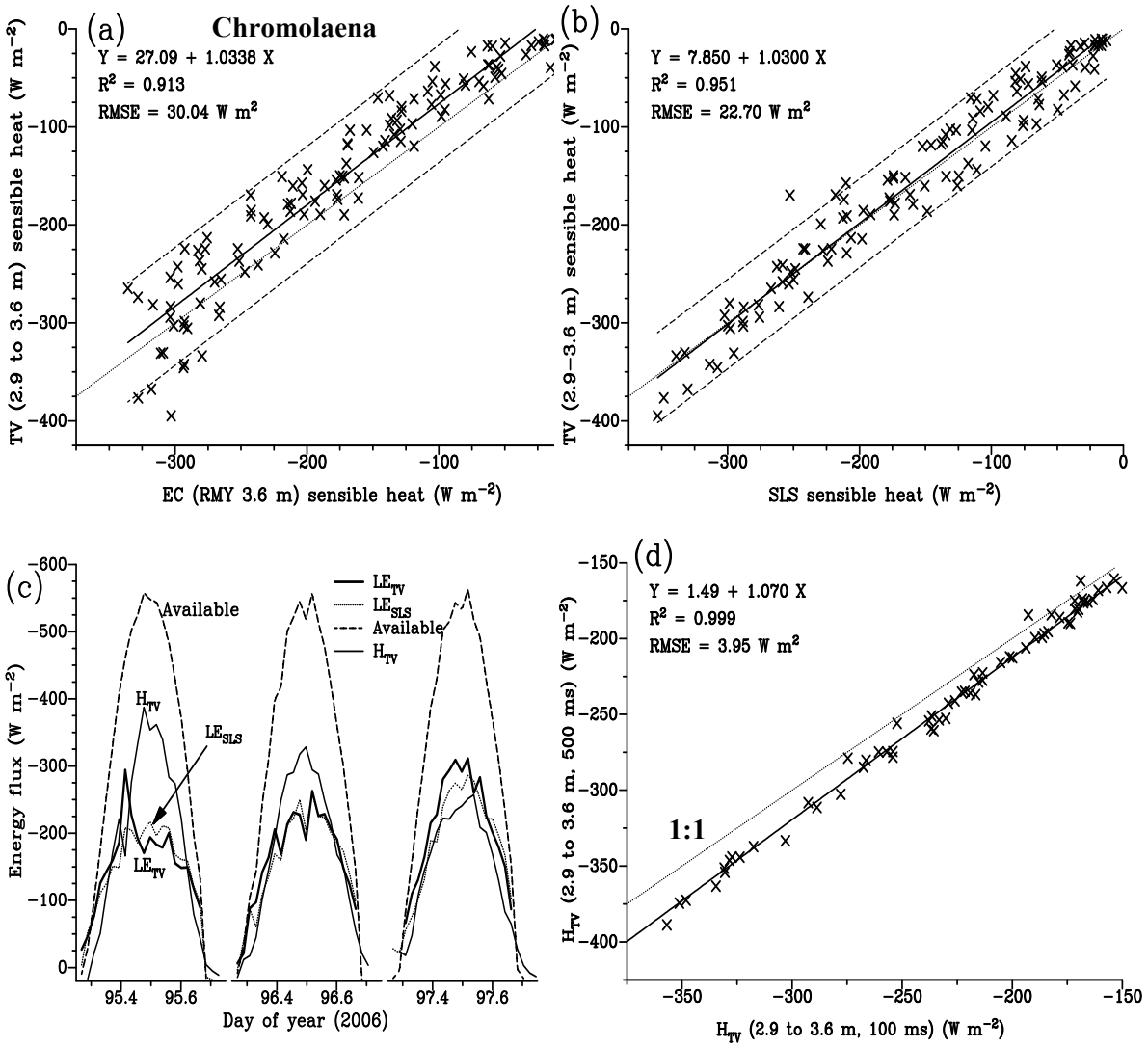

Fig. 7.2. Chromolaena site (a) Top left: The regression of the TV estimate of *H* (averaged for the 2.9- and 3.6-m heights) against the EC estimate at the 3.6-m height. Each point represents a 30-min average of the 2-min estimates for unstable conditions only. The confidence belts shown represent those for a single predicted value and the dotted line is the 1:1 line. (b) Top right: The regression of the TV estimate of *H* (averaged for the 2.9- and 3.6-m heights) against the SLS estimate at the 3.6-m height. Each point represents a 30-min average of the 2-min estimates for unstable conditions only. (c) Bottom left: The diurnal variation in some of the shortened energy balance components for day of year 95 to 97 for the TV and SLS methods. The available energy flux density is the sum of the net irradiance and the soil heat flux density. The latent energy amounts shown are estimated as a residual amount from the shortened energy balance. (d) Bottom right: A comparison between *H* estimated using the TV method using both the 100- and 500-ms datasets, for the 2.9- and 3.6-m heights. The dotted line is the 1:1 line.

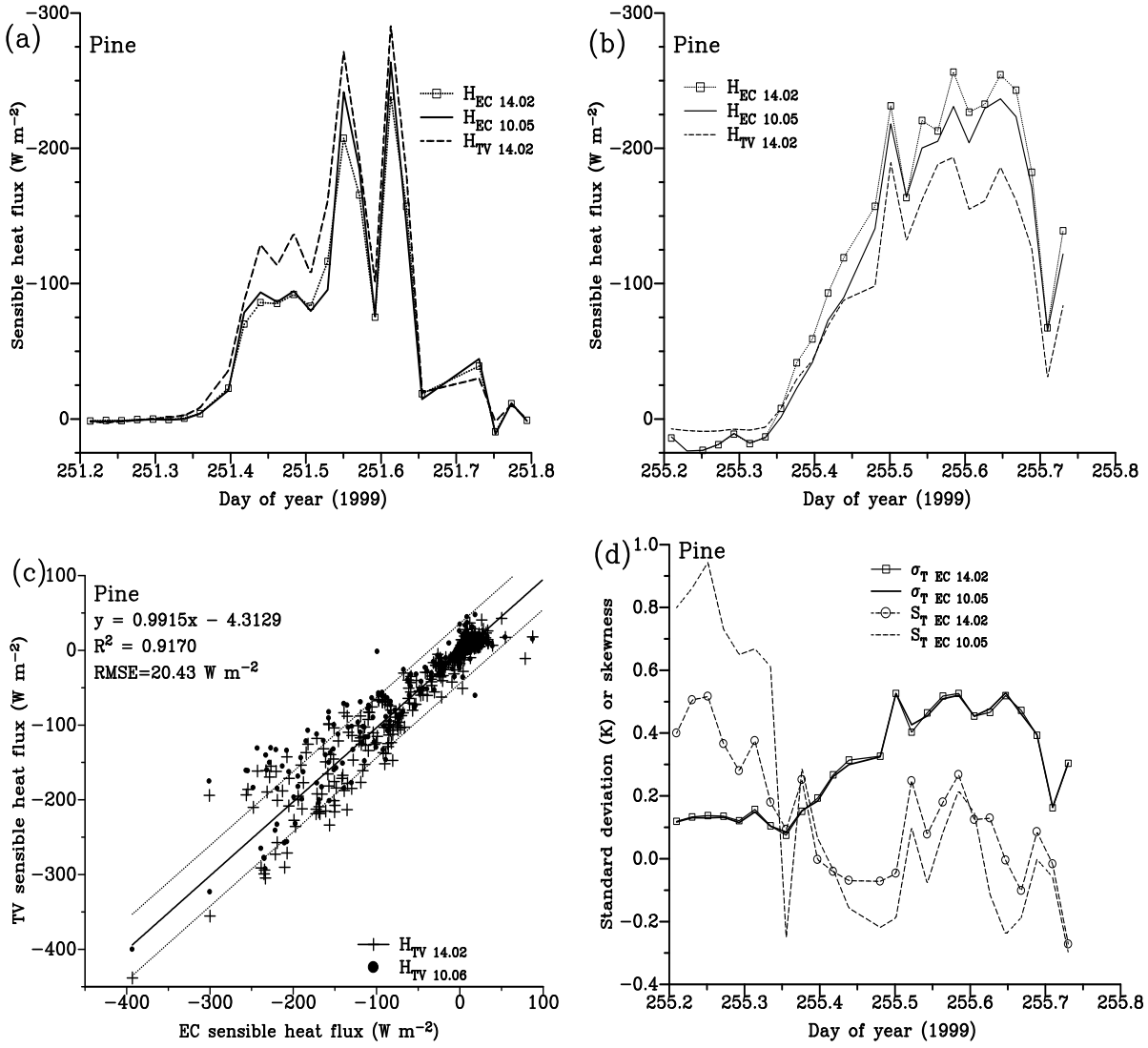

Fig. 7.3 Pine canopy site (a) Top left: Diurnal variation in *H* (half-hourly) for the Pine canopy site for day of year 251 with variable cloud cover conditions for the EC method at 14.02 m ($H_{EC\_14.02}$) and 10.05 m ($H_{EC\_10.05}$) heights as well as the *H* estimate using the TV method at the 14.02 m height ($H_{TV\_14.02}$).(b) Top right: Diurnal variation in *H* (half-hourly averages of 2-min estimates) for the Pine canopy site for day of year 255 for the EC method at 14.02 m ($H_{EC\_14.02}$) and 10.05 m ($H_{EC\_10.05}$) heights as well as the *H* estimate using the TV method at the 14.02 m height ($H_{TV\_14.02}$). (c) Bottom left: The regression of H_{TV} against the H_{EC} (half-hourly) compares favourably with the TV method for the same height ($H_{TV\_14.02}$) with a slope of 0.9915. The regression for the 10.06-m height ($H_{TV\_10.06}$) is also reasonable. The confidence belts shown represent those for a single predicted value. (d) Bottom right: The standard deviation in air temperature as measured by the EC system for the two heights (14.02 m and 10.05 m) agree well ($\sigma_{T\_14.02}$, $\sigma_{T\_10.05}$) with reduced agreement in the skewness ($S_{T\_14.02}$, $S_{T\_10.05}$).

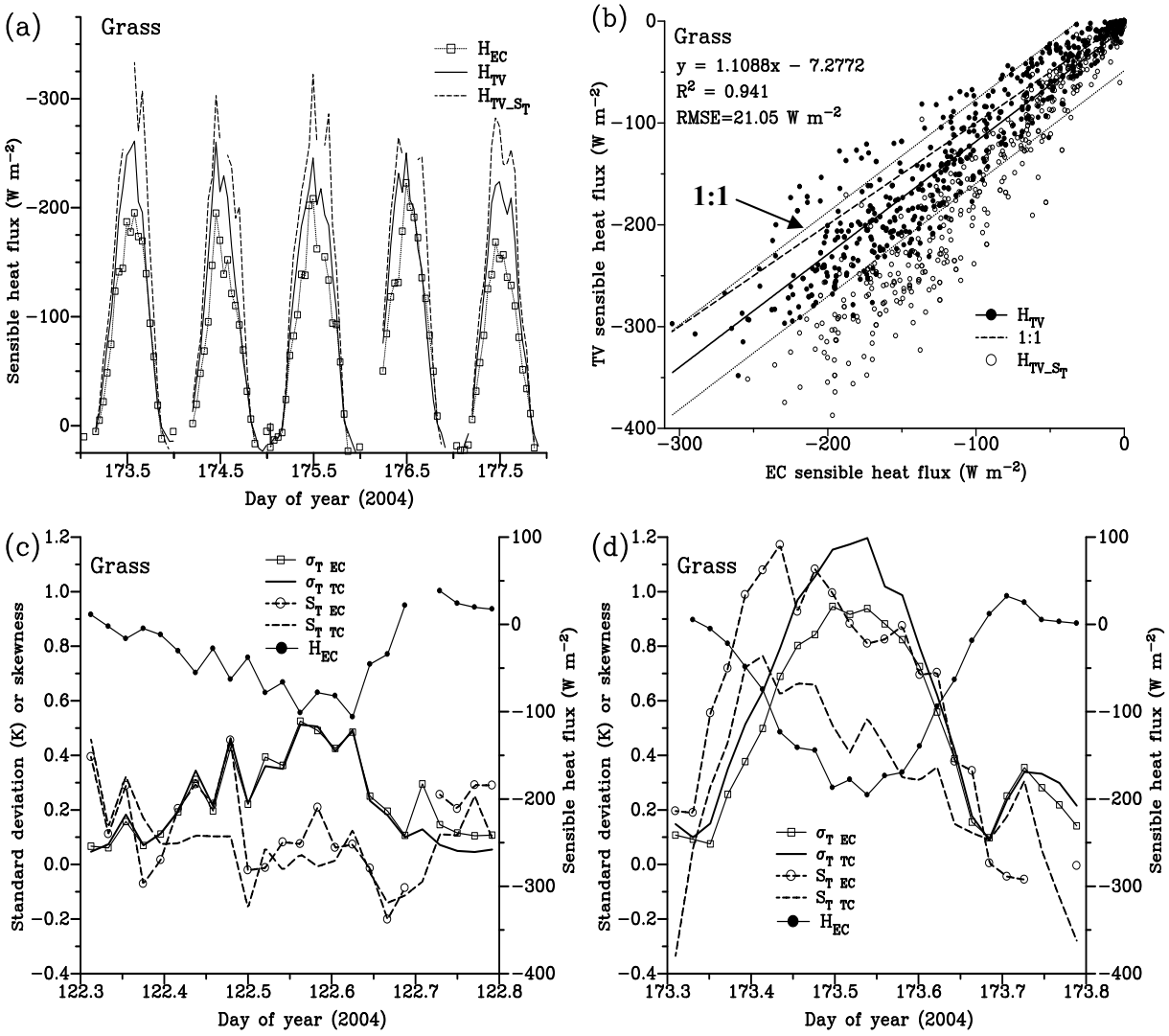

Fig. 7.4. Grassland site (a) Top left: Diurnal variation in *H* (half-hourly averages of 2-min estimates) for the Bellevue grassland site for five days. The temperature variance (H_{TV}) and the temperature variance adjusted for skewness ($H_{TV\,S_T}$) estimates of *H* for this period tends to overestimate compared to H_{EC}. (b) Top right: The regression of H_{TV} against H_{EC} (half-hourly) compares favourably with a slope of 1.1088. When adjusted for skewness, the comparison is biased. The confidence belts shown represent those for a single predicted value for the TV vs EC comparison and the dashed line is the 1:1 line. (c) Bottom left: The standard deviation in air temperature as measured by the EC and bare fine-wire thermocouple agree well ($\sigma_{T\_EC}, \sigma_{T\_TC}$) with reduced agreement in the skewness ($\sigma_{S_T\_EC}, \sigma_{S_T\_TC}$). Also shown is the eddy covariance H_{EC} (right-hand y-axis). (d) Bottom right: For this day, later in the season and with a greater *H* magnitude, the standard deviation in air temperature as measured by the EC and bare fine-wire thermocouple deviate somewhat ($\sigma_{T\_EC}, \sigma_{T\_TC}$) with poor agreement in the skewness ($\sigma_{S_T\_EC}, \sigma_{S_T\_TC}$). Also shown is the H_{EC} (right-hand y-axis).

8 BOWEN RATIO EVAPORATION MEASUREMENT IN A REMOTE MONTANE GRASSLAND: DATA INTEGRITY AND FLUXES[1]

8.1 Summary

Evaporation measurements using two Bowen ratio energy balance (BREB) systems in a remote high altitude montane grassland catchment of the Drakensberg Mountains, Cathedral Peak, South Africa are reported on. Various methods of data verification and rejection of inaccurate measured air temperature and water vapour pressure gradients are examined. A theoretical analysis, based on the equivalent temperature, results in data rejection procedures using the measurement of the air temperature profile difference. Data rejection is necessary whenever the Bowen ratio approaches -1, resulting in extremely inaccurate and impossibly large positive or negative sensible heat and latent energy fluxes. Using the shortened energy balance, it is shown that when the Bowen ratio approaches the limit of -1, for which the available energy flux approaches 0 W m^{-2}, conditions are pseudoadiabatic and isobaric and that such conditions can be depicted by the wet-bulb temperature isolines of the psychrometric chart. Disregarding evaporation estimates for which the Bowen ratio values are between arbitrarily chosen values remedies the problem to some extent. With this method, daily total evaporation may be reasonable but 20-min values unreasonable during mainly early morning and late afternoon periods. A more sensitive and dynamic approach is used to prevent BREB data from being excluded unnecessarily and to prevent rogue values escaping detection. Once the rejection procedures were applied, the 20-min BREB latent energy flux estimates compared well with measurements from a weighing lysimeter adjacent to the site. Three methods were used to estimate the exchange coefficient K which allowed flux estimation for when BREB data are invalid or lacking. One method involved calculating K from wind speed only and the second method was based on the MOST-dependent temperature-variance method for which the 20-min standard deviation of 1-Hz air temperature data were used. From independent measurements of sensible heat H and latent energy LE, a time-invariant exchange coefficient K was also determined from measurements of the air temperature profile difference. These methods were used when there were invalid water vapour pressure data due to condensation in the hoses or problems with the cooled dew point mirror or when the fine-wire thermocouples were damaged or when there were unreliable estimates of the air temperature gradient. The time-invariant value for K used in one of the methods, 0.239 m^2 s^{-1}, was confirmed for a mesic grassland using independent eddy covariance and surface-layer scintillometer measurements of H and Bowen ratio measurements of the air temperature profile difference.

Keywords:

Bowen ratio

Data rejection

Evaporation measurement

Grassland evaporation

K method

[1] Based on Savage et al. (1997, 2004, 2009)

Temperature-variance

Eddy covariance

Surface-layer scintillometer

8.2 Introduction

One of the most important factors affecting water supply from any catchment is the evaporative loss from the vegetative community, which in the Drakensberg, for example, in KwaZulu-Natal, South Africa is a fire-determined climax grassland. The loss of water in the gaseous phase may be estimated by measuring, *inter alia*, the flux of water vapour, in various parts of the soil-plant-atmosphere system, by various means.

The flux of an entity above and away from an exchanging surface is dependent on the gradient of that entity. Using the Bowen Ratio Energy Balance (BREB) micrometeorological method, the flux of water vapour, the latent energy flux , and the sensible heat flux from the surface are estimated. These flux densities are obtained simultaneously by measuring both the water vapour pressure difference and the air temperature difference between the same two vertical heights above the canopy or soil, and measuring the net irradiance and the soil heat flux.

The BREB method has been employed for the quantification of evaporation over various surfaces, from open water, to grassland to crop land and to forest. Specific studies include trees (Dawson, 1996), a vegetated clearcut in a sub-boreal region (Pypker and Freedeen, 2002), open water (Burba et al., 1999; Rohli et al., 2004), sheltered lemon orchard (Daamen et al., 1999), irrigated alfalfa advective environment (Todd et al., 2000), grass (Perez et al., 2008; Xing et al., 2008), semi-arid grass (Frank, 2003), short grass in a steppe region using a modified BREB system (Wolf et al., 2008), affect of spring burning in a tallgrass prairie (Bremer and Ham, 1999), reed beds (Sommer et al., 2003; Peacock and Hess, 2004); irrigated groundnut (Kara and Kumarb, 2007), ammonia fluxes over soybean (Walker et al., 2006), vineyard (Heilman et al., 1994) and vineyard in an arid desert region (Zhang et al., 2008). Henrici (1943) appears to have been the first to have attempted evaporation measurements in the Drakensberg catchments of South Africa, and these were entirely plant-based measurements. The water balance of a first-order catchment in the montane grasslands was reported on by Everson (2001).

Besides the measurement of how much water is lost from a surface, the Bowen ratio, by virtue of its formulation, provides additional valuable information about the distribution or partitioning of available energy at the surface (Suomi and Tanner, 1958; Tanner, 1961). Energy available at the earth's surface is consumed mainly as sensible heat H (temperature change with no phase change of water) and latent energy LE (the phase change of water with little temperature change). The relative significance of these terms is through the ratio H/LE, now more commonly known as the Bowen ratio β (Bowen, 1926; Sverdrup, 1943). The BREB method has traditionally been employed as a research tool over flat and only moderately hilly, extensive crop surfaces to determine crop responses to various treatments, most commonly different weather conditions causing different atmospheric demands and water stresses (Garratt, 1984). The use of the BREB method on a 22^{o} slope has been verified by Nie et al. (1992). The BREB method has also been tested and used over uniform agricultural crops but less often above natural grasslands such as in this work (Webb, 1960; Tanner, 1961; Fritschen, 1965;

Tanner and Fuchs, 1969; Lourens and Pruitt, 1971; Perrier et al., 1971; Verma et al., 1978; Tanner et al., 1987).

In the BREB method there are, apart from measurements for the estimation of soil heat flux and the net irradiance above the surface, no surface-based measurements of any kind. The problems associated with measuring or obtaining resistances, surface temperature, and saturation water vapour pressure as a function of surface temperature are therefore avoided. Furthermore, with the assumption that the exchange coefficients for *H* and *LE* are equal, stability dependence of the BREB method is removed (Savage, 2009).

It could be argued that the BREB method is obsolete. However, BREB measurements are still of interest since the method is less expensive than eddy covariance and scintillometry and there is reduced operator skill required with fewer corrections to the data needed. Furthermore, the method will remain of interest until the issue of lack of closure of eddy covariance measurements (Foken, 2008) is resolved. For example, Wolf et al. (2008) used a modified BREB method to investigate the effects of different eddy covariance correction schemes on energy balance closure and Savage (2009) used the BREB method to validate surface-layer scintillometer measurements.

Apart from the theoretical paper of Ohmura (1982) and work by Perez et al. (1999), there are few papers that deal with BREB data checking. The aim of this research is to use the BREB method to collect accurate and reliable evaporation measurements as part of a larger long-term study of the total evaporation in grassland systems but in particular in a remote montane grassland. The treatment of BREB data, including data rejection procedures, is emphasized. An additional aim included the estimation of *H* in the absence of either air temperature or water vapour pressure gradients. To this end, the use of an exchange coefficient *K*, calculated in different ways for estimating *H* and *LE,* was investigated.

8.3 Theory

8.3.1 Bowen ratio

The transfer of water vapour between a surface and the atmosphere of the surface is a fundamental aspect of the water balance of a plant community. From a consideration of the shortened energy balance of a vegetated surface, in the absence of advection flux and neglecting biochemical and physical storage by the canopy in comparison with the other terms:

$$R_{net} + LE + H + S = 0 \tag{8.1}$$

where R_{net}, *LE*, *H* and *S* are the net irradiance, latent energy flux , sensible heat flux and soil heat flux respectively. All terms are in W m^{-2}. Combining the energy balance equation with the definition of the Bowen ratio (Bowen, 1926):

$$LE = -(R_{net} + S) / (1 + \beta) \tag{8.2}$$

and

$$H = -\beta (R_{net} + S) / (1 + \beta) \tag{8.3}$$

where $\beta \neq -1$. When $\beta \to -1$, Eqs. (8.2) and (8.3) cannot be applied and $R_{net} + S \to 0$ (Eq. (8.1)). Assuming similarity between the exchange coefficients for *H* and *LE*:

$$\beta = \gamma \, \mathrm{d}T / \mathrm{d}e \tag{8.4}$$

where γ is the psychrometric constant (kPa $^{o}C^{-1}$), d*T* the profile air temperature difference (^{o}C) and d*e* the profile water vapour pressure difference (kPa). Both differences are averaged, typically over 20 min. If, in Eq. (8.4), $\beta = -1$, then $-\mathrm{d}e = \gamma \, \mathrm{d}T$ or $\mathrm{d}\theta = \mathrm{d}e + \gamma \, \mathrm{d}T = 0$ where the equivalent temperature θ (K) is defined by:

$$\theta = T + e / \gamma \tag{8.5}$$

where *T* (K) is the air temperature and *e* (kPa) the water vapour pressure. The psychrometric constant may be written as $c_p P / \varepsilon L$ where c_p is the specific heat capacity of air at constant pressure (J kg^{-1} $^{o}C^{-1}$), *P* the atmospheric pressure (kPa), $\varepsilon = 0.622$ the ratio of the molecular mass of water vapour to that of dry air and *L* the specific latent energy of vapourisation (≈ 2.45 MJ kg^{-1} at 20 ^{o}C). When the Bowen ratio $\beta = \gamma \, \mathrm{d}T / \mathrm{d}e = (c_p P / \varepsilon L) \cdot \mathrm{d}T / \mathrm{d}e$ equals -1, then $c_p \, \mathrm{d}T + L \, \mathrm{d}q = 0$ in terms of specific humidity *q* (kg kg^{-1}) = $w / (1 + w)$ [where mixing ratio $w = \varepsilon e / (P - e)$] or $c_p \, \mathrm{d}T + (\varepsilon L / P) \mathrm{d}e = 0$ in terms of water vapour pressure *e*. Noting that an adiabatic process is defined as one in which no energy is added or removed and considering what is referred to as a pseudoadiabatic process at constant pressure (a process used in meteorology), Byers (1974) showed that $c_p \, \mathrm{d}T + L \, \mathrm{d}q = 0$. Hence, since $\beta = -1$ is equivalent to $c_p \, \mathrm{d}T + L \, \mathrm{d}q = 0$, the conditions under which $\beta = -1$ are pseudoadiabatic and isobaric. For application of Eqs. (8.2) and (8.3), data collected during these conditions must be identified, excluded if necessary and if possible replaced. Such pseudoadiabatic conditions are depicted on the psychrometric chart by wet-bulb temperature isolines, since for such isolines $\mathrm{d}e / \mathrm{d}T = -\gamma$ or $\mathrm{d}\theta = 0$. Furthermore β = -1 implies *H* = -*LE* and therefore that the available energy is zero which corresponds to adiabatic conditions. Also, assuming adiabatic conditions prevail for which $H + LE = 0$ and hence $R_{net} + S = 0$ from Eq. (8.1), $1 + \beta = 0$ is a possibility using from Eq. (8.2).

8.3.2 Data rejection

By definition, *LE* estimates may need to be rejected when the Bowen ratio β approaches -1 (Eq. (8.2)). Use of Eq. (8.2) may result in inconsistent estimates, when $R_{net} + S \neq 0$, of *H* and *LE* when compared to values just before and just after this time.

Suppose that δT and δe are the respective measured air temperature and water vapour pressure differences. The resolution limits of the air temperature and hygrometer sensors are denoted as *E*(*T*) and *E*(*e*) respectively. Consider the difference in the equivalent temperature $\theta = T + e / \gamma$ where $\mathrm{d}\theta = \mathrm{d}T + \mathrm{d}e / \gamma$ is the true profile equivalent temperature difference. Assuming that the difference between the measured profile equivalent temperature difference $\delta\theta$ and the true profile equivalent temperature difference $\mathrm{d}\theta$ is less than twice the resolution limit in equivalent temperature $E(\theta)$

$$|\delta\theta - \mathrm{d}\theta| < 2E(\theta) \tag{8.6}$$

where $E(\theta) = E(T) + E(e)/\gamma$. (8.7)

For cases where $\beta = -1$, we previously showed that $\mathrm{d}\theta = 0$. This condition implies that the equivalent temperature is the same at both BREB levels in the atmosphere. Substituting $\mathrm{d}\theta = 0$, corresponding to $\beta = -1$, into Eq. (8.6) and expanding:

$$-2E(\theta) < \delta\theta < 2E(\theta) \tag{8.8}$$

where the measured profile equivalent temperature difference $\delta\theta = \delta T + \delta e/\gamma$ corresponds to measurements of the air temperature and water vapour pressure profile differences δT and δe respectively. Hence the limits of the measured profile temperature difference are defined by:

$$-2E(\theta) - \delta e/\gamma < \delta T < 2E(\theta) - \delta e/\gamma\,. \tag{8.9}$$

This inequation was employed as a data rejection criterion. This derivation results in a similar equation used by Ohmura (1982) in his data rejection methodology. The theory presented here is pedagogically simple and reinforces concepts from the psychrometric chart. Equivalently, by rearrangement of Eq. (8.9):

$$-2\gamma E(\theta) - \gamma\,\delta T < \delta e < 2\gamma E(\theta) - \gamma\,\delta T \tag{8.10}$$

$$\text{or } -1 - 2\gamma E(\theta)/\delta e < \beta_{measured} < -1 + 2\gamma E(\theta)/\delta e \tag{8.11}$$

for $\delta e > 0$ kPa or

$$-1 + 2\gamma E(\theta)/\delta e < \beta_{measured} < -1 - 2\gamma E(\theta)/\delta e \tag{8.12}$$

for $\delta e < 0$ kPa where $\beta_{measured}$ is estimated from profile measurements δT and δe. In both Eqs. (8.11) and (8.12), as δe approaches 0 kPa, $\beta_{measured}$ becomes undefined corresponding to $|H| \approx |LE|$. Eqs. (8.11) and (8.12) confirm the result of Perez et al. (1999) that the excluded values for $\beta_{measured}$ are dependent on the water vapour pressure profile difference δe and $E(\theta)$ and hence also dependent on $E(T)$ and $E(e)$. If the inequalities expressed by Eqs. (8.9) to (8.12) are satisfied then there is a high possibility that the true Bowen ratio will be very near -1 and therefore the calculated flux densities will not have numerical meaning (Eqs. (8.2), (8.3)). For the instruments used by Tanner et al. (1987), as an example, it is assumed that $E(T) \approx 0.006$ K and $E(e) \approx 0.01$ kPa. Then $E(\theta) \approx 0.006 + 0.01/\gamma$. In the case of the water vapour pressure measurements, a cooled dew point mirror system is often used, but alternatives such as a capacitive hygrometer have also been employed (Cellier and Olioso, 1993). Given the typical value for $\gamma = 0.066$ kPa K^{-1}, the value for $E(\theta)$ is dominated by $E(e)/\gamma$, and $E(\theta) \approx 0.1575$ K. Hence Eq. (8.11) reduces to:

$$-1 - 0.0208/\delta e < \beta_{measured} < -1 + 0.0208/\delta e \tag{8.13}$$

for $\delta e > 0$ kPa or from Eq. (8.12)

$$-1 + 0.0208 / \delta e < \beta_{measured} < -1 - 0.0208 / \delta e \tag{8.14}$$

for $\delta e < 0$ kPa. Perez et al. (1999) used a value of 0.019 kPa compared to the value of 0.0208 kPa in Eqs. (8.13) and (8.14).

Data rejection may therefore be based on limits being defined for the measured profile air temperature difference δT profile water vapour pressure difference δe or β using Eqs. (8.9) to (8.12).

A common rejection procedure (Tanner et al., 1987) involves rejecting data for which

$$-1.25 < \beta_{measured} < -0.75 \tag{8.15}$$

or using similar limits (for example, Ortega-Farias et al., 1996; Brotzge and Crawford, 2003). Comparing Eqs. (8.13) and (8.14), we note that Eq. (8.15) is equivalent to assuming limits for δe of -0.083 kPa and 0.083 kPa, the result of an arbitrary choice of limits for the measured Bowen ratio. Generalising Eq. (8.15) to $|\beta_{measured} + 1| < l_\beta$ where l_β is the Bowen ratio rejection limit (for which $l_\beta = 0.25$ yields Eq. (8.15)), then the limits for δe are $-2\gamma E(\theta) / l_\beta$ and $2\gamma E(\theta) / l_\beta$.

Other measurements including R_{net} and S may be in error (Savage, 2009; Savage and Heilman, 2009) besides those dealt with here. Furthermore, there is the possibility of a mismatch in the footprint of the convective fluxes, net irradiance and soil heat flux (Schmid, 1997). Guidelines for the possible correction and the validation of BREB data are discussed by Payero et al. (2003). These guidelines include ensuring that for normal evaporative conditions, $e_{lower\,arm} > e_{upper\,arm}$ and $T_{lower\,arm} > T_{upper\,arm}$. The air temperature condition, for example, ensures that the sensible heat is directed away from the surface for unstable conditions and toward when stable. Ohmura (1982) suggested data rejection should the following conditions, rewritten in terms of the equivalent temperature difference, not be met:

$-R_{net} - S < 0$ then $\delta\theta > 0$;

and $-R_{net} - S > 0$ then $\delta\theta < 0$.

These conditions are based on Eq. (8.2) and ensure that under normal evaporative conditions, the fluxes have the correct direction.

Occasionally however, the fine-wire thermocouples may be damaged causing data loss or the measurements are in error due to spider's webs or dirt. Error in δe may be due to cooled mirror problems or water condensation in either or both of the hoses or mixing bottles, if used. The next section is concerned with the estimation of H and LE in such cases using measured δT or measured δe values and knowledge of an exchange coefficient.

8.3.3 Determination of H from an exchange coefficient

If a method of obtaining a reliable estimate of *H* using the exchange coefficient *K* could be found, fluxes could still be estimated in spite of the lack of or invalid BREB data. Wang and Bras (1998), for example, used a time-invariant value for *K* for two field experiments FIFE and ABRACOS. Alternatively, if δe data are missing or in error, *K* could be calculated from horizontal wind speed using a method of Wang and Bras (1998) described by Wesson et al. (2001) or by using the temperature-variance method using the standard deviation in air temperature (σ_T, ^oC) and application of Monin-Obukhov similarity theory (MOST) (Tillman, 1972). Furthermore, it would be possible to patch data for which the δT or the δe measurements were invalid (Eqs. 8.9 to 8.12), inaccurate, unreliable or for which $\beta \to -1$. In the case of the K method, all that would be required to calculate *H* is a *K* value and either the air temperature profile difference or the measured water vapour pressure profile difference. The other methods for calculating *K* would require wind speed or σ_T. From the value of *K* determined, in conjunction with an estimate of the available energy, *LE* and *H* could be estimated.

One assumption of the BREB method is the "assumption of similarity" where the turbulent exchange coefficients for *H* and *LE*, K_h and K_w respectively, are assumed equal: ($K = K_h = K_w$) (Rider and Robinson, 1951; Rider, 1954; Tanner, 1963; Dyer, 1967; Swinbank and Dyer, 1967). It is assumed that the ratio of the exchange coefficients (or eddy diffusivities) for the two types of energy fluxes considered is not significantly different from unity under the conditions for which the method applies. Therefore only one *K* value is required - the assumed (common) *K* value.

The value of *K* may be calculated directly from the governing diabatic profile equations (Fuchs and Tanner, 1970). The transfer coefficient with the diabatic influence accounted for is given by Sellers (1965). This method requires *a priori* wind speed profile measurements and an assessment of the dependency of some of the parameters in the equations on atmospheric stability conditions by means of further measurements. It was therefore not attempted.

The value of *K* can also be calculated indirectly either from simultaneous lysimetric and BREB measurements (Verma et al., 1978), or from simultaneous eddy covariance and BREB measurements at one site (Motha et al., 1979). Rearranging the BREB and energy balance equations and substituting lysimetrically-determined (or similar) values for the flux densities would yield the best estimate of the unknown *K*.

The assumption of similarity between the two exchange coefficients ($K_h = K_w$) means that individual values for both exchange coefficients are not required (due to the assumption that the two diffusivities are equal and therefore cancel). Thus a common *K* value may be found using BREB measurements alone by back calculation, and is, due to the formulation of the Bowen ratio, identical in value whether calculated from *H* or *LE*.The back calculation method can reveal the value of *K* (= K_h = K_w) using standard flux-gradient relationships:

$$K_h = -(H / \rho c_p)\delta z / \delta T \tag{8.16}$$

and $$K_w = -(LE\,\gamma / \rho c_p)\delta z / \delta e \tag{8.17}$$

where δz is the profile height difference (m). If the calculated K value is now used in conjunction with the gradient measurements from another BREB system (or other independent source) to calculate the flux densities, a comparison of the results without any auto self-correlation is possible. Other published work has also used the K method. For example, Pypker and Freedeen (2002) and Wolf et al. (2008) used the K method and CO_2 measurements based on Eqs. (8.16) and (8.17), to obtain BREB measurements of H, LE and CO_2 flux. The BREB measurements of Wolf et al. (2008) were used to obtain eddy covariance closure correction schemes. It must be mentioned that K has a complex behaviour and that there have been many unsuccessful attempts to establish empirical relationships to determine K. Wind speed, atmospheric stability and canopy roughness are also known to influence K.

For four different surfaces Wesson et al. (2001) found that K_h, corrected for displacement height $d \approx 0.67$ times canopy height, can be estimated from $K_h \approx U(z-d)$ (Wang and Bras, 1998) where U is the horizontal wind speed and z the measurement height or $K_h \approx (h/3)U$ where h is the canopy height. They noted that their estimates performed as well as or better than the MOST parameterisation of K_h.

More often than not, δe measurements are in error compared to δT. In such cases, it is possible to use the MOST-dependent temperature-variance method (Tillman, 1972) to calculate K and hence estimate sensible heat. Following Tillman (1972) H may be estimated using air temperature data, for the upper measurement level. In spite of the lack of a stability correction, the temperature-variance method has been applied with satisfactory results for a range of canopy types (for example, Weaver, 1990; Albertson et al., 1995; Guo et al., 2009). Combining Eq. (8.16) and the temperature-variance method:

$$K_h = (kg/T)^{1/2}(z-d)^{1/2}(\sigma_T/C_1)^{3/2}/(\delta T/\delta z) \tag{8.18}$$

where $C_1 \approx 1$ for unstable conditions (Tillman, 1972 but with the von Kármán constant k adjusted from 0.35 to 0.41) and a different value for stable conditions (de Bruin and Hartogensis, 2005), g the acceleration of gravity (≈ 9.81 m s^{-2}) and T (K) the average air temperature and σ_T (^{o}C) the 20-min standard deviation in air temperature, the latter two from the upper and/or lower measurement level.

8.4 Materials and methods

The research location was Catchment VI of the Cathedral Peak Forestry Research Station, in the foothills of the Drakensberg, KwaZulu-Natal, South Africa at 29.00°S, 29.25°E, at an altitude of 1935 m and with a predominantly north-facing aspect and average slope of about 15^{o}. It is 0.677 km^2 (68 ha) in area and varies in altitude from 1847 to 2076 m (Schulze, 1975; Everson, 2001). Two locations were used in the catchment - an upslope site at which two BREB systems were employed for simultaneous measurement comparisons and a location within a riparian zone. A second site was used for BREB and eddy covariance measurements to confirm the value of the exchange coefficient used by the K method. For this site, BREB measurements were conducted above an open and mesic grassland at Bellevue farm, Ashburton and close to Pietermaritzburg, South Africa (29.64^{o}S, 30.43^{o}E, altitude of 671 m).

Initially two totally independent (separate) BREB systems were collocated at Cathedral Peak to later compare measurements at different sites in the same catchment. One system remained

permanently in the open grassland (upslope) site whilst the second system was moved to the riparian zone after the initial comparisons. Both systems had almost identical instrumentation.

The sensors at the ends of the BREB supporting arms were placed 1 m apart. To measure the dew point of air drawn in from 0.8 m and 1.8 m above ground, a single cooled dew point hygrometer (Dew-10, General Eastern, Wilmington, Massachusetts, USA) was employed with a solenoid valve to alternate the air flow between the two levels. For the first 40 s of each two-min interval, air was passed through a mixing bottle, one for each level. The dew point measurements, converted to water vapour pressure, were made every 1 s for the remaining 80-s period. The air temperature at 0.8 m and the air temperature difference between 0.8 and 1.8 m was measured using two unshielded type-E thermocouples each with a parallel combination of 75-µm diameter thermocouples. A frequent measurement period of either 1 or 10 s was employed in the case of all sensors except for the dew point hygrometer and fine-wire thermocouples. For the 80-s measurement period, the average air temperature and water vapour pressure were determined. These averages were in turn used to obtain the 20-min air temperature and water vapour pressure averages. The output storage data included the mean and standard deviation of all the above-mentioned micrometeorological variables for both levels.

An independent net radiometer and two soil heat flux plates (model Middleton CN2, Carter-Scott Design, Brunswick, Australia and model HFT-3, REBS, Seattle, Washington, USA respectively) and four soil temperature averaging thermocouples were used to calculate the remainder of the components of the energy balance. Two net radiometers (model Middleton CN1 and model REBS Q*6) and eight soil temperature sensors were used to measure the lysimeter *LE*, net irradiance, soil heat flux and soil temperature respectively. The net radiometers were placed 1.0 m above ground on a north-south axis with the net radiometer support on the south side to avoid shading of the ground surface by the supports. The soil heat flux plates were buried at a depth of 80 mm, on a north-south axis together with a liberal length of wire to reduce the influence of heat conduction along the surface-exposed wires to the sensor. Two sets of soil temperature sensors (type-E thermocouples mounted in tubes) buried at a depth of 20 and 60 mm and connected in parallel were used for obtaining the average soil temperature at four positions. All sensors were connected to a Campbell Scientific Inc. (Logan, Utah, USA) 21X datalogger. Gravimetric soil water content in the upper 80-mm layer was determined every 10 days. At the upslope site, data from an adjacent weighing lysimeter enabled *LE* to be measured directly for absolute verification of the calculated fluxes. The resolution of the lysimeter was 0.1 kg using a 1-m^3 undisturbed soil monolith.

For the Bellevue site, a similar BREB system was used except that the arms were 1.41 m apart. An eddy covariance system (EC) (SWS-211/3V, Applied Technologies, Boulder, Colorado, USA) and a surface-layer scintillometer (SLS) (model SLS40-A, Scintec Atmospärenmessetechnik, Tübingen, Germany) were used for independent measurements of *H* for the estimation of *K* which also required the BREB air temperature profile gradient (Eq. (8.16)). The EC system was maintained at a height of 1.5 m above the soil surface which was then increased to 2.12 m in summer. For the SLS, a beam distance of 101 m and beam height of 1.5 m was used. Further details of the EC and SLS measurements may be found in Savage (2009) and Odhiambo and Savage (2009). BREB data from Cathedral Peak between 1990 and 1994 and for 2004 for Bellevue were used in this study. A separate analysis was conducted using 2004 Bellevue data for the temperature-variance method of estimating *H* and calculating *K* to test the sensitivity of the frequency of measurements on the standard deviation

and mean of the 20-min air temperature values for sample measurement frequencies ranging between 1 and 10 Hz.

8.5 Results and discussion

8.5.1 Data rejection

The allowable range or ranges of each variable are tabled (Table 8.1). These ranges were used to exclude erroneous data. Results calculated from data within the range $-1.25 < \beta < -0.75$ should be carefully screened and those that are spurious should be rejected and if possible replaced. A further consideration at this stage is whether the resolution of the sensors has been exceeded. When the magnitude of the water vapour pressure difference is less than the 0.01-kPa dew point mirror system resolution, the data for that time are considered inconclusive and should be rejected. Similarly, if the profile air temperature difference is less than 0.006 K in magnitude, then these periods are not suitable for processing. These criteria were combined into a single method expressed by Eq. (8.9). The resolution thresholds for air temperature and water vapour pressure differences, incorporated into the method have particular relevance for dry periods when β is large, and even the smallest errors in either cause large error in *LE* (Angus and Watts, 1984). The method sets limits to the value that the profile air temperature difference can assume with respect to the value of the profile water vapour pressure difference and the measurement resolution of both sensors. The argument stems from the mathematical complication that occurs when the Bowen ratio tends to -1 with the available energy $-R_{net} - S = LE + H \to 0$. At these times, prevalently in the early morning and evening periods, evaporation is generally low (except under berg or foehne advective hot and dry conditions). Under these conditions physically inconsistent, and therefore extremely inaccurate and impossibly large positive and negative, fluxes are calculated. Simply disregarding Bowen ratio values between arbitrarily chosen values of -1.25 and -0.75 will to some extent remedy the problem. However, a more sensitive and dynamic approach is required to decrease the amount of data previously excluded unnecessarily, and prevent any rogue values escaping detection.

For this purpose an upper and lower limit to the value that the measured profile air temperature difference δT can hold, before β will be likely to be close to -1, is calculated as per the relationship of Eq. (8.9).

After initial implementation and success with the inequality as a rejection criterion (Eq. (8.9)), it was decided that data points not satisfying the inequality on the lower side had to be those when δT was large and negative. This set of circumstances is indicative of inversion conditions, which occur under either nocturnal condensation (dewfall) or periods of horizontal heat advection. The nocturnal *LE* gains (dew) are not included in daily total *LE* calculations, but advection can nearly double a windless day's water loss. Including *LE* gains for such times is of obvious importance. Fortunately, during the nocturnal inversions, the water vapour pressure gradient is very small, and the region of rejection small (Eq. (8.9)). However, during advective inversions, the magnitude of the water vapour pressure gradient is uncertain and therefore the air temperature difference values may not fall inside the rejection limits. Due to these uncertainties, we stipulated the upper limit of the Eq. (8.9) inequality as the rejection criterion:

$$\delta T < 2[E(T) + E(e)/\gamma] - \delta e/\gamma \tag{8.19}$$

(Fig. 8.1). Exclusions occur on almost every day (Fig. 8.1). Of note is that there are even large magnitudes for the δT limit on some days, as large as 0.3 ^{o}C (Fig. 8.1, day 201). For each BREB measurement level, the calculated saturation water vapour pressure e_s at the air temperature T_{air} recorded for that time period was used to reject measured water vapour pressures that were greater than saturation. Under dewfall or rainfall conditions, with the likelihood that the thermocouples are covered with water and possibly at the wet-bulb temperature, the measured water vapour pressure from the dew point mirror system can be greater than the saturation water vapour pressure corresponding to the temperature of the fine-wire thermocouple. If the fine-wire thermocouple is measuring the wet-bulb temperature T_w then the requirement that $T_w \leq T_{air}$, $e_s(T_w) \leq e_s(T_{air})$ allows for the easy automatic rejection of single level air temperatures and water vapour pressures. The absurd result that e can be greater than $e_s(T_{air})$ when the air is unsaturated at that time is referred to as the $e > e_s$ condition in Fig. 8.2. The times when the data need to be excluded, according to these criteria, are infrequent but it is necessary to apply the exclusion criteria (Fig. 8.2). The output data were tagged with a 1 if $e \leq e_s(T_{air})$ and 9999 (that is, out of range data) if $e > e_s(T_{air})$, and the $e > e_s(T_{air})$ water vapour pressures and air temperatures were then discarded from further analysis.

Early on in the evaporation measurement investigation, a loose hose to the dew point mirror of one of the systems caused water vapour pressures e to be greater than $e_s(T_{air})$ some of the time. The above procedures would have assisted in an earlier identification of the loose hose problem. On another occasion, the electronic bias of the dew point mirror of one system and much later on both systems was being set too infrequently, due to the remoteness of the site, with the result that water continually condensed on the mirror. The system therefore indicated a dew point too high with $e > e_s(T_{air})$. Again rejection procedures would have assisted in an earlier identification of the incorrect electronic bias setting.

Identifying tags were generated according to the class of rejection (Table 8.2). The identifying tags were used in order to be able to identify the cause of the problem. Data points not rejected were tagged "1". Water vapour pressures close to or above saturation were rejected and tagged "2" (the "WVP" criteria). If the upper and lower limit inequality (lower limit condition of Eq. (8.9)) was satisfied then there was a high possibility that the Bowen ratio will be very near -1 and therefore the calculated fluxes would not have numerical meaning (tagged "3"). Data fulfilling this inequality were therefore excluded from further processing. The majority of the data during clear days were not rejected, and all points rejected were done so justifiably when checked. The diurnal variation in δT and δe for a period of six days in summer are shown (Fig. 8.3) as well as the rejection periods. These variations demonstrate that data rejection occurred almost every day but with increasing frequency on cloudy or wet days or days with early morning mist. Tags 5 and 6 were used to identify problems with sensors at one level compared to those at the other.

The rejection method had the additional benefit of calculating condition-sensitive daily totals. In the case of missing data, the method thereby negates the requirement of calculating daylengths and adjusting evaporation calculations according to those daylengths. The procedure is sensitive to the times of day when reasonable fluxes occur, rejecting points other than the good data points. This allows an 18-hour day set of data to be used at all times, so avoiding having to decide when to start and stop data collection for each daylength.

Initially both the Upper Limit (UL) and Lower Limit (LL) values for δT (Eq. (8.9)) were used as rejection criteria. It was found that the periods when δT decreased below LL were those in the very early morning or late afternoon when $\beta \to -1$. These periods are often already rejected by the "WVP" criteria (case 2 in Table 8.2). A relatively small number of points not already rejected by the WVP criteria were rejected by the UL criterion. The reason for this is that at these times the net irradiance R_{net} is negative, with $S \approx -R_{net}$ (Eq. (8.1)), balanced by soil heat (flow towards the surface). Those that are not rejected by negative R_{net}, but occur during the early morning and late afternoon periods, are often rejected by the WVP criteria, since at these times, δe values approach the resolution limit of the sensor (and to a lesser extent, the measured water vapour pressures approach their saturation value).

The WVP criterion is made up of two components: the resolution limit check (Eq. (8.19)), and the check on each measured water vapour pressure with respect to its saturation value (Table 8.2). The additional points rejected by using only the upper limit rejection criterion (Eq. (8.19)) were found to be occasional large spurious δT values within the other rejection limits, as well as a few small values close to morning and evening times in which the classes of rejection have been separated out. These points, however, had already mostly been rejected by the WVP and negative R_{net} criteria. Comparisons of daily totals using both and then only the upper criterion, show that the disadvantage of rejecting the [good] low data values in the early morning or late afternoon periods are over-shadowed by the disadvantage of not rejecting the far fewer, but much larger, [bad] spurious values that also occurred, but that had escaped rejection by the other criteria (Table 8.3).

From Table 8.3, the benefits of applying these rejection criteria compared to not applying them are evidenced by the contribution that large spurious values make to the evaporation totals for each of the four days. Two days show "good" conditions (Day 4 and 16), and two are examples of "poor" conditions (Day 2 and 31), when net irradiance levels were low and/or variable. There was a small amount of precipitation on the mornings of Day 4 and 31. Fortuitously, the daily evaporation total based on $-1.25 < \beta < -0.75$ was reasonable but generally slightly over-estimated compared to estimates of LE obtained using Eqs. (8.9) or (8.19) but on some of the days the 20-min values were spuriously large negative and positive during early morning and/or late afternoon times.

Based on the above discussion, it was decided to flag all data periods when δT decreased below both the UL and the LL in the procedure used. Whether this is entirely justified under all conditions requires some clarification. For δT to decrease below the LL requires a large negative air temperature gradient (a strong inversion), as well as δe close to zero, or positive if δT is not large. This set of circumstances is indicative of inversion conditions, which occur under either nocturnal condensation (dewfall) or periods of positive horizontal heat advection. Dewfall renders both air intake levels saturated, thereby making water vapour pressure gradient determinations and flux calculations impossible using the BREB method. Wet thermocouples will measure the wet-bulb temperature, preventing the measurement of air temperature gradients. It follows that including periods of advection is of obvious importance. Under advective conditions, wind speeds are high enough to ensure a completely mixed or convective boundary layer. If the BREB sensors at the two levels are high enough above the surface to be out of any low-level inversion caused by advection, then this effect should not confound LE measurements by causing the data to be rejected. A local source of energy additional to the available energy (as defined by the assumption that excludes advection), will increase the flux densities flowing upwards from the surface. However, they will not

be perceived by sensors above the low-level inversion, and so introduce an error due to advection. Some way of obtaining measurements of the advective energy input must therefore be found to avoid this error.

8.5.2 Verification of BREB measurements

To verify the evaporative losses measured with the BREB systems, comparison against a more absolute method was necessary. The 20-min evaporative water losses measured from the adjacent weighing lysimeter, ignoring night-time condensing events, were used for this purpose (Fig. 8.4) and tracked reasonably well with the BREB *LE* values. BREB data during the early morning were rejected by the procedures discussed previously and *LE* replaced using the K method described later.

Since the overall time scale of much hydrological research is based on daily totals, further comparisons between BREB- and lysimeter-determined evaporation were based on daily totals (Table 8.4). Since lysimetric evaporation is often regarded as the standard for *LE* measurements, the reasonable agreement between the two verifies the accuracy and integrity of the BREB method.

Several days were chosen to show typical conditions — high radiation load in the morning, with commensurately high *LE* conditions, and periods of cloud in the afternoon when less than optimum conditions exist for BREB measurements.

The upper and lower air temperatures for the two BREB systems, and therefore δT, tracked well (data not shown). The upper and lower water vapour pressures may be in error if the hygrometer mirror becomes dirty and/or there is inadequate damping of the bias. Since the Bowen ratio is the product of the psychrometric constant γ and the ratio of the above profile differences, the agreement between two Bowen ratios measured was directly affected by the correlations of the two differences.

A weekly check between the two systems was made by comparing the many variables measured, especially the water vapour pressures and air temperatures and the respective differences. By its nature, water vapour pressure δe is extremely difficult to measure continuously and accurately. Thus almost weekly maintenance was required to keep the two systems measuring similar δT and δe values when the systems were at the same site. Eventually, from experience, the ability to accurately and consistently measure the differences was achieved. Having the two BREB systems next to each other allowed the development of any problems to be detected, while experience was being gained in the data collecting procedure. The BREB systems could then be moved apart and used individually with confidence. The results from the two individual systems at two different sites could then be compared.

The net radiometer for one BREB system (Middleton) always gave a slightly higher net irradiance than did the other (REBS). This was due ostensibly to a small constant calibration error in one or both of the instruments, if both net radiometers were exposed similarly. Using a paired *t* comparison, the daily total net radiant values for two collocated systems differed by about 5 %. The agreement between the overall soil heat flux of the two systems was fair (data not shown).

8.5.3 The back calculation method of obtaining K

It should be noted that an independent method of calculating (or preferably directly measuring) the exchange coefficient K is required to be able to simultaneously check the accuracy and precision of the method before it is applied. The method of calculation and the lack of a completely independent dataset preclude the drawing of definite and quantitative conclusions and the comparisons made all contain a degree of auto self-correlation. However, for the Cathedral Peak site, gradients used to calculate K were obtained from one BREB system and those to check the dependency of K from the other collocated system.

Confidence in the applicability of the assumption of similarity between exchange coefficients will be greater if the back calculated value of K, Eqs. (8.16) and (8.17), does not vary considerably from one measurement period to the next. That is, if the coefficient of variation is low, then the assumption of similarity is acceptable. But if the value of the calculated K varies considerably from one 20-min period to the next, then the likelihood that the two exchange coefficients are not similar is greater.

The exchange coefficient K during cloudless "normal" days was found to reach a fairly even and stable plateau, for both Cathedral and Bellevue sites, of around 0.2 to 0.3 $m^2\ s^{-1}$ for the period 10h00 to 16h00 (Fig. 8.5). At later times, the value decreased consistently slowly towards zero at sunset, temporarily becoming negative but remaining just above zero until the next sunrise. Large spurious spikes occurred at the expected times due to the available energy approaching zero in the early morning and evening. The results were consistent with the values reported by Motha et al. (1979) and Verma et al. (1978), although they reported a larger range of values, (0.1 to 0.7 $m^2\ s^{-1}$) and larger maximum values, probably since their studies were carried out under advective conditions. The values reported by Fuchs and Tanner (1970) were much lower than reported here, but their work was done over bare soil with the result that LE was much lower than H, indicating a lower midday common exchange coefficient of between 0.10 and 0.15 $m^2\ s^{-1}$, possibly due to the effect of lack of vegetative cover. Fritschen et al. (1985) found that the value of the eddy diffusivity increased with plant height, surface roughness and instability, and reported midday values of 0.08, 0.8 and 8 $m^2\ s^{-1}$ for alfalfa (0.5 to 0.8 m), saltcedar (2 to 6 m) and Douglas fir (30 m) respectively.

Night-time assessments of K were originally thought not possible due to the failure of the BREB method at these times (when the available energy approaches zero). From the measurements however, an extremely stable value of 0.01 to 0.02 $m^2\ s^{-1}$ was found after the rejection of data around sunrise and sunset time. Although the contribution that nocturnal evaporation makes is small, a continuous 24-hour calculation of fluxes seems possible with the proposed method, K is known and reasonably time-invariant and dew does not occur. Alternatively K could be estimated from Eq. (8.18) if σ_T measurements are available.

Analysis of the dependence of K on δT and δe showed that even though these were the "independent" variables used to calculate K (via the BREB-determined fluxes using Eqs. (8.16) and (8.17)), they alone were not responsible for the trends observed (data not shown). The ratio $\delta T / \delta e$ which constitutes the dynamic part of the Bowen ratio proved to account for much of the dependence. The dependence on wind speed (and therefore approximately on stability), was somewhat less. The net irradiance also had some effect on K, mainly by virtue of the fact that large fluxes are primarily caused

by large positive net irradiances. Less variability is encountered under high flux conditions with the result that the calculated value of K is more stable between measurement periods.

The mean and standard deviation of K over a typical period (Table 8.5) illustrates these points, and suggests that only "normal" cloudless days with large fluxes be used in the calculation of a representative K value for a site. The comparison of BREB-determined K values (Eqs. (8.16) and (8.17)) to results calculated with the average K value of 15 days (Table 8.6) and the independent temperature gradients were within 2 % over the period, even though the 20-min predictions were somewhat lagged. The LE comparisons were generally within 5 %.

The time-invariant value of K = 0.239 $m^2 s^{-1}$ was confirmed using independent measurements from the Bellevue site in a mesic grassland (Fig. 8.5, Table 8.5). These measurements were at a different time of year compared to the Cathedral Peak data shown. For the Bellevue estimates of K, H was measured using eddy covariance and surface-layer scintillometer systems and K calculated using Eqs. (8.16) and (8.17). The average K value obtained was 0.264 $m^2 s^{-1}$.

Comparisons between K estimated using Eq. (8.16) (back calculation method, x axis) and Eq. (8.18) (temperature-variance method for the upper-level air temperature measurements, y axis) for the Cathedral Peak site for day of year 181 to 189 (1990) were fair: slope = 0.775, intercept = 0.052 $m^2 s^{-1}$, coefficient of determination r^2 = 0.0456, root mean square error ($RMSE$) = 0.033 $m^2 s^{-1}$ for number of data pairs n = 171. The wind speed dependent method of estimating K (Wang and Bras, 1998; Wesson et al., 2001), by comparison with using Eqs. (8.16) or (8.18), overestimated K.

The influence of the frequency of air temperature measurement on the 20-min σ_T values, and hence on K estimated by temperature-variance (Eq. (8.18)), was investigated using data from the Bellevue site. Air temperature measurements using fine-wire thermocouples and a 3-D sonic anemometer, at frequencies of 1 and 10 Hz were used to calculate 20-min σ_T values. The normal frequency used for BREB air temperature measurements is 1 Hz. For almost all of 25 December 2004, when conditions ranged from convectively unstable to stable sporadic, σ_T (10 Hz, fine-wire) *vs.* σ_T (1 Hz, fine-wire) yielded a slope of 1.045 (r^2 = 0.923, RMSE = 0.060 °C) and σ_T (10 Hz 3-D sonic) *vs.* σ_T (1 Hz fine-wire) yielded a slope of 0.993 (r^2 = 0.894, $RMSE$ = 0.064 °C). Based on these reasonable comparisons, the 1-Hz BREB air temperature measurements, from which σ_T is calculated, were used to calculate K.

In the normal BREB formulation, all energy balance components other than H and LE must be measured, as well as gradients in both air temperature and water vapour pressure. But with the back calculation method once a K value has been found for a site, only net irradiance and soil heat flux, and either of the gradients are required for estimating both H and LE.

There is another important use for the K method for remote sites. Water entry into the hoses or dew point mirror problems invalidates the δe measurements. For such periods, the δT or σ_T, R_{net} and S measurements with a known or calculated value for K could be used to estimate LE with reasonable reliability.

Under certain conditions, equilibrium evaporation (Table 8.1), which can be shown theoretically to correspond to $\beta = \gamma / \Delta$ (□ 1 at 6 °C, 0.5 at 18 °C and 0.33 at 26 °C) was also used to patch evaporation data when both air temperature and water vapour pressure profile measurements were not available. In such cases, weather station data were used to confirm whether or not conditions were relatively calm and humid and the date and amount of the last rainfall event. For drier conditions, the Priestley-Taylor evaporation method was used, for which $\beta = -0.206 + 0.794\gamma / \Delta$ corresponding to $\beta = 0.588$ at 6 °C, $\beta = 0.191$ at 18 °C, and $\beta = 0.059$ at 26 °C.

8.6 Conclusions

The logistics of calculating sensible heat *H* and latent energy *LE* flux from measurements of net irradiance, soil heat flux and the measurement of time-averaged air temperature and water vapour pressure gradients are discussed. Criteria, underpinned by theory, are defined for the rejection of "bad" data corresponding to the Bowen ratio tending to -1 by logical limits imposed on the measured air temperature and water vapour pressure profile differences. When β approaches -1, conditions are pseudoadiabatic and isobaric. The major contributor to total error in *LE* is the error in the measurement of the water vapour pressure gradient. When evaporation rates are high, the relative accuracy in *LE* is good, even with a poorly measured Bowen ratio β. When β becomes large and *LE* less, the absolute error is smaller due simply to the smaller values, but the relative error increases.

The diurnal trend in the value of *K* over several months averaged 0.239 $m^2 s^{-1}$. More importantly, the lack of variability between measurement time intervals showed that the value of *K* is not changing markedly from one measurement period to another. This implies that the assumption of a time-invariant *K* is reasonable for when BREB data are invalid or lacking. Alternatively, *K* may be determined using the temperature-variance method based on the 20-min standard deviation in air temperature.

The requirements for long-term continuous monitoring of *H* and *LE* from one site may, by the proposed method, be significantly reduced. An initial period spanning at least a set of seasons should be used to find a representative value of *K* for further use at the site. The instrumental requirements would be decreased to a two-point air temperature gradient measurement and sensors to determine the available energy. One set of thermocouples for measurement of the air temperature profile gradient and standard deviation in air temperature, a net radiometer and soil heat flux plates, or some simpler estimate of available energy, are all that is required.

8.7 Acknowledgements

Funding from the Water Research Commission (South Africa) through projects K349 and K1335, University of KwaZulu-Natal, the National Research Foundation, and the CSIR which also provided technical support and infrastructure is gratefully acknowledged. The Department of Water Affairs and Forestry are also thanked for their initial funding of the project. The technical support of G. Molefe and K. Hudson, and the two Water Research Commission Steering Committees, was invaluable.

8.8 References

Albertson, J.D., Parlange, M.B., Katul, G.G., Chu, C.-R., Stricker, H., Tyler, S., 1995. Sensible heat flux from arid regions: A simple flux-variance method, Water Resour. Res. 31, 969–973.

Angus, D.E., Watts, P.J., 1984. Evapotranspiration - how good is the Bowen ratio method? Agric. Water Mgt. 8, 133–150.

Bowen, I.S., 1926. The ratio of heat losses by conduction and by evaporation from any water surface. Phys. Rev. 27, 779–787.

Bremer, D.J., Ham, J.M., 1999. Effect of spring burning on the surface energy balance in a tallgrass prairie. Agric. For. Meteorol. 97, 43–54.

Brotzge, J.A., Crawford, K.C., 2003. Examination of the surface energy budget: A comparison of eddy correlation and Bowen ratio measurement systems. J. Hydrometeorol. 4, 160–178.

Burba, G.G., Verma, S.B., Kim, J., 1999. Energy fluxes of an open water area in a mid-latitude prairie wetland. Boundary-Layer Meteorol. 91, 495–504.

Byers, H.R., 1974. General Meteorology, 4th ed., pp. 74–77. McGraw-Hill Book Company, New York.

Cellier, P., Olioso, A., 1993. A simple system for automated long-term Bowen ratio measurement. Agric. For. Meteorol. 66, 81–92.

Daamen, C.C., Dugas, W.A., Prendergast, P.T., Judd M.J., McNaughton, K.G., 1999. Energy flux measurements in a sheltered lemon orchard. Agric. For. Meteorol. 93, 171–183.

Dawson, T.E., 1996. Determining water use by trees and forests from isotopic, energy balance and transpiration analyses: the roles of tree size and hydraulic lift. Tree Physiol. 16, 263–272.

De Bruin, H.A.R., Hartogensis, O.K., 2005. Variance method to determine turbulent fluxes of momentum and sensible heat in the stable atmospheric surface layer. Boundary-Layer Meteorol. 116, 385–392.

Dyer, A.J., 1967. The turbulent transport of heat and water vapour. Quart. J. R. Meteorol. Soc. 93, 501–509.

Everson, C.S., 2001. The water balance of a first order catchment in the montane grasslands of South Africa. J. Hydrol. 241, 110–123.

Foken, T., 2008. The energy balance closure problem: an overview. Ecol. Appl. 18, 1351–1367.

Frank, A.B., 2003. Evapotranspiration from northern semiarid grasslands. Agron. J. 95, 1504–1509.

Fritschen, L.J., 1965. Accuracy of evapotranspiration rate of field crops determined by the Bowen ratio method. Bull. Internat. Assoc. Sci. Hydrol. 10, 38–48.

Fritschen, L.J., Gay, L.W., Simpson, R., 1985. Eddy diffusivity and instrument in relation to plant height. In: Hutchinson, B.A., Hichs, B.B. (Eds.), The Forest-Atmosphere Interaction. pp. 583–590, D Riedel Publishing Company, Dordrecht, Holland.

Fuchs, M., Tanner, C.B., 1970. Error analysis of Bowen ratio measured by differential psychrometry. Agric. Meteorol. 7, 329–334.

Garratt, J.R., 1984. The measurement of evaporation by meteorological methods. In Sharma, M.L. (Ed.) Evapotransipration from Plant Communities. Elsevier, Amsterdam.

Guo, X., Zhang, H., Cai, X., Kang, L., Zhu, T., Leclerc, M.Y., 2009. Flux-variance method for latent heat and carbon dioxide fluxes in unstable conditions. Boundary-Layer Meteorol. 131, 363–384.

Heilman, J.L., McInnes, K.J., Savage, M.J., Gesch, R.W., Lascano, R.J., 1994. Soil and canopy energy balances in a west Texas vineyard. Agric. For. Meteorol. 71, 99–114.

Henrici, M., 1943. Transpiration of grasses in the sour mountain grassveld of the Drakensberg in comparison with the water loss of indigenous forests. S. Afr. J. Sci. 39, 155–163.

Kara, G., Kumarb, A., 2007. Surface energy fluxes and crop water stress index in groundnut under irrigated ecosystem. Agric. For. Meteorol. 146, 94–106.

Lourens, F.J., Pruitt, W.O., 1971. Energy balance and water use of rice grown in the Central Valley of California. Agron. J. 63, 827–832.

Motha, R.P., Verma, S.B., Rosenberg, N.J., 1979. Exchange coefficients under sensible heat advection determined by eddy correlation. Agric. Meteorol. 20, 273–280.

Nie, D., Flitcroft, I.E., Kanemasu, E.T., 1992. Performance of Bowen ratio systems on a slope. Agric. For. Meteorol. 59, 165–181.

Odhiambo, G.O., Savage, M.J., 2009. Sensible heat flux by surface layer scintillometry and eddy covariance over a mixed grassland community as affected by Bowen ratio and MOST formulations for unstable conditions. J. Hydrometeorol. 10, 479–492.

Ohmura, A., 1982. Objective criteria for rejecting data for Bowen ratio flux calculations. J. Appl. Meteorol. 21, 595–598.

Ortega-Farias, S.O., Cuenca, R.H., Ek, M., 1996. Daytime variation of sensible heat flux estimated by the bulk aerodynamic method over a grass canopy. Agric. For. Meteorol. 81, 131–143.

Payero, J.O., Neale, C.M.U., Wright, J.L., Allen R.G., 2003. Guidelines for validating Bowen ratio data. Trans. ASAE 46, 1051–1060.

Peacock, C.E., Hess, T.M., 2004. Estimating evapotranspiration from a reed bed using the Bowen ratio energy balance method. Hydrol. Process. 18, 247–260.

Perez, P.J., Castellví, F., Ibañez, M., Rosell, J.I., 1999. Assessment of reliability of Bowen ratio method for partitioning fluxes. Agric. For. Meteorol. 97, 141–150.

Perez, P.J., Castellví, F., Martínez-Cob, A., 2008. A simple model for estimating the Bowen ratio from climatic factors for determining latent and sensible heat flux. Agric. For. Meteorol. 10, 25–37.

Perrier, E.R., Robertson, J.M., Millington, R.J., Peters, D.B., 1971. Spatial and temporal variation of wind above and within a soybean canopy. Agric. Meteorol. 10, 421–442.

Pypker, T.G., Fredeen, A.L., 2002. The growing season carbon balance of a subboreal clearcut 5 years after harvesting using two independent approaches to measure ecosystem CO_2 flux. Can. J. For. Res. 32, 852–862.

Rider, N.E., 1954. Eddy diffusion of momentum, water vapour, and heat near the ground. Phil. Trans., Royal Soc. Series A. 246, 481–501.

Rider, N.E., Robinson, G.D., 1951. A study of the transfer of heat and water vapour above a surface of short grass. Quart. J. Roy. Meteorol. Soc. 77, 375–401.

Rohli, R.V., Hsu, S.A., Lofgren, B.M., Binkley, M.R., 2004. Bowen ratio estimates over Lake Erie. J. Great Lakes Res. 30, 241–251.

Savage, M.J., 2009. Estimation of evaporation using a dual-beam surface layer scintillometer and component energy balance measurements. Agric. For. Meteorol. 149, 501–517.

Savage, M.J., Everson, C.S., Metelerkamp, B.R., 1997. Evaporation measurement above vegetated surfaces using micrometeorological techniques. Water Research Commission Report No. 349/1/97, p248, Pretoria, South Africa, ISBN 1-86845-363-4.

Savage, M.J., Everson, C.S., Metelerkamp, B.R., 2009. Bowen ratio evaporation measurement in emote montane grassland: Data integrity and fluxes. J. Hydrol. 376, 249-260.

Savage, M.J., Everson, C.S., Odhiambo, G.O., Mengistu M.G., Jarmain, C., 2004. Theory and practice of evaporation measurement, with special focus on surface layer scintillometry as an operational tool for the estimation of spatially averaged evaporation. Water Research Commission Report No. 1335/1/04, p204, Pretoria, South Africa, ISBN 1-77005-247-X.

Savage, M.J., Heilman, J.L., 2009. Infrared calibration of net radiometers and infra red thermometers. Agric. For. Meteorol. 149, 1279–1293.

Schmid, H.P., 1997. Experimental design for flux measurements: matching scales of observations and fluxes. Agric. For. Meteorol. 87, 179–200.

Schulze, R.E., 1975. Catchment evaporation in the Natal Drakensberg. Unpublished M.Sc. thesis. University of Natal, Pietermaritzburg.

Sellers, W.D., 1965. Physical Climatology. Univ. of Chicago Press, Chicago. pp. 272.

Sommer, R., Fölster, H., Vielhauer, K., Carvalho, E.J.M., Vlek, P.L.G., 2003. Deep soil water dynamics and depletion by secondary vegetation in the Eastern Amazon. Soil Sci. Soc. Amer. J. 67, 1672–1686.

Suomi, V.E., Tanner, C.B., 1958. Evapotranspiration from heat-budget measurements over a field crop. Trans. Am. Geophys. Union 39, 298–304.

Sverdrup, H.U., 1943. On the ratio between heat conduction from the sea surface and the heat used for evaporation. Ann. N. Y. Acad. Sci. 68, 81–88.

Swinbank, W.C., Dyer, A.J., 1967. An experimental study in micrometeorology. Quart. J. Roy. Meteorol. Soc. 93, 494–500.

Tanner, B.D., Greene, J.P., Bingham, G.E., 1987. A Bowen-ratio design for long term measurements. ASAE Paper No. 87–2503, Am. Soc. Agric. Eng., St. Joseph, MI, 1–6.

Tanner, C.B., 1961. A simple aero-heat budget method for determining daily evapotranspiration. Trans. Int. Congress Soil Science 1, 203–209.

Tanner, C.B., 1963. Basic instrumentation and measurements for plant environmental and micrometeorology. Soil Bulletin 6, 1–32.

Tanner, C.B., Fuchs, M., 1969. Error analysis of Bowen ratio measured by differential psychrometry. Agric. Meteorol. 7, 329–334.

Tillman, J.E., 1972. The indirect determination of stability, heat and momentum fluxes in the atmospheric boundary layer from simple scalar variable during dry unstable conditions. J. Appl. Meteorol. 11, 783–792.

Todd, R.W., Evett, S.R., Howell, T.A., 2000. The Bowen ratio-energy balance method for estimating latent heat flux of irrigated alfalfa evaluated in a semi-arid, advective environment. Agric. For. Meteorol. 103, 335–348.

Verma, S.B., Rosenberg, N.J., Blad, B.L., 1978. Turbulent exchange coefficients for sensible heat and water vapour under advective conditions. J. Appl. Meteorol. 17, 330–338.

Walker, J.T., Robarge, W.P., Wu, Y., Meyers, T.P., 2006. Measurement of bi-directional ammonia fluxes over soybean using the modified Bowen-ratio technique. Agric. For. Meteorol. 138, 54–68.

Wang J., Bras R.L., 1998. A new method for estimation of sensible heat flux from air temperature. Water Resour. Res. 34, 2281–2288.

Weaver, H.L., 1990. Temperature and humidity flux-variance relations determined by one-dimensional eddy correlation. Boundary Layer Meteorol. 53, 77–91.

Webb, E.K., 1960. On estimating evaporation with fluctuating Bowen ratio. J. Geophys. Res. 65, 3415–3417.

Wesson, K.H., Katul, G., Lai, C.-T., 2001. Sensible heat flux estimation by flux variance and half-order time derivative methods. Water Resour. Res. 37, 2333–2343.

Wolf, A., Saliendra, N., Akshalov, K., Johnson, D.A., Laca, E., 2008. Effects of different eddy covariance correction schemes on energy balance closure and comparisons with the modified Bowen ratio system. Agric. For. Meteorol. 148, 942–952.

Xing, Z., Chow, L., Meng, F.-R., Rees, H.W., Stevens, L., Monteith, J., 2008. Validating evapotranspiration equations using Bowen ratio in New Brunswick, Maritime, Canada. Sensors 8, 412–428.

Zhang, B., Kang, S., Li, F., Zhang, L., 2008. Comparison of three evapotranspiration models to Bowen ratio-energy balance method for a vineyard in an arid desert region of northwest China. Agric. For. Meteorol. 148, 1629–1640.

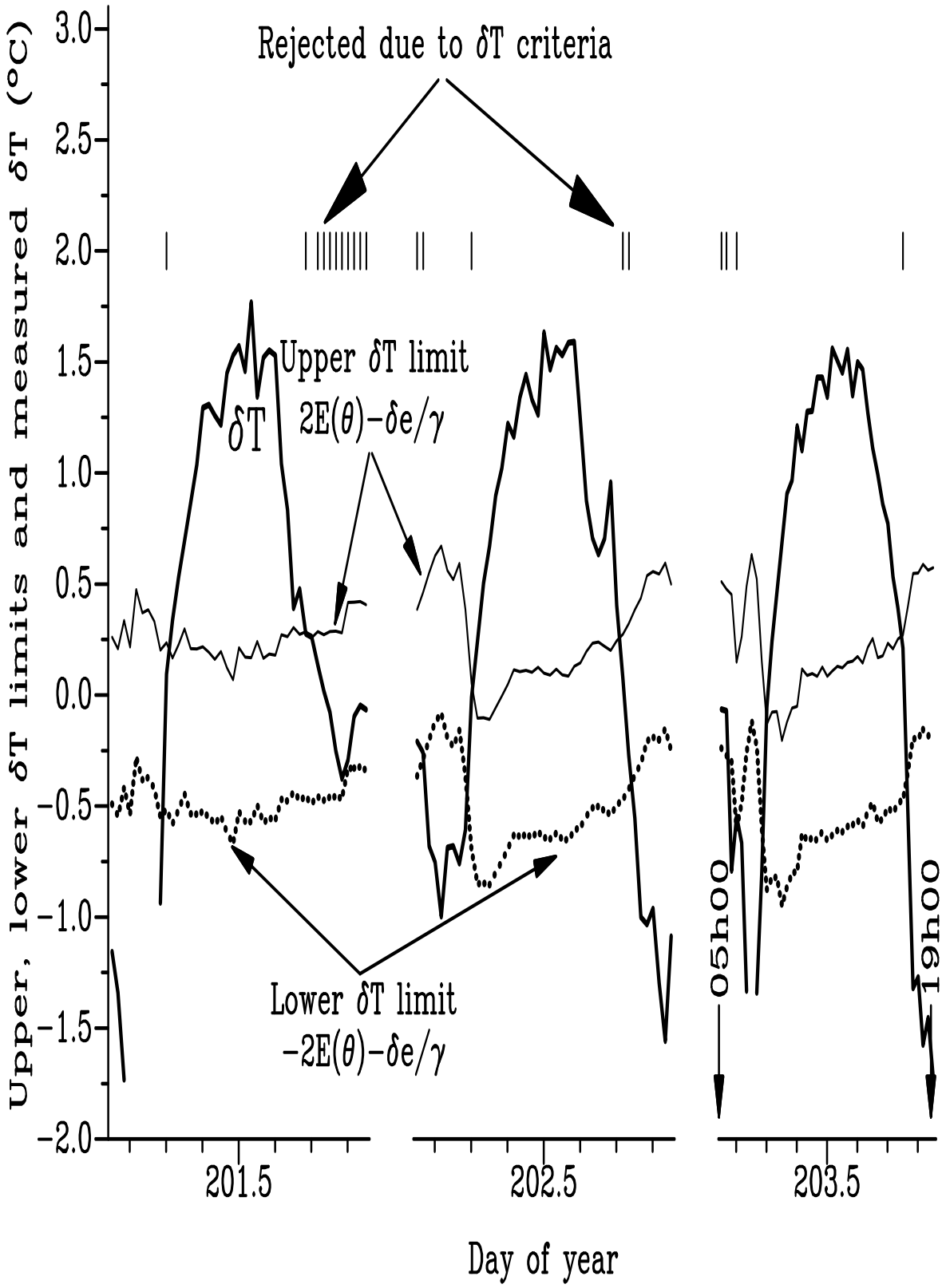
Rejected due to δT criteria
Upper δT limit
2E(θ)−δe/γ
δT
Lower δT limit
−2E(θ)−δe/γ
05h00
19h00
Upper, lower δT limits and measured δT (°C)
3.0
2.5
2.0
1.5
1.0
0.5
0.0
−0.5
−1.0
−1.5
−2.0
201.5
202.5
203.5
Day of year

Fig. 8.1. The 20-min variation in the measured profile air temperature difference δT (K) as a function of day (201 to 203, 1990) for Cathedral Peak Catchment for the times 05h00 to 19h00 (each small tick interval is 120 min). The vertical line ticks corresponding to δT = 2.0 K indicates rejection tags for the condition expressed in Eq. (8.9) (viz., that the Bowen ratio β is around -1, usually at early morning and late afternoon times). The upper limit curve is defined by $\delta T = 2E(\theta) - \delta e / \gamma$ and the lower by $\delta T = -2E(\theta) - \delta e / \gamma$. Rejection of air temperature and water vapour pressure data occurs if δT is within the lower and upper limit.

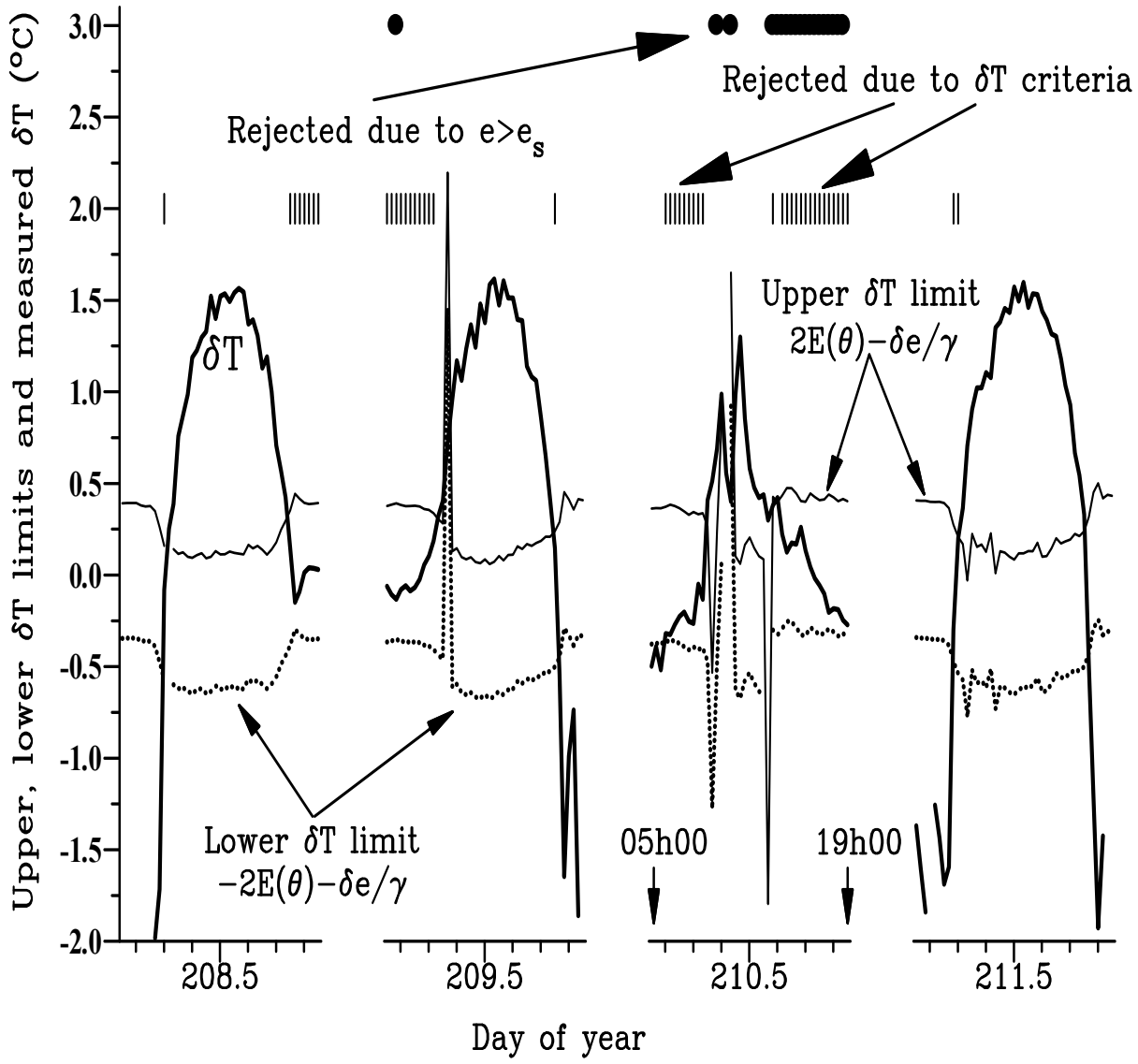

Fig. 8.2. The 20-min variation in the measured profile air temperature difference δT (K) as a function of day (208 to 211, 1990) for Cathedral Peak for the times 05h00 to 19h00 (each small tick interval is 120 min). The bullets corresponding to δT = 3.0 K indicates rejection tags for the absurd condition $e>e_s$ (usually corresponding to dewfall or rainfall wetting the fine-wire thermocouples completely). Note the large number of tags for this condition, due to a rainfall event on day 210.

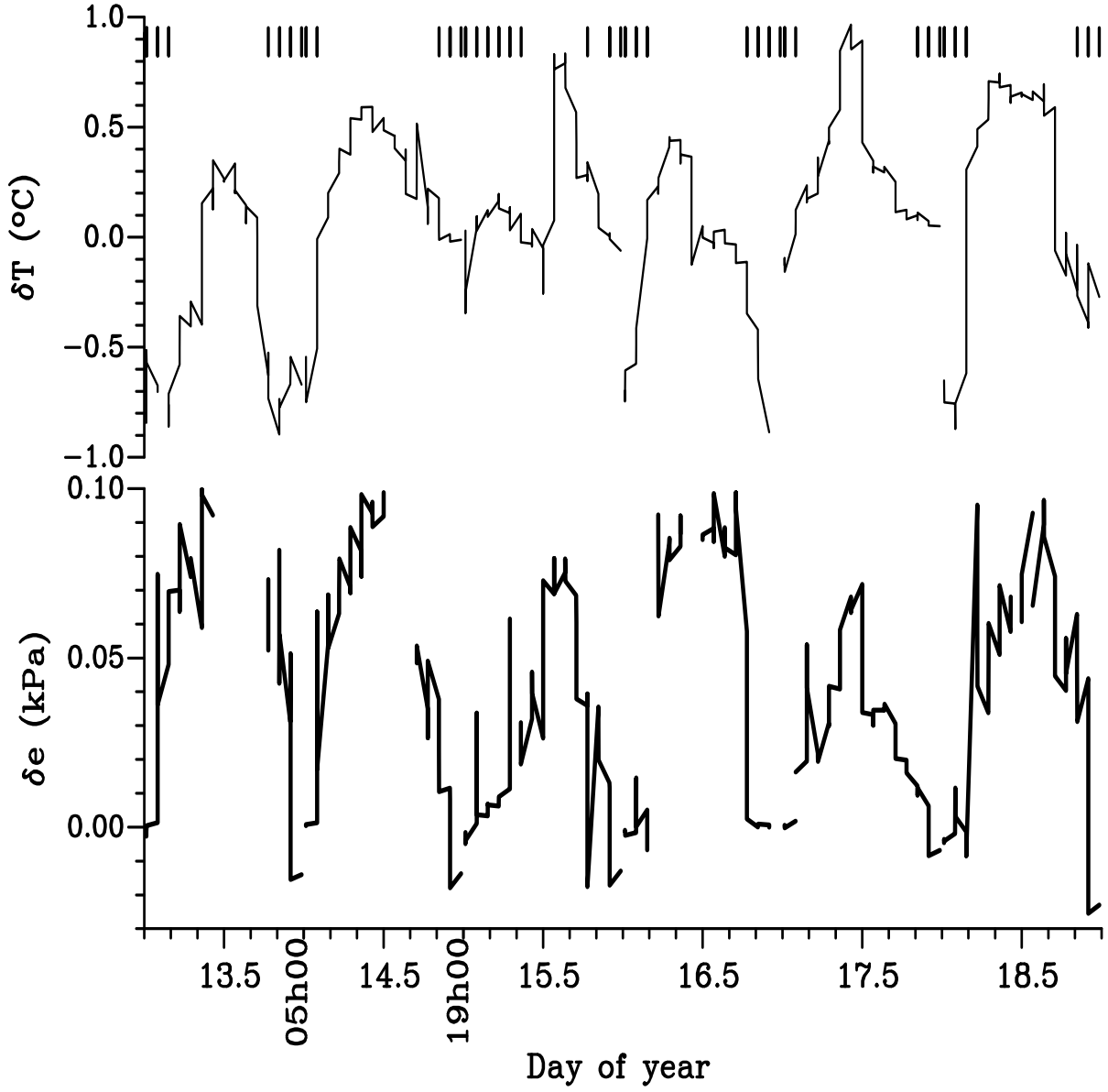

Fig. 8.3. Typical trends in the measured profile differences in air temperature (δT) and water vapour pressure (δe) between the two BREB measurement heights (Cathedral Peak, 1992). The periods for which data were rejected according to Eq. (8.9) are shown at the top of the graph by the vertical bars.

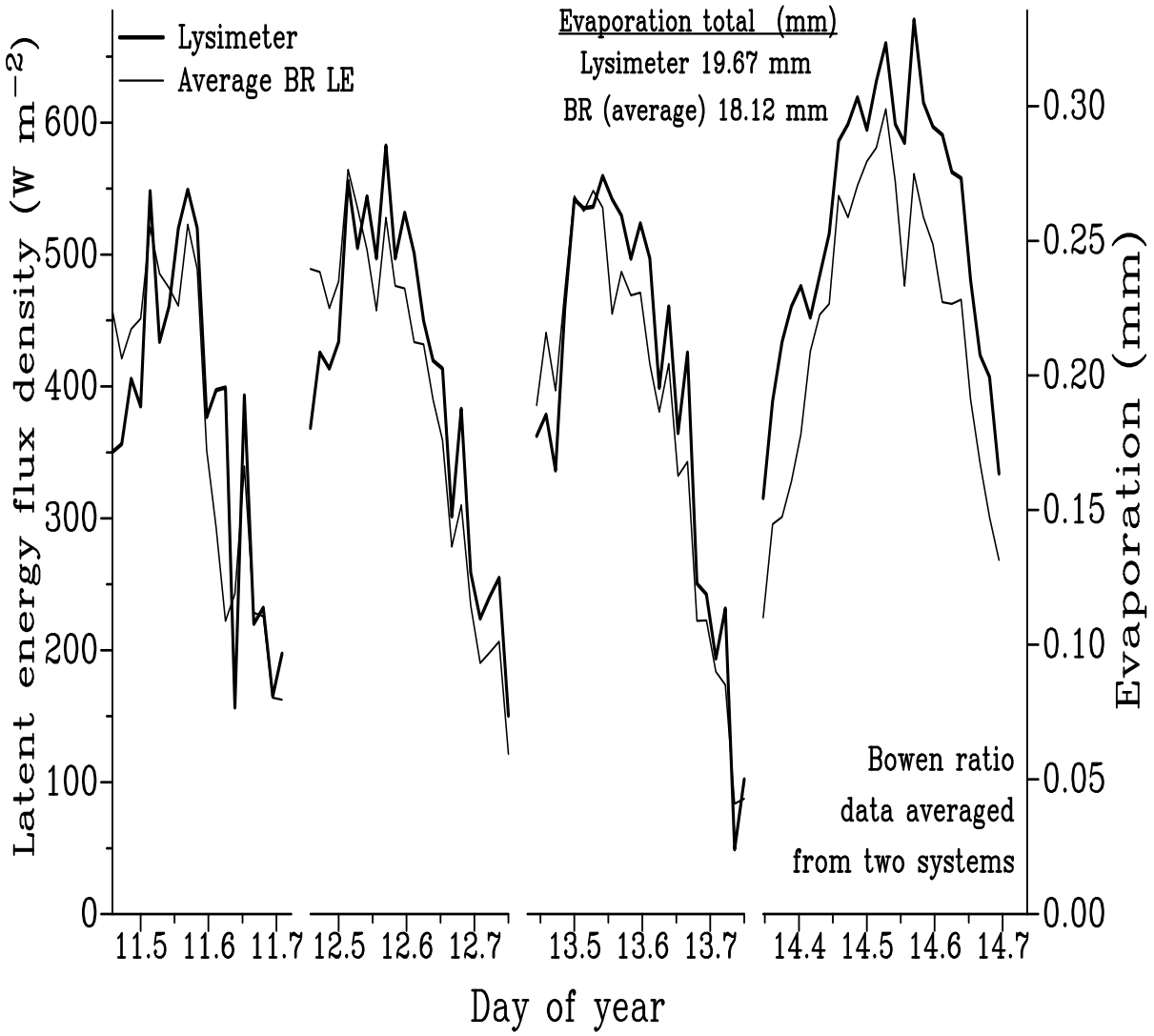

Fig. 8.4. Comparison of 20-min lysimeter and BREB evaporation for the upslope site. The BREB evaporation from the two systems was averaged. There was very good agreement between lysimeter and BREB (average) evaporation total for this four-day period (Cathedral Peak, 1991).

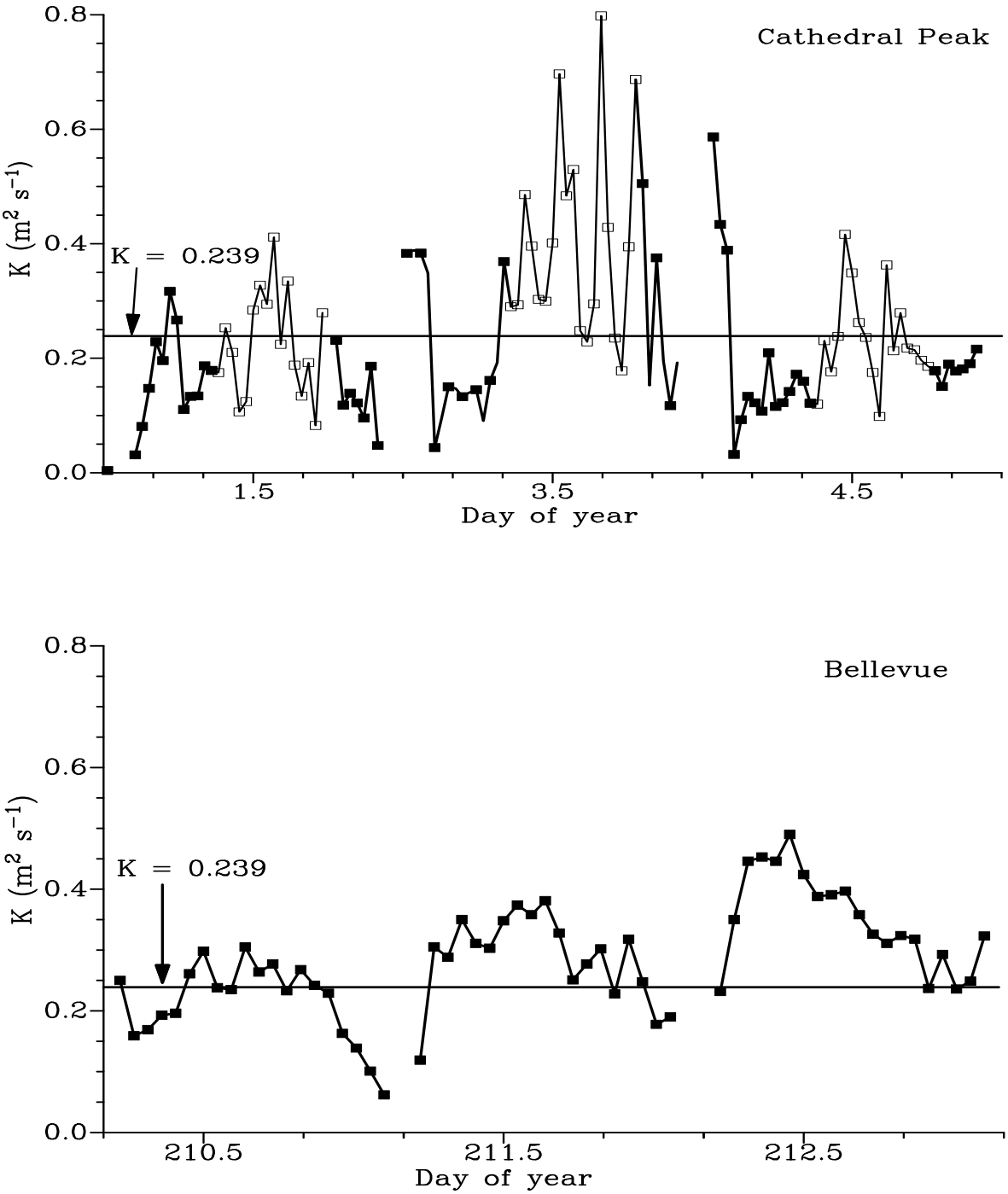

Fig. 8.5. Top: Diurnal trend of *K* on three typical days (1992) for Cathedral Peak. The "long" day (06h00 to 18h00 thin horizontal line) and "short" day (10h00 to 16h00 thick horizontal line) means are similar at this time of year. The overall mean for several month's data *K* = 0.239 m^2 s^{-1} is presented. The trend was consistent throughout the year, both in shape and value, and comparable with similar trends found by Motha et al. (1979); bottom: Bellevue site (2004).

Table 8.1. The ranges of the various parameters used to define limits, just greater than the probable, allowable and expected values.

Variable name	Allowable range	Units
D	1 to 366	
TOD	0500 to 1900	100 h + min
T_{lower} [lower air temperature]	-5 to 45	^{o}C
$T_{lower} - T_{upper}$ [air temperature profile difference]	-2.5 to 2.5	^{o}C
Standard deviation of T_{lower}, T_{upper}	0 to 2.5	^{o}C
Difference between standard deviation of T_{lower}, T_{upper}	0 to 0.5	^{o}C
e_{lower}, e_{upper} [lower/upper water vapour pressure]	0.01 to 5	kPa
$e_{lower} - e_{upper}$ [water vapour pressure profile difference]	-0.4 to 0.4	kPa
Standard deviation of e_{lower}, e_{upper}	0 to 0.1	kPa
Difference between standard deviation of e_{lower}, e_{upper}	-0.1 to 0.1	kPa
R_{net} [net irradiance]	-200 to 1000	W m^{-2}
SHF1 and 2 [plate-measured soil heat flux]	-100 to 100	W m^{-2}
G [stored soil heat flux]	-200 to 200	W m^{-2}
dT_{soil} [change in soil temperature over 20 min]	-3 to 3	^{o}C
θ [gravimetric soil water content]	0.1 to 0.99	kg kg^{-1}
I_s^* [solar irradiance]	0 to 1400	W m^{-2}
Wind speed	0 to 20	m s^{-1}
Wind direction	0 to 360	
K_h, K_w**	0 to 3	m^2 s^{-1}
β	-10 to 10	
LE	-800 to 300	W m^{-2}

Variable name	Allowable range	Units
H	-800 to 300	W m^{-2}
Equilibrium and Priestley-Taylor latent energy flux	-800 to 300	W m^{-2}

*A maximum of 1400 W m^{-2} for solar irradiance is to allow for such values when partly cloudy conditions result in direct and significant scattered irradiance.

**The exchange coefficients cannot be negative unless counter gradient flux densities occur.

Table 8.2. Summary of rejection or data replacement conditions and associated rejection tag identifiers.

Condition	Tag
No rejection	1
e_{lower} or $e_{upper} > (e_s + 0.01)$ or $\lvert e_{lower} - e_{upper} \rvert < 0.01$ kPa (i.e. $\lvert T_{dp\,lower} - T_{dp\,upper} \rvert < 0.003$ °C)†	2
Lower Limit < δT < Upper Limit	3
Both of the above (2 and 3)	4
Large standard deviation in T_{lower}, T_{upper} at one level compared to the other level	5
Large standard deviation in e_{lower}, e_{upper} at one level compared to the other level	6

† $T_{dp\,lower}$ and $T_{dp\,upper}$ are the dew point measurements at the lower and upper measurement levels respectively

Table 8.3. Comparison of daily total evaporation (mm) calculated with differing sets of rejection criteria for Day 2, 4, 16 and 31, 1992 (Cathedral Peak).

Rejection criterion type	Day 2	Day 4	Day 16	Day 31
No rejection criteria[1]	-3.37	2.63	10.80	3.20
Range limits only[2]	2.16	2.65	6.74	2.07
"WVP" limits[3]	1.65	2.24	6.63	1.60
LL < δT < UL[3,4]	0.41	2.14	6.23	0.70
δT < UL[3,4,5]	0.41	2.14	6.23	0.70
$-1.25 < \beta < -0.756$	0.676	2.36	6.50	0.80

Notes:

1 Other than missing data caused by division by zero when $\beta \to -1$.

2 The [from and to] range limits as listed in Table 8.1.

3 As well as the range limits which apply over and above this.

4 With the use of this criterion, a significant reduction in daily total evaporation occurred on Day 2 and 31 as a result of the large spurious negative and positive daytime evaporation values not rejected by the above criteria.

5 No change in the evaporation total was observed when only the UL was used because the few additional points rejected were very low values.

6 On some days, for example Days 2 and 31, there were large daytime spurious 20-min evaporation values, negative and positive, that were not rejected.

Table 8.4. Comparison of daily BREB (averaged from the two systems) and lysimeter *LE* totals (Cathedral Peak, 1991).

Day	Daily total evaporation				% difference
	(MJ m^{-2})		(mm)		
	Lysimeter	BREB	Lysimeter	BREB	
11	8.72	8.49	3.57	3.48	-2.52
12	10.74	10.33	4.40	4.23	-3.86
13	11.22	10.78	4.59	4.42	-3.70
14	17.38	14.63	7.11	5.99	-15.75

Table 8.5. Mean, standard deviation and percentage coefficient of variation (CV) of *K* over a typical 15-day period (Cathedral Peak, CVI) and for ten days for the Bellevue site.

Day (1991), Cathedral Peak	Average K (m^2 s^{-1})	$\sigma(K)$ (m^2 s^{-1})	CV (%)
121	0.231	0.045	19.5
122	0.242	0.058	23.8
123	0.248	0.062	24.9
124	0.239	0.070	29.0
125	0.219	0.059	26.7
126	0.220	0.047	21.4
127	0.225	0.055	24.6
128	0.203	0.048	23.8
129	0.210	0.075	35.8
130	0.349	0.088	25.3
132	0.270	0.055	20.4
133	0.267	0.056	21.0
134	0.219	0.084	38.5
135	0.239	0.149	85.9

Day (2004), Bellevue	Average K (m^2 s^{-1})	$\sigma(K)$ (m^2 s^{-1})	CV (%)
211	0.214	0.065	30.3
212	0.287	0.070	24.5
213	0.350	0.079	22.5
214	0.292	0.095	32.6
215	0.340	0.069	20.4
216	0.252	0.075	29.9
217	0.271	0.073	26.9
218	0.236	0.073	30.7
219	0.229	0.075	32.5
220	0.165	0.046	27.8

Table 8.6. Comparison of *LE* and *H* calculated with the conventional BREB method and that using the back calculated *K* (using independent δT and δe values respectively and *K* = 0.239 m^2 s^{-1}) (Cathedral Peak, 1991).

Day	*H* (MJ m^{-2})			*LE* (MJ m^{-2})		
	BREB	*K* and δT	Difference	BREB	*K* and δe	Difference
121	5.21	5.17	0.04	5.17	4.45	0.72
122	4.73	3.40	1.33	4.28	4.53	-0.25
123	3.49	4.16	-0.67	5.93	4.20	1.73
124	5.34	5.38	-0.04	4.10	1.18	2.92
125	4.65	4.43	0.22	4.93	0.25	4.68
126	4.36	4.96	-0.60	5.22	0.67	4.55
127	4.12	3.82	0.30	5.22	0.35	4.87
128	4.29	4.91	-0.62	4.85	0.31	4.54
129	3.61	3.66	-0.05	3.84	-0.34	4.18
130	1.33	0.57	0.76	0.40	-0.40	0.80
131	-2.72	4.36	-7.08	2.49	-0.55	3.04
132	2.32	0.89	1.43	1.51	-1.78	3.29
133	5.64	4.69	0.95	4.48	0.12	4.36
134				4.33	0.56	3.77
135	2.27	2.55	-0.28	6.12	0.68	5.44

9 PLACEMENT HEIGHT[1] AND "FOOTPRINTS"[2] OF EDDY COVARIANCE SENSORS ABOVE A SHORT TURF GRASS SURFACE

9.1 Abstract

Variation in measured *H* with sensor height above short turf grass during mainly unstable conditions was investigated using the eddy correlation (EC) technique. Our data showed that EC-measured sensible *H* at 0.25 and 0.38 m above the turf grass were 15 and 10 % lower, respectively, than that at the 1.00-m height. There was no statistical difference in the EC-measured *H* at 0.50, 1.00 and 1.25 m. These placement heights corresponded to fetch-to-height ratios from 520:1 to 95:1. Calculations based on fetch showed that the lowest four heights were within the equilibrium layer whereas the heights at or greater than 1.25 m were above the equilibrium layer. The greater *H* measurements above the 1.25-m height, compared to the lower heights, were probably from advected *H* from nearby tar roads and buildings. Measurements of atmospheric stability were obtained by calculating the ratio of height *z* above surface to the Obukhov length. Most measurements were obtained under unstable conditions when mixed convection prevailed. Our measurements show that it is possible for EC sensors to be placed as low as 0.50 m above the surface, during unstable periods, without significant difference from the *H* measurements at a height of 1.00 m. Data were obtained with a pan filled with soil placed 0.27 m below the fine wire thermocouple of an EC system placed 1.00 m above surface. These data demonstrated that the reduction in the sensible heat was not due to acoustic reflections from that surface. Possibly, the reduction was due to small-sized eddies near the surface being contained between the sonic separation distance. An analysis of "footprints" shows that, at least 90 % of the measured *H* at a height of 0.5 m was from our experimental site, decreasing to less than 70 % at the 1.5-m height. Calculations showed that the fetch requirement for micrometeorological measurements above a forest canopy was more stringent than for grassland canopy. Sensor placement at the 0.5-m height would result in little reduction, as did occur at heights less than 0.50 m, in the covariance between vertical wind speed fluctuation and air temperature fluctuation due to small-sized eddies being contained between the separation distance of the sonic anemometer transducers. We speculate that measurements closer than 0.5 m to the surface differed from those at 1.00 m due to small-sized eddies near the surface being contained between the sonic separation distance and therefore not completely detected by the sonic anemometer. A power spectrum analysis for 10-Hz vertical wind speed for decreasing measurement heights demonstrate a drop-off of measurements from the -5/3 Kolmogorov law for the inertial sub-range for the lower frequencies. The drop-off was not noticeable for sonic temperature.

9.2 Introduction

For certain chemically active substances, scalar flux measurements should be made as close to the surface as possible (Fitzjarrald and Lenschow, 1983; Kristensen and Fitzjarrald, 1984). Not much attention has been devoted to how close to vegetated surfaces eddy correlation (EC) sensors (Swinbank, 1951) may be placed without the measured scalar flux being significantly different from that further from the surface, but still within the equilibrium boundary layer. In the present study, we only consider the flux of sensible heat flux (*H*) at various heights above the canopy surface.

---

[1] Based on Savage at al. (1995, 1997)

[2] Based on Savage et al. (1996, 1997)

Fetch considerations aside (Heilman et al., 1989), EC sonic anemometer measurements of vertical wind speed fluctuation should ideally be at a height that allows even small-sized eddies between the anemometer transducer to be sensed. If sensor height is too close to the plant canopy surface, small- sized eddies between the anemometer transducer to be sensed. If sensor height is too close to the plant canopy surface, small-sized eddies may not be sensed and possible sonic reflections from vegetation may affect measurements. Presumably, small-sized eddies between the separation distance of the sonic anemometer will result in spectral attenuation of the eddy structures and an underestimation in *H*. On the other hand, any sonic reflections from the vegetation would be detected by the sensor but not discriminated from the nonreflected fluctuations by the sensor and would, in all likelihood, increase the measured *H*.

Kaimal (1975) showed theoretically that the minimum operating height of the sonic anemometer above plant canopy in an unstable surface layer is 6 π multiplied by the spatial resolution of the sonic anemometer to avoid spectral attenuation from spatial averaging between the anemometer transducers. These recommendations have been used by some workers (for e.g., Kizer and Elliott, 1991). Kaimal (1991, pers. comm.) however suggested that measurements, under unstable conditions, at a height of 1 m above plant canopy should be sufficiently valid without making any corrections for spectral attenuation from spatial averaging. There appears to have been some hesitation by researchers in placing their EC systems at heights approaching 1 m or closer above canopy.

Our goal was to compare EC sensible heat measured at various placement heights above short turf grass and determine the fraction of these measurements, at each height, emanating from within the adjacent upwind area.

Fast response sensors (Swinbank, 1951; Campbell and Unsworth, 1979) allow eddy correlation (EC) determination of sensible heat flux *H*, independent of the other terms of the surface energy balance, from the covariance of vertical wind speed fluctuation w' and the air temperature fluctuation T':

$$H = \rho c_p \overline{w'T'} \tag{9.1}$$

where ρ is the density of air (taken to be 1.17 kg m^{-3}, appropriate for a standard temperature of 25° C and a atmospheric pressure of 100 kPa), c_p the specific heat capacity of dry air (1056 J kg^{-1} K^{-1}) and the overbar shows a time average.

Heilman et al. (1989) investigated the fetch requirements of their Bowen ratio sensors by placement at various heights. Dyer (1961) and Dyer and Pruitt (1962) used a placement height of 4 m over an irrigated field for fetch distances of 190 m. Verma et al. (1992) placed their EC sensors at 3.5-m (3-D sonic anemometer) and 2.5-m (1-D sonic anemometer) heights above a peat surface for a site with at least 250 to 300 m of fetch. However, placement heights of several metres require large fetch distances to ensure adequate adjustment of the turbulent boundary layer and horizontal equilibrium of the measured vertical fluxes. Hicks et al. (1975) used various placement heights above a pine forest.

Ideally, measurements should be in that portion of the boundary layer that is in equilibrium with the surface. The equilibrium sublayer is defined as the region where the momentum flux is within 10 % of that at the surface (Brutsaert, 1982). As Brutsaert (1982) pointed out, this definition has led to formulations of minimum fetch-to-height ratios to ensure that Bowen ratio measurements are made in the equilibrium layer - ratios varying from 10:1 (Panofsky and Townsend, 1964) to 200:1 (Dyer, 1965) although 100:1 has been considered adequate for most measurements (Rosenberg et al., 1983).

Heilman *et al*. (1989) obtained adequate Bowen ratio measurements for ratios as low as 20:1. To avoid spectral attenuation from spatial averaging between the anemometer transducers, the minimum operating height of the sonic anemometer above plant canopy in an unstable surface layer is 6 π multiplied by the spatial resolution of the sonic anemometer (Kaimal, 1975). These recommendations have been used by some workers (for e.g., Kizer and Elliott, 1991). Kristensen and Fitzjarrald (1984) found no statistical difference between their measurements of H for five heights varying between 1.46 and 8.45 m for a 1-km upwind fetch consisting of patchy grass, 0.8-m tall. Similarly, Haugen et al. (1971) found sensible heat measurements at 5.66 and 22.6 m agreed to within 20 % for a site with a fetch of 500 m in all directions and no obstructions for tens of kilometres.

In spite of the theory presented by Kaimal (1975), he suggested (1991, pers. comm.) however that measurements, under unstable conditions, at a height of 1 m above plant canopy should be sufficiently valid without making any corrections for spectral attenuation from spatial averaging. To assess how close to canopy surfaces measurements may be obtained, we performed eddy correlation measurements using four systems placed at eight different heights above a short grassland surface of limited fetch (less than 200 m) with measurements at or below 2 m. We investigated the effect of placement height on measurements of H and using these measurements calculated, for different placement heights, for grassland and forest canopies, the fraction of sensible heat emanating from within an adjacent upwind area - the footprints of the measurements.

9.3 Materials and methods

Measurements were performed outside the Agricultural Engineering Workshop at Texas A & M University, College Station, TX, USA (altitude of 100 m, latitude $30^{o}\,30'$ N and longitude of 96^{o}W). The research area (Fig. 9.1) was a 1.6-ha short and flat bermudagrass (*Cynodon dactylon* L.) surface on a Boonville soil series (fine, montmorillonitic, thermic Mollic Albaqualfs). Measurements were obtained between 18 August and 13 October (Days 231 to 287, 1992).

Sensible heat flux H was determined using four EC systems. Fluctuations in vertical wind speed w' and the air temperature T' were measured initially every 0.1 s but later every 0.2 s using a CA27 sonic anemometer (Campbell and Unsworth, 1979) equipped with a fine wire (12.5-µm diameter) chromel-constantan thermocouple (Campbell Scientific, Logan, Utah, USA).

The thermocouple allowed a temperature difference measurement but not an absolute temperature measurement. Alterations to the sensors included insulating the reference thermojunction of the thermocouple and the metal arm containing the reference junction with pipe insulation material. We used extra insulation to increase the time constant of the reference junction to temperature change. This ensured a more stable reference junction temperature during our 12-min averaging period. Signals from two EC systems were measured with a 21X datalogger and signals from the other two

systems using a CR7X datalogger (Campbell Scientific). These commonly-used dataloggers have the limitation that a measurement frequency greater than 5 Hz is not possible without loss of data. The CR7X datalogger was also used to gather the wind speed, wind direction, net irradiance and air temperature data. Data collection priority was always given to the EC data. Real-time measurements of H were possible by programming the datalogger to calculate F_h every 12 min.

This choice of averaging period was based on the work of Kaimal (1969), who found that a 15-min averaging period was sufficient for sensible heat measurements, and Kaimal and Gaynor (1991) who used 10-min averaging periods.

The datalogger program enabled the determination of $\overline{w'T'}$ and other parameters such as $\overline{w}$, $\overline{T}$ and the standard deviations of these quantities. To minimize datalogger program execution time, we used fast and single-ended voltage measurements.

According to Kanemasu et al. (1979), much of the transport of sensible heat energy is associated with normalized frequencies, $f = nz / \overline{u}$, between 0.001 and 2 where n is the cyclical frequency, z the sensor placement height above the canopy and u the mean horizontal wind speed. Assuming that the normalized frequencies of importance are bounded by these limits (0.001 and 2), the averaging period used must under ideal conditions respond to normalized frequencies less than 0.001 and the datalogger measurement frequency must respond to high frequency eddies at normalized frequencies greater than 2. Measurement systems should therefore be fast enough to respond to fluctuations of at least $2 = \overline{u} / z$. The choice of sampling rate is to insure that the highest frequency of interest is included in the statistics (Kaimal, 1975). Based on sampling theory, he argued that the sampling rate should be at least twice the highest frequency of physical significance. The high frequency requirement for flux measurements is $f = 3$ corresponding to a cyclic frequency $m = 3\,\overline{u} / z$ in the data. Even at this rate, there will be some underestimation in sensible heat because of aliasing. Ideally, the measurement sampling rate should be varied according to the mean horizontal wind speed and sensor placement height. This procedure is not practical. A frequency of greater than 5 Hz was not possible with our equipment. Other workers using the identical equipment presumably faced similar problems. Furthermore, many commercially available sonic anemometer systems do not allow sampling rates greater than 10 Hz (varying from 5 to 20 Hz for the units that we are aware of). It appears that a sampling rate greater than 10 Hz is not possible for analogue measurements. However, some digital measurement systems may allow measurement frequencies greater than 10 Hz (varying from 5 to 20 Hz for the units that we are aware of). It appears that a sampling greater than 10 Hz is not possible for analogue measurements. However, some digital measurement systems may allow measurement frequencies greater than 10 Hz.

In our preliminary measurements, not reported here, a datalogger measurement frequency of 10 Hz was employed. However datalogger overrun occurred with the possibility of data loss during measurement periods with an even greater possibility whenever data were transferred to final storage every 12 minutes. These commonly-used dataloggers have this limitation - measurement frequencies greater than 5 Hz are not possible without loss of data if two eddy correlation systems are connected to one datalogger. However, preliminary comparisons of sensible heat, using two eddy correlation systems at the same height with one system operating at 5 Hz on one datalogger and another system at 10 Hz, were not statistically different (data not shown) for our site and conditions.

One sonic anemometer-fine wire temperature system (system #1) was positioned at a height of 1.00 m above the turf grass surface. The other three systems (#2, #3 and #4) were placed at a height of 0.25, 0.375, 0.50, 1.00, 1.25, 1.50, 1.75 or 2.00 m. These systems were kept at each of these heights until there were sufficient data to compare with measurements of H from system #1 at the 1.00-m height. Initial measurement comparisons were performed with all systems at the 1.00-m height.

In a separate experiment to assess the importance of sonic reflections (from a 0.22 m by 0.22 m metal pan placed 0.27 m directly beneath the fine wire thermocouple) on our measurements, EC systems #1 and #2 were placed at a height of 1.00 m above the turf grass (Fig. 9.2). Air temperature 1 m above the turf grass was measured as the average from five non-aspirated 50-µm diameter copper-constantan thermocouples. Wind speed was measured at 0.25, 0.50, 1.00, 1.25 and 1.50 m heights above the turf grass using model 12102 DC three-cup anemometers (R.M. Young, Traverse City, Michigan). For each 12-minute period, friction velocity plot of ($u*$) was determined from the slope of the plot of $\overline{u}$ (average wind speed for the 12-min period) *vs.* $\ln(z-d)$ where z is the height and d is the zero-plane displacement. Wind direction was measured using a model 12005 wind vane (R.M. Young). These measurements were at 2 m above the turf grass surface.

The CR7X datalogger was also used to gather the air temperature, net irradiance, wind speed and wind direction data. Data collection priority was always given to the EC data. Real-time measurements of H were possible by programming the datalogger to calculate H every 12 min.

Atmospheric stability was evaluated as the ratio of z/L, where L is the Obukhov length (m), defined as:

$$L = -u_*^3 / [k(g/T) \cdot H / (\rho c_p)] \tag{9.2}$$

where u_* is the friction velocity (m s^{-1}), k von Kármán's constant (≈ 0.41), g the acceleration due to gravity (9.795 m s^{-2}), and T the air temperature (K). Net irradiance was measured with a model Q*6 net radiometer (Radiation and Energy Balance Systems, Seattle, WA) at 1-s intervals and averaged over a 12-min period.

The placement height study was repeated but using three-dimensional sonic anemometers and included a spectral analysis of w and T_{sonic}. The study was above a short and flat 5.6–ha area adjacent the Rabie Saunders Building of the University of KwaZulu-Natal, Pietermaritzburg, South Africa (28^{o}35'S, 30^{o}26'E, altitude 684 m). The grass height was less than 0.05 m and the fetch distance was at least 200 m. Grass species included red grass (*Themeda triandrox* L.), trident grass (*Fristachya leucothrix* L.) and thatch grass (*Hyparrhenia hirta* L.) on a soil of the Mispah form. Two Applied Technologies (Boulder, CO) three-dimensional sonic anemometers, model SWS-2M/3V (path length of 100 mm) were used. Measurements were at 10 Hz and each microprocessor of each anemometer were separately powered using 150 A h, 12 V batteries. Two battery-powered personal computers were used to collect the data through a serial port at the end of each 12-min period. The clock times of each computer were synchronised prior to data collection. The sensor cables for each anemometer system were kept at least 0.3 m apart to avoid signal interference. Measurements before 09h00 and after 17h00 were invalid due to a significant amount of dew. One sonic anemometer was always positioned at a height of 1 m above the grass surface for the duration of the study and the other was

kept at one of the heights 0.25, 0.35, 0.5 or 1.0 m. The system for which height varied was kept at each height for at least a day.

A power spectral analysis of the vertical wind speed and sonic temperature measurements, for each height, were compared. The spectrum of turbulence in the boundary layer includes the inertial subrange for which energy neither enters the system nor is dissipated but cascades down to smaller and smaller eddies. Kolmogorov (1941) argued that the turbulent energy spectrum in the inertial subrange is a function of spectral wave number to the power of -5/3. Kaimal et al. (1972) showed that log-log plots could be used to demonstrate the -5/3 relationship for vertical wind speed and air temperature. Furthermore, such plots could demonstrate the adequacy of the measurements, particularly for systems close to the surface. To this end, power spectrum log-log plots for vertical wind speed and sonic temperature at the various measurement heights were used to compare with the log-log plot for sonic temperature. A fast Fourier transform was applied to the 100-ms sonic temperature data. For this purpose, the 100-ms data for the period 12h00 to 12h12 for each day (corresponding to 7200 data points) on days of year 132 (both systems at 1 m) and 134 (one system at 1 m and the other at 0.5 m), 135 (one system at 1 m and the other at 0.25 m) and 136 (one system at 1 m and the other at 0.35 m) were used. The fast Fourier transform analysis required 2^n data points and for the 100-ms data; this was achieved for n = 12 for each 12-min period.

9.4 Results and discussion

9.4.1 Texas study

During the study, winds were predominantly from the south with a uniform fetch distance of at least 190 m (Fig. 9.1). Sensible heat measurements for which the wind direction was between SW and ESE were only used for analysis. The thickness of the internal boundary layer ($\delta_{boundary}$) at the locations of the EC measurements was calculated using the Munro and Oke (1975) equation:

$$\delta_{boundary} = x^{0.8} z_o{}^{0.2} \tag{9.3}$$

where x is fetch, ($\approx 190\ m$) and z_o is the roughness length for momentum transport. For these values, $\delta_{boundary}$ varied between 18 and 21 m for z_o estimated as 13 % of canopy height. The height of the turf grass was between 0.005 and 0.02 m. All sensor heights were measured relative to the plant canopy. Since a rough-to-smooth transition existed at our site, the lowest 5 % of the boundary layer was assumed to be in equilibrium with the surface (Brutsaert, 1982, page 166). For a smooth-to-rough transition, the lowest 10 % of the boundary layer is assumed to be in equilibrium with the surface (Brutsaert, 1982, page 166). For our site

$$\delta_{equilibrium} = 0.05 \times \delta_{boundary} \tag{9.4}$$

with $\delta_{equilibrium}$ varying between about 0.90 and 1.05 m. The calculated thickness of the internal boundary layer at the measurement site, using the Munro and Oke (1975) equation, was therefore between 0.90 and 1.05 m. It is therefore likely that measurements at or below 1.00 m were within the equilibrium layer while measurements above 1.00 m were above the equilibrium layer. Stability during the period of measurements was assessed by examining the ratio of height above canopy z (m)

to the Obukhov length L (m). The length L was calculated from u_* determined from the wind profile measurements, the air temperature at 1 m and the H (Fig. 9.3) measured at 1.00 m using EC system 1. Under unstable conditions, free and mixed convection dominates. The magnitude of L for unstable conditions can be interpreted as the height above the zero plane displacement at which free convection becomes the dominant transfer mechanism. For unstable conditions and for a short grassland surface, free convection dominates when $z/L < -1$ and mixed convection dominates when $-1 < z/L < -0.01$. During the study, z/L varied between about -0.2 to -0.01 during the day and from about -0.01 to 0.02 during the night.

Typical data are shown (Fig. 9.3). During these periods, friction velocity u_* varied between 0.15 and 0.38 m s^{-1}. Throughout the experiment, unstable conditions ($z/L < -0.01$) occurred during daylight hours when mixed convection dominated but tended towards free convection during the noon hours (Fig. 9.3). Neutral conditions ($-0.01 < z/L < 0.01$) occurred close to sunrise or sunset and stable conditions ($0.01 < z/L < 0.02$) occurred during the night. The $z/\boldsymbol{L}$ ratio was used to calculate the stability-corrected footprints.

A three-dimensional plot of $3 = \overline{u} / z$ (Hz), the high frequency requirement for flux measurement corresponding to a normalized frequency $f = 3$, as a function of local time and height above grass canopy surface (Fig. 9.4) shows that the normalized frequency $3 = \overline{u} / z$ increases with height and increases progressively from morning periods from about 3 to 40 Hz in the late afternoon. Assuming a sampling time of 0.1 s (corresponding to a sampling rate of 10 Hz), it therefore seems that it would not be possible to obtain good correspondence between sensible heat measurements as a function of height, using a single 10 Hz sampling rate for all heights. However, a 10 Hz sampling rate must have allowed most of the frequencies to be included in the statistics. This statement is supported by the fact that, as we will show reasonable EC sensible heat comparisons as close as 0.5 m from the surface were possible.

In view of our aim of performing measurements close to the surface and in the light of Kaimal's (1991, pers. comm.) comments, we chose 1.00 m as a standard height above canopy. Before comparing measurements of sensible heat at the various heights, it was therefore important to first compare measurements from all EC systems at 1.00 m. There were no statistical differences in sensible heat flux measurements from all EC systems at 1.00 m above surface. The slope's 95 % confidence interval, for each system, contained the slope value of unity. Therefore, for the rest of the study, measurements from systems 2, 3 and 4 were treated as three independent measurements at the chosen height. These measurements were compared with the H measurements from system 1 at 1.00 m above surface.

Typical diurnal H measurements are shown (Fig. 9.5) for EC system 1 at 1.00 m and 2 and 3 both at 0.38 m. Of particular note is the underestimation in H at the 0.38-m height compared to 1.00 m. Measurements such as these were used to determine the dependence of the H measurements on placement height.

Sensible heat flux measurements from all EC systems 1.00 m above surface were compared and no differences were found. The unsystematic root mean square error was a small fraction of the total root mean square error for each EC system (Table 9.1, first three data columns).

Measurement comparisons between EC system #1 at 1.00 m and the other systems at 0.25 m, 0.38 m, 0.50 m and 1.00 m above turf grass are shown in Fig. 9.6. Of particular note is the gradual increase in the slope from 0.8636 for the *H* measurements from system #1 at 1.00 m (*x*-axis) and the other systems at 0.25 m (*y*-axis) measurement comparisons (Fig. 9.6a) to 0.9126 at 0.38 m (Fig. 9.6b), 1.0245 at 0.50 m (Fig. 9.6c) and 1.0076 at 1.00 m (Fig. 9.6d).

The slope of the curves of *H* at a known height, *vs.* that measured at a height of 1.00 m using EC system #1 (Fig. 9.6), as a function of height above turf grass is shown (Fig. 9.7). The bars above and below each datum point show the 95 % confidence limit in the slope. Statistically, there is a difference among the slopes at each of the 0.25-m, 0.38-m and 0.50-m heights (at the 95 % level of significance). There is also a difference among the slopes at 0.50, 1.75 and 2.00-m heights (Fig. 9.2). Slope of the ratio of *H* at height *z* over that at 1.00 m *vs.* the height *z* above turf grass relationships show three distinct regions (Fig. 9.7): (a) increasing slope between 0.25 and 0.50 m; (b) plateau region of constant slope between 0.50 and 1.25 m; (c) increasing slope (although not statistically significant) between 1.25 and 1.75 m. Root mean square errors (Table 9.2) show a decrease in the systematic mean square error (associated with a slope value different from unity) with height up to 1.00 m and then an increase in this error component above the 1.00-m height up to a height of 1.75 m.

The significance of the plateau region of Fig. 9.7 is that measurements at 0.50 m above the turf grass were no different from measurements at between 1.00 and 1.25 m (Table 9.2). For heights less than 0.50 m, there was a sudden reduction in the slope by nearly 10 % (at 0.38 m) and 15 % (at 0.25 m) (Fig. 9.7). The generally increasing slope region between placement heights of 1.00 and 2.00 m deserves comment. The experimental site was surrounded by asphalt roads on three sides with buildings to the southeast and southwest (Fig. 9.1), the predominant wind direction being from the south. Wind from a generally southerly direction would flow between two nearby buildings and across the asphalt roads and advect hot air to the experimental site. It was uncertain whether the EC values at either 0.50 or 1.00 m were actually measures of the true sensible heat flux at the site. However, we did obtain 543 12-minute comparisons between EC-measured sensible heat at 1.00 m and *H* determined using an independent surface temperature method (data not shown). The surface temperature sensible heat was about 0.96 of that measured using the EC technique at the 1.00 height, indicating that the 1.00-m height EC sensible heat adequately represented the true sensible heat at the site. There was however no statistical difference in measured sensible heat between the 1.25 and 2.00 m placement heights.

Koprov and Sokolov (1973) showed that sonic anemometer and thermocouple sensor separation can cause a discrepancy between measured and actual *H* values. It is not possible however to use their empirical relationship to correct for sensor separation as the closest separation between their sensors was 100 mm compared to the 20 mm in our case. Furthermore, the ratio of sensor separation distance to placement height for all our measurements was less than or equal to 0.01. This was considerably less than the 0.2 minimum value recommended by Koprov and Sokolov (1973) for application of their corrective empirical relationship.

The reason for the large reduction in the slope for heights less than 0.5 m (Fig. 9.7) was further investigated. We wished to determine if the reduction could be attributed to sonic reflections from the underlying vegetated surfaces. The reduction could also be due to small-sized eddies, contained

between the upper and lower arms of the sonic anemometer (100-mm separation), causing a reduction in the covariance between the vertical wind speed fluctuation and the air temperature fluctuation. Sensible heat flux measurements with and without the metal pan 0.27 m beneath the fine-wire thermocouple were obtained for a week using EC system #1 and #2. Typical diurnal measurements with the pan in position at 12h00 (Fig. 9.8) show no differences in sensible heat after the pan was in place. A statistical comparison between the measurements showed no significant difference (Table 9.1, last column of data). There was therefore no evidence for sonic reflections from the pan affecting our H measurements. Eddies were presumably able to envelope the square pan. This envelopment would not alter the covariance between the vertical wind speed fluctuation and air temperature. Therefore, we speculate that measurements close to the canopy surface differ from those at 1.00 m due to small-sized eddies near the surface being contained between the sonic separation distance. These eddies would not be correctly measured by the sonic anemometer. At a measurement height z above the canopy surface, under neutral conditions, the mean eddy diameter, given by the mixing length l, is typically $k\,(z - d)$ where $k = 0.41$ is the von Kármán constant (Thom, 1975). Therefore for a grassland surface (with $d << z$) for a placement height $z = 1.00$ m, l is 0.41 m. The mean eddy size, l, in the vertical direction is greater than $k\,(z - d)$ under unstable conditions (Thom, 1975). Eddies with typical diameters of 0.41 m were presumably able to envelope the square metal pan, filled with soil, of dimension 0.22 m This envelopment would not alter the actual sensible heat. Therefore, measurements close to the canopy surface differ from those at 1.00 m due to small-sized eddies near the surface being contained between the sonic separation distance. In order to conclusively demonstrate that the reduction in sensible heat near the surface is due to a loss of small-sized eddies, one would need to show that there is a loss of the high frequency contribution in the cospectral estimates of sensible heat. Typically, measurements at a sampling rate at 20 Hz would be required. These rates were not possible with our equipment.

Since EC H measurements are absolute, requiring one measurement height only, the EC technique appears to have some advantages compared to the Bowen ratio (BREB) technique. The BREB technique requires measurements at two heights maintained sufficiently far apart for the sensors to detect differences in air temperature and water vapour pressure between the two levels. Given that the lower measurement level is at 0.50 m above the canopy, the upper level would be at least 1.00 m above a canopy similar to ours and usually at a height of 1.50 m. The EC measurements at the 0.5-m above canopy height would be less affected under limited fetch conditions than BREB measurements at 0.50 and 1.50 m, say. For the 1-D sonic anemometers used, the minimum operating height of 6 π multiplied by sensor path length, for unstable conditions Kaimal (1975) would be equal to 1.8 m. Clearly then, adequate EC measurements of H are possible at heights much lower than previously thought. This fact has considerable importance for short-canopy situations where fetch may be limited.

If lower placement heights are also possible for other surfaces, the implication is that the fetch requirement for EC sensors is not as severe as was previously thought. For the less conservative fetch to placement height ratio of 20:1 found by Heilman et al. (1989), a Bowen ratio system would require a minimum fetch of 20 x 1.50 m = 30 m. The EC system, from our data, could be placed at a height above canopy of 0.50 m where the minimum fetch was 190 m.

Traditionally, the ratio of height z above the zero plane displacement d to the uniform upwind fetch distance x has been set to, say, 1:100 and then the maximum permissible $(z - d)$ calculated from the known fetch x. This is a simplistic approach. A much-improved approach is to use an approximate analytical solution to the two-dimensional diffusion equation for idealized surface boundary conditions (Philip, 1959; Wilson, 1982).

Under neutral conditions the fraction f of the measured H at a height z, that can be expected to emanate from within the adjacent upwind area a horizontal distance x from the measurement point is described by the relation:

$$f = \exp[-U(z-d)/(k\,u_* x)] \tag{9.5}$$

where U is the horizontal wind speed and k is von Kármán's constant (Gash, 1986; Leclerc and Thurtell, 1990; Schuepp et al., 1990). The fraction f, also referred to in the literature as the cumulative footprint prediction, is shown (Fig. 9.9) on the z-axis as a function of local time on the x-axis (every 12 min between 09h48 to 17h12 local time for day 259, 1992), for various placement heights z (y-axis) for our grassland site. For these calculations we used the actual measured wind speeds averaged between 0.25 m and the measurement height, the friction velocity u_* calculated from our wind profile data, and a value of between 25 and 190 m for upwind distance x. A correction for stability was applied by replacing $(z-d)$ in Eq. 6 by $\Phi_m(z-d)$ where $\Phi_m = [1-16(z-d)/L]^{-0.25}$ is the dimensionless stability function for momentum transfer (Thom, 1975) calculated using typical $(z-d)/L$ data depicted in Fig. 9.7. The fraction f exceeds 0.75 for z >1.00 m for x = 190 m and f > 0.94 for z = 0.50 m. Of particular note, from the three dimensional plots (Fig. 9.8), is the large reduction in f with increase in placement height z from 0.25 m to 1.50 m. Also, the diurnal variation in f is more pronounced at 1.25 m than at the 0.25 m placement height. The fraction is shown in Table 9.3 for two days (at midday) for various placement heights z, for the measured wind speed U at the different heights and a value of 190 m for x. The fraction exceeds 0.8 for z > 1.0 m but if corrections for stability are applied (Schuepp et al., 1990), the fraction is greater than 0.87. The position of the peak of the footprint, x_{max} (m), is calculated using:

$$x_{max} = U(z-d)/[2\,u_* k]. \tag{9.6}$$

This position describes the downwind distance to which the measurement is most sensitive (Schuepp et al., 1990). The x_{max} position is less than 36 m for $z \le 1.0$ m but less than 18 m if stability corrections are applied. The stability corrections markedly reduce x_{max} for the z = 1.25 and 1.5 m placement heights. Since we found no statistical difference between H measurements between the 0.5 and 1.0 m placement heights, the advantages of the lower placement height of 0.5 m is the larger f fraction and a smaller x_{max} (Table 9.3).

The three-dimensional graphs (Fig. 9.9) may be used to determine the correct siting of an automatic weather station. Accepting a f-value of at least 0.70 and a sensor placement height at or below 2.00 m, the minimum fetch requirement is in excess of 100 m for unstable conditions. A fetch of 125 m to 150 m would be more desirable, resulting in a f-value approaching 0.8 except in the early morning and late afternoon times when f may be less than 0.65.

It is possible to extrapolate our measurements to forest canopies. For this, a value for u_* for forests is required. We chose a value of 1 m s^{-1}, a value greater than that measured for our grassland site and greater than the typical value of 0.46 m s^{-1} used by Monteith and Unsworth (1990) for a tall crop. We used the logarithmic wind profile equation to estimate U where U is the average wind speed between height $z=d + z$ and z above the soil surface:

$$U = \int u \, dz / \int dz \tag{9.7}$$

The horizontal wind speed u was obtained from the wind profile equation:

$$u = (u_* / k) \ln[(z - d) / z_o] \tag{9.8}$$

where $d \approx 2/3\,h$ and $z_o \approx 1/10\,h$ where h is the canopy height. We chose a canopy height of 20 m. To correct the calculation of f for stability, we recalculated the Obukhov length L for a friction velocity u_* = 1 m s^{-1} allowing for a diurnal variation in L based on the z/L values shown in Fig. 9.5. The results of these calculations are shown (Fig. 9.10). Compared with the three dimensional plots for the grassland surface (Fig. 9.8), the fraction f for a forest canopy had little diurnal variation. However, there was a rapid reduction in f with a decrease in the upwind distance x = 25 to 190 m for all placement heights z = 0.25 to 2.00 m. The significance of these results is that the fetch requirements for above-forest canopy micrometeorological measurements are necessarily more stringent than those for measurements above grassland canopies at all placement heights between 0.25 and 1.50 m. Also, for a given fetch distance, there may be little advantage in using a low placement height for a forest canopy (f varying between 0.69 and 0.80 for a fetch of 190 m compared to between 0.75 an 0.98 for a grassland canopy with the same fetch).

There is another problem that needs to be considered with above-forest canopy micrometeorological measurements. Due to the aerodynamically rough nature of forest canopies (compared to a grassland surface), profile measurements such as is used with the Bowen ratio technique, would require a much larger distance between the lower and upper placement heights for the water vapour and air temperature differentials to be measurably large. Typically, one would use 0.50 and 2.00 m or even 0.50 and 2.50 m placement heights. These placement heights would impose greater fetch limitations on the measurements (Fig. 9.10).

9.4.2 Pietermaritzburg study

Unlike the Texas placement height study, this study allowed collection of the raw EC data. The bias (b), comparability (c), precision (s) and coefficient of variation s' for vertical wind speed and sonic temperature for the two 3D sonic anemometers maintained at the same 1-m height showed good agreement between the two instruments. Both anemometers were placed at 1 m above the canopy surface for an entire day (day 132) and the following morning (n = 56). Values of b, c, s and s' for vertical wind speed were 0.00727 m s^{-1}, 0.02339 m s^{-1}, 0.02224 m s^{-1}, 5.0 % respectively. For sonic temperature, the respective values of b, c, s and s' were 0.03251 ^{o}C, 0.07031 ^{o}C, 0.06234 ^{o}C and 8.1 %. These values are in good agreement with values obtained by Hoene (1971). The bias, comparability, precision and coefficient of variation values were greater for the vertical wind speeds but lower for sonic temperature than the values obtained by Hoehne (1971).

Sensible heat flux measurement comparisons for the EC system at 1.00 m and the other system at 0.5–, 0.35– and 0.25–m heights above the tufted grass showed a gradual decrease in the slope from 1.0 to the 0.25 m height, particularly for heights below 0.5 m (data not shown). This result confirms the conclusion of the Texas study using a one dimensional sonic anemometer placed above a short turfgrass surface that there are no significant differences between *H* measurements with sensors placed at the 0.50, and 1.0 m heights (Fig. 9.7). This result was in a different year, season and hemisphere.

The power spectrum log-log plot comparisons for vertical wind speed and sonic temperature for the 10-Hz measurements are shown. In each case, -5/3 Kolmogorov law for the inertial sub-range is indicated by the straight line shown in the log-log plots with the envelope of points approaching the -5/3 curve at the higher frequencies. The envelope of points is associated with the most unstable conditions. The power spectrum log-log plots for the lower heights, 0.25 and 0.35 m for vertical wind speed (Fig. 9.11) show a slight drop-off from the -5/3 law at the lower frequencies, particularly for the 0.25 m height. For sonic temperature, Fig. 9.12, the envelope for the measurements appears to obey the -5/3 law for all heights.

9.5 Conclusions

No significant differences between sensible heat (*H*) measurements with sensors placed at the 0.50, and 1.25 m heights were found to occur. Below 0.50 m, there was a significant reduction in *H*. At heights greater than 1.50 m above canopy there was a significant increase in *H* compared to that measured at the 1.00-m height above canopy but measurements between 1.25 and 2.00 m were not significantly different. We speculate that placement of the sensors at heights less than 0.50 m caused a reduction in the covariance between the vertical wind speed fluctuation and the air temperature fluctuation presumably due to a larger fraction of eddies of small size occurring between the separation distance of the sonic anemometer transducers. The reduction was not due to acoustic reflections from the surface. Footprint calculations showed that at least 90 % of the measured *H* at the 0.5-m height was from our experimental site. Footprint calculations showed that the fetch requirement for micrometeorological measurements above forest canopies is more stringent than above grassland canopies. Placement height to fetch ratio calculations to determine sensor placement height is too simplistic an approach. Footprint calculations should be routinely performed. A power spectrum analysis for 10-Hz vertical wind speed demonstrate a drop-off of measurements, for decreasing measurement heights, from the -5/3 Kolmogorov law for the inertial sub-range for the lower frequencies. This was particularly noticeable at the 0.25-m placement height. The drop-off was not noticeable for sonic temperature.

9.6 Acknowledgements

Texas A & M University and the United States Council for the International Exchange of Scholars for a Fulbright grant provided financial support for this research. Use of two of the EC systems from Dr W.A. Dugas, Blackland Research Centre, Texas Agricultural Experiment Station, Temple, Texas is gratefully acknowledged. The comments from anonymous reviewers for Agricultural and Forest Meteorology are gratefully acknowledged.

9.7 References

Brutsaert, W.H., 1982. Evaporation into the Atmosphere. Reidel, Dordrecht, Holland, 299 pp.

Campbell, G.S. and Unsworth, M.H., 1979. An inexpensive sonic anemometer for eddy correlation. J. Appl. Meteorol. 18, 1072–1077.

Dyer, A.J., 1961. Measurement of evaporation and heat transfer in the lower atmosphere by an automatic eddy correlation technique. Q. J. Roy. Meteorol. Soc. 87, 401–412.

Dyer, A.J. 1965. Discussion on change of terrain roughness and the wind profile by H.A. Panofsky and A.A. Townsend. Q. J. Roy. Meteorol. Soc. 91, 241.

Dyer, A.J. and Pruitt, W.O., 1962. Eddy flux measurements over a small irrigated area. J. App. Meteorol. 1, 471–473.

Fitzjarrald, D.R. and Lenschow, D.H., 1983. Mean concentration and flux profiles for chemically reactive species in the atmospheric surface layer. Atmos. Environ. 17, 2505–2512.

Gash, J.H.C., 1986. A note on estimating the effect of limited fetch on micrometeorological evaporation measurements. Boundary–Layer Meteorol. 35, 409–413.

Haugen, D.A., Kaimal, J.C. and Bradley, E.F., 1971. An experimental study of Reynolds stress and heat flux in the atmospheric surface layer. Q. J. R. Meteorol. Soc. 97, 168–180.

Heilman, J.L., Brittin, C.L. and Neale, C.M.U., 1989. Fetch requirements for Bowen ratio measurements of latent and sensible heat fluxes. Agric. For. Meteorol. 44, 261–273.

Hicks, B.B., Hyson, P. and Moore, C.J., 1975. A study of eddy fluxes over a forest. J. App. Meteorol. 14, 58–66.

Hoehne, W.E., 1971. Standardized functional tests. NOAA TM NWST&EL-12, Sterling, VA. U.S. Dept. of Commerce, 23 pp.

Kaimal, J.C., 1969. Measurement of momentum and heat flux variations in the surface boundary layer. Radio Science. 4, 1147–1153.

Kaimal, J.C., 1975. Sensors and techniques for direct measurement of turbulent fluxes and profiles in the atmospheric surface layer. Atmospheric Technol. 7, 7–14.

Kaimal, J.C. and Gaynor, J.E., 1991. Another look at sonic thermometry. Boundary–Layer Meteorol. 56, 401–410.

Kanemasu, E.T., Wesley, M.L., Hicks, B.B. and Heilman, J.L., 1979. Techniques for calculating energy and mass fluxes. In Modification of the Aerial Environment of Plants. Barfield, B.J. and Gerber, J.F. (eds). Kansas State University, Manhattan, USA, p. 156.

Kaimal, J.C., Wyngaard, J.C., Izumi, Y., Cote, O.R., 1972. Spectral characteristics of surface layer turbulence. Q. J. Roy. Meteorol. Soc. 98, 563–589.

Kizer, M.A. and Elliott, R.L., 1991. Eddy correlation systems for measuring evapotranspiration. Trans. Am. Soc. Agric. Eng. 34, 387–392.

Kolmogorov, A.N., 1941. Dissipation of energy in the locally isotropic turbulence (English translation 1991). Proc. Roy. Soc. London A434 15–17.

Koprov, B.M. and Sokolov, Yu., D., 1973. Spatial correlation functions of velocity and temperature components in the surface layer of the atmosphere. Izv., Atmos. Oceanic Physics. 9, 178–182.

Kristensen, L. and Fitzjarrald, D.R., 1984. The effect of line averaging on scalar flux measurements with a sonic anemometer near the surface. J. Atmos. Oceanic Tech. 1, 138–146.

Monteith, J.L. and Unsworth, M.H., 1990. Principles of Environmental Physics. Edward Arnold, London.

Munro, D.S. and Oke, T.R., 1975. Aerodynamic boundary layer adjustment over a crop in neutral stability. Boundary–Layer Meteorol. 9, 53–61.

Panofsky, H.A. and Townsend, A.A., 1964. Change of terrain roughness and the wind profile. Q. J. Roy. Meteorol. Soc. 91, 147–155.

Philip, J.R., 1959. The theory of local advection: 1. J. Meteorol. 16, 535–547.

Rosenberg, N.J., Blad, B.L. and Verma, S.B., 1983. Microclimate: The Biological Environment. Wiley, New York, 495 pp.

Savage, M.J., McInnes, K.J. and Heilman, J.L., 1995. Placement height of eddy correlation sensors above a short grassland surface. Agric. For. Meteorol. 74, 195–204.

Savage, M.J., McInnes, K.J. and Heilman, J.L., 1996. The "footprints" of eddy correlation sensible heat flux density, and other micrometeorological measurements. S. Afr. J. Sci. 92, 137–142.

Savage, M.J., Everson, C.S. and Metelerkamp, B.R., 1997. Evaporation measurement above vegetated surfaces using micrometeorological techniques. Water Research Commission Report No. 349/1/97, Pretoria, South Africa, p248, ISBN 1–86845–363–4.

Schuepp, P.H., Leclerc, M.Y., Macpherson, J.I. and Desjardins, R.L., 1990. Footprint prediction of scalar fluxes from analytical solutions of the diffusion equation. Boundary–Layer Meteorol. 50, 355–373.

Swinbank, W.C., 1951. The measurement of vertical transfer of heat and water vapor by eddies in the lower atmosphere. J. Meterol. 8, 135–145.

Thom, A.S., 1975. Momentum, mass and heat exchange of plant communities. In: J.L. Monteith (Editor), Vegetation and the Atmosphere, Volume 1. Academic Press, London, pp. 57–109.

Verma, S.B., Ullman, F.G., Billesbach, D., Clement, R.J., and Kim, J., 1992. Eddy correlation measurements of methane flux in a northern peatland ecosystem. Boundary–Layer Meteorol. 58, 289–304.

Wilson, J.D., 1982. An approximate analytical solution for the diffusion equation for short range dispersion from a continous ground level source. Boundary–Layer Meteorol. 23, 85–103.

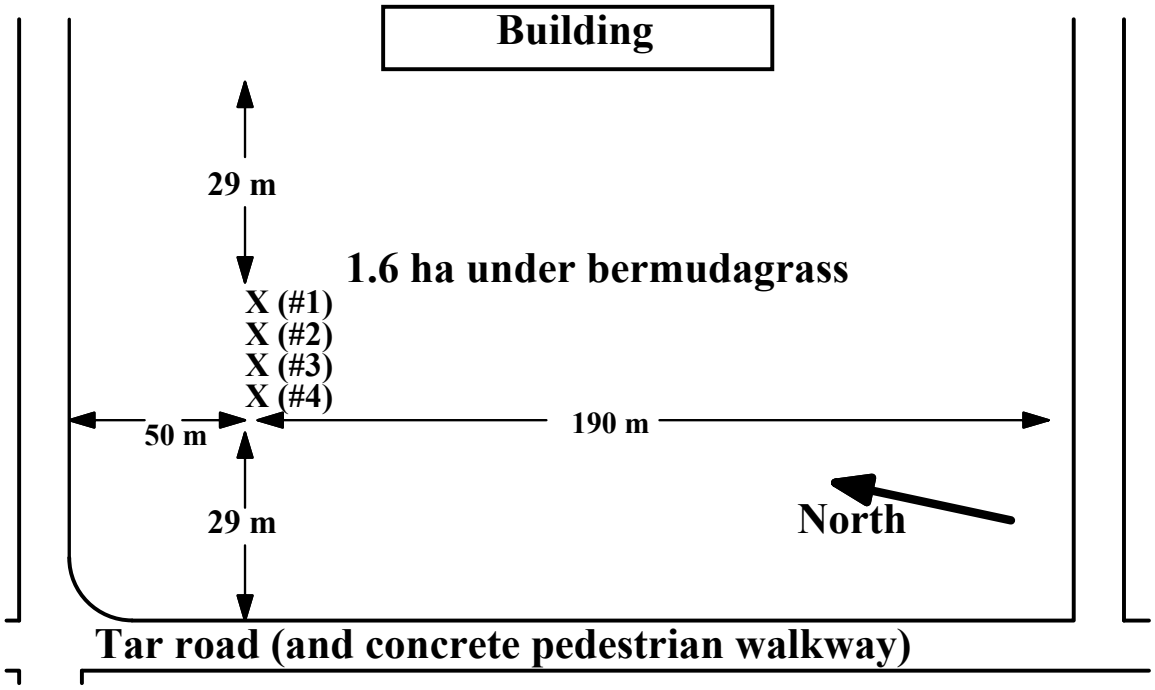

Fig 9.1. A diagram (in plain view and not to scale) of the experimental site. The positions of the four EC Systems are indicated by X's, each system 3 m from the next. EC system #1 was always positioned at 1.00 m above the turf grass surface.

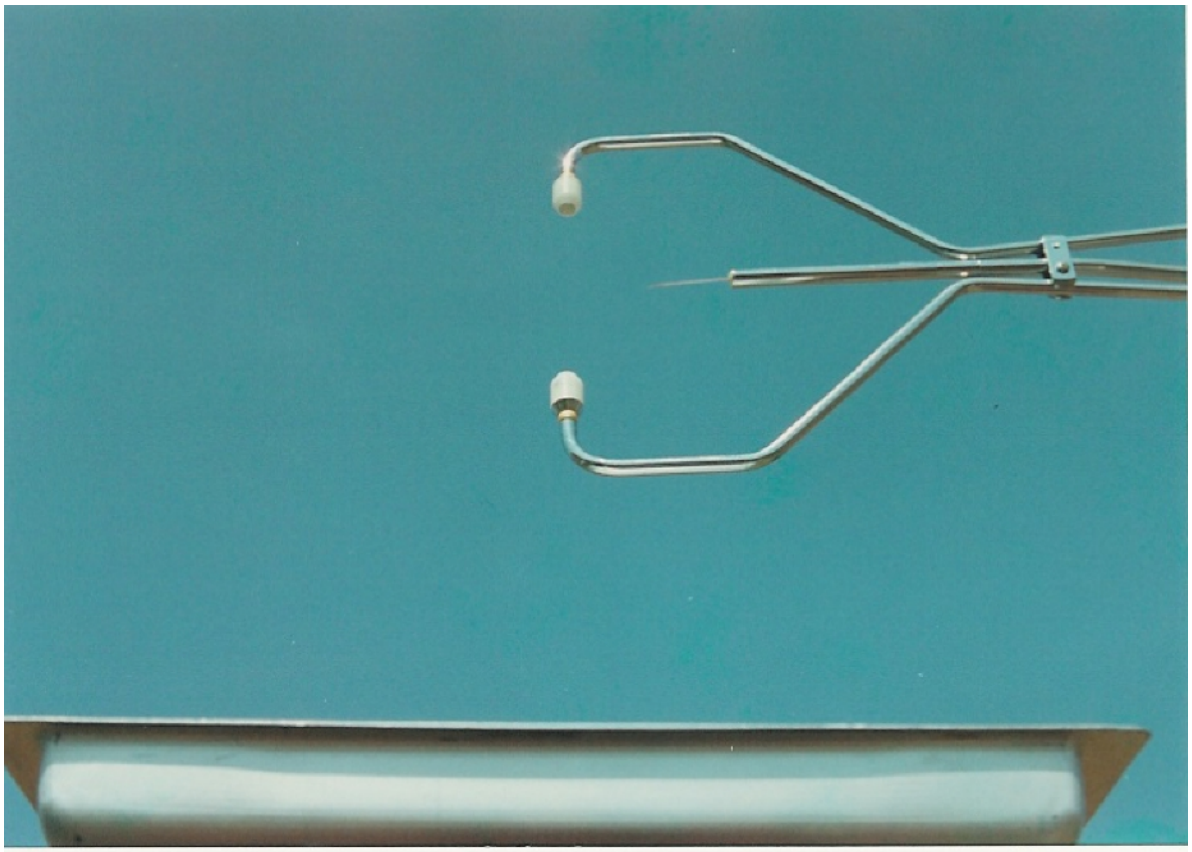

Fig. 9.2. A photograph showing the placement of a pan containing soil beneath an EC system to encourage acoustic reflections.

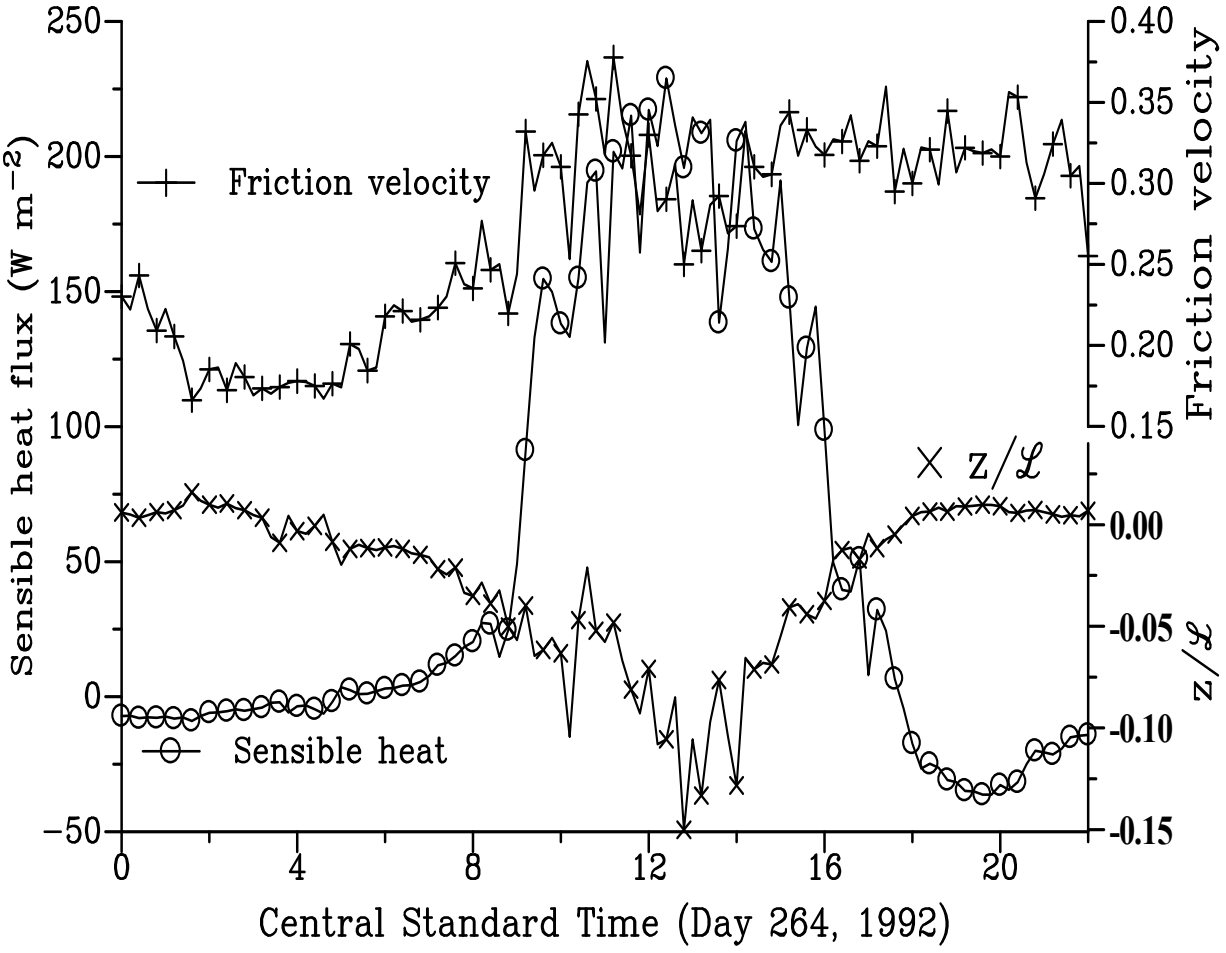

Fig 9.3. The variation in the friction velocity and the ratio of sensor height z (=10.00 m for system 1 used here) to the Obukhov length L and H for Day 264, 1992.

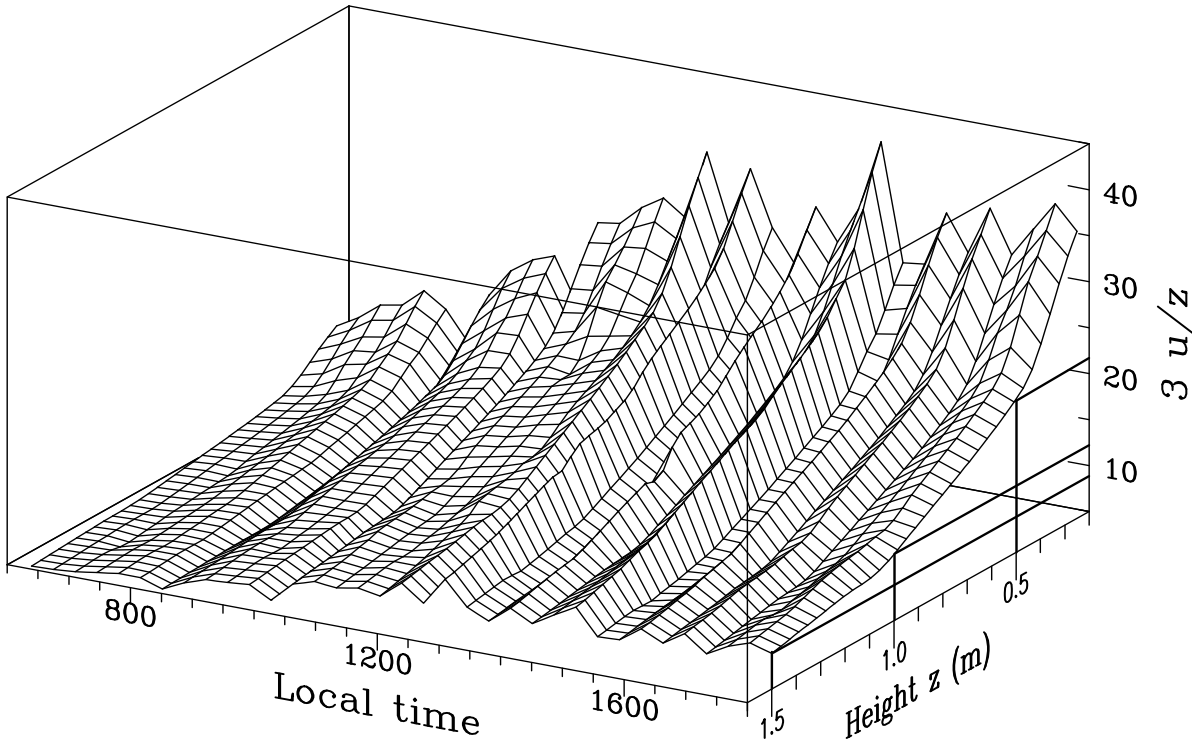

Fig 9.4. A three-dimensional representation of three times the ratio of horizontal speed to placement height *u*/*z*, corresponding to the high frequency requirement for flux measurement as a function of local time and placement height for Day 249.

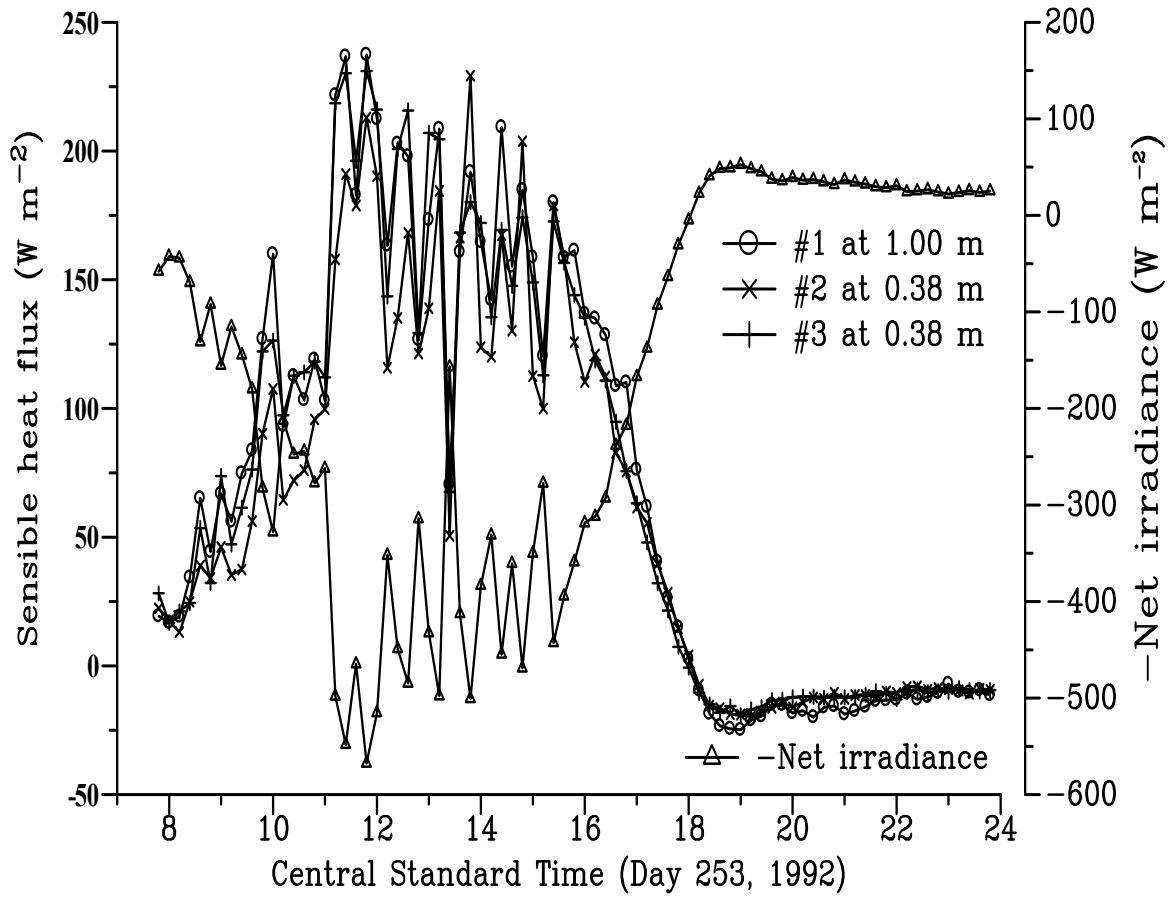

Fig. 9.5. Typical diurnal EC of measurements on Day 253, 1992. System 1 was at 1.00 m above the grassland surface 2 and 3 were both at 0.38 m. Also shown is the negative of the net irradiance (right-hand y-axis).

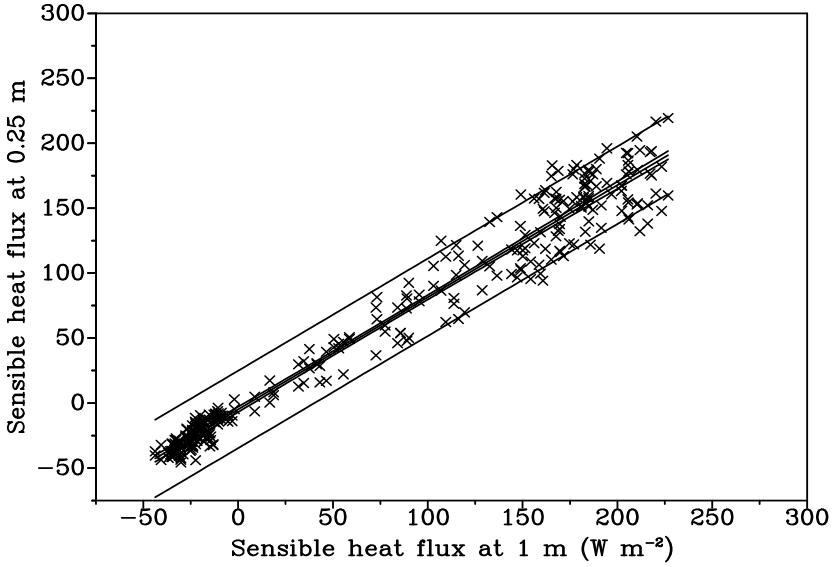

Fig. 9.6a. Measurement comparisons between EC system #1 at 1.00 m and the other systems at 0.25 m (Days 247 to 254) above the surface. The wide 95 % confidence belts are for an estimated single *y* value and the narrower limits are for the population mean.

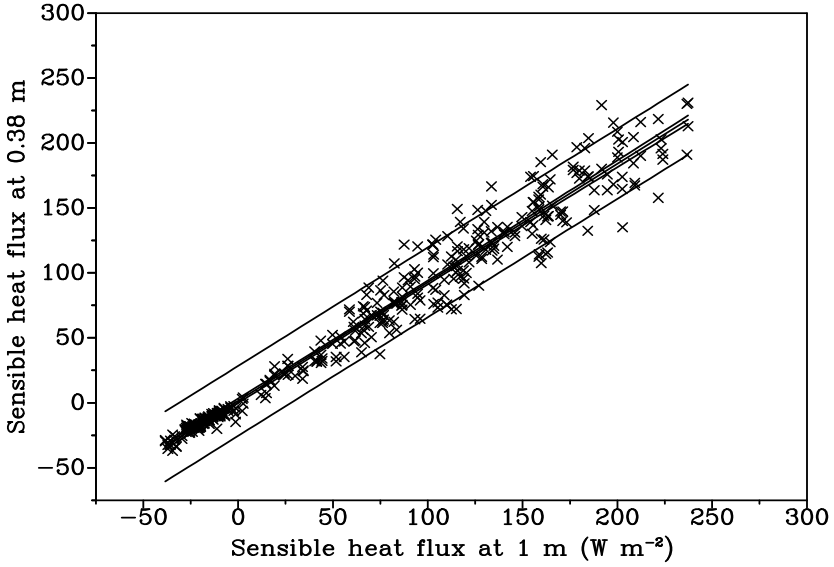

Fig. 9.6b. Measurement comparisons between EC system #1 at 1.00 m and the other systems at 0.38 m (Days 247 to 254) above the surface. The wide 95 % confidence belts are for an estimated single *y* value and the narrower limits are for the population mean.

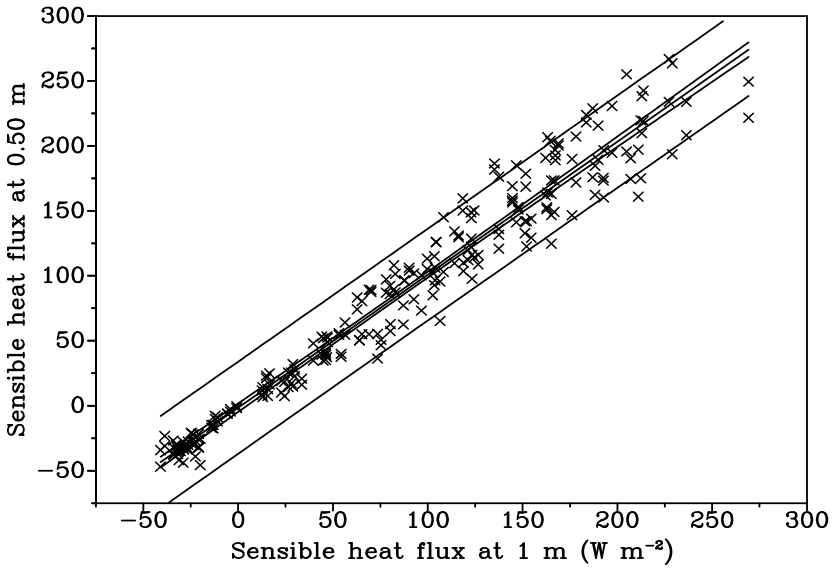

Fig. 9.6c. Measurement comparisons between EC system #1 at 1.00 m and the other systems at 0.50 m (Days 233 to 235) above the surface. The wide 95 % confidence belts are for an estimated single *y* value and the narrower limits are for the population mean.

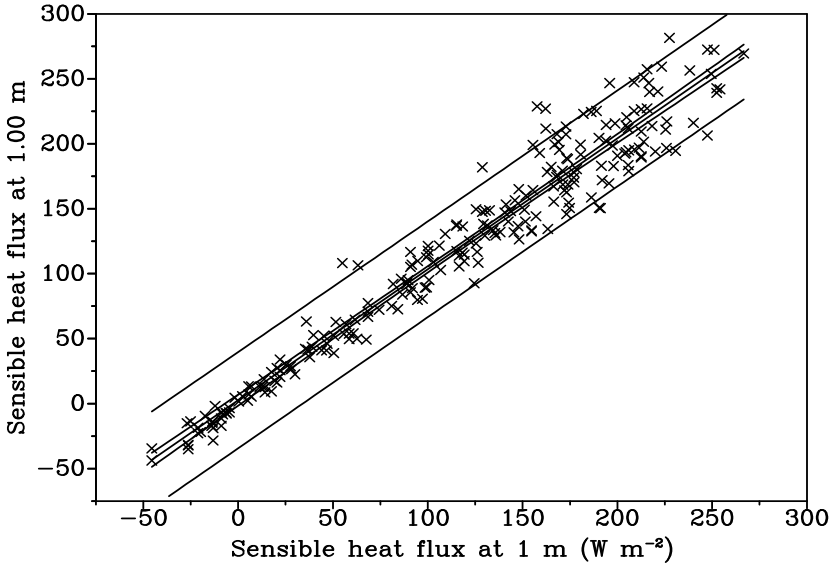

Fig. 9.6d. Measurement comparisons between EC system #1 at 1.00 m and the other systems at 1.00 m (Days 231, 232, 259 to 262) above the surface. The wide 95 % confidence belts are for an estimated single *y* value and the narrower limits are for the population mean.

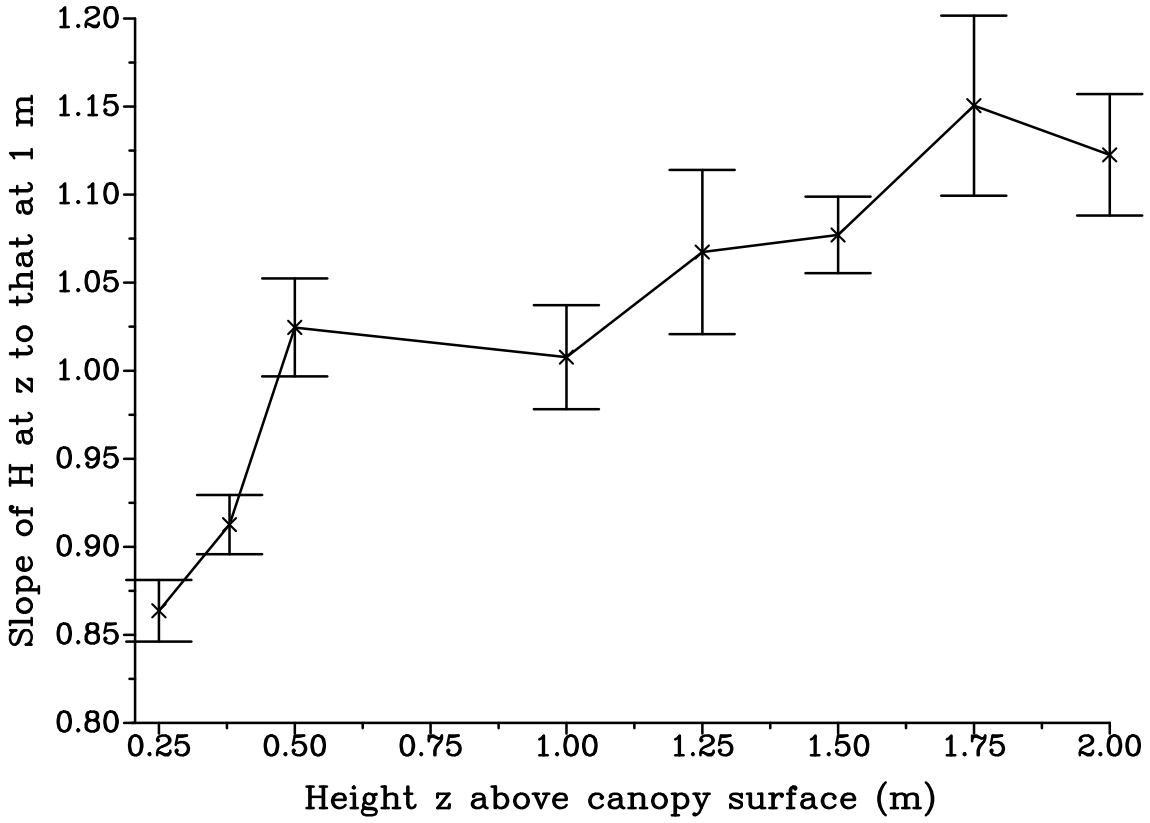

Fig. 9.7. The variation of the slope of the relationship sensible heat flux measured at height *z* as a function of that at height 1.00 m. The bars above and below each datum point show the 95 % confidence limit of the slopes measured at 1.00 m using system #1.

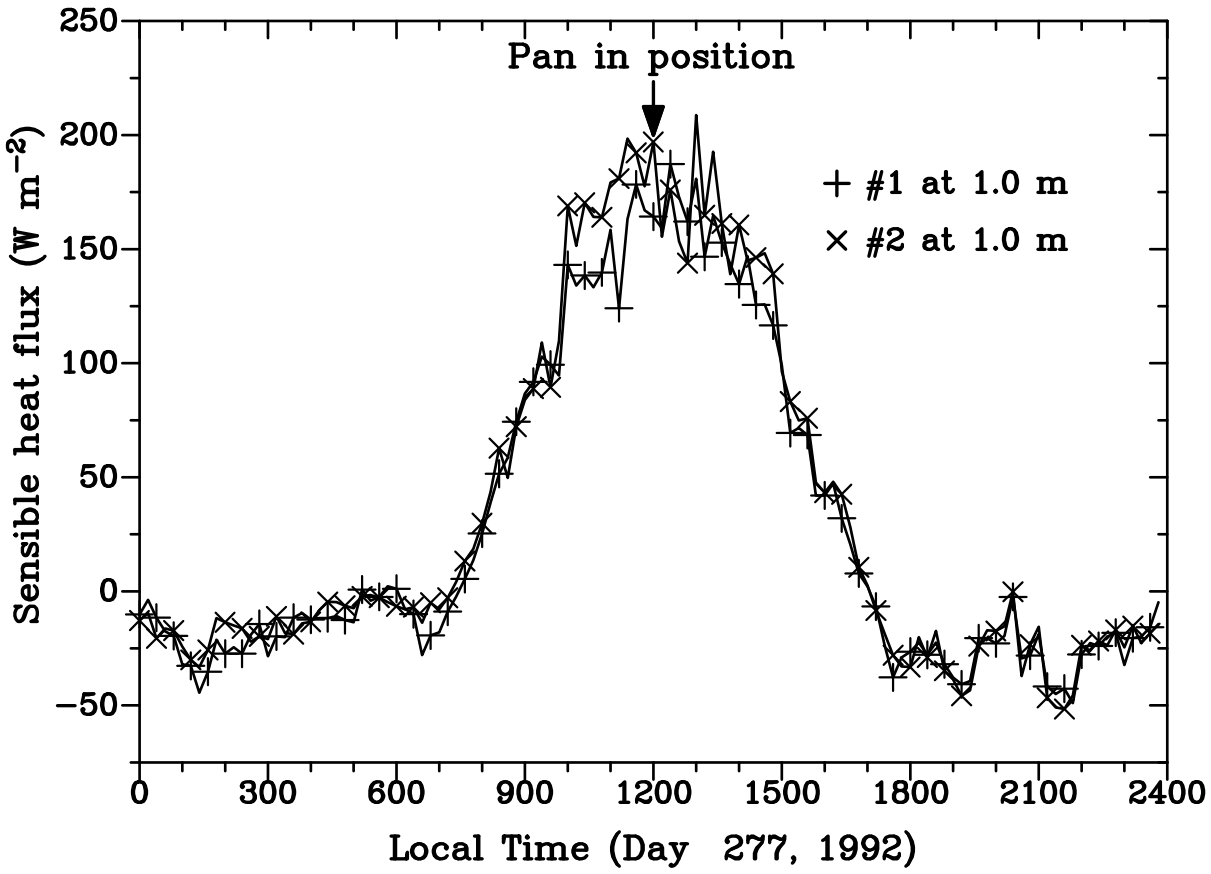

Fig. 9.8. The diurnal variation of Day 277, 1992 for system 1 placed at 1.00 m above the canopy and 2 also at 1.00 m above the grassland surface but with a metal pan located 0.27 m beneath the fine-wire thermocouple. The arrow shows the time at which the pan was placed beneath system 2 (and kept in position for the rest of the Day 277).

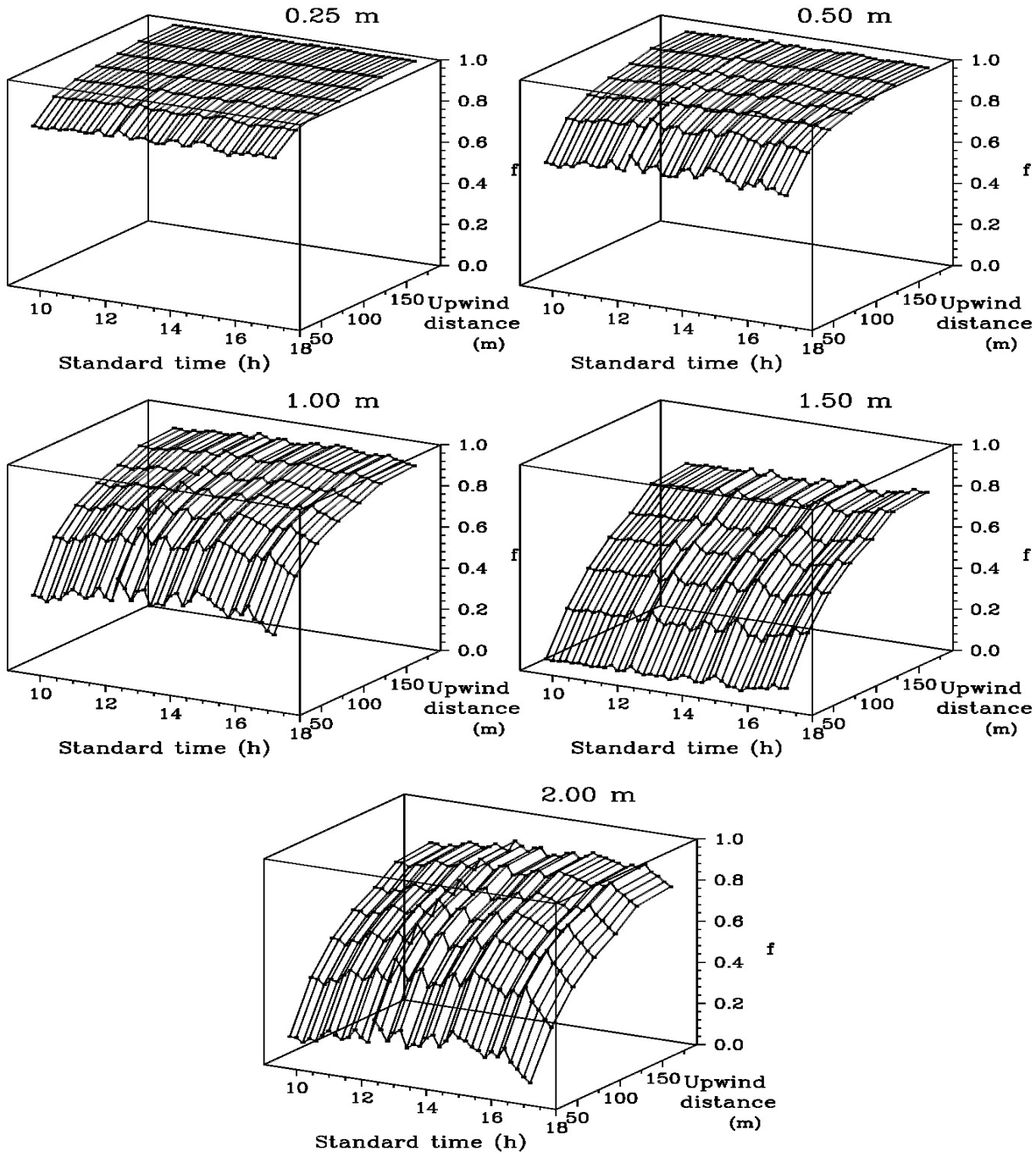

Fig. 9.9. Three dimensional representation of the diurnal variation for our grassland canopy in the cumulative footprint prediction, describing the fraction of sensible heat that can be expected to emanate from within the adjacent upwind area a horizontal distance *x* from the measurement point, for above-canopy placement heights between 0.25 and 2.00 m. The fraction *f* was corrected for stability.

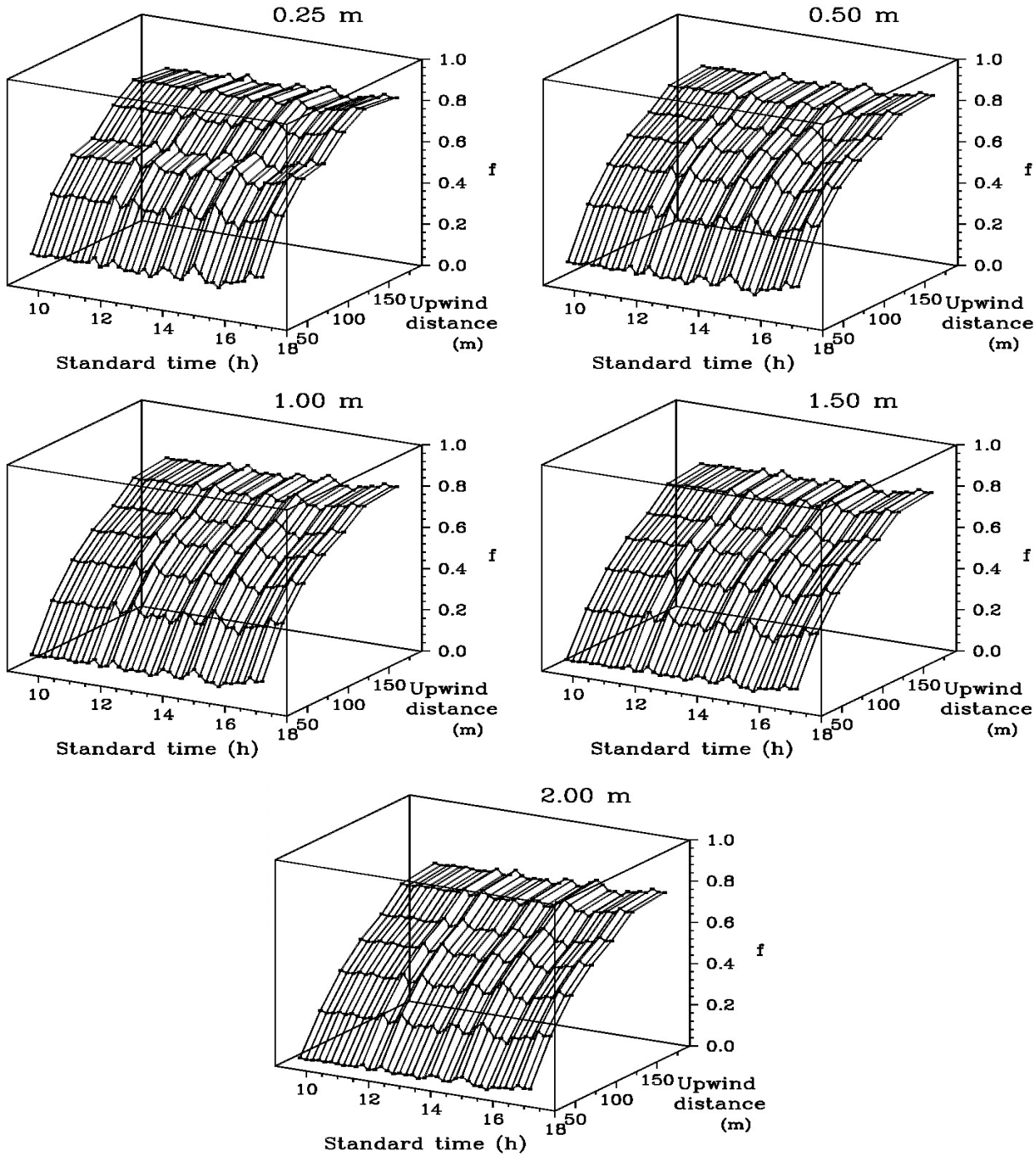

Fig. 9.10. Three dimensional representation of the diurnal variation for a forest canopy in the calculated footprint prediction for above-canopy placement heights 0.25 to 2.00 m. The fraction *f* was corrected for stability.

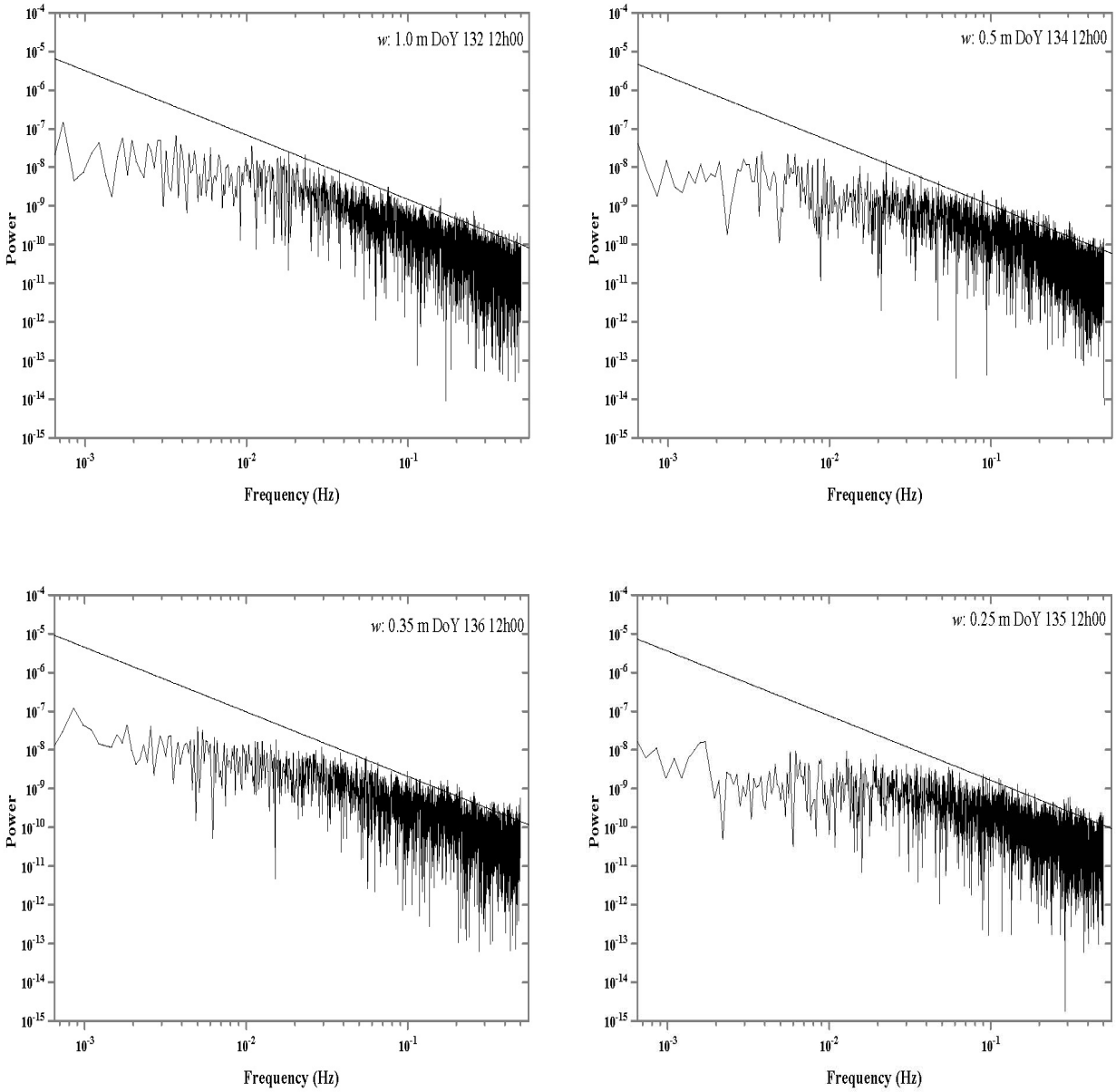

Fig. 9.11. Spectral analysis results for vertical wind speed for placement heights of 1, 0.5, 0.35 and 0.25 m above the grass surface. The -5/3 Kolmogorov law for the inertial sub-range is indicated by the straight line shown in the log-log plots with the envelope of points approaching the -5/3 curve at the higher frequencies.

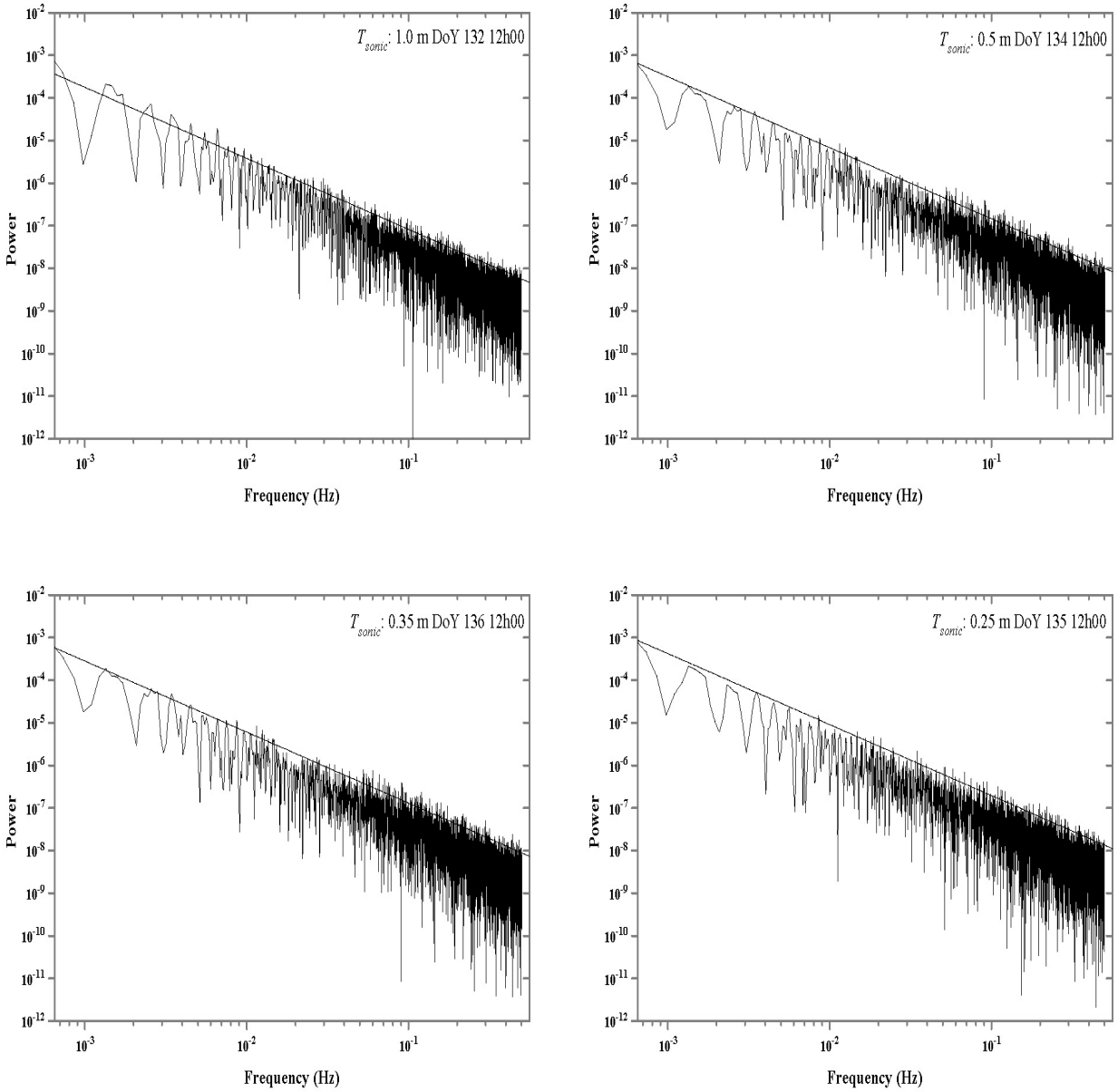

Fig. 9.12. Spectral analysis results for sonic temperature for placement heights of 1, 0.5, 0.35 and 0.25 m above the grass surface. The -5/3 Kolmogorov law for the inertial sub-range is indicated by the straight line shown in the log-log plots with the envelope of points approaching the -5/3 curve at the higher frequencies.

Table 9.1. First three data columns: associated statistical parameters for the linear regression of *H* at 1.00 m measured using systems #2 and #3 compared with that measured at 1.00 m using system #1; last data column: statistics for the comparison of *H* at 1.00 m using systems #2 placed at 1.00 m but with a pan placed 0.27 m beneath the fine-wire TC compared with that at 1.00 m using system #1.

	#2 (*y*) vs #1 (*x*) both at 1 m	#3 (*y*) vs #1 (*x*) both at 1 m	#2 and #3 (*y*) vs #1 (*x*) both at 1 m	#2 with pan 0.27 m beneath fine-wire TC (*y*) *vs* #1 (*x*) both at 1 m
n	155	82	237	496
Intercept (W m^{-2})	2.21	2.71	2.57	2.65
SE intercept (W m^{-2})	2.82	3.43	2.14	0.85
t value for zero intercept[a]	0.7823	0.7889	1.2024	3.1297[b]
Slope	1.0065	1.0150	1.0076	1.0032
SE slope	0.0190	0.0267	0.0151	0.0099
Slope confidence interval	(0.9690, 1.0441)	(0.9617, 1.0682)	(0.9779, 1.0374)	(0.9837, 1.0227)
t value for unit slope[a]	0.3428	0.5591	0.5049	0.3236
$S_{y\text{-}x}$ (W m^{-2})	17.97	20.21	18.67	16.77
r^2	0.9483	0.9474	0.9498	0.9540
t value[c]	36.96	26.48	46.51	70.74
$RMSE_{unsystematic}$[d]	17.855	19.966	18.595	16.736
$RMSE_{systematic}$	3.079	4.345	3.510	2.783
$RMSE_{total}$	18.118	20.433	18.923	16.966

[a] Null hypothesis is that slope is 1 and intercept is 0;

[b] Statistical significance at the 95 % level of significance;

[c] $t = r[(n-2)/(1-r^2)]^{0.5}$

[d] $MSE_{total} = MSE_{systematic} + MSE_{unsystematic}; MSE_{systematic} = \sum_{i=1}^{n}(\hat{y}_i - x_i)^2 / n; MSE_{unsystematic} = \sum_{i=1}^{n}(\hat{y}_i - y_i)^2 / n$

Table 9.2. Associated statistical parameters for the linear regression of *H* at various heights *z* (m) measured using systems #2, #3 and #4 compared with that measured at 1.00 m using system #1.

	Measurements at height *z* (*y*) *vs* #1 at 1.00 m (*x*)						
	***z* = 0.25 m**	***z* = 0.38 m**	***z* = 0.50 m**	***z* = 1.25 m**	***z* = 1.50 m**	***z* = 1.75 m**	***z* = 2.00 m**
N	327	412	246	103	308	63	223
Intercept (W m^{-2})	-4.98b	1.41	-1.62	6.73[b]	2.04	3.92	1.89
SE intercept (W m^{-2})	1.04	0.89	1.65	3.01	1.24	2.92	2.5
t value for zero intercept[a]	-4.7751[b]	1.5943	-0.9807	2.2344[b]	1.6432	1.3416	0.7534
Slope	0.8636b	0.9126[b]	1.0245	1.0673[b]	1.0771[b]	1.1505[b]	1.1226[b]
SE slope	0.0089	0.0086	0.0142	0.0235	0.0111	0.0256	0.0176
Slope confidence interval	(0.8460, 0.8811)	(0.8957, 0.9295)	(0.9966, 1.0524)	(1.0210, 1.1136)	(1.0553, 1.0988)	(1.0993, 1.2016)	(1.0879, 1.1572)
t value for unit slope[a]	-15.3116[b]	-10.1858[b]	1.7288	2.8646[b]	6.9711b	5.8800[b]	6.9681[b]
$S_{y\text{-}x}$ (W m^{-2})	15.12	13.66	17.92	20.01	17.54	16.61	22.16
r^2	0.9666	0.965	0.9554	0.9533	0.9688	0.9707	0.9485
t value[c]	96.98	106.32	72.3	45.41	97.44	44.95	63.83
$RMSE_{unsystematic}$ [d]	15.072	13.629	17.846	19.813	17.487	16.347	22.06
$RMSE_{systematic}$	19.346	8.183	2.024	14.417	9.987	20.111	19.004
$RMSE_{total}$	24.524	15.897	17.96	24.503	27.474	25.917	29.117

[a] Null hypothesis is that slope is 1 and intercept is 0;

[b] Statistical significance at the 95 % level of significance;

[c] $t = r[(n-2)/(1-r^2)]^{0.5}$ [d] $MSE_{total} = MSE_{systematic} + MSE_{unsystematic}; MSE_{systematic} = \sum_{i=1}^{n}(\hat{y}_i - x_i)^2 / n; MSE_{unsystematic} = \sum_{i=1}^{n}(\hat{y}_i - y_i)^2 / n$

Table 9.3. Cumulative footprint prediction f (for a fetch of 190 m) as a function of placement height above the turf grass surface for two days at midday, with and without stability correction. Also shown is the position of the peak of the footprint x_{max} (m), horizontal wind speed U (m s^{-1}) and z/L.

Placement height (m)	f	f (stability corrected)	x_{max} (m)	x_{max} (stability corrected) (m)	U (m s^{-1})	z/L
Day of year 259, CST 12h00, u_* = 0.19 m s^{-1}						
0.25	0.97	0.96	6.6	5.5	2.18	-0.07
0.50	0.91	0.93	16.0	10.2	2.59	-0.13
1.00	0.83	0.87	36.0	18.0	2.89	-0.26
1.25	0.74	0.83	58.4	24.9	3.12	-0.33
1.50	0.66	0.79	79.3	31.2	3.17	-0.40
Day of year 263, CST 12h00, u_* = 0.24 m s^{-1}						
0.25	0.97	0.96	5.5	4.7	2.25	-0.06
0.50	0.92	0.93	13.9	8.6	2.78	-0.12
1.00	0.85	0.88	32.0	15.3	3.17	-0.24
1.25	0.77	0.84	51.0	21.1	3.36	-0.30
1.50	0.69	0.81	70.8	26.5	3.49	-0.36

10 OPEN WATER EVAPORATION ESTIMATION FOR A SMALL SHALLOW RESERVOIR IN WINTER USING SURFACE RENEWAL[1]

10.1 Summary

Evaporation is one of the main components of the energy and water balance of reservoir water behind dams and is a major component of water loss. Measurements in winter of sensible heat (H) for the small and shallow reservoir of Midmar Dam, KwaZulu-Natal, South Africa were made using the surface renewal (SR) method, a renewal model method that uses the average cubic air temperature structure function and eddy covariance (EC). The small magnitude of H during winter makes it difficult to test the reliability of the H estimates obtained using instruments and sensors mounted above the water surface using the SR, renewal model and EC methods. Latent energy flux was estimated as a residual of the energy balance using additional measurements of net irradiance R_n above the water surface and the water-stored heat flux. The SR sensible heat flux (H_{SR}) was estimated for heights of 1.0, 1.3, 1.9 and 2.5 m above the water surface using two air temperature time lags r of 0.4 and 0.8 s of the 10-Hz measurements. The SR method depends on a weighting factor α which represents the capability of the atmospheric turbulence to mix the scalar, within the air parcel to be renewed. The factor α was determined for each measurement height and time lag from the slope of a linear regression relationship forced through the origin of measured EC sensible heat flux (H_{EC}) values on the y-axis *vs.* H_{SR} or renewal model H on the x-axis. All α values obtained using the renewal model method were not statistically different from that obtained using the SR method for z = 1.0 m for both time lags. Using a calibration dataset, an average α value for the 1.0- and 1.3-m heights of 0.198 for r = 0.4 s and 0.245 for r = 0.8 s for the SR and renewal model methods was obtained. The 30-min H_{SR}, renewal model and H_{EC} estimates were often the smallest component of the energy balance (generally -40 to 40 W m^{-2}) and compared reasonably well for the validation dataset. The heat storage flux G was larger in magnitude (0 to 200 W m^{-2}) compared to the sensible heat flux. The SR, renewal model and EC latent energy fluxes, each calculated as residuals of the energy balance, were almost the same in magnitude as the available energy flux $R_n - G$ due to the relatively small magnitude of the sensible heat flux during the winter measurement period. The daily evaporation ranged between 1.0 and 3.9 mm.

Keywords:

Sensible heat flux

Cubic air temperature structure function

Latent energy flux

Eddy covariance

Heat stored in water

[1] Based on Mengistu and Savage (2010)

10.2 Introduction

Evaporation from open water surfaces and from land surfaces covered with vegetation is one of the main components of the hydrologic cycle. Estimates of the amount and rate of evaporation from open water surfaces are required in water resource management for a variety of purposes, such as the design of storage reservoirs, catchment water balance studies, municipal and industrial water supply, irrigation of agricultural lands and management of wetlands (Brutsaert, 1982; Marsh and Bigras, 1988; Finch, 2001). However, studies of open water evaporation from fresh water systems are predominantly for reservoirs and larger lakes with relatively few investigations for smaller reservoirs and ponds (Rosenberry et al., 2007).

Different methods have been used in the past to estimate open water evaporation, such as the water balance method, mass transport approach, potential evaporation approach (Penman, 1948), floating pans, FAO-56 reference evaporation estimation using the Penman-Monteith method, Priestley-Taylor method, models based on meteorological data, Bowen ratio energy balance (BREB) method and the eddy covariance (EC) method (Rosenberg et al., 1983). A model based on the concept of an equilibrium temperature for the water body for the determination of the energy balance for a well-mixed body of water, which takes into account the heat stored in the water body was introduced by Edinger et al. (1968) and further developed by Keijman (1974) and de Bruin (1982). Short-term measurements of shallow lake evaporation using the EC and energy balance methods were compared by Stannard and Rosenberry (1991) and Assouline and Mahrer (1993). The accuracy and reliability of different methods for estimating open water evaporation are discussed in detail by Craig and Hancock (2004). Craig (2006) used the Penman-Monteith method and accurate water depth measurements using a pressure-sensitive transducer to estimate evaporation and seepage losses of agricultural water storages. Rosenberry et al. (2007) compared the BREB method with 15 different evaporation methods for a small mountain lake. Assouline et al. (2008) compared evaporation estimates from three water bodies of different sizes and climates.

Surface renewal (SR) analysis is a relatively low-cost and simple method for estimating sensible heat flux, latent energy flux, and other scalars (Paw U et al., 1995; Snyder et al., 1996; Spano et al., 1997a, b, 2000; Paw U et al., 2005; Castellví et al., 2006) that requires calibration and validation against a standard measurement method. The SR method has the advantage over other micrometeorological methods since it requires only temporal measurement of the scalar of interest at one point. The SR analysis for estimating sensible heat flux, used almost exclusively above canopies and bare soil, involves high frequency air temperature measurements, typically between 2 and 10 Hz, using unshielded and naturally-ventilated fine-wire thermocouples. The SR method has been used for estimating sensible heat flux and latent energy flux above different surfaces such as bare soil, short canopies and tall vegetation. Zapata and Martínez-Cob (2001) used the SR method to estimate latent energy flux from an endorreic salty lagoon, an aquatic environment characterized by short, sparse vegetation with high proportions of bare soil. However, we are unaware of previously reported studies in the scientific literature for estimating open water evaporation using the SR method.

This study presents the use of the SR and renewal model methods for estimating winter sensible heat flux and open water evaporation from a shallow reservoir. The SR method, and the renewal model method, have not been tested over open water surfaces. The aim of this study is therefore to calibrate the sensible heat flux obtained with the SR and renewal model methods against

measurements obtained using the EC method and to evaluate the performance of the SR and renewal model methods for estimating sensible heat flux, and latent energy flux as a residual of the energy balance, above an open water surface. The range of sensible heat is small and this presents an added difficulty in testing the reliability of these two air temperature based methods above open water, during periods of low sensible heat flux, and comparisons with EC measurements.

10.3 Theory

For the SR analysis, it is assumed that turbulent coherent structures exchange scalars, air temperature and water vapour pressure for example, between the surface and the atmosphere (Paw U et al., 1995, 2005; Snyder et al., 1996; Castellví et al., 2006). High frequency air temperature fluctuations exhibit organized coherent structures, as shown in Fig. 10.1, which resemble ramp events (Bergström and Högström, 1989; Gao et al., 1989; Shaw et al., 1989). The SR method assumes that the sensible heat flux $H = H_{\mathrm{SR}}$ at measurement height z is determined as:

$$H_{\mathrm{SR}} = \alpha z \rho c_p \frac{a}{\tau} \tag{10.1}$$

where α is a correction or weighting factor, ρ the air density, c_p the specific heat capacity of air at constant pressure and a the amplitude and τ the total ramp period corresponding to the inverse ramp frequency of the air temperature ramps. The variable αz in Eq. (10.1) represents the volume of air per unit ground area exchanged on average for each ramp in the sample period for the measurement height z (Paw U et al., 1995). Castellví et al. (2002) interpreted αz as the mean eddy size responsible for the renewal process. The amplitude a and inverse ramp frequency τ can be determined from the second, third, and fifth order of the structure function for air temperature (van Atta, 1977). The structure function is defined as:

$$S^n(r) = \frac{1}{m-j} \sum_{i=1+j}^{m} (T_i - T_{i-j})^n , \tag{10.2}$$

where n is the order of the air temperature structure function for which n = 2, 3 and 5 for SR analyses, m the number of data points measured at frequency f in Hz in the averaging time interval, T_i the i th air temperature sample, and j the number of lags between measurements corresponding to an air temperature time lag $r = j/f$.

Chen et al. (1997a, b) developed a renewal model method based on the formation of air temperature ramps, which estimates H from high frequency air temperature measurements using a cubic air temperature structure function corresponding to n = 3 in Eq. (10.2), and the additional measurement of friction velocity. According to the model, H is estimated in the roughness and inertial sublayers as:

$$H = -\alpha\beta^{2/3}\gamma\rho c_p \left[\frac{S^3_{(r_m)}}{r_m}\right]^{1/3} u_*^{2/3} \frac{z}{(z-d)^{2/3}}, \tag{10.3}$$

where $\alpha\beta^{2/3}\gamma$ is a combined empirical coefficient which is roughly 0.4 for bare soil, mulch and forest, $S^3_{(r_m)}$ the third order of the structure function for air temperature, r_m the time lag that maximizes $(S^3_{(r)}/r)^{1/3}$, u_* the friction velocity and d the zero-plane displacement height (Chen et al., 1997b). The zero-plane displacement height is approximately $2/3$ of the canopy height h. For this study over

water, h is zero and consequently d is assumed to be zero. Chen et al. (1997b) obtained values for the coefficients α, β and γ for bare soil, straw mulch and forest. The values for the coefficients β and γ obtained by Chen et al. (1997b) for bare soil are used for this study over water, corresponding to h and d equal to zero.

The heat flux stored in water G can be determined from profile measurements of water temperature (Brutsaert, 1982) as:

$$G = \rho_w c_w \Delta z \frac{\overline{\Delta T_w}}{\Delta t} \tag{10.4}$$

where ρ_w is the density of water, c_w the specific heat capacity of water, Δz the depth increment in water, $\overline{\Delta T_w}$ the average water temperature difference from one averaging time period to another for depth increment Δz and Δt the change in time for the averaging period. The vertical heat flux is assumed equal to 0 W m^{-2} at the bottom of the reservoir and it is also assumed that there is little or no horizontal or vertical advection of energy in the water.

The shortened energy balance equation may be used to estimate the latent energy flux λE above the water surface using the SR, renewal model and EC methods from measured net irradiance R_n above the water surface, the sensible heat flux H and the heat flux stored in water G using:

$$\lambda E = R_n - H - G\,. \tag{10.5}$$

10.4 Materials and methods

Field work was carried out at the reservoir behind Midmar Dam near Howick, in the midlands of KwaZulu-Natal, South Africa (29°30′ S, 30°10′ E, elevation 985 m) from day of year 186 to 201 (5th to 20th July, 2007). The reservoir is relatively small with a surface area of 1793.15 ha and a net volume capacity of 235.42 million m^3 (Department of Water Affairs and Forestry, 2007). The site has a summer rainy season and is characterized by warm and wet days with air temperatures exceeding 30 °C in summer. In winter, the days are dry and frequently cold with air temperatures less than 20 °C and decreasing to just less than 0 °C during the night. The mean annual rainfall is 992 mm (popular literature), with November to January being the wettest months. Prevailing winds are from the southeast, east and south which correspond to water to land wind flows at the measurement site.

A three-dimensional ultrasonic anemometer (model 81000, RM Young, Traverse City, Michigan, USA) was used to measure sensible heat flux and friction velocity, using the EC method, at 2.50 m above the water surface. All sensors were mounted on scaffolding which was installed inside the reservoir, 75 m from the shore line. The 3D sonic was connected to a CR3000 datalogger (Campbell Scientific Inc., Logan, Utah, USA). The 3D sonic was internally configured to sample at a frequency of 20 Hz and output data to the datalogger at a frequency of 10 Hz. The EC data were processed offline. Friction velocity u_* was calculated as $[(\overline{u'w'})^2 + (\overline{v'w'})^2]^{1/4}$ (Stull, 1988; Garratt, 1992), where u', v', and w' are the fluctuations from the mean of the three-dimensional orthogonal wind speeds $\overline{u}$, $\overline{v}$ and $\overline{w}$ respectively. Eddy covariance sensible heat flux H_{EC} was estimated as $H_{\mathrm{EC}} = \rho c_p \overline{w'T_s'}$, where w' is the vertical wind speed fluctuation and T_s' is the fluctuation from the mean sonic temperature. Corrections applied to the EC data (Oncley et al., 2007) included applying an

averaging coordinate rotation procedure (Kaimal and Finnigan, 1994) for removing instrument tilt and air flow irregularity effects, wake and crosswind corrections and the correction for water vapour pressure and the Bowen ratio (Odhiambo and Savage, 2009). Water vapour pressure was measured at two heights using two Vaisala/Campbell hygrometers (model HMP45C, Helsinki, Finland). The Bowen ratio was then estimated from the water vapour pressures and aspirated air temperature measurements, the latter from a pair of aspirated type-E fine-wire thermocouples. The heights for the Bowen ratio measurements were 1.0 and 2.5 m above the water surface.

For the SR and renewal model methods, four unshielded and naturally-ventilated type-E fine-wire thermocouples (75-μm diameter) were used to measure air temperature, placed at heights of 1.0, 1.3, 1.9 and 2.5 m above the water surface. The choice of thermocouple size was based on the finding by Duce et al. (1998) that compared to 12.5 and 25.4 μm thermocouples, use of the 75-μm diameter thermocouples resulted in the lowest root mean square error (RMSE) when comparing H_{SR} with H_{EC}. In the current Midmar study, thermocouple measurements were made differentially and air temperature data were sampled at a frequency of 10 Hz. Online time lags of 0.4 and 0.8 s, also used in many other studies, were used in obtaining the second, third and fifth air temperature structure function values as required by the van Atta (1977) approach (n = 2, 3 and 5 in Eq. (10.2)). An iterative procedure, discussed in an Appendix to the thesis, was used to calculate the amplitude a and the inverse ramp frequency τ. As a further justification of the choice of lag times, postdata calculations demonstrated that the coefficient of correlation (R^2) for the H_{EC} (y) and H_{SR} (x) linear regressions were generally lower for time lags of 0.1 to 0.3 s and with greater RMSE compared to that for 0.4 s with a similar R^2 and RMSE for 0.8 to 1.0 s (data not shown). The online air temperature structure function data were averaged and stored every two minutes in the datalogger. Subsequent to the collection of the structure functions, post-processing was required to calculate H_{SR}. Structure functions using the time lags and the analysis technique of van Atta (1977) were used to determine the amplitude a and the inverse ramp frequency τ characterizing the air temperature fluctuations and hence the sensible heat H_{SR} using Eq. (10.1) as presented by Snyder et al. (1996). The 2-min H_{SR} values were then averaged to 30 min. For the renewal model estimates of H, the coefficients of β and γ of Eq. (10.3) were set to 0.398 and 1.104 respectively, corresponding to values obtained by Chen et al. (1997b) for their experiment over bare soil. The value of $S_{(r)}^3/r$ in Eq. (10.3) was determined from the high frequency air temperature data. The parameter α in Eqs. (10.1) and (10.3) for each height was obtained from the slope of the linear regression, forced through the origin, of measured H_{EC} (y) *vs.* H_{SR} or H of the right-hand side of Eqs. (10.1) and (10.3) respectively using α = 1 (x) for all 30-min measurement periods. Data for the period 5th to 17th July (day of year 186.5 to 198.0) were used as the calibration dataset for which the SR and renewal model estimates of H were compared with H_{EC} using the linear regression analysis. The data for the period 18th to 21st July (day of year 198.0 to 201.0) were used for validation purposes.

Net irradiance was measured using a NR Lite domeless net radiometer (Kipp and Zonen, Delft, The Netherlands) at 2.40 m above the water surface. Water temperature (T_w) at different depths was measured using seven type-E thermocouples attached to a hollow aluminium pole with the one end attached to a polystyrene float to measure the surface temperature of the water. A sink load was connected to the other end of the pole to ensure a vertical position of the pole. A Campbell CR23X datalogger was used for these measurements, every 1.0 s, with averages obtained every two minutes which were in turn used to calculate 30-min averages for estimating the latent energy flux using Eq.

(10.5). The water temperature measurement depth was adjusted according to the decrease in reservoir water depth due to evaporation and stream flow reduction. At the beginning of the experiment, the reservoir water depth was 0.75 m and the T_w-measurement depths were 0 (surface of the water), 20, 40, 80, 160, 320 and 640 mm below the surface. The water depth decreased to 0.54 m on day of year 192 and the T_w-measurement depths were adjusted to 0, 20, 40, 80, 160, 260 and 520 mm. Towards the end of the experiment, on day of year 199, the water depth had decreased to 0.40 m and T_w measurements were taken at 0, 20, 40, 80, 140, 240 and 380 mm below the water surface. Measurements of the vertical heat flux at the bottom of the reservoir were obtained using soil heat flux plates (model HFT-3, REBS, Seattle, Washington, USA) but the magnitude of these measurements was negligibly small.

10.5 Results and discussion

10.5.1 Ramp amplitude and ramp period for the SR method

For the calibration dataset (5th to 17th July), the frequency distribution of the 2-min events for ramp amplitude a and ramp period τ are shown together with the cumulative probability distribution for the 1-m height for a lag time of 0.4 s (Fig. 10.2). Generally, there were fewer stable events corresponding to $a < 0$ ^{o}C compared to unstable events (Fig. 10.2a). More than 50 % of the 2-min ramp events were unstable with amplitudes between 0.4 and 1.0 ^{o}C. For the van Atta analysis, the 2-min calibration dataset was separated into two: data for which the ramp period was less than or equal to 20 s and data for which the ramp period exceeded 20 s (Fig. 10.2b). The former data subset, corresponding to events for which there are six ramps or more in a 2-min period, represented more than two-thirds of the ramp events of the calibration period. Fig. 10.2a and b therefore indicate reasonable ramp events for the 2-min interval dataset.

10.5.2 Sensible heat flux

The 30-min H_{EC} values (y) were plotted against SR sensible heat flux H_{SR} estimates (x) computed using Eq. (10.1) for the calibration dataset at measurement heights of 1.0, 1.3, 1.9 and 2.5 m above the water surface for time lags r = 0.4 and 0.8 s to indirectly determine the weighting or calibration factor α by forcing the linear regression through the origin (Table 10.1). About 20 % of the 2-min dataset, from which the 30-min dataset was generated, contained data pairs for which H_{SR} and H_{EC} were of opposite sign, corresponding to an impossible probable negative α value. These data pairs were therefore removed from the regression analysis resulting in the R^2 values for the H_{EC} and H_{SR} relationships increasing and the computed α value increasing by about 20 % (data not shown). Castellví et al. (2006) also noted that in some cases the H_{EC} and H_{SR} data pairs had different signs. The α values obtained for the SR method using Eq. (10.1) for the time lag of 0.8 s were significantly greater, at the 95 % level of significance, than those for the 0.4-s time lag for all SR datasets (Table 10.1). Furthermore, for all measurement heights and each time lag the SR Eq. (10.1) regressions for data for which $\tau >$ 20 s, corresponding to fewer than six ramps in a 2-min event period, resulted in a significantly increased α. There was a significantly decreased α for $\tau \leq$ 20 s. The α values corresponding to $\tau >$ 20 s and $\tau \leq$ 20 s were almost always significantly different at the 95 % level from the α for the full dataset (Table 10.1). There were fewer ramps within the 2-min periods for the 1.9- and 2.5-m heights, upon which the 30-min data were based, resulting in a reduced dataset compared to that for the 1.0- and 1.3-m heights. In general for the SR method using Eq. (10.1), α

decreased with increasing height for all datasets. As shown in Table 10.1, which excluded data for day of year 198 to 201 inclusive used for validation purposes, the α values obtained indirectly using Eq. (10.1) varied with measurement height and time lag. For each linear regression, R^2 and the Nash-Sutcliffe efficiency coefficient (Nash and Sutcliffe, 1970) were calculated. The efficiency coefficient provides a quantitative measure for the comparisons with a value of 1 corresponding to perfect agreement between H_{EC} and H_{SR} and varied between 0.28 and 0.47 for the various SR regressions shown in Table 10.1.

The combined empirical coefficient $\alpha\beta^{2/3}\gamma$ (Eq. (10.3)), a roughly constant value of 0.4 for bare soil, mulch and forest, resulted in H_{SR} being overestimated compared to the measured H_{EC}. The value 0.4 for the combined coefficient does not hold true for an open water surface. Therefore, the parameter α for the renewal model method using Eq. (10.3) for each height and time lag was determined from the slope of the linear regression forced through the origin of measured H_{EC} (y) values *vs.* the right-hand side of H (Eq. (10.3)) (x) using β = 0.398 and γ = 1.104, values obtained by Chen et al. (1997b) for bare soil. The α values for the renewal model method using Eq. (10.3) tend to be smaller for the time lags r = 0.4 compared to that for 0.8 s, but the differences are not statistically different at the 95 % level of significance. All α values obtained using Eq. (10.3) are not statistically different from those obtained using Eq. (10.1) for z = 1.0 m and both time lags. Average α values for all measurement heights of 0.203 for r = 0.4 s and 0.217 for r = 0.8 s were obtained using Eq. (10.3). Different α values for different time lags, shown also by Snyder et al. (1996), occur since the ramp period depends on time lag due in turn to the procedure used to estimate the ramp period.

There are no previously determined α values for an open water surface in the scientific literature reported against which the α values of Table 10.1 could be compared. Of note though is that for a bare soil surface, α = 0.69 (r = 0.1 s) for measurements at 0.03 m above the surface (Chen et al., 1997b). A value for α for rice of 0.38 was determined by Snyder et al. (undated). Also, α obtained for the renewal model method was not statistically different from that obtained for the 1.0-m height and a time lag of 0.4 s.

The SR and renewal model estimates of H using Eqs. (10.1) and (10.3) respectively were compared with H_{EC} values to investigate the performance of each of the methods. Typical diurnal variation of H_{EC}, H_{SR} and renewal model H, for the four heights, averaged for the two time lags and calibrated using α values (Table 10.1) is shown in Fig. 10.3 for two days of the calibration period and for the validation period. The sensible heat flux values were small (-40 to 40 W m^{-2}), and less than 30 W m^{-2} in magnitude for most days. Sensible heat flux values obtained from shallow water bodies in warm environments measured using the EC method were also small, generally between -50 to 50 W m^{-2} (Stannard and Rosenberry, 1991; Assouline and Mahrer, 1993). The sensible heat fluxes estimated using Eqs. (10.1) and (10.3) compared reasonably well with H_{EC} measurements for all heights (Fig. 10.3).

The sensible heat flux values peaked between 09h00 and 10h00 as shown in Fig. 10.3. Sensible heat flux was positive in the morning and negative in the afternoon. In the morning, the water temperature was greater (2 to 3 ^{o}C) than the air temperature and hence the sensible heat flux was from water to the air resulting in positive H_{EC}, H_{SR} and renewal model values. In the afternoon, water

temperatures were less than the air temperature resulting in a downward sensible heat flux and negative H_{EC}, H_{SR} and renewal model H. In general, the SR and renewal model methods, once calibrated, performed reasonably well in estimating H (Fig. 10.3, validation period).

10.5.3 Heat stored in water

Heat storage flux in water G was calculated from the 2-min temporal changes in mean water temperature using Eq. (10.4). The heat storage flux fluctuated from negative to positive for each 2-min period, due to turbulent water waves of varying temperature travelling past the thermocouples as also noted by Tanny et al. (2008). Following the procedure of Burba et al. (1999), the heat storage flux was smoothed by calculating hourly running means of G for the 2-min data. The smoothed 2-min data were then averaged to 30 min for the latent energy flux calculations. The diurnal variations of the 30-min sensible heat flux H_{SR} at the 1-m height estimated using Eq. (10.1) and H_{EC}, stored heat flux G (Eq. (10.4)), net irradiance R_n above the water surface, the mean water temperature T_w and air temperature T_a are shown in Fig. 10.4.

The heat storage flux followed the diurnal variation in R_n and peaked at the same time as the peak in R_n. The water temperatures were low (8 to 14 ^{o}C) and followed the pattern of R_n with G ranging from -100 to 100 W m^{-2} for most days with extremes of -200 to 200 W m^{-2} for day of years 188, 189 and 193 (data not shown). The heat storage flux was much larger in magnitude compared to the sensible heat flux and a significant proportion of R_n. Therefore G plays a significant role in the sub-hourly energy balance and consequent evaporation estimation using Eq. (10.5) of shallow water bodies.

10.5.4 Latent energy flux

The latent energy flux λE was estimated, using Eq. (10.5), as a residual of the shortened energy balance equation. The linear regression analysis of the average latent energy flux from the SR (λE_{SR}) and renewal model analyses for the four heights for r = 0.4 and 0.8 s *vs.* the latent energy flux λE_{EC} calculated from H_{EC}, R_n and G for a height of 2.5 m above the water surface are presented in Table 10.2. The λE_{SR} and renewal model λE estimates using H estimated using Eqs. (10.1) and (10.3) respectively gave good estimates of λE_{EC} as shown in Table 10.2 – largely due to the available energy flux $R_n - G$ being common to the λE values calculated.

The magnitudes of the 30-min λE_{EC} and λE_{SR} values ranged from 20 to 450 W m^{-2} during the day and 0 to 100 W m^{-2} during the night. Generally, the magnitude of λE_{SR} increased from 30 W m^{-2} at 09h00 to 200 W m^{-2} at 11h00. The latent energy fluxes, λE_{EC} and that for the SR and renewal model methods peaked between 13h00 and 14h00. The magnitudes of the three 30-min λE estimates were almost the same in magnitude as the available energy flux $R_n - G$, because of the relatively small magnitudes of the sensible heat fluxes during the winter measurement period.

The daily total evaporation (mm), for the entire measurement period, using the E_{EC}, E_{SR} and renewal model estimates at 1.0 m is shown in Fig. 10.5. The daily total evaporation ranged between 1.0 and 3.9 mm. The daily average evaporation for the measurement period was 2.16 mm. Previously reported values of the daily evaporation rates from open water surface range between 2 and 5 mm in

winter (de Bruin, 1982) and 5 to 10 mm in summer (Burba et al., 1999; Gianniou and Antonopoulos, 2007).

10.6 Overall discussion

The range of H is small and this presents an added difficulty in testing the reliability of these two air temperature based methods above open water, during periods of low H, and comparisons with EC measurements. Furthermore, the measured heat storage flux fluctuated from negative to positive for each averaging period, due to unavoidable turbulent water waves of varying temperature travelling past the thermocouples. As a result, the heat storage flux required smoothing by calculating hourly running means. Also, about 20 % of the original dataset contained data pairs for which H_{SR} and H_{EC} were of opposite sign, corresponding to an impossible probable negative α value. At the insistence of a reviewer, these data pairs were removed from the regression analysis with R^2 values for the H_{EC} and H_{SR} relationships increasing and the computed α value increasing by about 20 %. Indeed, many published works show graphs with H_{EC} and H_{SR} of opposite sign. However, since the H_{SR} and H_{EC} and were small in magnitude, and given that both SR and EC methods have measurement uncertainty, an opposite sign for H_{SR} and H_{EC} may not in fact imply a negative α value. If most of the dataset had values of opposite sign then α would be negative, but this is not the case. If this argument is accepted, the α values of Table 10.1 should be decreased by about 20 %. Another contestation with regard to the open-water evaporation work is the averaging period for the SR measurements of H. A reviewer maintained that for the averaging period used for the SR measurements of H, viz. 2 min, there should be at least six air temperature ramps, corresponding to a ramp period $\tau \leq$ 20 s. This condition was not investigated for the mesic grassland study for the reported data (Appendix to the thesis). More recent calculations (data not shown) for this site show that for unstable and stable conditions, for three weeks of half-hourly grassland SR estimates of H, less than 1 % of the H values should be excluded based on the condition that ideally $\tau \leq$ 300 s, i.e. that there be at least six ramps in the averaging period of 30 min. Furthermore, about 5 % of the SR and EC fluxes are opposite in sign. The Appendix to the thesis finds that for a two-week period for stable conditions, a value for H is obtained, by the iterative procedure, less than 40 % of the time compared to in excess of 95 % for unstable conditions. If both the $\tau \leq$ 300 s condition and the same flux sign condition are also applied to these results, then solutions or H would be possible for 37.1 and 88.7 % of the stable and unstable cases respectively. These percentages are lower than those reported in the literature and patching of data using another method may be required to allow calculation of daily total evaporation.

10.7 Summary and conclusions

Sensible heat flux was estimated using the eddy covariance EC, surface renewal SR and renewal model methods in winter 2007, over an open water surface, in the small and shallow reservoir behind Midmar Dam in the midlands of KwaZulu-Natal, South Africa. The performance of the SR and renewal model methods in estimating the sensible heat flux is evaluated at heights of 1.0, 1.3, 1.9 and 2.5 m above the water surface using two air temperature time lags r = 0.4 and 0.8 s. The calibration or weighting factor α for each height and time lag was indirectly determined from the slope of the linear regression forced through the origin of measured H_{EC} values (y) *vs.* H_{SR}, or *vs.* H (x) for the renewal model method. For the calibration dataset, due to the procedure used to estimate the ramp period, the average α value for the SR and renewal model methods for the 1.0- and 1.3-m heights differed for the two time lags used: α = 0.198 for r = 0.4 s and 0.245 for r = 0.8 s. All α values

obtained using the renewal model method were not statistically different from that obtained using the SR method for z = 1.0 m and for both time lags. The sensible heat flux values were small (-40 to 40 W m^{-2}) for all days during the measurement period. The water-stored heat flux was much larger in magnitude (0 to 200 W m^{-2}) compared to the sensible heat flux. Therefore, the storage heat flux plays an important role in the sub-hourly energy balance and evaporation estimation of shallow water bodies. The EC, SR and renewal model latent energy fluxes were almost the same in magnitude as the available energy flux, due to the relatively small magnitude of the sensible heat flux for the winter measurement period. The daily total evaporation ranged between 1.0 and 3.9 mm. The daily total evaporation estimates for the entire measurement period using the EC, SR and renewal model methods averaged 2.70 mm. The SR method is simple and low-cost and yields reasonable estimates of sensible heat, from which latent energy fluxes may be calculated over an open water surface once the weighting factor α is determined.

10.8 Acknowledgements

We acknowledge the staff of the Department of Water Affairs and Forestry offices at Midmar for allowing the use of their facilities for this work. This work would not have been possible without the technical support from Mr Eltayeb S. Nile and Mrs. J. Manickum, (University of KwaZulu-Natal) and Mr A.D. Clulow, Professor C.S. Everson and Dr C. Jarmain (Council for Scientific and Industrial Research, CSIR). Funding for this research from the University of KwaZulu-Natal, CSIR, and Water Research Commission (South Africa) as part of projects K1335 and K1567 is gratefully acknowledged.

10.9 References

Assouline, S., Mahrer, Y., 1993. Evaporation from Lake Kinneret. 1. Eddy correlation system measurements and energy budget estimates. Water Resour. Res. 29, 901–910.

Assouline, S., Tyler, S.W., Tanny, J., Cohen, S., Bou-Zeid, E., Parlange, M.B., Katul, G.G., 2008. Evaporation from three water bodies of different sizes and climates: Measurements and scaling analysis. Adv. Water Resour. 31, 160–172.

Bergström, H., Högström, U., 1989. Turbulent exchange above a pine forest: II. Organized structures. Boundary-Layer Meteorol. 49, 231–263.

Brutsaert, W.H., 1982. Evaporation Into the Atmosphere. Theory, History, and Applications. D. Reidel Publishing Co., Dordrecht, Holland, 299 pp.

Burba, G.G., Verma, S.B., Kim, J., 1999. Energy fluxes of an open water area in a Mid-Latitude prairie wetland. Boundary-Layer Meteorol. 91, 495–504.

Castellví, F., Martínez-Cob, A., Perez-Coveta, O., 2006. Estimating sensible and latent heat fluxes over rice using surface renewal. Agric. Forest Meteorol. 139, 164–169.

Castellví, F., Perez, P.J., Ibañez, M., 2002. A method based on high frequency temperature measurements to estimate sensible heat flux avoiding the height dependence. Water Resour. Res. 38 (6), WR000486–20, 1–10.

Chen, W., Novak, M.D., Black, T.A., Lee, X., 1997a. Coherent eddies and temperature structure functions for three contrasting surfaces. Part I: Ramp model with finite microfront time. Boundary-Layer Meteorol. 84, 99–123.

Chen, W., Novak, M.D., Black, T.A., Lee, X., 1997b. Coherent eddies and temperature structure functions for three contrasting surfaces. Part II: Renewal model for sensible heat flux. Boundary-Layer Meteorol. 84, 125–147.

Craig, I.P., 2006. Comparison of precise water depth measurements on agricultural storages with open water evaporation estimates. Agric. Water Manage. 85, 193–200.

Craig, I.P., Hancock, N., 2004. Methods for assessing dam evaporation - an introductory paper. In: IAA Conference, Adelaide, Australia, May 11–13, 16 pp.

de Bruin, H.A.R., 1982. Temperature and energy balance of a water reservoir determined from standard weather data of a land station. J. Hydrol. 59, 261–274.

Department of Water Affairs and Forestry, 2007. Information on South African dams. Hydrological services, Department of Water Affairs and Forestry. Available at (http://www.dwaf.gov.za/hydrology/dwafapp2_wma/). Accessed, July 18, 2009.

Duce, P., Spano D., Snyder, R.L., 1998. Effect of different fine-wire thermocouple design on high frequency temperature measurement. In: Proceedings of the 23rd Conference on Agric. Forest Meteorol. Albuquerque, New Mexico, Nov. 2–6, pp. 146–147.

Edinger, J.E., Duttweiler, D.W., Geyer, J.C., 1968. The response of water temperature to meteorological conditions. Water Resour. Res. 4, 1137–1143.

Finch, J.W., 2001. A comparison between measured and modelled open water evaporation from a reservoir in south-east England. Hydrological Processes 15, 2771–2778.

Gao, W., Shaw, R.H., Paw U, K.T., 1989. Observation of organized structure in turbulent flow within and above a forest canopy. Boundary-Layer Meteorol. 47, 349–377.

Garratt, J.R., 1992. The Atmospheric Boundary Layer. Cambridge University Press, Cambridge, 316 pp.

Gianniou, S.K., Antonopoulos, V.S., 2007. Evaporation and energy budget in Lake Vegoritis, Greece. J. Hydrol. 345, 212–223.

Kaimal, J.C., Finnigan, J.J., 1994. Atmospheric Boundary Layer Flows, Their Structure and Measurement. Oxford University Press, New York, 289 pp.

Keijman, J.Q., 1974. The estimation of the energy balance of a lake from simple weather data. Boundary-Layer Meteorol. 7, 399–407.

Marsh, P., Bigras, S.C., 1988. Evaporation from Mackenzie delta lakes, N.W.T., Canada. Arctic Alpine Res. 20, 220–229.

Mengistu, M.G., Savage, M.J., 2010. Open water evaporation estimation for a small shallow reservoir in winter using surface renewal. J. Hydrol. 380, 27–35.

Nash, J.E., Sutcliffe, J.V., 1970. River flow forecasting through conceptual models part I - A discussion of principles. J. Hydrol. 10, 282–290.

Odhiambo, G.O., Savage, M.J., 2009. Sensible heat flux by surface layer scintillometry and eddy covariance over a mixed grassland community as affected by Bowen ratio and MOST formulations for unstable conditions. J. Hydrometeorol. 10, 479–492.

Oncley, S.P., Foken, T., Vogt, R., Kohsiek, W., de Bruin, H.A.R., Bernhofer, C., Christen, A., van Gorsel, E., Grantz, D., Feigenwinter, C., Lehner, I., Liebethal, C., Liu, H., Mauder, M., Pitacco, A., Ribeiro, L., Weidinger, T., 2007. The energy balance experiment EBEX-2000. Part I: overview and energy balance. Boundary-Layer Meteorol. 123, 1–28.

Paw U, K.T., Qui, J., Su, H.B., Watanabe, T., Brunnet, Y., 1995. Surface renewal analysis: a new method to obtain scalar fluxes. Agric. Forest Meteorol. 74, 119–137.

Paw U, K.T., Snyder, R.L., Spano, D., Su, H.B., 2005. Surface renewal estimates of scalar exchange. In: Hatfield, J.L., Baker, J.M. (Eds), Micrometeorology in Agricultural Systems Agronomy Monograph no. 47, pp. 455–483.

Penman, H.L., 1948. Natural evaporation from open water, bare soil and grass. Proceedings of the Royal Society, London A193, No. 1032, 120–145.

Rosenberg, N.J., Blad, B.L., Verma, S.B., 1983. Microclimate: The Biological Environment. Second edition. John Wiley & Sons, New York, 495 pp.

Rosenberry, D.O., Winter, T.C., Buso, D.C., Likens, G.E., 2007. Comparison of 15 evaporation methods applied to a small mountain lake in the northern USA. J. Hydrol. 340, 149–166.

Shaw, R.H., Paw U, K.T., Gao, W., 1989. Detection of temperature ramps and flow structures at deciduous forest site. Agric. Forest Meteorol. 47, 123–138.

Snyder, R.L., Spano, D., Duce, P., Paw U, K.T., Anderson, F.E., undated. Surface renewal manual. Dept. of Land, Air, and Water Resources, University of California, Davis, California, USA, 16 pp.

Snyder, R.L., Spano, D., Paw U, K.T., 1996. Surface renewal analysis for sensible heat and latent heat flux density. Boundary-Layer Meteorol. 77, 249–266.

Spano, D., Duce, P., Snyder, R.L., Paw U, K.T., 1997a. Surface renewal estimates of evapotranspiration: tall canopies. Acta Hort. 449, 63–68.

Spano, D., Snyder, R.L., Duce, P., Paw U, K.T., 1997b. Surface renewal analysis for sensible heat flux density using structure functions. Agric. Forest Meteorol. 86, 259–271.

Spano, D., Snyder, R.L., Duce, P., Paw U, K.T., 2000. Estimating sensible and latent heat flux densities from grape vine canopies using surface renewal. Agric. Forest Meteorol. 104, 171–183.

Stannard, D.I., Rosenberry, D.O., 1991. A comparison of short-term measurements of lake evaporation using eddy correlation and energy budget methods. J. Hydrol. 122, 15–22.

Stull, R.B., 1988. An Introduction to Boundary Layer Meteorology. Kluwer Academic Publishers, Dordrecht, 666 pp.

Tanny, J., Cohen, S., Assouline, S., Lange, F., Grava, A., Berger, D., Teltch, B., Parlange, M.B., 2008. Evaporation from a small water reservoir: Direct measurements and estimates. J. Hydrol. 351, 218–229.

van Atta, C.W., 1977. Effect of coherent structures on structure functions of temperature in the atmospheric boundary layer. Archives Mechanics 29, 161–171.

Zapata, N., Martínez-Cob, A., 2001. Estimation of sensible and latent heat flux from natural sparse vegetation surface using surface renewal. J. Hydrol. 254, 215–228.

Table 10.1. Linear regression statistics for the calibration dataset for the period 5th to 17th July (day of year 186 to 198), where α_{ll} and α_{ul} are respectively the 95 % lower and upper limits for α, of 30-min H_{EC} (*y*) *vs.* H_{SR} (*x*) (Eq. (10.1) for all SR data, the data subset for which ramp period $\tau \leq$ 20 s and the subset for $\tau >$ 20 s) and H_{EC} (*y*) *vs. H* estimated using the renewal model (*x*) (Eq. (10.3)) for stable and unstable conditions for the four heights for time lags r = 0.4 and 0.8 s.

z (m)	Time lag (s)	Eq. (10.1)						Eq. (10.3)	
		α † (α_{ll}, α_{ul})	R^2	α (α_{ll}, α_{ul})	R^2	α (α_{ll}, α_{ul})	R^2	α †† (α_{ll}, α_{ul})	R^2
		All data		$\tau \leq$ 20 s		$\tau >$ 20 s			
1.0	0.4	0.199[a] (0.180, 0.218)	0.52	0.158 (0.141, 0.173)	0.74	0.268 (0.233, 0.301)	0.47	0.204[a] (0.189, 0.219)	0.62
1.0	0.8	0.282[A] (0.256, 0.307)	0.55	0.219 (0.196, 0.240)	0.75	0.385 (0.341, 0.429)	0.52	0.221[a] (0.206, 0.237)	0.64
1.3	0.4	0.183[a] (0.164, 0.202)	0.46	0.129 (0.110, 0.147)	0.66	0.233 (0.205, 0.261)	0.46	0.206[a] (0.191, 0.221)	0.62
1.3	0.8	0.255[A] (0.230, 0.279)	0.49	0.181 (0.155, 0.207)	0.67	0.315 (0.280, 0.349)	0.50	0.223[a] (0.208, 0.238)	0.65

z (m)	Time lag (s)	Eq. (10.1)						Eq. (10.3)	
		α † (α_{ll}, α_{ul}) All data	R^2	α (α_{ll}, α_{ul}) $\tau \leq$ 20 s	R^2	α (α_{ll}, α_{ul}) $\tau >$ 20 s	R^2	α †† (α_{ll}, α_{ul})	R^2
1.9	0.4	0.144[b] (0.129, 0.159)	0.45	0.087 (0.073, 0.100)	0.71	0.185 (0.164, 0.205)	0.48	0.200[a] (0.187, 0.214)	0.64
1.9	0.8	0.194[B] (0.175, 0.212)	0.50	0.123 (0.105, 0.140)	0.74	0.236 (0.212, 0.259)	0.52	0.214[a] (0.200, 0.229)	0.66
2.5	0.4	0.120[C] (0.107, 0.133)	0.46	0.069 (0.056, 0.082)	0.67	0.148 (0.131, 0.163)	0.49	0.200[a] (0.186, 0.215)	0.62
2.5	0.8	0.170[B] (0.154, 0.186)	0.51	0.108 (0.091, 0.123)	0.77	0.195 (0.175, 0.214)	0.53	0.210[a] (0.195, 0.225)	0.63

† Different superscripted lowercase letters for the full dataset column (third column) for the 0.4-s time lag indicates statistical significance at the 95 % level of significance. A capital letter is used for distinguishing significance for the 0.8-s time lag.

†† The superscripted letter next to the α value indicates no significant difference from that for Eq. (10.1) for the full dataset for the 1.0 m height for the 0.4 s time lag

Table 10.2. Regression statistics for the calibration period 5th to 17th July (day of year 186 to 198) for the four heights of 30-min λE_{SR} (average of two time lags r = 0.4 and 0.8 s) using H_{SR} (Eq. (10.1)) and λE using *H* from the renewal model method (Eq. (10.3)) (*x*) *vs.* λE_{EC} (*y*) estimates of latent energy flux.

z (m)	Slope		Intercept (W m^{-2})		R^2		RMSE (W m^{-2})	
	λE (1)	λE (3)	λE (1)	λE (3)	λE (1)	λE (3)	λE (1)	λE (3)
1.0	0.99	0.99	-0.16	0.88	0.99	0.99	10.58	11.94
1.3	0.99	0.99	0.81	0.95	0.99	0.99	11.64	12.51
1.9	0.98	0.99	-0.56	0.73	0.99	0.99	11.35	12.97
2.5	0.98	1.00	-1.01	0.17	0.99	0.99	11.29	12.09

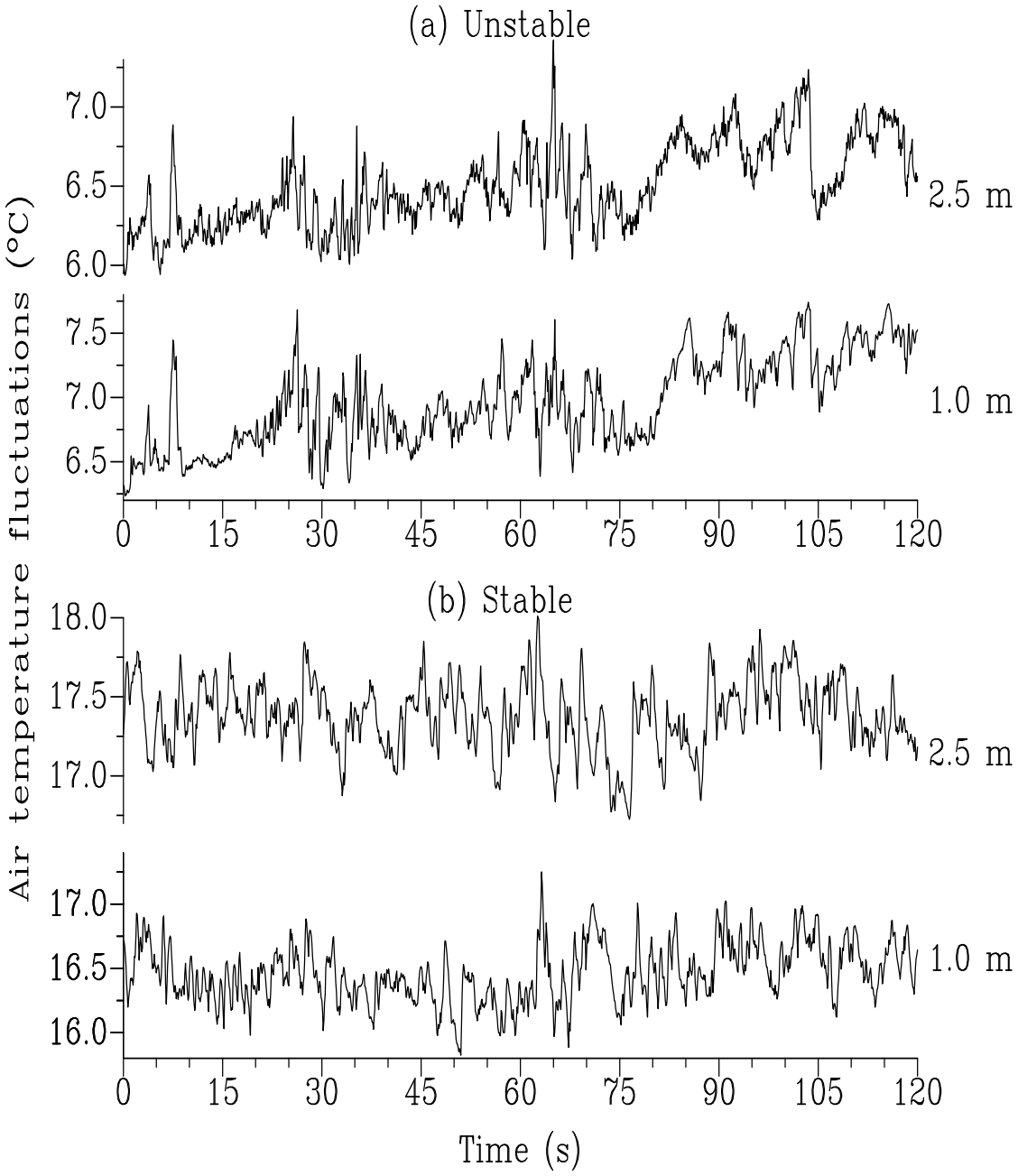

Fig. 10.1. Air temperature ramps observed in a sample of 120 s of 10-Hz air temperature traces. The measurements were at 1.0 and 2.5 m above open water in the reservoir behind Midmar Dam, South Africa for day of year 194 (13th July): (a) for unstable conditions (08h52), H_{EC} = 81.3 W m^{-2}; (b) for stable conditions (16h00), H_{EC} = -3.4 W m^{-2}.

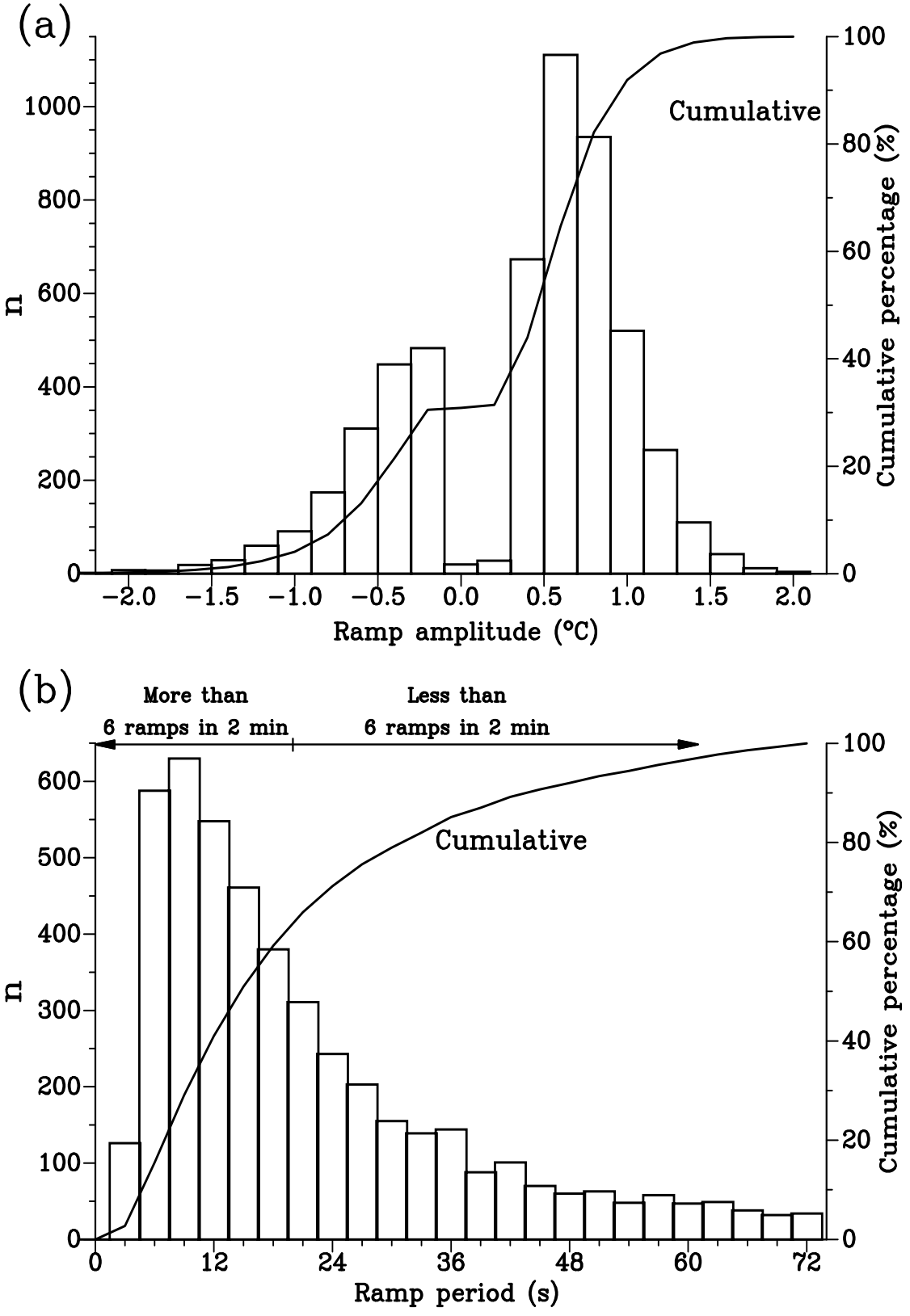

Fig. 10.2. Histogram and cumulative percentage plots for the 2-min ramp events for the calibration period for the 1-m height and lag of 0.4 s for (a) ramp amplitude and (b) ramp period.

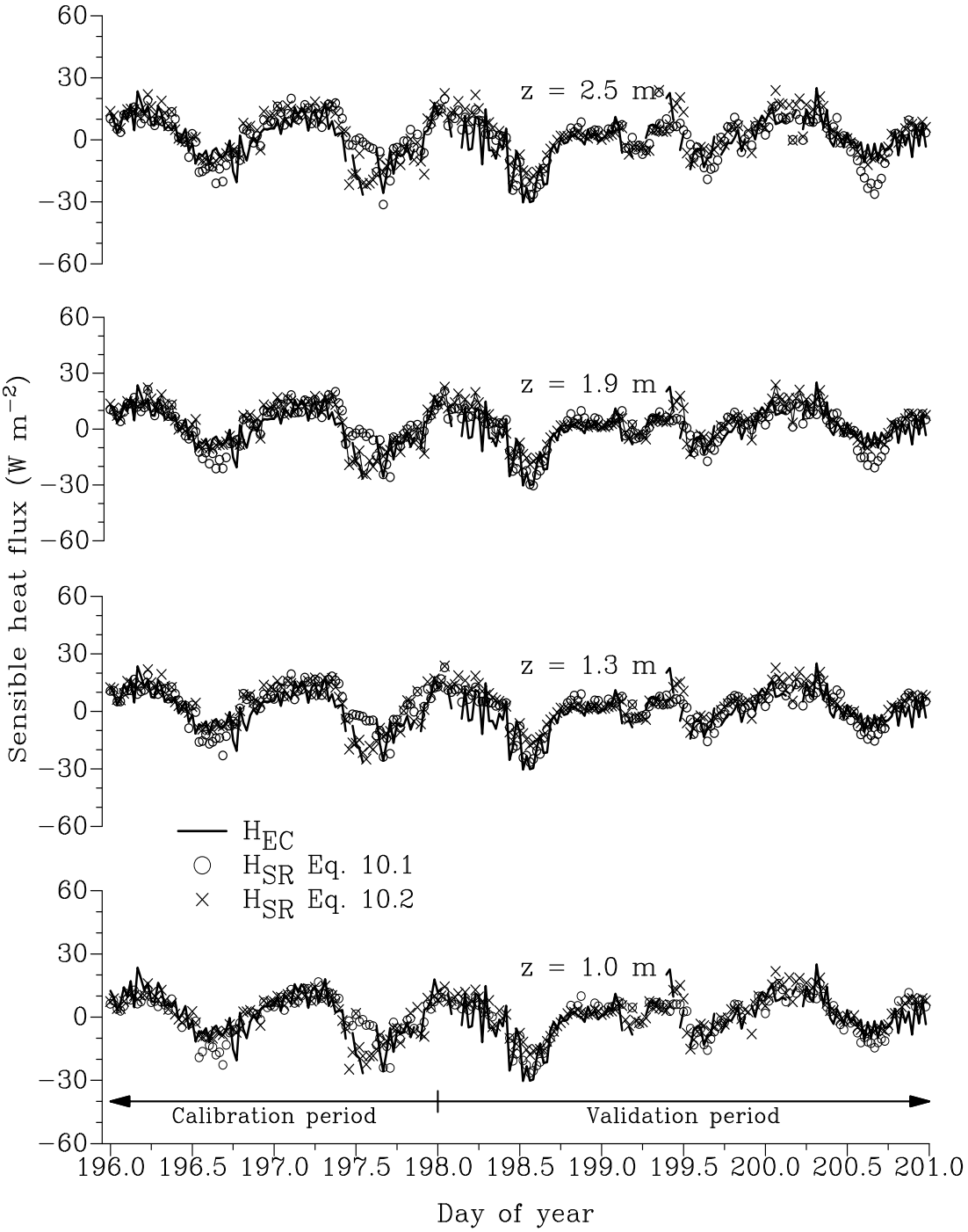

Fig. 10.3. Diurnal variations for the 30-min measured H_{EC} and estimated H_{SR} (Eq. (10.1)) and H estimated using the renewal model method (Eq. (10.3)) at 1.0, 1.3, 1.9 and 2.5 m above the water surface. The H_{SR} and renewal model estimates of H are the average for the two time lags r = 0.4 and 0.8 s using the α values shown in Table 10.1.

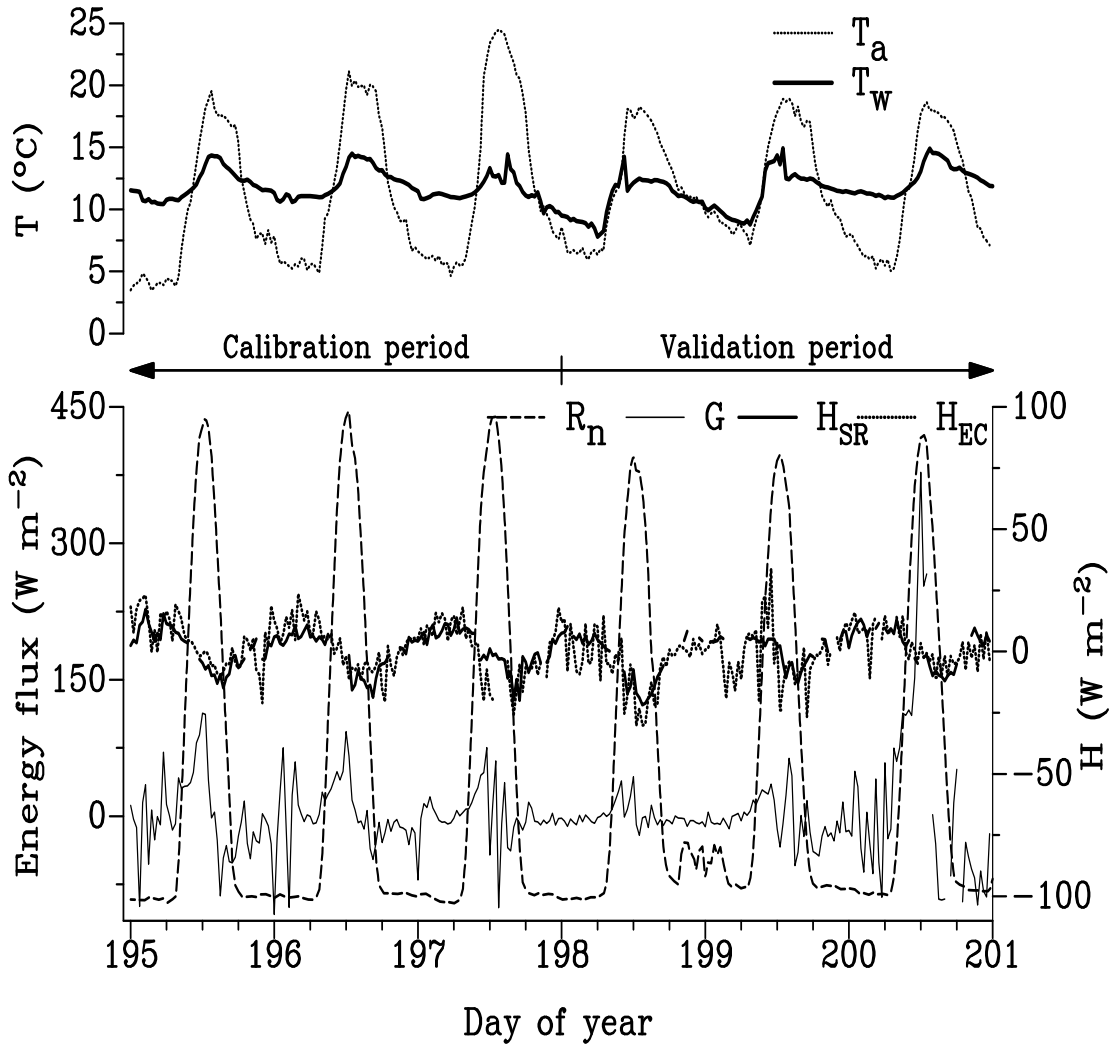

Fig. 10.4. Diurnal variations for bottom: 30-min stored heat G, measured net irradiance R_n (left-hand *y*-axis), H_{SR} for the 1-m height obtained using Eq. (10.1) and the α values of Table 10.1, H_{EC} (right-hand *y*-axis); top: 30-min mean water temperature T_w and air temperature T_a.

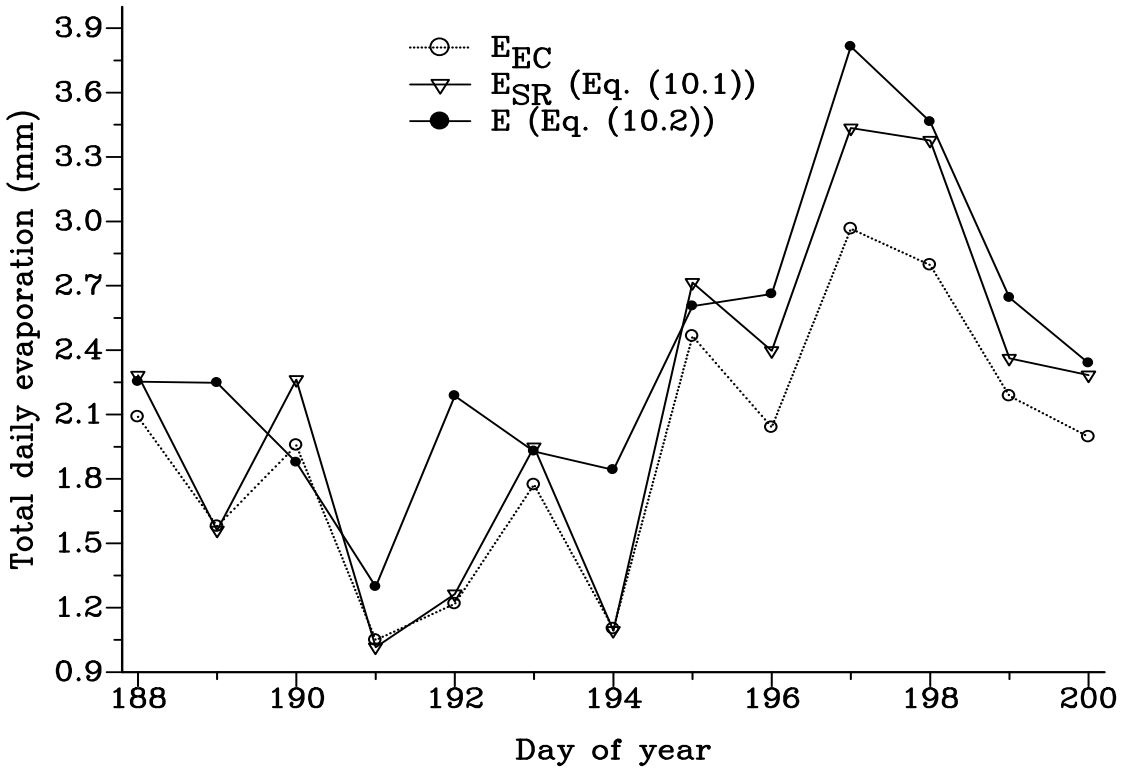

Fig. 10.5. Total daily evaporation estimates (mm) using EC, SR and renewal model methods for day of year 187 to 199 inclusive. The E_{SR} and *E* for the renewal model method were estimated using the sensible heat flux, Eqs. (10.1) and (10.3) respectively, at 1.0 m above the water surface.

11 INTEGRATION AND CONCLUSIONS

11.1 Abstract

The specific objective of this research centres on investigations of various methods for obtaining sensible heat flux (H) for estimating evaporation. The key for this approach is the application of the shortened energy balance equation, and in the case of methods based on the Monin-Obukhov similarity theory (MOST) and surface renewal (SR), the iterative procedures. The application of the shortened energy balance requires that errors associated with measurement of net irradiance (R_{net}) and soil heat flux (S) are kept to a minimum. To this end, methodology for the calibration of net radiometers for both the infrared and short wave irradiances receive attention. A field study attempts to quantify the error in soil heat flux measurement for a mesic grassland. A standard, convenient and accurate method for calibrating net radiometers would assist in unravelling reasons for the perplexing lack of surface energy balance closure when employing the eddy covariance (EC) flux estimation method as well as improve on the accuracy of the energy balance residual method for estimating evaporation. A relatively inexpensive, accurate and quick laboratory method, based on physical theory, for non-steady radiative conditions above a large water-heated or water-cooled radiator containing circulated water, with surface-embedded thermocouples is used to obtain reproducible net radiometer calibration factors for the infrared waveband for a wide range in net irradiance. When applied, the method would reduce error in the most important term of the shortened energy balance and assist in energy balance closure aspects of EC measurements. The surface-layer scintillometer (SLS) method, reliant on MOST, is used for estimating areally-averaged H for a mesic grassland for a 30-month period. Comparisons with EC measurements feature prominently in this unique study. These comparisons include using different MOST procedures and the influence of the Bowen ratio on SLS measurements of H is investigated. Furthermore, since there are reports in the literature that the EC method may underestimate H and/or latent energy flux (LE), resulting in the shortened energy balance not being closed, effort is devoted to this aspect. Other methods used for comparison purposes are the traditional Bowen ratio energy balance (BREB), SR, temperature variance (TV) and ETo (grass reference) methods. The TV and SLS and/or EC measurements of H are compared above three contrasting canopy surfaces. It is shown that other high frequency air temperature-based methods, for example, for the first time the TV method with adjustment for skewness (Tillman, 1972), may pave the way for evaporation stations from which real-time and sub-hourly estimates may be obtained relatively inexpensively. Another area of research that receives attention is the placement height of EC instruments above short-canopy surfaces and a spectral analysis of the vertical wind speed and sonic temperature measurements for close-canopy placement heights. The SR method is used to estimate, for the first time, open-water evaporation. The ideal SR method applied above canopies is the most inexpensive micrometeorological method for estimating H, but the SR weighting factor α needs to be determined using EC and for this reason, the TV method with adjustment for skewness was investigated. Finally, a unique implementation of SR uses an iterative method for calculating H. A similar iterative procedure is applied for MOST and ETo calculations.

11.2 Summary discussion and conclusions

The EC method allows independent estimation of H and LE provided sonic temperature, vertical wind speed and concentrations of water vapour are measured using fast-responding sensors. Alternatively, the EC method may be used to measure H with LE estimated as a residual from the shortened energy

balance. The BREB and SLS measurements allow *H* to be estimated from which *LE* is also estimated as a residual of the energy balance. Both BREB and SLS methods, by definition, force energy balance closure.

While the EC method, regarded by many as the standard for flux measurement, has many advantages including direct and separate measurement of for example *H* and *LE*, it is a complicated method (Castellví, 2007). While the EC method directly measures the turbulence, it is a stringent method, requiring many post-processing corrections (Mauder et al., 2007), favourable wind directions, careful sensor positioning and alignment. To overcome the energy balance closure problem (Foken, 2008) of direct EC measurements, correction schemes have been proposed (Twine et al., 2000; Wilson et al., 2002). For the mesic grassland and for *Chromolaena odorata*, there was no evidence for underestimation of *H* by the EC method, compared to SLS and BREB estimates for the grassland and SLS estimates for Chromolaena (Chapters 4 to 7). However, these studies are above relatively short canopies. Using a type of wavelet transformation, von Randow (2007) demonstrated that the contribution from the largest temporal and spatial scales of turbulent motions, corresponding to lower frequencies, is more important over the forest sites investigated than over grassland. He states that due to the high measurement height in forests, and other factors, it would be important in forests to extend the averaging interval to include the active contribution of low turbulent frequencies. He admits that there is a disadvantage to this approach, viz., that there would be an increase in the uncertainty of the estimated flux due to random errors. He recommends a more improved understanding of how the low-frequency motions affect the structure and scales of turbulence and hence the flux estimation.

The nagging question about the appropriateness of the shortened energy balance equation and its use for estimating evaporation remain. To this end, there is some evidence in the literature that as convective conditions are approached, the energy balance closure significantly worsens. The reasons need to be investigated further. This aspect is important and impacts on all of the methods used to estimate measurements of *H* for which *LE* is calculated using the simplified energy balance. Further research in this area would necessitate investigating low-frequency *H* transport. An approach, that includes flux contributions from large organised turbulent structures, would be to apply spatial averaging instead of temporal averaging for the calculation of fluxes that contribute to vertical transport.

In some senses, the placement height study of Chapter 9 may be a microcosm of a forest and grassland situation that von Randow (2007) investigated: measurements of *H* at different heights above the canopy surface. This study (Pietermaritzburg) above a short grassland surface demonstrated a gradual decrease in *H* with decrease in measurement height. The spectral analysis for vertical wind speed and sonic temperature shows an increased deviation from the -5/3 Kolmogorov law for the inertial sub-range, for the lower frequencies, for measurements closer to the canopy surface. The power spectrum log-log plots for vertical wind speed for the lowest heights, show a slight drop-off from the -5/3 law at the lower frequencies, particularly for the lowest height. It may therefore be inferred that for the lower measurement heights, energy balance closure is not satisfied, mainly due to not all of the turbulent motion frequencies being captured by the measurements. The rationale for this inference is that for a similar uppermost measurement height for the mesic grassland (Bellevue) studies (Chapters 4 to 6), there was good correspondence between *H* for the EC, SLS and BREB methods for EC measurement heights not close to the grassland canopy. In the case of the study by

von Randow (2007), in relation to turbulent frequencies, the opposite occurs – namely that with increase in height, reduced turbulent motion frequencies occur and these frequencies too are not captured by the half-hourly or similar averaging periods.

The SLS method, based on extremely high frequency measurements, 1 kHz, should on the surface not suffer from these frequency problems plaquing EC. Indeed, as already mentioned, there is good correspondence between EC, SLS and BREB measurements of H for the mesic grassland and Chromolaena studies. However, and more importantly though as far as the grassland study is concerned is that strictly, the EC and SLS methods are not independent – their dependence is due to the fact that the MOST functions used with the SLS method were developed with the use of EC data and then using stability functions derived from long-averaging periods (Chapter 4). This would apply to any method that uses MOST for which the semi-empirical MOST functions derived were based on EC measurements. So while the EC method does not directly depend on MOST for estimating H_{EC}, the form of the empirical MOST functions $f(\zeta)$ and $g(\zeta)$ were determined based on direct comparisons of H_{EC} with the MOST-determined H using the SLS method. Since the H_{EC} estimates were obtained for an unknown energy balance closure condition, there is a suggestion by Kohsiek et al. (2002) that the EC method is non-standard! Furthermore, SLS flux estimates use similarity functions derived from long averaging periods, claiming that there is no evidence that MOST is also valid for 1- to 10-min laser scintillometer fluxes.

Attention is devoted in Chapter 4 to a possible lack of energy balance closure where LE_{EC} is independently measured from the covariance between the vertical wind speed and water vapour concentration. We show that there is good agreement between H_{SLS} *vs* H_{EC} and H_{BR} *vs* H_{EC}. Therefore, if there is any underestimation in the magnitude of either H_{EC} or the directly-measured LE_{EC}, this could be due to the underestimation in the LE_{EC} magnitude – for if not we would have found significant underestimation in H_{EC} compared to H_{SLS} or compared to H_{BR}. Alternatively, the lack of closure could be due to energy fluxes not included in the shortened energy balance. This finding assumes that the R_{net} and S measurements are not the cause for a lack of closure (Chapter 3). However, possibly, an underestimation in H may not be a difficulty of MOST but it could also be a difficulty of the EC method which assumes that all parts of the turbulent fluxes are observable during the measurement period. In Chapter 5, we use differing averaging periods – 2, 20 and 60 min – for the EC data to demonstrate that this is not the case for the 10-Hz EC data apart from periods less than 10 min.

For the mesic grassland, from the H estimates using SLS and measurements of S and R_{net}, evaporation rates are calculated (Chapter 6) as a residual of the shortened energy balance equation and compared with ETo. Inconsistent hourly ETo values occur due to the incorrect assumption that S is 10 % of R_{net}. The SLS estimates of H, and evaporation rate as a residual, compared favourably with BREB and EC estimates for cloudless, cloudy and variable cloud days. The diurnal variation in SLS H is often asymmetrical, peaking before noon. Reasons for this asymmetry deserves more research attention. Practical aspects of SLS for the estimation of evaporation rate receive attention and the procedure for definition for rejection of out-of-range and bad or "doubtful" SLS data is also presented.

Can we measure H from a surface using a single air temperature sensor, in real-time? This important question was posed by Savage (2007). To this end, another MOST method, the TV method for the free convective range of turbulence is used in Chapter 7 for estimating H, for three contrasting

canopies: mesic grassland, Chromolaena and a pine canopy, for unstable conditions. As is the case with the SR method, the TV method involves high frequency (10 Hz) air temperature measurements using a fine-wire thermocouple at one or more heights above the canopy. The direction of the flux is determined from the sign of a third-order air temperature structure function. The main advantage of the TV method is that it is inexpensive compared to most methods and that friction velocity is not required when estimating *H*. Daytime TV estimates of *H* are compared with estimates obtained using SLS and/or EC estimates of the same. The skewness of air temperature (Tillman, 1972) is included in the analysis to extend the *H* estimates to include both the free and forced convective turbulence ranges. The comparison between *H* for the TV method and one or both of the SLS and the EC methods is quite good for the three canopy types. Given the theoretical limitation of the TV method, it performed remarkably well against the much more expensive SLS and EC methods. The requirement for 10-Hz air temperature data for the TV method is investigated by comparing *H* calculated from 10-Hz and 2-Hz datasets. The agreement in *H* for these two datasets is very good. The implication of this result is that the requirement for high frequency data may be relaxed somewhat, or that the sample rate should be greater than 10 Hz! The TV method with adjustment for skewness for estimating *H*, also investigated by Abraha (2010) and Nile (2010), shows considerable promise as an inexpensive method for providing real-time estimates at sub-hourly intervals. The method has the additional advantage of much reduced data processing and electrical power requirements compared to SLS and EC. The method also appears to be calibration-free.

It could be argued that the BREB method is obsolete. One examiner was of the opinion that the BREB method has been treated as outdated in recent years. Another examiner was critical of the work, and of the opinion that the the BREB method should have received "more admiration from the candidate". It was however pointed out in Chapter 8 that BREB measurements are still of interest since the method is less expensive than EC and SLS or large aperture scintillometry or boundary-layer scintillometry and there is reduced operator skill required with fewer corrections to the data applied. Furthermore, the method will remain of interest until the issue of lack of closure of EC measurements is resolved. For example, in Chapter 4, the BREB method is validated using SLS measurements. There are few papers that deal with BREB data checking, including theoretical aspects. This is the justification for the research on the use of the BREB method to collect accurate and reliable evaporation measurements as part of a larger long-term study of the total evaporation in grassland systems but in particular in a remote montane grassland (Chapter 8). The treatment of BREB data, including data rejection procedures, is emphasized. An additional aim includes the estimation of *H* in the absence of either air temperature or water vapour pressure gradients. To this end, the use of an exchange coefficient *K*, calculated in different ways for estimating *H* and *LE,* is investigated.

Possibly the most difficult measurement study of this report involved estimation of open-water evaporation (Chapter 10). The aim of this study is to calibrate *H* obtained with the SR and renewal model methods against EC measurements and to evaluate the performance of the SR and renewal model methods for estimating *H*, and *LE* as a residual of the energy balance. The range of *H* in this study was small and this presents an added difficulty in testing the reliability of these two air temperature based methods above open water, during periods of low *H*, and comparisons with EC measurements.

11.3 Broad overview of research products

A number of research products stem for the research conducted:

a number of unique and valuable long-term data sets have been collected, including the BREB measurements at Cathedral Peak and the SLS measurements at the Bellevue site;

calibration methodologies, including that for the calibration of net radiometers using a protocol that allows repeatable laboratory calibrations to be performed;

computational methodologies, and specifically the simple iteration methodologies used for estimating SLS and SR fluxes and ETo;

criteria for ensuring valid and representative measurements included, *inter alia*, the development of theory for excluding BREB data for the Bowen ratio approached -1 and valid data for SR measurements;

theoretical developments, including the correction of sonic temperature for water vapour pressure, atmospheric pressure and the Bowen ratio;

fetch and footprint considerations, including modification of an existing footprint model;

new evaporation estimation approaches, including the TV method with adjustment for air temperature skewness, amd fresh guidelines for the appropriate use of existing and new evaporation methodologies.

11.4 Detailed contributions

What has been achieved? Two scientific reviews, namely reviews on SLS and SR, highlight the use of these methods for measurement of H and estimation of LE. Currently, there is no similar review on these topics in the published literature.

The methodology for the laboratory calibration of net radiometers for both the infrared and the shortwave (Chapter 3) is directly relevant to the energy balance closure problem. Most research groups rely on new instruments, calibrated by the manufacturer, or use their own instrument intercomparison. The method details the procedures for calibration, based on physical theory, for the laboratory infrared and shortwave calibration, the latter using a reference pyranometer. Application of the method would also ensure that error in the most important component of the shortened energy balance, R_{net}, is minimized and therefore give confidence that any possible lack of energy balance closure is not due to the R_{net} measurements. This methodology should have significant impact.

Prior to the published work on the SLS (Chapters 4, 5 and 6), there had been no long-term study that also compared SLS, BREB and EC methods. The other significant contributions of the work included investigations of the different MOST functions (Chapters 4 and 5), the influence of the Bowen ratio (Chapter 5) and the important aspect of the averaging period on H (Chapter 5).

The TV method with adjustment for skewness is an original contribution that has not been applied elsewhere. The novelty is that the method, for the first time allows real-time and inexpensive estimates of *H* for the inertial sub-layer (Chapter 7). There is no doubt that this method will receive further attention, based on the research reported here.

The objectives of the BREB research in a remote montane grassland have been achieved. This significant work points out that, on the contrary, the BREB method is not obsolete. BREB measurements are still of interest since the method is less expensive than EC and scintillometry and there is reduced operator skill required with fewer corrections to the data applied. Furthermore, the method will remain of interest until the issue of lack of closure of EC measurements is resolved.

The significance of the placement height and spectral analysis investigations (Chapter 9) allow a more precise assessment of placement heights for EC instruments above short crops, in this case, short grass. This early study now has significance in terms of the issue of EC energy balance closure – as is evident by the work of von Randow (2007).

The open-water evaporation investigation, using SR, is original. This research presents many challenges and needs further investigation as far as methods for evaporation estimation without the need for the heat storage flux in water. In this regard, the procedures outlined in the Appendix would be useful in allowing application of a MOST method.

While much has been achieved here in the area of sensible heat flux for evaporation estimation, and in South Africa in particular, there are still many areas that need further investigation.

11.5 Brief assessment of advances made in terms of answering key questions and generating new knowledge and applicable technology

One of the important key questions was whether it would be possible to use integrative methods for which flux measurements represent a large area. This question was answered through the use of BREB, EC, SR and TV micrometeorological measurements of *H*. The question of which method of estimating evaporation using the shortened energy balance should be applied to which canopy surface was also answered through the use of the various methods. The placement height question received attention through the EC placement height study as well as TV measurement of *H* as different heights. In some cases, trial and error was used to initially determine measurement frequency, the averaging period and the placement height. Inexpensive methods for estimating *H* using high frequency measurements of air temperature received attention. These measurements allowed evaporation to be estimated using the simplified energy balance. Early research attempted to answer the question about a calibration standard for net irradiance measurements. Following on this research, work commenced on determining the impact of placement height on EC measurements for a short grassland surface.

The key decision made to emphasise research on scintillometry has proved to be the correct one. Research is this area led to unique measurements in a mesic grassland (Bellevue) site for which there were simultaneous measurements of *H* using BREB, EC and SLS measurements for an extended period of time. These measurements attempted to answer the questions surrounding placement height, fetch, measurement frequency, the uncertainties in the implementation of MOST, the contribution of

net irradiance measurements to the overall error in estimating evaporation, but more importantly, identifying inexpensive methods for estimating *H* and validating BREB and EC measurement of *H*.

11.6 Remaining key questions pointing the way for future research

A recognised deficiency of these investigations, due to lack of equipment funding, is the lack of more direct measures of *LE* – such as is possible with EC using an open-path H_2O/CO_2 infrared analyser – apart from a short period (Chapter 4). Such equipment would allow a more thorough investigation of energy balance closure and permit the application of SR and TV methods to scalars other than just air temperature for measurement of *H*.

Another area to be exploited is the possible application of the SR iterative procedure, outlined in an Appendix to the thesis, in real-time or near real-time in a datalogger. While methods that provide point values fail to describe the larger spatial scale (Teixeira et al., 2009a, b), such near real-time point measurement efforts could marry the remote sensing efforts of estimating *H* and calculating *LE* using the shortened energy balance by allowing almost real-time calibration of remotely-sensed estimates with ground-based estimates. As an alternative to SR, the TV method, with adjustment for skewness, should be applied with greater urgency to other canopy surfaces to determine its wider applicability. Furthermore, the datasets collected should be re-analysed to also check the wider applicability of the combination SR-similarity and SR-dissipation methods (Castellví, 2004; Castellví and Snyder, 2009a).

Inexpensive methods for estimation *H* and/or *LE*, such as SR and TV, are of considerable interest in agriculture (Castellví and Snyder, 2009b), particularly methods that may be applied close to the canopy surface. Many of the experimental sites suffer from fetch limitations and measurements at positions close to the canopy surface reduce the fetch requirements. Compared to EC and BREB measurements of *H*, SLS measurements may be obtained at heights closer to the surface – and this may present opportunities for estimation of evaporation for riparian areas.

Remote-sensing measurement comparisons using SLS, large-aperture or boundary-layer scintillometer turbulent fluxes and aerodynamic surface temperature estimates, including robust inexpensive temperature-based methods, should be pursued vigorously.

Evaporation estimation remains one of the important challenges for the agricultural and environmental sciences. Determination of reliable and representative evaporation data is an important issue of atmospheric research with respect to applications in agriculture, catchment hydrology and the environmental sciences, not only in South Africa. Long-term measurements of evaporation at different time scales and from different climate regions, are not yet readily available (Jarmain et al., 2009).

The most popular method currently for evaporation estimation is the ETo method, based on FAO56, for daily or hourly automatic weather station data. The method has a solid scientific basis and has been used for decades in many countries. Unfortunately in South Africa, the method has been underutilised and this should be rectified as a matter of urgency. The method may be applied real-time and applied to historic data with ETo estimations for short grass and a tall-crop (0.5-m tall) estimated.

Aside from the ETo estimations, the aerodynamic methods for estimating *H* or *LE* have received attention over the last decade or so. Improvements in datalogging, improvements in sensors and their

reduced cost, together with theoretical developments, have made their *in situ*, long-term, and unattended use in remote areas attractive. The EC and BREB methods have received the most attention but increasingly, the scintillometer and temperature-based aerodynamic methods are becoming more popular. The scintillometer has the advantage of the large areal representation of the measurements and real-time monitoring but the method is costly. The temperature-based methods, such as the SR and TV methods, have low cost, low power and reduced fetch requirements. In some cases real-time estimations of evaporation are now within reach for the temperature-based methods.

Five possible areas of future activity, stemming partly from the research reported on here, are presented here in relation to the progress made in the current programme of research:

1. There is a dearth of technologists trained in the area covered by this research. This has negative long-term consequences. The work of Jarmain et al. (2009) attempted to address this through a training workshop, based in Pietermaritzburg. This should be aggressively pursued through the conducting of similar workshops regularly. Outside South Africa, clearly, there is also such a lack so efforts in this regard would need to be regionalised and receive the support of statutory bodies as a matter of urgency. In this regard, it is noted that different agencies within South Africa are using different methods – hopefully there can be some sharing of knowledge and data and working towards a common approach in the future.

2. The aspect of fetch and the footprint of evaporation estimates are not the main focus of this research. However, these important aspects must receive attention. Some of the sites chosen for evaporation measurement are at the limit of adequate fetch and this aspect needs to be considered in more detail in relation to footprints. Only one footprint model was applied (Chapter 5). These aspects need to be pursued further for the dataset already collected by the application and comparison of the results using various footprint models. It is noted here again that some of the temperature-based methods, particularly SR, have reduced fetch requirements since measurements may be made close to the canopy surface.

3. The lack of energy balance closure is another area that has frustrated energy balance methods and the consequential estimation of evaporation. This aspect needs to be further pursued and in addition, needs to involve the estimation of evaporation from the high frequency measurements of water vapour pressure using an approach similar to the SR and/or TV approaches for high frequency air temperature.

4. Ground-based methods for estimating evaporation will always be in demand. These measurements are required to validate the remote estimates determined using spatial methods. The merging of these technologies will see much progress in the future.

5. It is now possible to obtain on site, real-time, sub-hourly, inexpensive estimates of evaporation, for measurements in the inertial sub-layer, using simple methodology. It is suggested that high frequency air temperature-based methods, which include SR and TV, may pave the way for evaporation stations from which real-time and sub-hourly estimates may be obtained. It is in this area that future research should also be continued.

Three other areas of future research, noted in the report by Jarmain et al. (2009), are worth repeating here.

An assumption of the shortened energy balance is that advection is ignored. In the case of arid environments for which riparian total evaporation is required, advection may be significant. What are the limitations of the evaporation measurements for such environmental and climatic conditions?

The focus of the reported research has been on SLS, with a pathlength less than a few hundred metres, and the focus by Jarmain et al. (2009) on LAS. Research in the area of microwave scintillometer systems, which may allow evaporation estimates over tens of kilometres, need attention. These efforts should allow for modelled and measured estimates of total evaporation for small catchments to be compared with remotely-sensed estimates.

The open-water evaporation research (Chapter 10) needs to be extended. Based on initial investigations stemming from this report, not reported here, it appears possible to apply the MOST iterative procedures of the Appendix to estimate open-water evaporation, and H, without resorting to water temperature measurements to obtain the heat storage flux in water.

In addition, as mentioned previously, the appropriateness of the shortened energy balance equation and its use for estimating evaporation remain. The reasons as to why energy balance closure significantly worsens as convective conditions are approached need to be investigated further. This aspect is important and impacts on all of the methods used to estimate measurements of H for which LE is calculated using the simplified energy balance. Further research in this area would necessitate investigating low-frequency H transport. An approach, that includes flux contributions from large organised turbulent structures, would be to apply spatial averaging instead of temporal averaging for the calculation of EC fluxes that contribute to vertical transport.

Since the TV, SLS and SR methods all process a single signal – the temperature fluctuations – through optical and/or digital filters to produce a heat flux a remaining question is: which filter works best?

11.7 References

Abraha, M.G., 2010. Sensible heat flux and evaporation for sparse vegetation using temperature-variance and a dual source model. Ph.D. thesis submitted, University of KwaZulu-Natal, pp. 217.

Castellví, F., 2004. Combining surface renewal analysis and similarity theory: a new approach for estimating sensible heat flux. Water Resour. Res. 40, W05201, 1-20.

Castellví, F., 2007. The estimation of latent heat flux: a reflection for the future. Tethys 4, 19–26.

Castellví, F., Snyder, R.L., 2009a. Combining the dissipation method and surface renewal analysis to estimate scalar fluxes from the time traces over rangeland grass near Ione (California). Hydrol. Process. 23, 842–857.

Castellví F., Snyder, R.L., 2009b. On the performance of surface renewal analysis to estimate sensible heat flux over two growing rice fields under the influence of regional advection. J. Hydrol. 375, 546–553.

Foken, T., 2008. The energy balance closure problem - An overview. Ecol. Appl. 18, 1351–1367.

Jarmain, C., Everson, C.S., Savage, M.J., Mengistu, M.G., Clulow, A.D., Gush, M.B., 2009. Refining tools for evaporation monitoring in support of water resources management. Water Research Commission Report No. 1567. Water Research Commission, Pretoria, South Africa. ISBN 978–1–77005–798–2. p137.

Kohsiek, W., Meijninger, W.M.L., Moene, A.F., Heusinkveld, B.G., Hartogensis, O.K., Hillen, W.C.A.M., de Bruin, H.A.R., 2002. An extra large aperture scintillometer for long range applications. Boundary-Layer Meteorol. 105, 119–127.

Lothon M., Couvreux, F., Donier S., Guichard F., Lacarrère P., Lenschow D.H., Noilhan J., Saïd F., 2007. Impact of coherent eddies on airborne measurements of vertical turbulent fluxes. Boundary-Layer Meteorol. 124, 425–447.

Mauder M., Desjardins R.L., Pattey E., Gao Z., van Haarlem, R., 2008. Measurement of the sensible eddy heat flux based on spatial averaging of continuous ground-based observations. Boundary-Layer Meteorol. 128, 151–172.

Mauder, M., Foken, T., Clement, R., Elbers, J.A., Eugster, W., Grünwald, T., Heusinkveld, B. and Kolle, O., 2008. Quality control of CarboEurope flux data – Part II: Inter-comparison of eddy-covariance software. Biogeosciences. 5, 451–462

Nile, E.S., 2010. Sensible heat flux estimation for unstable conditions for sugarcane using temperature variance and surface renewal. Ph.D. thesis submitted, University of KwaZulu-Natal, pp. 171.

Savage, M.J., 2007. Sensible heat estimation using a high frequency temperature-based method above various canopies. Proc. 13th S. Afr. Nat. Comm. Int. Assoc. of Hydro. Sci. (SANCIAHS) Symp, Sept 6–7, Cape Town, Republic of South Africa.

Teixeira, A.H. de C., Bastiaanssen, W.G.M., Ahmad, M.D., Bos, M.G., 2009a. Reviewing SEBAL input parameters for assessing evapotranspiration and water productivity for the Low-Middle São Francisco River basin, Brazil: Part A: Calibration and validation. Agric. Forest Meteorol. 149, 462–476.

Teixeira, A.H. de C., Bastiaanssen, W.G.M., Ahmad, M.D., Bos, M.G., 2009b. Reviewing SEBAL input parameters for assessing evapotranspiration and water productivity for the Low-Middle São Francisco River basin, Brazil: Part B: Application to the regional scale. Agric. Forest Meteorol. 149, 477–490.

Tillman, J.E., 1972. The indirect determination of stability, heat and momentum fluxes in the atmospheric boundary layer from simple scalar variable during dry unstable conditions. J. Appl. Meteorol. 11, 783–792.

Twine, T.E., Kustas, W.P., Norman, J.M., Cook, D.R., Houser, P.R., Meyers, T.P., Prueger, J.H., Starks, P.J., 2000. Correcting eddy covariance flux underestimates over a grassland. Agric. Forest Meteorol. 103, 279–300.

van Atta, C.W., 1977. Effect of coherent structures on structure functions of temperature in the atmospheric boundary layer. Archives Mechanics 29, 161–171.

Von Randow, C., 2007. On turbulent exchange processes over Amazonian forest. Ph.D. thesis, Wageningen University, Wageningen, The Netherlands, pp. 166.

Wilson, K., Goldstein, A., Falge, E., Aubinet, M., Baldocchi, D., Berbigier, P., Bernhofer, C., Ceulemans, R., Dolman, H., Field, C., Grelle, A., Ibrom, A., Law, B.E., Kowalski, A., Meyers, T., Moncrieff, J., Monson, R., Oechel, W., Tenhunen, J., Valentini, R., Verma, S., 2002. Energy balance closure at FLUXNET sites. Agric. Forest Meteorol. 113, 223–243.

APPENDIX: FLUX ESTIMATION USING A SIMPLE IMPLEMENTATION OF AN ITERATIVE METHOD: EXAMPLES USING MOST, SURFACE RENEWAL, PENMAN-MONTEITH GRASS REFERENCE EVAPORATION AND THE PSYCHROMETRIC EQUATION[1]

A.1 Abstract

Flux estimation using iterative procedures are necessary when using Monin-Obukhov similarity theory (MOST), Penman-Monteith (PM) grass reference evaporation (ETo) and surface renewal (SR) methods. The MOST iteration method was applied to surface-layer scintillometer measurements. A single-cell spreadsheet iterative method is described, with separate calculations for stable and unstable cases. For the SR method, the air temperature ramp and period and sensible heat flux (H) for the averaging period is calculated in a single-cell for stable and unstable conditions. The roots of a third-order polynomial in ramp amplitude, dependent on the second-, third- and fifth-order air temperature structure functions obtained for each averaging period, were efficiently determined by the iterative procedure with the result of the polynomial varying between -0.015 and 0.01. For SR measurements in a mesic grassland for a two-week period for stable conditions, a sensible heat flux value was obtained less than 40 % of the time compared to in excess of 95 % for unstable conditions. This is a weakness of the SR method. Using three months of 2-min SLS data, the spreadsheet procedure agreed well with the online estimates of H. Large negative differences occurred for large values for the structure parameter of refractive index, corresponding to large H. These outlier points represent less than 1 % of the dataset. For ETo, for short grass, an iterative procedure is required since the slope of the saturation water vapour pressure *vs* temperature relationship, theoretically, is that slope between the grass surface temperature and the air temperature. The Penman approximation of this slope was to replace the grass surface temperature with the wet bulb temperature. The iterative procedure showed differences between ETo with and without iteration. Maximum differences for Kaalrug, South Africa ranged between -0.9 and 0.4 mm compared to -0.5 to 0.3 mm for Pretoria. The aerodynamic term of ETo was more affected by not using the iterative procedure with the largest ETo differences occurring under large water vapour pressure deficit conditions. An iterative procedure was also used to estimate wet bulb temperature, used in estimating open-water evaporation, and compared with an approximation by Penman for the wet bulb based on air temperature, dew point temperature, the psychrometric constant and the slope of the saturation water vapour pressure *vs* temperature relationship evaluated at the average of the two temperatures. Generally, the Penman estimate of wet bulb overestimated and increasingly so with decreasing dew point (increasing air temperature) with the largest overestimation being as much as 4.6 ^{o}C at negative dew points with differences of 0.5 ^{o}C occurring for more than a third of the dataset. The iterative procedure is quick, accurate and convenient, easy to repeat following changes to equations or data and allows easy manipulation and convenient visual inspection of data and graphics compared to other methods involving programming.

A.2 Introduction

Iterative procedures are common in biometeorology. A brief scan of the literature shows that iterative procedures are in common use but there is little published description of the actual methodology used

[1] Based on Savage (2009, 2010) and Savage et al. (2004)

or any other simple, applicable methodology. An iterative procedure is usually required when, for example, solving for the real roots of:

$$g(x) = f(x, m_1, m_2, ...) + x^n \tag{A.1}$$

where x is real number, $f(x, m_1, m_2, ...)$ is a function of measurements m_1, m_2,… and n is a known real number. Frequently, there is no analytical solution to $g(x) = 0$. Computer programming is most-often resorted to, to obtain the values of x for which $g(x) = 0$. Generally, an inequality is used to solve for the roots for which

$$\left| f(x, m_1, m_2, ...) + x^n \right| < \delta \tag{A.2}$$

where δ is a pre-defined acceptance limit – say $\delta = 0.0001$. Depending on the complexity of $f(x, m_1, m_2, ...)$ and the value of n and the amount of temporal and spatial data for which Eq. (A.1) applies, the number of iterations used to obtain the value of x satisfying the limiting conditions may vary. Often, it is necessary to compromise between the value of δ and the number of iterations.

A simple method for solving for the roots of Eq. (A.1), for which $g(x) = 0$, often using the Newton-Raphson procedure, may be obtained by rearrangement:

$$x = \left(-f(x, m_1, m_2, ...) \right)^{1/n}. \tag{A.3}$$

The right-hand side of Eq. (A.3) may be entered into a single spreadsheet cell and the iteration performed by specifying the maximum number of iterations and the maximum change below which the iteration process terminates.

The procedures outlined here are usually more complex since, for example, stable atmospheric conditions for MOST application may require a different data analysis procedure compared to unstable cases. Also, there may be missing data or measurements preventing the iteration from starting or continuing, limits to measurements m_1, m_2,… imposed that need to be specified or are imposed by theory as well as limits that may need to be specified to ensure that mathematical absurdities or impossibilities do not occur. Furthermore, the choice of equation used for solving may not be unique. For example, by inverting Eq. (A.3), x could also be written as:

$$x = f^{-1}(-x^n) + h(m_1, m_2, ...) \tag{A.4}$$

assuming that the function $h(m_1, m_2, ...)$ exists and an easy-to-use form for $f^{-1}(-x)$ exists. It is also assumed that f^{-1} can be evaluated at $-x^n$. In all cases however, a check of the iterative solution(s) should be performed to ensure real roots. For example, if x_1 is an iteratively-obtained real root, using Eq. (A.2), a test of:

$$\left| f(x_1, m_1, m_2, ...) + x_1^n \right| < \delta \tag{A.5}$$

should be performed. Should the test not succeed, then either more iteration steps are required or no solution(s) exist, assuming that the methodology followed is correct.

A.3 Theory

The theory associated with the iterative methods is discussed using four examples: MOST, surface renewal, psychrometric equation for obtaining the wet bulb temperature and Penman-Monteith grass reference evaporation.

A.3.1 A simple iterative method for surface renewal

Snyder et al. (1996) used an air temperature structure function and the procedure of van Atta (1977) to calculate the amplitude a (^{o}C) and the ramp period τ (s) (also referred to as the inverse ramp frequency) of high frequency air temperature measurements above a canopy over an averaging period, typically sub-hourly. The surface renewal (SR) sensible heat flux is calculated using:

$$H_{SR} = \alpha z \rho c_p \frac{a}{\tau}. \tag{A.6}$$

The term α is a correction or weighting factor, z the measurement height above the soil surface, ρ the density of air (kg m^{-3}) and c_p the specific heat capacity of air at constant pressure (J kg^{-1} K^{-1}). The variable αz in Eq. (A.6) represents the volume of air per unit ground area exchanged on average for each ramp in the sample period for height z (Paw U et al., 1995). Castellví et al. (2002) interpreted αz as the mean eddy size responsible for the renewal process. The weighting factor α is determined from the slope of the linear regression of eddy covariance estimates of $H = H_{EC}$ (y) against $H = H_{SR}$ (x) using Eq. (A.6) but specifying $\alpha = 1$.

The amplitude a and inverse ramp frequency τ can be determined from the second-, third-, and fifth-order of the structure function for air temperature (van Atta, 1977). The structure function is defined as:

$$S_r^n(r) = \frac{1}{m-j} \sum_{i=1+j}^{m} (T_i - T_{i-j})^n, \tag{A.7}$$

where n is the order of the air temperature structure function for which n = 2, 3 and 5 for SR analyses, m the number of data points measured at frequency f (Hz) in the hourly or sub-hourly averaging time interval, T_i the ith air temperature sample measurement, and j the number of lags between measurements corresponding to an air temperature time lag $r = j/f$ (s).

The three air temperature structure functions S_r^2 (^{o}C^2), S_r^3 (^{o}C^3) and S_r^5 (^{o}C^5) are obtained in real-time using air temperature measurements lagged by one or two time lags. Typical lags are 0.4 and 0.8 s but this varies depending on the type of datalogger used as well as the scan rate of measurements. Older and therefore slower dataloggers such as Campbell Scientific (Logan, Utah, USA) CR10X, 21X and 23X dataloggers allow scan rates of 0.125 s with typical lags of 0.25 and 0.5 s used. The newer and faster dataloggers allow scan rates of 10 Hz with typical lags of 0.4 and 0.8 s. However, the newer loggers also allow storage of the high frequency air temperature data from which any desired time lag can then be used post-data collection.

Van Atta (1997) suggested that τ should be much greater than the time lag r, typically $\tau > 10r$, or otherwise the structure function theory is invalid. Snyder et al. (2007), using a procedure they referred to as SR_Excel, only computed τ if $\tau \geq 5r$ with an upper condition that $\tau \leq 600$ s.

Following van Atta (1997), an estimate of the mean value for ramp amplitude a during the averaging time interval is determined by solving for the real roots of:

$$a^3 + pa + q = 0 \tag{A.8}$$

where

$$p = 10S_r^2 - \frac{S_r^5}{S_r^3} \tag{A.9}$$

and

$$q = 10S_r^3. \tag{A.10}$$

The ramping period τ is calculated using:

$$\tau = -\frac{a^3 r}{S_r^3}. \tag{A.11}$$

By definition, τ in Eq. (A.11) is positive. For unstable conditions, $a > 0$ ^{o}C and therefore $a^3 r > 0$ and therefore the negative sign on the right-hand side of Eq. A.11 forces $S_r^3 < 0$ ^{o}C^3. Similarly, for stable conditions, $a < 0$ ^{o}C forces $S_r^3 > 0$ ^{o}C^3. The key to the SR approach is the solution of the real roots of Eq. (A.8) and that atmospheric stability is indicated by the sign of S_r^3 (Eq. (A.11)).

To date, there has been no simple methodology proposed for the solution of Eq. (A.8). The objective of this work is to obtain the real roots to the van Atta (1997) cubic polynomial in a single cell in a spreadsheet and hence calculate $H = H_{SR}$ for both stable and unstable conditions.

For

$$5r \leq \tau \leq 600 \tag{A.12}$$

and rearranging Eq. (A.8):

$$a = (-pa - q)^{1/3}. \tag{A.13}$$

Accounting for unstable conditions for which a > 0 ^{o}C is possible using the multiplicative term $-S_r^3 / |S_r^3|$ which equates to 1 for unstable conditions and -1 for stable conditions. Hence, combining Eqs (A.13), (A.9) and (A.10), in terms of the air temperature structure functions:

$$a = \frac{-S_r^3}{|S_r^3|}\left|\left(\left(-10S_r^2 + \frac{S_r^5}{S_r^3}\right)a - 10S_r^3\right)^{1/3}\right| . \quad \text{(A.14)}$$

Hence if $S_r^3 < 0$, then $a > 0$ °C which corresponds to unstable conditions for which $H_{SR} > 0$ W m^{-2}.

Hence, ramping period τ is calculated using Eq. (A.11) with the limiting conditions imposed by Eq. (A.12). The sensible heat flux H_{SR} is then calculated using Eq. (A.6) with α = 1.

A.3.2 A simple iterative method for surface-layer scintillometry

From scintillometer beam transmission measurements for a known horizontal beam distance and height, surface-layer scintillometry (SLS) allows measurements of four key quantities required for the estimation of sensible heat and momentum flux using the Monin-Obukhov similarity theory (MOST):

the structure parameter of refractive index C_n^2 (m$^{-2/3}$),

the structure parameter of temperature C_T^2 (K^2 m$^{-2/3}$),

the inner scale of refractive index fluctuations l_o (mm) and

the dissipation rate of turbulent kinetic energy ε (referred to as TKE in the literature, m^2 s^{-3}).

Large-aperture scintillometry (LAS), which only measures C_n^2, requires additional measurements of horizontal wind speed to estimate the friction velocity u_*, but both SLS and LAS methods also require measurements or estimates of atmospheric pressure P as well as the air temperature T and information about the direction of the sensible heat flux H. For the dissipation range of turbulence, the structure parameter of refractive index C_n^2 is calculated from measurements at the receiver position. The parameter C_n^2 provides the linkage between radiation transmission and atmospheric turbulence via the optical properties of the atmosphere. For the dissipation range, a function describing the decay of the refractive index fluctuations is used for calculating C_n^2 (Thiermann and Grassl, 1992). This function, proposed by Hill and Clifford (1978), includes the spectral "bump" in the dissipation range reported by Champagne et al. (1977) and Williams and Paulson (1977).

The dissipation rate of the turbulent kinetic energy ε is estimated using SLS measurements of l_o using the Hill and Clifford (1978) relationship for the dissipation range for which

$$\varepsilon = \nu^3 \left(\frac{7.4}{l_o}\right)^4 \quad \text{(A.15)}$$

where ν (m^2 s^{-1}) is the kinematic viscosity of air. The constant 7.4 is derived from $(12\beta_1 / \mathrm{Pr})^{3/4} = 7.37$ where β_1 = 0.86 is the Obukhov-Corrsin constant and Pr = 0.72 is the Prandtl number.

Invoking MOST, the temperature scaling parameter T_* (K) is given by

$$T_* = C_T \cdot (z-d)^{1/3} \cdot [f(\zeta)]^{-1/2} \quad \text{(A.16)}$$

where C_T is determined from measurements of C_n^2 and from air temperature T and atmospheric pressure P or equivalent, measurement height z (m) and the zero-plane displacement d (m) where $\zeta = \frac{z-d}{L}$ is the argument of the MOST semi-empirical and dimensionless function $f(\zeta)$ where L is the Obukhov stability length.

Using the convention that the Obukhov length $L < 0$ m for unstable conditions, corresponding to $H < 0$ W m^{-2}, where

$$L = \frac{T}{k\,g}\frac{\rho c_p u_*^3}{H} \text{ or equivalently } L = -\frac{T}{k\,g}\frac{u_*^2}{T_*} \tag{A.17}$$

where k is the von Kármán constant (0.4) and g the acceleration of gravity (m s^{-2}). Also from MOST,

$$u_* = \varepsilon^{1/3} \cdot [k \cdot (z-d)]^{1/3} \cdot [g(\zeta)]^{-1/3} \tag{A.18}$$

where ε is obtained using Eq. (A.15) from ν and l_o, the latter estimated from measurements at the SLS receiver, and where $g(\zeta)$ is the second MOST empirical and dimensionless function. Strictly,

$$L = \frac{T}{k\,g}\frac{\rho c_p u_*^3}{(H + 0.61 c_p T E)},$$

where E is the mass flux of water vapour (kg s^{-1} m^{-2}), to account for the contribution of buoyancy from evaporation effects (Businger and Yaglom, 1971). The shortened energy balance can be used to express E in terms of H, R_{net} and S. Hence:

$$L = \frac{T}{k\,g}\frac{\rho c_p u_*^3}{\left(H + 0.61 c_p T\left(-R_{net} - H - S\right)/\lambda\right)}$$

where λ is the specific latent heat of vapourisation. Different forms of the MOST functions $f(\zeta)$ and/or $g(\zeta)$ have been used in the literature (examples of which are presented in Chapter 4, Table 4.1). These functions allow T_* and u_* to be estimated (Eqs (A.16) and (A.18) respectively) from which H is then determined using

$$H = -\rho c_p u_* T_*. \tag{A.19}$$

The functions for $f(\zeta)$ and $g(\zeta)$ used are those from Thiermann and Grassl (1992).

Measurements of C_n^2 and ε and use of the MOST functions $f(\zeta)$ and $g(\zeta)$ respectively, allow T_* and u_* to be determined by iteratively varying L (Eq. (A.17)) obtained by combining Eqs (A.16) and (A.18). Sensible heat flux density $H = H_{SLS}$ is then calculated using Eq. (A.19). These calculations also require knowledge of T, P, z, and d. The shortened form of the energy balance is then used to determine λE.

In summary, SLS measurements allow for the determination of H_{SLS} using MOST, relying on the determination of the structure parameter for refractive index fluctuations C_n^2 from which T_* is estimated and from measurements of the inner scale of refractive index fluctuations l_o from which u_*

is calculated. This is in contrast with LAS instruments that allow determination of C_n^2 with u_* estimated from additional horizontal wind speed or eddy covariance measurements.

For unstable conditions, ($\zeta < 0$ and H_{SLS} < 0 W m^{-2}), the single-cell calculation for L is as follows:

if $L = 0$ then $L = L$ - 0.00001

else if C_T^2 or $\varepsilon = 0$

then $L =$ ""

else if $\left|f(\zeta)\right| < 0.000001$

then $L = -0.001$

else $L = -T\,(k\,g)^{-1}\,\varepsilon^{2/3}\left(k(z-d)\right)^{1/3}\left(C_T^2\right)^{-1/2}\left(g(\zeta)\right)^{-2/3}k^{1/3}\left(f(\zeta)\right)^{1/2}$.

For stable conditions, ($\zeta \geq 0$ and H_{SLS} > 0 W m^{-2}), the single-cell calculation for L is as follows:

if $L = 0$ then $L = L + 0.00001$

else if C_T^2 or $\varepsilon = 0$

then $L =$ ""

else $L = T\,(k\,g)^{-1}\,\varepsilon^{2/3}\left(k(z-d)\right)^{1/3}\left(C_T^2\right)^{-1/2}\left(g(\zeta)\right)^{-1/3}(z-d)^{-1/3}k^{1/2}\left(f(\zeta)\right)^{1/2}$.

For unstable conditions, the single-cell calculation for H_{SLS} is as follows:

if $L =$ "" then $H =$ ""

else $H = 1.1045\cdot 1000\left(0.4\varepsilon\cdot(z-d)\right)^{1/3}\left(1-3\zeta^{-1}-\zeta^{-1/3}\right)\left(C_T^2\right)^{1/2}\left(0.4\,(z-d)\right)^{1/3}\,0.4^{-1/3}6.34^{-1/2}\left(1-7\zeta+75\zeta^2\right)^{1/6}$.

The density of air value of 1.1045 kg m^{-3} and specific heat capacity of 1000 J kg^{-1} K^{-1} were used to ensure agreement with the Scintec (2006) estimates of H_{SLS}.

For stable conditions, the single-cell calculation for H_{SLS} is as follows:

if $L =$ "" then $H =$ ""

else

$H = 1.1045\cdot 1000\cdot\left(\varepsilon\cdot 0.4\cdot(z-d)\right)^{1/3}\left(1+4\zeta+16\zeta^2\right)^{-1/6}\left(C_T^2\right)^{1/2}\left(0.4\cdot(z-d)\right)^{1/3}\,0.4^{-1/3}6.34^{-1/2}\left(1+7\zeta+20\zeta^2\right)^{-1/6}$.

For unstable conditions, the single-cell calculation for momentum flux τ_{SLS} is as follows:

if $L =$ "" then $\tau =$ ""

else $\tau = 1.1045 \cdot \left(\left(\varepsilon \cdot 0.4 \cdot (z-d) \right)^{1/3} \left((1-3\zeta)^{-1} - 1 - \zeta \right)^{-1/3} \right)^2$.

For stable conditions, the single-cell calculation for τ_{SLS} is as follows:

if $L =$ "" then $\tau =$ ""

else $\tau = 1.1045 \cdot \left(\left(\varepsilon \cdot 0.4 \cdot (z-d) \right)^{1/3} \left(1 + 4\zeta + 16\zeta^2 \right)^{-1/6} \right)^2$.

In a remote sensing application, Gieske (2003) used a cubic spline approximation for the calculation of the MOST stability functions for momentum and sensible heat flux. In their case, the required number of calculations is large since their iterative numerical flux-profile method had to be applied to every pixel, typically 10^7 pixels in a Landsat 7 scene.

A.3.3 A simple iterative method for calculating wet bulb temperature

Models for estimating open-water evaporation require the wet bulb temperature (Edinger et al., 1968; Keijman and Koopmans, 1973; de Bruin, 1982). There is no accurate analytical method for calculating wet bulb from the dry bulb T_d – also referred to as T_z – and say the water vapour pressure e. Penman (1948) approximated the wet bulb temperature T_w (^{o}C) as a weighted mean between dry bulb and dew point T_d and T_{dp} respectively, in (^{o}C), using the psychrometric constant γ (kPa K^{-1}) and the slope of the saturation water vapour pressure *vs* dry bulb Δ (kPa K^{-1}):

$$T_w \approx \frac{\gamma \cdot (T_d + 273.15) + \Delta \cdot (T_{dp} + 273.15)}{\gamma + \Delta} - 273.15 \qquad \text{(A.20)}$$

where Δ is in this case evaluated at $(T_d + T_{dp})/2$. The psychrometric equation allows the water vapour pressure e to be calculated from T_d and T_w, requiring also information to calculate the atmospheric pressure P (kPa):

$$e = e_s(T_w) - (\gamma P / 100) \cdot (T_d - T_w) \cdot (1 + 0.00115 T_w) \qquad \text{(A.21)}$$

where

$$e = e_s(T_d) \cdot RH / 100, \qquad \text{(A.22)}$$

where RH is the relative humidity (%) and $e_s(T)$ the saturation water vapour pressure (kPa) at temperature T (^{o}C) that is given by:

$$e_s(T) = 0.6108 \cdot \exp\left(17.2694 T / (237.3 + T)\right). \qquad \text{(A.23)}$$

The psychrometric constant γ (Eq. (A.21)) is given by:

$$\gamma = \frac{c_p P}{\varepsilon \lambda} \tag{A.24}$$

where ε is the ratio of the molecular mass of water to that of dry air ε 0.622 and λ is the specific latent energy of vapourization (MJ kg^{-1}) at the wet bulb,

$$\lambda = 2.501 - 2.361 \times 10^{-3} T_w$$

and, from Savage et al. (1997),

$$c_p = 1004.722587 + 1148.84385 \cdot \left(\frac{e}{P - e} \right) + 1.256 \cdot \left(1 + \frac{T_d}{40} \right) \cdot \left(1 + \frac{RH}{100} \right). \tag{A.25}$$

Most texts give λ as a function of T_d – Ham (2005) maintains that in theory $\lambda = \lambda(T_w)$. However for a canopy surface, strictly, should λ of λE not be evaluated at canopy temperature T_o since evaporation is at the canopy surface? Why should λ be evaluated at the wet bulb of the atmosphere?

The atmospheric pressure P can be estimated from water vapour pressure e, T_d and altitude h (m):

$$P = 101.325 - \frac{(-10.94866 e_d + 2934.7773) \cdot 9.79267 h / 1000}{8.31451 \left(T_d + 273.15 \right) + 0.28362157 h}. \tag{A.26}$$

Testing to examine if:

$$\left| e_s(T_w) - (\gamma P / 100) \cdot (T_d - T_w) \cdot (1 + 0.00115 T_w) - e \right| < 0.005 \tag{A.27}$$

allows T_w to be evaluated, as in Eq. (A.2). If the condition is not met, the wet bulb can be incremented by a small value – say 0.005 °C for positive T_w values and -0.005 °C for negative T_w. The disadvantage of this method is that more than 6000 iterations may be required if wet bulb to two decimals is required.

A.3.4 A simple iterative method for Penman-Monteith grass reference evaporation

Evaporation from a surface can be calculated using the Penman-Monteith equation, or "combination" method:

$$\lambda E = \frac{\Delta \cdot (R_n - G) + \rho c_p \cdot \left(e_s(T_z) - e \right) / r_a}{\Delta + \gamma \cdot \left(1 + \frac{r_s}{r_a} \right)} \tag{A.28}$$

where R_n and G are the net irradiance and soil heat flux respectively, r_s the bulk surface resistance that describes the resistance to flow of water vapour from inside the leaf, vegetation canopy or soil to outside the surface and r_a is the aerodynamic resistance to turbulent heat energy and/or water vapour transfer from the surface to a height z above the surface (Allen et al., 2006). The Penman-Monteith equation is also often used to calculate, by back-calculation, the surface conductance to water vapour

(Wohlfahrt et al., 2009). As pointed out by Wohlfahrt et al. (2009), it is assumed in Eq. (A.28) that the energy balance is closed.

Commonly, λE is calculated using a crop factor and grass reference evaporation (Allen et al., 1998: FAO56; Allen et al., 2006), referred to as ETo, based on point atmospheric measurements at a single level, usually at 2 m, at an automatic weather station from measurements of solar irradiance, air temperature, water vapour pressure and wind speed. The crop factor is used as a multiplying factor for ETo to obtain λE, the crop factor effectively distinguishing the vegetation under consideration from a grass reference crop. The dual crop factor approach uses one crop factor for the soil surface and another for the crop. The extension of reference evaporation from daily (Allen et al., 1998) to hourly estimates has been recommended (Allen et al., 2006) for both grass (0.1-m tall) reference evaporation and tall vegetation (0.5-m lucerne). Allen et al. (2006) recommend that for application of the FAO-PM ETo method from FAO56 applied for hourly or shorter time intervals for short grass, a surface resistance r_s = 50 s m^{-1} is recommended for daytime and r_s = 200 s m^{-1} for night-time periods and an aerodynamic resistance of $208/U_2$ is used, where U_2 is the horizontal wind speed at a height of 2 m. These adjustments are based on best agreements with computations made on a 24-h time step basis lysimeter measurements. The daytime value of r_s = 50 s m^{-1} recommended by Allen et al. (2006) is also in agreement with that found by Savage et al. (1997) for a short grass surface.

Also for hourly or shorter time intervals for a 0.5-m tall canopy, r_s = 30 s m^{-1} for daytime and r_s = 200 s m^{-1} for night-time periods and an aerodynamic resistance of $118/U_2$ is recommended. Allen et al. (2006) based these adjustments on best agreement with 24-h time-step lysimeter measurements. For application of the FAO-PM method for daily (24-h) time steps, Allen et al. (2006) recommend use of r_s = 70 s m^{-1}.

The partitioning of the available energy flux is slightly different for short grass reference evaporation compared to that for tall-crop reference evaporation. For short grass, $S = 0.1R_{net}$ when R_{net} is positive (daytime) and $S = 0.5R_{net}$ (night-time). For tall-crop reference evaporation, it is assumed that $S = 0.04R_{net}$ when R_{net} is positive (daytime) and $S = 0.2R_{net}$ (night-time).

An examination of the literature shows that the details for determining Δ are often absent and sometimes incorrect. Grass reference λE using the Penman-Monteith approach (ETo) is frequently calculated using values for Δ and λ evaluated at the air temperature T_z at height z. More correctly however, $\Delta = \Delta(T_z, T_o)$ and $\lambda = \lambda(T_o)$ where T_o is the short-grass surface temperature, or that for tall-crop for ETo for tall-crop reference evaporation. To avoid the use of what is usually an unknown temperature, viz. T_o, most derivations make the assumption that

$$\Delta = \left(\frac{\delta e_s}{\delta T}\right)_{T=T_z} . \tag{A.29}$$

McArthur (1990) refers to this assumption as the first step in an iterative method for arriving at T_o. Some derivations instead make the assumption that $T_o \approx T_w$. The procedure for obtaining T_w has already been described so the focus here is on estimating T_o. The assumption that $T_o \approx T_w$ then allows Δ to be calculated using

$$\Delta = \frac{e_s(T_z) - e_s(T_w)}{T_z - T_w} \tag{A.30}$$

where $e_s(T_z)$ is the saturation water vapour pressure at T_z and $e_s(T_w)$ that at T_w. However, McArthur (1990) correctly indicates that

$$\Delta = \frac{e_s(T_z) - e_s(T_o)}{T_z - T_o}, \tag{A.31}$$

the theoretical formulation used by Penman (1948).

Bristow (1987) used an algorithm which employs Newton's iterative method for solving the non-linearized surface energy balance equation to obtain surface temperature to any desired degree of accuracy. Paw U and Gao (1988) found that use of the Penman-Monteith equation can introduce errors as large as 20 % when T_o exceeds T_z and suggested that this was due to the linearization used in the Penman-Monteith equation. McArthur (1990) found that errors in λE can arise if it is assumed that $\Delta = \Delta(T_z)$ – that is, if Eq. (A.29) is used. Further, he found that the error in λE introduced by the assumption that $\Delta = \Delta(T_z)$ depended on $T_o - T_z$ and on the absolute value of T_z and therefore recommended elimination of the error by a simple iterative procedure.

Using the shortened energy balance equation and resistance expressions for λE and H, an expression for T_o may be derived:

$$R_n - G = \lambda E + H \tag{A.32}$$

$$\lambda E = \frac{\rho c_p}{\gamma} \frac{e_s(T_z) - e_z}{r_s + r_v} \tag{A.33}$$

$$H = \rho c_p \frac{T_o - T_z}{r_h} \tag{A.34}$$

where r_s is the bulk surface resistance (s m^{-1}), referred to as r_c by McArthur (1990), r_v the boundary-layer resistance to water vapour flux (s m^{-1}) and r_h the boundary-layer resistance to sensible heat flux (s m^{-1}). For the MacArthur (1990) case, applied to grass reference evaporation, it is assumed that the short reference crop fully covers the soil, thereby making soil evaporation negligible. In the FAO56 formulation, r_h is equated to r_v – that is, similarity between sensible heat and latent energy flux is assumed. Assuming similarity, making $r_h = r_v = r_a$, and substituting Eqs (A.33) and (A.34) into (A.32) and rearranging to obtain T_o:

$$T_o = T_z + \frac{r_a \gamma_* \cdot (R_n - G)}{\rho c_p \cdot (\Delta + \gamma_*)} - \frac{e_s(T_z) - e_z}{\Delta + \gamma_*} \tag{A.35}$$

where a modified psychrometric constant, γ_* (kPa K^{-1}), is defined as:

$$\gamma_* = \gamma \cdot \frac{(r_s + r_a)}{r_a}. \tag{A.36}$$

If $T_o \leq T_z$, then

$$R_n - G \leq \frac{\rho c_p \left(e_s(T_z) - e_z\right)}{r_a \gamma_*} \tag{A.37}$$

or

$$R_n - G \leq \left(\lambda E\right)_{r_s=0,\, r_h=r_v=r_a} \tag{A.38}$$

where $\left(\lambda E\right)_{r_s=0,\, r_h=r_v=r_a}$ is the evaporation with a canopy resistance r_s of 0 s m^{-1} under similarity conditions $(r_h = r_v = r_a)$.

For daily measurements from a weather station, assuming a constant grass (or crop) height of 0.12 m and a standardized height for air temperature, wind speed and relative humidity of 2 m, the aerodynamic resistance r_a for neutral conditions is given by:

$$r_a = \frac{208}{U_z}, \tag{A.39}$$

where U_z is the measured horizontal wind speed at height z. The application of Eq. A.28 for short time periods (hourly or less) may require the inclusion of corrections for stability (Allen et al., 1998), for other than neutral stability conditions, but that when predicting ETo for a well-watered (grass) reference surface, the heat energy flux exchanged is small, and the stability correction is therefore not normally applied.

A.4 Materials and methods

Surface renewal and surface-layer scintillometer measurements were conducted above an open, mixed grassland community and summer rainfall site in the Hay Paddock area neighbouring Ashburton and close to the suburb of Bellevue of Pietermaritzburg, South Africa (29°38'S, 30°26'E) with an altitude of 671.3 m.

For the SR method, several unshielded and naturally-ventilated type-E thermocouples (75-µm diameter) were used to measure air temperature, placed at heights of 0.5, 0.8, 1.0 and 1.5 m above the soil surface. Each sensor consisted of a pair of thermocouples in parallel. Some of the thermocouples were connected to a Campbell CR10X datalogger that also had an insulated reference thermistor for thermocouple measurements. The datalogger panel was covered with insulation foam to reduce temperature changes in the vicinity of the thermistor and connecting thermocouple wires. The remaining thermocouples were connected to a Campbell CR23X datalogger. The thermocouples were pointed into the predominant wind direction which occurred during daylight hours. Measurements were made every 0.125 s, equivalent to a frequency of 8 Hz, and then lagged by 0.25 s and 0.5 s before calculating the second-, third- and fifth-order air temperature structure functions required by the van Atta (1977) approach for SR analysis and then these were averaged every two minutes. Similar measurement procedures were later used using the faster Campbell CR5000 datalogger except that measurements were made every 0.1 s and then lagged by 0.2 and 0.4 s. Software calculations, post-data collection, were used to calculate SR sensible heat fluxes using the van Atta (1977) approach. For this purpose, three methods were used to solve for the real roots of the cubic equation (Eq. A.14):

a Microsoft QuickBASIC 4.0 programme, under MS-DOS, provided by Snyder (2003, pers. comm.[2]). Since measurements from a number of thermocouples were stored in one datalogger, it was necessary to split the data so that each data file corresponded to data from just one thermocouple. For this purpose, the Split program, part of PC208 (version 3.08) or LoggerNet 2.1 (both from Campbell) was used. Following the data split, the data file the QuickBASIC program was executed. The program required two versions of the data file. Following successful execution of the program, the output file was created;

the SR_Excel spreadsheet of Snyder et al. (2007) was used. The spreadsheet contains 52 columns for performing the same SR calculations as in the QuickBasic programme for two thermocouples and two time lags;

the single-cell spreadsheet method for calculating each of a (Eq. (A.14)), τ (Eq. (A.11)) with conditions imposed by Eq. (A.12) and H_{SR} (Eq. (A.6)), based on the iterative method.

The procedures used for SLS sensible heat flux measurements are described in Chapter 4. The beam path length was kept at 101 m and the beam height varied between 1.5 and 1.65 m except near the end of the study. The canopy height h was measured regularly and this height was used to calculated $d + z_o$ where it was assumed that the zero plane displacement height $d \approx 0.67\ h$ and the roughness length $z_o \approx 0.1\ h$ (Brutsaert, 1982). The effective beam height input, which is required for SLS measurements, was set at beam height above the soil surface minus $d + z_o$. For some of the time, the voltage range was altered due to low voltage signals. The transmitter and receiver SLS units required little attention apart from inspecting for dirt and cobwebs obscuring the beam and occasional realignment following storms. The cables had to be replaced twice – once due to the accidental fire and a second time when the grass was accidentally cut.

A decade of weather station data (1993 to 2002 inclusive) for Pretoria, South Africa (latitude 25°44′31″S, longitude 28°11′59″E, altitude 1308 m) for the ETo calculations were provided by the South African Weather Service, Pretoria, South Africa. The daily data included maximum and minimum air temperature, daily solar radiation (MJ m^{-2}), water vapour pressure and wind speed. There were no missing air temperature, water vapour pressure and wind speed data. Missing solar radiation data – 78 occurrences in ten years – were computed from the air temperature range (Abraha and Savage, 2008). For confirmation of the results, more than 17 years of weather station data (1990 to July 2006 inclusive) for Kaalrug, Mpumalanga, South Africa (latitude 25°37′25″S, longitude 31°32′24″E, altitude 366 m) were provided by the South African Sugar Research Institute, Mount Edgecombe, South Africa.

[2] Dr. R.L. Snyder, Department of Land, Air and Water Resources, University of California, Davis, California, USA

A.5 Results and discussion

A5.1 SR iterative procedure

The QuickBASIC approach of determining the ramp amplitude a suffers from a resolution limitation (Figs A.1, A.2). The check of the solution, viz., that $a^3 + pa + q = 0$ (Eq. (A.8)) is satisfied shows that $a^3 + pa + q$ varies between about -1.0 and 1.0 for the QuickBASIC method compared to between -0.015 and 0.01 for the single-cell iterative method. The results of the two spreadsheet methods shows good correspondence for the majority of the data but unpredictable H values for the QuickBASIC method for when a is not an exact root of Eq. (A.8) (Fig. A.3). The single-cell iterative method for both stable and unstable cases is quick, accurate and convenient, easy to repeat following changes to equations or data, allows easy manipulation and allows convenient visual inspection of data and graphics, compared to other methods involving Fortran, Visual Basic, C or other language programming. For half-hourly SR measurements above a mixed community grassland surface for a month (day of year 291 to 321, 2004) for stable conditions, less than 40 % of the time a sensible heat flux value was obtained by iteration compared to in excess of 95 % for unstable conditions. The inability of the SR method to obtain a solution for most of the stable conditions is a significant weakness of the method. In defence of the SR method for such cases, Castellví et al. (2008) point out that the fetch requirements are more demanding for stable cases and that the fluxes are small and more affected by (measurement) errors.

A5.2 SLS MOST iterative procedure

For three months of two-min SLS data (January 2004), estimates of H_{SLS} (y) using the online method, for unstable events is almost identical to the estimates from the iterative procedure (x): slope of 0.9819, intercept -1.49 W m^{-2}, R^2 of 0.9970 and RMSE of 3.94 W m^{-2} (Fig. A.4). For about 1.6 % of the data pairs, the difference in H was more than 3 W m^{-2}, with some exceptional differences as large as 5.0 and as low as -157.2 W m^{-2}. The large negative differences generally occurred when C_n^2 was large – greater than 0.25 $\times$ 10^{-12} m$^{-2/3}$ and in some cases equal to 99.99 $\times$ 10^{-12} m$^{-2/3}$. In general, the two methods were in very good correspondence. The set of points not falling on the 1:1 line shown in Fig. A.4 represent less than 1.5 % of the set of data but need further investigation.

A5.3 Iterative procedure for wet bulb estimation

For the Kaalrug site, the wet and dry bulb temperatures were used to calculate water vapour pressure for the 08h00 and 14h00 datasets using Eq. (A.21). The iterative procedure and the method of Penman (1948) were used to calculate T_w using Eqs (A.27) and (A.20) respectively. The paired T_w datasets for 08h00 and 14h00 were then compared using normal linear regression analysis. For the Pretoria dataset, the average daily air temperature and water vapour pressures were used and the two wet bulbs calculated as described previously. In general, the $T_{w\ \mathrm{Penman}}$ estimates were lower than the $T_{w\ \mathrm{iterative}}$ values. For Kaalrug, the largest deviations tended to occur at low wet bulbs with the maximum $T_{w\ \mathrm{Penman}} - T_{w\ \mathrm{iterative}}$ deviation of 2.1 ^{o}C at 08h00 and 4.6 ^{o}C at 14h00. The RMSE was greater at 14h00 (0.40 ^{o}C) compared to 08h00 (0.11 ^{o}C). The 14h00 data also showed more variability compared to the 08h00 data. For Pretoria, the maximum deviation was 2.1 ^{o}C. For both sites, the greatest deviations tended to occur at low T_{dp}, particularly negative T_{dp} for Kaalrug at 14h00 (Fig. A.5, A.6).

A5.4 Iterative procedure for grass reference ETo

The comparison between ETo calculated iteratively using $\Delta = \Delta(T_o, T_z)$ (Eq. (A.31)) and ETo calculated using $\Delta = \Delta(T_z)$ (Eq. (A.29)) showed differences that varied between -0.89 and 0.43 mm for the 16-year dataset from Kaalrug with a tendency for $\mathrm{ETo}(T_z)$ to underestimate compared to $\mathrm{ETo}(T_o)$ at greater ETo values (Figs A.7, A.8). The differences varied between -0.51 and 0.34 mm for the Pretoria site, respectively. The aerodynamic component of ETo was consistently underestimated using $\mathrm{ETo}(T_z)$ compared to $\mathrm{ETo}(T_o)$ (Fig. A.9) whereas the radiative component of ETo was generally slightly overestimated (Fig. A.10). The slight underestimation of the aerodynamic component of ETo tended to cancel with the over-estimated radiative component.

A.6 Acknowledgements

The weather station data for Pretoria for the ETo and wet bulb calculations were provided by the South African Weather Service, Pretoria, South Africa and that for Kaalrug by the South African Sugar Research Institute. We acknowledge financial support from the UKZN, CSIR, and WRC as part of projects K349, K1335 and K1567. Thanks to my postgraduates for pestering me to work on these procedures.

A.7 References

Abraha, M.G. and M.J. Savage, 2008. Comparison of estimates of daily solar radiation from air temperature range for application in crop simulations. Agric. Forest Meteorol. 148, 401-416.

Allen, R.G, Pereira, L.S., Raes, D., Smith, M., 1998. Crop evapotranspiration - Guidelines for computing crop water requirements - FAO Irrigation and drainage paper 56 FAO - Food and Agriculture Organization of the United Nations Rome., Italy. 315 pp.

Allen, R.G., Pruitt, W.O., Wright, J.L., Howell, T.A., Ventura, F., Snyder, R., Itenfisu, D., Steduto, P., Berengena, J., Yrisarry, J.B., Smith, M., Pereira, L.S., Raes, D., Perrier, A., Alves, I., Walter, I., Elliott, R., 2006. A recommendation on standardized surface resistance for hourly calculation of reference ETo by the FAO56 Penman-Monteith method. Agric. Water Manage. 81, 1–22.

Bristow, K.L., 1987. On solving the surface energy balance equation for surface temperature. Agric. Forest Meteorol. 39, 49–54.

Brutsaert, W.H., 1982. Evaporation into the Atmosphere. Reidel, Dordrecht, Holland, 299 pp.

Businger, J.A., Yaglom, A.M., 1971. Introduction to Obukhov's paper on turbulence in an atmosphere with a non-uniform temperature. Boundary-Layer Meteorol. 2, 3–6.

Castellví, F., Perez, P.J., Ibañez, M., 2002. A method based on high frequency temperature measurements to estimate sensible heat flux avoiding the height dependence. Water Resour. Res. 38 (6), WR000486–20, 1–10.

Castellví, F., Snyder, R.L., Baldocchi, D.D., 2008. Surface energy-balance closure over rangeland grass using the eddy covariance method and surface renewal analysis. Agric. Forest Meteorol. 148, 1147–1160.

Champagne, F.H., Friehe, C.A., La Rue, J.C., Wyngaard, J.C., 1977. Flux measurements, flux estimation techniques, and fine scale turbulence measurements in the unstable surface layer over land. J. Atmos. Sci. 34, 515–530.

de Bruin, H.A.R., 1982. Temperature and energy balance of a water reservoir determined from standard weather data of a land station. Journal of Hydrology 59, 261–274.

Edinger, J.E., Duttweiler, D.W., Geyer, J.C., 1968. The response of water temperature to meteorological conditions. Water Resources Research 4, 1137–1143.

Gieske, A., 2003. The iterative flux-profile method for remote sensing applications. Int. J. Remote Sensing 16, 3291–3310.

Hill, R.J., Clifford, S.F., 1978. Modified spectrum of atmospheric temperature fluctuations and its application to optical propagation. J. Opt. Soc. Am. 68, 1201–1211.

Keijman, J.Q., Koopmans, R.W.R., 1973. A comparison of several methods of estimating evaporation of Lake Flevo. In Hydrology of Lakes. IAHS publication no 109, Helsinki. Pp 225–232.

McArthur, A.J., 1990. An accurate solution to the Penman equation. Agric. Forest Meteorol. 51, 87–92.

Paw U, K.T., Gao, W., 1988. Applications of solutions to non-linear energy budget equations. Agric. Forest Meteorol. 43, 121–145.

Paw U, K.T., Qui, J., Su, H.B., Watanabe, T., Brunet, Y., 1995. Surface renewal analysis: a new method to obtain scalar fluxes. Agric. Forest Meteorol. 74, 119–137.

Penman, H.L., 1948. Natural evapotranspiration from open water, bare soil and grass. Proc. Roy. Soc. London, Ser. A, 193, 120–145.

Savage, M.J., 2009. Estimation of evaporation using a dual-beam surface layer scintillometer and component energy balance measurements. Agric. Forest Meteorol. 149, 501–517.

Savage, M.J., 2010. Sensible heat flux and evaporation using iteration. Paper presentation to the Combined Congress 2010, South African Society for Horticultural Sciences, Weed Science Society, Crop Production Society and Soil Science Society of South Africa, 18 to 21 Jan, 2010, Bloemfontein, South Africa.

Savage, M.J., Everson, C.S., Metelerkamp, B.R., 1997. Evaporation measurement above vegetated surfaces using micrometeorological techniques. South African Water Research Commission Report No. 349/1/97, Pretoria, South Africa, 248 pp., ISBN 1–86845–363–4.

Savage, M.J., Odhiambo, G.O., Mengistu, M.G., Jarmain, C., 2004. Theory and practice of evapotranspiration measurement, with special focus on surface layer scintillometer (SLS) as an operational tool for the estimation of spatially-averaged evaporation. Water Research Commission (WRC) Report No. 1335/1/04. WRC, Pretoria, Republic of South Africa, 204 pp., ISBN 1-77005-247-X.

Scintec, 2006. Surface Layer Scintillometer, SLS20/SLS20-A/SLS40/SLS40-A. User's Manual. pp 100. Scintec Atmosphärenmessetechnik, Tübingen, Germany.

Snyder, R.L., Anderson, F.E., Spano, D., Duce, P., Paw U, K.T., Russo, A.E., 2007. An Excel application program to compute surface renewal estimates of sensible heat flux from the 2nd, 3rd and 5th moments of a structure function using high frequency temperature data and to compute ET and crop coefficients using energy balance. University of California, Davis, California.

Snyder, R.L., Spano, D., Paw U, K.T., 1996. Surface renewal analysis for sensible heat and latent heat flux density. Boundary-Layer Meteorol. 77, 249–266.

Thiermann, V., Grassl, H., 1992. The measurement of turbulent surface-layer fluxes by use of bichromatic scintillation. Boundary-Layer Meteorol. 58, 367–389.

van Atta, C.W., 1977. Effect of coherent structures on structure functions of temperature in the atmospheric boundary layer. Archives Mechanics 29, 161–171.

Williams, R.M., Paulson, C.A., 1977. Microscale temperature and velocity spectra in the atmospheric boundary layer. J. Fluid Mech. 83, 547–567.

Wohlfahrt, G., Haslwanter, A., Hörtnagl, L., Jasoni, R.L., Fenstermaker, L.F., Arnone, J.A., Hammerle, A., 2009. On the consequences of the energy imbalance for calculating surface conductance. Agric. Forest Meteorol. 149, 1556–1559.

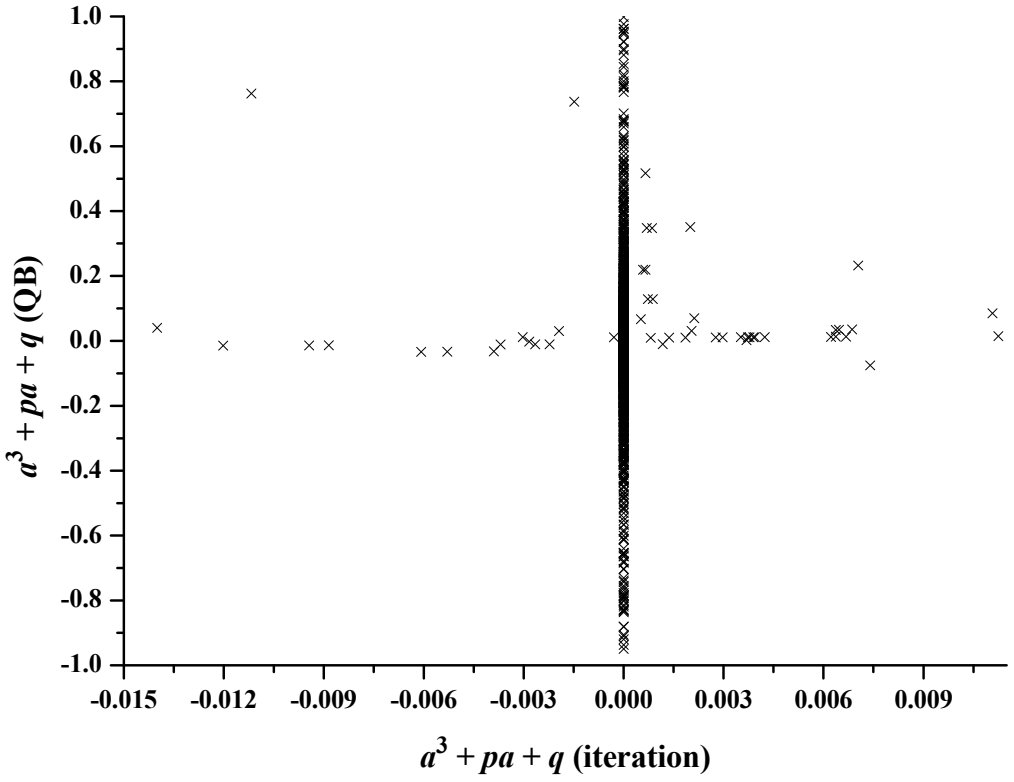

Fig. A.1. A comparison of the root of the SR polynomial, checked by evaluating $a^3 + pa + q$ for 0, using the QuickBASIC and spreadsheet iterative methods, for a month of 30-min SR data from the Bellevue mesic grassland site.

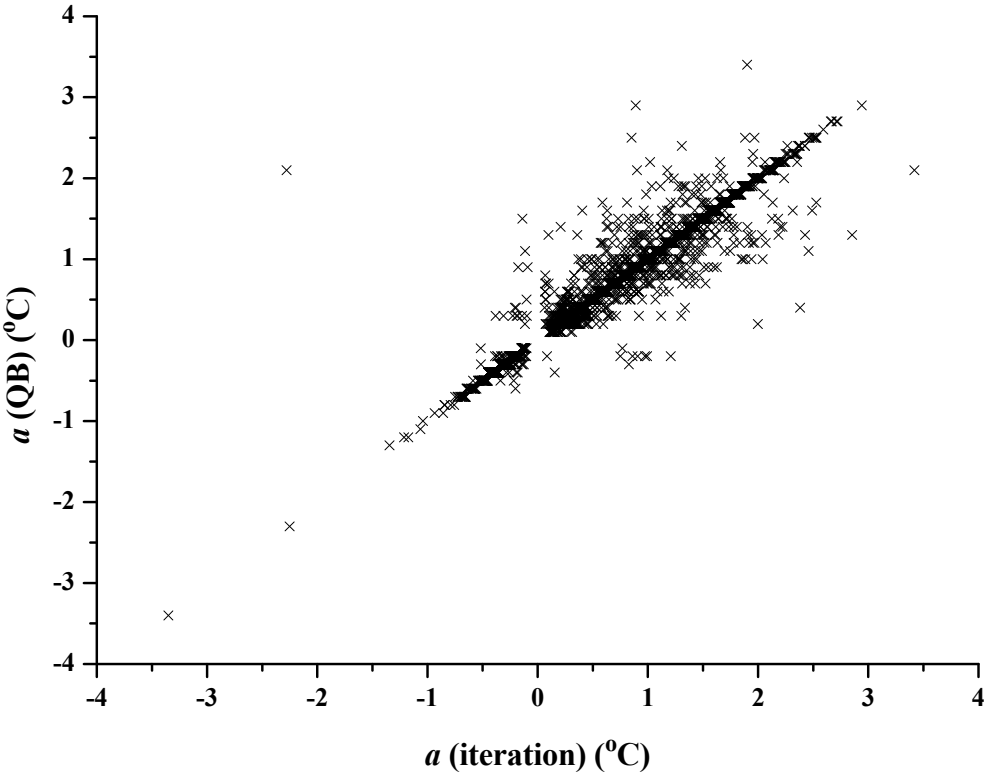

Fig. A.2. A comparison of 30-min SR air temperature ramp amplitude *a* (°C), using the QuickBASIC and spreadsheet iterative methods, for a month of data from the Bellevue mesic grassland site.

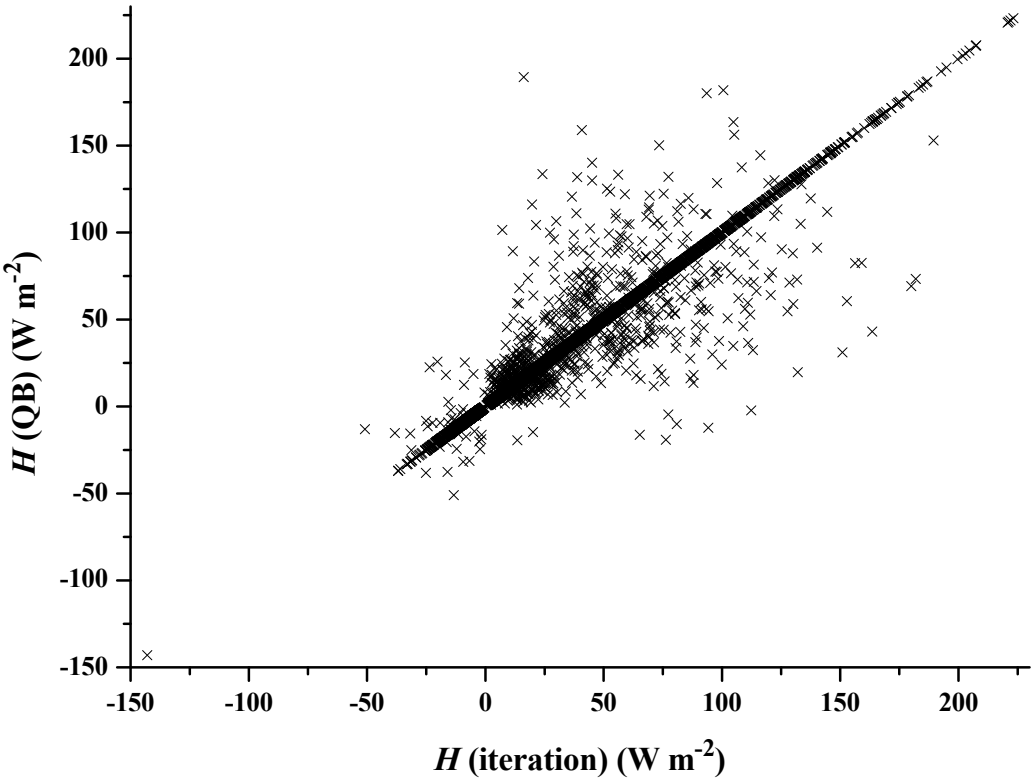

Fig. A.3. A comparison of 30-min H_{SR} (W m^{-2}) estimates, using the QuickBASIC and spreadsheet iterative methods, for a month of data from the Bellevue mesic grassland site.

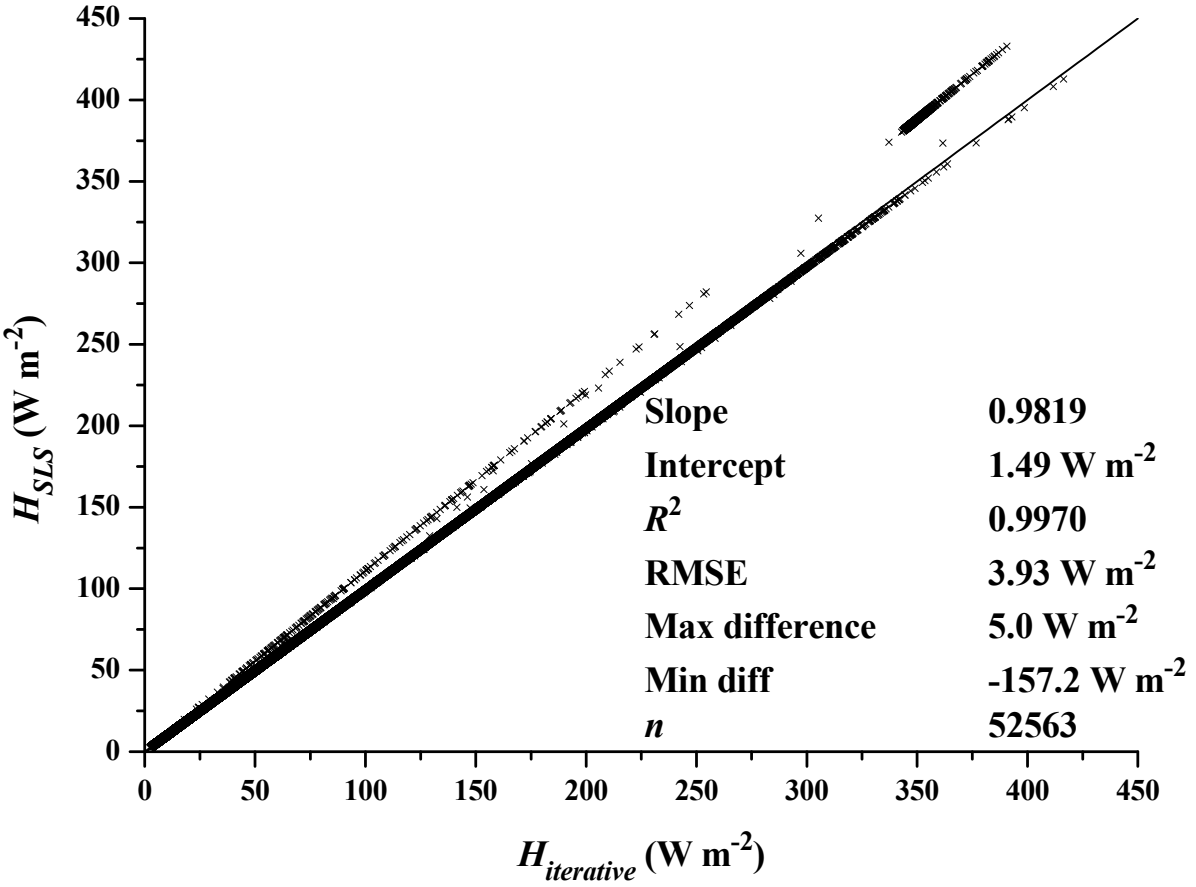

Fig. A.4. A comparison of 2-min H_{SLS} (W m^{-2}), using the QuickBASIC and spreadsheet iterative methods, for a three months' of data from the Bellevue mesic grassland site.

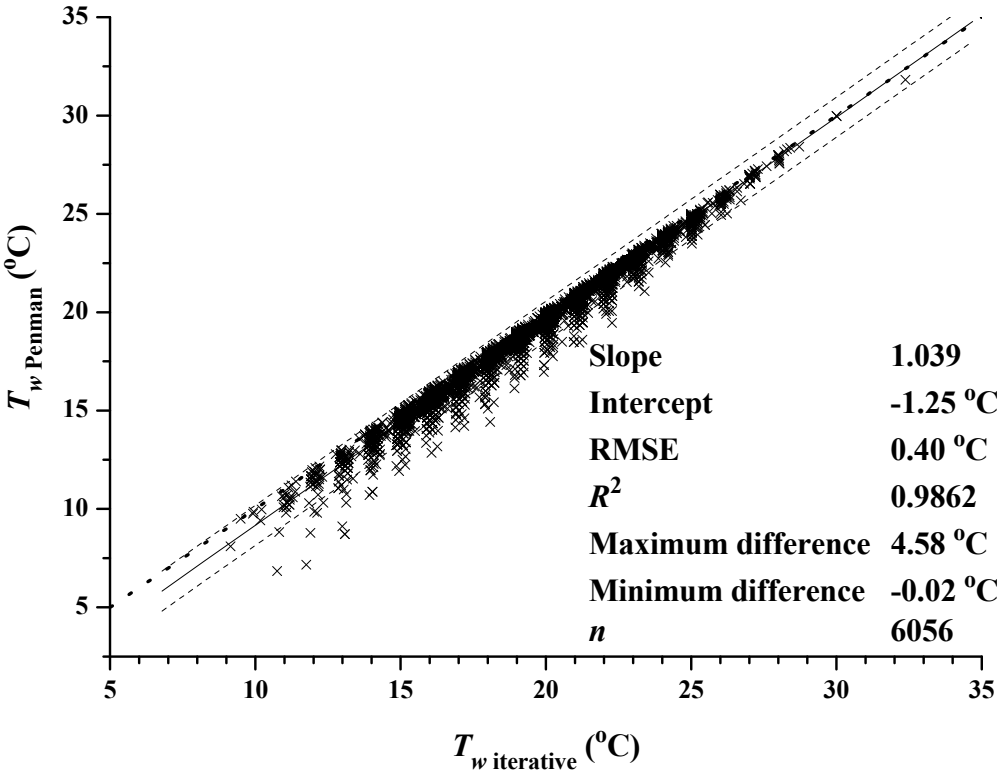

Fig. A.5. A comparison of the daily 14h00 wet bulb temperature (°C), estimated using the Penman method (Eq. (A.20)), against that obtained using the single-cell spreadsheet method (Eq. (A.27)) for the Kaalrug site (1990 to 2006 dataset).

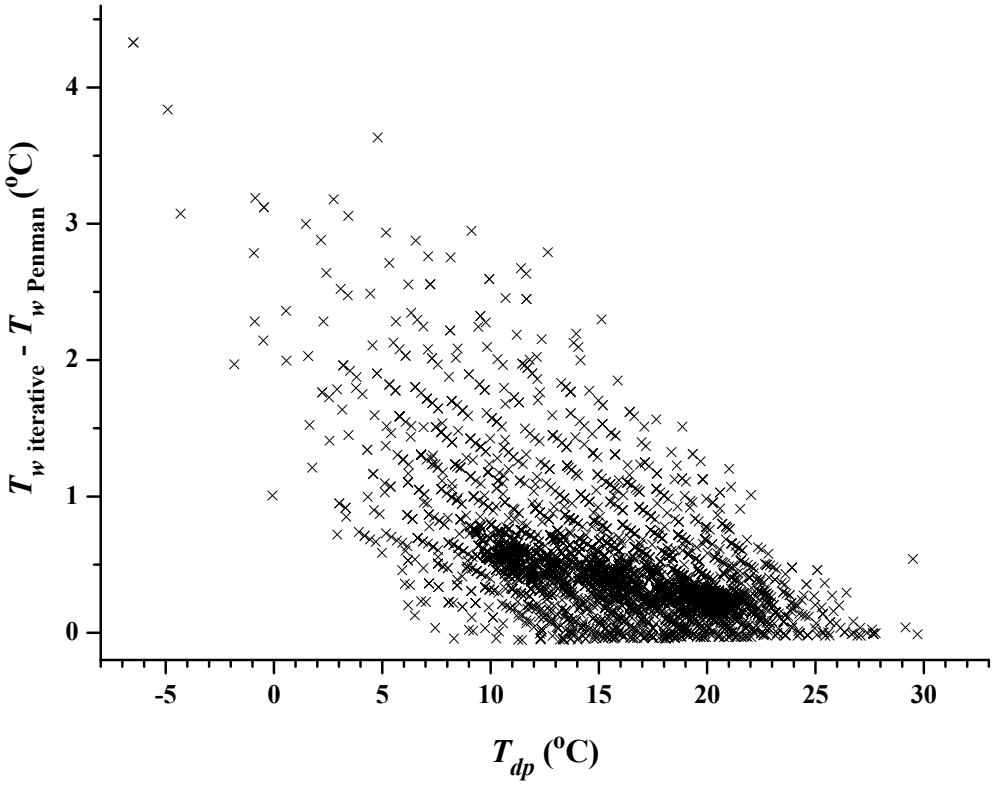

Fig. A.6. The difference in the daily 14h00 wet bulb temperature between the iterative and Penman methods (Eqs (A.20) and (A.27) respectively), as a function of the dew point temperature, for the Kaalrug site (1990 to 2006 dataset).

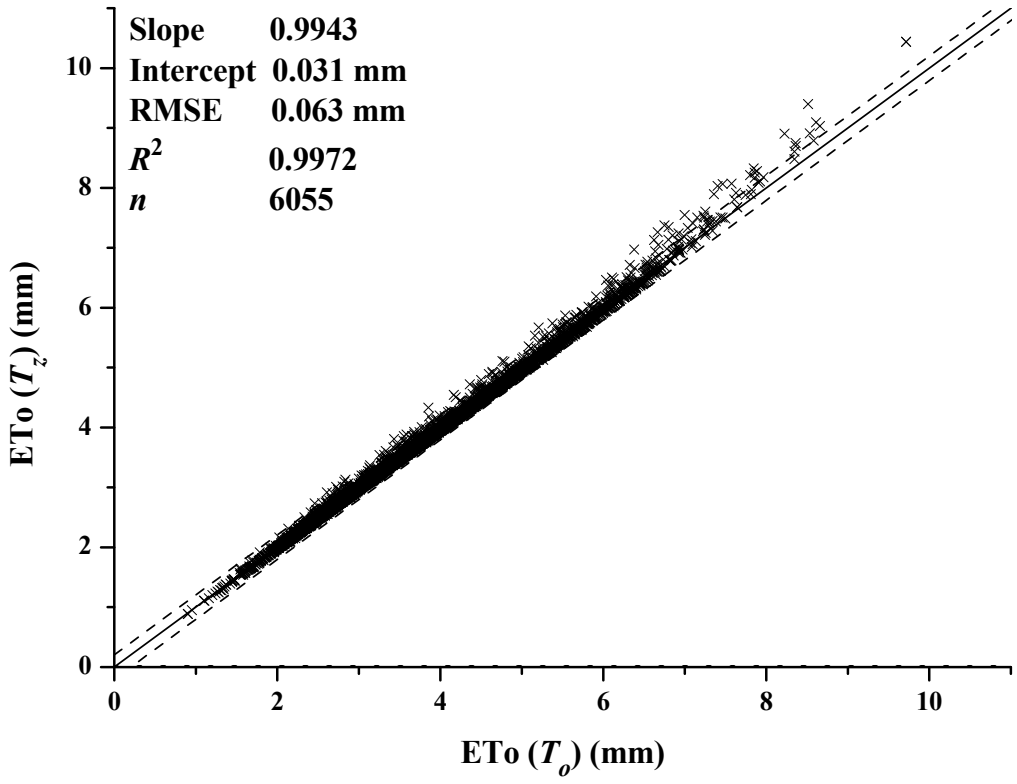

Fig. A.7. A comparison between daily grass reference ETo(T_z) and ETo(T_o) (mm) for the Kaalrug 16-year dataset.

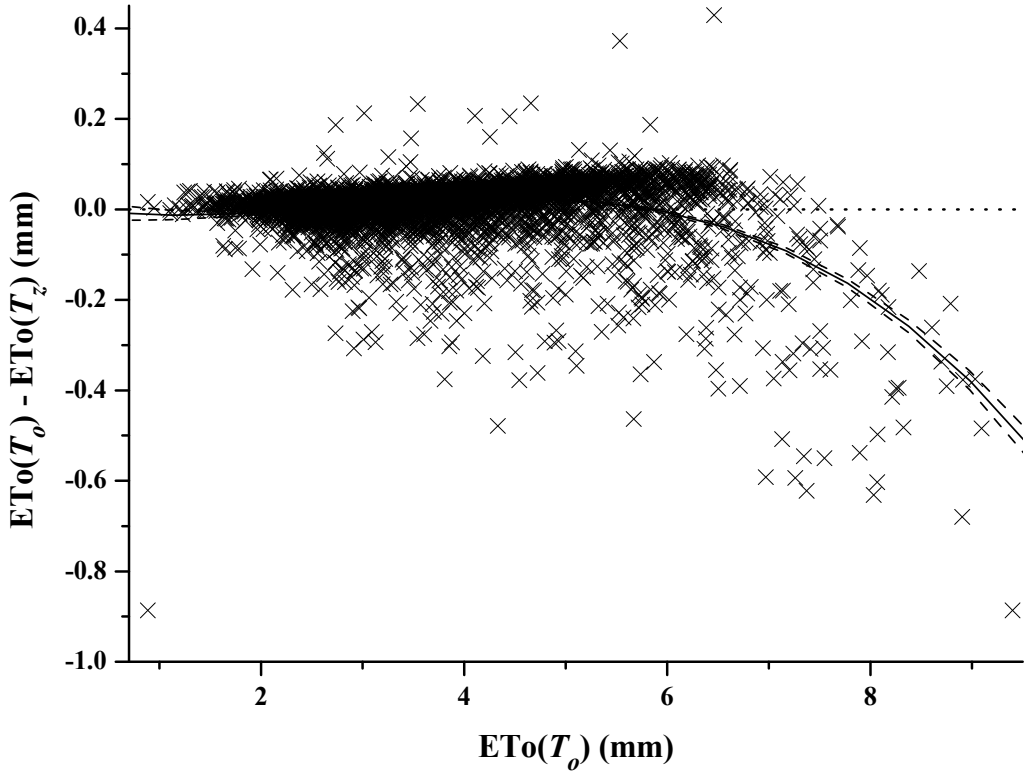

Fig. A.8. A plot of the difference between daily ETo(T_z) *vs* ETo(T_o) and ETo(T_o) (mm) for the Kaalrug 16-year dataset.

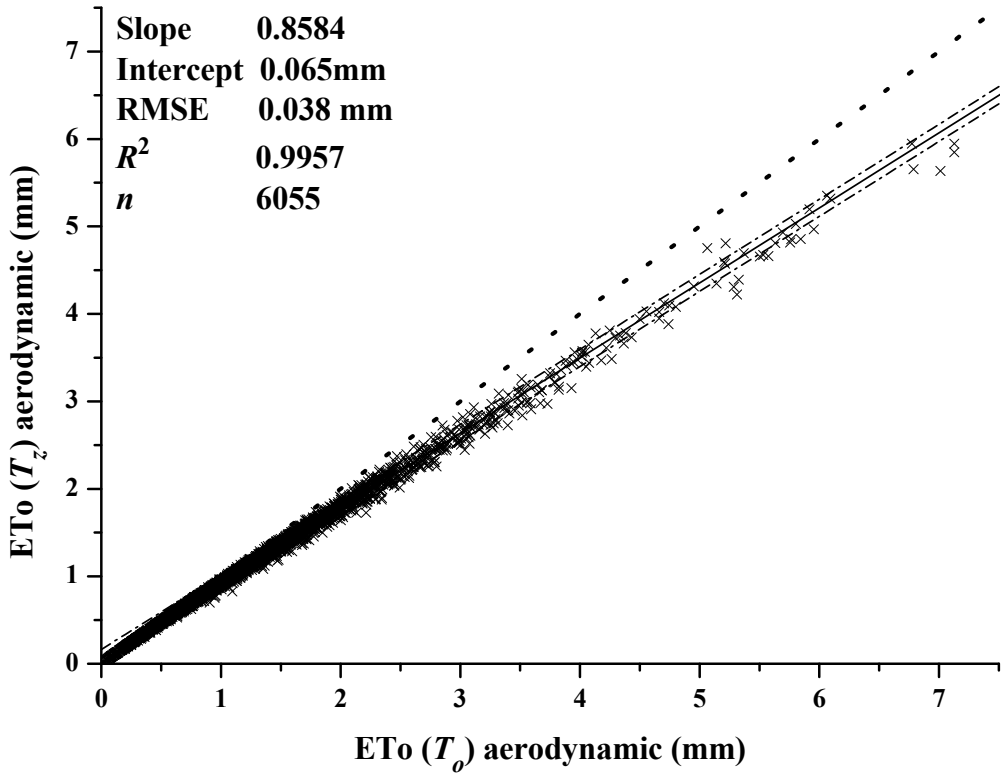

Fig. A.9. A comparison between the daily aerodynamic component of ETo(T_z) and that of ETo(T_o) (mm) for the Kaalrug 16-year dataset.

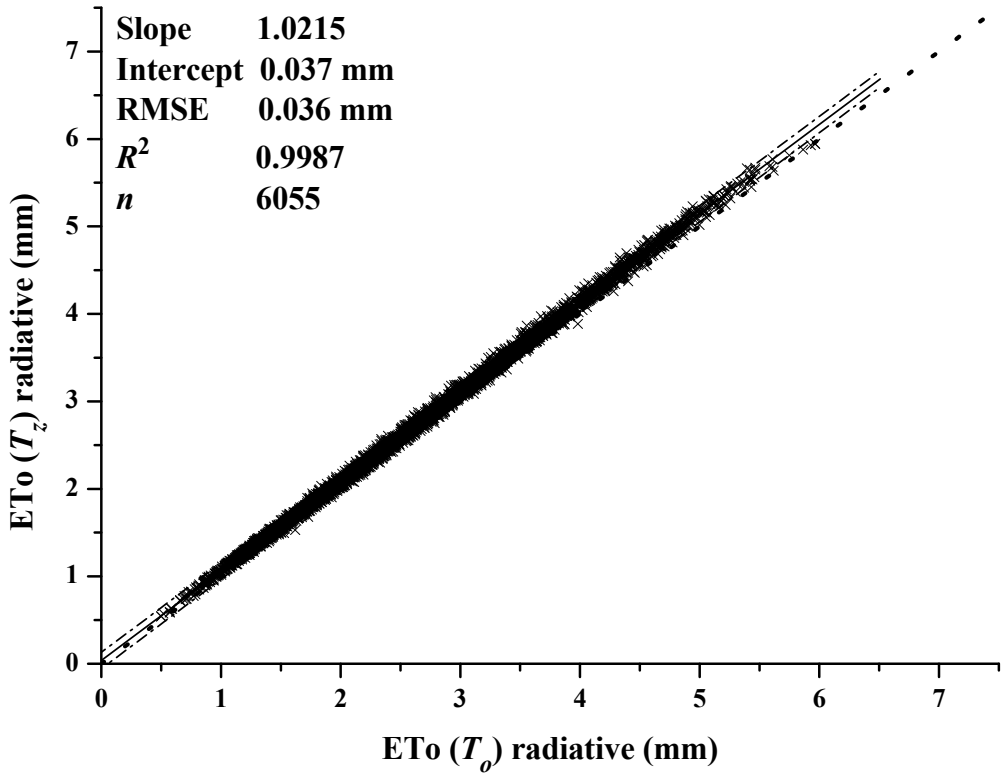

Fig. A.10. A comparison between the daily radiative component of ETo(T_z) and that of ETo(T_o) (mm) for the Kaalrug 16-year dataset.

Calculation of Obukhov length and sensible heat and momentum fluxes for unstable and stable conditions using a single-cell spreadsheet implementation of an iterative procedure

Obukhov length *L* (unstable)
=IF(*L*=0,*L*-0.00001,IF(OR(*CT2*=0,ε=0),"",IF(ABS((1-7*(*z* - *d*)/*L*+75*((*z* - *d*)/*L*)^2)^(-1/6))<0.000001,-0.001,-(*T*+273.15)*(0.4*9.81)^(-1)*ε^(2/3)*(0.4*(*z* - *d*))^(1/3)**CT2*^(-1/2)*((1-3*(*z* - *d*)/*L*)^(-1)-(*z* - *d*)/*L*)^(-2/3)*(0.4)^(1/3)*(6.34)^(1/2)*(1-7*(*z* - *d*)/*L*+75*((*z* - *d*)/*L*)^2)^(-1/6))))

Sensible heat flux *H* (unstable)
=IF(*L*="","",1.1045*1000*(ε*0.41*(*z* - *d*))^(1/3)*((1-3*(*z* - *d*)/*L*)^-1-(*z* - *d*)/*L*)^(-1/3)**CT2*^(1/2)*(0.4*(*z* - *d*))^(1/3)*0.4^(-1/3)*(6.34)^(-1/2)*(1-7*(*z* - *d*)/*L*+75*((*z* - *d*)/*L*)^2)^(1/6))
Comment: 1.1045*1000 corresponds to $\rho\, c_p$

Momentum flux τ (unstable)
=IF(*L*="","",1.1045*((ε*0.4*(*z* - *d*))^(1/3)*((1-3*(*z* - *d*)/*L*)^-1-(*z* - *d*)/*L*)^(-1/3))^2)
Comment: 1.1045 corresponds to ρ

Obukhov length *L* (stable)
=IF(*L*=0,*L*+0.00001,IF(OR(*CT2*=0,ε=0),"",(*T*+273.15)*(0.4*9.81)^(-1)*ε^(2/3)*(0.4*(*z* - *d*))^(1/3)**CT2*^(-1/2)*(1+4*(*z* - *d*)/*L*+16*((*z* - *d*)/*L*)^2)^(-1/3)*(((*z* - *d*))^(-1/3))*0.4^(1/3)*(6.34)^(1/2)*(1+7*(*z* - *d*)/*L*+20*((*z* - *d*)/*L*)^2)^(1/6)))
Comment: 9.81 corresponds to the acceleration of gravity (m s^{-2}) *g* and 6.34 to $4\beta_l/k^{2/3}$where β_l is the Obukhov-Corrsin constant (= 0.86) and *k* is the von Kármán constant (= 0.4). The coefficient 6.34 is obtained from $4\beta_1 / k^{2/3}$ where β_1 = 0.86 is the Obukhov-Corrsin constant and k = 0.4. Thiermann and Grassl (1992) used k = 0.41 for which $4\beta_1 / k^{2/3}$ = 6.23.

Sensible heat flux *H* (stable)
=IF(*L*="","",-1.1045*1000*(ε*0.4*(*z* - *d*))^(1/3)*(1+4*(*z* - *d*)/*L*+16*((*z* - *d*)/*L*)^2)^(-1/6)**CT2*^(1/2)*(0.4*(*z* - *d*))^(1/3)*0.4^(-1/3)*(6.34)^(-1/2)*(1+7*(*z* - *d*)/*L*+20*((*z* - *d*)/*L*)^2)^(-1/6))

Momentum flux τ (stable)
=IF(*L*="","",1.1045*((ε*0.4*(*z* - *d*))^(1/3)*(1+4*(*z* - *d*)/*L*+16*((*z* - *d*)/*L*)^2)^(-1/6))^2)

Calculation of surface renewal ramp amplitude, ramp period and sensible heat flux for unstable and stable conditions using a single-cell spreadsheet implementation of an iterative procedure

Notes:
1. The input measurements for the SR method are S_r^2, S_r^3 and S_r^5, the second-, third- and fifth-order of the air temperature structure function.
2. the cell for ramp amplitude should refer to the current cell for the iterative procedure to function.
3. Both the lag time r (= j/f), and the measurement height z above the soil surface need to be specified as fixed cell references.
4. A positive sign is attached to the ramp amplitude a if $S_r^3 > 0$, corresponding to unstable conditions. This condition allows the calculation in a single-cell.
5. Once the roots have been obtained, a check is performed in a fourth cell to ensure that the value is indeed a root.

Ramp amplitude a
= (- S_r^3 /ABS(S_r^3))*ABS(-10* S_r^2 *a +(S_r^5 / S_r^3)*a -10* S_r^3)^(1/3)

Ramp period τ
= IF(AND(-$a^{3*}r$/ S_r^3 >=5*r,-$a^{3*}r$/ S_r^3 <=600),-$a^{3*}r$/ S_r^3 ,"")

Sensible heat flux H
=IF(ABS(*check*)<0.001,IF(τ<=5*r,"",1216*z*a/τ),"")

check
=a^3+(10* S_r^2 - S_r^5 / S_r^3)*a+10* S_r^3

Ramp amplitude a (with ISERROR function to trap any error value (#N/A, #VALUE!, #REF!, #DIV/0!, #NUM!, #NAME?, or #NULL!).
=IF(ISERROR((- S_r^3 /ABS(S_r^3))*ABS(-10* S_r^2 *a +(S_r^5 / S_r^3)*a -10* S_r^3)^(1/3)),"",(- S_r^3 /ABS(S_r^3))*ABS(-10* S_r^2 *a +(S_r^5 / S_r^3)*a -10* S_r^3)^(1/3))

Ramp period τ
=IF(ISERROR(IF(AND(-$a^{3*}r$/ S_r^3 >=5*r,-$a^{3*}r$/ S_r^3 <=600),-$a^{3*}r$/ S_r^3 ,"")),"",IF(AND(-$a^{3*}r$/ S_r^3 >=5*r,-$a^{3*}r$/ S_r^3 <=600),-$a^{3*}r$/ S_r^3 ,""))

Sensible heat flux H
=IF(ISERROR(IF(ABS(*check*)<0.001,IF(τ<=5*r,"",1216*z*a/τ),"")),"",IF(ABS(*check*)<0.001,IF(τ<=5*r,"",1216*z*a/τ),""))

check
=IF(ISERROR(a^3+(10* S_r^2 - S_r^5 / S_r^3)*a+10* S_r^3),"",a^3+(10* S_r^2 - S_r^5 / S_r^3)*a+10* S_r^3)

Calculation of the wet bulb temperature using the psychrometric equation and a single-cell spreadsheet implementation of an iterative procedure

L_v (MJ kg^{-1})
=2.501-T_w*2.361*10^-3

P (kPa)
=101.325-((-0.01094866*e*1000+2934.7773)/(8.31451*(T_d+273.15)+0.28362157**altitude_m*)*9.79267**altitude_m*/1000)

c_p (MJ kg^{-1} K^{-1})
=10^-6*(1004.722587+1148.254385*e/(P-e)+1.256*(1+T_d/40)*(1+(e/(0.6108*EXP((17.2694*T_d)/(237.3+T_d))))))

γ (kPa K^{-1})
=c_p*P/(0.622*λ)

T_w (^{o}C)
=IF(ABS(0.6108*EXP((17.2694*T_w)/(237.3+ Tw))-γ*(P/100)*(T_d - T_w)*(1+0.00115*T_w)-e)>0.01,T_w+0.01,T_w)

Calculation of Penman-Monteith grass reference evaporation using an iterative procedure

Declination (rad)
=-0.409*SIN((2*PI()/365)*doy-1.39)

Hour angle (rad)
=IF(lat>0,ACOS(-TAN((2*PI()/360)*-1*lat)*TAN(decl)),ACOS(TAN((2*PI()/360)*lat)*TAN(decl)))

Tz (^{o}C)
=(((360/(2*PI()))*(2/15)*hourangle)*Tzmax+(24-((360/(2*PI()))*(2/15)*hourangle))*Tzmin)/24

Tdp (^{o}C)
=IF(ez=0,-273.16+(273.16-2.0765067*LN((ez+0.001)/0.6108))/(1-0.0579059*LN((ez+0.001)/0.6108)),-273.16+(273.16-2.0765067*LN(ez/0.6108))/(1-0.0579059*LN(ez/0.6108)))

vpd (kPa)
=(0.6108*(EXP(17.27*Tzmax/(Tzmax+237.3))+EXP(17.27*Tzmin/(Tzmin+237.3)))/2)-ez

Tw (^{o}C)
=IF(Twet>=Tz,Tz,IF(ABS(0.6108*EXP((17.2694*Twet)/(237.3+Twet))-gamma*((101.325-((-0.01094866*ez*1000+2934.7773)/(8.31451*(Tz+273.15)+0.28362157*alt))*9.79267*alt/1000)/100)*(Tz-Twet)*(1+0.00115*Twet)-ez)>0.01,Twet+0.02,Twet))

Twet check (^{o}C)
=0.6108*EXP((17.2694*Twet)/(237.3+Twet))-gamma*((101.325-((-0.01094866*ez*1000+2934.7773)/(8.31451*(Tz+273.15)+0.28362157*alt))*9.79267*alt/1000)/100)*(Tz-Twet)*(1+0.00115*Twet)-ez

Twet Penman (1948) (^{o}C)
=(gamma*Tz+delta_Tz*Tdp)/(gamma+delta_Tz)

Twet check for Penman (1948) (^{o}C)
=0.6108*EXP((17.2694*X55)/(237.3+Twet))-gamma*((101.325-((-0.01094866*ez*1000+2934.7773)/(8.31451*(Tz+273.15)+0.28362157*alt))*9.79267*alt/1000)/100)*(Tz-((gamma*Tz+delta_Tz*Tdp)/(gamma+delta_Tz)))*(1+0.00115*((gamma*Tz+delta_Tz*Tdp)/(gamma+delta_Tz)))-ez
Comment: delta_Tz is the slope of the saturation water vapour pressure vs temperature relationship evaluated at Tz

Uz (m s^{-1})
=IF(u="",2,u*4.87/(LN(67.8*zu-5.42)))
Comment: Uz is the wind speed at height z and zu is the wind speed measurement height

Is0 (MJ m^{-2})
=118.08*((1+0.033*COS(2*PI()*doy/365))/PI())*(hourangle*SIN((2*PI()/360)*-1*lat)*SIN(decl)+SIN(hourangle)*COS((2*PI()/360)*-1*lat)*COS(decl))

Is (MJ m^{-2})
=IF(Is>0,Is,0.17*(((293.15-0.01*alt)/293.15)^(9.8/(0.01*286.9)))*((Tzmax-Tzmin)^0.5)*Is0)

Net solar (ins) (MJ m^{-2})
=IF(Is>0,(1-0.23)*Is,(1-rfrac)*0.17*(((293.15-0.01*alt)/293.15)^(9.8/(0.01*286.9)))*((Tzmax-Tzmin)^0.5)*Is0)

Net infrared (inl) (MJ m^{-2})
=IF(Is>0,(1.35*Is/(0.75*Is0)-0.35)*4.9*10^-9*(0.34-0.14*ez^0.5)*((Tzmax+273)^4+(Tzmin+273)^4)/2,(1.35*(ins/(1-0.23))/(0.75*Is0)-0.35)*4.9*10^-9*(0.34-0.14*ez^0.5)*((Tzmax+273)^4+(Tzmin+273)^4)/2)

fsoil (MJ m^{-2})
=IF(ISERROR(J54+K54),"",IF(Tzmax>0,0.38*(Tz-(J54+K54)/2),0))
Comment: fsoil is the soil heat flux. This calculation assumes that the cursor is currently on row 55 and that the Tzmax and Tzmin values for the previous day are in cells J54 and K54 respectively

gamma (kPa K^{-1})
=0.00163*101.35*((293.15-0.01*alt)/293.15)^(9.8/(0.01*286.9))/((2.501-(2.361*10^-3)*Twet))

delta_Tz (kPa K^{-1})
=4098*0.611*EXP(17.27*Tz/(Tz+237.3))/(Tz+237.3)^2
Comment: delta_Tz is the slope of the saturation water vapour pressure vs temperature relationship evaluated at Tz

Erad_Tz (mm)
=IF(ISERROR((0.408*delta_Tz*(ins-inl-fsoil))/(delta_Tz+gamma*(1+0.34*Uz))),"",(0.408*delta_Tz*(ins-inl-fsoil))/(delta_Tz+gamma*(1+0.34*Uz)))
Comment: This is the radiative component of ETo computed using delta calculated from Tz; ins is the net solar irradiance; inl is the net infrared irradiance; fsoil is the soil heat flux

Eaero_Tz (mm)
=(gamma*900*Uz*vpd/((Tz+273))/(delta_Tz+gamma*(1+0.34*Uz)))
Comment: This is the aerodynamic component of ETo computed using delta calculated from Tz; Uz is the wind speed at height z

ETo_Tz (mm)
=IF(ISERROR(K54+L54),"",(0.408*delta_Tz*(ins-inl-fsoil)+gamma*900*Uz*vpd/(Tz+273))/(delta_Tz+gamma*(1+0.34*Uz)))

To (^{o}C)
=IF(ISERROR(Tz+(208/Uz)*gamma*(70+208/Uz)/(208/Uz)*(ins-inl-fsoil)/((1/(8.3143*(Tz+273.15)))*(18.02*ez+28.96*(101.35*((293.15-0.01*alt)/293.15)^(9.8/(0.01*286.9))))*(1004.723+1148.254*ez/((101.35*((293.15-0.01*alt)/293.15)^(9.8/(0.01*286.9)))-ez)+1.256*(1+Tz/40)*((1+(ez/(0.6108*EXP(17.27*Tz/(Tz+237.3))))/100)))*(delta_esTo_esTz+gamma*(70+208/Uz)/(208/Uz)))-vpd/(delta_esTo_esTz+gamma*(70+208/Uz)/(208/Uz))),Tz,Tz+(208/Uz)*gamma*(70+208/Uz)/(208/Uz)*(ins-inl-fsoil)/((1/(8.3143*(Tz+273.15)))*(18.02*ez+28.96*(101.35*((293.15-0.01*alt)/293.15)^(9.8/(0.01*286.9))))*(1004.723+1148.254*ez/((101.35*((293.15-0.01*alt)/293.15)^(9.8/(0.01*286.9)))-ez)+1.256*(1+Tz/40)*((1+(ez/(0.6108*EXP(17.27*Tz/(Tz+237.3))))/100)))*(delta_esTo_esTz+gamma*(70+208/Uz)/(208/Uz)))-vpd/(delta_esTo_esTz+gamma*(70+208/Uz)/(208/Uz)))

Delta (esTo-esTz)/(To-Tz)
=IF(ISERROR((0.6108*EXP(17.27*To/(To+237.3))-0.6108*EXP(17.27*Tz/(Tz+237.3)))/(To-Tz)),delta_Tz,(0.6108*EXP(17.27*To/(To+237.3))-0.6108*EXP(17.27*Tz/(Tz+237.3)))/(To-Tz))

Erad To (mm)
=IF(ISERROR(0.408*delta_esTo_esTz*(ins-inl-fsoil)/(delta_esTo_esTz+gamma*(1+0.34*Uz))),"",0.408*delta_esTo_esTz*(ins-inl-fsoil)/(delta_esTo_esTz+gamma*(1+0.34*Uz)))
Comment: This is the radiative component of ETo computed using delta calculated from To and Tz
Eaero To (mm)
=(gamma*900*Uz*vpd/(To+273))/(delta_esTo_esTz+gamma*(1+0.34*Uz))
Comment: This is the aerodynamic component of ETo computed using delta calculated from To and Tz

ETo_To (mm)

```
=IF(ISERROR((0.408*delta_esTo_esTz*(ins-inl-
fsoil)+gamma*900*Uz*vpd/(Tz+273))/(delta_esTo_esTz+gamma*(1+0.34*Uz))),"",(0.408*delta_esTo_esTz*(ins-inl-
fsoil)+gamma*900*Uz*vpd/(Tz+273))/(delta_esTo_esTz+gamma*(1+0.34*Uz)))
```